BEILSTEIN JOURNAL OF ORGANIC CHEMISTRY

Superstructures with cyclodextrins: Chemistry and applications

Edited by Helmut Ritter

Imprint

Beilstein Journal of Organic Chemistry
www.bjoc.org
ISSN 1860-5397
Email: journals-support@beilstein-institut.de

The *Beilstein Journal of Organic Chemistry* is published by the Beilstein-Institut zur Förderung der Chemischen Wissenschaften.

Beilstein-Institut zur Förderung der Chemischen Wissenschaften
Trakehner Straße 7–9
60487 Frankfurt am Main
Germany
www.beilstein-institut.de

Beilstein Journal of Organic Chemistry

Superstructures with cyclodextrins: Chemistry and applications

Helmut Ritter

Editorial

Open Access

Address:
Institute of Organic Chemistry and Macromolecular Chemistry II, Heinrich-Heine-University of Düsseldorf, Universitätsstraße 1, D-40225 Düsseldorf, Germany

Email:
Helmut Ritter - h.ritter@uni-duesseldorf.de

Keywords:
cyclodextrins; superstructures

Beilstein J. Org. Chem. **2012,** *8,* 1303–1304.
doi:10.3762/bjoc.8.148

Received: 16 July 2012
Accepted: 17 July 2012
Published: 16 August 2012

This article is part of the Thematic Series "Superstructures with cyclodextrins: Chemistry and applications".

Guest Editor: H. Ritter

Cyclodextrins (CDs) are cyclic oligosaccharides consisting of 6 (α), 7 (β) and 8 (γ) 1,4-glycosidically linked α-D-glucose units. Production of these compounds is accomplished by enzymatic degradation of starch using CD-glycosyl transferase.

Since their discovery more than 100 years ago, a significant development in CD research has taken place. Right after their discovery, CDs were very expensive due to the fact that only small quantities were available. In addition to this, it was assumed that CDs are toxic to human beings. Meanwhile, things have changed. Now, large quantities of CDs are available at low prices. Additionally, it could be demonstrated that CDs are not toxic to humans. Various applications of CDs can be found, e.g. the binding of odors and flavors. Even drugs can be complexed and set free after a while by CDs. This enables the transfer of hydrophobic substances into aqueous media, which is of great interest in pharmaceutical chemistry. For instance, release and molecular dispersion of antihistamines in the tear fluid are achieved very quickly by means of amylase catalysis.

Regarding the interactions of CDs with low-molecular and macromolecular compounds, respectively, the reactivity of complexed molecules is another key factor besides solubility effects. For example, differences in the absorption spectra of some compounds are caused by complexation with CDs.

For analytical purposes, CDs are used as chiral hosts. Thus, the application of CDs in column chromatography and HPLC to isolate and separate suitable racemic mixtures is broadly established. More recently, the use of CDs as food additives was approved. For example, dispersion of triglycerides can be achieved by the addition of α-CD.

In organic synthesis and polymer chemistry, the interest in CDs has increased significantly during the past decades. For instance, in the latter case covalent attachment of CDs to macromolecules and threading of CD molecules onto suitable macromolecular chains could be demonstrated. Unlike other macrocycles such as crown ethers or calixarenes, the cavity of CDs is

big enough to include more or less hydrophobic molecules completely. In contrast to macrocyclic cucurbiturils, CDs show a better solubility in water. On top of that, they are also biodegradable.

Considering the importance of CDs as demonstrated above, we felt encouraged to summarize some of the latest results achieved in CD research. Contributions from leading research groups dealing with CDs can be found in this Thematic Series of the Beilstein Journal of Organic Chemistry.

Helmut Ritter

Düsseldorf, July 2012

Beilstein Journal of Organic Chemistry

Cyclodextrin nanosponge-sensitized enantiodifferentiating photoisomerization of cyclooctene and 1,3-cyclooctadiene

Wenting Liang[1], Cheng Yang[*1], Masaki Nishijima[1], Gaku Fukuhara[1], Tadashi Mori[1], Andrea Mele[*2], Franca Castiglione[2], Fabrizio Caldera[3], Francesco Trotta[*3] and Yoshihisa Inoue[*1]

Letter

Open Access

Address:
[1]Department of Applied Chemistry and Center for Advanced Science and Innovation, Osaka University, 2-1 Yamada-oka, Suita 565-0871, Japan, [2]Department of Chemistry, Materials and Chemical Engineering "G. Natta" – Politecnico di Milano, Piazza L. Da Vinci 32, 20133 Milano, Italy and [3]Department of Chemistry, University of Torino, Via P. Giuria 7, 10125 Torino, Italy

Email:
Cheng Yang[*] - c.yang@chem.eng.osaka-u.ac.jp; Andrea Mele[*] - andrea.mele@polimi.it; Francesco Trotta[*] - francesco.trotta@unito.it; Yoshihisa Inoue[*] - inoue@chem.eng.osaka-u.ac.jp

* Corresponding author

Keywords:
cyclodextrins; 1,3-cyclooctadiene; cyclooctene; nanosponge; photochirogenesis; photoisomerization

Beilstein J. Org. Chem. **2012,** *8,* 1305–1311.
doi:10.3762/bjoc.8.149

Received: 05 April 2012
Accepted: 27 June 2012
Published: 16 August 2012

This article is part of the Thematic Series "Superstructures with cyclodextrins: Chemistry and applications".

Guest Editor: H. Ritter

Abstract

Enantiodifferentiating geometrical photoisomerizations of (*Z*)-cyclooctene and (*Z,Z*)-1,3-cyclooctadiene were performed by using the pyromellitate-linked cyclodextrin network polymer, termed "cyclodextrin nanosponge (CDNS)", as a supramolecular sensitizing host. The photochirogenic behavior of the nanosponges incorporating β- or γ-cyclodextrin was significantly different from that reported for the conventional sensitizer-appended monomeric cyclodextrins, affording chiral (*E*)-cyclooctene and (*E,Z*)-cyclooctadiene in enantiomeric excesses critically dependent on the solution pH and solvent composition employed, revealing the active roles of chiral void spaces of CDNS in the photochirogenic reaction.

Introduction

The precise control of chiral photoreactions, or photochirogenesis, is one of the most challenging topics in current photochemistry [1-3]. Weak intermolecular interactions, short lifetime and high reactivity of the excited-state substrate are the major causes that prevent efficient asymmetric induction in chiral photochemistry. A supramolecular approach to photochirogenesis provides a convenient and also promising tool to facilitate the excited-state chirality transfer from chiral host to prochiral substrate through the long-lasting intimate supramolecular contacts of guest substrate(s) with the chiral host in

both the ground and excited states [4-10]. Various types of chiral supramolecular hosts, including modified zeolites [11], hydrogen-bonding templates [12], cyclodextrins [13-21] and serum albumins [22,23], have hitherto been employed to mediate chiral photoreactions. External factors, such as temperature [13], solvent [17], pressure [18] and irradiation wavelength [24], have also been found to play crucial roles in controlling supramolecular photochirogenesis.

Amongst the chiral supramolecular hosts that have been applied to photochirogenesis, cyclodextrin (CD) is undoubtedly the most frequently employed, probably due to its ready availability, modifiability, inherently chiral cavity, and optical transparency down to the UV region [3,4]. Nevertheless, the foregoing studies on CD-based supramolecular photochirogenesis have focused primarily on the use of native and singly or doubly modified monomeric CDs. In this communication, we report the results of the first supramolecular photochirogenesis to use pyromellitate-linked polymeric β- and γ-CDs, termed "cyclodextrin nanosponges" (CDNSs) [25-33], as sensitizing hosts for the enantiodifferentiating photoisomerization of (*Z*)-cyclooctene (**1Z**) [34-37] and (*Z,Z*)-1,3-cyclooctadiene (**2ZZ**) [38-40] (Scheme 1). Enantiodifferentiating photosensitization of **1Z** and **2ZZ** was extensively studied by using different kinds of conventional and supramolecular chiral photosensitizers (Scheme 2). The enantioselectivity obtained is generally low to moderate, despite that fact that some reactions were performed at very low temperatures (below −100 °C).

Results and Discussion

CDNSs **3**, **4** and **5** were prepared in almost quantitative yields by reacting pyromellitic dianhydride (PDA) with β-CD or γ-CD in the presence of triethylamine in dimethyl sulfoxide at room temperature (Scheme 1) and purified by extensive Soxhlet extraction with acetone, as reported previously [41]. We termed these cross-linked CD network polymers as "nanosponges", because these CD-based polymers show a nanoporous structure and a property of swelling upon absorption of water. The ability to entrap organic molecules can be ascribed to both the pores generated by the polymerization reaction and to the CD cavities. Recently, the relationship between the networking properties of CD nanosponges and the CD/cross linker ratio employed upon synthesis, was revealed by inelastic light-scattering experiments. Thus, the CD/cross linker ratio can be conveniently used as a descriptor of the degree of cross linking and the elastic properties [42]. By using Raman and Brillouin scattering experiments, we found that increasing the PMA/CD ratio leads to an increase in the degree of cross linking, with the frequency of the maximum boson peak in cross-polarized Raman spectra shifting to higher wavenumbers. On the other hand, the stiffness of the polymeric network of CDNSs is more affected by the PMA/CD ratio, rather than the type of CD used.

The adsorption, absorption and inclusion properties of these new materials have been demonstrated for a large variety of substrates, including some pharmaceuticals [25], enzymes [26], pollutants [27], polymers [28], agrochemicals [29], and metal ions [30].

The complexation behavior of **1Z** and **2ZZ** with CDNSs was examined by means of circular dichroism spectroscopy, showing negative induced circular dichroism (ICD) at the ^1L_a band and more weakly at the ^1L_b band in aqueous solution (Figure 1a). On the basis of the sector rule proposed by Kajtar et al. [43,44], the pyromellitate (PM) units in the polymer network are deduced to be perching on or shallowly included in the CD cavity, placing the ^1L_a and ^1L_b transitions in the negative region (Figure 1c). The addition of **1Z** to the solution of **3** caused a small but steady enhancement of the negative ICD (Figure 1b), which is rationalized by assuming that the PM unit is excluded from the cavity to better accommodate guest **1Z** and hence becomes more parallel to the portal plane, inducing

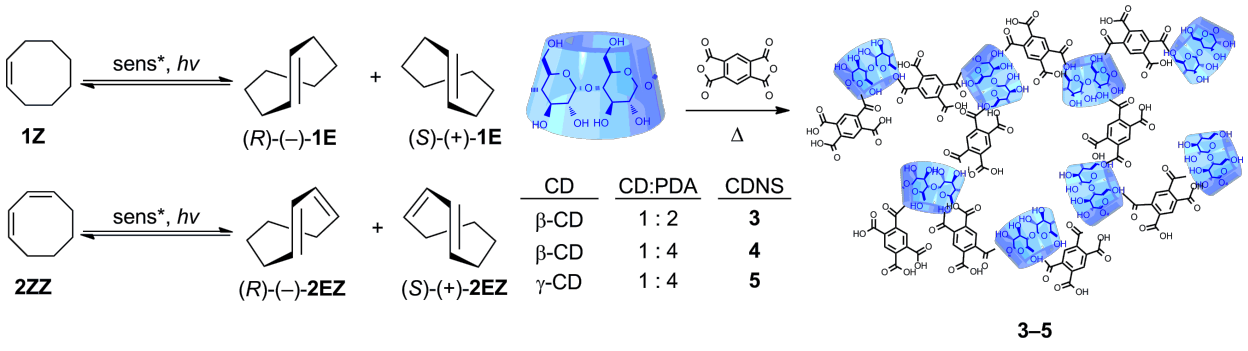

Scheme 1: Enantiodifferentiating photoisomerizations of **1Z** and **2ZZ** sensitized by β- and γ-cyclodextrin nanosponges (CDNSs) cross linked by pyromellitic dianhydride (PDA).

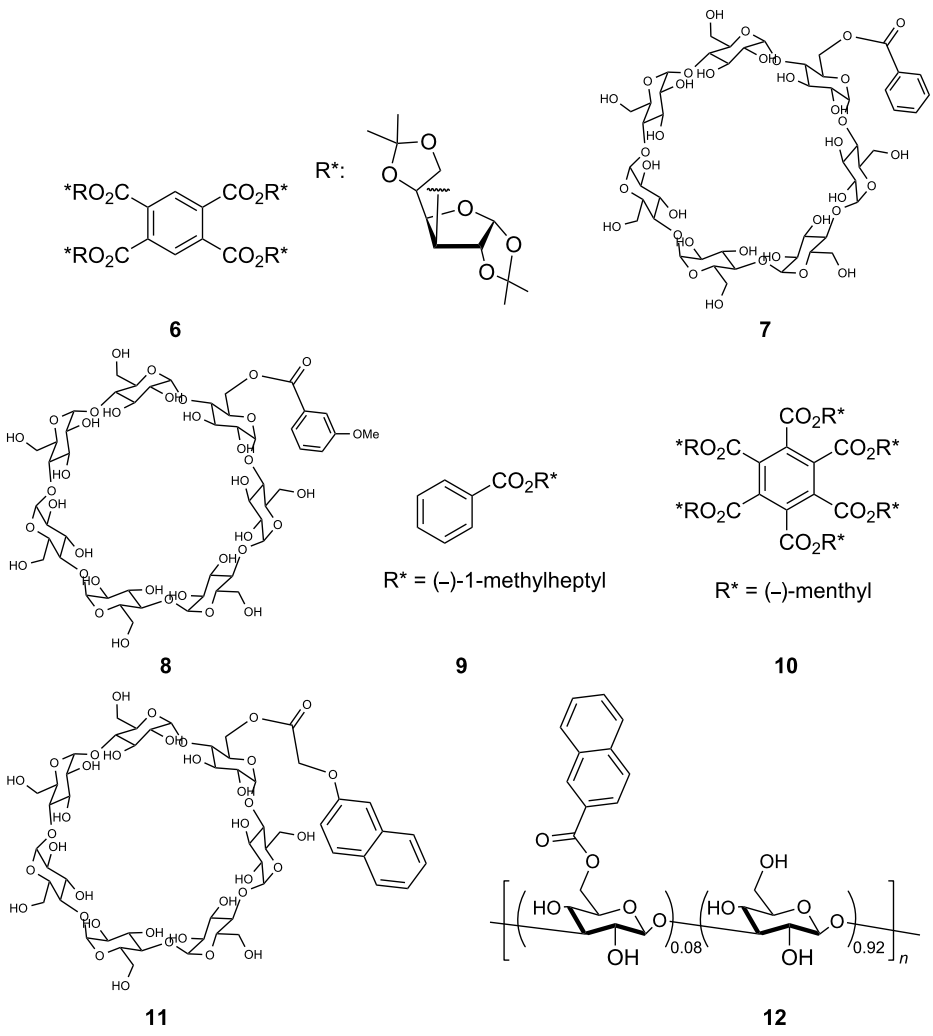

substrate	chiral sensitizer	*T* / °C	% ee	reference
1Z	**6**	–110	73	[35]
	7	25	11	[9]
	8	–5	46	[37]
	9 in zeolite	25	–4.5	[34]
2ZZ	**10**	–40	17.6	[38]
	11	0.5	4.6	[39]
	12	–160	11.7	[40]

Scheme 2: Representative enantiodifferentiating photosensitization of **1Z** and **2ZZ** with conventional and supramolecular photosensitizers.

stronger ICD at the ^1L_a band (Figure 1c). Assuming the 1:1 stoichiometry, we calculated the apparent binding constant, averaged over the CD units of CDNS, as 4000 M^{-1} in water at 25 °C. This value is smaller than those obtained with the sensitizer-modified CDs reported previously [36], for which the steric hindrance in the network polymer and/or the less efficient complexation inside the nanoparticle of CDNS would be responsible. The circular dichroism spectral changes observed for the more cross-linked CDNSs **4** and **5** upon binding **1Z** or **2ZZ** were too small to allow quantitative evaluation of the binding affinity.

CDNSs **3**–**5** were dissolved in water to make aqueous solutions with concentrations of 45–60 μM in terms of the monomer unit, which were apparently clear at these concentrations but should be a suspension of swollen polymer. In view of the excess

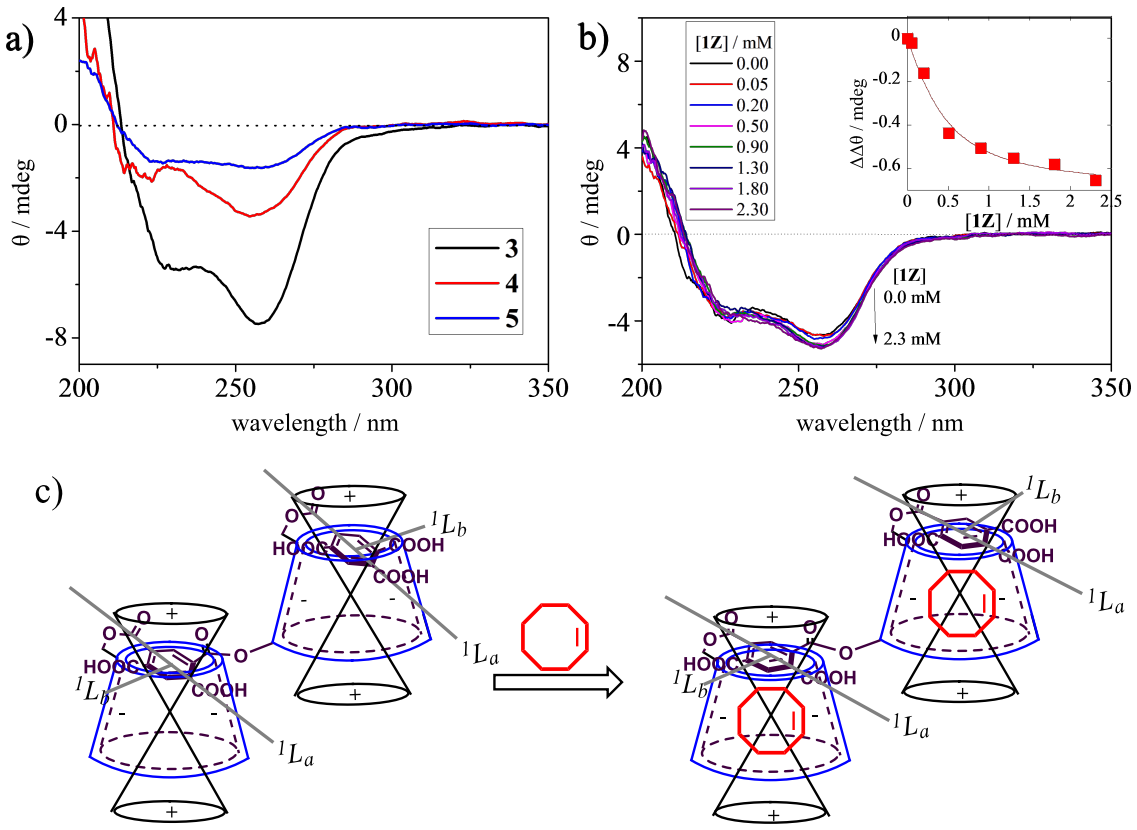

Figure 1: (a) Circular dichroism spectra of **3** (67 μg/mL) (black), **4** (67 μg/mL) (red) and **5** (50 μg/mL) (blue) in pure water at 25 °C, and (b) of **3** (560 μg/mL) in the presence of 0–2.3 mM **1Z**; Inset shows the nonlinear least-squares curve fit of the ellipticity changes at 257 nm, assuming the 1:1 stoichiometry, from which the apparent binding constant was determined to be 4000 ± 1000 M^{-1}. (c) Schematic illustrations of the conformational change of CDNS upon inclusion of **1Z**.

amount of PDA used in the preparation of CDNSs, it is likely that some of the carboxyl groups in PDA are not incorporated in the polymer chain, and hence, the solution pH may change the ionic state of the remaining carboxyl groups, affecting the sensitizer conformation and also the product selectivity. The conformational change of the PM units with pH was examined by circular dichroism spectroscopy. As shown in Figure 2a, increasing the solution pH caused a significant enhancement of

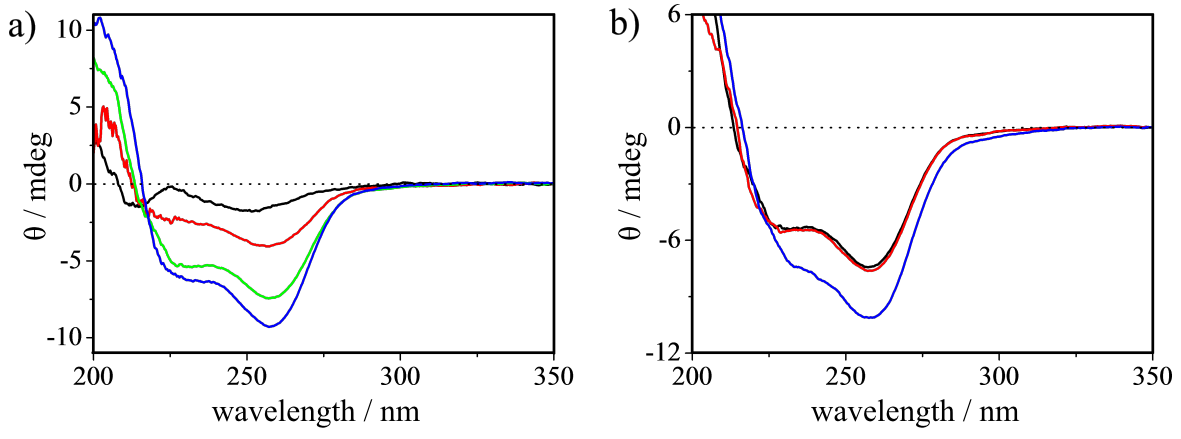

Figure 2: Circular dichroism spectra of **3** (67 μg/mL) (a) in water at pH 1.9 (black), 4.0 (red), 7.5 (green) and 10 (blue) and (b) in water at pH 7.5 (black), in 10% ethanol (red) and in 50% ethanol (blue).

the negative ICD of CDNS **3**. This seems reasonable, as the ionization of the carboxylic acid moieties on the PM units (pK_{a1} = 2.93 for pyromellitic acid; pK_{a1} = 2.98 and pK_{a2} = 5.28 for phthalic acid) [45] will drive out the shallowly included PM from the cavity but still keep it near the portal with the short ester linker, orienting the ^1L_a transition in the more negative region of the sector rule (parallel to the portal plane).

Photoisomerizations of **1Z** and **2ZZ** sensitized by CDNSs were performed at 254 nm under nitrogen in aqueous solutions at different pH values by using a xenon lamp fitted with a band-pass filter (Asahi Spectra MAX-301). As shown in Table 1, the photosensitizations of **1Z** and **2ZZ** with CDNSs gave **1E** and **2EZ** in modest enantioselectivities. Interestingly, the enantiomeric excess (ee) was a critical function of the solution pH. For instance, **3** gave (+)-**1E** in 4.4% ee at pH 1.9 but a doubled 9.0% ee at pH 10. The largest pH-induced ee change was observed for **5**, which afforded (−)-**1E** in 4.8% ee at pH 6.5 but antipodal (+)-**1E** in 9.8% at pH 10. Similar ee behavior was observed upon photoisomerization of **2ZZ** sensitized by **5**, showing a significant increase from 1.0% ee at pH 1.9–6.5 to 7.4% ee at pH 10. These results nicely coincide with the conformational changes of PM units caused by altering the solution pH, providing us with a convenient and also powerful tool for manipulating the stereochemical outcomes of supramolecular photochirogenesis.

Table 1: Enantiodifferentiating photoisomerization of **1Z** and **2ZZ** sensitized by CDNSs in aqueous solution at different pH values.

guest	host	pH	*E*/*Z*	% ee
1Z	**3**[a]	1.9	0.03	+4.4
		4.0	0.02	+4.5
		7.5	0.04	+7.5
		10	0.03	+9.0
	4[a]	1.9	0.03	−0.1
		4.0	0.05	+1.4
		5.2	0.07	+2.1
		10	0.01	+4.3
	5[a]	1.9	0.06	+0.1
		4.0	0.09	+0.6
		6.5	0.06	−4.8
		10	0.01	+9.8
2ZZ	**3**[a]	1.9	0.04	+5.0
		4.0	0.04	+1.7
		7.5	0.03	+4.6
		10	0.01	+2.7
	4[a]	1.9	0.02	+4.0
		4.0	0.07	+1.0
		5.2	0.03	+4.9
		10	0.02	+4.9
	5[a]	1.9	0.03	+1.0
		4.0	0.07	+1.0
		6.5	0.13	+0.7
		10	0.01	+7.4

[a][**1Z**] = [**2ZZ**] = 1.5 mM; [CDNS] = 0.2 mg/mL; irradiated for 1 h at 254 nm in aqueous buffer solutions of pH 1.9–10.0 at 0.5 °C.

It should be noted that γ-CD-based nanosponge **5** gave the highest ee values for both **1E** and **2EZ**. This is in sharp contrast to the result reported for the photosensitization with conventional sensitizer-modified CDs [9,39], in which the more size-matched β-CD, rather than the larger-sized γ-CD, sensitizers consistently afforded **1E** and **2EZ** in (much) higher ee's. This unusual behavior observed for β- and γ-CDNSs implies the operation of photosensitization and/or enantiodifferentiation mechanisms differing from those proposed for the sensitizer-modified monomeric CDs [9,39]. A plausible alternative mechanism, available for the cross-linked CD polymers, is the photosensitization in a chiral void space surrounded by CD and PM units.

In order to obtain experimental support for the alternative mechanism, we examined the solvent effects on the chromophore conformation of CDNS by circular dichroism spectroscopy and also on the CDNS-sensitized photoisomerization. Indeed, the ICD intensity was enhanced upon the addition of ethanol to an aqueous solution of CDNS (Figure 2b), which encouraged us to further investigate the effect of solvent composition on the photoisomerization. As shown in Table 2, the

Table 2: Enantiodifferentiating photoisomerization of **1Z** sensitized by CDNSs in water containing methanol or ethanol.

sens*	solvent	*E*/*Z*	% ee
3[a]	H_2O	0.04	+7.5
	5% MeOH	0.07	+7.8
	10% MeOH	0.02	+9.3
	25% MeOH	0.04	+9.0
	50% MeOH	0.04	+8.5
	5% EtOH	0.06	+11.7
	10% EtOH	0.05	+9.8
4[a]	H_2O	0.07	+2.7
	10% MeOH	0.04	+2.8
	15% MeOH	0.05	+3.2
	25% MeOH	0.02	+1.5
5[a]	H_2O	0.06	−4.8
	10% MeOH	0.02	−4.5
	25% MeOH	0.01	−1.6

[a][**1Z**] = 1.5 mM; [CDNS] = 0.2 mg/mL; irradiated for 30 min at 254 nm in distilled water containing a varying amount of methanol or ethanol at 0.5 °C.

addition of 10% methanol or 5% ethanol enhanced the product's ee from 7.5 to 9.8 or 11.7%, respectively, upon sensitization with **3**, while the further addition of methanol (up to 50%) or ethanol (up to 10%) led to less pronounced enhancements. In contrast, the ee of **1E** obtained with the more heavily cross-linked **4** and **5** was not greatly affected or even reduced at high alcohol contents. Crucially, such ee enhancement caused by increasing alcohol content has never been observed for the supramolecular photoisomerization mediated by conventional sensitizer-modified CDs [9], since the addition of alcohol simply reduces the guest affinity [46,47] and hence the ee of the product. This unusual solvent effect upon the addition of alcohol to the aqueous solution of CDNS reinforces the above hypothesis that the enantiodifferentiating photosensitization occurs not in the CD cavity but in the chiral polymer void of CDNS.

Conclusion

The pyromellitate-linked cyclodextrin nanosponges, employed for the first time as supramolecular reaction media for sensitizing the enantiodifferentiating photoisomerization of **1Z** and **2ZZ**, exhibited unique photochirogenesis behavior significantly different from the conventional sensitizer-modified CDs. Thus, the variation of solution pH and solvent composition enabled us to critically control the stereochemical outcomes, leading to the switching of product chirality and the enhancement of the ee of the product by adding alcohol. The latter result in particular revealed the active roles of chiral voids in CDNS as novel photochirogenic reaction media, encouraging the further application of CDNS to chiral photochemistry.

Acknowledgement

This work was supported by JST (CY) and JSPS (YI), which are gratefully acknowledged. WL thanks the financial support by the "Global 30" Program (MEXT) at Osaka University.

References

1. Inoue, Y. *Chem. Rev.* **1992,** *92,* 741–770. doi:10.1021/cr00013a001
2. Inoue, Y.; Ramamurthy, V., Eds. *Chiral Photochemistry;* Marcel Dekker: New York, 2004.
3. Yang, C.; Inoue, Y. Photochirogenesis. In *CRC Handbook of Organic Photochemistry and Photobiology,* 3rd ed.; Griesbeck, A. G.; Oelgemöller, M.; Ghetti, F., Eds.; Taylor & Francis: Boca Raton, 2012; pp 125–176.
4. Yang, C.; Inoue, Y. Supramolecular Photochirogenesis. In *Supramolecular Photochemistry: Controlling Photochemical Processes;* Ramamurthy, V.; Inoue, Y., Eds.; John Wiley & Sons, Inc.: Hoboken, NJ, 2011; pp 115–154. doi:10.1002/9781118095300.ch4
5. Griesbeck, A. G.; Meierhenrich, U. J. *Angew. Chem., Int. Ed.* **2002,** *41,* 3147–3154. doi:10.1002/1521-3773(20020902)41:17<3147::AID-ANIE3147>3.0.CO;2-V
6. Yang, C.; Inoue, Y. Supramolecular Photochirogenesis with Cyclodextrin. In *Cyclodextrin Materials Photochemistry, Photophysics and Photobiology;* Douhal, A., Ed.; Elsevier: Amsterdam, 2006; pp 241–265. doi:10.1016/B978-044452780-6/50012-7
7. Inoue, Y. *Nature* **2005,** *436,* 1099–1100. doi:10.1038/4361099a
8. Bauer, A.; Westkämper, F.; Grimme, S.; Bach, T. *Nature* **2005,** *436,* 1139–1140. doi:10.1038/nature03955
9. Inoue, Y.; Dong, F.; Yamamoto, K.; Tong, L.-H.; Tsuneishi, H.; Hakushi, T.; Tai, A. *J. Am. Chem. Soc.* **1995,** *117,* 11033–11034. doi:10.1021/ja00149a037
10. Lu, R.; Yang, C.; Cao, Y.; Wang, Z.; Wada, T.; Jiao, W.; Mori, T.; Inoue, Y. *Chem. Commun.* **2008,** 374–376. doi:10.1039/b714300a
11. Sivaguru, J.; Natarajan, A.; Kaanumalle, L. S.; Shailaja, J.; Uppili, S.; Joy, A.; Ramamurthy, V. *Acc. Chem. Res.* **2003,** *36,* 509–521. doi:10.1021/ar020269i
12. Aechtner, T.; Dressel, M.; Bach, T. *Angew. Chem., Int. Ed.* **2004,** *43,* 5849–5851. doi:10.1002/anie.200461222
13. Nakamura, A.; Inoue, Y. *J. Am. Chem. Soc.* **2003,** *125,* 966–972. doi:10.1021/ja016238k
14. Nakamura, A.; Inoue, Y. *J. Am. Chem. Soc.* **2005,** *127,* 5338–5339. doi:10.1021/ja050704e
15. Yang, C.; Ke, C.; Liang, W.; Fukuhara, G.; Mori, T.; Liu, Y.; Inoue, Y. *J. Am. Chem. Soc.* **2011,** *133,* 13786–13789. doi:10.1021/ja202020x
16. Ke, C.; Yang, C.; Mori, T.; Wada, T.; Liu, Y.; Inoue, Y. *Angew. Chem., Int. Ed.* **2009,** *48,* 6675–6677. doi:10.1002/anie.200902911
17. Yang, C.; Fukuhara, G.; Nakamura, A.; Origane, Y.; Fujita, K.; Yuan, D.-Q.; Mori, T.; Wada, T.; Inoue, Y. *J. Photochem. Photobiol., A: Chem.* **2005,** *173,* 375–383. doi:10.1016/j.jphotochem.2005.04.017
18. Yang, C.; Nakamura, A.; Fukuhara, G.; Origane, Y.; Mori, T.; Wada, T.; Inoue, Y. *J. Org. Chem.* **2006,** *71,* 3126–3136. doi:10.1021/jo0601718
19. Yang, C.; Nakamura, A.; Wada, T.; Inoue, Y. *Org. Lett.* **2006,** *8,* 3005–3008. doi:10.1021/ol061004x
20. Yang, C.; Nishijima, M.; Nakamura, A.; Mori, T.; Wada, T.; Inoue, Y. *Tetrahedron Lett.* **2007,** *48,* 4357–4360. doi:10.1016/j.tetlet.2007.04.104
21. Yang, C.; Mori, T.; Inoue, Y. *J. Org. Chem.* **2008,** *73,* 5786–5794. doi:10.1021/jo800533y
22. Wada, T.; Nishijima, M.; Fujisawa, T.; Sugahara, N.; Mori, T.; Nakamura, A.; Inoue, Y. *J. Am. Chem. Soc.* **2003,** *125,* 7492–7493. doi:10.1021/ja034641g
23. Nishijima, M.; Wada, T.; Mori, T.; Pace, T. C. S.; Bohne, C.; Inoue, Y. *J. Am. Chem. Soc.* **2007,** *129,* 3478–3479. doi:10.1021/ja068475z
24. Wang, Q.; Yang, C.; Ke, C.; Fukuhara, G.; Mori, T.; Liu, Y.; Inoue, Y. *Chem. Commun.* **2011,** *47,* 6849–6851. doi:10.1039/c1cc11771h
25. Trotta, F. Cyclodextrin Nanosponges and Their Applications. In *Cyclodextrins in Pharmaceutics, Cosmetics, and Biomedicine: Current and Future Industrial Applications;* Bilensoy, E., Ed.; John Wiley & Sons, Inc.: Hoboken, NJ, 2011; pp 323–342. doi:10.1002/9780470926819.ch17
26. Di Nardo, G.; Roggero, C.; Campolongo, S.; Valetti, F.; Trotta, F.; Gilardi, G. *Dalton Trans.* **2009,** 6507–6512. doi:10.1039/b903105g
27. Li, D. Q.; Ma, M. *CHEMTECH* **1999,** *29,* 31–37.
28. Alongi, J.; Poskovic, M.; Frache, A.; Trotta, F. *Carbohydr. Polym.* **2011,** *86,* 127–135. doi:10.1016/j.carbpol.2011.04.022
29. Seglie, L.; Martina, K.; Devecchi, M.; Roggero, C.; Trotta, F.; Scariot, V. *Plant Growth Regul.* **2011,** *65,* 505–511. doi:10.1007/s10725-011-9621-y

30. Berto, S.; Bruzzoniti, M. C.; Cavalli, R.; Perrachon, D.; Prenesti, E.; Sarzanini, C.; Trotta, F.; Tumiatti, W. *J. Inclusion Phenom. Macrocyclic Chem.* **2007,** *57,* 637–643. doi:10.1007/s10847-006-9270-3
31. Castiglione, F.; Crupi, V.; Majolino, D.; Mele, A.; Panzeri, W.; Rossi, B.; Trotta, F.; Venuti, V. *J. Inclusion Phenom. Macrocyclic Chem.*, in press. doi:10.1007/s10847-012-0106-z
32. Raffaini, G.; Ganazzoli, F.; Mele, A.; Castiglione, F. *J. Inclusion Phenom. Macrocyclic Chem.*, in press. doi:10.1007/s10847-012-0126-8
33. Mele, A.; Castiglione, F.; Malpezzi, L.; Ganazzoli, F.; Raffaini, G.; Trotta, F.; Rossi, B.; Fontana, A.; Giunchi, G. *J. Inclusion Phenom. Macrocyclic Chem.* **2011,** *69,* 403–409. doi:10.1007/s10847-010-9772-x
34. Wada, T.; Shikimi, M.; Inoue, Y.; Lem, G.; Turro, N. J. *Chem. Commun.* **2001,** 1864–1865. doi:10.1039/b105381g
35. Inoue, Y.; Tsuneishi, H.; Hakushi, T.; Tai, A. *J. Am. Chem. Soc.* **1997,** *119,* 472–478. doi:10.1021/ja963160c
36. Lu, R.; Yang, C.; Cao, Y.; Wang, Z.; Wada, T.; Jiao, W.; Mori, T.; Inoue, Y. *Chem. Commun.* **2008,** 374–376. doi:10.1039/B714300A
37. Lu, R.; Yang, C.; Cao, Y.; Tong, L.; Jiao, W.; Wada, T.; Wang, Z.; Mori, T.; Inoue, Y. *J. Org. Chem.* **2008,** *73,* 7695–7701. doi:10.1021/jo801439n
38. Inoue, Y.; Ikeda, H.; Kaneda, M.; Sumimura, T.; Everitt, S. R. L.; Wada, T. *J. Am. Chem. Soc.* **2000,** *122,* 406–407. doi:10.1021/ja993542t
39. Yang, C.; Mori, T.; Wada, T.; Inoue, Y. *New J. Chem.* **2007,** *31,* 697–702. doi:10.1039/b615353d
40. Fukuhara, G.; Imai, M.; Yang, C.; Mori, T.; Inoue, Y. *Org. Lett.* **2011,** *13,* 1856–1859. doi:10.1021/ol2003644
41. Berto, S.; Bruzzoniti, M. C.; Cavalli, R.; Perrachon, D.; Prenesti, E.; Sarzanini, C.; Trotta, F.; Tumiatti, W. *J. Inclusion Phenom. Macrocyclic Chem.* **2007,** *57,* 631–636. doi:10.1007/s10847-006-9273-0
42. Rossi, B.; Caponi, S.; Castiglione, F.; Corezzi, S.; Fontana, A.; Giarola, M.; Mariotto, G.; Mele, A.; Petrillo, C.; Trotta, F.; Viliani, G. *J. Phys. Chem. B* **2012,** *116,* 5323–5327. doi:10.1021/jp302047u
43. Kajtar, M.; Horvath-Toro, C.; Kuthi, E.; Szejtli, J. *Acta Chim. Acad. Sci. Hung.* **1982,** *110,* 327–333.
44. Berova, N.; Nakanishi, K.; Woody, R. W., Eds. *Circular Dichroism: Principles and Applications,* 2nd ed.; Wiley-VCH: New York, 2000.
45. Baude, E. A.; Nachod, F. C. *Determination of Organic Structures by Physical Methods;* Academic Press: New York, 1955.
46. Rekharsky, M. V.; Inoue, Y. *Chem. Rev.* **1998,** *98,* 1875–1918. doi:10.1021/cr970015o
47. Inoue, Y.; Yamamoto, K.; Wada, T.; Everitt, S.; Gao, X.-M.; Hou, Z.-J.; Tong, L.-H.; Jiang, S.-K.; Wu, H.-M. *J. Chem. Soc., Perkin Trans. 2* **1998,** 1807–1816. doi:10.1039/a801858h

License and Terms

Beilstein Journal of Organic Chemistry

Interaction of cyclodextrins with pyrene-modified polyacrylamide in a mixed solvent of water and dimethyl sulfoxide as studied by steady-state fluorescence

Akihito Hashidzume[1], Yongtai Zheng[1] and Akira Harada[*1,2]

Full Research Paper

Open Access

Address:
[1]Department of Macromolecular Science, Graduate School of Science, Osaka University, 1-1 Machikaneyama-cho, Toyonaka, Osaka 560-0043, Japan and [2]Japan Science and Technology Agency (JST), Core Research for Evolutional Science and Technology (CREST), 7 Gobancho, Chiyoda-ku, Tokyo 102-0076, Japan

Email:
Akira Harada[*] - harada@chem.sci.osaka-u.ac.jp

* Corresponding author

Keywords:
cyclodextrins; interaction; pyrene-modified polyacrylamide; steady-state fluorescence; water/DMSO mixed solvent

Beilstein J. Org. Chem. **2012,** *8,* 1312–1317.
doi:10.3762/bjoc.8.150

Received: 20 April 2012
Accepted: 31 July 2012
Published: 16 August 2012

This article is part of the Thematic Series "Superstructures with cyclodextrins: Chemistry and applications".

Guest Editor: H. Ritter

Abstract

The interaction of β- and γ-cyclodextrins (β-CD and γ-CD, respectively) with polyacrylamide modified with pyrenyl (Py) residues (pAAmPy) was investigated in a mixed solvent of water and dimethyl sulfoxide (DMSO) by steady-state fluorescence. In the absence of CD, the fluorescence spectra indicated that the formation of Py dimers became less favorable with increasing volume fraction of DMSO (x_{DMSO}). The fluorescence spectra at varying x_{DMSO} and CD concentrations indicated that β-CD and γ-CD included monomeric and dimeric Py residues, respectively. Using the fluorescence spectra, equilibrium constants of the formation of Py dimers and the complexation of β-CD and γ-CD with Py residues were roughly estimated based on simplified equilibrium schemes.

Introduction

Cyclodextrins (CDs) are cyclic oligomers composed of glucopyranose units linked through α-1,4-glycoside bonding. They bear a tapered structure with a narrower rim of primary hydroxy groups and a wider rim of secondary hydroxy groups. CDs of 6, 7, and 8 glucopyranose units are called α-CD, β-CD, and γ-CD, respectively. CDs have a hydrophilic exterior and a rather hydrophobic cavity, and thus, recognize guest compounds of a size and shape matching their cavity, to form inclusion complexes [1-5]. Since CDs are nontoxic, they have been utilized in a variety of fields, including food additives, cosmetics, and personal care items [6-12]. In the past decade, the formation of inclusion complexes of CDs with guest residues attached on water-soluble polymers has attracted increasing interest from a number of research groups because these systems are applicable to stimuli-responsive systems [13-18].

We have been working on the interaction of CDs with water-soluble polymers bearing various guest residues, including linear, branched, and cyclic aliphatics, as well as aromatics [19-21], and realized stimuli-responsive hydrogels [22-27] and macroscopic assemblies based on molecular recognition [28-31]. Aromatic residues absorb light to become excited, and subsequently they can transfer energy and electrons. The interaction of CDs with water-soluble polymers carrying aromatic residues may allow one to construct functional systems that convert photo energy based on molecular recognition. Among aromatic compounds, pyrene is the most examined as a fluorescence probe or label because it shows a relatively high fluorescence quantum yield and a relatively long fluorescence lifetime in both monomer and excimer states [32,33]. Since pyrene is very hydrophobic, it may tend to form aggregates, e.g., dimers, in aqueous solutions. It is also known that pyrene forms inclusion complexes with β-CD and γ-CD in different manners; β-CD includes monomeric pyrene whereas γ-CD includes dimeric pyrene [34-36]. Recently, we have demonstrated this selectivity switching on macroscopic molecular recognition for polyacrylamide-based gels carrying pyrenyl (Py) and CD residues, by changing the composition of a mixed solvent of water and dimethyl sulfoxide (DMSO) [37]. In the present study, the interaction of β-CD and γ-CD with Py-modified polyacrylamide (pAAmPy, Scheme 1) was investigated in the water/DMSO mixed solvent of varying composition by steady-state fluorescence to elucidate the mechanism of the selectivity switching.

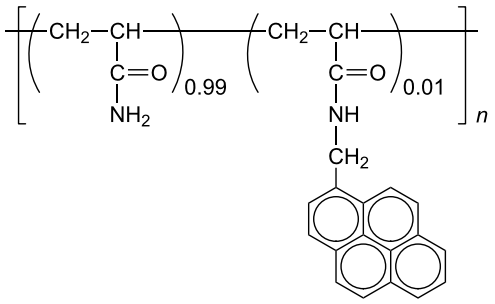

Scheme 1: Structure of pAAmPy.

cularly under the dilute conditions (0.04 g L^{-1}) in this study. These spectra indicate that the intensity of excimer fluorescence decreases whereas that of monomer fluorescence increases with increasing x_{DMSO}. This observation indicates that the formation of Py dimer becomes less favorable, because the Py residue becomes more solvophilic with x_{DMSO}. Using the spectra, the ratios (I_{480}/I_{376}) of the intensities at 480 and 376 nm, which are predominantly due to the Py excimer and monomer, respectively, were calculated and plotted in Figure 1b against x_{DMSO}. I_{480}/I_{376} decreases monotonously from 0.125 to 0.025 with increasing x_{DMSO} from 0 to 1.

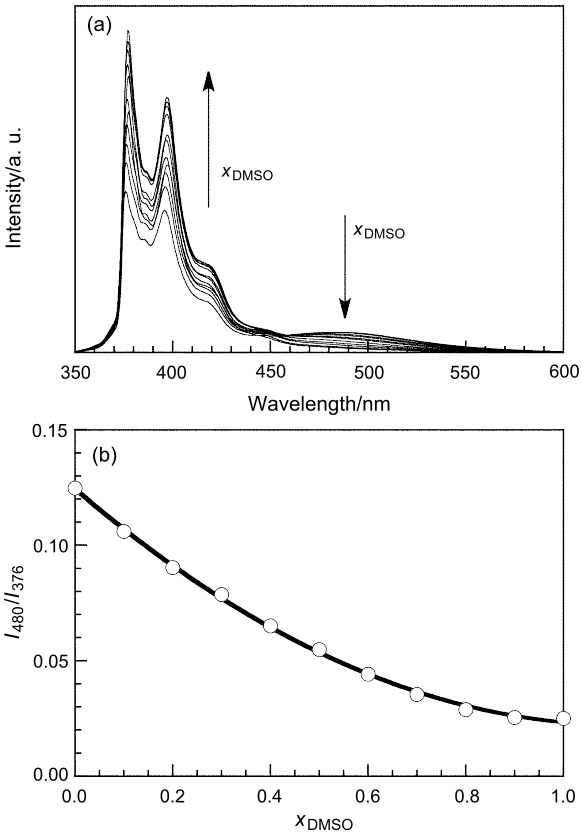

Figure 1: Steady-state fluorescence spectra for 0.04 g L^{-1} pAAmPy at varying x_{DMSO} from 0 to 1 with excitation at 335 nm (a) and I_{480}/I_{376} as a function of x_{DMSO} (b).

Results

Figure 1a demonstrates the steady-state fluorescence spectra measured for 0.04 g L^{-1} pAAmPy (5 μM in Py residue) at varying volume fractions of DMSO (x_{DMSO}) in the water/DMSO mixed solvent in the absence of CD. At x_{DMSO} = 0 (i.e., in water), the spectrum exhibits not only emission bands ascribable to monomeric Py in the region of 370–430 nm, but also a broad band assignable to a Py excimer around 480 nm, indicating that Py residues tend to form dimers because of the hydrophobicity. It is likely that Py residues associate intramole-

The interaction of β-CD and γ-CD with pAAmPy was also investigated at varying x_{DMSO} by steady-state fluorescence. Figure 2 exhibits fluorescence spectra for the β-CD/pAAmPy system at x_{DMSO} = 0.1 and for the γ-CD/pAAmPy system at x_{DMSO} = 0 as typical examples, showing remarkable tendencies. In the spectra of the β-CD/pAAmPy system at x_{DMSO} = 0.1, the intensity of Py excimer fluorescence decreases whereas that of Py monomer fluorescence increases with the increasing concentration of CD ($[CD]_0$), indicating that β-CD forms inclusion complexes with monomeric Py residues, and dimeric Py

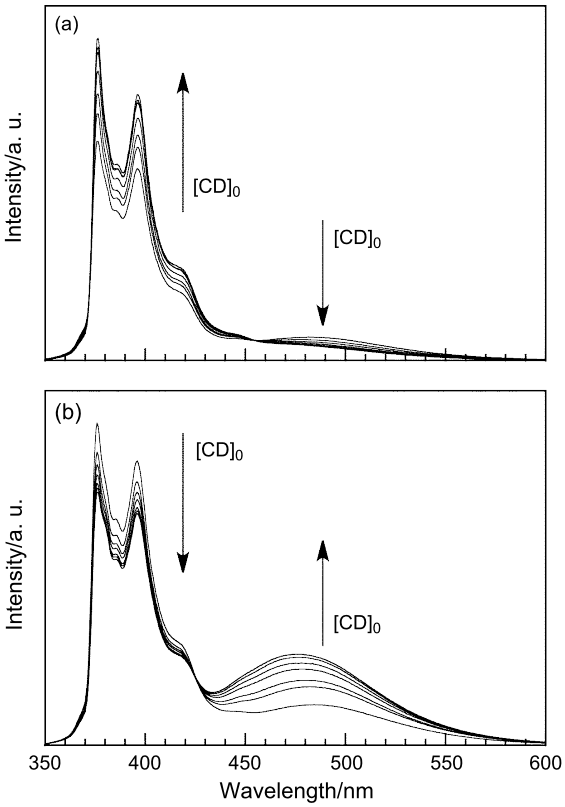

Figure 2: Steady-state fluorescence spectra for 0.04 g L^{-1} pAAmPy with excitation at 335 nm in the presence of varying concentrations of β-CD at x_{DMSO} = 0.1 (a) and of γ-CD at x_{DMSO} = 0 (b).

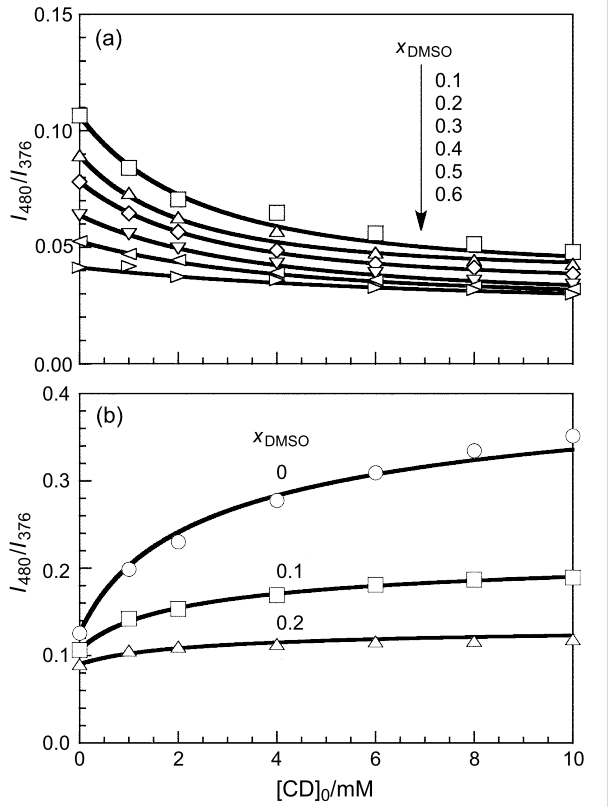

Figure 3: I_{480}/I_{376} as a function of $[CD]_0$ for β-CD/pAAmPy (a) and γ-CD/pAAmPy (b) at different x_{DMSO}.

residues dissociate to the monomers. In the spectra of the γ-CD/pAAmPy system at x_{DMSO} = 0, on the other hand, the intensity of the excimer fluorescence increases whereas that of the monomer fluorescence decreases with increasing $[CD]_0$, indicating that γ-CD forms inclusion complexes with dimeric Py residues, and monomeric Py residues further associate to form the dimers. Using the steady-state fluorescence spectra, I_{480}/I_{376} values were calculated. Figure 3 compares I_{480}/I_{376} as a function of $[CD]_0$ for the β-CD/pAAmPy system at x_{DMSO} = 0.1–0.6 and for the γ-CD/pAAmPy system at x_{DMSO} = 0–0.2. At other x_{DMSO}, I_{480}/I_{376} was practically independent of $[CD]_0$, indicative of no significant interaction of β-CD or γ-CD with pAAmPy. For the β-CD/pAAmPy system (Figure 3a), I_{480}/I_{376} decreases with increasing $[CD]_0$ at x_{DMSO} = 0.1–0.6. For the γ-CD/pAAmPy system (Figure 3b), on the other hand, I_{480}/I_{376} increases with $[CD]_0$ at x_{DMSO} = 0–0.2.

Discussion

Detailed study of the equilibria of the inclusion complex formation of CDs with Py-modified water-soluble polymers, including the formation of the dynamic excimer, requires not only steady-state fluorescence measurements but also time-resolved fluorescence measurements [38-43]. In this study, however, equilibrium constants are roughly estimated by analyzing the steady-state fluorescence data, assuming that dynamic excimer formation is negligible. In the absence of CD, I_{480}/I_{376} for pAAmPy decreases from 0.125 to 0.025 with increasing x_{DMSO} from 0 to 1. It should be noted here that the fluorescence of the Py monomer is dominant compared to that of the Py excimer even at x_{DMSO} = 0 (i.e., in water), implying that there are a significant fraction of Py residues (Py°) that cannot form Py dimers (Py_2). Since the steady-state fluorescence measurements were performed under dilute conditions in this study, most of the Py_2 were formed intramolecularly. Thus, Py residues in pAAmPy carrying a Py residue may not form Py_2. The fraction of Py° is defined as *f*. Scheme 2a indicates a simplified equilibrium of the formation of Py_2 from two Py residues. On the basis of the derivation of equations in the Supporting Information File 1, the equilibrium constant for the Py_2 formation (K_{Py}) can be calculated as

$$K_{Py} = \frac{x^2 - 1}{8(1-f)[Py]_0} \quad (1)$$

where $[Py]_0$ is the total concentration of Py residue and *x* as given in Equation 2.

$$x = \frac{2\left(\frac{I_{480}}{I_{376}}A_{1,376} - A_{1,480}\right)(f-2)[\mathrm{Py}]_0 + \left(\frac{I_{480}}{I_{376}}A_{2.376} - A_{2.480}\right)(1-f)[\mathrm{Py}]_0 - 2\left(\frac{I_{480}}{I_{376}}B_{376} - B_{480}\right)}{2\left(\frac{I_{480}}{I_{376}}A_{1,376} - A_{1,480}\right)f[\mathrm{Py}]_0 + \left(\frac{I_{480}}{I_{376}}A_{2.376} - A_{2,480}\right)(1-f)[\mathrm{Py}]_0 - 2\left(\frac{I_{480}}{I_{376}}B_{376} - B_{480}\right)} \quad (2)$$

Here, $A_{1,376}$, $A_{1,480}$, $A_{2,376}$, and $A_{2,480}$ are constants corresponding to the products of the molar extinction coefficient and the fluorescence quantum yield (subscripts 1 and 2 indicate monomeric and dimeric Py residues, respectively, and subscripts 376 and 480 indicate the wavelengths), and B_{376} and B_{480} are constants corresponding to the background. If it is assumed that all the Py residues are in the monomer state at $x_{\mathrm{DMSO}} = 1$ (i.e., in DMSO), $f = 0.5$, $A_{2,480}/A_{1,376} = 0.5$, and $B_{376} = B_{480} = 0$, K_{Py} can be calculated as can be seen in Figure 4a. This figure indicates that K_{Py} decreases monotonously from 6.2×10^4 to 0 M^{-1} with increasing x_{DMSO} from 0 to 1.

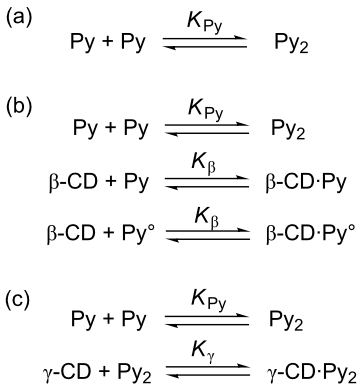

Scheme 2: Simplified equilibria of CDs/pAAmPy systems.

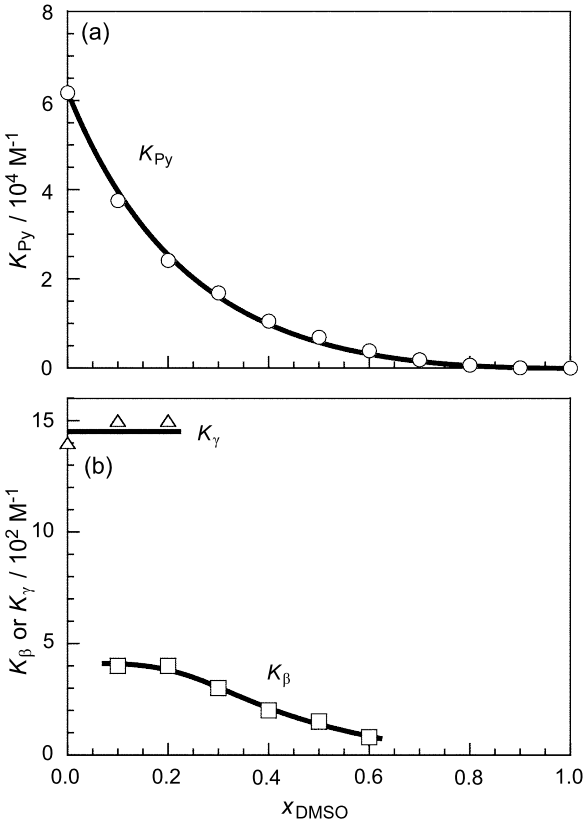

Figure 4: K_{Py}, K_β, and K_γ as a function of x_{DMSO}.

In the β-CD/pAAmPy system, β-CD forms inclusion complexes with both Py and Py° (Scheme 2b). On the basis of the derivation described in the Supporting Information File 1, the concentrations of all species can be calculated by using the equilibrium constant (K_β) for the inclusion complex formation, and I_{480}/I_{376} can be also obtained as given in Equation 3.

Here [Py], [Py°], [CD], [CD·Py], and [CD·Py°] denote the concentrations of Py, Py°, free CD, and the complexes of CD with Py and with Py°, respectively, and $A'_{1,376}$ and $A'_{1,480}$ are constants. In this study, $A'_{1,480}/A'_{1,376}$ is fixed at 0.025 (Supporting Information File 1). It is also likely that $A_{2,376} = 0$. When K_β and $A'_{1,376}/A_{1,376}$ are chosen appropriately, the calculated I_{480}/I_{376} values agree with the experimental data, as can be seen in Figure 3a. The K_β values were plotted in Figure 4b against x_{DMSO}. As x_{DMSO} increases from 0.1 to 0.6, K_β decreases from 4×10^2 to 8×10^1 M^{-1}. This observation indicates that the formation of inclusion complexes becomes less favorable with increasing x_{DMSO}.

In the γ-CD/pAAmPy system, γ-CD forms inclusion complexes with Py_2, in which Py° is not involved. On the basis of the

$$I_{480}/I_{376} = \frac{A_{1,480}([\mathrm{Py}]+[\mathrm{Py°}]+A'_{1,480}([\mathrm{CD\cdot Py}]+[\mathrm{CD\cdot Py°}])+A_{2,480}[\mathrm{Py_2}]+B_{480}}{A_{1,376}([\mathrm{Py}]+[\mathrm{Py°}]+A'_{1,376}([\mathrm{CD\cdot Py}]+[\mathrm{CD\cdot Py°}])+A_{2,376}[\mathrm{Py_2}]+B_{376}} \quad (3)$$

$$I_{480}/I_{376} = \frac{A_{1,480}([\mathrm{Py}]+[\mathrm{Py}^{\circ}]+A_{2,480}([\mathrm{Py}_2]+A'_{2,480}[\mathrm{CD}\cdot\mathrm{Py}_2]+B_{480}}{A_{1,376}([\mathrm{Py}]+[\mathrm{Py}^{\circ}]+A_{2,376}([\mathrm{Py}_2]+A'_{2,376}[\mathrm{CD}\cdot\mathrm{Py}_2]+B_{376}} \quad (4)$$

derivation described in the Supporting Information File 1, the concentrations of all species can be calculated by using the equilibrium constant (K_γ) for the inclusion complex formation, and I_{480}/I_{376} can be also obtained as given in Equation 4.

Here [CD·Py_2] denotes the concentration of the complex of CD with Py_2, and $A'_{2,480}$ is a constant. It is also likely that $A_{2,376}$ = $A'_{2,376}$ = 0. When K_γ and $A'_{2,480}/A_{1,376}$ are chosen appropriately, the I_{480}/I_{376} values calculated agree with the experimental data, as can be seen in Figure 3b. The K_γ values were also plotted in Figure 4b against x_{DMSO}. This figure indicates that K_γ is practically constant (ca. 1.5×10^3 M^{-1}) independent of x_{DMSO} in the region of $0 \le x_{DMSO} \le 0.2$.

It should be noted here that the values of K_{Py}, K_β, and K_γ were estimated rather qualitatively based on the simplified equilibria and a number of assumptions, but the K_β and K_γ values are in good agreement with the values reported for pyrene (4.9×10^2 and 1.1×10^3 M^{-1} for β-CD and γ-CD, respectively) [44].

Experimental

1-Pyrenemethylamine hydrochloride was purchased from Sigma-Aldrich Co. Ltd. Acryloyl chloride was obtained from Tokyo Chemical Industry Co. Ltd. Triethylamine, acrylamide (AAm), ammonium peroxodisulfate (APS), acetone, methanol, DMSO (spectroscopic grade), $NaHCO_3$, and NaOH were purchased from Nacalai Tesque Inc. *N*,*N*-Dimethylformamide (DMF) and dichloromethane (DCM) were purified by utilizing a glass contour solvent dispensing system. Water was purified by a Millipore Milli-Q system. β-CD and γ-CD were purchased from Junsei Chemical Co. Ltd. and recrystallized twice from water before use. *N*-1-Pyrenylmethylacrylamide (APy) was prepared from 1-pyrenemethylamine hydrochloride and acryloyl chloride according to the procedure reported previously [37]. Other reagents were reagent grade and used without further purification.

The polymer (pAAmPy) was prepared by radical copolymerization of AAm and APy using APS as the initiator. A predetermined amount of AAm and APy were dissolved in DMF. After purging with dry argon for 30 min, APS (3 mg, 13 μmol) was added to the monomer solution. The reaction mixture was placed into a cuvette equipped with a stirrer and sealed. The cuvette was warmed with an oil bath thermostated at 60 °C overnight. The reaction mixture was poured into an excess of methanol to give a precipitate. The polymer obtained was recovered by filtration and dried under vacuum. The molecular weight of the polymer was estimated to be 4×10^3 by size exclusion chromatography (SEC), and the Py content was determined to be ca. 1 mol % by ^{1}H NMR.

Steady-state fluorescence spectra were obtained on a HITACHI F-2500 spectrophotometer with excitation at 335 nm by using a 1 cm quartz cuvette. The slit widths for both excitation and emission sides were kept at 2.5 nm during measurement. SEC analysis was carried out at 40 °C on a TOSOH CCP & 8020 system equipped with two TOSOH TSKgel α-M columns connected in series, using formamide as the eluent at a flow rate of 0.3 mL min^{-1}. TOSOH UV-8020 and TOSOH RI-8021 detectors were used. The molecular weights were calibrated by polystyrene sulfonate sodium-salt samples (American Polymer Standards). ^{1}H NMR spectra were measured on a JEOL JNM-ECA500 spectrometer by using a mixed solvent of DMSO-d_6 and D_2O (1/1, v/v) as a solvent, and chemical shifts were referenced to the solvent value (i.e., 2.49 ppm for DMSO).

Supporting Information

Supporting Information File 1

Equilibria for the CDs/pAAmPy systems.
[http://www.beilstein-journals.org/bjoc/content/supplementary/1860-5397-8-150-S1.pdf]

Acknowledgements

The authors are grateful to Associate Professor Hiroyasu Yamaguchi and Assistant Professor Yoshinori Takashima, Department of Macromolecular Science, Graduate School of Science, Osaka University, for fruitful discussion and suggestions.

References

1. Bender, M. L.; Komiyama, M. *Cyclodextrin Chemistry;* Springer: Berlin, Germany, 1978.
2. Szejtli, J. *Cyclodextrins and Their Inclusion Complexes;* Akadémiai Kiadó: Budapest, Hungury, 1982.
3. Szejtli, J.; Osa, T., Eds. *Cyclodextrins;* Pergamon: Oxford, U.K., 1996.
4. Harada, A. In *Large Ring Molecules;* Semlyen, J. A., Ed.; Wiley & Sons: Chichester, U.K., 1996; pp 407–432.
5. Dodziuk, H., Ed. *Cyclodextrins and Their Complexes: Chemistry, Analytical Methods, Applications;* Wiley-VCH: Weinheim, Germany, 2006.

6. Uekama, K.; Hirayama, F.; Irie, T. *Chem. Rev.* **1998,** *98,* 2045–2076. doi:10.1021/cr970025p
7. Uekama, K.; Hirayama, F.; Arima, H. Pharmaceutical Applications of Cyclodextrins and Their Derivatives. In *Cyclodextrins and Their Complexes: Chemistry, Analytical Methods, Applications;* Dodziuk, H., Ed.; Wiley-VCH: Weinheim, Germany, 2006; pp 381–422. doi:10.1002/3527608982.ch14
8. Hashimoto, H. In *Cyclodextrins and Their Complexes: Chemistry, Analytical Methods, Applications;* Dodziuk, H., Ed.; Wiley-VCH: Weinheim, Germany, 2006; pp 452–459.
9. Szejtli, J.; Szente, L. *Eur. J. Pharm. Biopharm.* **2005,** *61,* 115–125. doi:10.1016/j.ejpb.2005.05.006
10. Brewster, M. E.; Loftsson, T. *Adv. Drug Delivery Rev.* **2007,** *59,* 645–666. doi:10.1016/j.addr.2007.05.012
11. Astray, G.; Gonzalez-Barreiro, C.; Mejuto, J. C.; Rial-Otero, R.; Simal-Gándara, J. *Food Hydrocolloids* **2009,** *23,* 1631–1640. doi:10.1016/j.foodhyd.2009.01.001
12. Loftsson, T.; Brewster, M. E. *J. Pharm. Pharmacol.* **2010,** *62,* 1607–1621. doi:10.1111/j.2042-7158.2010.01030.x
13. Wenz, G.; Han, B.-H.; Müller, A. *Chem. Rev.* **2006,** *106,* 782–817. doi:10.1021/cr970027+
14. Harada, A.; Hashidzume, A.; Yamaguchi, H.; Takashima, Y. *Chem. Rev.* **2009,** *109,* 5974–6023. doi:10.1021/cr9000622
15. Zhou, J.; Ritter, H. *Polym. Chem.* **2010,** *1,* 1552–1559. doi:10.1039/c0py00219d
16. Yuen, F.; Tam, K. C. *Soft Matter* **2010,** *6,* 4613–4630. doi:10.1039/c0sm00043d
17. Chen, G.; Jiang, M. *Chem. Soc. Rev.* **2011,** *40,* 2254–2266. doi:10.1039/c0cs00153h
18. Harada, A.; Hashidzume, A.; Yamaguchi, H.; Takashima, Y. *Polymeric Materials;* John Wiley & Sons, Inc., 2012; pp 1–31.
19. Hashidzume, A.; Tomatsu, I.; Harada, A. *Polymer* **2006,** *47,* 6011–6027. doi:10.1016/j.polymer.2006.06.021
20. Harada, A.; Hashidzume, A. *Aust. J. Chem.* **2010,** *63,* 599–610. doi:10.1071/CH09609
21. Hashidzume, A.; Harada, A. *Polym. Chem.* **2011,** *2,* 2146–2154. doi:10.1039/c1py00162k
22. Tomatsu, I.; Hashidzume, A.; Harada, A. *Macromolecules* **2005,** *38,* 5223–5227. doi:10.1021/ma050670v
23. Tomatsu, I.; Hashidzume, A.; Harada, A. *Macromol. Rapid Commun.* **2006,** *27,* 238–241. doi:10.1002/marc.200500793
24. Tomatsu, I.; Hashidzume, A.; Harada, A. *J. Am. Chem. Soc.* **2006,** *128,* 2226–2227. doi:10.1021/ja058345a
25. Tamesue, S.; Takashima, Y.; Yamaguchi, H.; Shinkai, S.; Harada, A. *Angew. Chem., Int. Ed.* **2010,** *49,* 7461–7464. doi:10.1002/anie.201003567
26. Tamesue, S.; Takashima, Y.; Yamaguchi, H.; Shinkai, S.; Harada, A. *Eur. J. Org. Chem.* **2011,** 2801–2806. doi:10.1002/ejoc.201100077
27. Nakahata, M.; Takashima, Y.; Yamaguchi, H.; Harada, A. *Nat. Commun.* **2011,** *2,* No. 511. doi:10.1038/ncomms1521
28. Harada, A.; Kobayashi, R.; Takashima, Y.; Hashidzume, A.; Yamaguchi, H. *Nat. Chem.* **2011,** *3,* 34–37. doi:10.1038/nchem.893
29. Yamaguchi, H.; Kobayashi, R.; Takashima, Y.; Hashidzume, A.; Harada, A. *Macromolecules* **2011,** *44,* 2395–2399. doi:10.1021/ma200398y
30. Zheng, Y.; Hashidzume, A.; Takashima, Y.; Yamaguchi, H.; Harada, A. *Langmuir* **2011,** *27,* 13790–13795. doi:10.1021/la2034142
31. Yamaguchi, H.; Kobayashi, Y.; Kobayashi, R.; Takashima, Y.; Hashidzume, A.; Harada, A. *Nat. Commun.* **2012,** *3,* No. 603. doi:10.1038/ncomms1617
32. Turro, N. J. *Modern Molecular Photochemistry;* University Science Books: Sausalito, CA, 1991.
33. Valeur, B. *Molecular Fluorescence: Principles and Applications;* Wiley-VCH: Weinheim, Germany, 2002.
34. Yorozu, T.; Hoshino, M.; Imamura, M. *J. Phys. Chem.* **1982,** *86,* 4426–4429. doi:10.1021/j100219a031
35. Hamai, S. *J. Phys. Chem.* **1989,** *93,* 6527–6529. doi:10.1021/j100354a048
36. Ueno, A. *Supramol. Sci.* **1996,** *3,* 31–36. doi:10.1016/0968-5677(96)00016-8
37. Zheng, Y.; Hashidzume, A.; Takashima, Y.; Yamaguchi, H.; Harada, A. *Nat. Commun.* **2012,** *3,* No. 831. doi:10.1038/ncomms1841
38. Siu, H.; Duhamel, J. *J. Phys. Chem. B* **2008,** *112,* 15301–15312. doi:10.1021/jp801105q
39. Siu, H.; Duhamel, J. *J. Phys. Chem. B* **2012,** *116,* 1226–1233. doi:10.1021/jp208168r
40. Duhamel, J. *Polymers* **2012,** *4,* 211–239. doi:10.3390/polym4010211
41. Duhamel, J. *Langmuir* **2012,** *28,* 6527–6538. doi:10.1021/la2047646
42. de Melo, J. S.; Costa, T.; da G. Miguel, M.; Lindman, B.; Schillén, K. *J. Phys. Chem. B* **2003,** *107,* 12605–12621. doi:10.1021/jp0346054
43. de Melo, J. S. S.; Costa, T.; Oliveira, N.; Schillén, K. *Polym. Int.* **2007,** *56,* 882–899. doi:10.1002/pi.2219
44. Blyshak, L. A.; Warner, I. M.; Patonay, G. *Anal. Chim. Acta* **1990,** *232,* 239–243. doi:10.1016/S0003-2670(00)81238-6

License and Terms

Beilstein Journal of Organic Chemistry

Restructuring polymers via nanoconfinement and subsequent release

Alan E. Tonelli

Review

Open Access

Address:
Fiber & Polymer Science Program, North Carolina State University, Campus Box 8391, Raleigh, NC, 27695-8301, USA

Email:
Alan E. Tonelli - alan_tonelli@ncsu.edu

Keywords:
cyclodextrins; inclusion compounds; nanoconfinement; organization; polymers; properties; release; urea

Beilstein J. Org. Chem. **2012,** *8,* 1318–1332.
doi:10.3762/bjoc.8.151

Received: 30 March 2012
Accepted: 13 July 2012
Published: 16 August 2012

This article is part of the Thematic Series "Superstructures with cyclodextrins: Chemistry and applications".

Guest Editor: H. Ritter

Abstract

During the past several years my students and I have been utilizing certain small-molecule hosts to create nanostructured polymers. This is accomplished by first forming noncovalently bonded inclusion complexes (ICs) between these small-molecule hosts and guest polymers, followed by the careful removal of the host crystalline lattice to obtain a coalesced bulk polymer. We have repeatedly observed that such coalesced polymer samples behave distinctly from those produced from their solutions or melts. Coalesced amorphous homopolymers exhibit higher glass-transition temperatures, while crystallizable homopolymers coalesced from their ICs display higher melting and crystallization temperatures, and sometimes different crystalline polymorphs. When ICs are formed with block copolymers or with two or more different homopolymers, the resulting coalesced samples can exhibit intimate mixing between the copolymer blocks, or between entire homopolymer chains. Each of the distinct behaviors observed for polymers coalesced from their ICs is a consequence of the structural organization of the polymer–host-ICs. Polymer chains in host-IC crystals are confined to occupy narrow channels (diameter ~0.5–1.0 nm) formed by the small-molecule hosts around the included guest polymers during IC crystallization. This results in the separation and high extension of the included guest polymer chains, which leads, following the careful removal of the host molecule lattice, to unique behaviors for the bulk coalesced polymer samples. Apparently, substantial degrees of the extended and unentangled natures of the IC-included chains are retained upon coalescence. In this review we summarize the behaviors and uses of coalesced polymers, and attempt to draw conclusions on the relationship between their behavior and the organization/structures/conformations of the constituent polymer chains achieved upon coalescence from their ICs.

Introduction

The behaviors and properties of polymer materials are closely related to the organizations, structures, and morphologies of their constituent chains, which can be significantly altered during their processing, unlike the case of atomic and small molecule solids. Because the conformations and arrangements of their inherently flexible long chains are amenable to modifications through processing, materials made from the same polymer can behave very distinctly when the means used to process them are also different. For example, gel-spun Spectra poly(ethylene) (PE) fibers are extremely strong in the fiber direction, and may be fabricated into light-weight armor. On the other hand, molded articles, such as melt-blown PE garbage bags, are not nearly as strong, but have a much greater elasticity, even though the same polymer is used in both applications. The differences in their behaviors are a result of the different organizations, structures, and morphologies of their polymer chains, which are produced by the widely different means used to process PE Spectra fibers and garbage bags.

In this review, a means to reorganize polymers by nanoprocessing them into solids with unique properties is presented. This is achieved by first forming noncovalently bonded inclusion complexes (ICs) between certain small-molecule hosts and guest polymers, followed by the careful removal of the host molecules to obtain a coalesced bulk polymer sample. This process is illustrated in Figure 1, in which the cyclic starches, cyclodextrins (CDs), are the host molecules used to form ICs with guest polymers [1,2]. In polymer ICs formed with CDs and other small-molecule hosts, such as urea, thiourea, cyclotriphosphazenes, and perhydrotriphenylenes, the polymer guests are included in very narrow channels (~0.5–1.0 nm in diameter) of the crystalline lattice formed by the host molecules. This results in the isolation and high extension of each included guest polymer chain. By careful removal of the crystalline lattice of host molecules, it was hoped that the resulting coalesced polymer chains (c-polymers) would retain a significant degree of their prior extended and unentangled natures (Figure 1), and thus be organized in a manner quite different from samples processed from their solutions or melts, in which polymer chains randomly coil and entangle. This was indeed found to be the case, and the behaviors and properties of such c-polymer samples were observed to differ significantly from, and to be improved with respect to those of ordinarily processed samples [2-66].

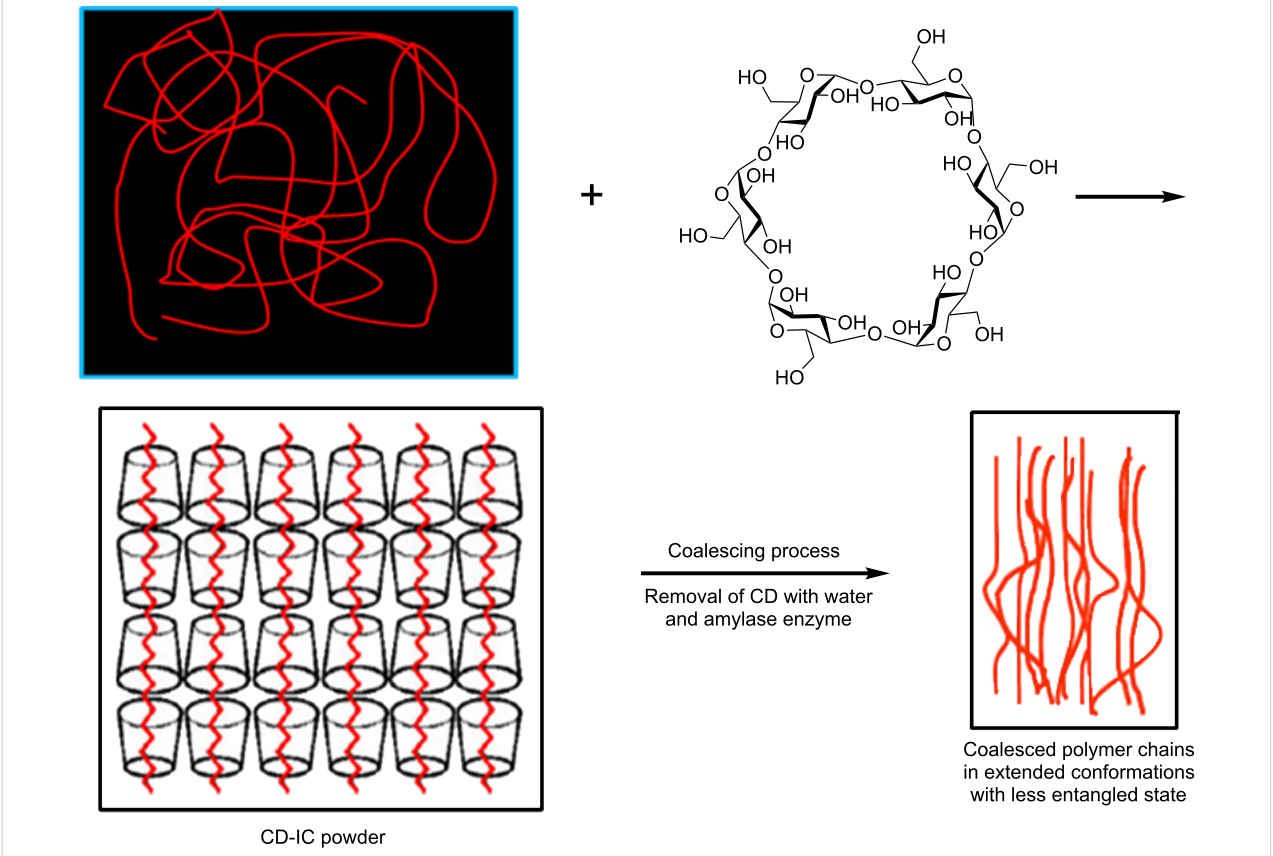

Figure 1: Formation of and coalescence of a polymer sample from its crystalline cyclodextrin inclusion complex [2].

Here, by way of several examples, we attempt to demonstrate the restructuring of polymers by nanoconfinement and subsequent release from their noncovalently bonded ICs. In each case a comparison is made between the behaviors and properties of such c-polymers and samples of the same polymer that were processed in the normal manner. In addition, we demonstrate the use of crystallizable c-polymers to serve as self-nucleants for the melt-crystallization of chemically identical polymers. The behaviors and properties of such self-nucleated polymers are examined and discussed, and their use as reinforcement in the formation of single-component polymer composites is suggested.

Review

Because the vast majority of the polymer-ICs that we have formed employed CDs as hosts, we herein simply outline the procedures used to form and characterize polymer–CD ICs and to coalesce guest-polymer samples from them. More detailed procedures, as well as the means used to characterize them, may be found in the cited references.

Formation and characterization of polymer–CD ICs

Polymer–CD ICs are most often produced [2,5,6,17] by combining polymer and CD solutions, usually gradually and with stirring or sonication, followed by filtering off of the resultant IC crystals. These are usually sequentially washed with the same solvents used to make their solutions, to remove any free unthreaded guest polymer and/or host CD, and are then dried.

In some instances, suspension of solid host CDs in polymer solutions or in polymer melts can also lead to IC formation [36,66]. In a related study [67] it was observed that when the α-CD IC containing guest poly(L-lactic acid) (PLLA) chains was suspended overnight in a solution containing poly(ε-caprolactone) (PCL), the resulting solid α-CD IC contained included PCL chains, while the displaced PLLA chains had moved into solution.

Polymer–CD ICs are readily characterized by FTIR, NMR, DSC, and X-ray observations [6,8,17,20]. The presence of both guest polymer and host CD can be confirmed by FTIR and NMR spectroscopy, while solid-state ^{13}C NMR and X-ray diffraction can confirm the columnar IC structure. For example, in Figure 2 the crystal structures of as-received cage and columnar IC γ-CDs are easily distinguished [20]. Finally, examination by DSC can determine whether the guest polymer has been included in the columnar CD lattice or not, by the absence or presence, respectively, of the thermal signature(s) characteristic of the polymer, i.e., T_g and/or T_m.

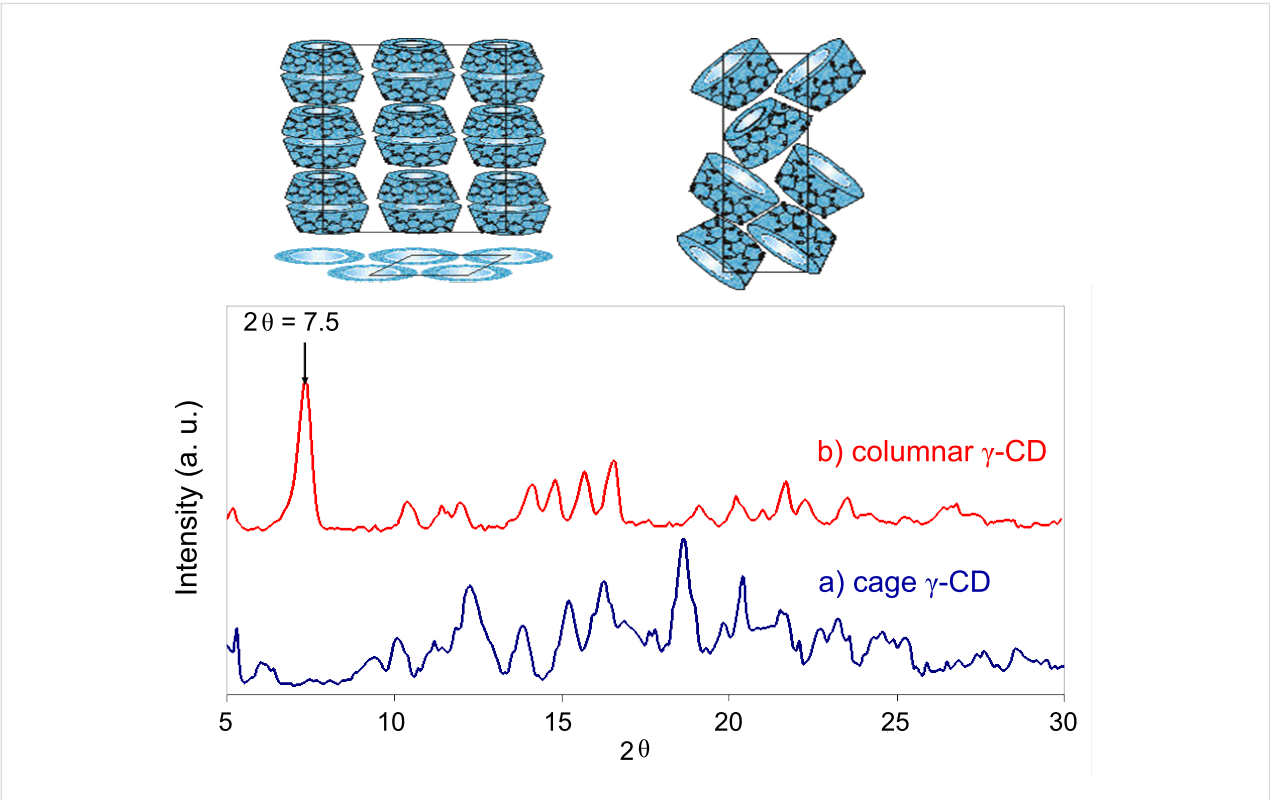

Figure 2: Crystal structures and wide-angle X-ray diffractograms of neat (a) cage and (b) columnar IC γ-CD [20].

The formation of polymer ICs with host urea (U) and their characterization are similar to those of polymer–CD ICs [69].

Coalescence and characterization of polymers from their CD ICs

Guest polymers may be coalesced from their CD ICs in several ways [65]. Depending on their mode of formation, they may be washed with warm water, briefly treated with an acidic aqueous solution, or treated with an aqueous solution of an amylase enzyme. Their characterization is accomplished by the same experimental means mentioned above for polymer–CD ICs. In addition, details of the polarizing micrographs, permeabilities, mechanical properties, and rheological behaviors of the c-polymer samples discussed here may be found in references [8,64,65,68-70]. Polymer ICs made with host U are usually coalesced by washing with water and methanol [68].

Formation and characterization of single-component polymer composites

Single-component polymer composites consist of both a matrix and reinforcement made with the same polymer to provide compatible and strong interfaces. This is achieved by forming reinforcing films or fibers with crystallizabilities and mechanical properties superior to those of the matrix they are embedded in. When a crystallizable polymer is coalesced from its CD IC, it is observed to be more readily crystallized upon cooling of its melt [62,64,65], as indicated by a higher crystallization temperature, T_c, and a larger and narrower crystallization exotherm, as can be seen in Figure 3 for nylon-6 (N-6) [58,64].

Consequently, when coalesced-N-6 (c-N-6) is added in small amounts to as-received N-6 (asr-N-6) the resulting sample (nuc-N-6) crystallizes in a manner similar to neat c-N-6. Such self-nucleated polymers can be effectively used as reinforcement in single-component polymer composites [64], and will be discussed later.

Coalesced amorphous polymers

We begin describing the behaviors of amorphous polymers coalesced from their CD ICs, with atactic poly(vinyl acetate) (PVAc) as an example [44,71]. In Figure 4 we can see that the T_g of c-PVAc is more than 12 °C higher than that of asr-PVAc,

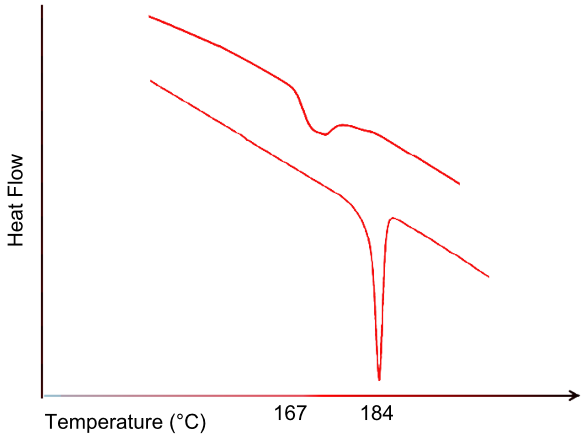

Figure 3: DSC cooling scans of as-received (upper) and coalesced N-6 (lower) [58].

an observation typical of amorphous polymers coalesced from their CD ICs [42]. Table 1 presents the densities of both PVAc samples measured [71] below and above their T_g's. The higher T_g of c-PVAc is consistent with its higher density, which remains higher than that of asr-PVAc even after being annealed at well above their T_g's, at 70 °C, for several weeks.

The high-temperature stability of the reorganized structures and resultant behaviors of c-polymers, as typified here by c-PVAc, has been repeatedly observed [17,52,63,71] and will be revisited and discussed further after we have completed our presentation of c-polymer behaviors. Also we have recently observed that PVAc coalesced from its IC formed with host urea (U) behaves quite similarly to PVAc coalesced from its γ-CD IC [72].

Coalesced semicrystalline polymers

Poly(ε-caprolactone) (PCL) is a biodegradable/bioabsorbable aliphatic polyester that is often used in biomedical applications, such as drug delivery and suture manufacturing. However, its relatively poor physical properties limit its use in load-bearing applications. An attempt to improve the strength of PCL was made by processing with α-cyclodextrin (α-CD). First an inclusion complex (IC) between PCL and α-CD was formed, and

Table 1: Measured densities for as-received and coalesced PVAcs [71].

sample	density at 25 °C (g/cm^3) (below T_g)	density at 58 °C (g/cm^3) (above T_g)
asr-PVAc	1.093	1.040
c-PVAc	1.156	1.077

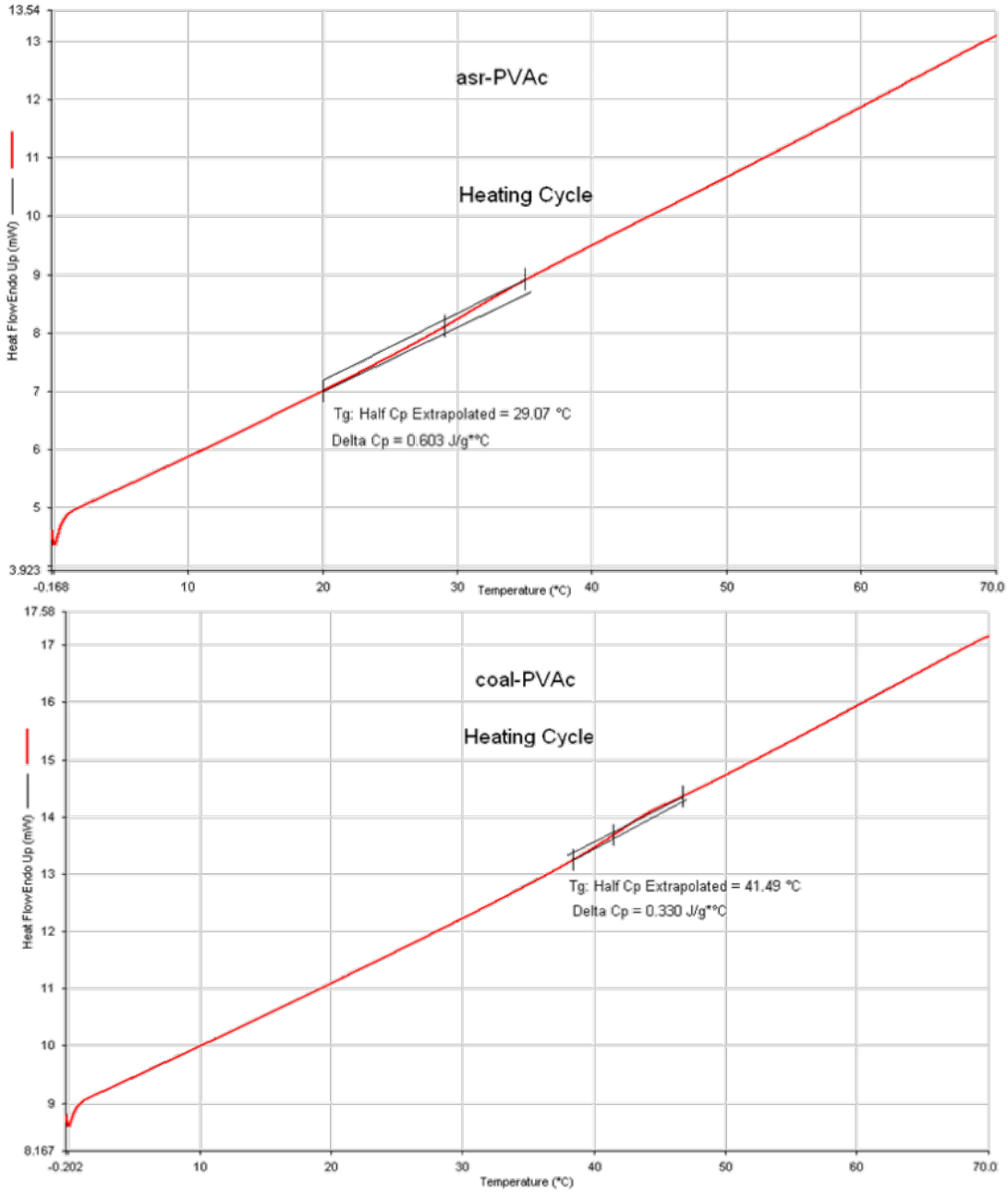

Figure 4: DSC heating scans for asr-PVAc (upper) and c-PVAc coalesced from its γ-CD IC (lower) [72].

then the host α-CD was stripped away to yield bulk coalesced PCL (c-PCL), a process referred to as coalescence [65]. The thermal, physical, and melt rheological properties of c-PCL resulting from this coalescence process were observed to be improved, as a result of the largely extended, unentangled coalesced PCL chains. This also resulted in substantial increases in melt-crystallization temperatures, T_c's (up to 25 °C higher, depending on the cooling rate from the melt), as illustrated in Figure 5, even though PCL is ordinarily an inherently "fast melt-crystallizer". Similarly enhanced crystallizabilities were also observed for PCLs of various molecular weights when coalesced from their U ICs [68].

Density and DSC measurements [70] revealed a closer packing of chains in the noncrystalline sample regions, but this did not affect the overall crystallinity of the c-PCL films. Increased elastic storage modulus, decreased tan δ, increased average hardness (33%), and increased Young's modulus (53%) [65] were observed for the c-PCL films. Annealing c-PCL well above T_m (90 °C) for a month, did not cause the reorganized

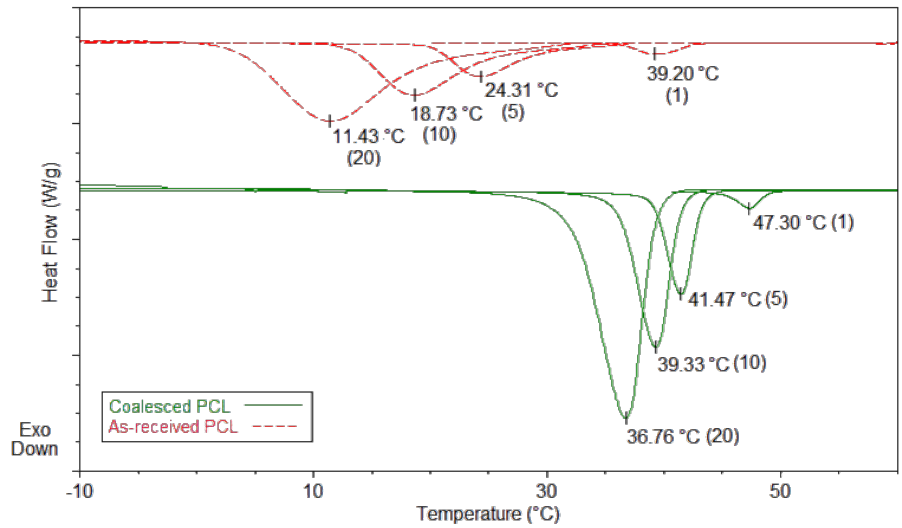

Figure 5: Melt-crystallization curves of as-received and coalesced PCL observed at 20, 10, 5, and 1 °C/min cooling rates [65].

c-PCL chains in the noncrystalline regions to revert to the normal randomly coiled entangled melt. This permitted c-PCL to be used as a homogeneous nucleant in the melt-crystallization of as-received PCL (asr-PCL), because when a few percent of c-PCL was added to asr-PCL its melt-crystallization was also found to be accelerated. Thus, by means of melt-processing with c-PCL added as a nucleant, the semi-crystalline morphology of PCL may be controlled. Of course, not only is the c-PCL nucleant necessarily nontoxic and biodegradable/bioabsorbable, it is also chemically compatible and has a "stealthy" nature.

Bulk, as-received poly(ethylene terephthalate) (asr-PET) has been observed to reorganize both morphologically and conformationally, either by formation of a crystalline inclusion complex (IC) between guest PET and host γ-cyclodextrin (γ-CD), followed by removal of the host γ-CD and coalescence of the guest PET (c-PET), or by precipitation (p-PET) from its solution in trifluoroacetic acid upon gradual addition to a large excess of rapidly stirred acetone [17,52,69]. The c- and p-PETs showed very similar behaviors, but p-PET can be more easily produced in larger quantities. DSC and density observations of p-PET imply structures/morphologies and chain conformations and packing in the noncrystalline sample regions that are different from those of asr-PET obtained by standard processing techniques.

In comparison to slowly crystallizing/easily melt-quenched asr-PET, p-PET repeatedly crystallizes rapidly from the melt. Upon subsequent heating, its noncrystalline domains do not show a glass transition or undergo crystallization, but only a melting endotherm that is virtually identical in magnitude to the crystallization exotherm observed during its prior rapid cooling from the melt, is observed (see DSC results and further discussion of p-PET below). These observations suggest that p-PET readily attains higher crystallinity even when repeatedly cooled rapidly from the melt. Apparently the extended conformations of largely unentangled chains in p-PET do not become coiled and entangled even after spending substantial time in the melt.

As a consequence, we have demonstrated [69] that p-PET can be used in small quantities (a few percent) as an effective self-nucleating agent to control the bulk semicrystalline morphology of melt-processed asr-PET, and the resulting properties of nucleated PET (nuc-PET) were assessed. For instance, comparison of asr- and nuc-PET films, each with ~10% crystallinity, reveals that the nuc-PET film has significantly increased density, hardness and Young's modulus and is also much less permeable to CO_2 than the asr-PET film. Undrawn nuc-PET fibers also exhibited significantly higher tenacities and moduli than undrawn asr-PET fibers. Self-nucleated PET not only possesses improved properties, but contains no incompatible additives, and so may be readily recycled.

Coalesced block copolymers

The triblock copolymer PCL-PPG-PCL, with noncrystallizable central poly(propylene oxide blocks), was synthesized by coordinated ring-opening polymerization of ε-caprolactone with PPG-diol as the initiator [21]. In the IC of PCL-PPG-PCL formed with α-CD, only PCL blocks were included. In contrast, both PCL and PPG blocks were included in the IC of PCL-PPG-PCL formed with γ-CD, which has larger channels. Conse-

quently, coalescence of the triblock copolymer chains from these two CD ICs yielded samples showing opposite changes in the segregation and crystallinity (X_c) of the PCL blocks.

As can be seen in Table 2, the crystallinity of the sample coalesced from the triblock-α-CD IC is obviously higher than that of the as-synthesized triblock copolymer. On the contrary, the crystallinity of the sample coalesced from the γ-CD IC is lower than that of the as-synthesized triblock copolymer [21]. This difference is a result of the fact that the entire triblock is included in the crystalline channels of the γ-CD IC, while only the PCL blocks are included in the α-CD IC (Figure 1).

Table 2: Thermal properties and crystallinities of various PCL-PPG-PCL triblock copolymer samples, as revealed by DSC [21].

sample	T_m (°C)	ΔH_m (J/g)	X_c (%)
as-synthesized copolymer	57.3	58.6	56.5
coalesced from α-CD IC	63.8	76.8	74.1
coalesced from γ-CD IC	63.0	51.3	49.5

As a result, the segregation or mixing of PCL and PPO blocks in their CD-ICs is carried over to the coalesced tri-block copolymer samples, explaining the divergent crystallinities of the PCL blocks.

The fact that the PCL-PPG-PCL triblock coalesced from its γ-CD IC is not dramatically less crystalline than the fully segregated as-synthesized sample, is likely a result of the ability of two PCL blocks to occupy the same γ-CD IC channels [73], which are larger and, consequently, lead to partial segregation of the crystallizable PCL blocks.

When PCL-*b*-PLLA [poly(L-lactic acid)] was obtained by first forming its IC with α-CD, followed by coalescence of the guest diblock copolymer chains, a readily biodegradable sample of the block copolymer with very low crystallinity was produced [16]. Compression molding between Teflon plates produced film samples of asr- and c-PCL-*b*-PLLA, PCL and PLLA homopolymers of approximately the same chain lengths as the corresponding blocks in PCL-*b*-PLLA, and a physical blend of PCL/PLLA homopolymers with the same molar composition as the PCL-*b*-PLLA. The in vitro biodegradation behaviors of these films were observed in phosphate buffer solution containing lipase from *Rhizopus arrhizus* by means of ultraviolet and attenuated total reflectance FTIR spectroscopy, DSC, wide-angle X-ray diffraction, and weight-loss analysis.

The PCL segments in all of the above films were found to degrade much faster than the PLLA segments. As expected, suppression of the phase segregation that resulted from mixing of PCL and PLLA blocks leading to decreased crystallinity in the c-diblock copolymer film, resulted in a much faster enzymatic degradation than that of either the asr-diblock copolymer or the PCL/PLLA physical blend. The biodegradation of the c-diblock was observed to be especially enhanced during the early stages. The disappearance of amorphous scattering and a sharpening of the crystalline peaks in the X-ray diffractograms seen in Figure 6 make clear that it is the well-mixed amorphous portions of the c-PCL-*b*-PLLA diblock copolymer film that are preferentially degraded by the enzyme. Regulation of their biodegradation behavior, through formation of and coalescence from CD ICs, may enhance the use of block copolymers in drug delivery and controlled release systems, because of its decisive importance in these applications.

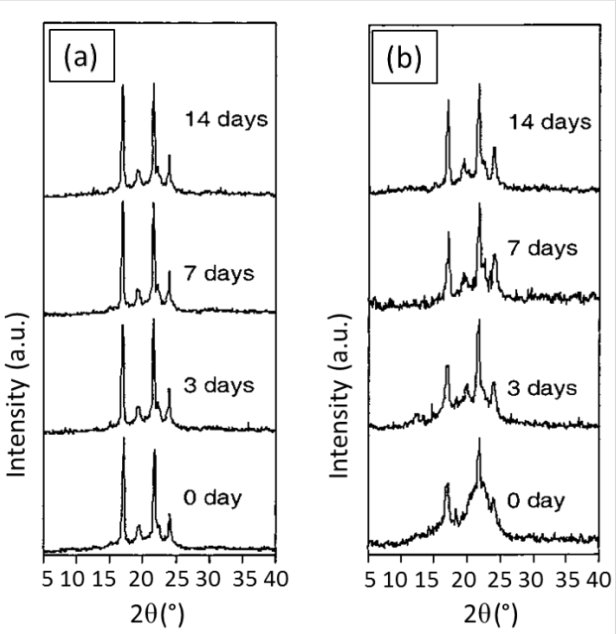

Figure 6: X-ray diffraction patterns of as-synthesized PCL-*b*-PLLA films (a) and coalesced PCL-*b*-PLLA films (b), after various enzymatic degradation times [16,25].

Coalesced polymer blends

Intimately mixed PCL/PLLA blends were obtained upon coalescence from their common α-CD IC [7], as suggested by the polarized micrographs and X-ray diffractograms shown in Figure 7 and Figure 8, respectively. Two-dimensional spin-diffusion NMR observations [40] of these blends demonstrated that individual PCL and PLLA chains are indeed in intimate contact.

A ternary PVAc/poly(methyl methacrylate) (PMMA)/polycarbonate (PC) blend was coalesced from their common IC formed with host γ-CD [28]. Intimate mixing of all three polymers was

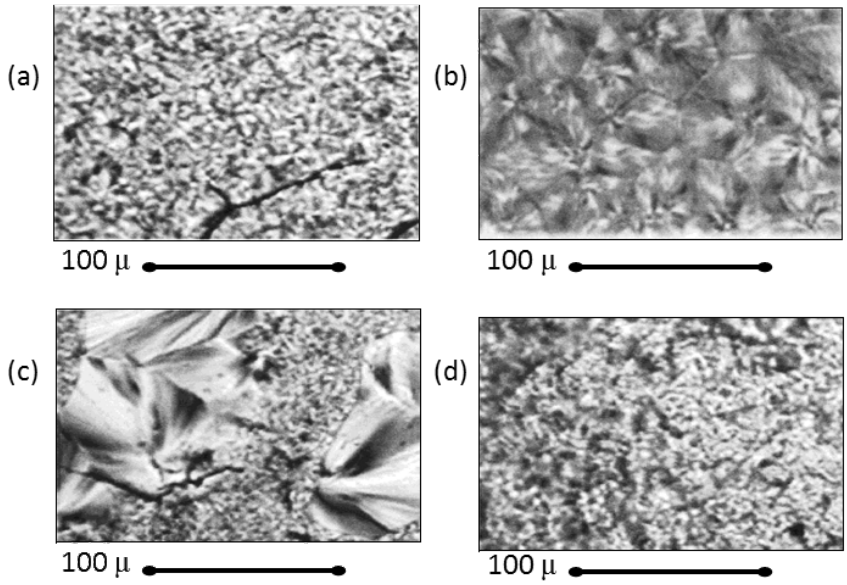

Figure 7: Polarizing photomicrographs of (a) PLLA, (b) PCL, (c) solution-cast, and (d) coalesced PLLA/PCL blends [8].

observed, as indicated by the single T_g exhibited in DSC observations of their ternary coalesced blend (Figure 9). Solid-state NMR observations [^{13}C observed ^{1}H spin-lattice relaxation times recorded in the rotating frame, $T_{1\rho}(^{1}H)$] of the three polymers in their ternary blend confirmed their intimate molecular mixing on a scale less than 5 nm.

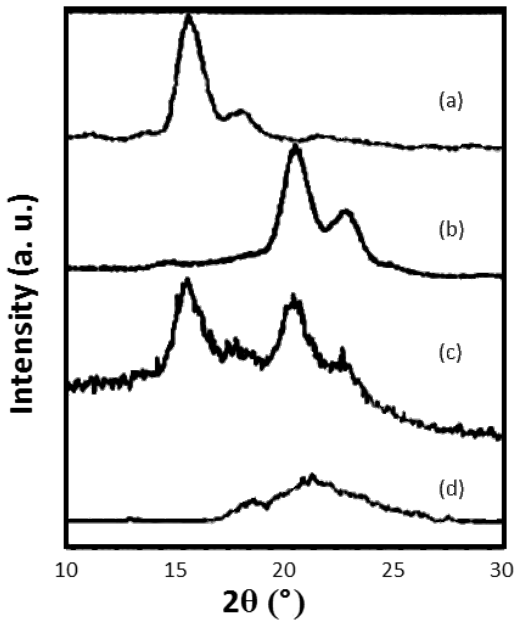

Figure 8: X-ray diffractograms of (a) pure PCL and (b) PLLA and PCL/PLLA blends obtained by casting from dioxane solution (c) and hot-water coalescence from PCL/PLLA–CD IC (d) [16,25].

Thermal stability of coalesced polymer structures and behaviors

As noted in passing above, in our discussion of coalesced polymers both amorphous and crystallizable, the many unusual behaviors and properties they exhibit are stable to long periods of high-temperature annealing, above their T_g's and T_m's [57,74]. These observations suggest solid-state organizations/structures/morphologies for coalesced polymers that are distinct

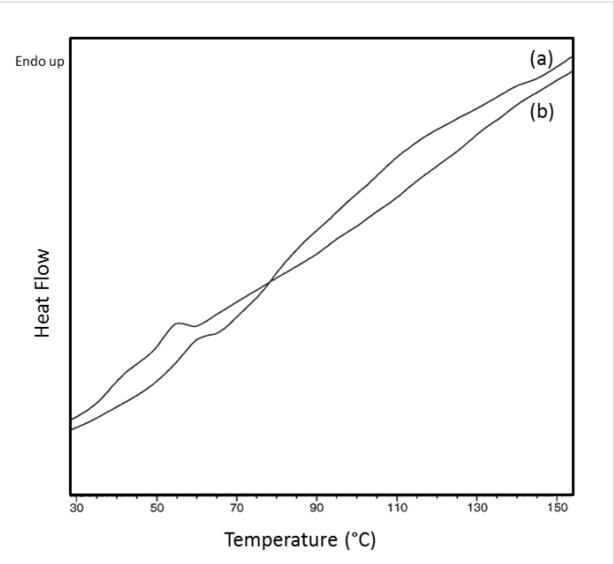

Figure 9: MDSC scans of the (a) first and (b) second heating runs recorded for the PC/PMMA/PVAc-2 blend. The sample was held for 3 min at 170 °C after the first heating [28].

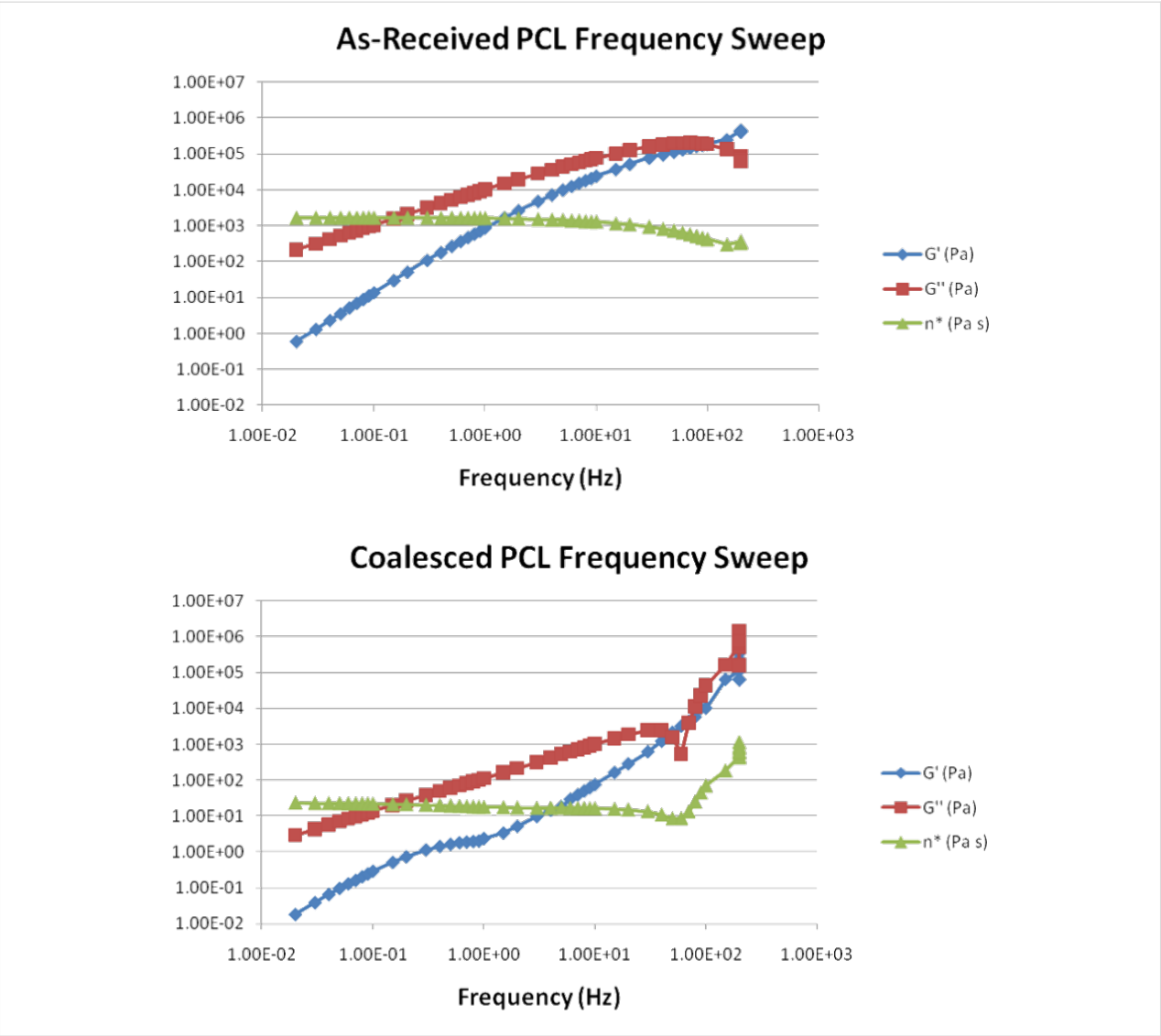

Figure 10: Storage modulus, loss modulus, and apparent viscosity (G', G'', and n*, respectively) for asr- and c-PCL melts, (top and bottom, respectively), as obtained through oscillatory melt rheology (T = 90 °C; testing stress = 750 Pa; pretest hold time = 1 minute) [65,70].

from those that are normally processed from their solutions and melts. Furthermore, their stability to long periods of high-temperature annealing also indicates that their melts are and remain distinct from those samples that are processed normally.

For example, in Figure 10 the rheological behaviors of asr- and c-PCL melts, the latter obtained from PCL-α-CD IC, are compared and seen to be quite distinct [65,70]. The zero shear viscosity of the c-PCL melt is about two orders of magnitude less than that of the asr-PCL melt. Repetitive rheological runs on the same asr- and c-PCL samples demonstrated that the distinct rheological responses of their melts were independent of long-time melt annealing, as well as long exposures to rheological stresses.

So, what are the organizations/structures in c-polymer melts?

What we do know [2,57,65,70,74]:

1. They behave differently:
   (a) They crystallize more readily and apparently without chain folding.
   (b) They have elevated T_g's and T_c's.
   (c) Their blends are intimately mixed.
   (d) Their amorphous regions are denser.
   (e) Their melts have much lower zero shear viscosities.
   (f) They produce stronger, less extensible films and fibers.
   (g) They are less permeable to gases (CO_2).

2. All the above behaviors remain, even after extensive periods (weeks) spent in their melts [57,65,68,69,72,74] and, though only mentioned very briefly here, are independent of their molecular weights and their IC host (CD or U).
3. We anticipate that upon coalescence from their ICs, the resulting coalesced polymer samples will consist of small disoriented regions (smaller than the sizes of their IC crystals) of extended, unentangled, and oriented chains (Figure 1), because polymer ICs are generally obtained as crystalline powders. That is not to say that the initial overall macroscopic orientation of all extended and unentangled chains is a result of this. Instead, the macroscopic organization of polymer chains in the melt may initially resemble a grouping of small, randomly arranged "nematic-like" regions, i.e., without a preferred orientation of their directors. For a discussion of Vectra, a liquid-crystalline ester/arylate copolymer, which exhibits a macroscopically anisotropic melt, much like that suggested above locally for coalesced polymers and with similar rheological behavior (Beers and Ramirez [75]).
4. This anticipated structure is consistent with their behaviors noted in point 1, including their melt rheologies. Though we have discussed potential reasons for the long-time, high-temperature stability noted in point 2 [57,74], we have yet to connect it to the structures of coalesced polymer samples.

So the question remains, how can we directly observe the structure(s) of coalesced polymers in their melts? To date we have been unable to answer this question, and, so, invite the reader to offer suggestions.

Coalesced polymer applications: Scientific and commercial

Our brief discussion above concerning the behaviors of c- and p-PETs, and how they may be used to self-nucleate the melt-crystallization of asr-PET to produce nuc-PET materials with improved properties, may not only have commercial significance, but may in addition enhance our understanding of the underlying bases for polymer structure–property relations in PET and other polymers.

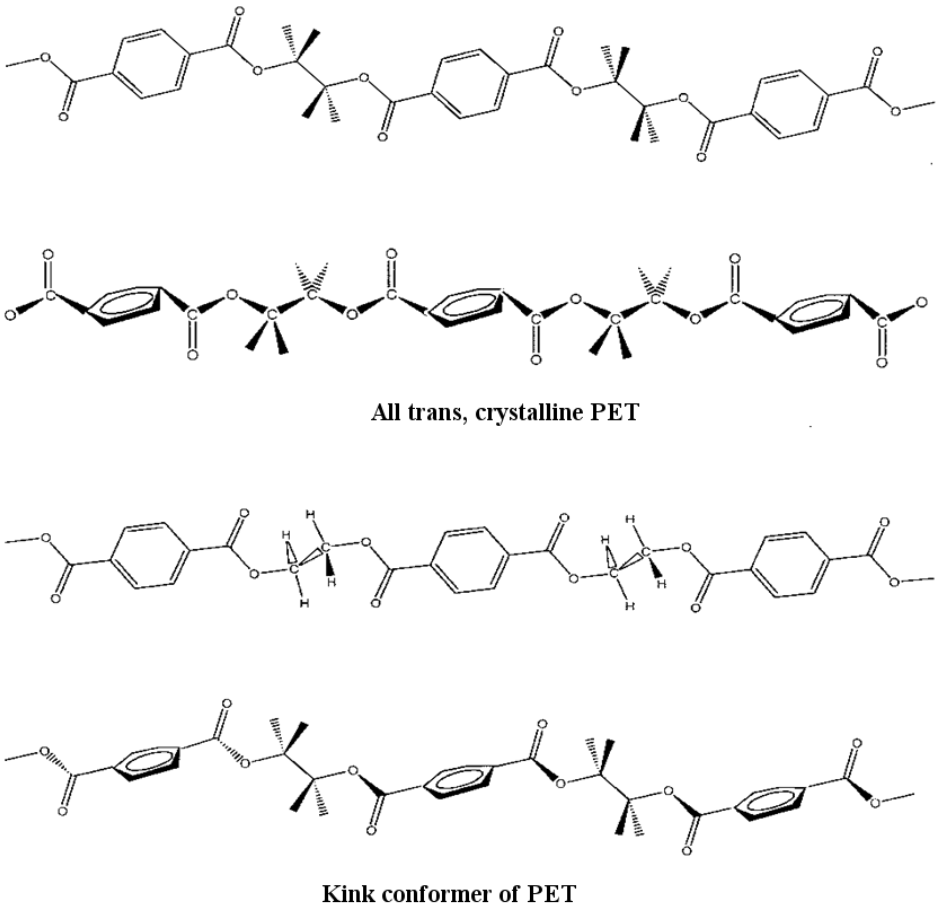

Figure 11: Crystalline all *trans* (*t*) and γ-CD-included *g*±*tg*∓ conformations of PET [76].

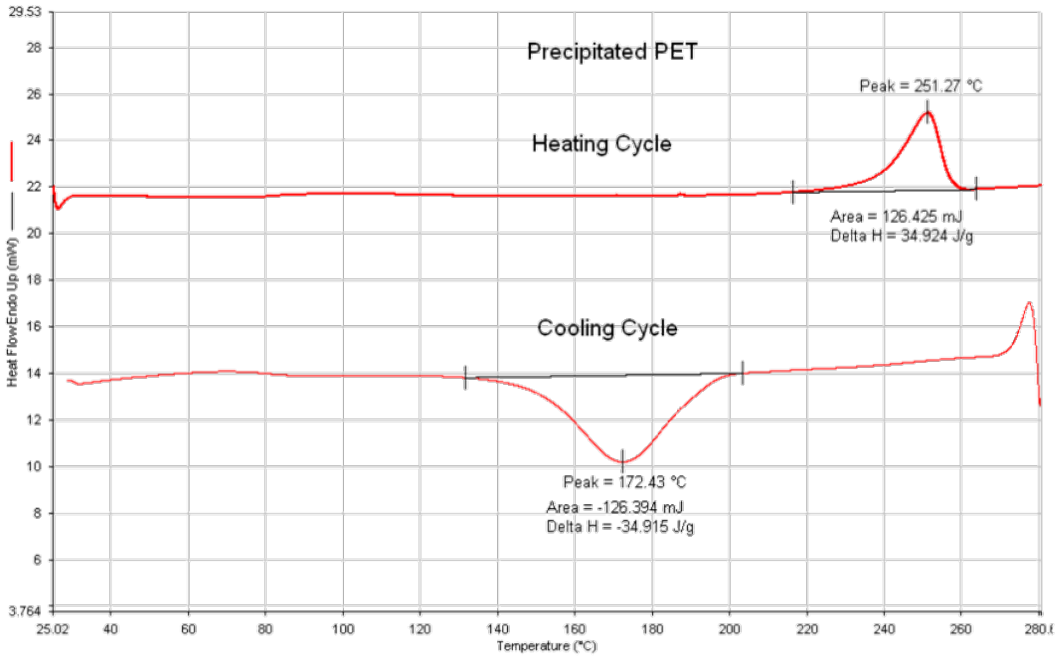

Figure 12: DSC scans for p-PET [70].

As described previously [17,52], γ-CDs are capable of forming an inclusion compound with PET. Modeling of PET conformations able to thread through CDs suggested that the *gauche*± *trans gauche*∓ ethylene glycol conformations illustrated in Figure 11 have a narrower cross section than the all trans crystalline PET conformation also illustrated there [76]. Analyses of the FTIR [17] and solid-state ^{13}C NMR [27] spectra of PET coalesced from its γ-CD IC (c-PET) are consistent with the narrower *gauche*± *trans gauche*∓ conformations for the noncrystalline portions of the coalesced sample. Unlike normal as-received PET (asr-PET), c-PET was observed to be repeatedly rapidly crystallizable from its melt. During the course of forming the PET-γ-CD IC [17], several control experiments were conducted that led to the observation that PET that was slowly precipitated (p-PET) from TFA solution with rapidly stirred acetone, exhibited thermal behavior very similar to that of c-PET [52,69], which can be seen in Figure 12.

It has been suggested [17,52,69] that the chains of c- and p-PETs in their noncrystalline regions largely adopt the extended *gauche*± *trans gauche*∓ conformations, with *trans* $–CH_2–CH_2–$ bonds, as in their crystals. Normally in the melt, the $–CH_2–CH_2–$ bond is predominantly *gauche*± [77,78], and so must rotate to *trans* during crystallization. This conformational transition is not possible without sweeping out a large volume. On the other hand, crystallization of c- or p-PETs into the all-trans conformation proceeds rapidly from preponderantly *gauche*± $–O–CH_2–$, *trans* $–CH_2–CH_2–$ and *gauche*∓ $–CH_2–O–$ bond conformers through facile counter rotations about the $–O–CH_2–$ and $–CH_2–O–$ bonds, requiring only a very modest amount of swept-out volume [17,52,69]. Thus, it may not be surprising that asr-PET crystallizes slowly from its melt, while c- and p-PETS crystallize rapidly.

Quenched asr- and nuc-PET films (5 wt % p-PET/95 wt % asr-PET) are clear in appearance. DSC scans of the two films are not shown here, but indicate [69] that both PET films have the same level of crystallinity (~10%). Their densities obtained by using the flotation technique are summarized in Table 3 [69,71]. The higher density of the nuc-PET film (~1.3% higher) with the same low level of crystallinity as in the asr-PET film can likely be attributed to the higher orientation and increased order and packing of its extended unentangled chains in its predominant amorphous domains, which is seen even after the polymer film was quenched from the melt into ice water. This shows that nuc-PET has a tendency to organize differently to asr-PET, even when the melt is quenched at very high cooling rates.

Table 3: Densities of asr-PET and nuc-PET [69].

sample	density at 25 °C (g/cm^3)
asr-PET	1.368
nuc-PET	1.386

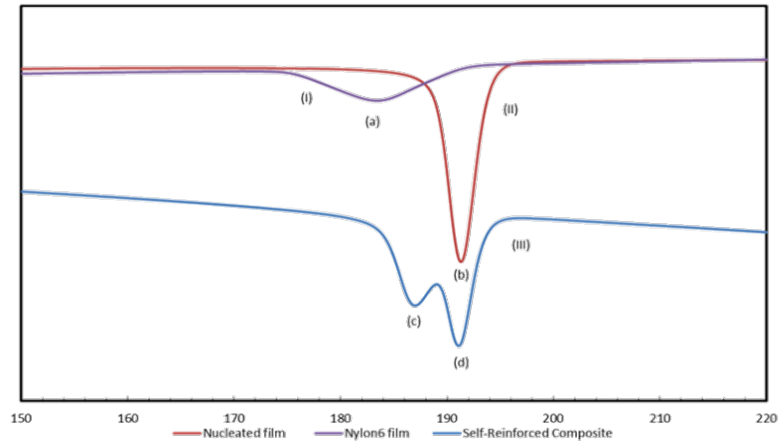

Figure 13: DSC cooling scans from the melts of (I) asr-N-6, (II) nuc-N-6, and (III) asr/nuc N-6 film sandwich. Melt-crystallization peaks (a), (b), (c), and (d) in the DSC scans correspond to T_c = 183, 192, 186, and 191 °C, respectively [64].

As clearly demonstrated in the case of PET, much can be learned about polymer structure–property relationships by forming polymer ICs, coalescing the guest polymers, and observing and comparing their behaviors and properties to those of samples normally processed from their solutions and melts.

Previously in Figure 3, we demonstrated that N-6 coalesced from its α-CD IC (c-N-6) crystallizes more readily. When 2 wt % c-N-6 is added to 98 wt % asr-N-6 to produce nuc-N-6, we similarly observe the nuc-N-6 to crystallize rapidly (Figure 13) [64]. This leads to improved mechanical properties for nuc-N-6, as illustrated in Figure 14, in which asr-N-6 film has also been annealed to exhibit very similar crystallinity to the nuc-N-6 film.

As a consequence, we created film sandwiches formed with two layers of asr-N-6 and a composite sandwich with one layer each of asr- and nuc-N-6 films. Note in Figure 13 the composite N-6 sandwich retains distinct thermal responses for each of its constituent layers despite ~10 min of melt processing. The mechanical properties of the asr-N6/asr-N-6 control and asr-N-6/nuc-N-6 composite sandwiches are presented in Figure 15.

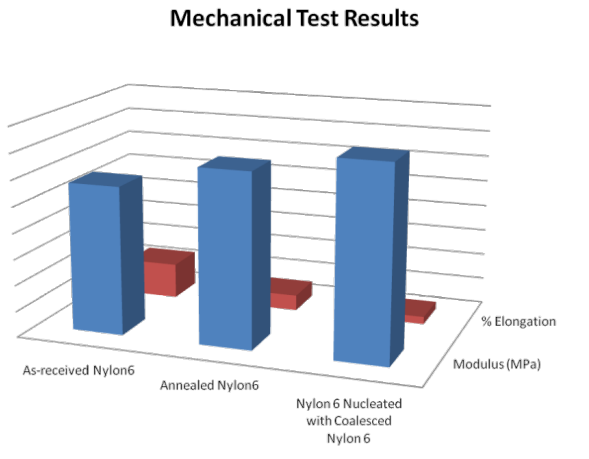

	As-received Nylon6	Annealed Nylon6	Nylon 6 Nucleated with Coalesced Nylon 6
Modulus (MPa)	571.01	667.85	739.4
% Elongation	136	59.7	28.7

Figure 14: Mechanical properties of N-6 films [62].

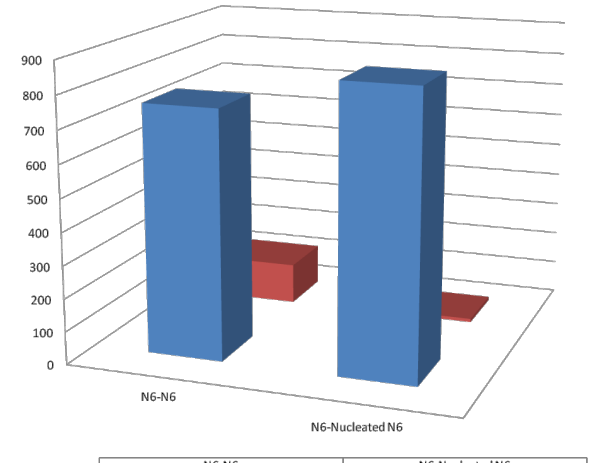

	N6-N6	N6-Nucleated N6
Modulus(MPa)	757.41	860.6
Elongation(%)	125	10.3

Figure 15: Tensile testing of as-received/as-received and as-received/nucleated nylon-6 film sandwiches conducted according to ASTM D-882-97. Each value of the mechanical properties reported is an average of at least five film-sandwich specimens [64].

Stress-strain observations (not shown) of both film sandwiches reveal, unsurprisingly, very strong interfaces for both sandwiches [64].

This work has been extended to melt-spun N-6 fibers, with similar results, confirming that c-polymers can serve to nucleate the melt-crystallization of chemically identical polymers, resulting in improved mechanical properties for the nuc-polymers. Such nuc-polymers can be effectively used as reinforcements in single-component composites, which necessarily have strong interfaces, and which show improved properties in comparison to the asr-polymer matrices.

Conclusion

We have attempted to demonstrate the utility of restructuring polymers, through nanoconfinement in and subsequent release/coalescence from their noncovalently bonded inclusion compounds, for the reorganization of their resulting bulk samples, thereby improving their properties. Because c-polymers remain reorganized despite long-term melt-annealing, they may be successfully melt-processed into improved materials. The examples of coalesced polymers discussed here were all obtained from their CD ICs. However, we have recently observed [68,72] very similar behavior for polymers coalesced from their U ICs, for which in this case the host molecules cannot thread over the included polymer chains. We therefore conclude that the unique behaviors of polymer samples coalesced from their CD ICs is not a consequence of remnant host CDs threaded over their chains.

Though mentioned only in passing here, significant information regarding the conformations, mobilities and supramolecular assembly of polymers can be obtained by observing and modeling both the formation of polymer ICs [47,73,76] and the behaviors of their included, highly extended, and isolated guest polymer chains [73,76]. Finally, we have also tried to indicate that examination and modeling of the behaviors of coalesced polymer samples, and their resulting properties, can usefully contribute to our understanding of the bases for structure–property relations observed in polymer materials.

Acknowledgements

I am indebted to the many students and collaborating colleagues listed in the references who have made possible the research summarized herein. Funding received from the National Textile Center (U.S. Commerce Dept.), the National Science Foundation, and North Carolina State University is also appreciated.

References

1. Harada, A.; Kamachi, M. *Macromolecules* **1990,** *23,* 2821. doi:10.1021/ma00212a039
   First reported formation of polymer–CD-ICs formed between poly(ethylene oxide) oligomers and α-CD. Since that time a large number of polymer-CD-ICs have been reported, and many can be found in the references cited here.
2. Tonelli, A. E. *Adv. Polym. Sci.* **2009,** *222,* 55. doi:10.1007/12_2008_2
3. Huang, L.; Vasanthan, N.; Tonelli, A. E. *J. Appl. Polym. Sci.* **1997,** *64,* 281. doi:10.1002/(SICI)1097-4628(19970411)64:2<281::AID-APP8>3.0.CO;2-N
4. Huang, L.; Allen, E. G.; Tonelli, A. E. In *Recent Research Developments in Macromolecular Research;* Pandalai, S. G., Ed.; Research Signpost: Trivandrum, India, 1997; Vol. 2, p 175.
5. Huang, L.; Tonelli, A. E. *J. Macromol. Sci, Revs. Macromol. Chem. Phys.* **1998,** *38,* 781. doi:10.1080/15583729808546037
6. Huang, L.; Allen, E.; Tonelli, A. E. *Polymer* **1998,** *39,* 4857. doi:10.1016/S0032-3861(97)00568-5
7. Huang, L.; Tonelli, A. E. Inclusion Compounds as a Means to Fabricate Controlled Release Materials. In *Intelligent Materials for Controlled Release;* Dinh, S. M.; DeNuzzio, J. D.; Comfort, A. R., Eds.; ACS Symposium Series No. 728; American Chemical Society: Washington, D.C., 1999; Chap. 10.
8. Rusa, C. C.; Tonelli, A. E. *Macromolecules* **2000,** *33,* 5321. doi:10.1021/ma000746h
9. Huang, L.; Gerber, M.; Taylor, H.; Lu, J.; Tapaszi, E.; Wutkowski, M.; Hill, M.; Nunalee, F. N.; Harvey, A.; Rusa, C. C.; Porbeni, F. E.; Edeki, E.; Tonelli, A. E. Creation of Polymer Films with Novel Structures by Processing with Inclusion Compounds. In *Film Formation in Coatings: Mechanisms, Properties, and Morphology;* Povder, T.; Urban, M. W., Eds.; ACS Symposium Series No. 790; American Chemical Society: Washington, D.C., 2001; Chap. 14.
10. Lu, J.; Mirau, P. A.; Rusa, C. C.; Tonelli, A. E. Cyclodextrin: From Basic Research to Market. In *Proceedings of the 10th International Cyclodextrin Symposium (CD-2000),* Ann Arbor, Mich., May 21–24, 2000; Szejtli, J., Ed.; Mira Digital Publishing: Saint Louis, MO, 2001.
11. Rusa, C. C.; Lu, J.; Huang, L.; Tonelli, A. E. Cyclodextrin: From Basic research to Market. In *Proceedings of the 10th International Cyclodextrin Symposium (CD-2000),* Ann Arbor, Mich., May 21–24, 2000; Szejtli, J., Ed.; Mira Digital Publishing: Saint Louis, MO, 2001.
12. Rusa, C. C.; Luca, C.; Tonelli, A. E. *Macromolecules* **2001,** *34,* 1318. doi:10.1021/ma001868c
13. Wei, M.; Tonelli, A. E. *Macromolecules* **2001,** *34,* 4061. doi:10.1021/ma010235a
14. Shuai, X.; Porbeni, F. E.; Wei, M.; Shin, I. D.; Tonelli, A. E. *Macromolecules* **2001,** *34,* 7355. doi:10.1021/ma0109626
15. Huang, L.; Gerber, M.; Taylor, H.; Lu, J.; Tapazsi, E.; Wutkowski, M.; Hill, M.; Lewis, C.; Harvey, A.; Wei, M.; Rusa, C. C.; Tonelli, A. E. *Macromol. Symp.* **2001,** *176,* 129. doi:10.1002/1521-3900(200112)176:1<129::AID-MASY129>3.0.CO;2-M
16. Shuai, X.; Wei, M.; Porbeni, F. E.; Bullions, T. A.; Tonelli, A. E. *Biomacromolecules* **2002,** *3,* 201. doi:10.1021/bm015609m
17. Bullions, T. A.; Wei, M.; Porbeni, F. E.; Gerber, M. J.; Peet, J.; Balik, M.; White, J. L.; Tonelli, A. E. *J. Polym. Sci., Part B: Polym. Phys.* **2002,** *40,* 992. doi:10.1002/polb.10152

18. Shuai, X.; Porbeni, F. E.; Wei, M.; Bullions, T.; Tonelli, A. E. *Macromolecules* **2002,** *35,* 3126. doi:10.1021/ma011954s
19. Wei, M.; Davis, W.; Urban, B.; Song, Y.; Porbeni, F. E.; Wang, X.; White, J. L.; Balik, C. M.; Rusa, C. C.; Fox, J.; Tonelli, A. E. *Macromolecules* **2002,** *35,* 8039. doi:10.1021/ma020765m
20. Rusa, C. C.; Bullions, T. A.; Fox, J.; Porbeni, F. E.; Wang, X.; Tonelli, A. E. *Langmuir* **2002,** *18,* 10016. doi:10.1021/la0262452
21. Shuai, X.; Porbeni, F. E.; Wei, M.; Bullions, T.; Tonelli, A. E. *Macromolecules* **2002,** *35,* 2401. doi:10.1021/ma012085+
22. Wei, M.; Shuai, X.; Tonelli, A. E. *Biomacromolecules* **2003,** *4,* 783. doi:10.1021/bm034078u
23. Bullions, T. A.; Edeki, E. M.; Porbeni, F. E.; Wei, M.; Shuai, X.; Rusa, C. C.; Tonelli, A. E. *J. Polym. Sci., Part B: Polym. Phys.* **2003,** *41,* 139. doi:10.1002/polb.10366
24. Abdala, A. A.; Tonelli, A. E.; Khan, S. A. *Macromolecules* **2003,** *36,* 7833. doi:10.1021/ma034173v
25. Tonelli, A. E. *J. Tex. Appar. Tech. Mgmt.* **2003,** *3,* 1.
26. Tonelli, A. E. *Macromol. Sympos.* **2003,** *203,* 71. doi:10.1002/masy.200351306
27. Wei, M.; Bullions, T. A.; Rusa, C. C.; Wang, X.; Tonelli, A. E. *J. Polym. Sci., Part B: Polym. Phys.* **2004,** *42,* 386. doi:10.1002/polb.10681
28. Rusa, C. C.; Uyar, T.; Rusa, M.; Hunt, M. A.; Wang, X.; Tonelli, A. E. *J. Polym. Sci., Part B: Polym. Phys.* **2004,** *42,* 4182. doi:10.1002/polb.20273
29. Abdala, A. A.; Wu, W.; Olesen, K. R.; Jenkins, R. D.; Tonelli, A. E.; Khan, S. *J. Rheol.* **2004,** *48,* 979. doi:10.1122/1.1773781
30. Wei, M.; Shin, I. D.; Urban, B.; Tonelli, A. E. *J. Polym. Sci., Part B: Polym. Phys.* **2004,** *42,* 1369. doi:10.1002/polb.20018
31. Rusa, C. C.; Shuai, X.; Bullions, T. A.; Wei, M.; Porbeni, F. E.; Lu, J.; Huang, L.; Fox, J.; Tonelli, A. E. *J. Polym. Environ.* **2004,** *12,* 157. doi:10.1023/B:JOOE.0000038547.36750.78
32. Uyar, T.; Rusa, M.; Tonelli, A. E. *Makromol. Rapid Commun.* **2004,** *25,* 1382. doi:10.1002/marc.200400165
33. Rusa, C. C.; Wei, M.; Bullions, T. A.; Rusa, M.; Gomez, M. A.; Porbeni, F. E.; Wang, X.; Shin, I. D.; Balik, C. M.; White, J. L.; Tonelli, A. E. *Cryst. Growth Des.* **2004,** *4,* 1431. doi:10.1021/cg049821w
34. Rusa, C. C.; Wei, M.; Shuai, X.; Bullions, T. A.; Wang, X.; Rusa, M.; Uyar, T.; Tonelli, A. E. *J. Polym. Sci., Part B: Polym. Phys.* **2004,** *42,* 4207. doi:10.1002/polb.20272
35. Rusa, M.; Aboelfotoh, O.; Kolbas, R. M.; Tonelli, A. E. *PMSE Prepr.* **2004,** *90,* 620.
36. Rusa, M.; Wang, X.; Tonelli, A. E. *Macromolecules* **2004,** *37,* 6898. doi:10.1021/ma040081+
37. Rusa, C. C.; Wei, M.; Bullions, T. A.; Shuai, X.; Uyar, T.; Tonelli, A. E. *Polym. Adv. Technol.* **2005,** *16,* 269. doi:10.1002/pat.566
38. Rusa, C. C.; Rusa, M.; Gomez, M.; Shin, I. D.; Fox, J. D.; Tonelli, A. E. *Macromolecules* **2004,** *37,* 7992. doi:10.1021/ma0489164
39. Hernández, R.; Rusa, M.; Rusa, C. C.; López, D.; Mijangos, C.; Tonelli, A. E. *Macromolecules* **2004,** *37,* 9620. doi:10.1021/ma048375i
40. Jia, X.; Wang, X.; Tonelli, A. E.; White, J. L. *Macromolecules* **2005,** *38,* 2775. doi:10.1021/ma047838h
41. Uyar, T.; Rusa, C. C.; Wang, X.; Rusa, M.; Hacaloglu, J.; Tonelli, A. E. *J. Polym. Sci., Part B: Polym. Phys.* **2005,** *43,* 2578. doi:10.1002/polb.20546
42. Rusa, C. C.; Bridges, C.; Ha, S.-W.; Tonelli, A. E. *Macromolecules* **2005,** *38,* 5640. doi:10.1021/ma050340a
43. Uyar, T.; Rusa, C. C.; Hunt, M. A.; Aslan, E.; Hacaloglu, J.; Tonelli, A. E. *Polymer* **2005,** *46,* 4762. doi:10.1016/j.polymer.2005.04.002
44. Uyar, T.; Aslan, E.; Tonelli, A. E.; Hacaloglu, J. *Polym. Degrad. Stab.* **2006,** *91,* 1. doi:10.1016/j.polymdegradstab.2005.05.002
45. Uyar, T.; Hunt, M. A.; Gracz, H. S.; Tonelli, A. E. *Cryst. Growth Des.* **2006,** *6,* 1113. doi:10.1021/cg050500+
46. Uyar, T.; Oguz, G.; Tonelli, A. E.; Hacaloglu, J. *Polym. Degrad. Stab.* **2006,** *91,* 2471. doi:10.1016/j.polymdegradstab.2006.03.006
47. Rusa, C. C.; Rusa, M.; Peet, J.; Uyar, T.; Fox, J.; Hunt, M. A.; Wang, X.; Balik, C. M.; Tonelli, A. E. *J. Inclusion Phenom. Macrocyclic Chem.* **2006,** *55,* 185. doi:10.1007/s10847-005-9038-1
48. Pang, K.; Schmidt, B.; Kotek, R.; Tonelli, A. E. *J. Appl. Polym. Sci.* **2006,** *102,* 6049. doi:10.1002/app.25217
49. Uyar, T.; Gracz, H. S.; Rusa, M.; Shin, I. D.; El-Shafei, A.; Tonelli, A. E. *Polymer* **2006,** *47,* 6948. doi:10.1016/j.polymer.2006.07.054
50. Uyar, T.; Tonelli, A. E.; Hacaloğlu, J. *Polym. Degrad. Stab.* **2006,** *91,* 2960. doi:10.1016/j.polymdegradstab.2006.08.028
51. Tonelli, A. E. In *Nanofibers and Nanotechnology in Textiles;* Brown, P.; Stevens, K., Eds.; Woodhead Publ. Ltd.: Cambridge, UK, 2007.
52. Vedula, J.; Tonelli, A. E. *J. Polym. Sci., Part B: Polym. Phys.* **2007,** *45,* 735. doi:10.1002/polb.21098
53. Uyar, T.; Rusa, C. C.; Tonelli, A. E.; Hacaloğlu, J. *Polym. Degrad. Stab.* **2007,** *92,* 32. doi:10.1016/j.polymdegradstab.2006.10.002
54. Martínez, G.; Gómez, M. A.; Villar-Rodil, S.; Garrido, L.; Tonelli, A. E.; Balik, C. M. *J. Polym. Sci., Part A: Polym. Chem.* **2007,** *45,* 2503. doi:10.1002/pola.22014
55. Tonelli, A. E. *J. Inclusion Phenom. Macrocyclic Chem.* **2008,** *60,* 197. doi:10.1007/s10847-007-9372-6
56. Tonelli, A. E. *Polymer* **2008,** *49,* 1725. doi:10.1016/j.polymer.2007.12.003
57. Tonelli, A. E. *J. Polym. Sci., Part B: Polym. Phys.* **2009,** *47,* 1543. doi:10.1002/polb.21753
58. Mohan, A.; Joyner, X.; Kotek, R.; Tonelli, A. E. *Macromolecules* **2009,** *42,* 8983. doi:10.1021/ma901599c
59. Busche, B. J.; Tonelli, A. E.; Balik, C. M. *Polymer* **2010,** *51,* 454. doi:10.1016/j.polymer.2009.11.069
60. Busche, B. J.; Tonelli, A. E.; Balik, C. M. *Polymer* **2010,** *51,* 1465. doi:10.1016/j.polymer.2010.01.019
61. Busche, B. J.; Tonelli, A. E.; Balik, C. M. *Polymer* **2010,** *51,* 6013. doi:10.1016/j.polymer.2010.10.024
62. Mohan, A.; Gurarslan, A.; Joyner, X.; Child, R.; Tonelli, A. E. *Polymer* **2011,** *52,* 1055. doi:10.1016/j.polymer.2010.12.049
63. Williamson, B. R.; Tonelli, A. E. *J. Inclusion Phenom. Macrocyclic Chem.* **2012,** *72,* 71. doi:10.1007/s10847-011-9940-7
64. Gurarslan, A.; Tonelli, A. E. *Macromolecules* **2011,** *44,* 3856. doi:10.1021/ma200530w
65. Williamson, B. R.; Krishnaswany, R.; Tonelli, A. E. *Polymer* **2011,** *52,* 4517. doi:10.1016/j.polymer.2011.07.043
66. Peet, J.; Rusa, C. C.; Hunt, M. A.; Tonelli, A. E.; Balik, C. M. *Macromolecules* **2005,** *38,* 537. doi:10.1021/ma048103f
67. Rusa, C. C.; Fox, J.; Tonelli, A. E. *Macromolecules* **2003,** *36,* 2742. doi:10.1021/ma021755o
68. Gurarslan, A.; Shen, J.; Tonelli, A. E. *Macromolecules* **2012,** *45,* 2835. doi:10.1021/ma300270g
69. Joijode, A. S.; Hawkins, K.; Tonelli, A. E. *Polymer* **2012,** *54,* in press.
70. Williamson, B. R. Ph.D. Thesis, North Carolina State University, 2010.

71. The densities of asr- and c-PVAc samples were measured as described in [65] by floatation using water and aq NaBr (21 wt %) (densities of 1.0 and 1.184 g/cm^3, respectively, lower and higher than that of PVAc). Into a known volume of water, vol(H_2O), containing a magnetic stirring bar, were placed small pieces of both PVAc films pressed at 70 °C, which sank to the bottom. The NaBr/H_2O solution was slowly added from a burette, under stirring, until each PVAc film in turn rose from the bottom and was suspended in the aq solution, and the volume of added NaBr/H_2O, vol(NaBr/H_2O), was noted. The densities of asr- and c-PVAc films were then obtained as
$$\rho = \frac{[\text{vol}[H_2O) \times \rho(H_2O) + \text{vol}(\text{NaBr}/H_2O) \times \rho(\text{NaBr}/H_2O)]}{\text{vol}(H_2O) + \text{vol}(\text{NaBr}/H_2O)}$$
both below and above their glass-transition temperatures.
72. Joijode, A. S.; Gurarslan, A.; Tonelli, A. E. *Macromolecules* **2012,** *45,* in press.
73. Lu, J.; Mirau, P. A.; Tonelli, A. E. *Prog. Polym. Sci.* **2002,** *27,* 357. doi:10.1016/S0079-6700(01)00045-4
74. Gurarslan, A.; Joijode, A. S.; Tonelli, A. E. *J. Polym. Sci., Part B: Polym. Phys.* **2012,** *50,* 813. doi:10.1002/polb.23074
75. Beers, D. E.; Ramirez, J. E. *J. Text. Inst.* **1990,** *81,* 561.
76. Tonelli, A. E. *Comput. Theor. Polym. Sci.* **1992,** *2,* 80.
77. Williams, A. D.; Flory, P. J. *J. Polym. Sci., Part A-2* **1967,** *5,* 417.
78. Kaji, H.; Schmidt-Rohr, K. *Macromolecules* **2002,** *35,* 7993. doi:10.1021/ma020246j

License and Terms

Beilstein Journal of Organic Chemistry

Impact of cyclodextrins on the behavior of amphiphilic ligands in aqueous organometallic catalysis

Hervé Bricout[1], Estelle Léonard[2], Christophe Len[2], David Landy[3], Frédéric Hapiot[*1] and Eric Monflier[*1]

Full Research Paper

Open Access

Address:
[1]Université Lille Nord de France, CNRS UMR 8181, Unité de Catalyse et de Chimie du Solide - UCCS, UArtois, Faculté des Sciences Jean Perrin, SP18, 62307 Lens Cedex, France, [2]Université de Technologie de Compiègne, Transformation Intégrée de la Matière Renouvelable, EA 4297 UTC/ESCOM Centre de recherches de Royallieu, BP 20529, F-60205 Compiègne Cedex, France and [3]Université Lille Nord de France, UCEIV, ULCO, 145, Avenue Maurice Schumann, MREI 1, F-59140 Dunkerque, France

Email:
Frédéric Hapiot[*] - frederic.hapiot@univ-artois.fr; Eric Monflier[*] - eric.monflier@univ-artois.fr

* Corresponding author

Keywords:
amphiphilic phosphanes; biphasic system; cyclodextrins; micelles

Beilstein J. Org. Chem. **2012,** *8,* 1479–1484.
doi:10.3762/bjoc.8.167

Received: 05 June 2012
Accepted: 08 August 2012
Published: 06 September 2012

This article is part of the Thematic Series "Superstructures with cyclodextrins: Chemistry and applications".

Guest Editor: H. Ritter

Abstract

In this study, we showed that the addition of randomly modified β-cyclodextrin (RAME-β-CD) in aqueous medium could have a beneficial impact on the catalytic performances of phosphane-based aggregates in the Pd-catalyzed cleavage of allyl carbonates (Tsuji–Trost reaction). The RAME-β-CD/phosphane supramolecular interactions helped explain the catalytic results. The presence of RAME-β-CD in the aqueous compartment improved the phosphane-based aggregate dynamics. The exchanges between the hydrophobic substrate-containing aggregate core and the catalyst-containing aqueous phase were then greatly favored, resulting in an increase in the catalytic performances.

Introduction

Facing the need of developing a greener chemistry, chemists have recently focused their investigations on clean transformation processes to convert organic molecules into products. Traditional solvents have especially been incriminated due to the pollution problems they raise. Thus, in the context of increased awareness about environmental safety, nonconventional media appeared to be a promising alternative to toxic solvents. The use of supercritical fluids, ionic liquids and water especially appeared to be an effective solution to limit the environmental impact of chemical reactions [1-3]. Although these media all display eco-friendly characteristics such as non-flammability and chemical stability, water has an additional advan-

tage of being cheap, nontoxic and available in large amounts. As an example, the concept of aqueous-phase organometallic catalysis implemented by E. Kuntz in the 70s clearly illustrates the potential of water as a reaction medium [4,5]. However, while hydrophilic substrates can be readily converted in water, the conversion of hydrophobic substrates constitutes a real challenge not completely solved so far. Recently, we showed that an association of cyclodextrins (CDs) and amphiphilic phosphanes could significantly improve the catalytic performances in an aqueous rhodium-catalyzed hydroformylation of higher olefins [6]. Herein we clearly demonstrate that the beneficial effect of CDs on a catalytic micellar system can be generalized to another reaction and other amphiphilic phosphanes. To this end, we undertook a study using the randomly methylated β-cyclodextrin (RAME-β-CD) as an additive in an aqueous Pd-catalyzed cleavage reaction of allyl carbonates (Tsuji–Trost reaction) and four amphiphilic phosphanes as aggregate-building blocks. The RAME-β-CD/phosphane interaction and its consequence on the catalytic results are discussed.

Results and Discussion

To expand the scope of the CD/amphiphilic phosphane combination in aqueous-phase organometallic catalysis, four amphiphilic phosphanes **1**–**4** (Figure 1) were considered [6-8].

These phosphanes have been chosen for the information they could give under catalytic conditions by considering their structures and their amphiphilic properties. In this study, each phosphane has been proven to supramolecularly interact with β-CDs. For example, addition of a stoichiometric amount of RAME-β-CD on aqueous solutions of water-soluble phosphanes **1**–**4** led to the formation of phosphane⊂RAME-β-CD supramolecular complexes. The stoichiometry and association constant K_{ass} of these complexes were measured by isothermal titration calorimetry (ITC), at a suitable RAME-β-CD/phosphane concentration ratio ensuring the absence of micelles during the whole experiment. Under these conditions, the values reflect the interaction between a single CD with a single phosphane only. A 1/1 stoichiometry was found whatever the phosphane, according to the fit between theoretical and experimental heats. The K_{ass} values were very dependent upon the phosphane structure. The K_{ass} values measured for **1** and **2** (300 and 590 M^{-1}, respectively) were three orders of magnitude lower than those measured for **3** and **4** (326 000 and 210 000 M^{-1}, respectively) indicative of the deleterious role played by the diazo function on the inclusion phenomenon. In fact, two distinct parameters could be implicated to explain the low K_{ass} values observed for **1** and **2**. First, the hydrophilic diazo function had less affinity for the hydrophobic CD cavity than the biphenyl moiety. Additionally, the phosphane nonlinear geometry resulting from the zig-zag diazo structure also disfavored the recognition process between the phosphane and the CD cavity.

The existence of phosphane⊂CD supramolecular complexes was confirmed by using a 2D NMR T-ROESY sequence sensitive to dipolar contacts between the CD host and the phosphane guest. Correlations were detected on T-ROESY spectra of stoichiometric mixtures of RAME-β-CD and phosphanes **1**–**4**. However, a clear assignment of the CD and phosphane protons could not be properly made due to a severe broadening of the NMR signals (ESI). Accordingly, the native β-CD was chosen as host by default. The CD protons could then be assigned as illustrated in Figure 2 for the **4**⊂β-CD supramolecular complex.

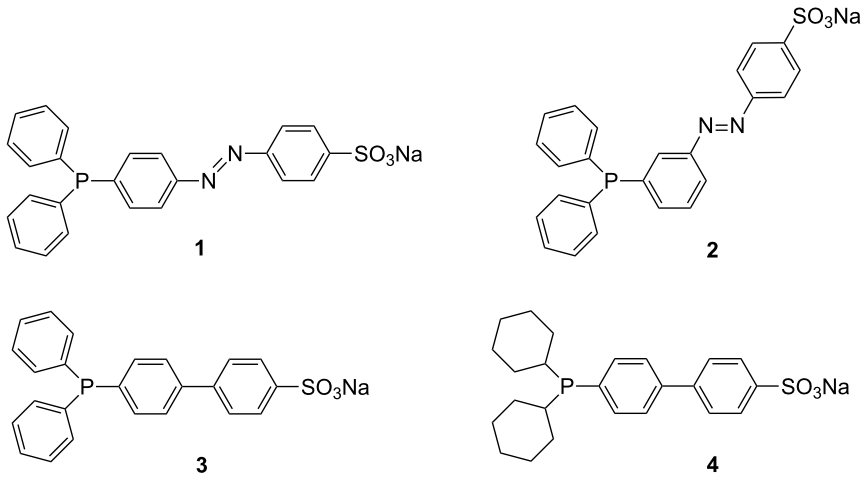

Figure 1: Water-soluble phosphanes **1**–**4**.

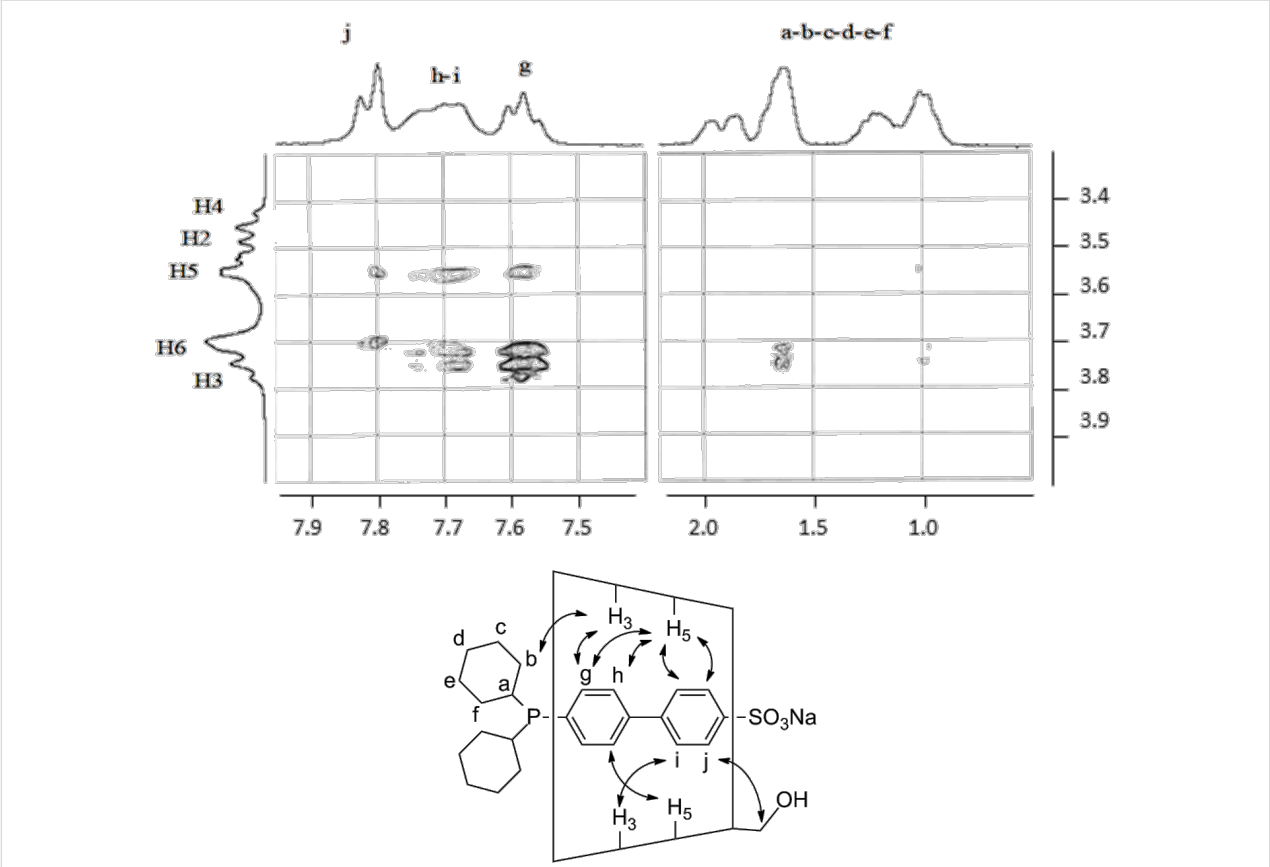

Figure 2: 2D T-ROESY NMR spectrum of a stoichiometric mixture of β-CD and **4** (3 mM each) in D_2O at 20 °C.

Cross peaks were detected between the inner CD protons H-3/H-5 and the phosphane aromatic protons. A correlation was also detected between some of the cyclohexyl protons and H-3 suggesting a deep phosphane inclusion into the CD cavity. For the other phosphanes, mixtures of supramolecular complexes could be detected because of the additional inclusion of the phosphorus-bound phenyl groups into the CD cavities (ESI). It should be noted that the signal broadening observed for phosphane protons suggested the presence of aggregates in the medium. Thus, though a 1/1 CD/phosphane mixture was used, phosphane-based aggregates and native β-CD/phosphane complexes coexisted in water in this concentration range [9]. In fact, the mixture of CD/phosphane complexes and aggregates was a consequence of the competitive equilibria of CD/phosphane complexation and phosphane self-assembly to form micelles.

The surface activity of the four studied phosphanes has already been the subject of investigations [7,8]. Phosphanes **1**–**4** proved to be very surface active as expected from their amphiphilic structure (ESI). However, we show in this study that the addition of increasing amounts of native β-CD or RAME-β-CD in phosphane-containing solutions produced a significant rise of the surface tension (Figure 3). This phenomenon was interpreted in terms of CD/amphiphilic phosphane interaction leading, for high CD concentrations, to an aggregate-destruc-

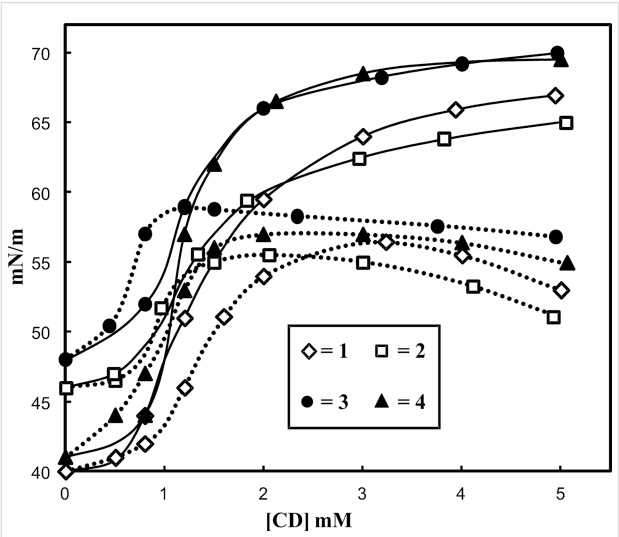

Figure 3: Effect of increasing concentrations of β-CD (solid lines) and RAME-β-CD (dotted lines) on the surface tension of 1 mM aqueous solutions of phosphanes **1**–**4** (20 °C).

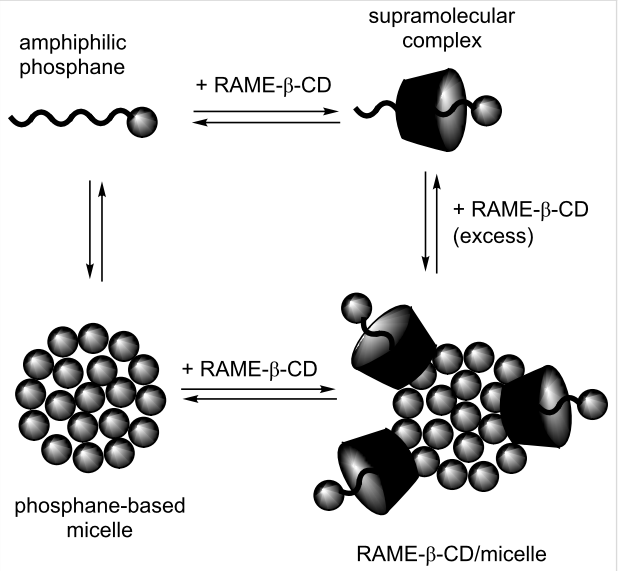

Figure 4: Equilibria in a phosphane-based micelle/RAME-β-CD mixture.

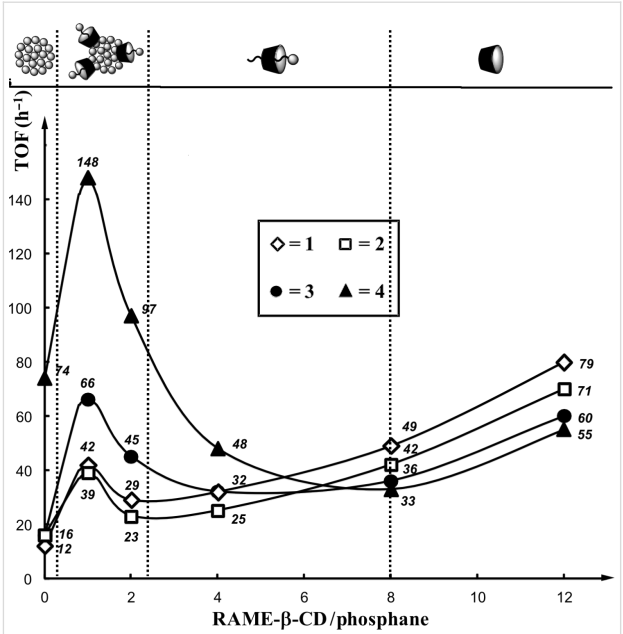

Figure 5: Turnover frequency (TOF) as a function of the RAME-β-CD/phosphane ratio in the Pd-catalyzed cleavage of allyl undecyl carbonate. Reaction conditions: $Pd(OAc)_2$ = 2.23 μmol, phosphane = 20.1 μmol, RAME-β-CD = 0–241 μmol, H_2O = 2 g, allyl undecyl carbonate = 223 μmol, diethylamine = 446 μmol, dodecane = 110 μmol, heptane = 2 g, 1250 rpm, room temperature. The TOF was defined as the number of moles of allyl undecyl carbonate converted per mole of palladium and per hour in the early stage of the reaction (20–40% of conversion).

turing process. Indeed, in the post-micellar region, increasing the CD amount resulted in a displacement of the equilibria towards the CD/phosphane complex. The aggregates were then partially or totally destroyed depending on the CD concentration. Mixtures of modified and unaltered phosphane-based aggregates probably coexisted in water (Figure 4). The above results corroborate previous studies on CD/amphiphilic phosphane interactions [9-13].

The catalytic performances of the CD/amphiphilic phosphane combination have been evaluated in the aqueous Pd-catalyzed cleavage reaction of allyl undecyl carbonate (Scheme 1).

The reactions were performed at room temperature under nitrogen by using palladium acetate as a catalyst precursor, phosphanes **1**–**4** as hydrosoluble ligands, and diethylamine as an allyl scavenger. RAME-β-CD was chosen as an additive because of its ability to adsorb at the aqueous/organic interface [14-17]. The RAME-β-CD/phosphane ratio was varied to evaluate the impact of the CD concentration on the catalytic micellar system. The catalytic results have been translated in terms of turnover frequency (TOF) to RAME-β-CD/phosphane ratio, thus highlighting the role of RAME-β-CD on the catalytic performances of the phosphane-based aggregates (Figure 5).

Nonlinear curves were obtained indicative of different processes depending on the CD concentration. The highest TOFs were measured for a RAME-β-CD/phosphane ratio of 1:1, while a huge drop in TOF was observed for a RAME-β-CD/phosphane ratio of 2:1. Conversely, high RAME-β-CD/phosphane ratios yielded an increase in TOF. The results could be interpreted as follows. First, for a RAME-β-CD/phosphane ratio of around 1:1, the micelle structure was slightly altered because of the interaction of RAME-β-CD with the micelle constituents, especially the inclusion process (Figure 4).

As the micelle dynamics was improved, the exchanges between the hydrophobic substrate-containing micelle core and the catalyst-containing aqueous solution were then greatly favored, thus leading to an increase in TOF. In that case, the substrate concentration within the core of the phosphane-based aggregates remained high. Note that the beneficial effect of RAME-

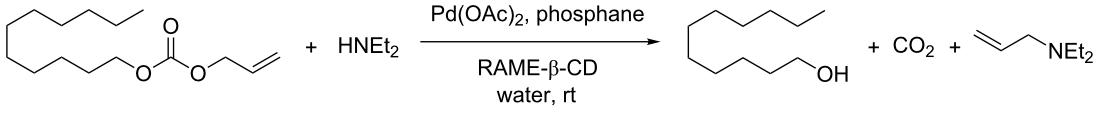

Scheme 1: Tsuji–Trost reaction mediated by a phosphane-based micelle/RAME-β-CD combination.

β-CD on the aggregates was observed in a well-defined concentration range for each phosphane. The concentration range was narrow for aggregates constituted by diazo phosphanes **1** or **2** and rather broad for aggregates constituted by **3** or **4**. Second, above a stoichiometric RAME-β-CD/phosphane ratio, the RAME-β-CD impact on aggregates became deleterious to the point that the aggregates were destroyed. Most of the RAME-β-CD cavities were then filled with phosphanes and the equilibria were greatly displaced towards the RAME-β-CD/phosphane complex. In that case, neither the amphiphilic phosphanes nor RAME-β-CD could favor the substrate–catalyst binding anymore. On the contrary, their interaction was counterproductive as both components annihilated their interfacial properties. The observed TOFs measured in this concentration range probably resulted from the intrinsic catalyst activity. Finally, the TOF variations observed for very high RAME-β-CD/phosphane ratios could be easily rationalized considering the ability of RAME-β-CD to supramolecularly recognize not only the phosphane but also the substrate. When mixed in excess with amphiphilic phosphanes, a proportion of the RAME-β-CD included phosphanes in their cavities, but the majority of RAME-β-CD interacted with allyl carbonates and acted as mass transfer promoters between the substrate-containing organic phase and the aqueous component [10-13].

It should be noted that the above catalytic performances were mainly related to the K_{ass} values. Indeed, the spread between the highest and the lowest TOF was larger for phosphanes **3** and **4** for which K_{ass} values over 200 000 M^{-1} were measured. With the RAME-β-CD/interaction being strong, the aggregate dynamics was greatly favored at a CD/phosphane ratio of around 1:1 (high TOF). In that case, the intensity of the aggregate destructuring process was stronger at a higher CD/phosphane ratio (low TOF) as a result of the formation of stable RAME-β-CD/phosphane complexes. Conversely, because of the low K_{ass} values measured for phosphanes **1** and **2**, the amplitude between the highest and the lowest TOF was moderate, illustrative of the weak interaction between both components. However, for stoichiometric RAME-β-CD/phosphane mixtures (10 mM each, catalytic conditions), the percentages of RAME-β-CD/phosphane complexes were calculated to be 56.6, 66.4, 98.3 and 97.8% for phosphanes **1**, **2**, **3** and **4**, respectively. Thus, even for phosphanes **1** and **2** whose K_{ass} were low, a significant amount of RAME-β-CD/phosphane complexes were present in the aqueous medium and significantly contribute to the beneficial effect observed for stoichiometric RAME-β-CD/phosphane mixtures.

Accordingly, in this study we showed that RAME-β-CD could positively interact with phosphane-containing aggregates in a very narrow concentration range to improve the exchanges between the hydrophobic aggregate core and the aqueous catalyst-containing solution. The result is in line with the conclusions previously drawn by using other modified β-CDs as additives [6]. The beneficial effect of the CD/amphiphilic phosphane interaction thus appeared generalizable to other phosphanes and other reactions and to reinforce the view of a synergetic relationship between both components.

Conclusion

In our constant effort to elaborate an effective catalytic system aiming at converting hydrophobic substrates in water, the CD/amphiphilic phosphane combination proved to be a versatile solution provided that the ratio between both components had been carefully defined. The CD positively affects the phosphane-constituted aggregate structure by supramolecular means to the point that the substrate–catalyst binding becomes favorable. Given the above catalytic results, we are currently widening the scope of the CD/amphiphilic phosphane interaction in other aqueous-phase organometallic reactions.

Supporting Information

Supporting Information File 1

Experimental procedures and characterization of the supramolecular complexes.
[http://www.beilstein-journals.org/bjoc/content/supplementary/1860-5397-8-167-S1.pdf]

Acknowledgements

Roquette Frères (Lestrem, France) is gratefully acknowledged for the generous donation of cyclodextrins.

References

1. Adams, D. J.; Dyson, P. J.; Tavener, S. J. *Chemistry in Alternative Reaction Media;* John Wiley & Sons: Chichester, U.K., 2004. doi:10.1002/0470869666
2. Kerton, F. M. *Alternative Solvents for Green Chemistry;* Royal Society of Chemistry: Cambridge, U.K., 2009. doi:10.1039/9781847559524
3. Mohammed, A.; Inamuddin, Eds. *Green Solvents – Properties and Applications in Chemistry;* Springer: Dordrecht, 2012. doi:10.1007/978-94-007-1712-1
4. Kuntz, E. G. *CHEMTECH* **1987,** 570–575.
5. Shaughnessy, K. H. *Chem. Rev.* **2009,** *109,* 643–710. doi:10.1021/cr800403r
6. Ferreira, M.; Bricout, H.; Azaroual, N.; Landy, D.; Tilloy, S.; Hapiot, F.; Monflier, E. *Adv. Synth. Catal.* **2012,** *354,* 1337–1346. doi:10.1002/adsc.201100837
7. Bricout, H.; Banaszak, E.; Len, C.; Hapiot, F.; Monflier, E. *Chem. Commun.* **2010,** *46,* 7813–7815. doi:10.1039/c0cc02458a
8. Ferreira, M.; Bricout, H.; Azaroual, N.; Gaillard, C.; Landy, D.; Tilloy, S.; Monflier, E. *Adv. Synth. Catal.* **2010,** *352,* 1193–1203. doi:10.1002/adsc.201000014

9. Cepeda, M.; Daviña, R.; García-Río, L.; Parajó, M. *Chem. Phys. Lett.* **2010,** *499,* 70–74. doi:10.1016/j.cplett.2010.09.017
10. De Lisi, R.; Milioto, S.; Muratore, N. *J. Phys. Chem. B* **2002,** *106,* 8944–8953. doi:10.1021/jp013648m
11. De Lisi, R.; Lazzara, G.; Milioto, S.; Muratore, N. *J. Phys. Chem. B* **2003,** *107,* 13150–13157. doi:10.1021/jp034105a
12. De Lisi, R.; Lazzara, G.; Milioto, S.; Muratore, N.; Terekhova, I. V. *Langmuir* **2003,** *19,* 7188–7195. doi:10.1021/la0342316
13. García-Río, L.; Méndez, M.; Paleo, M. R.; Sardina, F. J. *J. Phys. Chem. B* **2007,** *111,* 12756–12764. doi:10.1021/jp073510p
14. Bricout, H.; Hapiot, F.; Ponchel, A.; Tilloy, S.; Monflier, E. *Curr. Org. Chem.* **2010,** *14,* 1296–1307. doi:10.2174/138527210791616920
15. Hapiot, F.; Ponchel, A.; Tilloy, S.; Monflier, E. *C. R. Chim.* **2011,** *14,* 149–166. doi:10.1016/j.crci.2010.04.003
16. Six, N.; Guerriero, A.; Landy, D.; Peruzzini, M.; Gonsalvi, L.; Hapiot, F.; Monflier, E. *Catal. Sci. Technol.* **2011,** *1,* 1347–1353. doi:10.1039/c1cy00156f
17. Hapiot, F.; Leclercq, L.; Azaroual, N.; Fourmentin, S.; Tilloy, S.; Monflier, E. *Curr. Org. Synth.* **2008,** *5,* 162–172. doi:10.2174/157017908784221585

License and Terms

Beilstein Journal of Organic Chemistry

Synthesis and characterization of low-molecular-weight π-conjugated polymers covered by persilylated β-cyclodextrin

Aurica Farcas*, Ana-Maria Resmerita, Andreea Stefanache, Mihaela Balan and Valeria Harabagiu

Full Research Paper

Open Access

Address:
Inorganic Polymers, "Petru Poni" Institute of Macromolecular Chemistry, Grigore Ghica Voda Alley, 700487-Iasi, Romania

Email:
Aurica Farcas* - afarcas@icmpp.ro

* Corresponding author

Keywords:
alternating fluorene-bithiophene copolymer; cyclodextrins; interlocked molecules; macrocycles; persilylated β-cyclodextrin; polyrotaxanes

Beilstein J. Org. Chem. **2012,** *8,* 1505–1514.
doi:10.3762/bjoc.8.170

Received: 30 May 2012
Accepted: 13 August 2012
Published: 11 September 2012

This article is part of the Thematic Series "Superstructures with cyclodextrins: Chemistry and applications".

Guest Editor: H. Ritter

Abstract

The paper reports the preparation of a poly[2,7-(9,9-dioctylfluorene)-*alt*-5,5'-bithiophene/PS-βCD] (**PDOF-BTc**) polyrotaxane copolymer, through a Suzuki coupling reaction between the 5,5'-dibromo-2,2'-bithiophene (**BT**) inclusion complex with persilylated β-cyclodextrin (PS-βCD), and 9,9-dioctylfluorene-2,7-bis(trimethylene borate) (**DOF**) as the blocking group. The chemical structure and the thermal and morphological properties of the resulting polyrotaxane were investigated by using NMR and FT-IR spectroscopy, TGA, DSC and AFM analysis. The encapsulation of **BT** inside the PS-βCD cavity results in improvements in the solubility, as well as in different surface morphology and thermal properties of the **PDOF-BTc** rotaxane copolymer compared to its noncomplexed **PDOF-BT** homologue. In contrast, the number-average molecular weight (M_n) of **PDOF-BTc** rotaxane copolymer indicated lower values suggesting that the condensation reaction is subjected to steric effects of the bulkier silylated groups, affecting the ability of the diborate groups from the **DOF** molecule to partially penetrate the PS-βCD cavity.

Introduction

Organic materials with extended π-conjugation have attracted considerable attention in recent years as a new class of active organic materials for optoelectronic applications [1-4]. Among the conjugated polymers, a number of poly(9-alkylfluorene)s (**PF**s) and poly(9,9-dioctylfluorene) (**PDOF**) polymers in particular have been the focus of much research as encouraging candidates for organic light-emitting diodes (OLEDs) due to their pure blue luminescence and high efficiency [5-10]. The application of **PF**s and **PDOF** conjugated polymers is limited by unwanted side effects, such as aggregation and a wide emission band during operation [8]. Taking into account the relevant photophysical properties of these organic compounds, new synthetic approaches were developed. Copolymerization of fluorene with thiophene, bithiophene or other aromatic

comonomers is an alternative method for tuning the optical, electronic and thermal properties [11-18]. However, as a consequence of intramolecular interactions, these synthetic methods are often accompanied by undesirable side effects influencing the optoelectronic properties, e.g., red shifting or lower fluorescence.

As a route to candidate materials for use in molecular devices, the construction of mechanically interlocked molecules, such as rotaxanes and polyrotaxanes, has attracted considerable attention [19-23]. A rotaxane assembly comprises a macrocyclic component (host) encircling an axle (guest) through noncovalent interactions; bulky groups (also known as stoppers) are attached at the ends of the axle to prevent dethreading of the host.

In the past few years many authors have demonstrated that the encapsulation of conjugated polymers into macrocycle cavities plays an important role in the construction of diverse polymeric architectures. Moreover, the fabrication of mechanically interlocked molecules, such as polyrotaxanes, has been investigated as a method for the further improvement of thermal and electro-optical properties through the insulating backbones of conjugated polymers [20-24]. The studies revealed an attractive approach to achieve a higher degree of control over molecular rigidity, prevention of aggregation, fluorescence efficiency, improved solubility, and surface-morphological properties of the resulting conjugated polyrotaxanes [5,11,21,23,25-31].

Among the several known host molecules, e.g., crown ethers [32], cyclodextrins (CDs) have been employed for the synthesis of polyrotaxanes with π-conjugated polymers. As a result, many CD-based rotaxanes and polyrotaxanes have been reported until now [5,11,12,19-31]. In spite of the extended use of new compounds as hosts for inclusion-complex formation, CD derivatives have received less attention when compared to native CDs. Very few polyrotaxanes within CD derivatives were reported [12,33,34]. Recently, we have exemplified such improvements on the photophysical properties of **PF**s by using persilylated γ-CD as a new host molecule [33]. Inclusion of bithiophene into persilylated β-cyclodextrin, randomly methylated β-cyclodextrin, or chemically modified CD derivatives, followed by copolymerization with fluorene monomers results in significant changes in the thermal as well as photophysical stability, and the ability to form good films [12,34].

Herein, we report the preparation and characterization of a main-chain polyrotaxane with alternating fluorene–bithiophene moieties covered by persilylated β-cyclodextrin (PS-βCD). Thus, poly[2,7-(9,9-dioctylfluorene)-*alt*-5,5'-bithiophene/PS-βCD] (**PDOF-BTc**), was synthesized by Suzuki cross-coupling reaction between 5,5'-dibromo-2,2'-bithiophene (**BT**), as an inclusion complex in PS-βCD cavities, and the bulky molecule 9,9-dioctylfluorene-2,7-bis(trimethylene borate) (**DOF**), (Scheme 1). Of particular interest is the ability of cross-coupling reaction of **BT** and **DOF** to proceed close to the cavity surface of PS-βCD, which will provide a deeper insight into the use of these new host molecules (more soluble in nonpolar organic solvents) for the construction of mechanically interlocked molecules with conjugated polymers.

Results and Discussion

The paper describes the preparation of poly[2,7-(9,9-dioctylfluorene)-*alt*-5,5'-bithiophene/PS-βCD] (**PDOF-BTc**) main-chain polyrotaxane and its noncomplexed **PDOF-BT** counterpart copolymer by Suzuki cross-coupling reaction. The preparation of copolymer polyrotaxane (**PDOF-BTc**) involves a 1:1 5,5'-dibromo-2,2'-bithiophene inclusion complex in PS-βCD (**BTc**) and 9,9-dioctylfluorene-2,7-bis(trimethylene borate) (**DOF**) as a bulky molecule followed by a small excess of **DOF** at the end of polymerization and, finally, 3-bromothiophene (**3T**) as a monofunctional end-capping reagent, as illustrated in Scheme 1. In order to analyse the influence of end-capping reagents on the photophysical properties we changed the termination of the growing chains to **3T** instead of bromobenzene, as in previously reported results [12]. A noncomplexed **PDOF-BT** copolymer was also synthesized by polycondensation reaction between **DOF** and **BT**, and its properties were compared with the rotaxane **PDOF-BTc** copolymer.

The first step in the preparation of **PDOF-BTc** polyrotaxane is the threading of the **BT** monomer through the PS-βCD cavity to form the **BTc** inclusion complex. **BTc** obtained as a precipitate from a 2:1 mol/mol mixture of PS-βCD and **BT** in acetone was isolated, purified and characterized by ^{1}H NMR, as can be seen in Figure 1. The average number of PS-βCD macrocycles per **BT** unit was calculated by using the ratio of the integrated area of the peak assigned to the H from $-CH_3$ groups of PS-βCD (0.09–0.11 ppm, $I_{H\text{-}CH3}$) and the proton peaks of **BT** (6.85–7.97 ppm, I_{BT}), Figure 1. The average number of PS-βCD macrocycles per **BT** unit was calculated as $(I_{BT}/4)/(I_{H\text{-}CH3}/63)$ and found to be 0.95 (i.e., ca. 95% coverage).

Not surprisingly, due to the presence of PS-βCD the rotaxane **PDOF-BTc** copolymer showed a marked contrast compared with **PDOF-BT**. The **PDOF-BTc** rotaxane copolymer was soluble (~10% by weight) in petroleum ether (after vortex stirring at room temperature for 15 minutes). The ^{1}H NMR spectrum of a soluble fraction in petroleum ether indicated a higher coverage with PS-βCD. From this spectrum a PS-βCD/**BT** molar ratio of about 1/1.5 was determined, as can be seen in Figure S1 in the Supporting Information File 1.

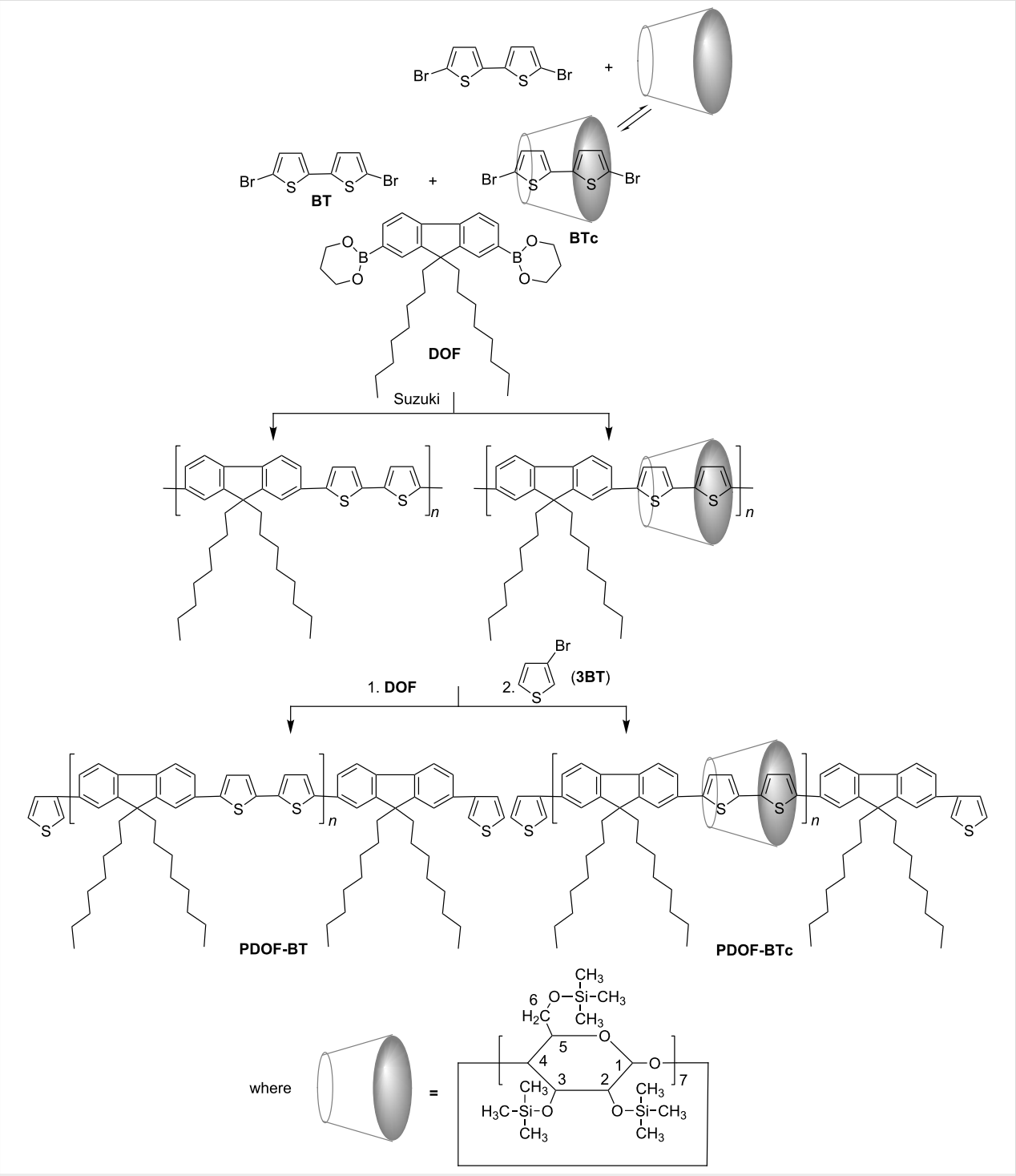

Scheme 1: Synthesis of **PDOF-BT** and **PDOF-BTc** copolymers.

The chemical structure of **PDOF-BTc** (insoluble part in petroleum ether) and **PDOF-BT** copolymers was proved by ^{1}H NMR and FTIR analysis. The infrared spectrum of the **PDOF-BTc** (Figure 2B) shows all the characteristic bands of **PDOF-BT** and additional bands located in the 748–1251 cm^{-1} region. Note that the peaks at 792 and 817 cm^{-1}, assigned to the C–H out-of-plane bending vibrations, and the peak at 880 cm^{-1}, assigned to the C–H in-plane vibrations of the aromatic rings, were at distinctly lower energy in **PDOF-BTc** as compared to the corresponding peaks of the non-rotaxane **PDOF-BT** copolymer.

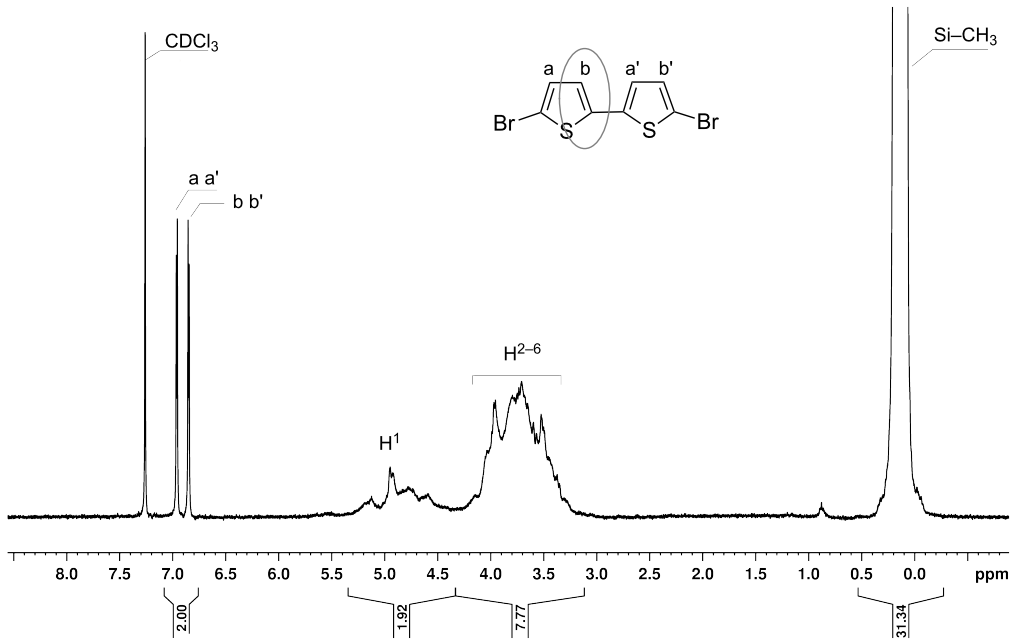

Figure 1: ^{1}H NMR spectrum ($CDCl_3$) of the **BTc** inclusion complex.

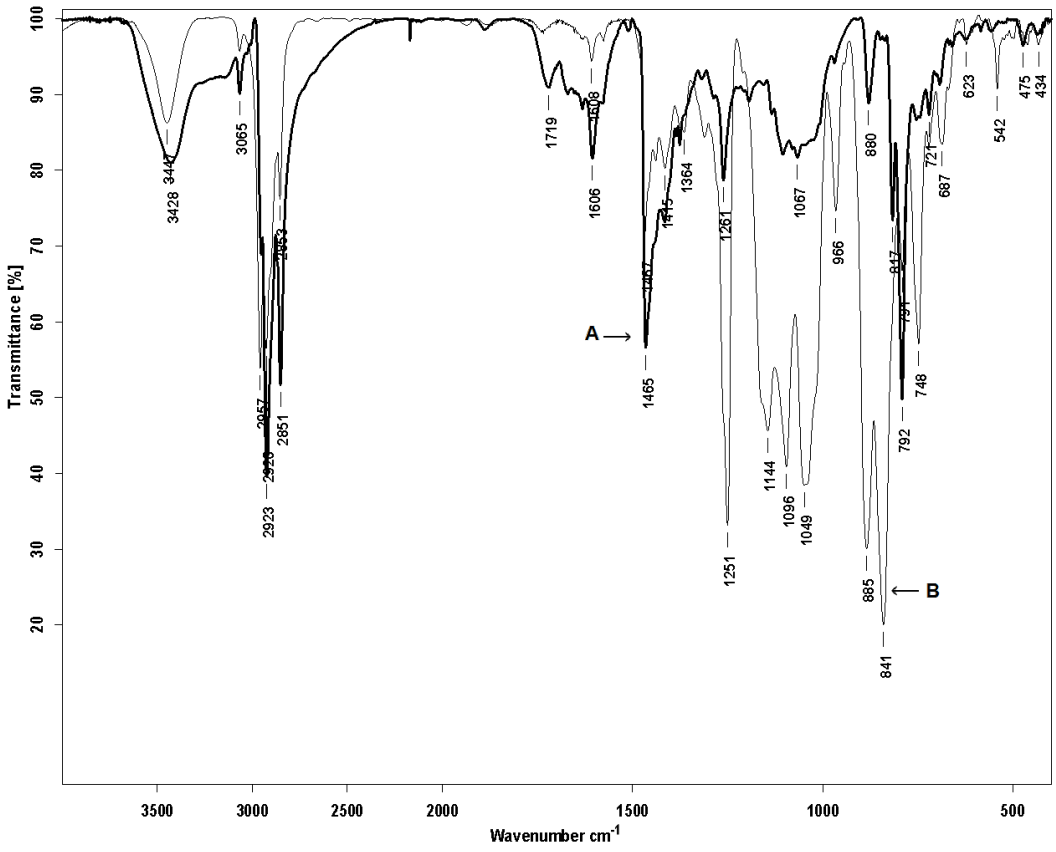

Figure 2: FTIR spectra (KBr pellet) of **PDOF-BT** (A) and **PDOF-BTc** (B) copolymers.

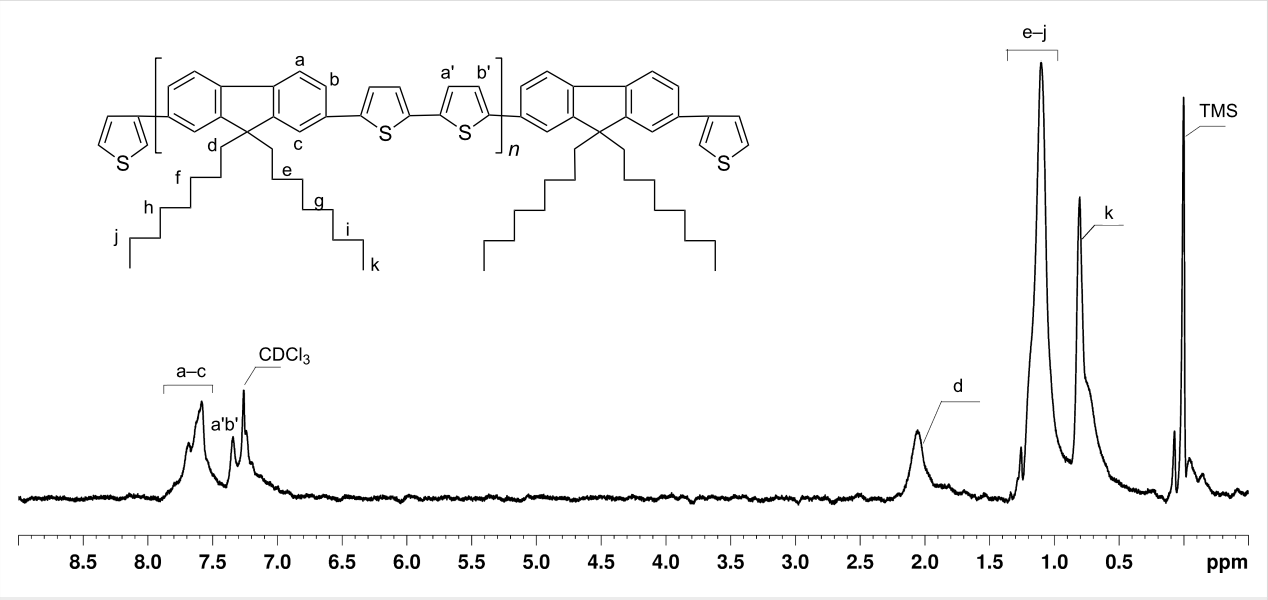

Figure 3: ^{1}H NMR spectrum of **PDOF-BT** copolymer ($CDCl_3$).

^{1}H NMR spectra of **PDOF-BT** and **PDOF-BTc** (insoluble part in petroleum ether) are presented in Figure 3 and Figure 4, respectively. The NMR spectrum of **PDOF-BT** shows characteristic peaks for both **DOF** and **BT** chains in good agreement with the proposed structures.

The coverage of the rotaxane copolymer with the macrocycle, i.e., the average number of PS-βCD macrocycles per repeating unit [23], was determined from the NMR spectral analysis and was calculated from the ratio of the integrated area of the peak assigned to the H from –CH_3 groups of PS-βCD (0.121–0.249

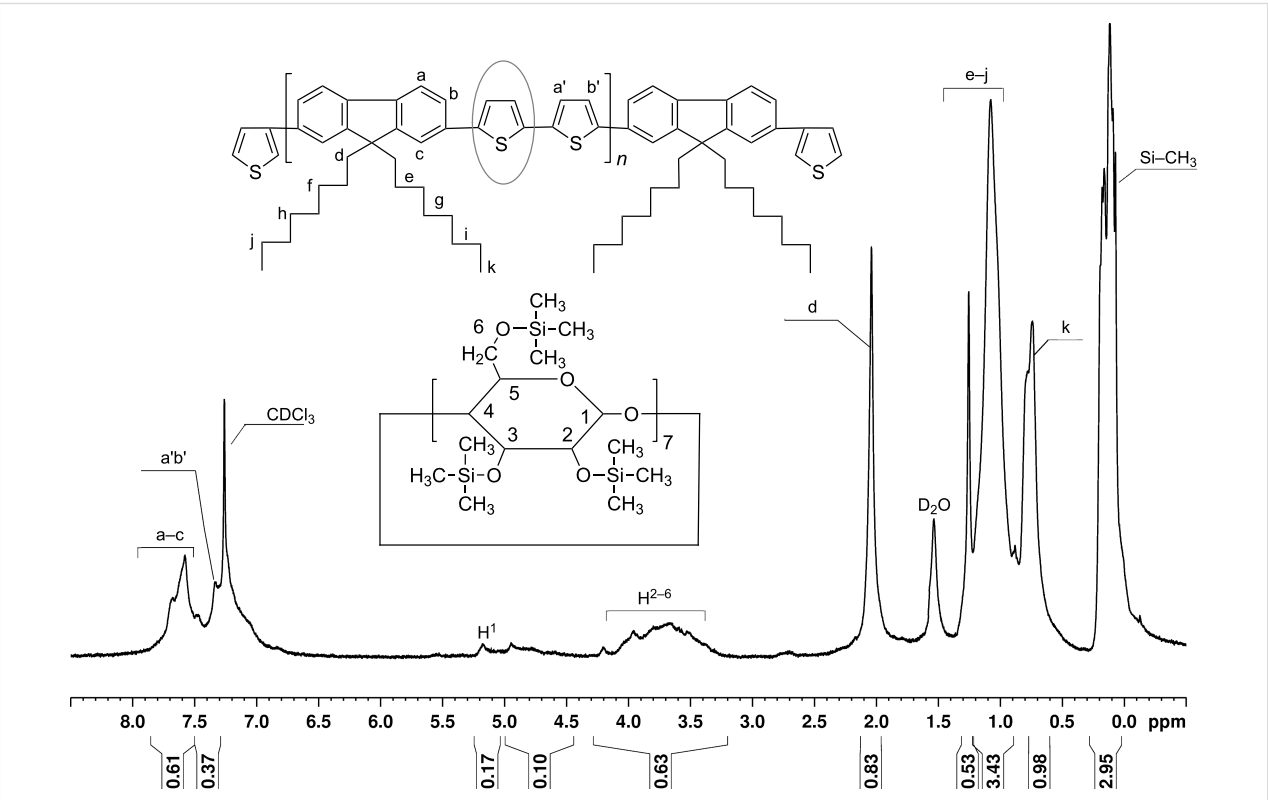

Figure 4: ^{1}H NMR spectrum of **PDOF-BTc** copolymer ($CDCl_3$).

ppm, $I_{H\text{-}CH3}$) and the proton peaks of **BT** (7.247–7.412 ppm, I_{BT}), as shown in Figure 4. The average number of PS-βCD macrocycles per repeat unit was calculated as (I_{BT} /4)/($I_{H\text{-}CH3}$/63) and found to be 0.32 (i.e., ca. 32% coverage). The peaks corresponding to the fluorene copolymer chains in **PDOF-BTc** were down-field shifted by 0.03–0.08 ppm, as compared to the noncomplexed **PDOF-BT** sample (Figure 4).

The weight-average molecular weight (M_w) and number-average molecular weight (M_n), with the polydispersity index PDI (PDI = M_w/M_n), of **PDOF-BTc** and **PDOF-BT** samples were determined by gel-permeation chromatography (GPC) analysis, using polystyrenes as standards and CH_2Cl_2 as eluent. GPC data are listed in Table 1 and shown in Figure S2 and Figure S3 in the Supporting Information File 1. On the basis of the molecular weight, the numbers of repeat units for **PDOF-BTc** and **PDOF-BT** samples are 10 and 40, respectively. **PDOF-BT** non-rotaxane copolymer has higher molecular weights than the **PDOF-BTc** sample, an expected result owing to the lower accessibility of diborate to bromine groups encapsulated in the PS-βCD cavity. The higher PDI values of the **PDOF-BTc** copolymer compared to **PDOF-BT** can be attributed to variations in the average number of PS-βCD units per macromolecular chain (see incomplete coverage determined by ^{1}H NMR above). It is important to note that the lower molecular weights of **PDOF-BTc** rotaxane copolymer, which have not been observed for other polyrotaxanes [5,29,31,34], can be assigned to the contribution from the structure of the PS-βCD macrocycle, which provides a deeper insight into the blocking effect of silylated groups on the cross-coupling reaction. In order to obtain higher-molecular-weight polyrotaxanes the optimal reaction time has to be taken into consideration.

Table 1: The molecular weights of the polymers.

Polymer	M_n	M_w	M_w/M_n
PDOF-BTc	14771	24805	1.67
PDOF-BT	23286	34461	1.48

The thermal stability of the inclusion-complex **BTc**, **PDOF-BT** and the **PDOF-BTc** copolymers was investigated by differential scanning calorimetry (DSC) and thermogravimetric analysis (TGA), as shown in Figure 5 and Figure 6, and the results are summarized in Table 2. The endothermic peak attributed to the melting temperature of **BT** (144 °C), as a result of a decomplexation process (17%) was present in the second heating scan of **BTc** (Figure 5). The presence of two broadening peaks accompanied by a shift to a lower melting temperature for **BTc** (133 °C, ΔH = 5.22 J/g) with a strong reduction of intensity could be attributed to a heating-favoured loosening of the crystal forces of **BT** included in the amorphous PS-βCD cavities.

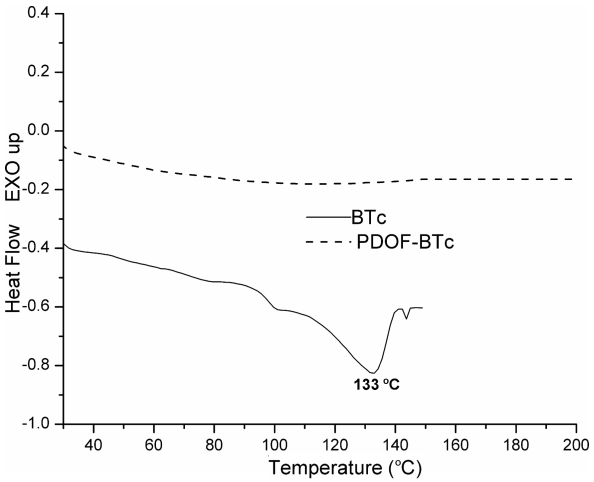

Figure 5: DSC curves of **BTc** and **PDOF-BTc** from second-heating DSC measurements.

On the cooling cycle (not shown) the exothermal sharp peak attributed to the crystallization process of **BTc** was found at lower temperature (108 °C, ΔH = 7.66 J/g)) compared with non-complexed **BT** (111 °C). DSC profiles of **PDOF-BTc** copolymer does not indicate T_g or melting temperature in the 30–200 °C interval, as can be seen in Figure 6. These findings indicated their amorphous nature and rigid chains.

The effect of PS-βCD on the thermal stability of the samples was further supported by TGA in a nitrogen atmosphere, which revealed the stage of the degradation process, shown in Figure 6 and Figure S4 in the Supporting Information File 1.

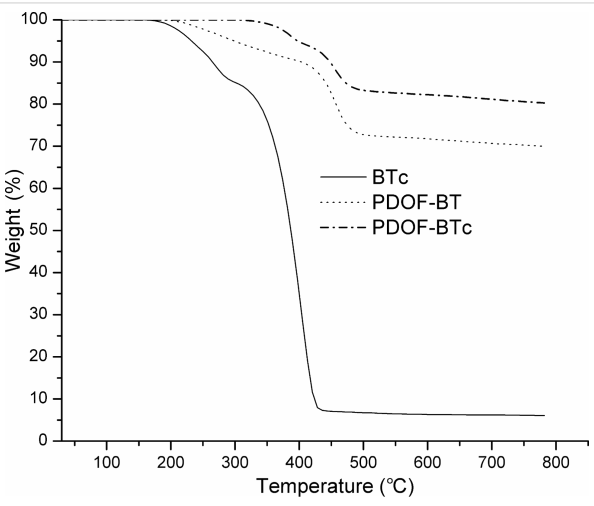

Figure 6: Thermogravimetric curves (TG) for **BTc**, **PDOF-BT**, and **PDOF-BTc** compounds.

Table 2: Thermal properties.

Sample	Step	T_{onset}[a]	T_{endset}[b]	T_{peak}[c]	W%[d]	Residue[e] %
BTc	I	196	287	271	15.49	63.18
	II	350	433	401	79.72	
PDOF-BT	I	212	330	264	9.78	69.07
	II	426	480	456	21.15	
PDOF-BTc	I	341	396	383	6.38	80.94
	II	431	480	456	12.68	

[a]The onset temperature of the degradation process. [b]The temperature of complete degradation process. [c]The maximum degradation temperature. [d]The mass percentage loss recorded in each stage. [e]The amount of residue at the end of degradation process.

As one can see from Figure 6, **BTc**, **PDOF-BT** and **PDOF-BTc** samples present two thermal decomposition steps. For the **PDOF-BT** sample the decomposition process starts at 212 °C, while the degradation of its **PDOF-BTc** complex homologue begins at a higher temperature (341 °C). Thus, a stabilizing effect of the inclusion of the **BT** chain into the PS-βCD cavity for the first decomposition step is evidenced. The maximum degradation process of the samples is around 271 °C for **BTc**, 264 °C for **PDOF-BT** and 383 °C for **PDOF-BTc**, i.e., not much higher than the decomposition temperature of PS-βCD (380 °C). The TGA data revealed that the **PDOF-BTc** rotaxane copolymer is stable up to 300 °C. The improvement of the thermal stability provides an indication that the rotaxane formation increases the stability of the **PDOF-BT** macromolecular chains.

The rotaxane copolymer has good solubility in common organic solvents, such as $CHCl_3$, CH_2Cl_2, THF, and toluene, and allows the formation of homogeneous and transparent films. In order to analyse the influence on the surface morphological properties induced by using **3T** as an end-capping reagent instead of bromobenzene [12], AFM experiments were also performed. The 2D AFM images of the top surface of both copolymer films, within the same scan areas of 2 × 2 μm^2 are shown in Figure 7a and Figure 7b (insets show the 3D images). They afforded the root-mean-square roughness of the formations (S_q)

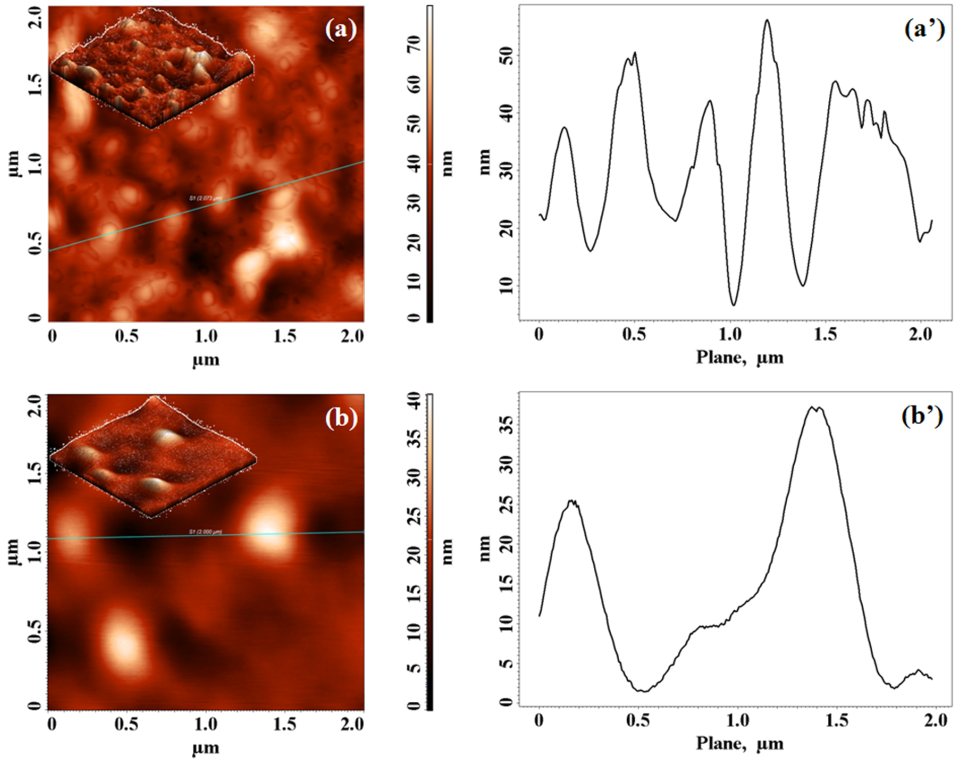

Figure 7: High-resolution tapping-mode AFM images and cross-section plots (along the solid line in the images) of the **PDOF-BT** (a, a') and **PDOF-BTc** (b, b').

Table 3: Roughness and grain parameters collected from 2 × 2 μm² AFM images.

Material	S_q[a]/nm	μ[b]/nm	H_a[c]/nm
PDOF-BT	12.43	9.83	34.40
PDOF-BTc	5.29	3.70	17.34

[a]Root-mean-square roughness. [b]Average roughness. [c]Average heights.

and the average roughness (μ) as well as the average heights (H_a), see Table 3.

The 3D AFM images of the complexed **PDOF-BTc** film (insets Figure 7b) show more favourable surface parameters in comparison to the noncomplexed copolymer (insets Figure 7a). **PDOF-BT** showed an agglomeration tendency and globular formations with S_q and μ values of 12.43 and 9.83 nm, whereas the **PDOF-BTc** sample showed a uniform and smooth surface, covered with individual small, spherically shaped formations, with smaller S_q and μ values of 5.29 and 3.70 nm. The average AFM heights of the **PDOF-BT** and **PDOF-BTc** decreased from 34.40 to 17.34 nm, respectively, as shown in Figure 7a' and Figure 7b' and documented in Table 3.

The trend toward a more uniform and smoother surface, already observed for rotaxane copolymers [12,23,27,31], continues for the **PDOF-BTc** polymer rotaxane, where a decrease of the S_q and the value of the H_a parameter (the first moment of the height distribution) indicated that the rotaxane architecture changed the morphology of **PDOF-BT** copolymer. These results could provide microscopic evidence for reduced interchain interactions, which allow the polyrotaxane chains to pack densely. A better quality of the film, with higher uniformity, flatness, and better mechanical properties, is always desirable for optoelectronic applications.

The optical properties of the **PDOF-BT** and **PDOF-BTc** compounds (not shown) recorded in $CHCl_3$ solution, as well as in thin film, upon excitation at the maximum absorption value (λ_{max} = 380 nm) indicate no significant difference in the electronic absorption and emission spectra of both copolymers, consistent with previously reported results [12]. The similarity between the absorption and fluorescence excitation spectra shows that major structural changes have not occurred, and that emissions arose from the compounds and not from the thienyl end-capping, as has been previously reported for PFO with perylene derivative as end-units [35].

Conclusion

The present study confirms that PS-βCD can be used as a host macrocycle molecule in the synthesis of a main-chain polyrotaxane with alternating fluorene-bithiophene moieties. Lower values of number-average molecular weight (M_n) of the rotaxane copolymer suggested that the condensation reaction is subjected to steric effects of the bulkier silylated groups from PS-βCD, thus requiring a longer reaction time. We have demonstrated that PS-βCD covered bithiophene-fluorene copolymer has beneficial effects on the solubility in nonpolar solvents, and on the thermal properties and surface characteristics.

Experimental

Materials and methods

PS-βCD was obtained by the silylation of native βCD with 1-trimethylsilylimidazole [36]. 9,9-dioctylfluorene-2,7-bis(trimethylene borate) (**DOF**, 97%), tetrakis(triphenylphosphane)palladium (99%), and 5,5'-dibromo-2,2'-bithiophene (**BT**) were purchased from Aldrich and used as received; 3-bromothiophene (**3BT**, 97%) was purchased from Lancaster. All solvents were analytical grade and used without further purification.

^{1}H NMR spectra were recorded in $CDCl_3$ on a Bruker Advance 400 MHz instrument. FTIR analyses of the powder polymers were performed in a Specord Carl Zeiss Jena FTIR spectrophotometer. The molecular weights of copolymers were determined by gel permeation chromatography (GPC) in CH_2Cl_2 by using a Water Associates 440 instrument and polystyrene calibrating standards. Differential scanning calorimetry (DSC) was performed with a Mettler Toledo DSC-12E calorimeter with two repeated heating-cooling cycles at a heating rate of 10 °C·min^{-1} under a N_2 atmosphere. Thermogravimetric analysis (TGA) was performed under constant nitrogen flow (20 mL·min^{-1}) with a heating rate of 15 °C·min^{-1} by using a Mettler Toledo TGA/SDTA 851e balance. The heating scans were performed with 1.5 to 3 mg of the sample in a temperature range 25–800 °C. Absorption spectra were measured on a Specord 200 spectrophotometer in $CHCl_3$ solution and on thin films. Fluorescence spectra were obtained with a Perkin Elmer LS55 luminescence spectrophotometer. The surface images were obtained with a Solver PRO-M scanning probe microscope (NT-MDT, Zelenograd, Moscow, Russia), in atomic force microscopy (AFM) configuration. The scan area was 2 × 2 μm². Rectangular silicon cantilevers NSG10 (NT-MDT, Russia) with tips of high aspect ratio were used. All images were acquired in air, at room temperature (23 °C), in tapping mode at a scanning frequency of 1.56 Hz. The AFM image processing and the calculation of the surface texture parameters were realized by Nova v.1.26.0.1443 for Solver Software, NT-MDT Russia. Films of copolymers were prepared by spin coating from CH_2Cl_2 solutions at 3000 rpm for 60 s on a WS-400B-6NPP-Lite Single Wafer Spin Processor (Laurel Technologies Corporation, USA).

Synthesis of the **BTc** inclusion complex

BT (0.124 g, 0.4 mmol) was added to the solution of PS-βCD (2.58 g, 0.96 mmol) in acetone (15 mL) and the mixture was vigorously stirred for 24 h. The precipitate was filtered, washed thoroughly twice with 5 mL of petroleum ether and 5 mL of acetone, and finally dried under vacuum at 60 °C for 24 h to yield 0.607 g of **BTc** as a light-yellow solid (42.9% yield). ^{1}H NMR **BTc** ($CDCl_3$): 6.97–6.96 (d, 2H), 6.85–6.86 (d, 2H), 5.12–4.95 (m, 7H, H^1), 4.93–4.60 (m, OH^{2+3}), 3.97–3.35 (m, 42H, H^{2-6}), 0.19–0.09 (m, 63, Si–CH_3).

Synthesis of the **PDOF-BTc** copolymer

To a three-necked flask, 0.602 g (0.202 mmol) of **BTc** and 0.112 g (0.2 mmol) of **DOF** was added. The flask was equipped with a condenser, evacuated, and filled with argon several times to remove traces of air. Degassed toluene (6 mL) was added as solvent into the flask and subsequently 4.8 mg (0.42×10^{-2} mmol) of $(Ph_3P)_4Pd(0)$, dissolved in 5 mL of degassed toluene, and 2 mL of 5 M Na_2CO_3 solution were added. The mixture was vigorously stirred in the dark under an argon atmosphere for 72 h at 85–87 °C. An excess of 0.0113 g (0.02 mmol) of **DOF** dissolved in 3 mL of toluene was then added and the reaction was continued for 12 h in order to obtain the macromolecular chains terminated with borate units. Finally, 0.2 μL of **3BT** was added as the end-capper of the copolymer chain, and the reaction was continued overnight. After cooling, the mixture was poured into the stirred mixture of methanol and deionised water (10:1). The fibrous solid obtained by filtration was solubilised in 20 mL of toluene, washed with water three times to completely remove the alkali solution, dried over anhydrous $MgSO_4$, and concentrated by vacuum evaporation of the solvents. The residue was dissolved in a minimum volume of $CHCl_3$ (10 mL) and poured into 10 times the volume of stirred methanol, and then filtered, thoroughly washed with 5 mL of acetone, and dried under reduced pressure at 60 °C. **PDOF-BTc** was obtained in 0.125 g (approximately 23.0% yield) as a light-orange solid. After drying, the solid was immersed in petroleum ether, vortex stirred for 15 min, and then filtered. The precipitate was filtered and dried under vacuum. The soluble part in petroleum ether was concentrated by vacuum evaporation. Both fractions of **PDOF-BTc** were found to be also soluble in THF, CH_2Cl_2, $CHCl_3$ and toluene. FTIR (KBr, cm^{-1}): 3447, 2957, 2923, 1608, 1415, 1364, 1251, 1144, 1096, 1049, 966, 885, 841, 748, 687, 542, 475, 434. ^{1}H NMR ($CDCl_3$): 7.67–7.57 (m, 6 H), 7.33–7.24 (m, 4H), 5.13–4.95 (m, 7H, H^1), 4.95–4.79 (m, OH^{2+3}), 3.96–3.53 (m, 42H, H^{2-6}), 2.04 (s, 4H), 1.25–0.88 (m, 24H), 0.74 (d, 6H), 0.18–0.07 (m, 63, Si–CH_3).

Synthesis of the **PDOF-BT** copolymer

PDOF-BT was synthesized under similar experimental conditions as those described for **PDOF-BT**, except that **BT** was used instead of **BTc**. The copolymer was obtained as a brownish solid in 78% yield. The **PDOF-BT** sample was insoluble in petroleum ether. FTIR (KBr, cm^{-1}): 3428, 3065, 2923, 2851, 1719, 1606, 1465, 1261, 1067, 880, 817, 721, 475, 434. ^{1}H NMR ($CDCl_3$): 7.68–7.58 (m, 6 H), 7.34–7.24 (m, 4H), 2.05 (m, 4H), 1.26–1.10 (m, 24H), 0.91–0.80 (d, 6H).

Supporting Information

Supporting Information File 1

Gel permeation chromatography and derivative thermogravimetric curves.
[http://www.beilstein-journals.org/bjoc/content/supplementary/1860-5397-8-170-S1.pdf]

Acknowledgements

This research was supported by a grant of the Romanian National Authority for Scientific Research, CNCS – UEFISCDI, project number PN-II-ID-PCE-2011-3-0035.

References

1. Chochos, C. L.; Choulis, S. A. *Prog. Polym. Sci.* **2011,** *36,* 1326–1414. doi:10.1016/j.progpolymsci.2011.04.003
2. Fang, Y. K.; Liu, C. L.; Li, C.; Lin, C.-J.; Mezzenga, R.; Chen, W.-C. *Adv. Funct. Mater.* **2010,** *20,* 3012–3024. doi:10.1002/adfm.201000879
3. Thompson, B. C.; Fréchet, J. M. J. *Angew. Chem., Int. Ed.* **2008,** *47,* 58–77. doi:10.1002/anie.200702506
4. Günes, S.; Neugebauer, H.; Sariciftci, N. S. *Chem. Rev.* **2007,** *107,* 1324–1338. doi:10.1021/cr050149z
5. Farcas, A.; Gosh, I.; Jarroux, N.; Guégan, P.; Harabagiu, V.; Nau, W. M. *Chem. Phys. Lett.* **2008,** *465,* 96–101. doi:10.1016/j.cplett.2008.09.058
6. Beinhoff, M.; Appapillai, A. T.; Underwood, L. D.; Frommer, J.; Carter, K. R. *Langmuir* **2006,** *22,* 2411–2414. doi:10.1021/la051878c
7. Grisorio, R.; Mastrorilli, P.; Nobile, C. F.; Romanazzi, G.; Suranna, G. P.; Acierno, D.; Amendola, E. *Macromol. Chem. Phys.* **2005,** *206,* 448–455. doi:10.1002/macp.200400306
8. Scherf, U.; List, E. J. W. *Adv. Mater.* **2002,** *14,* 477–487. doi:10.1002/1521-4095(20020404)14:7<477::AID-ADMA477>3.0.CO;2-9
9. Kim, J. H.; Lee, H. *Chem. Mater.* **2002,** *14,* 2270–2275. doi:10.1021/cm011553r
10. Bernius, M. T.; Inbasekaran, M.; O'Brien, J.; Wu, W. *Adv. Mater.* **2000,** *12,* 1737–1750. doi:10.1002/1521-4095(200012)12:23<1737::AID-ADMA1737>3.0.CO;2-N
11. Farcas, A.; Stoica, I.; Stefanache, A.; Peptu, C.; Farcas, F.; Marangoci, N.; Sacarescu, L.; Harabagiu, V.; Guégan, P. *Chem. Phys. Lett.* **2011,** *508,* 111–116. doi:10.1016/j.cplett.2011.04.027

12. Farcas, A.; Hitruc, E. G. *Dig. J. Nanomater. Bios.* **2011,** *6,* 1649–1656. http://www.chalcogen.infim.ro/1649_Farcas.pdf
13. Zhao, D.; Tang, W.; Ke, L.; Tan, S. T.; Sun, X. W. *ACS Appl. Mater. Interfaces* **2010,** *2,* 829–837. doi:10.1021/am900823b
14. Tang, W. H.; Chellappan, V.; Liu, M. H.; Chen, Z. K.; Ke, L. *ACS Appl. Mater. Interfaces* **2009,** *1,* 1467–1473. doi:10.1021/am900144b
15. Pal, B.; Yen, W.-C.; Yang, J.-S.; Su, W.-F. *Macromolecules* **2007,** *40,* 8189–8194. doi:10.1021/ma071126k
16. Blouin, N.; Leclerc, M.; Vercelli, B.; Zecchin, S.; Zotti, G. *Macromol. Chem. Phys.* **2006,** *207,* 175–182. doi:10.1002/macp.200500429
17. Surin, M.; Sonar, P.; Grimsdale, A. C.; Müllen, K.; Lazzaroni, R.; Leclère, P. *Adv. Funct. Mater.* **2005,** *15,* 1426–1434. doi:10.1002/adfm.200500241
18. Liu, B.; Yu, W. L.; Lai, Y. H.; Huang, W. *Macromolecules* **2000,** *33,* 8945–8952. doi:10.1021/ma000866p
19. Huang, F.; Gibson, H. W. *Prog. Polym. Sci.* **2005,** *30,* 982–1018. doi:10.1016/j.progpolymsci.2005.07.003
20. Wenz, G.; Han, B.-H.; Müller, A. *Chem. Rev.* **2006,** *106,* 782–817. doi:10.1021/cr970027+
21. Frampton, M. J.; Anderson, H. L. *Angew. Chem., Int. Ed.* **2007,** *46,* 1028–1064. doi:10.1002/anie.200601780
22. Harada, A.; Hashidzume, A.; Yamaguchi, H.; Takashima, Y. *Chem. Rev.* **2009,** *109,* 5974–6023. doi:10.1021/cr9000622
23. Farcas, A.; Ghosh, I.; Nau, W. M. *Chem. Phys. Lett.* **2012,** *535,* 120–125. doi:10.1016/j.cplett.2012.03.069
24. Farcas, A.; Fifere, A.; Stoica, I.; Farcas, F.; Resmerita, A.-M. *Chem. Phys. Lett.* **2011,** *514,* 74–78. doi:10.1016/j.cplett.2011.08.007
25. Frampton, M. J.; Sforazzini, G.; Brovelli, S.; Latini, G.; Townsend, E.; Williams, C. C.; Charas, A.; Zalewski, L.; Kaka, N. S.; Sirish, M.; Parrott, L. J.; Wilson, J. S.; Caciali, F.; Anderson, H. L. *Adv. Funct. Mater.* **2008,** *18,* 3367–3376. doi:10.1002/adfm.200800653
26. Farcas, A.; Jarroux, N.; Guegan, P.; Fifere, A.; Pinteala, M.; Harabagiu, V. *J. Appl. Polym. Sci.* **2008,** *110,* 2384–2392. doi:10.1002/app.28760
27. Farcas, A.; Jarroux, N.; Harabagiu, V.; Guégan, P. *Eur. Polym. J.* **2009,** *45,* 795–803. doi:10.1016/j.eurpolymj.2008.11.047
28. Farcas, A.; Jarroux, N.; Ghosh, I.; Guégan, P.; Nau, W. M.; Harabagiu, V. *Macromol. Chem. Phys.* **2009,** *210,* 1440–1449. doi:10.1002/macp.200900140
29. Zalewski, L.; Wykes, M.; Brovelli, S.; Bonini, M.; Breiner, T.; Kastler, M.; Dotz, F.; Beljonne, D.; Anderson, H. L.; Cacialli, F.; Samorì, P. *Chem.–Eur. J.* **2010,** *16,* 3933–3941. doi:10.1002/chem.200903353
30. Broveli, S.; Cacialli, F. *Small* **2010,** *6,* 2796–2820. doi:10.1002/smll.201001881
31. Zalewski, L.; Broveli, S.; Bonini, M.; Mativetsky, J. M.; Wykes, M.; Orgiu, E.; Breiner, T.; Kastler, M.; Dötz, F.; Meinardi, F.; Anderson, H. L.; Beljonne, D.; Caciali, F.; Samori, P. *Adv. Funct. Mater.* **2011,** *21,* 834–844. doi:10.1002/adfm.201001135
32. Gibson, H. W.; Farcas, A.; Jones, J. W.; Ge, Z.; Huang, F.; Vergne, M.; Hercules, D. M. *J. Polym. Sci., Part A: Polym. Chem.* **2009,** *47,* 3518–3543. doi:10.1002/pola.23435
33. Farcas, A.; Jarroux, N.; Guegan, P.; Harabagiu, V.; Melnig, V. *J. Optoelectron. Adv. Mater.* **2007,** *9,* 3484–3488. http://joam.inoe.ro/download.php?idu=1050
34. Farcas, A.; Ghosh, I.; Grigoras, V. C.; Stoica, I.; Peptu, C.; Nau, W. M. *Macromol. Chem. Phys.* **2011,** *212,* 1022–1031. doi:10.1002/macp.201000727
35. Ego, C.; Marsitzky, D.; Becker, S.; Zhang, J.; Grimsdale, A. C.; Müllen, K.; MacKenzie, J. D.; Silva, C.; Friend, R. H. *J. Am. Chem. Soc.* **2003,** *125,* 437–443. doi:10.1021/ja0205784
36. Harabagiu, V.; Simionescu, B. C.; Pinteala, M.; Merrienne, C.; Mahuteau, J.; Guègan, P.; Cheradame, H. *Carbohydr. Polym.* **2004,** *56,* 301–311. doi:10.1016/j.carbpol.2003.12.007

License and Terms

Beilstein Journal of Organic Chemistry

Influence of cyclodextrin on the solubility of a classically prepared 2-vinylcyclopropane macromonomer in aqueous solution

Helmut Ritter*, Jia Cheng and Monir Tabatabai

Full Research Paper

Open Access

Address:
Heinrich-Heine-Universität Düsseldorf, Institut für Organische Chemie und Macromolekulare Chemie, Universitätsstraße 1, 40225 Düsseldorf, Germany, Fax: (+49) 211-811-5840

Email:
Helmut Ritter* - h.ritter@uni-duesseldorf.de

* Corresponding author

Keywords:
branched poly(NiPAAm); cloud point; cyclodextrins; graft copolymer; macromonomer; ring-opening free radical polymerization; 2-vinylcyclopropane

Beilstein J. Org. Chem. **2012,** *8,* 1528–1535.
doi:10.3762/bjoc.8.173

Received: 03 May 2012
Accepted: 25 July 2012
Published: 13 September 2012

This article is part of the Thematic Series " Superstructures with cyclodextrins: Chemistry and applications".

Associate Editor: B. Stoltz

Abstract

A macromonomer **5** consisting of a polymerizable vinylcyclopropane end group and a poly(*N*-isopropylacrylamide) (poly(NiPAAm)) chain was obtained from amidation of 1-ethoxycarbonyl-2-vinylcyclopropane-1-carboxylic acid (**4**) with an amino-terminated poly(NiPAAm) **3** as an example. This macromonomer **5** showed an LCST effect after complexation of the vinyl end group with ß-cyclodextrin in water. Via radical ring-opening copolymerization of **5** and NiPAAm a graft copolymer **8** with a clouding point of 32 °C was synthesized. The branched unsaturated polymer was treated with ozone to cleave the double bonds of the main chain.

Introduction

Macromonomers are polymers or oligomers with at least one functional end group that is capable of further polymerization. The molecular weight of macromonomers generally ranges between 1000 and 20000 g/mol [1]. In the last decades, a considerable amount of studies on the synthesis and applications of macromonomers has been reported [2-5]. They enable easy and direct synthesis of a variety of graft copolymers [6], which consist of a linear main chain and randomly distributed side chains. Graft copolymers have found many applications, for example in the field of coatings, adhesives, compatibilizers, emulsifiers or biomaterials [1]. For the synthesis of graft copolymers, free radical copolymerization of macromonomers with suitable low molecular weight vinylmonomers is a widely studied area [7,8].

β-Cyclodextrins (β-CDs) are cyclic oligomers consisting of seven α-1,4-glycosidically linked glucopyranose units which are present in the chair conformation [9-12]. The molecule resembles a truncated cone with approximate C_n-symmetry [13]. The cyclic 1,4-linked glucose units in the molecule arrange themselves in a way that a hydrophilic exterior and a hydrophobic interior are created [14-16] and β-CDs are easily dissoluble in

polar solvents such as water. The interior height of β-CDs is 7.9 Å and the interior width is between 6.0–6.5 Å, which allows an inclusion of different types of molecules with fitting size through van-der-Waals interactions. By formation of such host–guest complex properties, the dissolution behavior of the guest molecules can be changed. Based on this fact numerous applications of β-CDs are reported [17-25].

Generally, 2-vinylcyclopropane monomers (2-VCPs) are known for their low volumetric shrinkage or even small expansion during free radical ring-opening polymerization (Scheme 1) [26-28]. However, this behavior is not in focus of the present work. The resulting polymer bears mainly 1,5-ring-opened units with a partially unsaturated backbone [29-31], which is suitable for further modifications.

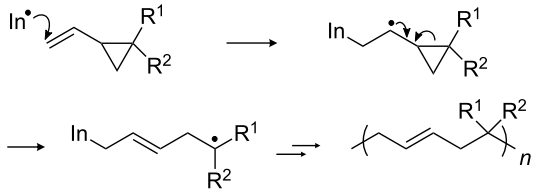

Scheme 1: Mechanism of free radical ring-opening polymerization of 2-VCPs (In: initiator) [29-31].

As mentioned above, polymerization reactions and mechanical and chemical modifications of vinylcyclopropane derivates have been carefully investigated in recent years. However, up to now, nothing is known in literature about the behavior of vinylcyclopropane-containing macromonomers. Thus, in this paper we are going to report our findings about the preparation and characterization of a new type of macromonomers based on a 2-vinylcyclopropane derivative bearing a thermoresponsive poly(NiPAAm) moiety as an example, with the intention to demonstrate the great potentials of this class of 2-vinylcyclopropane monomers. Additionally, the degradation of unsaturated poly(vinylcyclopropan) backbones using ozone is first reported.

Results and Discussion

1-Ethoxycarbonyl-2-vinylcyclopropane-1-carboxylic acid (**4**) was synthesized following a procedure described in [32]. Diethyl 2-vinyl-1,1-cyclopropanedicarboxylate could be obtained according to [33] from sodium ethoxide, diethyl malonate and *trans*-1,4-dichloro-2-butene in ethanol (Scheme 2).

The desired macromonomer **5** was prepared in two steps according to Scheme 3. The intermediate amino-terminated poly(NiPAAm) **3** was obtained from the reaction of NiPAAm (**1**) and 2-aminoethanethiol hydrochloride (**2**) via radical polymerization either in water using **2** and ammonium persulfate as redox initiator [34] or in ethanol using 2,2'-azobis(isobutyronitrile) (AIBN) as radical initiator and **2** as chain transfer agent. The implementation in aqueous solution represents an environmentally friendly alternative to conventional polymerization. To avoid the Michael addition between the amino group and the acryloyl group, the ammonium salt of **2** was used instead of uncharged nucleophilic 2-aminoethanethiol. After treating with triethylamine, amino-terminated polymer **3** was obtained. The

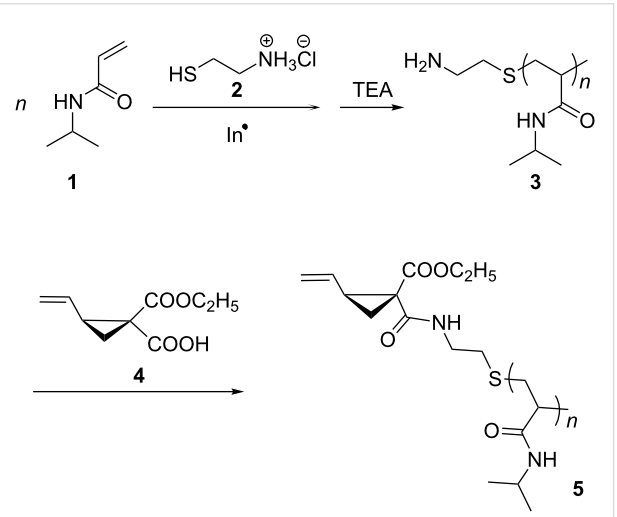

Scheme 3: Two-step synthesis of the macromonomer **5** (In: Initiator, TEA: triethylamine).

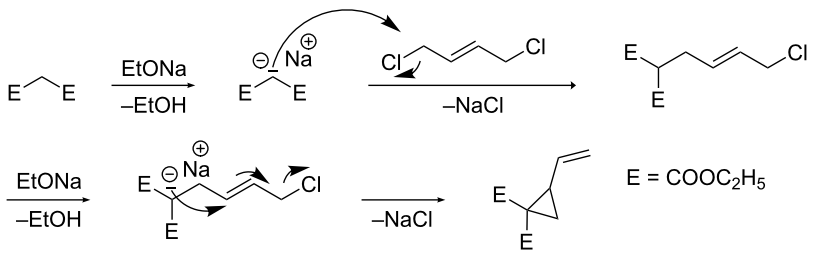

Scheme 2: Synthesis of diethyl 2-vinyl-1,1-cyclopropanedicarboxylate [33].

amidation of the amino group of **3** with 1-ethoxycarbonyl-2-vinylcyclopropane-1-carboxylic acid (**4**) in the presence of *N,N′*-dicyclohexylcarbodiimide (DCC) as condensation agent led to the formation of macromonomer **5**.

Compared to the FTIR spectrum of NiPAAm (**1**), the spectrum of **3** shows the disappearance of the C=C bonds band at 1619 cm^{-1} and the appearance of a new band of primary amino groups at 3436 cm^{-1}. In the ^1H NMR spectrum, the chemical shifts of the methylene protons adjacent to the amino group at δ 2.85 ppm and the methylene protons adjacent to the thio group at δ 2.68 ppm which also confirms the structure of **3**. The mass differences between the signals of the main series in MALDI-TOF MS correspond to the molar mass of the monomer NiPAAm units equal to 113 g/mol and the mass of end group agrees with the molar mass of 2-aminoethanethiol (77 g/mol, Figure 1), as expected. The number average molecular weight (M_n) and the dispersity index (DI) of **3** were measured with GPC and were 10300 g/mol and 2.8, respectively (Table 1). The hydrodynamic diameter (d_n) of **3** determined by means of DLS was about 4.1 nm. DSC measurement showed the glass-transition temperature (T_g) at about 123.5 °C. Due to the hydrophilicity of the amino end groups of **3** a typical LCST (lower critical solution temperature) was observed close to that of unmodified poly(NiPAAm) at about 33.4 °C (Figure 2).

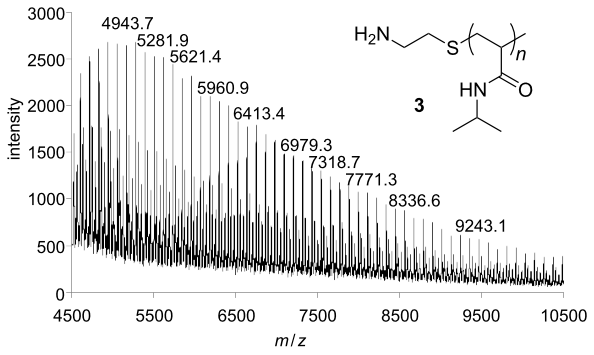

Figure 1: MALDI-TOF MS of amino-terminated poly(NiPAAm) **3**.

Table 1: Properties of synthesized macromonomers and polymers.

	M_n (10^4 g/mol)	DI	d_n[a] (nm)	cloud point[b] (°C)	T_g (°C)	yield (%)
3	1.0	2.8	4.1	33.4	123.5	54[c] or 66[d]
5	1.2	2.5	5.0	–	129.1	86
7			–	31.7		–
6	2.3	1.7	5.6	29.9	135.3	53
8	4.8	2.5	6.4	32.2	133.7	65

[a]5 mg/mL in acetone at 25 °C; [b]20 mg/mL in water; [c]polymerization in water; [d]polymerization in ethanol.

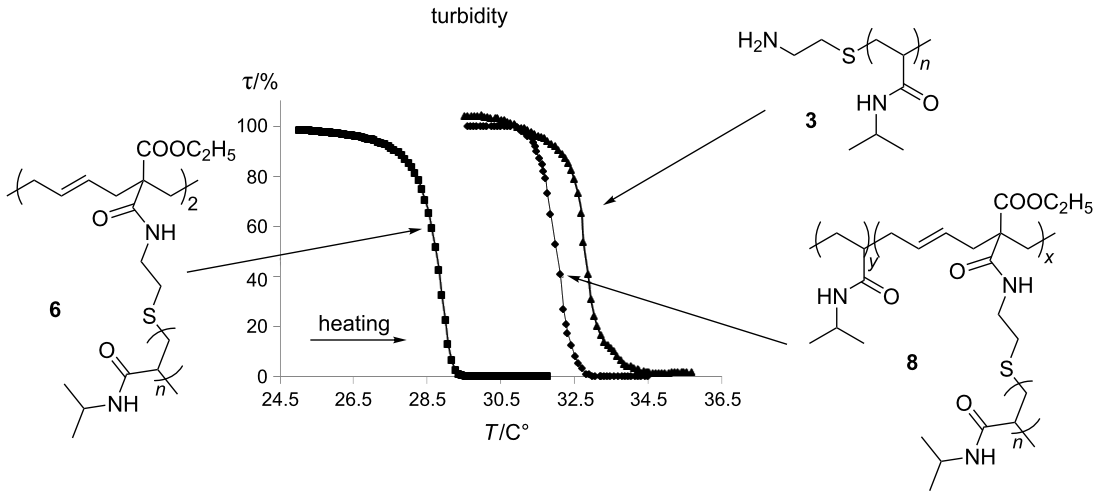

Figure 2: Optical transmittance of aqueous solutions (*c* = 20 mg/mL) of **3**, **6** und **8** during heating.

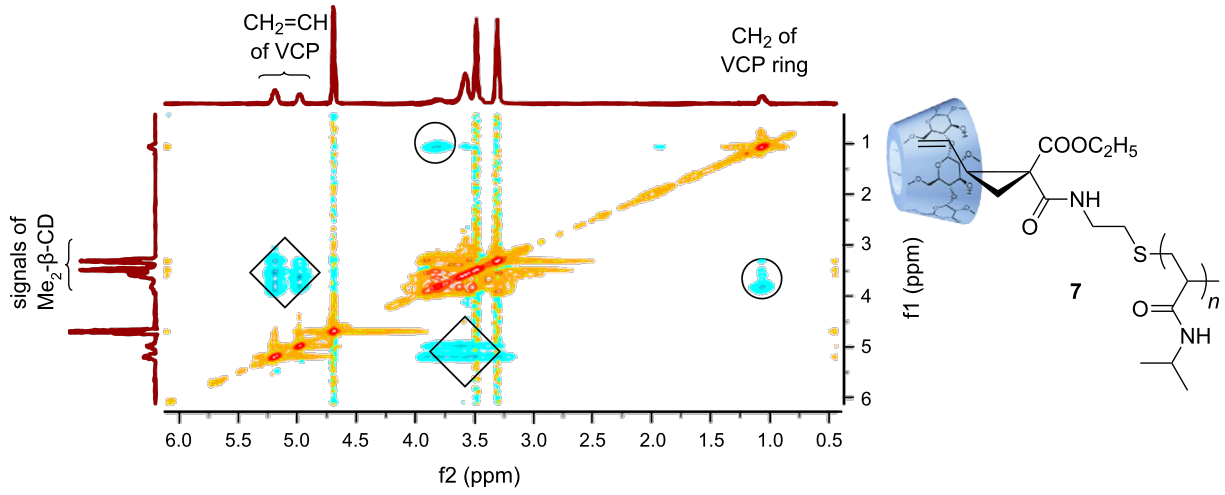

Figure 3: 2D ROESY NMR spectrum of a **5**/Me_2-β-CD deuterated water solution.

Via condensation of the amino end group of **3** with the carboxyl group of **4** the corresponding macromonomer **5** with M_n = 11540 g/mol und T_g = 129.1 °C was obtained. The ^{1}H NMR spectrum confirms the existence of a vinylcyclopropane unit by the presence of the multiplets at δ 1.48–1.61 ppm and δ 4.98–5.19 ppm, assignable to the CH of the cyclopropane ring and of the vinyl group, respectively. The FTIR spectrum shows the typical absorption band of ester groups at 1726 cm^{-1} and the disappearance of the band of primary amino groups; this also proves the successful condensation between **3** and **4**. Due to the faintly voluminous vinylcyclopropane unit **5** possesses a slightly larger d_n than **3** (by ca. 0.9 nm, Table 1).

In general, the cloud point of poly(NiPAAm) with relative low molecular weight can be influenced by the structure of end groups. The relatively hydrophobic vinylcyclopropane end group hampers the aqueous solubility of **5** at room temperature (about 25 °C). However, the turbid dispersion becomes completely clear by the addition of methylated β-cyclodextrin (Me_2-β-CD). This means that a water-soluble inclusion complex **7** of **5** with Me_2-β-CD is formed (Figure 3). The 2D ROESY NMR spectrum of **7** indicates the noncovalent interaction between the Me_2-β-CD ring and the vinyl end group of macromonomer **5** (Figure 2). It can be noticed that the protons of the vinyl groups (CH_2=CH) at δ 4.98–5.19 ppm and the protons of the cyclopropan units at δ 1.48–1.61 ppm correlated to the protons of Me_2-β-CD at δ 3.3–3.9 ppm. Therefore, we came to the conclusion that the Me_2-β-CD ring preferably includes the vinylcyclopropane unit instead of the isopropyl unit. The supramolecular complex **7** shows the typical LCST behavior (31.7 °C) of poly(NiPAAm) (Figure 4).

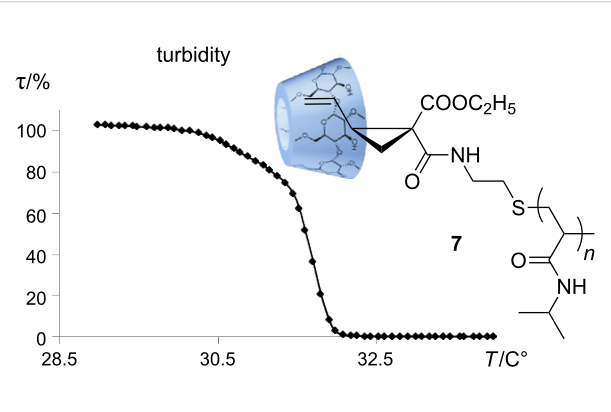

Figure 4: Temperature-dependent transparency measurements of aqueous solution of the supramolecular complex **7** (*c* = 20 mg/mL in water).

After free radical initiated ring-opening polymerization of **5**, a product **6** was formed (Scheme 4). However, GPC of **6** shows only a preferred dimerization of macromonomer **5**, which may result from the relative bulky poly(NiPAAm) side chains. Therefore, copolymerization of **5** and NiPAAm was carried out. In this case, as expected, a copolymer **8** was obtained with much higher M_n value of 48300 g/mol according to GPC measurement. The disappearance of NMR-signals of the vinylcyclopropane unit of **5** at δ 4.98–5.19 ppm and the appearance of a new peak at δ 5.6 ppm, which is assigned to the protons of CH=CH in the poly(vinylcyclopropane) main chain, prove the ring-opening polymerization of **5**. In addition, the product has only shown one glass-transition temperature T_g at 133.7 °C. This confirmed the formation of a copolymer **8**. If two homopolymers coexist, two glass-transition temperatures should

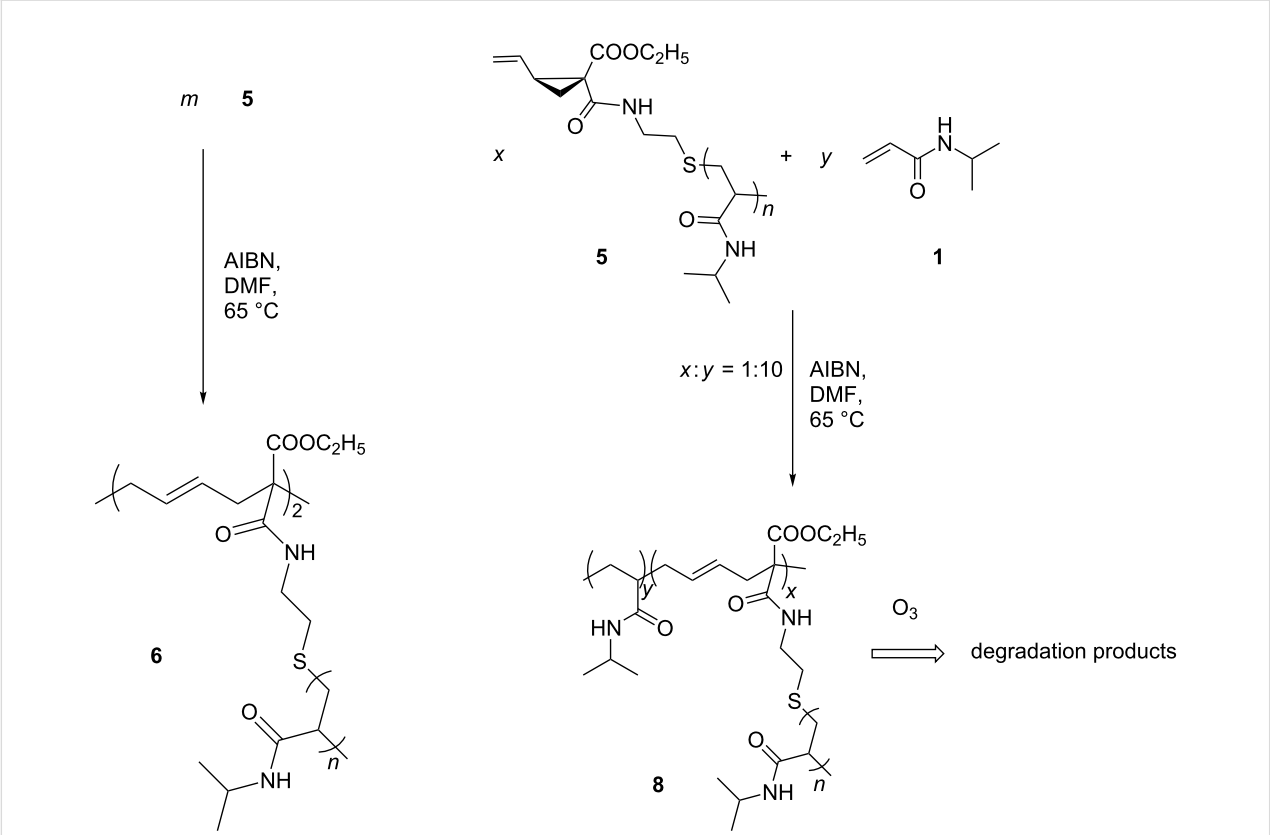

Scheme 4: Homo- and copolymerization of macromonomer **5**.

be measured. Both products **6** and **8** show the LCST behavior, respectively (Figure 2). After ozonolytic degradation of **8** in methanol, the disappearance of the protons of the double bond signal at δ 5.6 ppm in ^{1}H NMR spectrum and the appearance of the aldehyde protons at δ 8.5 ppm evidence the effective degradation of copolymer. The M_n of the degradation products amounts to 1.8×10^4 g/mol with DI equal to 2.2. Altogether, the successful ozonolytic degradation is proved.

Conclusion

A new macromonomer **5** was synthesized via amidation of 1-ethoxycarbonyl-2-vinylcyclopropane-1-carboxylic acid (**4**) with an amino-terminated poly(NiPAAm) **3** as an example. Thanks to its relative hydrophobic vinylcyclopropane unit, this water insoluble macromonomer **5** is able to form a host–guest complex with Me_2-β-CD, which is located at the polymerizable vinyl end group. This supramolecular complex **7** becomes completely water-soluble, so that a typical LCST effect could be observed. Since the bulky macromonomer **5** prefers to form only dimers in presence of a radical initiator rather than a homopolymer, a graft copolymer **8** was formed via radical ring-opening copolymerization of **5** and NiPAAm. The double bonds of the main chain can be cleaved simply by ozone treatment.

Experimental

All chemicals were commercially available and used as received without further purification. All solvents were distilled and dried over molecular sieve before use. ATR-FTIR-spectra were recorded with an FTIR-5SXB by Nicolet at room temperature. NMR spectra were recorded with an AVIII-300 instrument at 300 MHz at 25 °C. Tetramethylsilane (TMS) was used to calibrate the δ-scale. Chemical shifts were referenced to the residual solvent peaks (for example δ 2.09 ppm for acetone-d_6 and δ 2.22 ppm for D_2O). Dynamic light scattering (DLS) measurements were performed on a Malvern high performance particle sizer-extended temperature (HPPS-ET) instrument equipped with a He–Ne-laser and an Avalanche photodiode detector. The turbidity measurements were carried out using a power-regulated semiconductor laser (λ = 670 nm) and a silicon photodiode in a TP1 turbidity photometer from TEPPER-Analytik. Glass-transition temperatures (T_g) were measured using differential scanning calorimetry (DSC) with a Perkin-Elmer Model DSC-7 in nitrogen atmosphere; about 10 mg samples were used at a scan rate of 15 K/min. T_g was taken as the average of three measurements using the midpoint method. LCST were determined by transmission changes (at 500 nm) of the solutions heated at 1 °C/min^{-1} in a magnetically stirred cell;

values of the cloud points were defined as the temperature at which the deepest point of the derivative curve was achieved. MALDI-TOF MS was performed on a Bruker Ultraflex TDF mass spectrometer using a 337 nm nitrogen laser. GPC analyses were performed with a Viscotek GPC_{max} VE2001 using DMF as the eluent at 60 °C (flow rate: 1 mL/min). The ozonolysis was carried out on an ozone generator by Fischer Technology. In this ozone generator 45–50 liters of oxygen per hour was provided.

Synthesis of amino-terminated poly(*N*-isopropylacrylamide) **3**

A) In water: An aqueous solution of NiPAAm (12.45 g, 110 mmol) and 2-aminoethanethiol hydrochloride (0.31 g, 2.7 mmol) was deaerated with nitrogen bubbling for 1 h, and then, a 40 wt % aqueous solution of ammonium persulfate (0.62 g, 2.7 mmol) was added. The homogenous solution was stirred at room temperature (about 25 °C) for 4 h. After that, 1 mL Et_3N was dropped into the solution. Then, the solution was warmed to 40 °C and the polymer **3** precipitated thereby completely because of LCST. After filtration, washing with hot water for several times and drying, the polymer **3** (6.66 g, yield 54%) was obtained as a white powder.

B) In ethanol: A solution of NiPAAm (12.45 g, 110 mmol) and 2-aminoethanethiol hydrochloride (0.31 g, 2.7 mmol) in anhydrous ethanol (100 mL) was deaerated with nitrogen bubbling for 1 h. Subsequently, a solution of AIBN (54 mg, 0.33 mmol) in anhydrous ethanol (1 mL) was added. Afterwards, the solution was stirred at 65 °C for 12 h. Then, 1 mL of Et_3N was dropped into the solution. After evaporation of ethanol in vacuo the solid was dissolved in acetone. The precipitate formed was removed by filtration. The polymer **3** (8.17 g, yield 66%) was obtained as a white powder after it had been precipitated from ethanol in hexane, filtered off and dried.

FTIR (diamond) $\tilde{\nu}$ (cm^{-1}): 3436 (ν NH of NH_2), 3280 (ν NH of amide), 2970–2928 (ν CH aliphatic), 1655 (ν C=O, amide I), 1535 (δ NH, amide II); ^{1}H NMR (D_2O, 300 MHz) δ (ppm) 3.86 (*CH*NH), 2.85 (CH_2NH_2), 2.68 (CH_2CH_2S), 2.47 (*CH*CO), 2.10 (SCH_2CH), 1.41–1.01 (CH_2, CH_3).

Synthesis of macromonomer **5**

Ethoxycarbonyl-2-vinylcyclopropane-1-carboxylic acid (**4**) was synthesized following a procedure described in [32]. A solution of **3** (2 g) and **4** (0.5 g, 2.7 mmol) in 50 mL of anhydrous dichlormethane in a one-necked flask equipped with a calcium chloride drying tube was cooled to 0–5 °C. Subsequently, DCC (0.56 g, 2.7 mmol) in 2 mL anhydrous dichlormethane was slowly added. After a further 30 min at 0–5 °C the mixture was stirred for 24 h at room temperature. The precipitated dicyclohexylurea was filtered off and the organic solution was washed with three 20 mL portions of 5% HCl, three 20 mL portions of saturated $NaHCO_3$ solution and three 20 mL portions of water and then dried over Na_2SO_4. After precipitation from dichlormethane in hexane, the macromonomer **5** (1.72 g, yield 86%) was obtained as a white powder. FTIR (diamond) $\tilde{\nu}$ (cm^{-1}): 3280 (ν NH), 2970–2930 (ν CH aliphatic), 1726 (ν C=O of ester), 1639 (ν C=O, amide I), 1545 (δ NH, amide II); ^{1}H NMR (acetone-d_6, 300 MHz) δ (ppm) 7.13 (N*H*), 5.19–4.98 (CH_2=C*H*), 4.11 (COOCH_2), 3.85 (*CH*NH), 2.99 (C*H* of cyclopropane), 2.82 (CH_2NH_2), 2.68 (CH_2CH_2S), 2.47 (*CH*CO), 2.10 (SCH_2CH), 1.61–1.48 (CH_2 of cyclopropane), 1.40–1.01 (CH_2, CH_3).

Oligomerization of macromonomer **5** to **6**

A solution of **5** (0.7 g) in anhydrous DMF (50 mL) was deaerated with nitrogen bubbling for 1 h. Subsequently, a solution of AIBN (0.42 mg, 2.56 μmol) in anhydrous DMF (0.5 mL) was added. The polymerization was carried out at 65 °C for 12 h. The synthesized polymer **6** was purified by precipitation from DMF into diethylether. An amount of 0.37 g of **6** (yield 53%) was obtained as a white powder. FTIR (diamond) $\tilde{\nu}$ (cm^{-1}): 3291 (ν NH), 2970–2930 (υ CH aliphatic), 1726 (ν C=O of ester), 1636 (ν C=O, amide I), 1541 (δ NH, amide II); ^{1}H NMR (D_2O, 300 MHz) δ (ppm) 5.5 (C*H*=C*H*), 4.01 (COOCH_2), 3.80 (*CH*NH), 2.88 (CH_2NH_2), 2.70 (CH_2CH_2S), 2.52 (*CH*CO), 2.28 (SCH_2CH), 1.45–0.95 (CH_2, CH_3).

Copolymerization of macromonomer **5** with NiPAAm to **8**

A solution of **5** (0.7 g, 0.06 mmol) and NiPAAm (68.6 mg, 0.6 mmol) in anhydrous DMF (10 mL) was deaerated with nitrogen bubbling for 1 h. Subsequently, a solution of AIBN (0.2 mg, 1.32 μmol) in anhydrous DMF (0.2 mL) was added. The polymerization was carried out at 65 °C for 24 h. After removal of the solvent under reduced pressure the polymeric material was dissolved in water, dialyzed for three days at rt and then freeze-dried. An amount of 0.5 g of **8** (yield 65.1%) was obtained. FTIR (diamond) $\tilde{\nu}$ (cm^{-1}): 3331 (ν NH), 2970–2930 (ν CH aliphatic), 1728 (ν C=O of ester), 1655 (ν C=O, amide I), 1561 (δ NH, amide II); ^{1}H NMR (D_2O, 300 MHz) δ (ppm) 5.6 (C*H*=C*H*), 4.21 (COOCH_2), 3.85 (*CH*NH), 2.89 (CH_2NH_2), 2.72 (CH_2CH_2S), 2.55 (*CH*CO), 2.28 (SCH_2CH), 1.55–1.05 (CH_2, CH_3).

Complex formation of **5** with Me_2-β-CD

Compound **5** (100 mg) was dispersed in 5 mL of distilled water at rt. While stirring, Me_2-β-CD was gradually added until a clear solution was obtained. Then, the amount of Me_2-β-CD that has been used was calculated; in this case ca. 500 mg, corresponding [Me_2-β-CD]/[**5**] ratio of about 0.02:1.

Ozonolysis of copolymer **8**

A condensation trap with 1 g of copolymer **8** is filled up with methanol until the inlet is immersed in the solution. The cold trap is connected with the ozone generator and flushed with nitrogen for 10 min. Then, the solution is cooled to −74 °C and finally flushed with oxygen. After starting the ozone generator the oxygen is converted to ozone. The ozonolysis continues until the solution turns blue due to the excess of ozone. After shutting off the ozone generator, the solution is flushed with nitrogen until it is colorless. Then, 4 mL of dimethyl sulfide (DMS) are added to the solution. The reaction mixture is stirred overnight at rt. Methanol is removed under reduced pressure. M_n = 1.8 × 10^4 g/mol, DI = 2.2; d_n = 5.2 nm.

References

1. Pooley T., S. A.; Rivas, B. L.; San Martín, C. *J. Chil. Chem. Soc.* **2003,** *48,* 85–88. doi:10.4067/S0717-97072003000100015
2. Rempp, P. F.; Franta, E. Macromonomers: Synthesis, characterization and applications. *Polymerization Reactions;* Advances in Polymer Science, Vol. 58; 1984; pp 1–53. doi:10.1007/3-540-12793-3_6
3. Stephan, T.; Muth, S.; Schmidt, M. *Macromolecules* **2002,** *35,* 9857–9860. doi:10.1021/ma025711r
4. Hayashi, M.; Kojima, K.; Hirao, A. *Macromolecules* **1999,** *32,* 2425–2433. doi:10.1021/ma981673t
5. Nakawaga, O.; Kitayama, T.; Hatada, K. *Polym. Bull.* **2002,** *48,* 445–450. doi:10.1007/s00289-002-0053-8
6. Peruch, F.; Lahitte, J.-F.; Isel, F.; Lutz, P. J. *Macromol. Symp.* **2002,** *183,* 159–164. doi:10.1002/1521-3900(200207)183:1<159::AID-MASY159>3.0.CO;2-7
7. Eguiburu, J.; Fernandez-Berridi, M. J.; San Román, J. *Polymer* **1996,** *37,* 3615–3622. doi:10.1016/0032-3861(96)00184-X
8. Furch, M.; Eguiburu, J. L.; Fernandez-Berridi, M. J.; San Román, J. *Polymer* **1998,** *39,* 1977–1982. doi:10.1016/S0032-3861(97)00481-3
9. Wenz, G. *Angew. Chem.* **1994,** *106,* 851–870. doi:10.1002/ange.19941060804
10. Ley, S. V.; Priepke, H. W. M.; Warriner, S. L. *Angew. Chem.* **1994,** *106,* 2410–2412. doi:10.1002/ange.19941062226
11. Villiers, A. *C. R. Hebd. Seances Acad. Sci.* **1891,** 536–538.
12. Schardinger, F. Z. *Z. Unters. Nahr.- Genußm. Gebrauchsgegenstände* **1903,** *6,* 865–880.
13. Sakurai, M.; Kitagawa, M.; Hoshi, H.; Inoue, Y.; Chûjô, R. *Carbohydr. Res.* **1990,** *198,* 181–191. doi:10.1016/0008-6215(90)84291-2
14. Saenger, W. *Structural Aspects of Cyclodextrins and their Inclusion Complexes;* Academic Press: London, 1984.
15. Lindner, K.; Saenger, W. *Angew. Chem.* **1978,** *90,* 738–740. doi:10.1002/ange.19780900932
16. Lindner, K.; Saenger, W. *Carbohydr. Res.* **1982,** *99,* 103–115. doi:10.1016/S0008-6215(00)81901-1
17. Wenz, G., Ed. *Inclusion Polymers;* Advances in Polymer Science, Vol. 222; Springer: Berlin, Heidelberg, 2009. doi:10.1007/978-3-642-01410-9
18. Kretschmann, O.; Choi, S. W.; Miyauchi, M.; Tomatsu, I.; Harada, A.; Ritter, H. *Angew. Chem., Int. Ed.* **2006,** *45,* 4361–4365. doi:10.1002/anie.200504539
19. Harada, A.; Hashidzume, A.; Takashima, Y. Cyclodextrin-Based Supramolecular Polymers. *Supramolecular Polymers Polymeric Betains Oligomers;* Advances in Polymer Science, Vol. 201; 2006; pp 1–43. doi:10.1007/12_056
20. Amajjahe, S.; Ritter, H. *Macromolecules* **2008,** *41,* 3250–3253. doi:10.1021/ma702593s
21. Wang, Z.; Takashima, Y.; Yamaguchi, H.; Harada, A. *Org. Lett.* **2011,** *13,* 4356–4359. doi:10.1021/ol201575x
22. Takashima, Y.; Osaki, M.; Ishimaru, Y.; Yamaguchi, H.; Harada, A. *Angew. Chem., Int. Ed.* **2011,** *50,* 7524–7528. doi:10.1002/anie.201102834
23. Harada, A.; Kawaguchi, Y.; Nishiyama, T.; Kamachi, M. *Macromol. Rapid Commun.* **1997,** *18,* 535–539. doi:10.1002/marc.1997.030180701
24. Yamaguchi, H.; Kobayashi, R.; Takashima, Y.; Hashidzume, A.; Harada, A. *Macromolecules* **2011,** *44,* 2395–2399. doi:10.1021/ma200398y
25. Oi, W.; Hashidzume, A.; Harada, A. *Polymer* **2011,** *52,* 746–751. doi:10.1016/j.polymer.2010.12.027
26. Moszner, N.; Völkel, T.; Zeuner, F.; Rheinberger, V. *Macromol. Symp.* **2000,** *153,* 151–159. doi:10.1002/1521-3900(200003)153:1<151::AID-MASY151>3.0.CO;2-H
27. Moszner, N.; Zeuner, F.; Völkel, T.; Rheinberger, V. *Macromol. Chem. Phys.* **1999,** *200,* 2173–2187. doi:10.1002/(SICI)1521-3935(19991001)200:10<2173::AID-MACP2173>3.0.CO;2-A
28. Choi, S. W.; Hessamian, A.; Tabatabai, M.; Fischer, U. K.; Moszner, N.; Ritter, H. *e-Polym.* **2005,** 078.
29. Alupei, V.; Ritter, H. *e-Polym.* **2002,** 051.
30. Okazaki, T.; Sanda, F.; Endo, T. *Macromolecules* **1995,** *28,* 6026–6028. doi:10.1021/ma00122a007
31. Sugiyama, J.; Ohashi, K.; Ueda, M. *Macromolecules* **1994,** *27,* 5543–5546. doi:10.1021/ma00098a005
32. Alupei, V.; Ritter, H. *Macromol. Rapid Commun.* **2001,** *22,* 1349–1353. doi:10.1002/1521-3927(20011101)22:16<1349::AID-MARC1349>3.0.CO;2-T
33. Hosomi, A.; Mikami, M.; Sakurai, H. *Bull. Chem. Soc. Jpn.* **1983,** *56,* 2784–2794. doi:10.1246/bcsj.56.2784
34. Strotmann, F.; Bezdushna, E.; Ritter, H.; Galla, H. J. *Adv. Eng. Mater.* **2011,** *13,* B172–B180. doi:10.1002/adem.201080104

Beilstein Journal of Organic Chemistry

Mannose-decorated cyclodextrin vesicles: The interplay of multivalency and surface density in lectin–carbohydrate recognition

Ulrike Kauscher and Bart Jan Ravoo*

Full Research Paper

Open Access

Address:
Organic Chemistry Institute, Westfälische Wilhelms-Universität Münster, Corrensstraße 40, 48149 Münster, Germany

Email:
Bart Jan Ravoo* - b.j.ravoo@uni-muenster.de

* Corresponding author

Keywords:
carbohydrates; cyclodextrins; lectins; molecular recognition; multivalency; vesicles

Beilstein J. Org. Chem. **2012,** *8,* 1543–1551.
doi:10.3762/bjoc.8.175

Received: 25 May 2012
Accepted: 17 August 2012
Published: 17 September 2012

This article is part of the Thematic Series "Superstructures with cyclodextrins: Chemistry and applications".

Guest Editor: H. Ritter

Abstract

Cyclodextrin vesicles are versatile models for biological cell membranes since they provide a bilayer membrane that can easily be modified by host–guest interactions with functional guest molecules. In this article, we investigate the multivalent interaction of the lectin concanavalin A (ConA) with cyclodextrin vesicles decorated with mannose–adamantane conjugates with one, two or three adamantane units as well as one or two mannose units. The carbohydrate–lectin interaction in this artificial, self-assembled glycocalyx was monitored in an agglutination assay by the increase of optical density at 400 nm. It was found that there is a close relation between the carbohydrate density at the cyclodextrin vesicle surface and the multivalent interaction with ConA, and the most efficient interaction (i.e., fastest agglutination at lowest concentration) was observed for mannose–adamantane conjugates, in which both the cyclodextrin–adamantane and the lectin–mannose interaction is inherently multivalent.

Introduction

The surface modification of materials with carbohydrates has attracted much attention due to the fact that such materials can be compared to and compatible with the cell surface [1]. The "glycocalyx" is a dense layer on the surface of the cell, which serves as a responsive interface with its environment and also serves as a natural protective shield. The glycocalyx consists of various numbers and arrangements of polysaccharides and is found in eukaryotic as well as in prokaryotic cells. A well-known example of the pivotal role of oligosaccharides on cell surfaces is the fact that human blood types (A, B, AB and 0) are solely determined by minor changes in the composition of the erythrocyte glycocalyx. Additionally, many biological mecha-

nisms are mediated by multivalent recognition of carbohydrates. For example, lectins are proteins that bind to specific carbohydrates on the cell surface and activate biochemical responses [2]. In this way, protein–carbohydrate interactions regulate cell division, protein synthesis, the immune system, and the adhesion of cells. A well-known lectin is concanavalin A (ConA), which can be readily obtained from jack-beans. It has four identical binding sides and binds α-mannose, α-glucose and their derivatives. Because of the importance of carbohydrates and their multivalent recognition by lectins in physiological processes, they are also considered a promising tool for the development of drug-delivery systems [3].

Synthetic bilayer vesicles are a versatile model for biological cell membranes, and there are a substantial number of reports on synthetic glycolipids that mimic the glycocalyx [4-23]. Multivalent guest interaction with the surface of the vesicles has become a useful system to investigate recognition, adhesion and fusion of biological cell membranes [24-26]. In this context, amphiphilic cyclodextrins are a promising platform due to their ability to form stable bilayer vesicles that can be functionalized by self-assembly [27]. To this end, cyclodextrins are modified with long alkyl chains ("tails") and short oligo(ethylene glycol) head groups. These macrocyclic amphiphiles form unilamellar bilayer vesicles in aqueous solution upon hydration of a thin film cast by evaporation from organic solution and extrusion through a 0.1 μm polycarbonate membrane [27]. The cavities of each cyclodextrin are available to form inclusion complexes with hydrophobic guest molecules. Adamantane is known to be an excellent guest for β-cyclodextrin cavities (K_a = (2–3) × 10^4 M^{-1}). We were able to recently demonstrate the interaction of monovalent bifunctional guest molecules, containing a maltose or lactose unit and an adamantane unit, with cyclodextrin vesicles, and their ability to agglutinate with lectins [28]. We also showed that agglutination requires a critical density of carbohydrate ligand on the cyclodextrin vesicle surface [29]. In this work we investigate the influence of multivalent recognition by guest molecules with an increasing number of adamantane and mannose units. It is our hypothesis that more adamantane units in the guest molecule lead to higher affinity for the cyclodextrin vesicles due to multivalent interaction at the vesicle surface. In addition, we increased the number of mannose units in the guest molecule, assuming that a high density of carbohydrate is essential for multivalent lectin binding at the vesicle surface.

Results and Discussion

Four different guest molecules were synthesized to study the effect of multivalency, each with a distinct number of adamantane or mannose functions. The adamantane unit can bind into the cavity of cyclodextrins embedded at the vesicle surface. Additionally, all guest molecules possess α-mannose units, which bind to lectins such as concanavalin A (ConA, Figure 1). Guest **1** contains a single mannose and a single adamantane unit. Guest **2** and guest **3** contain a single mannose and two or three adamantane units, respectively. Guest **4** contains two mannose as well as two adamantane units. The synthesis of **1**–**4** is described in Supporting Information File 1. The analytical data for **1**–**4** are fully consistent with their molecular structure. The synthesis of amphiphilic β-cyclodextrin **5** has been reported previously [30]. Unilamellar vesicles with a diameter of 100–150 nm are obtained by extrusion [27,30].

To investigate the ability of adamantane functions to bind into the cavity of cyclodextrins, the synthesized guest molecules were investigated regarding their 1:1 complexation behavior towards β-cyclodextrin. Isothermal titration calorimetry (ITC) was carried out with β-cyclodextrin and each of the synthesized guest molecules **1**–**4**. The concentrations were chosen to provide one cyclodextrin cavity for each adamantane unit and are displayed in Table 1. The effective adamantane concentration describes the concentration of adamantane units. A guest with two adamantane units (**2** or **4**) results in an effective adamantane concentration that is twice the concentration of the divalent guest molecule. For guest **3**, the effective adamantane concentration is three times the concentration of the trivalent guest molecule. The results of these titrations can be seen in Table 1 and Figure 2.

The thermodynamic parameters of guests **1**–**4** are characteristic of the formation of a 1:1 inclusion complex of each adamantane unit with β-cyclodextrin. Based on the effective adamantane concentration, the stoichiometry, the binding constants, and the thermodynamic parameters (negative ΔH and positive ΔS) are very similar for each guest, with the exception of guest **3**. This implies that in guests **1**, **2** and **4**, each and every adamantane unit is able to complex a β-cyclodextrin host molecule independent of the other adamantanes on the guest molecule. A significant deviation of this behavior is observed only for guest **3**, which carries three adamantane units. In this case, the stoichiometry appears to be less than 1:1, the binding constant is somewhat lower, and the thermodynamic parameters are different (notably, ΔS is negative). This observation can be explained by steric hindrance in the trivalent host–guest complex: apparently, three β-cyclodextrins are too large to interact efficiently with each of the three adamantane units. The steric bulk of the cyclodextrins hinders the deep intrusion of adamantane functions into the cavity (Figure 3).

The results of the titration calorimetry show that each adamantane on guests **1**–**4** is able to bind to β-cyclodextrin. Accordingly, the guest molecules are expected to form inclusion

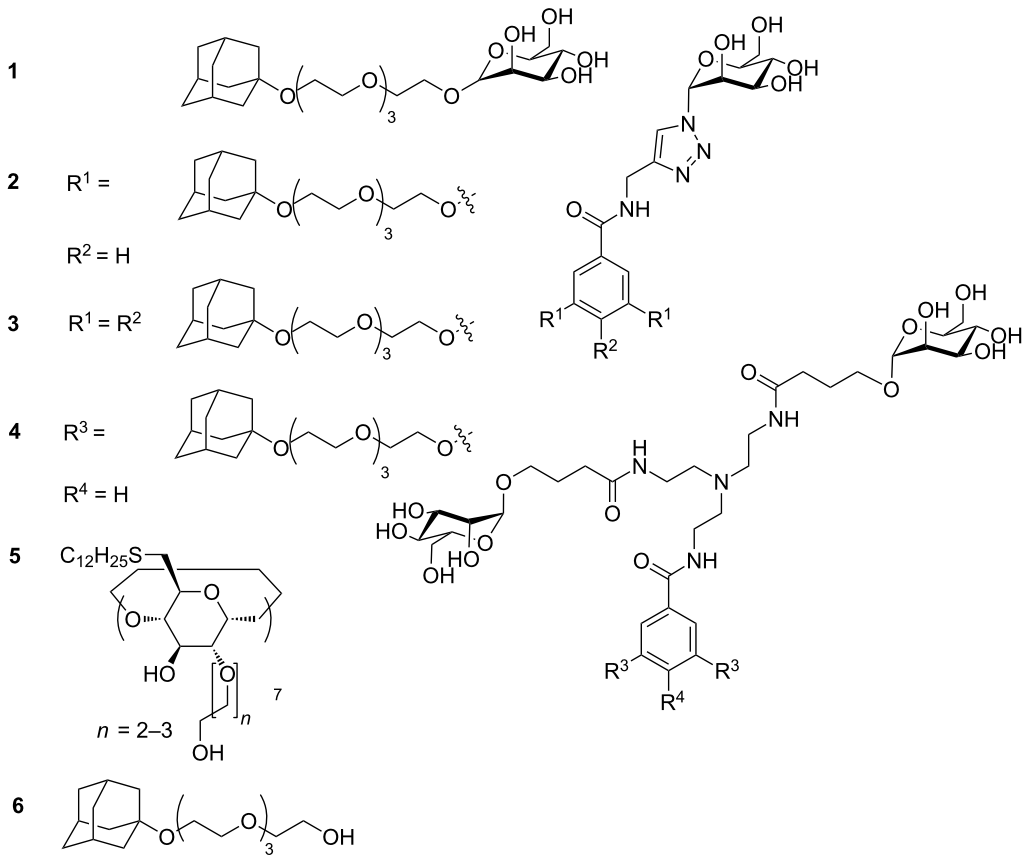

Figure 1: Mannose–adamantane conjugates **1**–**4** and amphiphilic cyclodextrin **5**.

Table 1: Thermodynamic parameters measured with isothermal titration calorimetry.

compound	host	[guest][a] mM	[host] mM	Δ*H* kJ/mol	Δ*G* kJ/mol	Δ*S* J/(K·mol)	K_a M^{-1}
1	β-CD	5.00	0.41	−18.93	−27.71	29.47	7.2×10^4
2[b]	β-CD	0.38	5.0	−16.96	−25.98	30.28	3.6×10^4
3[b]	β-CD	0.29	3.6	−28.78	−23.47	−17.82	1.3×10^4
4	β-CD	20.0	2.4	−12.62	−24.59	40.19	2.1×10^4

[a]Effective adamantane concentration. [b]Due to the low solubility of guest molecules the titration was carried out in reverse mode (host added to guest).

complexes at the surface of vesicles of amphiphilic cyclodextrin **5**. More importantly, guest molecules **2**–**4** are expected to form multivalent host–guest complexes with a much higher effective binding constant than the monovalent binding constant reported in Table 1. According to a quantitative treatment of multivalent host–guest interactions at surfaces, it may be expected that for a 1:1 monovalent interaction with a binding constant of $\approx 10^4$ M^{-1}, a divalent interaction can have an apparent binding constant of $\approx 10^7$ M^{-1} and a trivalent interaction can lead to an apparent binding constant of $\approx 10^{10}$ M^{-1} [31].

In view of the high affinity binding of the (multivalent) guest molecules **1**–**4** and assuming that these polar molecules are not able to permeate through the membrane, it is our hypothesis that even at submillimolar concentrations of guest **1**–**4** and host **5**, most guest molecules are confined to the outer vesicle surface. Moreover, since in all experiments the effective guest concentration is only half of the host concentration, it can be assumed that most cyclodextrin cavities at the vesicle surface are occupied by an adamantane unit. As a consequence, the density of mannose molecules on the surface of the vesicles is expected to be relatively high, resulting in the formation of an artificial

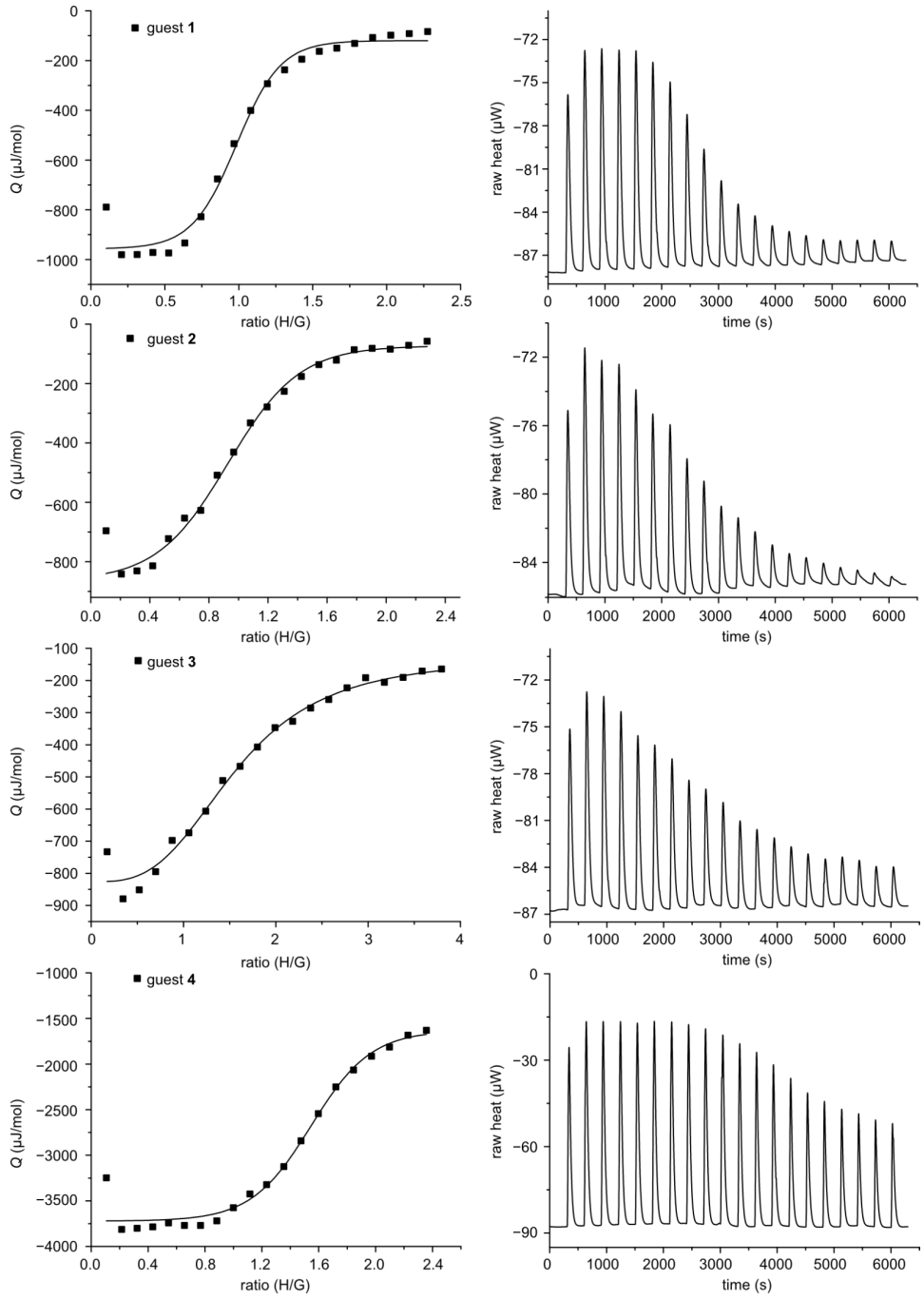

Figure 2: Integrated peak area (left) and raw titration curves (right) for the ITC measurements of **1**–**4** with β-CD. The concentrations used are listed in Table 1.

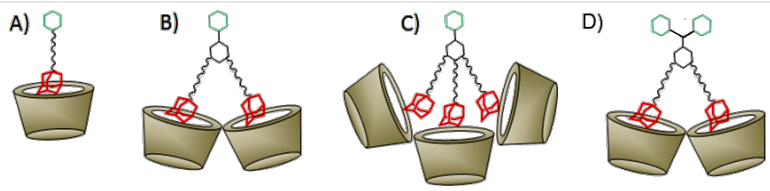

Figure 3: Schematic presentation of the binding between β-cyclodextrin and (A) monovalent guest **1**, (B) divalent guest **2**, (C) trivalent guest **3**, and (D) divalent guest **4**.

glycocalyx by self-assembly. Therefore, the addition of the lectin ConA should lead to agglutination of the vesicles due to the specific interaction of mannose and ConA at the vesicle surface. Optical density measurements were carried out at a wavelength of 400 nm to investigate the agglutination behavior of each guest molecule.

In the case of monovalent guest **1**, a typical time-dependent agglutination was found due to the specific interaction of ConA with mannose at the cyclodextrin vesicle surface (Figure 4). In these experiments, the concentration of cyclodextrin **5** was 0.2 mM and the concentration of guest **1** was 0.1 mM. It was also found that agglutination can be gradually suppressed by the substitution of guest **1** by an "inert" guest (adamantyl tetraethyleneglycol, **6**) that binds cyclodextrin but not ConA (Figure 4). It is evident that as the surface density of mannose is decreased in the glycocalyx, the effective separation of mannose ligands increases, and hence the multivalent interaction of mannose and ConA is suppressed. In fact, a critical threshold is observed around a mannose surface density of 50%: if the mannose density is reduced even further, the average distance of the mannose units on the vesicle surface is larger than the binding site separation of ConA, and hence multivalent interaction is no longer observed. The average distance between two cyclodextrins at the vesicle surface is approximately 2.2 nm [30]. The distance between two mannose molecules is expected to be the same when using a maximum surface coverage of the cyclodextrin host surface with guest **1**. The binding site separation for ConA is 3.6 to 4.9 nm [21,22], which roughly corresponds to the average spacing of mannose at 50% surface coverage of guest **1**. These observations are entirely consistent with our previous investigation of an artificial glycocalyx of lactose and maltose and its interaction with ConA and peanut agglutinin (PNA) [28,29].

Interestingly, if guests **2**–**4** (0.1 mM adamantane) were added to cyclodextrin vesicles (0.2 mM) an aggregation effect was detected even in the absence of ConA (Figure 5). This effect is due to noncovalent cross-linking of the vesicles by guest **2**–**4**. Each of the adamantane units on guest **2**–**4** can bind to a different cyclodextrin vesicle (intervesicular binding) and hence cause vesicle aggregation. We have previously observed this effect for homobifunctional guest molecules equipped with two azobenzene, methylbenzoyl, or *tert*-butylbenzyl groups [32-34]. It should be noted that in the case of guest **3** the aggregation due to cross-linking is much smaller, almost invisible, compared to the effect found for guests **2** and **4**. This can possibly be explained by the orientation of the adamantane units in the guest molecules. Guests **2** and **4** have two adamantane units and the average distance between these units is significantly larger than the average distance of the three adamantane units in guest **3**. We propose that due to the adjacency in the case of guest **3**, the binding of one adamantane unit directs the other two units to bind to the same vesicle (intravesicular binding), whereas the larger distance between the adamantane units in guest **2** and **4** allows the adamantane functions to bind to different vesicles (intervesicular binding). As discussed above for guest **1**, the surface density of guests **2**–**4** can be reduced by replacement with "inert" guest **6**. It can be seen from Figure 5 that addition of a substantial amount of this inert competitor effectively reduces the tendency to cross-link the vesicles. As can be seen in the plot of the maximum agglutination induced by guest **2**, a linear dependence (rather than a threshold) between the guest surface coverage and the extent of aggregation is observed. If a higher percentage of cross-linker is present on the vesicle surface, more noncovalent cross-links between vesicles are formed and more extensive aggregation is observed.

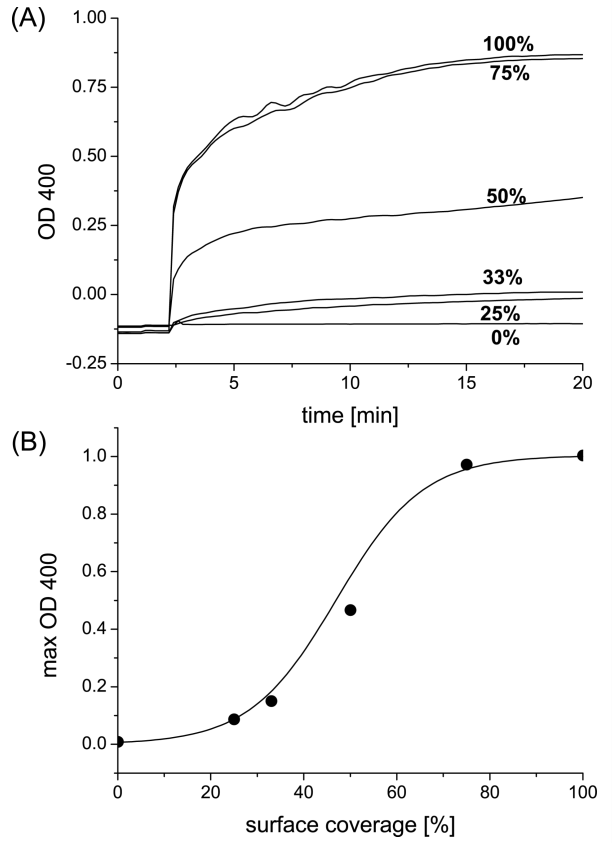

Figure 4: (A) Agglutination of β-cyclodextrin vesicles in the presence of monovalent guest **1** and ConA. The surface coverage of guest **1** is gradually reduced by substitution with "inert" guest **6**. Concentrations: [5] = 0.2 mM, [1] = 0–0.1 mM, [6] = 0–0.1 mM, [ConA] = 0.1 mg/mL. (B) Maximum agglutination depending on surface coverage of guest **1**.

In line with the observations discussed above, a tenfold dilution of the concentration of host ([5] = 20 μM) and guest ([2] = [4] = 5.0 μM and [3] = 3.3 μM) results in a complete suppression of

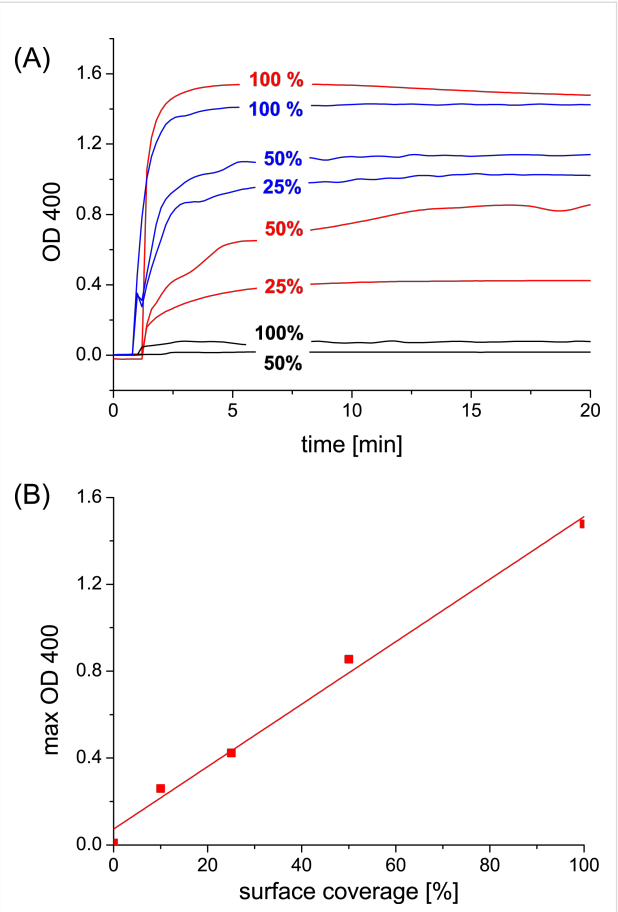

Figure 5: (A) Agglutination dependence of β-cyclodextrin vesicles in the presence of guests **2**–**4**. Legend: red = guest **2**, black = guest **3**, blue = guest **4**. The surface coverage of guests **2**–**4** is gradually reduced by substitution with "inert" guest **6**. Concentrations: [5] = 0.2 mM, [2] = 0–0.05 mM, [3] = 0–0.033 mM, [4] = 0–0.05 mM, [6] = 0–0.075 mM. (B) Maximum agglutination depending on surface coverage of guest **2**.

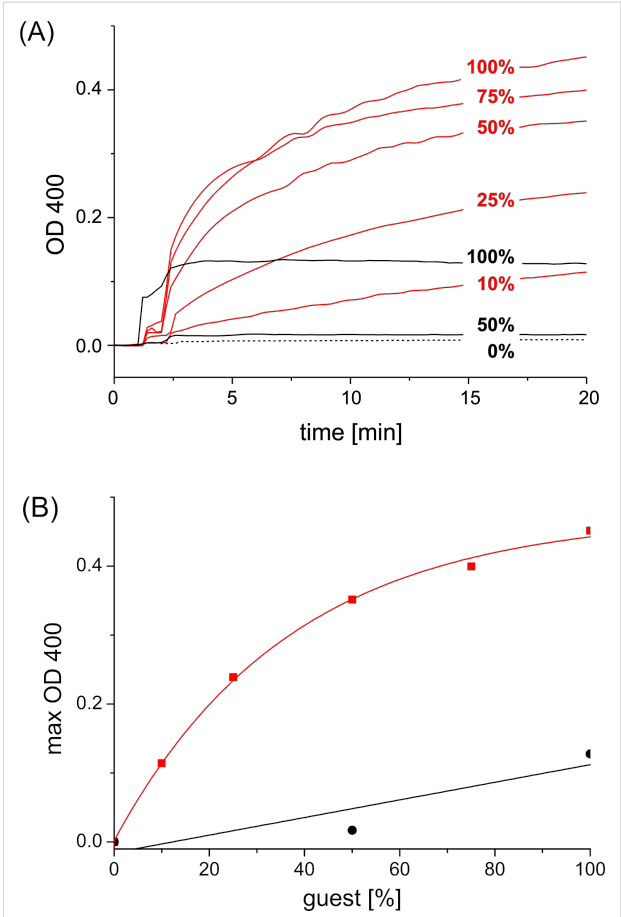

Figure 6: (A) Agglutination of β-cyclodextrin vesicles in the presence of guest **2** or **3** and ConA. Legend: red = guest **2**, black = guest **3**. The surface coverage of guests **2** and **3** is gradually reduced by substitution with "inert" guest **6**. Concentrations: [5] = 20 μM, [2] = 0–5.0 μM, [3] = 0–3.3 μM, [6] = 0–10 μM; [ConA] = 0.1 mg/mL. (B) Maximal aggregation depending on surface coverage of guest **2** or **3**.

cross-linking of the vesicles. Apparently, at this concentration intravesicular binding is favored over intervesicular binding, and vesicle aggregation is negligible. These findings are again consistent with earlier observations [32]. Hence, in this concentration window the agglutination in the presence of ConA can be investigated. Indeed, cyclodextrin vesicles functionalized with guests **2**–**4** aggregate in the presence of ConA. However, the extent and rate of agglutination is very different for each guest. The observations for divalent guest **2** and trivalent guest **3** are shown in Figure 6.

Perhaps counter intuitively, the extent of agglutination *decreases* with an increasing number of adamantane functions present in the guest molecule. In other words, agglutination is less efficient for **3** compared to **2** in spite of the higher surface affinity of trivalent guest **3** compared to divalent guest **2**. This observation can be explained by the density of mannose on the surface of the vesicles. The average distance between two cyclodextrins at the vesicle surface is approximately 2.2 nm [30]. The distance between two mannose molecules d_{CH} is expected to be the same when using a 100% surface coverage of cyclodextrin vesicles with monovalent guest **1**. A decrease in the surface density of mannose due to replacement of guest **1** by "inert" guest **6** decreases the agglutination by ConA (see Figure 4 and Figure 7) since eventually the average spacing of mannose on the vesicle surface (d_{CH}) exceeds the binding-site separation of ConA (d_{BS}) [21]. However, the surface density of mannose also decreases if the guest molecule occupies two or even three cyclodextrin cavities but yet carries only one mannose unit (Figure 7).

In the case of divalent guest **2** (with two adamantane units and a single mannose) the maximum surface density of mannose is only half of the surface density that can be achieved with monovalent guest **1**. As a consequence, the average distance d_{CH} of

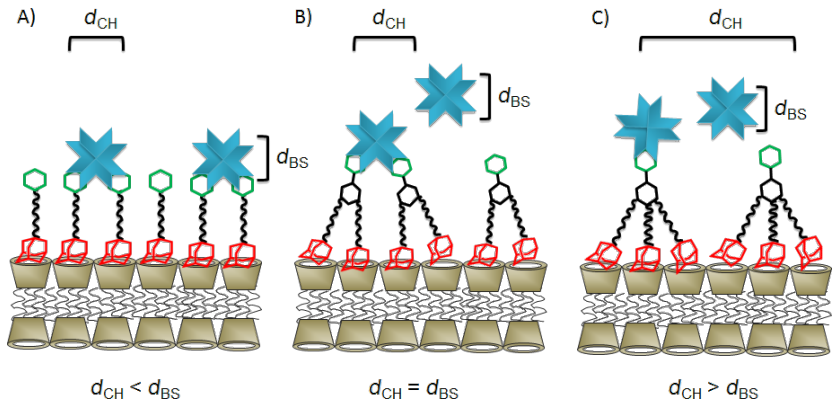

Figure 7: Schematic presentation of the binding of (A) a monovalent, (B) a divalent, or (C) a trivalent guest onto the surface of cyclodextrin vesicles and their interaction with ConA. d_{CH}: average spacing of carbohydrates, d_{BS}: effective binding-site separation of ConA.

the mannose residues is similar to the effective binding-site separation of ConA, and agglutination is quite efficient. However, it can be seen that although agglutination can be completely suppressed by replacement with guest **6**, the concentration dependence is completely different from that observed for guest **1**: rather than showing a threshold value, agglutination persists even at a rather low percentage of guest **2** compared to inert guest **6**. In the case of trivalent guest **3** (with three adamantane units and a single mannose) the maximum surface density of mannose on the cyclodexrin vesicle is only one third of the maximum surface density for guest **1**. As a consequence, the average distance of the mannose residues exceeds the effective binding-site separation of ConA, and very little agglutination is observed upon addition of ConA. Thus, it could be said that more adamantane units in the guest molecule in fact diminish the agglutination by ConA, since they result in a substantially lower surface coverage of mannose.

Finally, we investigated the agglutination behavior of cyclodextrin vesicles decorated with guest **4**. Guest **4** contains two adamantane units as well as two mannose residues. A 100% surface coverage of the cyclodextrin vesicles with guest **4** is therefore expected to give an average distance of 2.2 nm between the mannose functions, similar to the average spacing obtained for guest **1**. However, due to the inherent multivalency of guest **4**, it should have a much higher affinity both for the cyclodextrin vesicle surface as well as for ConA. Indeed it was found that guest **4** ([4] = 10 μM) can induce the agglutination of cyclodextrin vesicles ([5] = 20 μM) in the presence of ConA. Figure 8 shows the results of the optical density measurements for guest **4** compared to guest **2**. It can be seen that the extent and rate of agglutination of the vesicles induced by guest **4** is substantially higher than for guest **2**, in particular at low surface coverage (i.e., below 50 %). At higher surface coverage, the rate of agglutination is much higher for guest **4**, but the extent of agglutination is similar. These observations can be rationalized as illustrated in Figure 9. Since guest **4** has two mannose units, it can bind in a divalent fashion to ConA

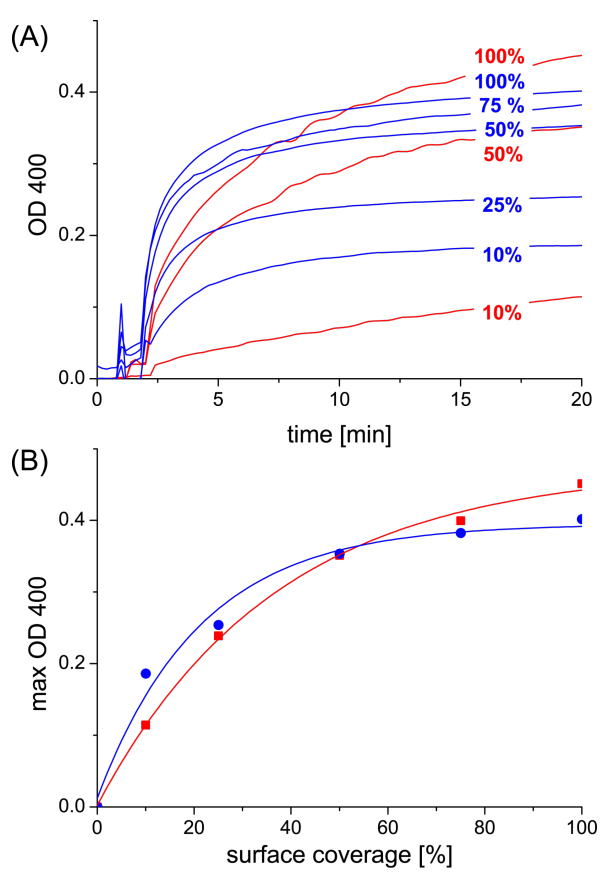

Figure 8: (A) Agglutination of β-cyclodextrin vesicles in the presence of guest **2** or **4** and ConA. Legend: red = guest **2**, blue = guest **4**. The surface coverage of guests **2** and **4** is gradually reduced by substitution with "inert" guest **6**. Concentrations: [5] = 20 μM, [2] = 0–5.0 μM: [4] = 0–5.0 μM, [6] = 0–10 μM; [ConA] = 0.1 mg/mL. (B) Maximal aggregation depending on surface coverage of guest **2** or **4**.

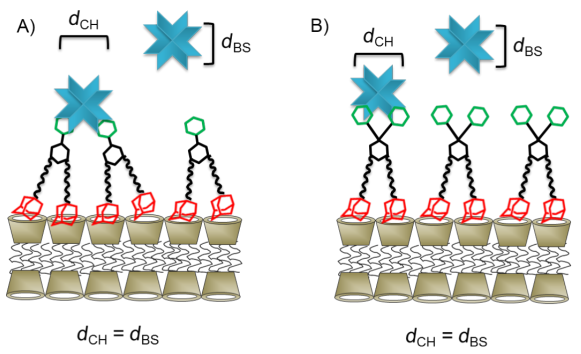

Figure 9: Schematic presentation of the binding of guest molecules with (A) one or (B) two mannose functions onto the surface of cyclodextrin vesicles and their interaction with ConA. d_{CH}: average spacing of carbohydrates, d_{BS}: effective binding site separation of ConA.

irrespective of the surface coverage. Nevertheless, the agglutination should still be surface coverage dependent, since multivalent intervesicular binding is more likely to occur when more mannose is presented on the cyclodextrin vesicles. Since guest **2** has only one mannose unit, one would expect that ConA can only bind in a divalent fashion to the cyclodextrin vesicle if the surface coverage is rather high. However, as can be seen from Figure 6 and Figure 8, the extent of agglutination can be very high (as high as for guest **4**) even at rather low surface coverage, albeit with a substantially lower rate of agglutination. These observations can be explained on the basis of a clustering of mannose residues in the mixed glycocalyx of guest **2** and "inert" guest **6**: clusters of guest **2** could offer multivalent "adhesive patches" for ConA even if the average surface coverage of guest **2** is far below 50%. The low rate of agglutination could be a consequence of a slow rearrangement of the glycocalyx, i.e., a "receptor-induced clustering" of mannose in the presence of ConA.

Conclusion

In this study we described a biomimetic model for the glycocalyx of a cell membrane based on multivalent adamantane–mannose conjugates that bind to cyclodextrin vesicles. In this dynamic supramolecular system the guest molecules bind with their adamantane units to the cyclodextrin cavity, which acts as a receptor, and as a consequence the vesicle surface is covered by mannose. In turn, the mannose units are ligands for the lectin ConA, which induces agglutination due to multivalent cross-linking of the vesicles. Strikingly, the multivalency of the guest molecules was found to have a detrimental effect on the glycocalyx: divalent and trivalent guest molecules can induce cross-linking of the vesicles even in the absence of ConA, and the interaction with ConA is reduced due to the lower surface coverage with mannose. The optimal binder therefore is a divalent guest molecule that carries two mannose residues: this molecule binds inherently divalent to the cyclodextrin vesicle surface as well as to ConA and, hence, is able to mediate fast agglutination at low overall concentration as well as low surface coverage. These findings should further the understanding of the complex and dynamic interactions of oligosaccharides on cell surfaces.

Experimental

Materials: Throughout this work, chemicals were used as received from Acros Organics (Schwerte, Germany) or Sigma-Aldrich Chemie (Taufkirchen, Germany) without further purification. The synthesis and analysis of guest molecule **1**–**4** is reported in Supporting Information File 1. Amphiphilic β-cyclodextrin **5** was synthesized as described in the literature [30].

Methods: Isothermal titration calorimetry (ITC) measurements were performed on a Nano-Isothermal Titration calorimeter III (model CSC 5300; Calorimetry Sciences Corporation, London, Utah, USA). All samples were measured in distilled water at 23 °C by using a stirring rate of 250 rpm. For each experiment 20 injections with 10 µL volume were carried out with a 250 µL syringe, into the measurement cell (V = 980.5 µL). Concentrations of host and guest molecules are reported in Table 1. β-Cyclodextrin vesicles are formed by extrusion of cyclodextrin **5** in a HEPES-buffer solution with a Liposofast manual extruder through a polycarbonate membrane with a pore size of 100 nm. Unilamellar vesicles with an average diameter of 100–140 nm are obtained [30,35]. Optical density measurements were performed in 1 mL small-volume disposable PMMA cuvettes at 400 nm by using an Uvikon 923 double-beam photospectrometer. All measurements were recorded at 23 °C in HEPES buffer (20 mM, pH 7.45) containing 1 mM $CaCl_2$ and 1 mM $MnCl_2$. Reagents were added in the following order: To 1 mL vesicle solution, 10 µL of guest molecule stock solution is added after 1 min, and 10 µL ConA stock solution after 2 min.

Supporting Information

Supporting Information File 1

Synthesis, NMR and mass spectra of guest molecules **1**–**4**.
[http://www.beilstein-journals.org/bjoc/content/supplementary/1860-5397-8-175-S1.pdf]

Acknowledgements

We acknowledge the synthesis of starting materials by Christian Wendeln. β-Cyclodextrin was kindly donated by Wacker Chemie AG.

References

1. Lindhorst, T. K. *Essentials of Carbohydrate Chemistry and Biochemistry;* Wiley-VCH: Weinheim, 2007.
2. Lis, H.; Sharon, N. *Chem. Rev.* **1998,** *98,* 637–674. doi:10.1021/cr940413g
3. Gabor, F.; Wirth, M. *STP Pharma Sci.* **2003,** *13,* 3–16.
4. Kitano, H.; Sodha, K.; Kosaka, A. *Bioconjugate Chem.* **1995,** *6,* 131–134. doi:10.1021/bc00031a016
5. Tagawa, K.; Sendai, N.; Ohno, K.; Kawaguchi, T.; Kitano, H.; Matsunaga, T. *Bioconjugate Chem.* **1999,** *10,* 354–360. doi:10.1021/bc980083x
6. Kitano, H.; Sumi, Y.; Tagawa, K. *Bioconjugate Chem.* **2001,** *12,* 56–61. doi:10.1021/bc000047+
7. Kitano, H.; Ishino, Y.; Yabe, K. *Langmuir* **2001,** *17,* 2312–2316. doi:10.1021/la000910u
8. Luzardo, M. D.; Lanio, M. E.; Alvarez, C.; Pazos, I. F.; Figueroa, S.; Vérez, V.; Disalvo, E. A. *Colloids Surf., B* **2002,** *26,* 281–289. doi:10.1016/S0927-7765(02)00009-7
9. Faivre, V.; de Lourdes Costa, M.; Boullanger, P.; Baszkin, A.; Rosilio, V. *Chem. Phys. Lipids* **2003,** *125,* 147–159. doi:10.1016/S0009-3084(03)00088-4
10. Guo, C. X.; Boullanger, P.; Liu, T.; Jiang, L. *J. Phys. Chem. B* **2005,** *109,* 18765–18771. doi:10.1021/jp052580y
11. Ballut, S.; Makky, A.; Loock, B.; Michel, J. P.; Maillard, P.; Rosilio, V. *Chem. Commun.* **2009,** 224–226. doi:10.1039/b816128c
12. Makky, A.; Michel, J. P.; Kasselouri, A.; Briand, E.; Maillard, P.; Rosilio, V. *Langmuir* **2010,** *26,* 12761–12768. doi:10.1021/la101260t
13. Bondurant, B.; Last, J. A.; Waggoner, T. A.; Slade, A.; Sasaki, D. Y. *Langmuir* **2003,** *19,* 1829–1837. doi:10.1021/la0262295
14. Mazzaglia, A.; Forde, D.; Garozzo, D.; Malvagna, P.; Ravoo, B. J.; Darcy, R. *Org. Biomol. Chem.* **2004,** 957–960. doi:10.1039/b400988f
15. Mazzaglia, A.; Valerio, A.; Villari, V.; Rencurosi, A.; Lay, L.; Spadaro, S.; Scolaro, L. M.; Micali, N. *New J. Chem.* **2006,** *30,* 1662–1668. doi:10.1039/b608495h
16. McNicholas, S.; Rencurosi, A.; Lay, L.; Mazzaglia, A.; Sturiale, L.; Perez, M.; Darcy, R. *Biomacromolecules* **2007,** *8,* 1851–1857. doi:10.1021/bm070055u
17. Lee, H.-K.; Park, K. M.; Jeon, Y. J.; Kim, D.; Oh, D. H.; Kim, H. S.; Park, C. K.; Kim, K. *J. Am. Chem. Soc.* **2005,** *127,* 5006–5007. doi:10.1021/ja042172s
18. Bandaru, N. M.; Sampath, S.; Jayaraman, N. *Langmuir* **2010,** *21,* 9591–9596. doi:10.1021/la051433o
19. Tamiaki, H.; Azefu, Y.; Shibata, R.; Sato, R.; Toma, K. *Colloids Surf., B* **2006,** *53,* 87–93. doi:10.1016/j.colsurfb.2006.08.001
20. Hassane, F. S.; Frisch, B.; Schuber, F. *Bioconjugate Chem.* **2006,** *17,* 849–854. doi:10.1021/bc050308l
21. Park, J.; Rader, L. H.; Thomas, G. B.; Danoff, E. J.; English, D. S.; DeShong, P. *Soft Matter* **2008,** *4,* 1916–1921. doi:10.1039/b806059b
22. Thomas, G. B.; Rader, L. H.; Park, J.; Abezgauz, L.; Danino, D.; DeShong, P.; English, D. S. *J. Am. Chem. Soc.* **2009,** *131,* 5471–5477. doi:10.1021/ja8076439
23. Noble, G. T.; Flitsch, S. L.; Liem, K. P.; Webb, S. J. *Org. Biomol. Chem.* **2009,** *7,* 5245–5254. doi:10.1039/b910976e
24. Kunitake, T. *Angew. Chem., Int. Ed. Engl.* **1992,** *31,* 709–7026. doi:10.1002/anie.199207091
25. Paleos, C. M.; Sideratou, Z.; Tsiourvas, D. *ChemBioChem* **2001,** *2,* 305–310. doi:10.1002/1439-7633(20010504)2:5<305::AID-CBIC305>3.0.CO;2-9
26. Voskuhl, J.; Ravoo, B. J. *Chem. Soc. Rev.* **2009,** *38,* 495–505. doi:10.1039/b803782p
27. Ravoo, B. J.; Darcy, R. *Angew. Chem., Int. Ed.* **2000,** *39,* 4324–4326. doi:10.1002/1521-3773(20001201)39:23<4324::AID-ANIE4324>3.0.CO;2-O
28. Voskuhl, J.; Stuart, M. C.; Ravoo, B. J. *Chem.–Eur. J.* **2010,** *16,* 2790–2796. doi:10.1002/chem.200902423
29. Vico, R. V.; Voskuhl, J.; Ravoo, B. J. *Langmuir* **2011,** *27,* 1391–1397. doi:10.1021/la1038975
30. Falvey, P.; Lim, C. W.; Darcy, R.; Revermann, T.; Karst, U.; Giesbers, M.; Marcelis, A. T. M.; Lazar, A.; Coleman, A. W.; Reinhoudt, D. N.; Ravoo, B. J. *Chem.–Eur. J.* **2005,** *11,* 1171–1180. doi:10.1002/chem.200400905
31. Huskens, J.; Mulder, A.; Auletta, T.; Nijhuis, C. A.; Ludden, M. J. W.; Reinhoudt, D. N. *J. Am. Chem. Soc.* **2004,** *126,* 6784–6797. doi:10.1021/ja049085k
32. Nalluri, S. K. M.; Ravoo, B. J. *Angew. Chem., Int. Ed.* **2010,** *49,* 5371–5374. doi:10.1002/anie.201001442
33. Nalluri, S. K. M.; Bultema, J. L.; Boekema, E. J.; Ravoo, B. J. *Chem.–Eur. J.* **2011,** *17,* 10297–10303. doi:10.1002/chem.201100789
34. Nalluri, S. K. M.; Bultema, J. L.; Boekema, E. J.; Ravoo, B. J. *Chem. Sci.* **2011,** *2,* 2383–2391. doi:10.1039/c1sc00422k
35. Torchilin, V.; Weissig, V. *Liposomes: A Practical Approach;* Oxford University Press: Oxford, 2003.

License and Terms

Beilstein Journal of Organic Chemistry

Supramolecular hydrogels formed from poly(viologen) cross-linked with cyclodextrin dimers and their physical properties

Yoshinori Takashima, Yang Yuting, Miyuki Otsubo, Hiroyasu Yamaguchi and Akira Harada*§

Full Research Paper

Open Access

Address:
Department of Macromolecular Science, Graduate School of Science, Osaka University, Toyonaka, Osaka 560-0043, Japan

Email:
Akira Harada* - harada@chem.sci.osaka-u.ac.jp

* Corresponding author
§ Telephone +81-6-6850-5445; Fax +81-6-6850-5445

Keywords:
cyclodextrins; poly(viologen); supramolecular hydrogel

Beilstein J. Org. Chem. **2012,** *8,* 1594–1600.
doi:10.3762/bjoc.8.182

Received: 28 May 2012
Accepted: 17 August 2012
Published: 20 September 2012

This article is part of the Thematic Series "Superstructures with cyclodextrins: Chemistry and applications".

Guest Editor: H. Ritter

Abstract

Supramolecular materials with noncovalent bonds have attracted much attention due to their exclusive properties differentiating them from materials formed solely by covalent bonds. Especially interesting are rotor molecules of topological complexes that shuttle along a polymer chain. The shuttling of these molecules should greatly improve the tension strength. Our research employs cyclodextrin (CD) as a host molecule, because CD effectively forms polyrotaxanes with polymers. Herein we report the formation of supramolecular hydrogels with an α-CD dimer (α,α-CD dimer) as a topological linker molecule, and a viologen polymer (VP) as the polymer chain. The supramolecular hydrogel of α,α-CD dimer/VP forms a self-standing gel, which does not relax ($G' > G''$) in the frequency range 0.01–10 rad·s^{-1}. On the other hand, the supramolecular hydrogel decomposes upon addition of bispyridyl decamethylene ($PyC_{10}Py$) as a competitive guest. Moreover, the β-CD dimer (β,β-CD dimer) with VP does not form a supramolecular hydrogel, indicating that complexation between the C_{10} unit of VP and the α-CD unit of the α,α-CD dimer plays an important role in the formation of supramolecular hydrogels.

Introduction

Development of functional soft materials has attracted much attention due to the numerous practical applications [1-3]. Typically, soft materials fall into one of two types of gels: physical gels and chemical gels [4-9]. Recently, topological cross-linked polyrotaxanes have been identified as tertiary gels, which should create a new paradigm in materials science [10]. Polyrotaxanes form topological gels, because the rotor molecules, which act as cross-linkers, slide on the axial polymer chain. In contrast, chemical gels do not exhibit cross-linker slippage.

Previously, there have been some reports of supramolecular complexes with cyclodextrin (CD) dimers. A supramolecular hydrogel, which was constructed by the formation of an inclusion complex between the copolymer with an adamantyl group

and CD dimer, showed a lower critical solution temperature (LCST) [11]. Another report indicated that adding selenium or platinum complexes yields supramolecular assemblies of bis(molecular tube)s cross-linked with the β-CD dimer, which form nanofibers [12-15]. Moreover, mechanically linked polyrotaxane with the α-CD and poly(ethylene glycol) (PEG) produces a hydrogel material, which exhibits unique physical properties [10].

Previously, we have prepared a polyrotaxane using α-CD and PEG [16,17]. The α-CD/PEG polyrotaxane forms a hydrogel material in high concentrations [18]. Using polyelectrolytes as threading molecules results in complexation between the polyelectrolyte and α-CD within the range of the ^{1}H NMR time scale due to the slow equilibrium [19,20]. Cationic groups, such as pyridinium and pyridylpyridinium terminal groups, inhibit the decomposition of polyrotaxane and stabilize the complexes between α-CD and cationic alkanediyl compounds [21-23]. Herein, to study the formation of supramolecular hydrogels with the α,α-CD dimer, we chose the viologen polymer (VP), which possesses multiple cations, as the axis molecules. Decamethylene units function as recognition sites of α-CD, and bipyridyls work as electric barriers.

Results and Discussion

Preparation of CD dimers and viologen derivatives

Figure 1 depicts the chemical structures of the cyclodextrin dimers (α,α-CD dimer, α,β-CD dimer, and β,β-CD dimer) and pyridyl derivatives ($PyC_{10}Py$ and viologen polymer (VP)). The α,α-CD and β,β-CD dimers are prepared by reacting the corresponding 6-amino-CDs and terephthalic acid using 4-(4,6-dimethoxy-1,3,5-triazin-2-yl)-4-methylmorpholinium chloride *n*-hydrate (DMT-MM) as a condensing reagent in DMF. The α,β-CD dimer is prepared by reacting 6-amino-α-CD and 6-*O*-(4-carboxylphenylamide)-β-CD using DMT-MM in DMF. These CD dimers are purified by preparative reversed-phase chromatography using DIAION HP-20 beads. As described in the experimental section, the reaction of 1,10-dibromodecane with 4,4'-bipyridyl in DMF gives VP, where the number of VP units is 20 and was determined by the ratio of integral values of the end group and the main chain unit in the ^{1}H NMR spectrum.

Hydrogelation between the CD dimer and viologen polymer

Mixing the α,α-CD dimer and VP in aqueous solutions at room temperature slightly increases the viscosity of the α,α-CD

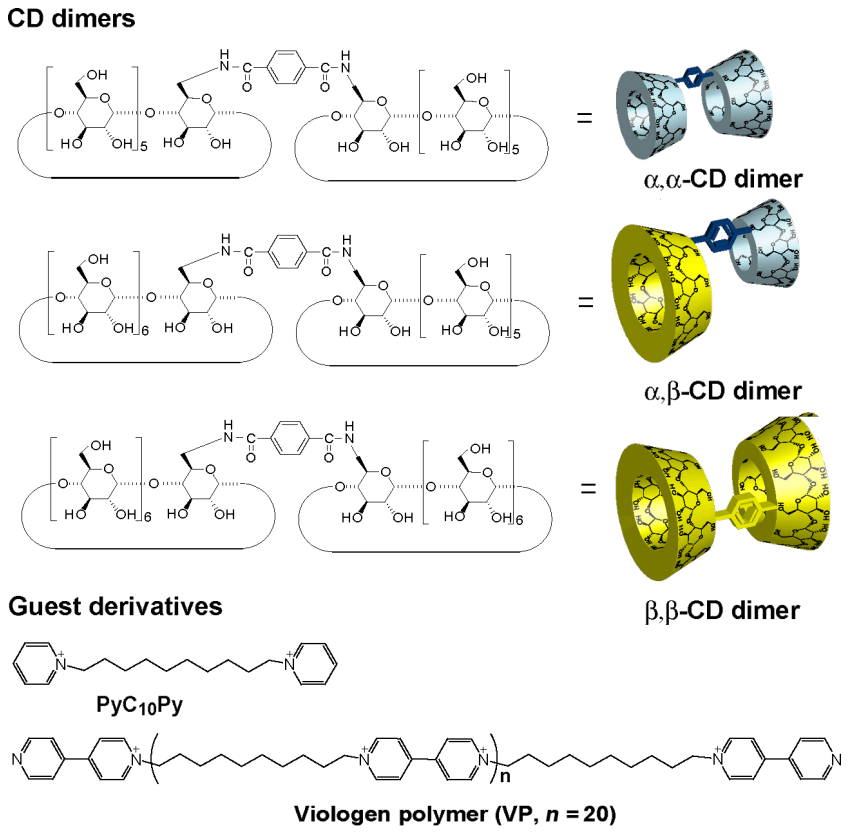

Figure 1: Chemical structures of the CD dimer (α,α-CD dimer, α,β-CD dimer, and β,β-CD dimer) and guest derivatives [$PyC_{10}Py$ and viologen polymer (VP)]. Bromonium anions are omitted in guest derivatives.

dimer/VP, but hydrogels are not formed. On the other hand, after heating at 100 °C for 7 h, an aqueous solution of the α,α-CD dimer/VP forms a supramolecular hydrogel containing over 30 mM (VP unit/CD unit 4:1) (Figure 2). The bipyridyl group of VP functions as an electric barrier, which prevents threading and dethreading of the α-CD unit in the α,α-CD dimer onto the decamethylene unit of VP at 30 °C; this observation suggests that the α-CD unit of the α,α-CD dimer cannot exceed the electric barrier at 30 °C, whereas after heating at 100 °C, the α-CD unit exceeds the barrier to form polyrotaxanes.

To confirm complementarity between the CD dimer and VP, we then investigated the formation of supramolecular hydrogels of VP with the α,β-CD dimer and the β,β-CD dimer. For each sample, the CD concentration was adjusted to 120 mM (VP unit/CD unit 4:1). Even with a dimer/VP concentration greater than 60 mM, the α,β-CD dimer/VP and β,β-CD dimer/VP do not form supramolecular hydrogels. These results indicate that complexation between the C_{10} unit of VP and the α-CD unit of the α,α-CD dimer is important for the formation of cross-links between VPs (Figure 3). The cavity size of β-CD is too large to allow formation of a stable cross-linked polyrotaxane complex.

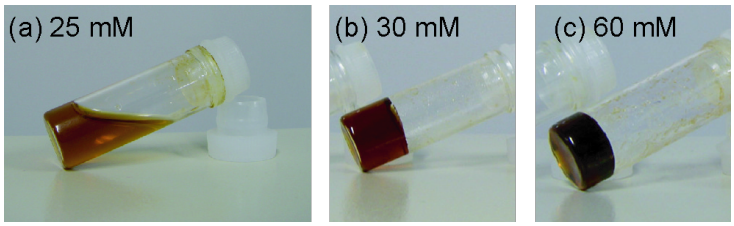

Figure 2: Photographs of hydrogelation with various concentrations of α,α-CD dimer/VP in water. Aqueous solution of α,α-CD dimer/VP forms the hydrogel at concentrations above 30 mM.

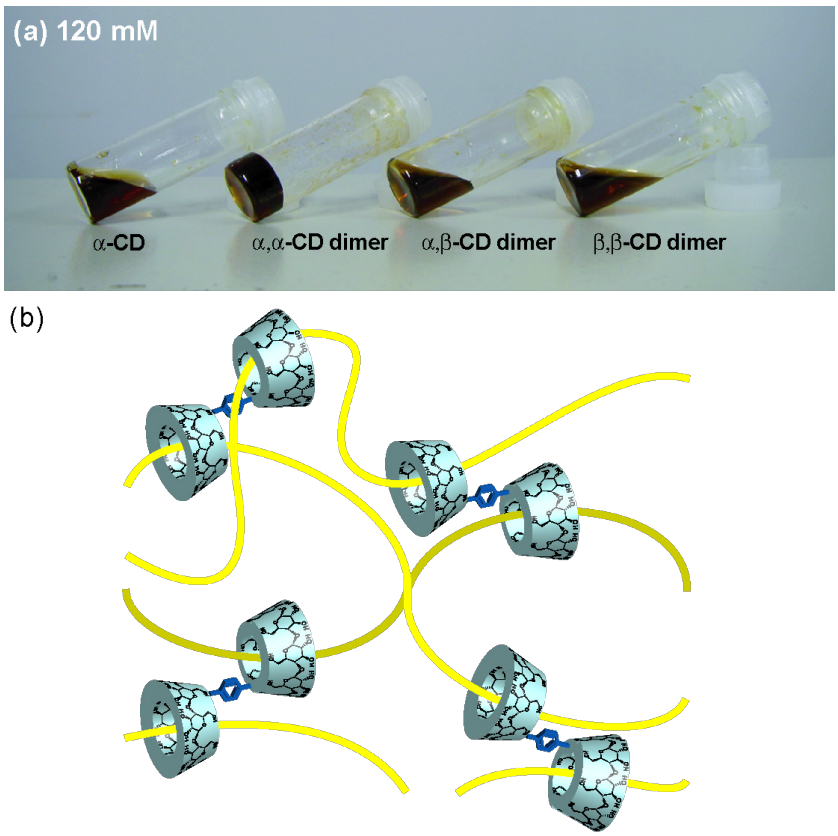

Figure 3: Hydrogelation of VP with various CD derivatives (VP unit/CD 4:1) at 25 °C. (a) Concentrations of CDs are 120 mM. (b) Proposed structure of the α,α-CD dimer/VP supramolecular hydrogel.

The α,β-CD dimer and β,β-CD dimer do not function as crosslinking molecules between VP and β-CD. Actually, the association constant of α-CD with decamethylene is much higher than that of β-CD with decamethylene [24]. Consequently, the association constant plays an important role in gel formation.

To confirm a supramolecular hydrogel formed by crosslinking VP with the α,α-CD dimer, we added $PyC_{10}Py$ as a competitive guest to the supramolecular hydrogel of the α,α-CD dimer/VP. After adding $PyC_{10}Py$ ($PyC_{10}Py$/VP unit/α,α-CD dimer 8:8:1) and heating at 100 °C, the supramolecular hydrogel of the α,α-CD dimer/VP changes to the sol even at a high concentration ([α,α-CD dimer] = 60 mM), because the α-CD unit of the α,α-CD dimer forms an inclusion complex with $PyC_{10}Py$. This inclusion-complex formation causes the cross-links between the α,α-CD dimer and VP to decompose.

^{1}H NMR study of complexation of the α,α-CD dimer/VP

To observe the competitive effect of $PyC_{10}Py$, we conducted ^{1}H NMR studies on complexation between α-CD/VP and a competitive experiment using $PyC_{10}Py$. Figure 4 shows ^{1}H NMR spectra of VP/$PyC_{10}Py$, VP/α-CD, and VP/α-CD/$PyC_{10}Py$. Addition of α-CD causes peak splitting of the decamethylene and pyridyl protons of VP (VP unit/α-CD 1:2), indicating the formation of a polyrotaxane VP/α-CD complex. The association–dissociation equilibrium between VP and α-CD is slow on the NMR time scale. On the other hand, upon addition of $PyC_{10}Py$ to the VP/α-CD complex (VP unit/α-CD/$PyC_{10}Py$ 1:2:8), the splitting peaks of the VP/α-CD complex disappear, and then signals of $PyC_{10}Py$ split due to complexation between $PyC_{10}Py$ and α-CD (Figure 4c). These results indicate that the excess $PyC_{10}Py$ disturbs complexation of α-CD and VP. The sol state of the α,α-CD dimer/VP in the presence of $PyC_{10}Py$ is attributed to the dissociation of VP and the α,α-CD dimer, suggesting that complexation between VP and the α-CD units is necessary to form the gel.

Viscoelastic property of the α,α-CD dimer/VP hydrogel

Figure 5 shows the storage elastic modulus (G') and loss elastic modulus (G'') for an α,α-CD dimer/VP hydrogel (60 mM) at 20 °C. The master curve of the hydrogel is similar to the Voigt Model. G'' relaxes as the frequency increases. However, the hydrogel does not relax ($G' > G''$) in the frequency range 0.01–10 rad·s^{-1}, indicating a self-standing gel. This behavior are similar to chemically cross-linked gels even though the α,α-CD dimer/VP hydrogel is topologically cross-linked between VPs with the α,α-CD dimer. This result confirms that complexation of VP and the α,α-CD dimer is stable and responsible for the stability of the hydrogel.

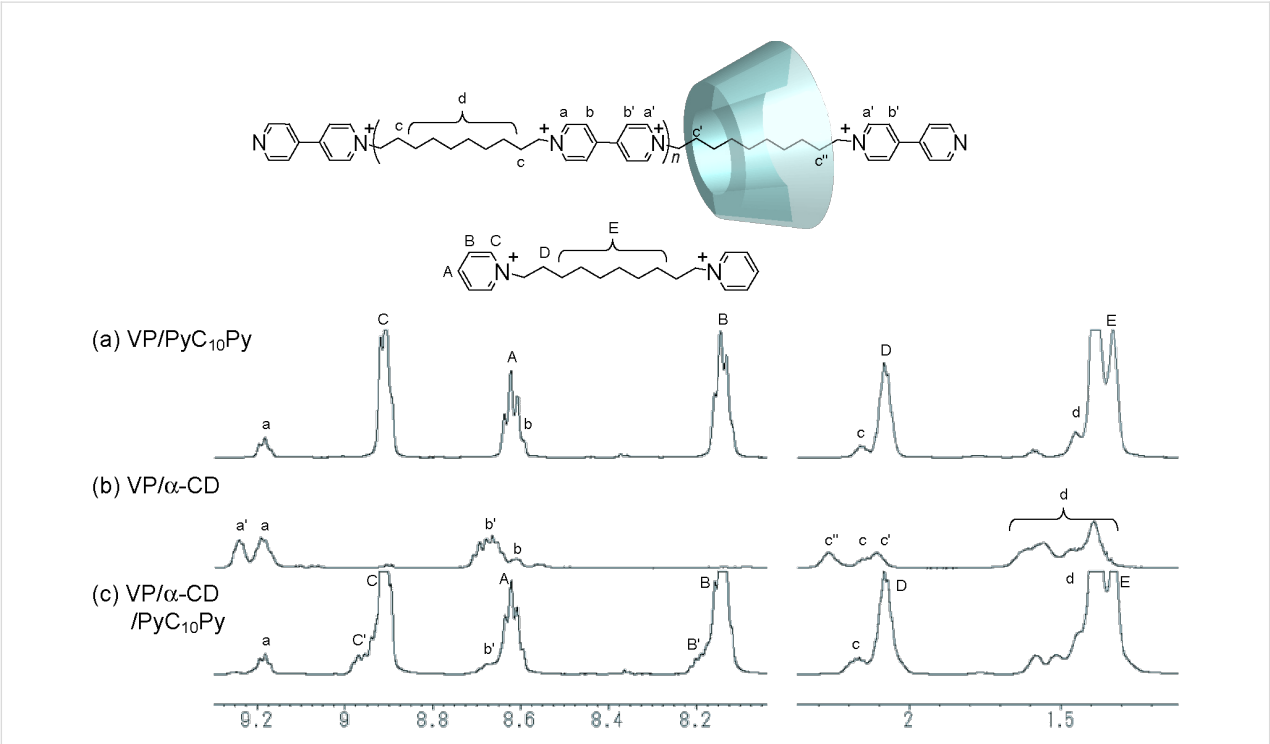

Figure 4: 500 MHz ^{1}H NMR spectra of VP (VP unit 2 mM) with α-CD and $PyC_{10}Py$ (VP unit/CD/$PyC_{10}Py$ 1:2:8) in D_2O at 30 °C: (a) VP and $PyC_{10}Py$, (b) VP and α-CD, and (c) VP, $PyC_{10}Py$, and α-CD.

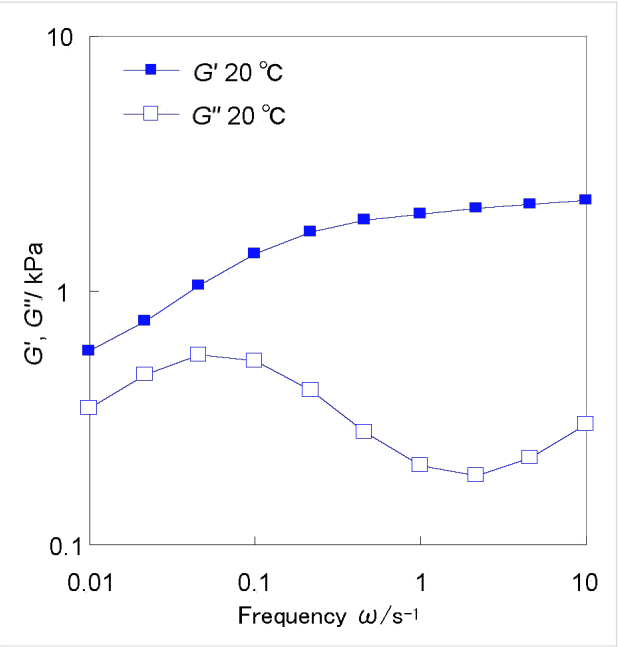

Figure 5: *G′* and *G″* of the α,α-CD dimer/VP hydrogel as a function of frequency (ω). Applied shear strain amplitude is 1%.

Conclusion

Mixing VP and the α,α-CD dimer creates a hydrogel, which is expected to realize supramolecular materials with a high tensile strength and self-healing abilities. The complementarity between α-CD and the decamethylene units plays an important role in the formation of supramolecular hydrogels composed of α,α-CD dimer/VP. VP has an electric barrier between the decamethylene units, which is a unique feature of this supramolecular hydrogel. The electric barrier prevents dethreading of α-CD from VP, yielding a self-standing supramolecular hydrogel. We will electrochemically control the elasticity of the α,α-CD dimer/VP hydrogel.

Experimental

Preparation of α,α-CD dimer

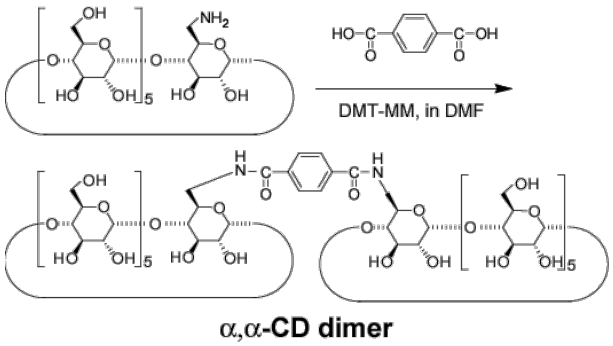

6-NH_2-α-CD (120 mg, 0.12 mmol) and terephthalic acid (8 mg, 0.50 mmol) were dissolved in dried DMF (20 mL). DMT-MM (34 mg, 0.12 mmol) was added and the mixture was stirred at rt for 4 days. After evaporation of the solvent, the residue was dissolved in water (10 mL) and poured into acetone (100 mL). The product was collected and purified by reversed-phase chromatography (elution: water–acetonitrile) to give α,α-CD dimer as a white solid in 22% yield. ^{1}H NMR (DMSO-d_6, 500 MHz) δ 8.36 (t, 2H, -N*H*), 7.88 (s, 4H, *Ph*), 5.59–5.40 (m, 24H, O(2,3)*H* of α-CD), 4.97–4.78 (m, 12H, C(1)*H* of α-CD), 4.55–4.41 (m, 10H, O(6)*H* of α-CD), 3.84–3.48 (m, C(3,6,5,3,4)*H* of α-CD); MALDI–TOF *m*/*z*: 2095 [M + Na]$^+$.

Preparation of α,β-CD dimer

a) Methyl terephthalate-β-CD

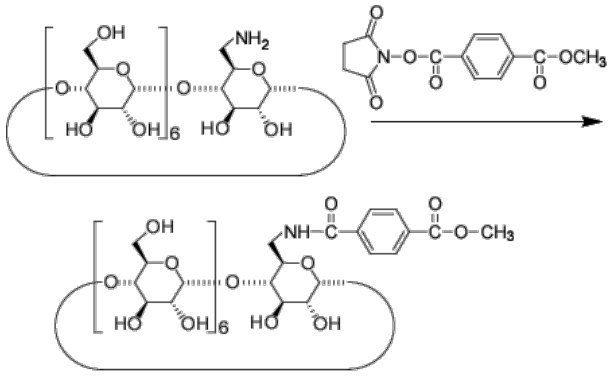

To a solution of 6-NH_2-β-CD (566 mg, 0.50 mmol) in dried DMF (7 mL) was added methyl terephthalate succinimidyl ester (137.6 mg, 0.50 mmol). After stirring for 2 days at rt, the solution was poured into acetone (100 mL) to give methyl terephthalate-β-CD as a yellow solid in 43% yield. ^{1}H NMR (DMSO-d_6, 500 MHz) δ 8.46 (t, 1H, -N*H*), 8.00 (d, 2H, *Ph*), 7.95 (s, 3H, -CH_3), 7.94 (d, 2H, *Ph*), 5.83–5.59 (m, 14H, O(2,3)*H* of β-CD), 4.95–4.79 (m, 7H, C(1)*H* of β-CD), 4.45–4.32 (m, 6H, O(6)*H* of β-CD), 3.74–3.51 (m, C(3,6,5,3,4)*H* of α-CD); TLC: R_f 0.22 (*n*-butanol/ethanol/water 5:4:3).

b) Terephthalic acid-β-CD

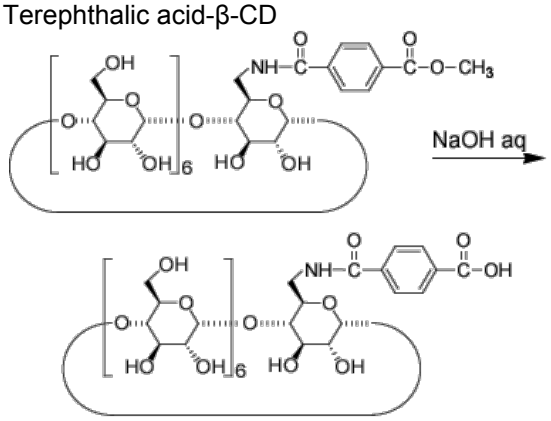

To a solution of methyl terephthalate-β-CD (605 mg, 0.47 mmol) in water (120 mL) was added NaOH (0.1 M, 7 mL). After stirring for 12 hours at rt, the solution was concentrated

and purified by DIAION HP-20 column. The column was flushed with water (500 mL) and then eluted with water/methanol 80:20 (v/v). The fraction was concentrated to give terephthalic acid-β-CD as a yellow solid in 70% yield. ^{1}H NMR (DMSO-d_6, 500 MHz) δ 8.39 (t, 1H, -NH), 7.98 (d, 2H, Ph), 7.90 (d, 2H, Ph), 5.83–5.59 (m, 14H, O(2,3)*H* of β-CD), 4.95–4.79 (m, 7H, C(1)*H* of β-CD), 4.45–4.32 (m, 6H, O(6)*H* of β-CD), 3.74–3.51 (m, C(3,6,5,3,4)*H* of α-CD); TLC: R_f 0.32 (*n*-butanol/ethanol/water 5:4:3).

c) α,β-CD dimer

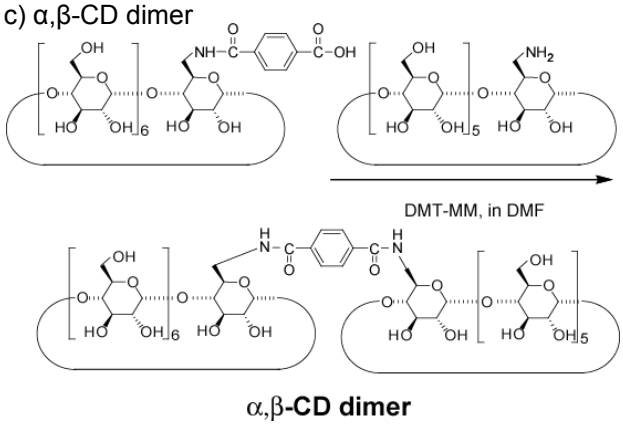

α,β-CD dimer

The synthetic procedure was the same as α,α-CD dimer, using terephthalic acid-β-CD (65 mg, 50 μmol), 6-NH_2-α-CD (59 mg, 60 μmol), DMT-MM (17 mg, 60 μmol), dried DMF (8 mL) to give α,β-CD dimer in 36% yield as a white solid. ^{1}H NMR (DMSO-d_6, 500 MHz) δ 8.32, 8.27 (m, 2H, -NH), 7.89 (s, 4H, Ph), 5.80–5.44 (m, 26H, O(2,3)*H* of CDs), 4.97–4.78 (m, 13H, C(1)*H* of CDs), 4.53–4.35 (m, 11H, O(6)*H* of CDs), 3.86–3.37 (m, C(3,6,5,3,4)*H* of α-CD); TLC: R_f 0.04 (*n*-butanol/ethanol/water 5:4:3); MALDI–TOF *m*/*z*: 2259 $[M + Na]^+$.

Preparation of β,β-dimer

β,β-Dimer was prepared according to our previous report [25].

Preparation of viologen polymer (VP)

1,10-Dibromodecane (7.3 g, 24 mmol) was added to a solution of 4,4'-bipyridyl (4 g, 24 mmol) in DMSO (40 mL). After being stirred at 100 °C for 2 d, the solution became turbid. The precipitate was collected and washed with acetone three times. The product was purified by dialysis for 4 d to give VP in 20% yield as a brown solid. ^{1}H NMR (D_2O, 500 MHz) δ 9.25 (m, 92H, 2-position of bipyridyl in the middle of the axle), 9.14 (m, 4H, 2-position of bipyridyl at the end of the axle near the decamethylene part), 8.94 (m, 4H, 2-position of bipyridyl at the end of the axle apart from the decamethylene part), 8.69 (m, 92H, 3-position of bipyridyl in the middle of the axle), 8.58 (m, 4H, 3-position of bipyridyl at the end of the axle near the decamethylene part), 8.18 (m, 4H, 3-position of bipyridyl at the end of the axle apart from the decamethylene part), 4.85 (m, 96H, α methylene in decamethylene), 2.21 (m, 96H, β methylene in decamethylene), 1.72–1.30 (m, 288H, χ, δ, ε methylene in decamethylene).

Preparation of $[Py\text{-}(CH_2)_{10}\text{-}Py]^{2+}\cdot 2Br^-$ ($PyC_{10}Py$)

Pyridine (158 mg, 2.0 mmol) and 1,10-dibromodecane (315 mg, 0.80 mmol) were dissolved in acetone and heated under reflux for 3 d. After evaporation of the solvent, the residue was dissolved in methanol (20 mL) and poured into diethyl ether (200 mL). The product was collected by centrifugation to give $PyC_{10}Py$ in 91% yield as a brown solid. ^{1}H NMR (D_2O, 500 MHz) δ 8.90 (d, J = 6.6 Hz, 4H, 2-position of pyridine), 8.62 (t, J = 8.2 Hz, 2H, 4-positon of pyridine), 8.14 (t, J = 7.7 Hz, 4H, 3-positon of pyridine), 4.67 (t, J = 7.3 Hz, 4H, α methylene in decamethylene), 2.08 (m, 4H, β methylene in decamethylene), 1.42–1.30 (m, 12H, χ, δ, ε methylene in decamethylene).

Rheological measurements

Dynamic viscoelasticity were measured by using an Anton Paar MCR301 rheometer at a strain of 0.1%. The storage elastic modulus (G') and loss elastic modulus (G'') were measured at 20 °C. The sample concentration was adjusted to 1.0 wt %.

Supporting Information

Supporting Information File 1

Additional information and ^{1}H NMR spectra of all new compounds.
[http://www.beilstein-journals.org/bjoc/content/supplementary/1860-5397-8-182-S1.pdf]

Acknowledgements

This work was supported by the "Core Research for Evolutional Science and Technology" program of the Japan Science and Technology Agency.

References

1. Gandhi, M. V.; Thompson, B. S. *Smart Materials and Structures;* Chapman & Hall: London, 1992.
2. Urban, M. W., Ed. *Handbook of Stimuli-Responsive Materials;* Wiley-VCH Verlag GmbH: Weinheim, Germany, 2011.
3. Minko, S., Ed. *Responsive Polymer Materials: Design and Applications;* Blackwell Pub.: Ames, IA, USA, 2006.
4. Beaty, C. E.; Saltzman, W. M. *J. Controlled Release* **1993,** *24,* 15–23. doi:10.1016/0168-3659(93)90165-2
5. Kim, S.; Healy, K. E. *Biomacromolecules* **2003,** *4,* 1214–1223. doi:10.1021/bm0340467
6. Mahoney, M. J.; Anseth, K. S. *Biomaterials* **2006,** *27,* 2265–2274. doi:10.1016/j.biomaterials.2005.11.007

7. Petka, W. A.; Harden, J. L.; McGrath, K. P.; Wirtz, D.; Tirrell, D. A. *Science* **1998,** *281,* 389–392. doi:10.1126/science.281.5375.389
8. Shen, W.; Lammertink, R. G. H.; Sakata, J. K.; Kornfield, J. A.; Tirrell, D. A. *Macromolecules* **2005,** *38,* 3909–3916. doi:10.1021/ma048348s
9. Hennink, W. E.; van Nostrum, C. F. *Adv. Drug Delivery Rev.* **2002,** *54,* 13–36. doi:10.1016/S0169-409X(01)00240-X
10. Okumura, Y.; Ito, K. *Adv. Mater.* **2001,** *13,* 485–487. doi:10.1002/1521-4095(200104)13:7<485::AID-ADMA485>3.0.CO;2-T
11. Kretschmann, O.; Choi, S. W.; Miyauchi, M.; Tomatsu, I.; Harada, A.; Ritter, H. *Angew. Chem., Int. Ed.* **2006,** *45,* 4361–4365. doi:10.1002/anie.200504539
12. Liu, Y.; You, C.-C.; Zhang, H.-Y.; Kang, S.-Z.; Zhu, C.-F.; Wang, C. *Nano Lett.* **2001,** *1,* 613–616. doi:10.1021/nl015550p
13. Liu, Y.; Li; Fan, Z.; Zhang, H.-Y.; Wu, X.; Guan, X.-D.; Liu, S.-X. *Nano Lett.* **2002,** *2,* 257–261. doi:10.1021/nl015670x
14. Liu, Y.; Li; Zhang, H.-Y.; Zhao, Y.-L.; Wu, X. *Macromolecules* **2002,** *35,* 9934–9938. doi:10.1021/ma025541i
15. Liu, Y.; Song, Y.; Wang, H.; Zhang, H.-Y.; Li, X.-Q. *Macromolecules* **2004,** *37,* 6370–6375. doi:10.1021/ma049929k
16. Harada, A.; Kamachi, M. *Macromolecules* **1990,** *23,* 2821–2823. doi:10.1021/ma00212a039
17. Harada, A.; Kamachi, M. *J. Chem. Soc., Chem. Commun.* **1990,** 1322–1323. doi:10.1039/C39900001322
18. Li, J.; Harada, A.; Kamachi, M. *Polym. J.* **1994,** *26,* 1019–1026. doi:10.1295/polymj.26.1019
19. Kawaguchi, Y.; Harada, A. *J. Am. Chem. Soc.* **2000,** *122,* 3797–3798. doi:10.1021/ja9943647
20. Harada, A.; Adachi, H.; Kawaguchi, Y.; Okada, M.; Kamachi, M. *Polym. J.* **1996,** *28,* 159–163. doi:10.1295/polymj.28.159
21. Meier, L. P.; Heule, M.; Caseri, W. R.; Shelden, R. A.; Suter, U. W.; Wenz, G.; Keller, B. *Macromolecules* **1996,** *29,* 718–723. doi:10.1021/ma946428y
22. Wenz, G.; Gruber, C.; Keller, B.; Schilli, C.; Albuzat, T.; Müller, A. *Macromolecules* **2006,** *39,* 8021–8026. doi:10.1021/ma061033n
23. Nelson, A.; Belitsky, J. M.; Vidal, S.; Joiner, C. S.; Baum, L. G.; Stoddart, J. F. *J. Am. Chem. Soc.* **2004,** *126,* 11914–11922. doi:10.1021/ja0491073
24. Saito, H.; Yonemura, H.; Nakamura, H.; Matsuo, T. *Chem. Lett.* **1990,** *19,* 535–538. doi:10.1246/cl.1990.535
25. Ohga, K.; Takashima, Y.; Takahashi, H.; Kawaguchi, Y.; Yamaguchi, H.; Harada, A. *Macromolecules* **2005,** *38,* 5897–5904. doi:10.1021/ma0508606

License and Terms

Beilstein Journal of Organic Chemistry

Polysiloxane ionic liquids as good solvents for β-cyclodextrin-polydimethylsiloxane polyrotaxane structures

Narcisa Marangoci[1], Rodinel Ardeleanu[1], Laura Ursu[1], Constanta Ibanescu[1,2], Maricel Danu[1], Mariana Pinteala[*1] and Bogdan C. Simionescu[1,2]

Full Research Paper

Open Access

Address:
[1]Centre of Advanced Research in Bionanoconjugates and Biopolymers, "Petru Poni" Institute of Macromolecular Chemistry, 700487 Iasi, Romania and [2]Department of Natural and Synthetic Polymers, "Gheorghe Asachi" Technical University of Iasi, 700050 Iasi, Romania

Email:
Mariana Pinteala[*] - pinteala@icmpp.ro

* Corresponding author

Keywords:
cyclodextrins; imidazolium salt; ionic liquid; polyrotaxanes; polysiloxanes

Beilstein J. Org. Chem. **2012,** *8,* 1610–1618.
doi:10.3762/bjoc.8.184

Received: 31 May 2012
Accepted: 17 August 2012
Published: 24 September 2012

This article is part of the Thematic Series "Superstructures with cyclodextrins: Chemistry and Applications".

Guest Editor: H. Ritter

Abstract

An ionic liquid based on polydimethylsiloxane with imidazolium salt brushes was synthesized as a good solvent for β-cyclodextrin-polydimethylsiloxane rotaxane. As expected the PDMS-Im/Br ionic liquid had a liquid-like non-Newtonian behavior with rheological parameters dependent on frequency and temperature. The addition of rotaxane to the ionic liquid strengthened the non-Newtonian character of the sample and a type of stable liquid-like network was formed due to the contribution of weak ionic interactions. The structure is stable in the 20 to 80 °C domain as proved by the oscillatory and rotational rheological tests.

Introduction

Ionic liquids (ILs) are environmentally friendly solvents with great potential for chemical and nonchemical applications due to their low melting points, nonvolatile and noncorrosive properties at room temperature. They possess good conductivities [1,2] and often they present a good thermal stability up to 400 °C [1,3]. The potential applications of ILs made them the subject of a number of works that showed their use as solvents or as solvents for synthesis and catalysis [4-6]. In this context ILs, which have polar and nonpolar regions, could play an important role in the field of supramolecular organization of different supramolecular structures (such as polyrotaxanes or supermolecules formed by ILs with different host molecules),

leading to interesting phenomena, properties and applications [7-12]. This includes the dissolution of cellulose and cyclodextrins (CDs) with ILs [12], synthesis of ILs containing slide-ring gels [7], synthesis of IL-CD inclusion complexes [10], etc.

Polyrotaxane structures based on cyclodextrins and different linear (co)polymers are well known as supramolecular ensembles. They consist of cyclodextrin molecules whose hydrophobic cavities are penetrated by a linear polymer chain terminating with bulky stoppers, which prevent the macrocycle from slipping out [13-22]. Unfortunately, the properties and mechanisms of CD-polymer polyrotaxanes have been rarely evaluated due to a lack of good solvents. In general, the CD-polymer polyrotaxanes are soluble only in DMSO and aqueous sodium hydroxide solution, even if each component of their structure is soluble in a large number of solvents [8]. Research for new solvents has led to the discovery of ionic liquids as a good option for pseudo- or polyrotaxane structures [7,8,17,18]. It should be also mentioned that the mobility of the carrier ions of ILs decreases when their glass-transition temperature (T_g) increases [23]. In this respect, we have synthesized ILs based on polydimethylsiloxane with imidazolium salt brushes (PDMS-Im/S) with low T_g values in order to avoid a macroscopic phase separation in a mixture of ILs and CD-polydimethylsiloxane polyrotaxane structures. Also, in the present study, we report how the rheological properties are influenced when CD-polydimethylsiloxane rotaxane is dissolved in PDMS-Im/S ionic liquid.

Results and Discussion

A class of polymers that possesses a unique combination of properties, such as very low T_g values, high chain flexibility, good thermal, oxidative and UV stability, high gas permeability, surface activity, hydrophobicity, etc., is the class of polysiloxanes, especially polydimethylsiloxanes [24]. It is worth mentioning that ionic liquids based on polydimethylsiloxane and imidazolium salt groups have been used for capillary gas chromatography [25,26] and as biocides [27]. Furthermore, one of our interests is to combine the properties of polydimethylsiloxanes with the versatility of synthetic approaches in designing well-defined macromolecular systems [17,21,27]. In this context, we synthesized polysiloxanes with a pendant imidazolium bromide derivative (PDMS-Im/Br) through a multistep procedure (Scheme 1) as an ionic liquid, which serves as a good solvent for β-CD-polydimethylsiloxane polyrotaxane (PRot).

The copolymer PDMS-Im is characterized by a $(CH_3)_2SiO$/$Im(CH_3)SiO$ molar ratio of 3/1, as determined from its ^{1}H NMR spectrum. PRot is characterized by a M_n = 1250 of polydimethylsiloxane (PDMS) and β-CD/PDMS chain ratio of 2/1,

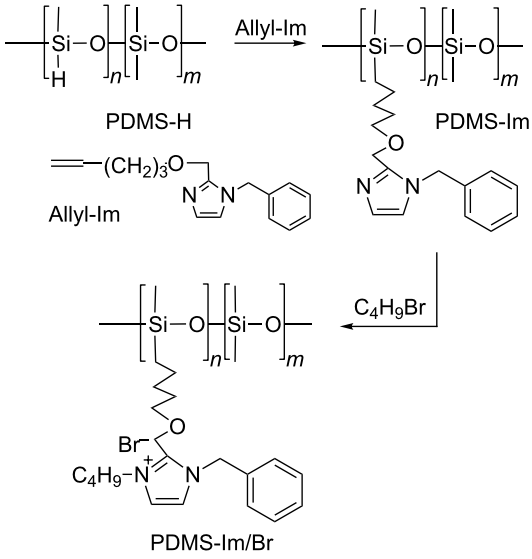

Scheme 1: Synthesis of PDMS-Im/Br ionic liquid.

both determined from the integrals of characteristic peaks in its ^{1}H NMR spectrum [21].

After 24 hours of stirring at 90 °C under nitrogen atmosphere, the mixture of 10 wt % PRot with PDMS-Im/Br turned into a viscous clear solution, suggesting a complete dissolution. Cooling the sample to room temperature in a dry box caused an increase in the apparent viscosity; it should also be mentioned that the mixture remained clear for the next five weeks (Figure 1).

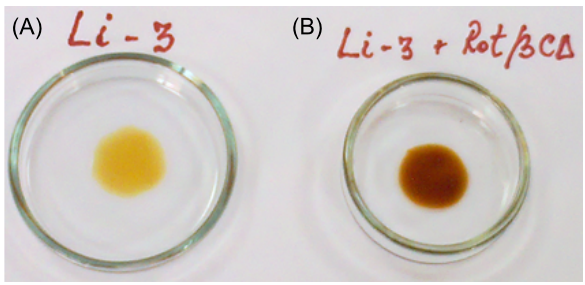

Figure 1: Appearance of (A) pure PDMS-Im/Br ionic liquid; (B) PDMS-Im/Br ionic liquid containing 1 wt % PRot.

This observation indicates the complete dissolution of PRot in PDMS-Im/Br ionic liquid. This may be due to the disruption of the intermolecular hydrogen bonds that exist in β-CD-polymer polyrotaxane structures by the ionic liquid [9]. In addition, an ordered morphology was observed from wet-STEM images of the mixture, which also indicates a good dissolution of PRot in the PDMS-Im/Br ionic liquid (Figure 2).

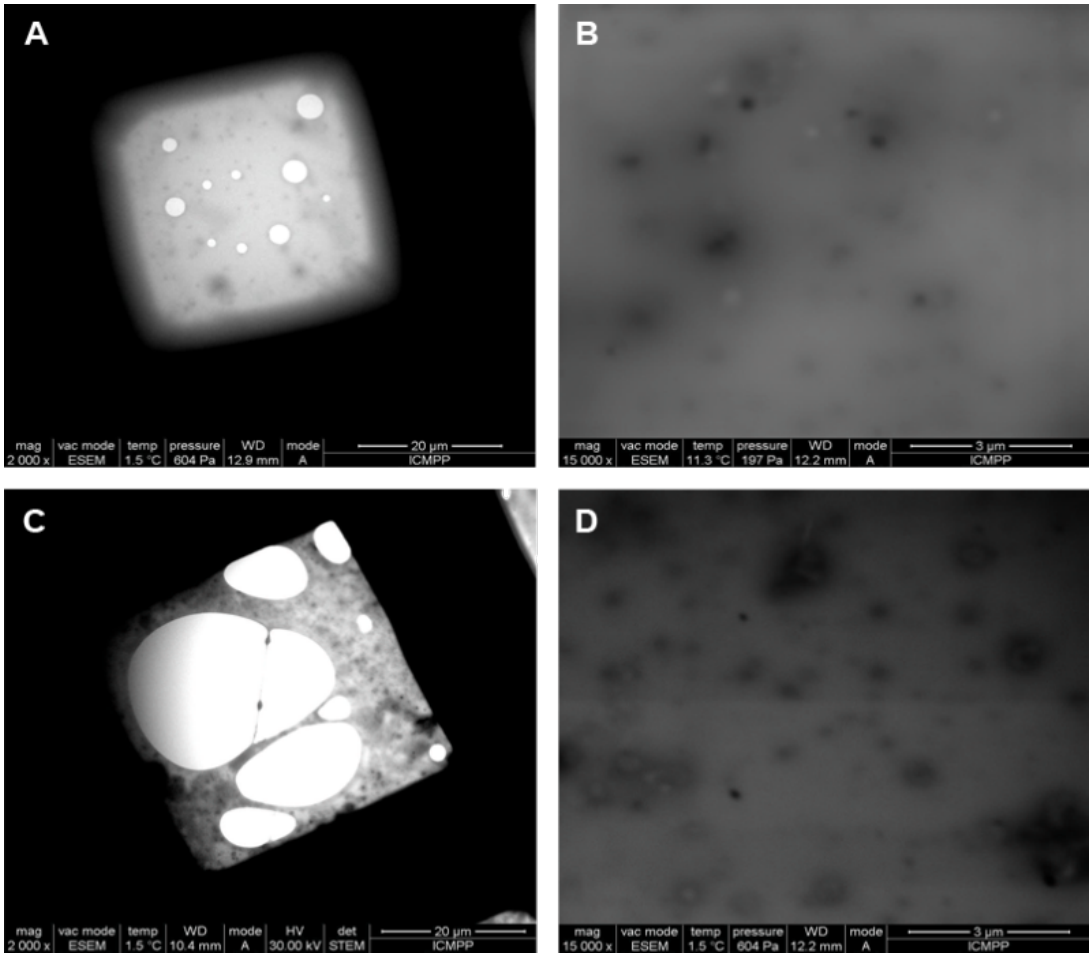

Figure 2: Wet-STEM images at 30 kV in bright field mode of: PDMS-Im/Br ionic liquid (A,B) and mixture of PDMS-Im/Br with PRot (C,D).

Apparently, the size of the morphology is maintained in PDMS-Im/Br with PRot mixture (Figure 2C,D) when we compare it with those corresponding to the ionic liquid (Figure 2A,B). The rheological properties of the PDMS-Im/Br ionic liquid and its mixture with PRot give important information on the interaction between IL and PRot and can explain the dissolution behavior of polyrotaxane in the ionic liquid [28-33]. The rheology of the mixture was studied by using both oscillatory and rotational shear measurements. A solution with a concentration of 10 wt % was used for all tests. The first test, prior to all the oscillatory measurements, was the strain (amplitude) sweep at a fixed frequency of 1 Hz and a shear stress varying from 0.1 to 50 Pa. In Figure 3, the storage modulus *G*', the loss modulus *G*", and the phase shift angle δ, as a function of shear stress, are presented.

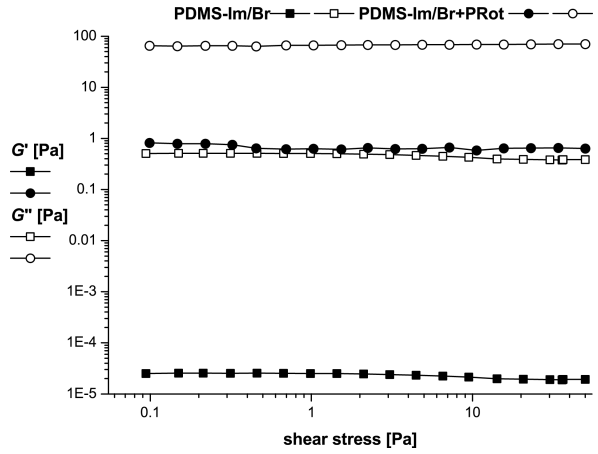

Figure 3: Amplitude sweep results for PDMS-Im/Br and PDMS-Im/Br+PRot at 25 °C.

As long as *G*" > *G*' for the entire experimental domain, we can suppose a stable liquid-like structure with an extended linear

viscoelastic plateau. The limits of the linear viscoelastic region (LVR) were established at 7.5 Pa for the ionic liquid and 43.7 Pa for the ionic liquid with rotaxane. The presence of rotaxane, therefore, extended the LVR domain. Even if, as usual, the amplitude sweep is used only to determine the limiting values of strain or shear stress, which are necessary for all the subsequent oscillatory tests, interesting data regarding the rheological behavior of solutions of complex fluids can be also obtained.

As mentioned in the literature [28], different strain-dependent behaviors may be recognized in the amplitude sweeps for various types of polymer solutions taking into consideration their complex microstructure. For both the ionic liquid alone and its mixture with rotaxane, a kind of liquid-like stable network is characteristic. This may be due to different electrostatic interactions. The shift angle δ has a constant value of 90° (ideal viscous behavior) for the ionic liquid and 89.5° for the mixture with rotaxane. The frequency sweep test was conducted in the linear viscoelastic region (LVR), as confirmed from the amplitude sweep test; the angular-frequency range was 0.1–100 rad/s (Figure 4).

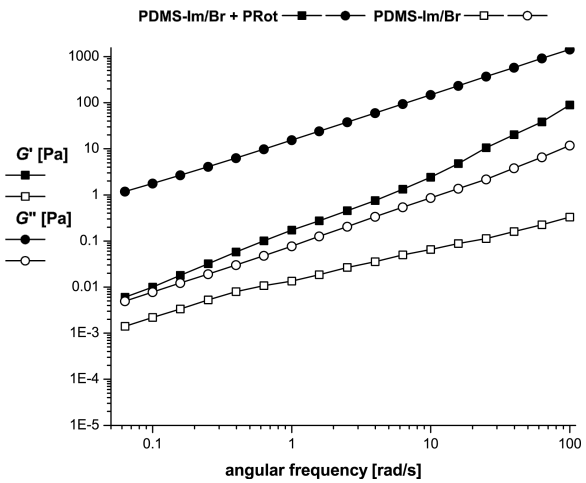

Figure 4: Storage (*G*') and loss (*G*") moduli dependence on frequency for PDMS-Im/Br and PDMS-Im/Br+PRot at 25 °C.

For both samples the loss modulus (*G*") dominates the storage modulus (*G*') over the entire measurement domain. This is an indication of the liquid-like (viscous) character of the systems. The shape of the curves for the mixture (PDMS-Im/Br+PRot) is typical for polymer solutions with a strong dependence on frequency for both moduli. Obviously, no frequency-dependent crossover point of the dynamic moduli appears in the considered frequency range, but it could be supposed at a higher frequency. The addition of rotaxane into the ionic liquid increases the loss modulus by almost three orders of magnitude and the storage modulus by one order.

The next step in the study was to check the influence of temperature on the rheological behavior of the ionic liquid and its mixture with rotaxane. For this purpose an oscillatory temperature test was performed. The temperature-sweep test was carried out in a temperature range between 20 and 80 °C, with a heating rate of 0.5 °C/min, at a constant frequency of 1 Hz and a constant strain amplitude $\gamma = 5\%$.

As it can be easily seen in Figure 5 the liquid-like stable structure is not disrupted during heating, with *G*' being almost parallel to *G*" over the entire temperature domain. For both samples the value of the dynamic moduli decreases when the temperature is increased.

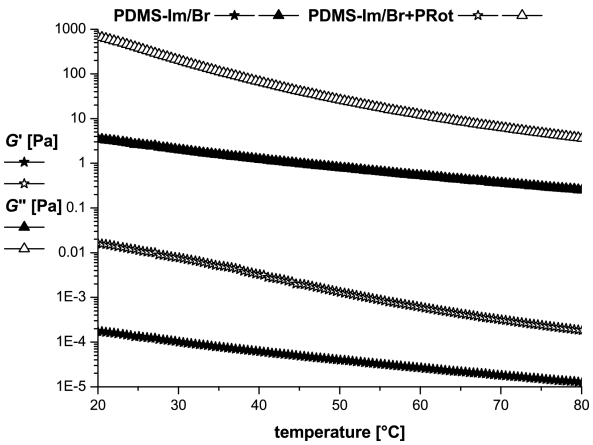

Figure 5: Storage (*G*') and loss (*G*") moduli dependence on temperature for PDMS-Im/Br and PDMS-Im/Br+PRot.

Rotational measurements were also carried out for a better understanding of the rheological behavior of the analyzed samples. The flow curves were recorded both in terms of the shear stress (τ) and viscosity (η) (Figure 6).

The ionic liquid exhibits Newtonian behavior for almost the entire measurement domain, with a viscosity that is independent of the shear rate. A deviation from linearity appears only for high shear rates. An important increase, both in terms of viscosity and shear stress, is noticed when rotaxane is added to the ionic liquid. The first Newtonian domain is obvious as well as the beginning of the shear-thinning behavior. The experimental results were fitted with the Carreau–Yasuda model by

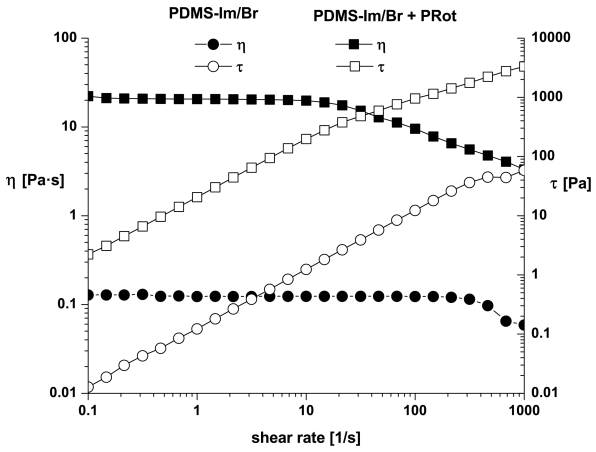

Figure 6: Flow curves for PDMS-Im/Br and PDMS-Im/Br + PRot at 25 °C.

using the rheometer software (Rheoplus) [29,30]. The parameters are listed in Table 1.

In this model, η_0 is the zero-shear viscosity, η_∞ is infinite-shear viscosity while a, n and Λ are the regression parameters of the model calculated by using the rheometer software, with Λ being the characteristic relaxation time related to the onset of non-Newtonian behavior or shear-thinning behavior [30]. The experimental data proved to be in very good concordance with the Carreau–Yasuda model.

Flow curves recorded at seven different temperatures between 20 and 80 °C (Figure 7 and Figure 8) showed a clear increase of the dynamic viscosity for the ionic liquid alone (Figure 7) and even more obviously for the mixture of ionic liquid with rotaxane (Figure 8). This remark concurs with reports in the literature [31-33], namely that the viscosity is strongly temperature-dependent.

Table 1: Parameters of the Carreau–Yasuda model.

Sample	η_0 [Pa·s]	η_∞ [Pa·s]	a	n	Λ [s]	R^2
PDMS-Im/Br	0.12399	$6.99 \cdot 10^{-9}$	4.5866	0.2949	0.00288	0.9944
PRot + PDMS-Im/Br	20.654	$3.95 \cdot 10^{-7}$	2.5312	0.5529	0.05846	0.9994

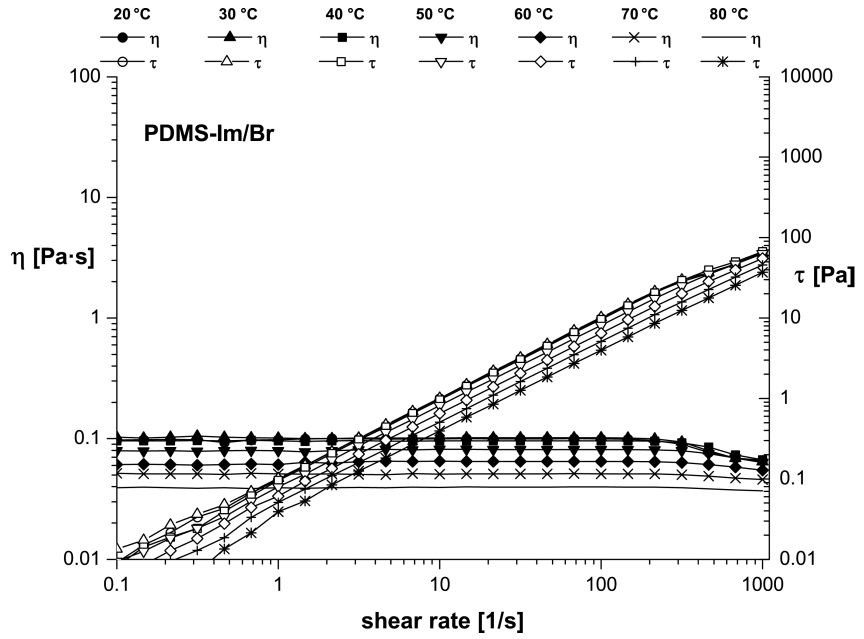

Figure 7: Temperature dependence of flow curves for PDMS-Im/Br ionic liquid.

Since the PDMS-Im/Br IL is liquid at room temperature, with T_g values at −117 and 22 °C, and PRot is in the solid state (T_g: −117 and 25 °C), their mixture presents T_g values at −112 and 23 °C (Figure 9). In addition, the negative T_g values are caused by the presence of siloxane chains, while the positive T_g values are attributed to the imidazolium salt sequences.

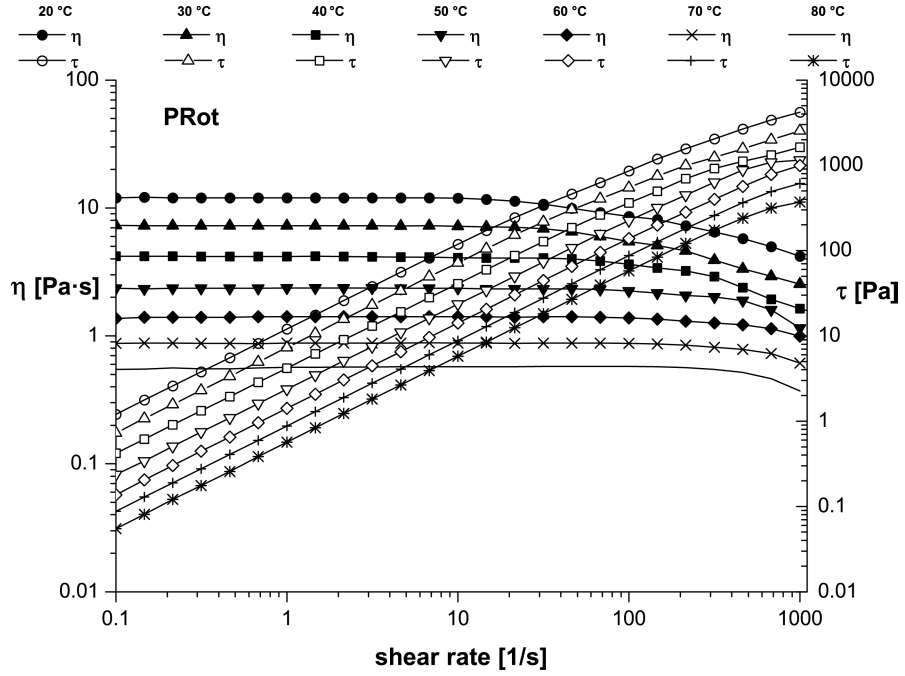

Figure 8: Temperature dependence of flow curves for PDMS-Im/Br+PRot.

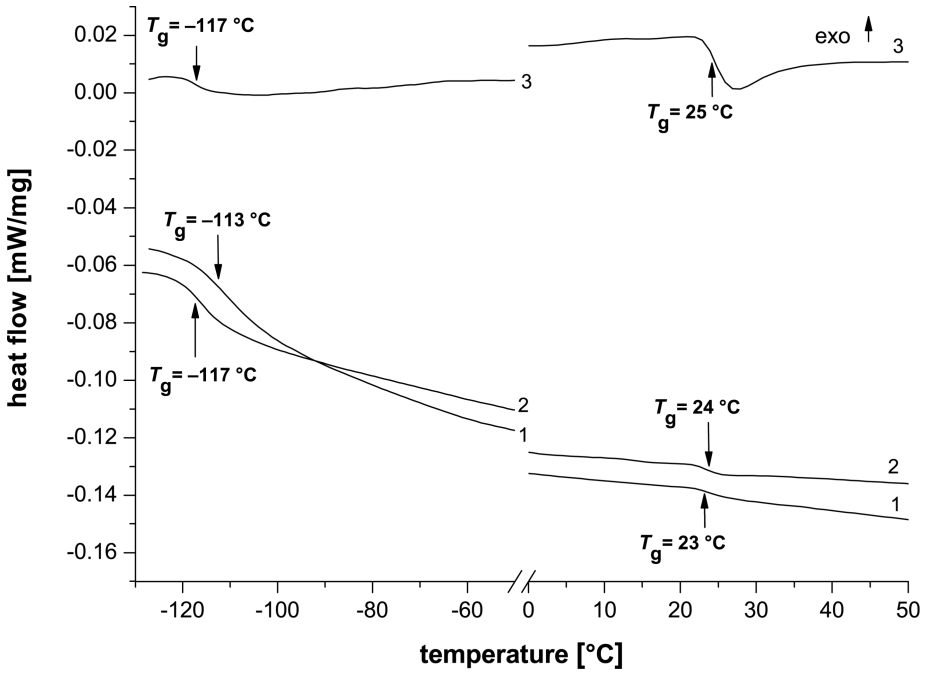

Figure 9: DSC second heating curves of: (1) PDMS-Im/Br ionic liquid, (2) mixture of PDMS-Im/Br with Prot and (3) Prot.

Conclusion

We synthesized, through a multistep procedure (Scheme 1), PDMS-Im/Br ionic liquid with a $(CH_3)_2SiO/Im(CH_3)SiO$ molar ratio of 3/1 and β-CD-polydimethylsiloxane polyrotaxane (PRot) with a β-CD/PDMS chain ratio of 2/1 (PDMS with M_n = 1250). The obtained ionic liquid proved to be a good solvent for PRot structures (Figure 1).

As expected, the PDMS-Im/Br ionic liquid had a liquid-like non-Newtonian behavior with rheological parameters dependent on frequency and temperature. The addition of rotaxane to the ionic liquid strengthened the non-Newtonian character of the sample and a type of stable liquid-like network was formed due to the contribution of weak ionic interactions. The structure is stable in the 20 to 80 °C domain as proved by the oscillatory and rotational rheological tests.

Experimental

Synthesis of ionic liquid

Synthesis of poly{dimethylsiloxane-co-([5-(1-benzylimidazole-2-yl-oximethyl)pentyl](methyl)siloxane)} (PDMS-Im). PDMS-lm was synthesized as previously described [22] and the compound was obtained as a yellow viscous product (approximately 78% yield). 2-[(Pent-4-en-1-yl)oxymethyl]-1-benzylimidazole (Allyl-Im, 6.8 g, 0.026 mmol), toluene (10 mL) and Karstedt catalyst (molar ratio: Allyl-Im/Pt(II) 542/1) were placed in a Schlenck reactor. The mixture was stirred at room temperature for 0.5 h. Then, 8.0 g of poly[dimethylsiloxane-co-(H-methyl)siloxane] copolymer (PDMS-H) (molar ratio: $SiH(CH_3)$/Allyl-Im 1/1.01) was introduced dropwise at 90 °C. The mixture was stirred at 90 °C for 3 d. The reaction progress was monitored by ^{1}H NMR and FTIR spectroscopy by the disappearing of peaks from 4.9 ppm and 2140 cm^{-1}, respectively. Finally, the solvent was evaporated and the resulting raw product was purified by column chromatography. ^{1}H NMR (400 MHz, $CDCl_3$) δ 0.09 (s, 37H, $SiCH_3$), 0.51 (t, 2H, $SiCH_2$), 1.25–1.57 (m, 6H, $SiCH_2CH_2CH_2CH_2$), 3.39 (t, 2H, CH_2CH_2O), 4.54 (s, 2H, OCH_2C), 5.23 (s, 2H, NCH_2Ar), 6.88 (s, 1H, =N-CH=CHNCH_2), 7.15 (m, 5H, Ar), 7.26–7.36 (m, 2H, $ArCH_2NCH$=CH).

Synthesis of poly{[(1-benzyl-3-*n*-butylimidazole-2-yl-3-ium)methyloxypent-5-yl](methyl)siloxane-co-(dimethylsiloxane)} (PDMS-Im/Br): The compound was obtained as a brown viscous product (approximately 99% yield). Butyl bromide (5 mL) was added dropwise at 0 °C to a stirred solution of PDMS-Im (26.59 g) in acetonitrile (70 mL). The reaction mixture was stirred for 5 d at 30 °C. The solvent was removed by vacuum distillation [34,35]. FTIR (KBr, cm^{-1}): 3064 and 3032 (Ar-H), 2962 and 2858 (C-H), 1676 (C=N), 1456 and 192 (C=C), 1261 (Si-C), 1091–1000 (Si-O-Si), 802 (Si-C); ^{1}H NMR (400 MHz, $CD_3OD + D_2SO_4$) δ 0.01–0.20 (s, $SiCH_3$), 0.35–0.65 (m, $SiCH_2$), 0.95–1.05 (s, C-CH_3), 1.25–1.87 (m, $SiCH_2CH_2CH_2CH_2$, $CH_3CH_2CH_2CH_2$), 3.35–3.40 (t, $CH_2CH_2OCH_2$), 4.63 (s, OCH_2C), 5.23 (s, NCH_2Ar), 6.98 (s, 1H, CH_2N-CH=CH), 7.15–7.23 (m, 5H, Ar), 7.35–7.55 (m, butyl-NCH=CH).

Synthesis of β-CD-polydimethylsiloxane polyrotaxane (PRot) was carried out according to a method previously described [17,22] and the compound was obtained as a white powder (approximately 55% yield). PRot was prepared by mixing β-CD in dimethylformamide (DMF, saturated solution) with α,ω-bis(3-glycidoxypropyl)polydimethylsiloxane prepolymer with M_n = 1250 until the solution became turbid (after approximately 72 h) at 65 °C, followed by the reaction of epoxide functionalities with 4-aminophenyltriphenylmethane (APhTPhM) (saturated solution in isopropyl alcohol) for 8 h at 65 °C. The slurry was then poured into cold water, washed quickly with ethanol, dried, and suspended in diethyl ether overnight to remove the traces of unreacted α,ω-bis(3-glycidoxypropyl)polydimethylsiloxane. After being filtered, the sample was dried at 40 °C for 8 h. The obtained crude PRot contains a significant amount of free β-CD. To remove the noncomplexed β-CD (until the β-CD/siloxane ratio remained unchanged), two successive precipitations in a DMF/water system were made. ^{1}H NMR (400 MHz, DMSO-d_6) δ −0.05 (s, CH_3Si chain), 0.04–0.06 (large, CH_3Si end), 0.44–0.53 (m, CH_2CH_2Si), 1.46–1.52 (m, CH_2CH_2Si), 3.32–3.66 (m, $CH_2OCH_2CH(OH)$-, $CH(OH)CH_2NH$- and H2–6 from CD), 4.53 (t, OH6 from CD), 4.89 (d, H1 from CD), 5.73–5.77 (two superposed doublets OH2+3 from CD), 6.45–6.47 (d, *ortho* to amino group from APhTPhM), 6.74–6.76 (d, *meta* to amino group from APhTPhM), 7.12–7.29 (m, triphenyl protons from APhTPhM); ^{13}C NMR (400 MHz, DMSO-d_6) δ −0.09–0.05 (CH_3Si chain), 13.30 (CH_2CH_2Si), 22.60 (CH_2CH_2Si), 30.46 (tertiary *C* from APhTPhM), 35.58 ($CH(OH)CH_2NHPh$), 59.70 (C6 from CD), 63.47 ($CH_2OCH_2CH(OH)$-), 70.60 ($OCH_2CH(OH)CH_2NH$), 71.90, 72.32, 72.64 (C2,3,5 from CD), 72.77 ($CH_2CH(OH)CH_2NH$-), 101.40 (C1 from CD), 112.80–162.14 (*C* from APhTPhM).

Morphological characterization using the Wet-STEM technique

The morphological characterization of samples was performed with a FEI Quanta 200 ESEM. The environmental scanning electron microscope (ESEM) equipped with a Wet-STEM detector enables wet samples to be observed, without potentially damaging them, through the use of partial water vapor pressure in the microscope specimen chamber.

Samples preparation

A holey-carbon-coated copper grid was placed on a TEM sample holder and positioned on a Peltier cooling stage. The samples were diluted in THF, and then a small amount of solution was dropped on the grid with a micropipette. The examination of samples was achieved at 1.5 °C, using a gaseous secondary electron detector (GSED) and a STEM detector with two semiannular detectors A and B for bright- or dark-field images. An acceleration voltage of 30 kV was chosen to optimize resolution and sample contrast.

Rheological measurements

The rheological measurements were performed on a Physica MCR 501 rheometer (Anton Paar, Austria) with a Peltier device for temperature control, equipped with an electronically commutated synchronous motor, allowing rheological measurements in controlled-stress and controlled-strain modes [29]. To avoid slippage, a parallel plate geometry with serrated plates was used. The upper plate, of stainless steel, was 50 mm in diameter, and a gap of 0.5 mm was fixed. The samples were introduced onto the plate with great care to avoid shear effects in the solutions. A solvent trap was used in all rheological tests to diminish the solvent evaporation. All isothermal measurements were made at 25 °C. Strain sweeps at a fixed frequency of 1 Hz were carried out to establish the limits of the linear viscoelastic region (LVR) both in terms of shear stress and amplitude of deformation. Various rheological parameters were calculated by using the Rheoplus software.

Differential scanning calorimetry (DSC)

DSC measurements were conducted on a DSC 200 F3 Maia device (Netzsch, Germany). About 10 mg of each sample was heated in pressed and pierced aluminum crucibles. A heating rate of 10 °C/min was applied. Nitrogen purge gas was used as an inert atmosphere at a flow rate of 50 mL/min. The apparatus was temperature- and sensitivity-calibrated with indium, according to standard procedures.

FTIR spectra

FTIR spectra were recorded on a Bruker Vertex 70 FTIR spectrometer from KBr pellets in transmittance mode in the 370–4000 cm^{-1} range, in ambient air at room temperature, with 2 cm^{-1} resolution and accumulation of 32 scans.

^{1}H NMR spectra

The ^{1}H NMR spectra were recorded on a Bruker Avance DRX 400 spectrometer operating at 400.1 MHz. ^{1}H NMR spectroscopy of PDMS-Im was performed in $CDCl_3$, and ^{1}H NMR spectroscopy of PDMS-Im/Br was performed in fully deuterated methanol (CD_3OD) with deuterated sulfuric acid (D_2SO_4) [35].

Acknowledgements

This research was financially supported by European Social Fund "Cristofor I. Simionescu" Postdoctoral Fellowship Programme (ID: POSDRU/89/1.5/S/55216), Sectoral Operational Programme Human Resources Development 2007–2013, and the PN-II-ID-PCCE-2011-2-0028 Grant.

References

1. Welton, T. *Chem. Rev.* **1999,** *99,* 2071–2084. doi:10.1021/cr980032t
2. Jarosik, A.; Krajewski, S. R.; Andrzej Lewandowski, A.; Radzimski, P. *J. Mol. Liq.* **2006,** *123,* 43–50. doi:10.1016/j.molliq.2005.06.001
3. Cornils, B.; Herrmann, W. A., Eds. *Aqueous-Phase Organometallic Catalysis: Concepts and Applications;* Wiley-VCH: Weinheim, Germany, 1998.
4. Villar-Garcia, I. J.; Abebe, A.; Chebude, Y. *Inorg. Chem. Commun.* **2012,** *19,* 1–3. doi:10.1016/j.inoche.2012.01.014
5. Pârvulescu, V. I.; Hardacre, C. *Chem. Rev.* **2007,** *107,* 2615–2665. doi:10.1021/cr050948h
6. Schoffers, E. *Eur. J. Org. Chem.* **2003,** *7,* 1145–1152. doi:10.1002/ejoc.200390168
7. Shen, X.; Chen, Q.; Zhang, J.; Fu, P. Supramolecular Structures in the Presence of Ionic Liquids. In *Supramolecular Structures in the Presence of Ionic Liquids: Theory, Properties, New Approaches;* Kokorin, A., Ed.; InTech: Croatia, 2011; pp 427–482. doi:10.5772/15586 Available from: http://www.intechopen.com/books/ionic-liquids-theory-properties-new-approaches/supramolecular-structures-in-the-presence-of-ionic-liquids.
8. Araki, J.; Ito, K. *Soft Matter* **2007,** *3,* 1456–1473. doi:10.1039/b705688e
9. Samitsu, S.; Araki, J.; Kataoka, T.; Ito, K. *J. Polym. Sci., Part B: Polym. Phys.* **2006,** *44,* 1985–1994. doi:10.1002/polb.20849
10. Amajjahe, S.; Ritter, H. *Macromolecules* **2008,** *41,* 3250–3253. doi:10.1021/ma702593s
11. Li, J. J.; Zhao, F.; Li, J. *Appl. Microbiol. Biotechnol.* **2011,** *90,* 427–443. doi:10.1007/s00253-010-3037-x
12. Zhu, S.; Wu, Y.; Chen, Q.; Yu, Z.; Wang, C.; Jin, S.; Ding, Y.; Wu, G. *Green Chem.* **2006,** *8,* 325–327. doi:10.1039/b601395c
13. Lehn, J.-M. *Supramolecular Chemistry: Concept and Perspectives;* Wiley-VCH: Weinheim, Germany, 1995. doi:10.1002/3527607439
14. Lehn, J.-M. *Science* **2002,** *295,* 2400–2403. doi:10.1126/science.1071063
15. Harada, A.; Kamachi, M. *Macromolecules* **1990,** *23,* 2821–2823. doi:10.1021/ma00212a039
16. Harada, A.; Hashidzume, A.; Takashima, Y. *Adv. Polym. Sci.* **2006,** *201,* 1–43. doi:10.1007/12_056
17. Farcas, A.; Marangoci, N.; Fifere, A.; Pinteala, M.; Harabagiu, V.; Simionescu, B. C. Polyrotaxanes with Cyclodextrins. In *New Trends in Nonionic (Co)Polymers and Hybrids;* Dragan, E., Ed.; Nova science Publishers, Inc., 2006; pp 53–78.
18. Ito, K. *Curr. Opin. Solid St. M.* **2010,** *14,* 28–34. doi:10.1016/j.cossms.2009.08.005
19. Jing, B.; Chen, X.; Hao, J.; Qiu, H.; Chai, Y.; Zhang, G. *Colloids Surf., A* **2007,** *292,* 51–55. doi:10.1016/j.colsurfa.2006.06.002
20. Okumura, H.; Kawaguchi, Y.; Harada, A. *Macromolecules* **2001,** *34,* 6338–6343. doi:10.1021/ma010516i

21. Marangoci, N.; Farcas, A.; Pinteala, M.; Harabagiu, V.; Simionescu, B. C.; Sukhanova, T.; Bronnikov, S.; Grigoryev, A.; Gubanova, G.; Perminova, M.; Perichaud, A. *High Perform. Polym.* **2008,** *20,* 251–266. doi:10.1177/0954008307079538
22. Marangoci, N.; Farcas, A.; Pinteala, M.; Harabagiu, V.; Simionescu, B. C.; Sukhanova, T.; Perminova, M.; Grigoryev, A.; Gubanova, G.; Bronnikov, S. J. *Incl. Phen. Macrocycl. Chem.* **2009,** *63,* 355–364. doi:10.1007/s10847-008-9529-y
23. Besner, S.; Prud'homme, J. *Macromolecules* **1989,** *22,* 3029–3037. doi:10.1021/ma00197a026
24. Mark, J. E. Overview of Silicone Polymers. In *Silicones and Silicone-Modified Materials;* Clarson, S. J.; Fitzgerald, J. J.; Owen, M. J.; Smith, S. D., Eds.; ACS Symposium Series 729; Washington DC, 2000; pp 1–10.
25. Wei, Q. Q.; Qi, M. L.; Fu, R. N. *Chin. Chem. Lett.* **2009,** *20,* 1111–1114. doi:10.1016/j.cclet.2009.04.002
26. Sun, X.; Wu, C.; Xing, J. *J. Sep. Sci.* **2010,** *33,* 3159–3167. doi:10.1002/jssc.201000030
27. Iojoiu, C.; Pinteala, M.; Simionescu, B. C.; Sanchez, J.-Y.; Abadie, M. J. M. *Curr. Trends Polym. Sci.* **2006,** *10,* 55–67.
28. Hyun, K.; Kim, S. H.; Ahn, K. H.; Lee, S. J. *J. Non-Newton. Fluid* **2002,** *107,* 51–65. doi:10.1016/S0377-0257(02)00141-6
29. Mezger, T. G. *The Rheology Handbook. For users of rotational and oscillatory rheometers,* 2 revised ed.; Vincentz Network: Hannover, Germany, 2006.
30. Rusu, M. C.; Ibanescu, C.; Ichim, I. C.; Riess, G.; Popa, M.; Rusu, D.; Rusu, M. *J. Appl. Polym. Sci.* **2009,** *111,* 2493–2506. doi:10.1002/app.29253
31. Okoturo, O. O.; VanderNoot, T. J. *J. Electroanal. Chem.* **2004,** *568,* 167–181. doi:10.1016/j.jelechem.2003.12.050
32. Tshibangu, P. N.; Ndwandwe, S. N.; Dikio, E. D. *Int. J. Electrochem. Sci.* **2011,** *6,* 2201–2213.
33. Mukherjee, I.; Manna, K.; Dinda, G.; Ghosh, S.; Moulik, S. P. *J. Chem. Eng. Data* **2012,** *57,* 1376–1386. doi:10.1021/je200938k
34. Min, G.-H.; Yim, T.-e.; Lee, H.-Y.; Huh, D.-H.; Lee, E.-j.; Mun, J.-y.; Oh, S. M.; Kim, Y.-G. *Bull. Korean Chem. Soc.* **2006,** *27,* 847–852. doi:10.5012/bkcs.2006.27.6.847
35. Mizerska, U.; Fortuniak, W.; Chojnowski, J.; Hałasa, R.; Konopacka, A.; Werel, W. *Eur. Polym. J.* **2009,** *45,* 779–787. doi:10.1016/j.eurpolymj.2008.11.045

License and Terms

Beilstein Journal of Organic Chemistry

Molecular solubilization of fullerene C_{60} in water by γ-cyclodextrin thioethers

Hai Ming Wang and Gerhard Wenz*

Full Research Paper

Open Access

Address:
Organische Makromolekulare Chemie, Saarland University, Campus Geb. C4.2, D-66123, Saarbrücken, Germany

Email:
Gerhard Wenz* - g.wenz@mx.uni-saarland.de

* Corresponding author

Keywords:
C_{60}; cyclodextrins; dynamic light scattering; particle size; solubilization; UV spectrum

Beilstein J. Org. Chem. **2012,** *8,* 1644–1651.
doi:10.3762/bjoc.8.188

Received: 18 June 2012
Accepted: 27 August 2012
Published: 28 September 2012

This article is part of the Thematic Series "Superstructures with cyclodextrins: Chemistry and applications".

Guest Editor: H. Ritter

Abstract

Various hydrophilic γ-cyclodextrin (CD) thioethers, containing neutral or ionic side arms were found to form molecular disperse solutions of C_{60} in water reaching concentrations of 15 mg/L. Equilibrium state was approached after seven days without the use of organic cosolvents. The 1:2 stoichiometry of the C_{60}/γ-CD thioether complexes was demonstrated by a parabolic phase-solubility diagram. In contrast, native γ-CD forms nanoparticles with C_{60}. Particle sizes of C_{60} were determined by dynamic light scattering.

Introduction

Since the first spectroscopic discovery of buckminsterfullerene, C_{60}, by Kroto, Heath, Curl and Smalley in 1985 [1], and its first macroscopic synthesis by Krätschmer et al. in 1990 [2], this third allotropic modification of carbon has been the subject of more than 10,000 publications giving rise to many interesting potential applications both in the biomedical field [3-5] and materials science [6-9].

A good solubility of C_{60} in water is especially required for biological applications; however, this is not the case at all. Solubility of C_{60} was estimated to be as low as 10^{-8} ng/L, equivalent to 10 C_{60} molecules per millilitre of water [10,11]. Therefore, hydrophilic derivatives of C_{60} have been synthesized and utilized for the inhibition of therapeutically important enzymes, such as HIV-1 protease [12], for the prevention of bacterial growth [13,14], or for photodynamic therapy of cancer by scission of DNA [3]. Despite these successes, there are still several issues relating to the chemical modification of C_{60}. The regioselectivity of derivatization is difficult to control [15], and derivatization reduces aromaticity, which leads to a change of the distinct electronic and photonic properties of C_{60}.

Dispersions of C_{60} nanoparticles in water have been discussed as alternatives for molecular solutions. Such C_{60} dispersions are

generally obtained by the so-called solvent-exchange method [16,17], where C_{60} is dissolved primarily in an organic solvent, such as benzene, THF, or acetone, and afterwards diluted with water. After evaporation of the organic solvent, clusters of C_{60} in water remain, which are temporarily stable. The biological activities of those dispersions strongly increase with decreasing size of the C_{60} nanoparticles [13]. Also micellar dispersions of C_{60} in water stabilized by detergents such as Tween, Triton, or SDS are known [18]. Applications of these C_{60} dispersions are hampered by the toxicities of the employed organic solvents or surfactants.

The most successful strategy to carry the extremely hydrophobic C_{60} molecule into water is the use of appropriate water-soluble carriers that can form host–guest complexes, such as calixarenes [19,20] and cyclodextrins (CDs) [21,22]. CDs are cyclic oligosaccharides consisting of six, seven, eight or more glucose subunits connected through α-1,4 glycosidic linkages, called α-, β-, and γ-CD, respectively. CD molecules resemble truncated cones comprising a hydrophilic outer surface and a relatively hydrophobic cavity [23-25]. CDs form water-soluble inclusion complexes with many hydrophobic or amphiphilic guest molecules [26], mainly driven by hydrophobic interactions [27]. Among the commercially available CDs, γ-CD with a clear width of d = 0.74 nm [28] is only large enough to partially accommodate C_{60}, which has a still greater van der Waals diameter of 1.0 nm [2]. Molecular dynamics studies strongly favour a sandwich-like structure of the complex, in which two γ-CD molecules tightly interact through hydrogen bonds between their secondary rims and in which C_{60} is situated in the middle at the widest sites of both CDs (see Figure 1, [29]).

Andersson et al. reported that C_{60} formed a water-soluble 1:2 inclusion complex with γ-CD after heating under reflux in water [21]. Mixing of an aqueous solution of γ-CD with a methanolic solution of C_{60} led to a C_{60} dispersion with a concentration of ca. 70 mg/L [30]. Even higher concentrations of up to 1 g/L were reached by high-speed vibration milling of C_{60} in aqueous solutions of γ-CD [31]. The main drawbacks of these aqueous systems are still (a) their lack of stability, leading to crystallization of the C_{60} complex after some days [31]; and (b) their pronounced tendency to form nanoparticular aggregates [21,32], both of which limit their practical application.

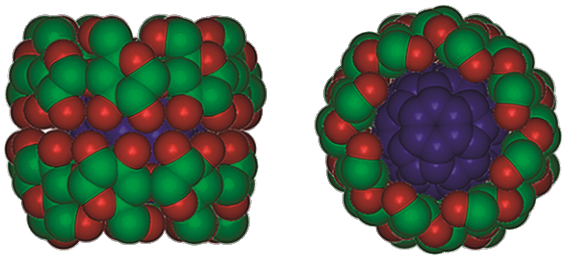

Figure 1: Space-filling model of the most stable complex between γ-CD and C_{60} with 1:2 stoichiometry, calculated in vacuo. Reprinted with permission from reference [29]. Copyright (2010) American Chemical Society.

Recently, we developed a new class of highly water-soluble per-6-deoxy-thioethers of β- and γ-CD (>20% w/w), which showed exceptionally high solubilization abilities for several aromatic molecules, such as anthracene and acenaphthylene, in water [33-35]. In this work, we investigated solubilization of C_{60} by these γ-CD thioethers (compounds **1**–**7** in Scheme 1) with the hope of achieving high concentrations of solubilized C_{60}. The hydrophilic substituents at the primary face of γ-CD should increase solubility and avoid aggregation, because they cannot form intermolecular hydrogen bonds like the primary hydroxyls of native γ-CD.

Results and Discussion

UV–vis spectra of C_{60} solutions

Powdered C_{60} was stirred at 25 °C in 6 mM aqueous solutions of γ-CD and γ-CD thioethers **1**–**7** giving rise to clear, dark yellow solutions of C_{60}, which show a narrow absorption band at λ_{max} = 335 nm quite similar to that of a solution of C_{60} in THF (λ_{max} = 327 nm), shown in Figure 2. Extensive centrifugation caused only a small reduction of signal intensity (less than

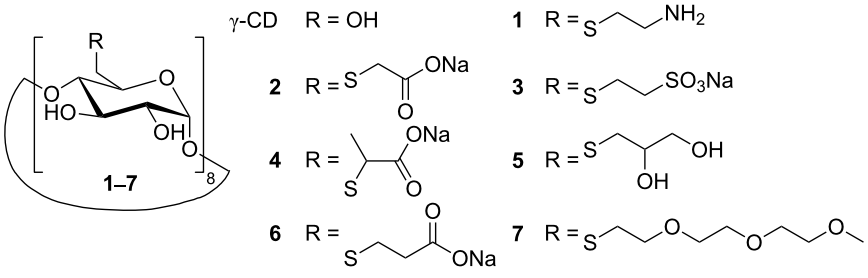

Scheme 1: Chemical structures of γ-CD and γ-CD thioether **1**–**7** used to solubilize C_{60} in water.

8%, Figure 2), which clearly precludes the existence of aggregates, which would otherwise sediment to the bottom. Therefore the molar concentration of C_{60} could be calculated by using the known molar extinction coefficient of C_{60} molecularly dissolved in *n*-hexane at 328 nm, i.e, ε = 52,000 $M^{-1}·cm^{-1}$ as published previously [36].

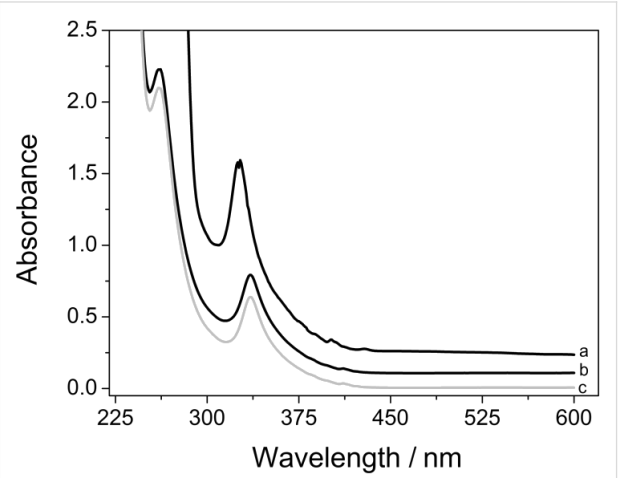

Figure 2: UV–vis spectra of (a) C_{60} solution in THF, (b) aqueous solutions of C_{60} with 6 mM γ-CD thioether **5** before centrifugation, and (c) after centrifugation (13,000 rpm) for 60 min. The absorbance intensities of (a) and (b) are shifted by 0.2 and 0.1 AU, respectively.

Dissolution kinetics

After the dissolution of C_{60} by γ-CD thioethers had been demonstrated, we were interested in how long it takes to reach equilibrium, within experimental error. Therefore a thinly casted film of C_{60} was incubated with an aqueous solution of γ-CD thioether **7** at 50 °C and stirred according to Kuroda et al. [37]. The slow increase of C_{60} concentration was monitored by the increase in absorption intensity at 335 nm. The observed first-order dissolution kinetics of C_{60} came nearly to an end after 7 d, as shown in Figure 3. The obtained rate constant, k = 0.021 h^{-1} was somewhat higher than the one already found for native γ-CD, k = 0.011 h^{-1}, which also showed first-order dissolution kinetics [37].

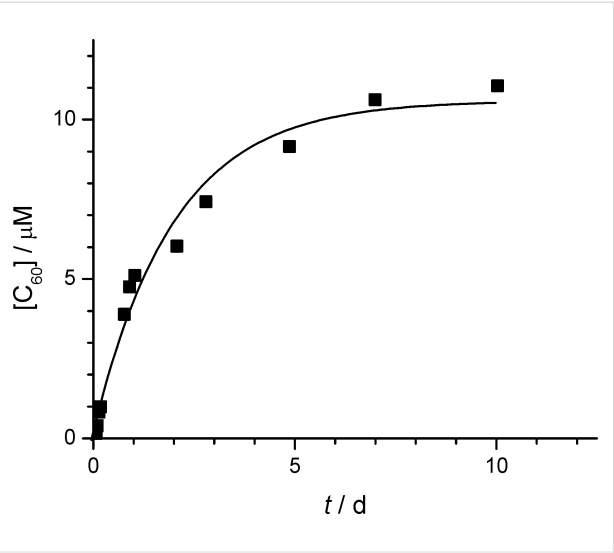

Figure 3: Isothermal kinetics of the dissolution of C_{60} in the presence of 10 mM CD **7** in water. Curve: best fit of first-order kinetics k = 0.5 d^{-1} = 0.021 h^{-1}.

The observed simple first-order kinetics was puzzling for us, because the concentration of the CD host does not go down significantly (<<1%) over the course of the dissolution of C_{60}. Therefore other reasons for the observed continuous decrease of dissolution rate had to be found.

Dissolution of C_{60} can be described by a two-step process, originally proposed by Kuroda et al. [37]. Alternatively, a one-step process, in which a C_{60} molecule is trapped by two CD rings at the same time, appeared reasonable to us. Both models are shown in Scheme 2.

The two-step model (a) employs a slow, rate-determining complexation of the guest C_{60} by the first CD molecule and a fast further complexation by the second. The second step is much faster than the first due to the strong stabilization exerted by multiple hydrogen bonds between both CD rings. For the back process, the first dissociation step should be slow and rate determining, because of the necessary cleavage of these intermolec-

a)

$$G_{solid} \rightleftharpoons G \underset{-CD,\,k_{-1}}{\overset{+CD,\,k_1}{\rightleftharpoons}} G\cdot CD \underset{-CD,\,k_{-2}}{\overset{+CD,\,k_2}{\rightleftharpoons}} G\cdot CD_2$$

$$K' = \frac{k_1}{k_{-2}} = \frac{[G\cdot CD_2]_{equ}}{[CD][G]} \cong \frac{[G\cdot CD_2]_{equ}}{[CD]_0[G]_0}$$

b)

$$G_{solid} \rightleftharpoons G \underset{-2CD,\,k_-}{\overset{+2CD,\,k}{\rightleftharpoons}} G\cdot CD_2$$

$$K = \frac{k}{k_-} = \frac{[G\cdot CD_2]_{equ}}{[CD]^2[G]} \cong \frac{[G\cdot CD_2]_{equ}}{[CD]_0^2[G]_0}$$

Scheme 2: Mechanistic description of the two possible mechanisms for the complexation of C_{60} (G) by CD hosts, in (a) two steps, and (b) one step.

ular hydrogen bonds. These assumptions lead to an apparent equilibrium constant K' in which the CD concentration is only present in first order. The initial rate of complexation is predicted to be proportional to CD concentration, which was already experimentally found for native γ-CD [37].

On the other hand, the one step model (b) leads to the classical binding constant K. The initial complexation rate should be proportional to the square of the host concentration, as shown in Supporting Information File 1.

Both models have in common that the formation of the complex follows pseudo-zero-order kinetics whereas dissociation follows first-order kinetics. Consequently, the integrations of the rate equations for both models (described in Supporting Information File 1) lead to the same final kinetics (Equation 1), a simple first-order equation converging to the equilibrium solubility of the guest $[C_{60}{\cdot}CD_2]_{equ}$ in agreement with the observed experimental data. According to both new models, the obtained rate constants k_{-2} and k_{-}, respectively, are not due to formation of the complex as proposed previously [37], but due to its dissociation.

$$[C_{60}\cdot CD_2] = [C_{60}\cdot CD_2]_{equ}\left(1-\exp(-k_{-2}t)\right) \qquad (1)$$

Dependence of the equilibrium concentration of C_{60} on the host and its concentration

Equilibrium concentrations of C_{60} in aqueous solutions of 6 mM γ-CD and γ-CD thioethers **1**–**7**, determined from the absorptions (λ_{max} = 335 nm) after being stirred for 7 d, are listed in Table 1. C_{60} concentrations obtained with γ-CD thioethers were up 35 times higher than the one obtained with native γ-CD, in accordance with previous results for other hydrophobic guests [38]. The improved solubilization potential of the thioethers was attributed to the higher hydrophobicity of sulfur compared to oxygen. The highest concentration of C_{60} in water, 14.9 μM, was found for CD derivative **5** with attached neutral diol substituents. In general, neutral γ-CD thioethers **1**, **5**, and **7** performed better than the anionic ones **2**, **3**, **4**. Coulomb repulsion between the anionic groups in between the two CD molecules was held responsible for the reduced binding affinity. Astonishingly, the amino derivative **1** also showed a high solubilization potential, which may originate from the addition of the amine to a double bond of C_{60}, as was already observed by Geckeler for other amino compounds [39].

The phase-solubility diagram of C_{60} in the presence of γ-CD thioether **3**, according to the method established by Higuchi and Connors [40], was obtained by plotting the concentration of the dissolved C_{60} versus the concentration of the host, as depicted in Figure 4. The observed parabolic A_P-type phase concentration dependence is typical for the formation of complexes with 1:2 stoichiometry [40,41]. The equation for the best fit $[C_{60}] = 10^{-3}(0.21 + 0.17[CD] + 0.11[CD]^2)$ indicates that the two-step process (first order in [CD]) as well as the one-step process (second order in [CD]), discussed above, contribute to the dissolution of C_{60}.

Table 1: C_{60} concentration in 6.0 mM aqueous solutions of γ-CD and γ-CD thioethers **1**–**7**.

host	$[C_{60}]$ (μM)
γ-CD	0.4
1	10.3
2	2.9
3	5.3
4	2.1
5	14.9
6	7.6
7	9.3

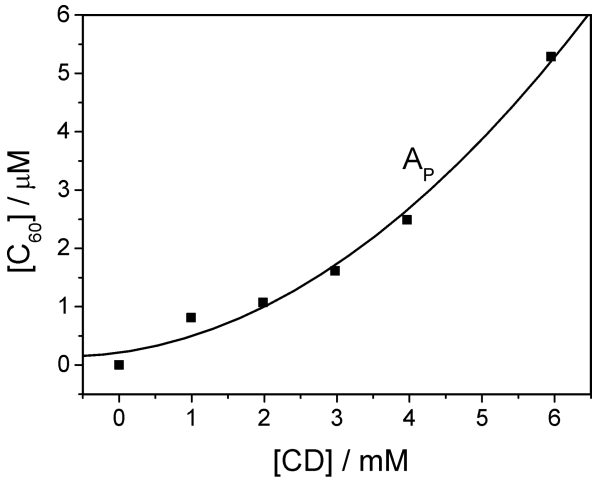

Figure 4: Phase-solubility diagram of C_{60} in aqueous solution in the presence of CD **3**.

Preparation of C_{60} complexes with the aid of organic solvents

Because equilibration took a long time (7 d) and occupancies of the γ-CD thioethers are still low (<0.3%), organic solvents, such as toluene, DMF or CS_2 were added to the aqueous solutions of γ-CD and γ-CD thioether **5**, in the hope of accelerating and improving the dissolution of C_{60} as reported by Murphy et al. [42]. The resulting solutions were characterized by UV–vis spectroscopy. The saturation concentrations of C_{60} are listed in Table 2.

Table 2: C_{60} concentration in 6.0 mM aqueous solutions of γ-CD and γ-CD thioether **5**.

CD	[C_{60}] (μM) procedure **a** water	procedure **b** water/toluene	procedure **c** water/DMF/toluene [42]	procedure **d** water/CS_2
γ-CD	0.4	7.5	4.9	10.8
5	14.9	21.4	6.3	18.6

Indeed, for native γ-CD much higher C_{60} concentrations could be achieved in water with the aid of organic solvents. But careful examination of the UV–vis spectra of the C_{60} solutions produced according to procedure **c** [42] before filtration, after filtration, and after centrifugation, as shown in Figure 5, revealed significant differences. The unfiltered solution of the C_{60}/γ-CD complex showed an additional absorption maximum 475 nm, which is typical for C_{60} nanoparticles (nC_{60}) such as those formed by dilution of a solution of C_{60} in THF with water [16,43]. After centrifugation nearly no C_{60} was left. Consequently, apparent improvements of the solubilization obtained with the aid of organic solvents were mostly due to the formation of nanoparticulate dispersions. Since these organic solvents are also hazardous for most cells, applications in biomedicine are prohibited. Therefore, organic solvents were avoided for the dissolution of C_{60} by γ-CD thioethers, because they also did not improve the solubilization process significantly.

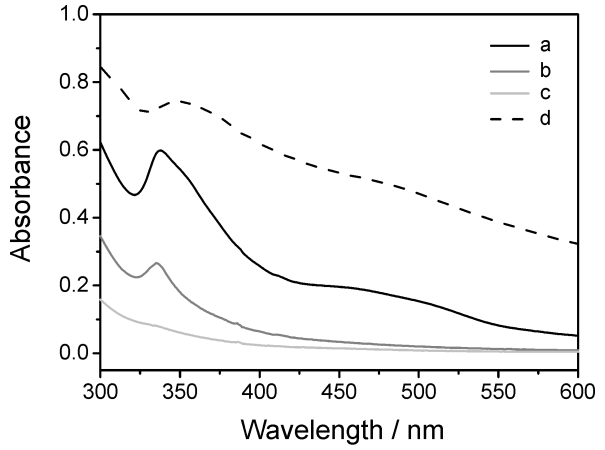

Figure 5: UV–vis spectra of the water solution of C_{60} produced by stirring C_{60} in 6mM γ-CD solution in DMF/toluene (v/v 1:1) at rt for 7 d, followed by dissolution of the resulting complex in water after evaporation of the solvents (procedure **c**): (a) before filtration, (b) after filtration, and (c) after centrifugation; (d) nC_{60} made from THF [43] before filtration.

Investigation of aggregation by dynamic light scattering

Since aggregation of CDs and CD inclusion compounds was already found in previous work [44,45], dynamic light scattering (DLS) investigations were performed to check for any aggregation during solubilization of C_{60} by γ-CD thioethers. DLS is a relatively fast method for the determination of the particle size distributions of proteins, polymers, micelles, and nanoparticles [46]. In particular, DLS is able to distinguish between a homogenous molecular solution and a dispersion of aggregates [47,48].

The size distribution of the solution of C_{60} in 6 mM γ-CD thioether **5** before centrifugation, shown in Figure 6, comprised two peaks at particle sizes of 3 and 300 nm. The first peak was attributed to the molecular CD/C_{60} complex, the second to aggregates of it. Since the intensity of the scattered light increases with the sixth power of the particle size, the content of aggregates is highly overestimated [45]. For getting the right picture, this intensity profile had to be transformed to the volume distribution profile, by using the Mie theory [49]. In the resulting volume distribution profile (Figure 6b) only one peak remains, which corresponds to the molecular complex. Consequently, this solution mainly consists of molecularly dissolved C_{60}. This finding is in accordance with the negligible decrease of C_{60} absorption caused by centrifugation, shown in Figure 2.

After centrifugation (13,000 rpm) for 60 min, shown in Figure 6c, only a sharp peak at 1 nm was observed for both the intensity and the volume size distributions, which demonstrates the validity of the DLS measurement. For comparison, the corresponding intensity and volume size distributions of a freshly prepared C_{60} solution in the presence of 6.0 mM native γ-CD according to procedure **c** [42] (Figure 7) only showed one peak at a diameter of 166 nm, very similar to nC_{60} prepared from THF. Consequently, the DLS investigations confirmed our previous finding that solubilization of C_{60} in water with the aid of organic solvents results in dispersions of C_{60} nanoparticles.

Conclusion

Neutral γ-CD thioethers are especially well suited as solubilizers for C_{60}. Sandwich-like 1:2 complexes are formed at room temperature without the necessity of adding organic cosolvents. These complexes show a much lower aggregation tendency than the corresponding ones of native γ-CD. Molecular solubilization of fullerene C_{60} in water, reaching concentrations as high

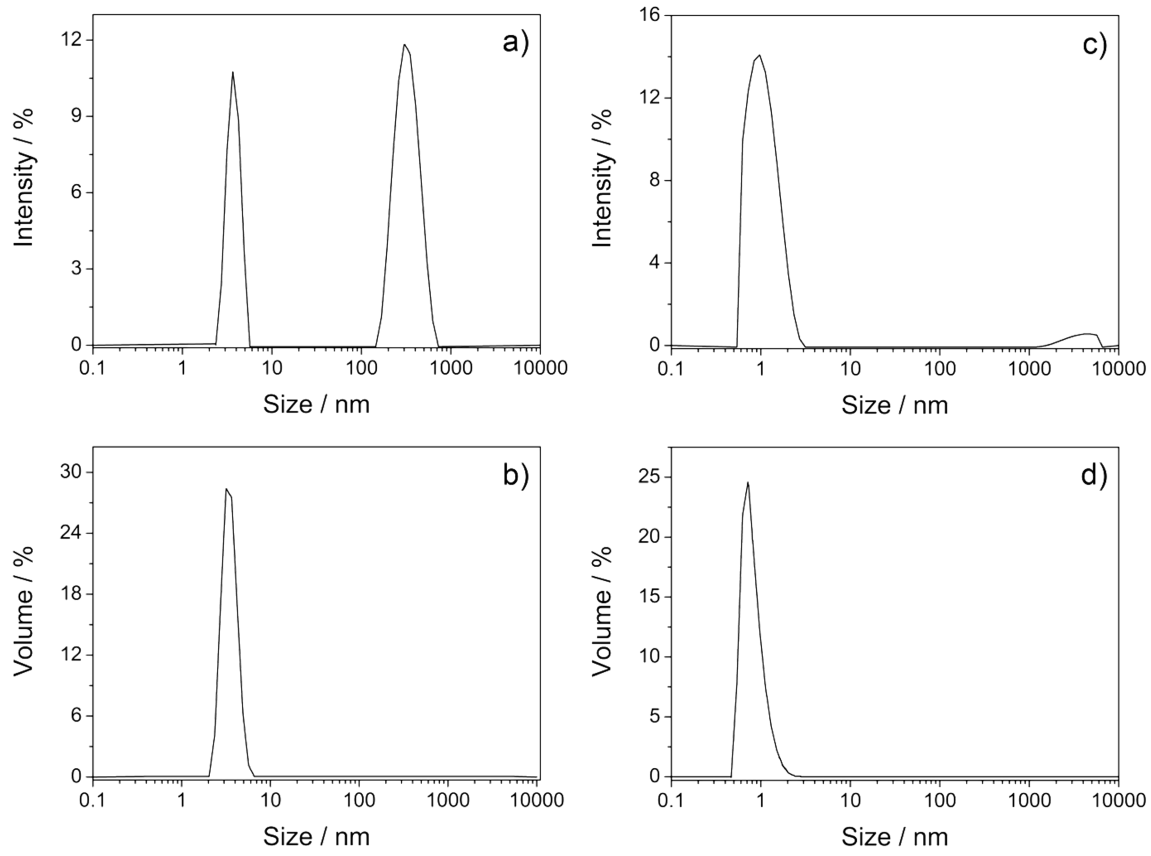

Figure 6: Size distribution of the molecular solution of C_{60} with 6 mM CD **5** in water at 25.0 °C: before centrifugation (a) by intensity, and (b) by volume; and after centrifugation (c) by intensity, and (d) by volume.

as 15 μM, was achieved in the presence of 6.0 mM of a γ-CD thioether. The resulting aqueous molecular solutions of C_{60} free of toxic organic solvents will hopefully find interesting applications in biomedicine, such as in photodynamic therapy or HIV-protease inhibition.

Experimental

General

Unless otherwise stated, all chemicals were used as received. Powdered fullerene C_{60} (> 99%) was purchased from Sigma Aldrich. Teflon syringe filters from Roth, Karlsruhe, Germany (0.45 μm) were used to remove insoluble material before UV–vis spectrophotometric analysis. UV–vis spectra of aqueous samples were performed on a Perkin Elmer Lambda 2 spectrometer (λ: 200–600 nm), by using quartz cells with a 1 cm or 1 mm optical path at 298 K.

Synthetic procedures

Hydrophilic thioethers **1**–**7** at all primary carbon atoms of γ-CD were synthesized from octakis(6-deoxy-6-iodo)-γ-CD by nucleophilic displacement reaction with sulfur nucleophiles by using standard procedures described previously [38].

Phase-solubility investigations

Solubility measurements of C_{60} in the presence of γ-CD and γ-CD derivatives in water were carried out according to the method proposed by Higuchi and Connors [40]. In glass vials containing excess amounts of C_{60}, aqueous solutions of γ-CD or γ-CD derivatives with different concentrations were added. The vials were sealed, protected from light, and magnetically stirred at room temperature for seven days. The solid residues were removed by filtration with syringe filter. According to the Lambert–Beer law, the concentrations of C_{60} in pure water and in CDs solutions were determined from UV–vis extinctions at the absorption maxima (log ε = 4.717, λ_{max} = 335 nm) [18].

Procedures for the solubilization of C_{60}

Several procedures were employed for the solubilization of C_{60}. **Procedure a:** C_{60} stirred in water in the presence of 6 mM γ-CD thioether at rt for 7 d. **Procedure b** was modified from a previously described method [21]: heated under reflux in water/toluene (v/v 1:1) for 3 d (γ-CD thioether concentration 6 mM), and then the resulting mixture dissolved in water after evaporation of the solvents. **Procedure c** was taken from a previous paper [42]: C_{60} stirred in DMF/toluene (v/v 1:1) at rt for 7 d

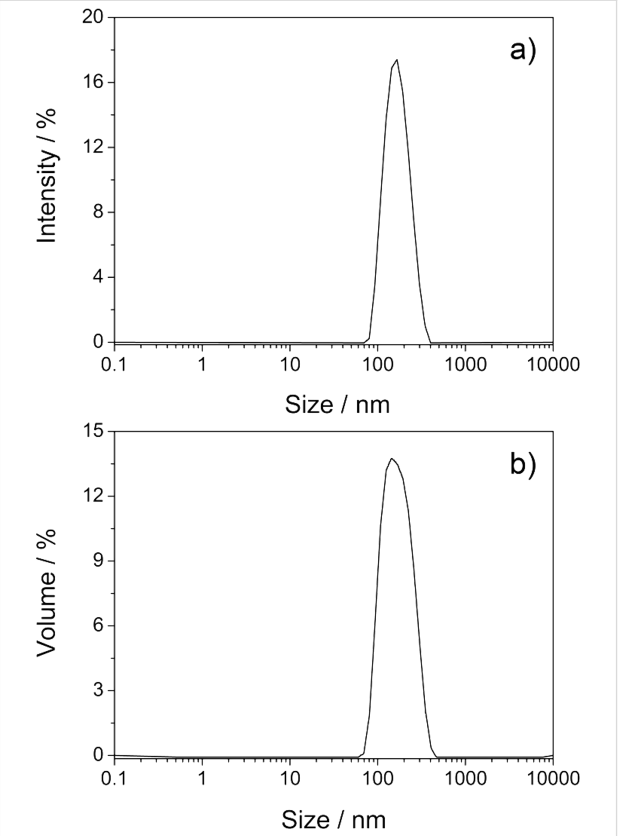

Figure 7: Size distributions of the aqueous C_{60} dispersions after filtration, produced by stirring C_{60} in 6mM γ-CD solution in DMF/toluene (v/v 1:1) according to procedure **c**) [42]: (a) by intensity and (b) by volume.

with 6 mM γ-CD thioether, and then the obtained inclusion complex dissolved in water after evaporation of the solvents. **Procedure d:** C_{60} stirred in water/CS_2 (v/v 1:1) at rt for 7 d with 6 mM γ-CD thioether, and then the obtained inclusion complex dissolved in water after evaporation of the solvents. *n*C_{60} was prepared following a method similar to that reported by Deguchi et al. (**procedure e**) [16]. ***n*C$_{60}$:** A saturated solution of C_{60} in THF was prepared by adding an excess amount of solid C_{60} (>2 mg) into THF (20 mL) and stirring overnight under a nitrogen atmosphere at room temperature. Excess solid was filtered off with a syringe filter. Saturated C_{60}/THF solution (500 mL) was placed in a flask and an equal volume of water was added at a rate of ca. 25 mL/min under vigorous stirring. A rotary evaporator was used to remove THF by using a stepwise evaporation approach. The start temperature was set at 30 °C. When the mixture volume had decreased to 500 mL, the temperature was increased at 1 °C/min to 70 °C and maintained at 70 °C until the volume had decreased to 250 mL, at which time an additional 250 mL volume of water was added. The last step was repeated once. The resulting *n*C_{60} solution could be diluted by adding water or concentrated by evaporation as needed.

Isothermal kinetic measurement

The procedure for performing isothermal kinetic investigations was modified from a previously described method [37]: A solution of C_{60} in chloroform (ca. 0.5 mg/mL, 0.5 mL) was carefully evaporated in a 1 cm quartz cell under nitrogen flow. After the addition of 3 mL of an aqueous solution containing the necessary amount of γ-CD derivative, the cell was sealed, protected from light, and maintained at 50 °C under gentle shaking. The UV–vis spectra of the resultant solution at appropriate time intervals were measured directly.

Dynamic light scattering measurement

Particle size distributions of the aqueous solution or dispersions of C_{60} were determined by dynamic light scattering (DLS) with a ZetaSizer Nano ZS (Malvern Instruments Ltd., Malvern, United Kingdom). From the diffusion coefficient the radius of the particle was determined via the Stokes–Einstein equation. The samples were filtered through a 0.45 μm syringe filter prior to particle-size measurements. Both intensity and volume size distribution curves were calculated from the scattering data by using the software of the instrument.

Supporting Information

Supporting Information File 1

Detailed dissolution kinetics.
[http://www.beilstein-journals.org/bjoc/content/supplementary/1860-5397-8-188-S1.pdf]

Acknowledgements

We gratefully thank the technical support from Annegret Engelke. Financial supports from Saarland University and China Scholarship Council are gratefully acknowledged.

References

1. Kroto, H. W.; Heath, J. R.; O'Brien, S. C.; Curl, R. F.; Smalley, R. E. *Nature* **1985,** *318,* 162–163. doi:10.1038/318162a0
2. Krätschmer, W.; Lamb, L. D.; Fostiropoulos, K.; Huffman, D. R. *Nature* **1990,** *347,* 354–358. doi:10.1038/347354a0
3. Nakamura, E.; Isobe, H. *Acc. Chem. Res.* **2003,** *36,* 807–815. doi:10.1021/ar030027y
4. Da Ros, T.; Prato, M. *Chem. Commun.* **1999,** 663–669. doi:10.1039/a809495k
5. Jensen, A. W.; Wilson, S. R.; Schuster, D. I. *Bioorg. Med. Chem.* **1996,** *4,* 767–779. doi:10.1016/0968-0896(96)00081-8
6. Hirsch, T.; Kettenberger, H.; Wolfbeis, O. S.; Mirsky, V. M. *Chem. Commun.* **2003,** 432–433. doi:10.1039/b210554c
7. Hebard, A. F.; Rosseinsky, M. J.; Haddon, R. C.; Murphy, D. W.; Glarum, S. H.; Palstra, T. T. M.; Ramirez, A. P.; Kortan, A. R. *Nature* **1991,** *350,* 600–601. doi:10.1038/350600a0

8. Dai, L. M. *Polym. Adv. Technol.* **1999,** *10,* 357–420. doi:10.1002/(SICI)1099-1581(199907)10:7<357::AID-PAT886>3.0.CO;2-9
9. Halls, J. J. M.; Pichler, K.; Friend, R. H.; Moratti, S. C.; Holmes, A. B. *Appl. Phys. Lett.* **1996,** *68,* 3120–3122. doi:10.1063/1.115797
10. Semenov, K. N.; Charykov, N. A.; Keskinov, V. A.; Piartman, A. K.; Blokhin, A. A.; Kopyrin, A. A. *J. Chem. Eng. Data* **2010,** *55,* 13–36. doi:10.1021/je900296s
11. Heymann, D. *Fullerene Sci. Technol.* **1996,** *4,* 509–515. doi:10.1080/10641229608001567
12. Sijbesma, R.; Srdanov, G.; Wudl, F.; Castoro, J. A.; Wilkins, C.; Friedman, S. H.; DeCamp, D. L.; Kenyon, G. L. *J. Am. Chem. Soc.* **1993,** *115,* 6510–6512. doi:10.1021/ja00068a006
13. Lyon, D. Y.; Adams, L. K.; Falkner, J. C.; Alvarez, P. J. J. *Environ. Sci. Technol.* **2006,** *40,* 4360–4366. doi:10.1021/es0603655
14. Fortner, J. D.; Lyon, D. Y.; Sayes, C. M.; Boyd, A. M.; Falkner, J. C.; Hotze, E. M.; Alemany, L. B.; Tao, Y. J.; Guo, W.; Ausman, K. D.; Colvin, V. L.; Hughes, J. B. *Environ. Sci. Technol.* **2005,** *39,* 4307–4316. doi:10.1021/es048099n
15. Hirsch, A.; Lamparth, I.; Karfunkel, H. R. *Angew. Chem., Int. Ed. Engl.* **1994,** *33,* 437–438. doi:10.1002/anie.199404371
16. Deguchi, S.; Alargova, R. G.; Tsujii, K. *Langmuir* **2001,** *17,* 6013–6017. doi:10.1021/la010651o
17. Scrivens, W. A.; Tour, J. M.; Creek, K. E.; Pirisi, L. *J. Am. Chem. Soc.* **1994,** *116,* 4517–4518. doi:10.1021/ja00089a067
18. Torres, V. M.; Posa, M.; Srdjenovic, B.; Simplício, A. L. *Colloids Surf., B* **2011,** *82,* 46–53. doi:10.1016/j.colsurfb.2010.08.012
19. Haino, T.; Yanase, M.; Fukunaga, C.; Fukazawa, Y. *Tetrahedron* **2006,** *62,* 2025–2035. doi:10.1016/j.tet.2005.07.121
20. Ikeda, A.; Suzuki, Y.; Yoshimura, M.; Shinkai, S. *Tetrahedron* **1998,** *54,* 2497–2508. doi:10.1016/S0040-4020(98)00012-X
21. Andersson, T.; Nilsson, K.; Sundahl, M.; Westman, G.; Wennerström, O. *J. Chem. Soc., Chem. Commun.* **1992,** 604–606. doi:10.1039/C39920000604
22. Yoshida, Z.-i.; Takekuma, H.; Takekuma, S.-i.; Matsubara, Y. *Angew. Chem., Int. Ed. Engl.* **1994,** *33,* 1597–1599. doi:10.1002/anie.199415971
23. Wenz, G. *Angew. Chem., Int. Ed. Engl.* **1994,** *33,* 803–822. doi:10.1002/anie.199408031
24. Wenz, G. *Adv. Polym. Sci.* **2009,** *222,* 1–54. doi:10.1007/978-3-642-01410-9
25. Dodziuk, H. *Cyclodextrins and their Complexes: Chemistry, Analytical Methods, Applications;* Wiley-VCH: Weinheim, Germany, 2006. doi:10.1002/3527608982
26. Rekharsky, M. V.; Inoue, Y. *Chem. Rev.* **1998,** *98,* 1875–1918. doi:10.1021/cr970015o
27. Liu, L.; Guo, Q.-X. *J. Inclusion Phenom. Macrocyclic Chem.* **2002,** *42,* 1–14. doi:10.1023/A:1014520830813
28. Müller, A.; Wenz, G. *Chem.–Eur. J.* **2007,** *13,* 2218–2223. doi:10.1002/chem.200600764
29. Raffaini, G.; Ganazzoli, F. *J. Phys. Chem. B* **2010,** *114,* 7133–7139. doi:10.1021/jp911812j
30. Priyadarsini, K. I.; Mohan, H.; Tyagi, A. K.; Mittal, J. P. *J. Phys. Chem.* **1994,** *98,* 4756–4759. doi:10.1021/j100068a044
31. Komatsu, K.; Fujiwara, K.; Murata, Y.; Braun, T. *J. Chem. Soc., Perkin Trans. 1* **1999,** 2963–2966. doi:10.1039/A904736K
32. Konstantaki, M.; Koudoumas, E.; Couris, S.; Janot, J. M.; Eddaoudi, H.; Deratani, A.; Seta, P.; Leach, S. *Chem. Phys. Lett.* **2000,** *318,* 488–495. doi:10.1016/S0009-2614(00)00037-3
33. Wenz, G.; Strassnig, C.; Thiele, C.; Engelke, A.; Morgenstern, B.; Hegetschweiler, K. *Chem.–Eur. J.* **2008,** *14,* 7202–7211. doi:10.1002/chem.200800295
34. Steffen, A.; Thiele, C.; Tietze, S.; Strassnig, C.; Kämper, A.; Lengauer, T.; Wenz, G.; Apostolakis, J. *Chem.–Eur. J.* **2007,** *13,* 6801–6809. doi:10.1002/chem.200700661
35. Wang, H. M.; Soica, C. M.; Wenz, G. *Nat. Prod. Commun.* **2012,** *7,* 289–291.
36. Bensasson, R. V.; Bienvenue, E.; Dellinger, M.; Leach, S.; Seta, P. *J. Phys. Chem.* **1994,** *98,* 3492–3500. doi:10.1021/j100064a035
37. Kuroda, Y.; Nozawa, H.; Ogoshi, H. *Chem. Lett.* **1995,** *24,* 47–48. doi:10.1246/cl.1995.47
38. Wang, H. M.; Wenz, G. *Chem.–Asian J.* **2011,** *6,* 2390–2399. doi:10.1002/asia.201100217
39. Geckeler, K. E.; Hirsch, A. *J. Am. Chem. Soc.* **1993,** *115,* 3850–3851. doi:10.1021/ja00062a091
40. Higuchi, T.; Connors, K. *Adv. Anal. Chem. Instrum.* **1965,** *4,* 117–212.
41. Singh, R.; Tonnesen, H. H.; Vogensen, S. B.; Loftsson, T.; Másson, M. *J. Inclusion Phenom. Macrocyclic Chem.* **2010,** *66,* 335–348. doi:10.1007/s10847-009-9651-5
42. Murthy, C. N.; Geckeler, K. E. *Chem. Commun.* **2001,** 1194–1195. doi:10.1039/b102142g
43. Hou, W.-C.; Jafvert, C. T. *Environ. Sci. Technol.* **2009,** *43,* 362–367. doi:10.1021/es802465z
44. Jansook, P.; Moya-Ortega, M. D.; Loftsson, T. *J. Inclusion Phenom. Macrocyclic Chem.* **2010,** *68,* 229–236. doi:10.1007/s10847-010-9779-3
45. Puskás, I.; Schrott, M.; Malanga, M.; Szente, L. *J. Inclusion Phenom. Macrocyclic Chem.* **2012,** 1–8. doi:10.1007/s10847-012-0127-7
46. Ruf, H.; Georgalis, Y.; Grell, E. *Methods Enzymol.* **1989,** *172,* 364–390. doi:10.1016/S0076-6879(89)72024-3
47. Alexander, M.; Dalgleish, D. G. *Food Biophys.* **2006,** *1,* 2–13. doi:10.1007/s11483-005-9000-1
48. Burchard, W. *Adv. Polym. Sci.* **1983,** *48,* 1–124. doi:10.1007/3-540-12030-0_1
49. Mie, G. *Ann. Phys.* **1908,** *330,* 377–445. doi:10.1002/andp.19083300302

License and Terms

Beilstein Journal of Organic Chemistry

Self-assembled organic–inorganic magnetic hybrid adsorbent ferrite based on cyclodextrin nanoparticles

Ângelo M. L. Denadai[1,2], Frederico B. De Sousa[3], Joel J. Passos[3], Fernando C. Guatimosim[3], Kirla D. Barbosa[3], Ana E. Burgos[4], Fernando Castro de Oliveira[1], Jeann C. da Silva[1], Bernardo R. A. Neves[5], Nelcy D. S. Mohallem[6] and Rubén D. Sinisterra[*3]

Full Research Paper

Open Access

Address:
[1]Centro Federal de Educação Tecnológica (CEFET-MG), Campus VII, Timóteo, MG, Brazil 35183-006, [2]Universidade Federal de Juiz de Fora (UFJF), Governador Valadares, 35010-177, MG, Brazil, [3]Laboratório de Encapsulamento Molecular e Biomateriais (LEMB) – Departamento de Química, Instituto de Ciências Exatas, Universidade Federal de Minas Gerais (UFMG), Belo Horizonte, 31270-901, MG, Brazil, [4]Universidad Nacional de Colombia Bogotá – DC, Colombia, [5]Departamento de Física, ICEx, Universidade Federal de Minas Gerais (UFMG) Belo Horizonte – MG, 31270-901, Brazil and [6]Laboratório de Materiais Nanoestruturados, Departamento de Química, ICEx, Universidade Federal de Minas Gerais (UFMG) Belo Horizonte – MG, 31270-901, Brazil

Email:
Rubén D. Sinisterra* - sinisterra@ufmg.br

* Corresponding author

Keywords:
assembled particles; colloids; cyclodextrin; ferrite; hybrid materials

Beilstein J. Org. Chem. **2012,** *8,* 1867–1876.
doi:10.3762/bjoc.8.215

Received: 01 June 2012
Accepted: 04 October 2012
Published: 01 November 2012

This article is part of the Thematic Series "Superstructures with cyclodextrins: Chemistry and applications".

Guest Editor: H. Ritter

Abstract

Organic–inorganic magnetic hybrid materials (MHMs) combine a nonmagnetic and a magnetic component by means of electrostatic interactions or covalent bonds, and notable features can be achieved. Herein, we describe an application of a self-assembled material based on ferrite associated with β-cyclodextrin (Fe-Ni/Zn/βCD) at the nanoscale level. This MHM and pure ferrite (Fe-Ni/Zn) were used as an adsorbent system for Cr^{3+} and $Cr_2O_7^{2-}$ ions in aqueous solutions. Prior to the adsorption studies, both ferrites were characterized in order to determine the particle size distribution, morphology and available binding sites on the surface of the materials. Microscopy analysis demonstrated that both ferrites present two different size domains, at the micro- and nanoscale level, with the latter being able to self-assemble into larger particles. Fe-Ni/Zn/βCD presented smaller particles and a more homogeneous particle size distribution. Higher porosity for this MHM compared to Fe-Ni/Zn was observed by Brunauer–Emmett–Teller isotherms and positron-annihilation-lifetime spectroscopy. Based on the pKa values, potentiometric titrations demonstrated the

presence of βCD in the inorganic matrix, indicating that the lamellar structures verified by transmission electronic microscopy can be associated with βCD assembled structures. Colloidal stability was inferred as a function of time at different pH values, indicating the sedimentation rate as a function of pH. Zeta potential measurements identified an amphoteric behavior for the Fe-Ni/Zn/βCD, suggesting its better capability to remove ions (cations and anions) from aqueous solutions compared to that of Fe-Ni/Zn.

Introduction

Organic–inorganic hybrid materials (HMs) are often prepared by assembling organic and inorganic molecules based on electrostatic interactions or chemical bonding between them, which will leads to an unpredictable stoichiometry [1]. The structures and properties of HMs depend on the nature of both components, organic and inorganic, and also on the synthesis process, which can be carried out by metal or organic hydrolyses [2,3]. Controlling the method of HM synthesis could lead to a predictable crystal structure and homogeneous particle size distribution [4]. Additionally, surface properties could be modulated by selecting an appropriate organic molecule with desirable functional groups in its structure. In particular, magnetic organic–inorganic hybrid materials (MHMs) have attracted considerable attention based on their multifunctional and biocompatible properties [2,5,6]. Moreover, MHMs can present a greater number of applications than nonmagnetic hybrid materials when their suspensions are used.

These MHMs systems are susceptible to external magnetic fields because of the strong magnetic interactions existing among the magnetized particles, which are able to modify the colloidal and rheological properties of the solutions. Thus, functions based on their magnetic characteristics such as conduction and accumulation in a system under an external magnetic field can be realized. In this sense, colloidal systems of MHMs have shown an increasing number of applications in many different technologies, including ferrofluids [7], magnetic separators [8], magnetic resonance imaging [9], hyperthermia [10], and water treatment [4].

Nickel-zinc ferrites (Fe-Ni/Zn) are one of these versatile magnetic materials, since these systems present high magnetic saturation, Curie temperature and chemical stability. Additionally, low coercivity and biodegradability have been observed in Fe-Ni/Zn, being an interesting part of the inorganic component in the MHM structure [11]. The organic molecule in the MHM should present specific characteristics in order to improve the material application, including available binding sites, to bond or interact through intermolecular forces with the inorganic matrix, and high surface area, which is important to improve the MHM adsorption and adhesion properties. In order to design a MHM based on Fe-Ni/Zn with adsorption properties for environmental use, cyclodextrins (CDs) can be associated with the inorganic matrix as an interesting strategy, since these macromolecules have been used for several devices with different properties, from light-responsive matrices to molecular recognition materials [12,13].

CDs are oligosaccharides commonly formed by six, seven or eight α(1→4) linked-D-glucopyranoside units, named αCD, βCD and γCD, respectively. These macromolecules have a rigid and well-defined structure with a toroidal shape, in which a variety of organic and inorganic guest molecules can be inserted into their cavities, resulting in the formation of inclusion complexes [14-17]. Beyond these characteristics, it has been reported in the literature that CDs self-assemble into large aggregates [18-20], suggesting their uses as size-modulator molecules [21], similar to other amphiphilic molecules [22-25]. Based on these interesting properties for both systems, CDs and Fe-Ni/Zn can be used to synthesize a MHM with large number of applications. Moreover, due to the arrangement of CDs, their primary and secondary hydroxy groups may be able to interact with a ferrite structure, through covalent bonds or also by intramolecular interactions. These hydroxy groups could improve the adsorption properties of the MHM by including guest molecules in CD cavities or also by allowing the assembly process. Recently, adsorption materials have become one of the most versatile and widely used technologies to remove heavy metals from industrial wastewater, including chrome in its different oxidation states [4,26]. Although activated carbon has been frequently applied for this purpose, magnetic adsorbent materials have also demonstrated their potential applicability in the past few years, because of their easy separation properties.

Herein, Fe-Ni/Zn and the MHM prepared by using Fe-Ni/Zn and βCD (Fe-Ni/Zn/βCD) were synthesized by adapting a method previously described in the literature [7]. These magnetic materials were characterized in the solid state by X-ray powder diffraction (XRD), Fourier transform infrared spectroscopy (FTIR), and thermal analysis (TG/DTA), and by their magnetic behavior in aqueous suspension (see Supporting Information File 1). Fe-Ni/Zn and Fe-Ni/Zn/βCD nanoparticles morphologies were investigated in the solid state by scanning electronic microscopy (SEM), transmission electronic

microscopy (TEM), and atomic force microscopy (AFM). Size distribution and colloidal suspension stability were characterized by dynamic light scattering (DLS) and sedimentation kinetic studies by using UV–vis spectroscopy. Ferrite binding sites were characterized by zeta potential (ZP) and potentiometric titration. The free volume for both materials was evaluated by Brunauer–Emmett–Teller isotherm (BET) and positron-annihilation-lifetime spectroscopy (PALS). Thus, considering the advanced functional properties achieved by βCD insertion in the inorganic matrix identified by the above experiments and the MHM capability to self-assemble, the adsorption properties for both ferrites using chrome ions (Cr^{3+} and $Cr_2O_7^{2-}$) in aqueous solutions were tested and evaluated by ZP measurements.

Results and Discussion

Fe-Ni/Zn and Fe-Ni/Zn/βCD size characterization

In order to investigate the Fe-Ni/Zn and Fe-Ni/Zn/βCD morphology and size distribution at different aggregation levels, these materials were investigated in the solid state by SEM, TEM and AFM and also in aqueous suspension by using DLS. AFM images of Fe-Ni/Zn and Fe-Ni/Zn/βCD are presented in Figure 1. Based on these images, nanoparticles below 100 nm were verified for these materials. Looking closer, Fe-Ni/Zn/βCD presents smaller nanoparticles in a range of 20 to 50 nm, while the Fe-Ni/Zn consisted of domains higher than 50 nm. The smaller particles observed for the Fe-Ni/Zn/βCD particles could be due to the size-modulator effect of CDs [19,20,27,28], which could act as a nanoreactor for ferrite synthesis, preventing the particles growing during the ferrite synthesis (nucleation process).

In order to gain insight into the microstructure of these assembled materials, SEM and TEM were also carried out. TEM images of the magnetic materials, demonstrating their structure from the nanoscale level up to the aggregate particles, are shown in Figure 2a and Figure 2b. In addition, the TEM image for the Fe-Ni/Zn/βCD showed aligned structures in the nanoparticle matrix, which can correspond to the assembled βCD structures in the MHM. These lamellar self-assembled structures are similar to the βCD crystals described previously in the literature [29], confirming the presence of the macromolecule in the ferrite nanoparticles matrix. SEM images, Figure 2c and Figure 2d, demonstrate larger assembled particles (above 500 nm). It is interesting to note that when βCD is used to prepare the ferrite nanoparticles, size domains are smaller than those observed for the material prepared without the macromolecule. These results corroborate the hypothesis considering the size-modulator effect of βCD proposed previously based on the analysis of the AFM images.

Fe-Ni/Zn and Fe-Ni/Zn/βCD were also analyzed in aqueous suspensions, at pH 7, (Figure 3). The ferrite aggregation process was confirmed, Figure 3a and Figure 3b, in which particle size distributions of about 2.8 and 2.3 μm were observed for Fe-Ni/Zn and Fe-Ni/Zn/βCD, respectively. In the presence of βCD a more homogeneous size distribution was verified, suggesting that βCD is able to minimize the ferrite coalescence process in aqueous solution. The ferrite aggregation process may occur in low zeta potential values (−10 mV, see zeta potential data) and is insufficient to avoid van der Waals attraction [30]; however, at pH 7 this self-assembly behavior can also be verified. Evidence for the ferrite aggregation process is observed in aqueous suspensions when these materials are sonicated, Figures 3c and

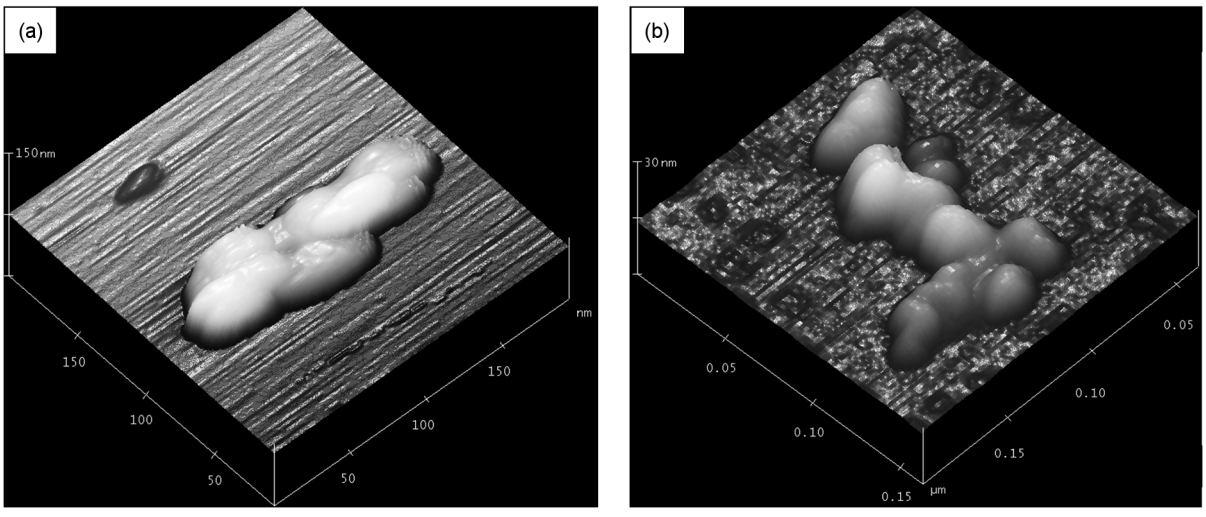

Figure 1: AFM images of (a) Fe-Ni/Zn and (b) Fe-Ni/Zn/βCD.

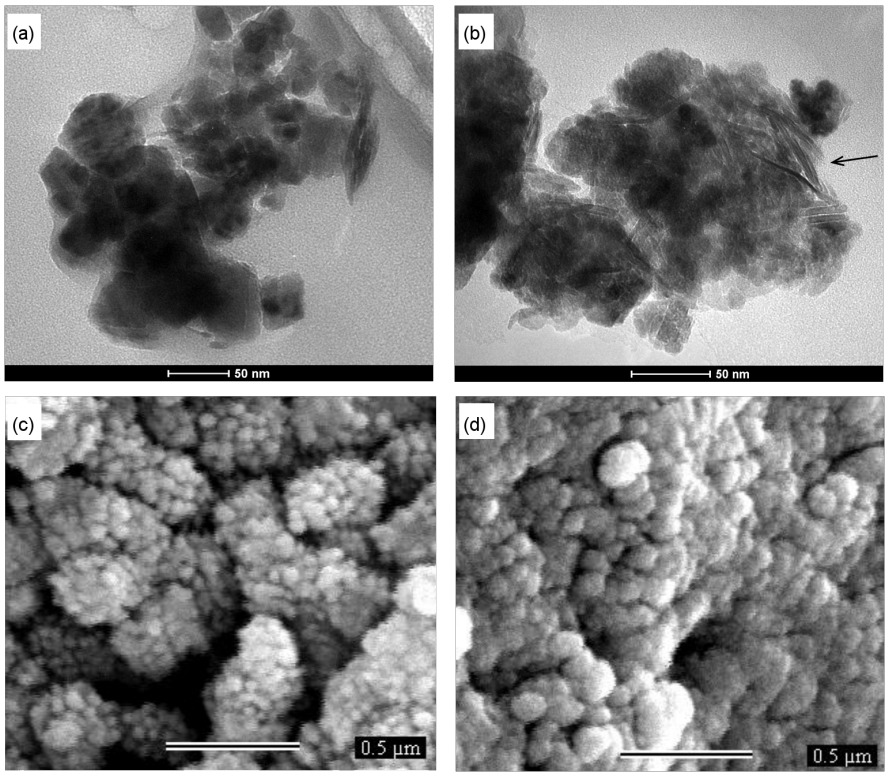

Figure 2: TEM images of (a) Fe-Ni/Zn and (b) Fe-Ni/Zn/βCD and SEM images of (c) Fe-Ni/Zn and (d) Fe-Ni/Zn/βCD.

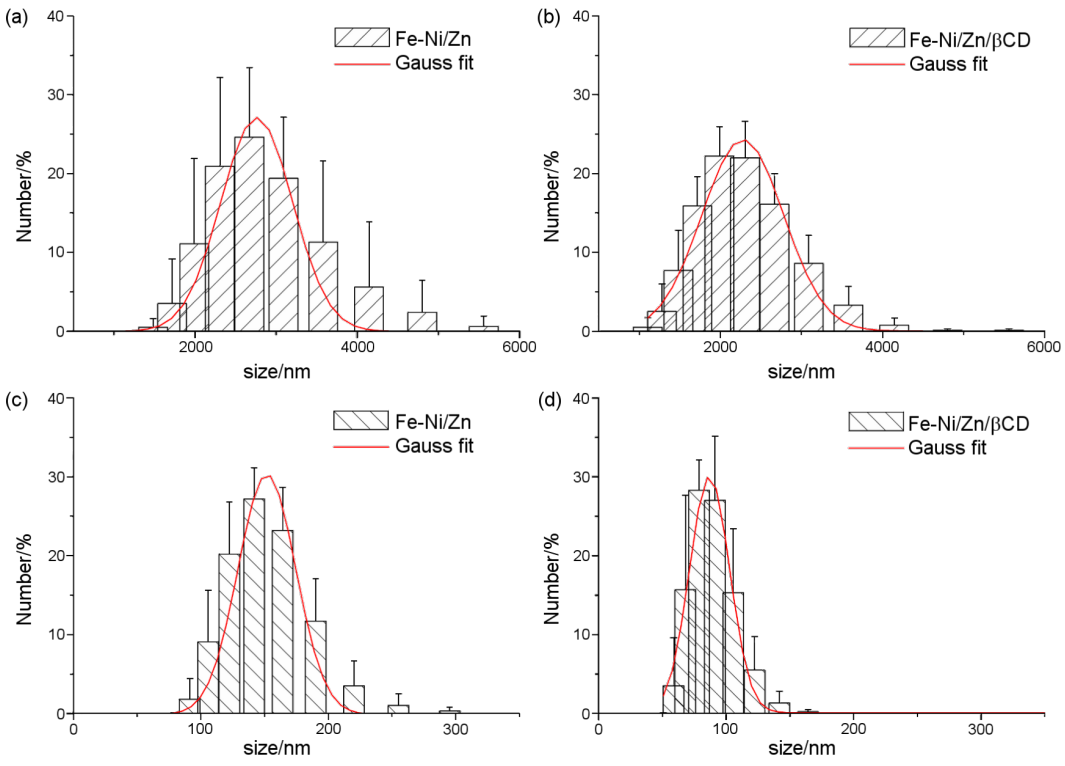

Figure 3: DLS measurements for before (a) and (b) and after (c) and (d) the sonication process.

Figure 3d, in which the assembled structures are disrupted in order to obtain the nanoparticles. Once again, Fe-Ni/Zn/βCD presented a smaller particles distribution (average size of about 85 nm) with a more homogenous size distribution than that prepared without βCD (Fe-Ni/Zn about 150 nm). These results are in accordance with those verified by AFM and TEM, in which Fe-Ni/Zn/βCD presented smaller nanoparticles than pure ferrite in the solid state. Although some discrepancy between the DLS and AFM particle size distributions has been observed, it has been previously reported in the literature for other systems [31,32].

Textural characterization by gas adsorption

BET isotherms were carried out to investigate the free volume of the ferrites. Fe-Ni/Zn was able to adsorb gas at 115 cm^3 g^{-1}, showing a type IV isotherm by (Brunauer, Deming, Deming, and Teller) BDDT classification [33], which is characteristic of mesoporous materials, and its hysteresis loop closed at p/p_0 = 0.2. Adsorbing capacity for the Fe-Ni/Zn/βCD was 125 cm^3 of gas per gram, presenting an intermediary isotherm characteristic that changes from meso- to microporosity, and its hysteresis loop closed at p/p_0 = 0.4, demonstrating that the presence of βCD implies a minor difficulty in adsorption.

Textural characteristics for the ferrite (Fe-Ni/Zn), which has a specific surface area of 127 m^2 g^{-1}, changed substantially with the inclusion of βCD in the inorganic matrix, increasing the specific surface area to 191 m^2 g^{-1} (an increase of 50.4%). This surface area variation is mainly due to the microporosity increasing by the inclusion of the βCD in the inorganic matrix. Fe-Ni/Zn presented a fractal dimension (D) of 2.772, which increased to 2.934 with the macromolecule insertion, showing a significant growth in the surface roughness, since the D value of a surface with maximum roughness is 3. This result is in accordance with microscopy analysis in the solid state, which shows different morphologies for these two samples.

Determination of free volume by PALS

The free volume was measured by positron probe through the PALS technique, where the longest component of the positron-lifetime spectrum, τ_3 (the o-Ps pick-off lifetime), can be correlated with free volume holes in condensed matter. According to this model, τ_3 grows leading to an increasing in the free volume radius, based on a spherical-cavity model [34,35]. The calculated free volume dimension has values of V_f = 69.9 $Å^3$ and V_f = 115.9 $Å^3$ for Fe-Ni/Zn and Fe-Ni/Zn/βCD, respectively; corresponding to an increase of 65% of the free volume (ΔV_f = 46 $Å^3$). These results corroborate BET isotherm studies, which pointed out a greater porosity in the material prepared by using βCD.

Potentiometric titrations

Potentiometric titrations were recorded in order to determine the number of ionizable sites for the magnetic materials through the first derivative of the titration curve. As can be seen in Figure 4a and Figure 4b, the first derivative of the titration curves pointed out several transitions, demonstrating that ferrite could be considered a polyprotic acid, probably due to the ionization of the different groups on the ferrite surfaces. It can also be observed that the potentiometric curve for Fe-Ni/Zn/βCD exhibits at least four transitions, two in addition to the pure Fe-Ni/Zn. The pKa values of the ferrites were calculated by using the Henderson–Hasselbalch Equation 1, at the point where $[A^-]$ = [HA] [36]:

$$\mathrm{pH} = \mathrm{pK_a} + \log\frac{[\mathrm{A^-}]}{[\mathrm{HA}]} \quad (1)$$

Transitions at pKa 6.5 and 13.5 were attributed to the ionization of ferrite groups in the MHM system, since Fe-Ni/Zn also presented close transition values (pKa 6.5 and 12.6). Thus, transitions at pKa 5.5 and 9.4 in the Fe-Ni/Zn/βCD were attributed to the ionization of βCD primary and secondary hydroxy

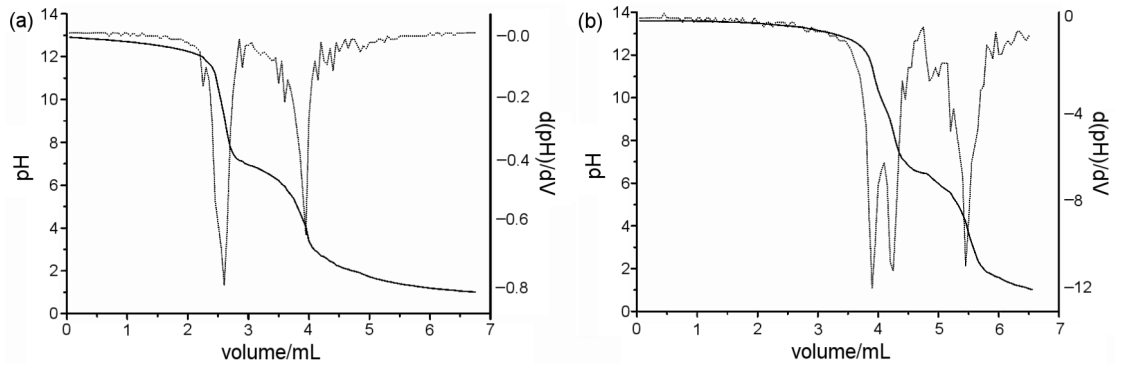

Figure 4: Potentiometric curves of the (a) Fe-Ni/Zn and (b) Fe-Ni/Zn/βCD.

groups. These results emphasize that βCD is part of the inorganic matrix, corroborating the data obtained by TEM, in which lamellar assembled structures were observed in the MHM matrix.

Zeta potential

Particles in contact with an aqueous electrolyte solution acquire a surface charge as a result of adsorption or ionization processes. In order to evaluate the electrostatic repulsion between dispersed ferrite particles in solution, the electrical surface potential was evaluated by using ZP, computed from electrophoretic mobility measurements [37]. Figure 5 depicts the ZP variation as a function of the pH for the aqueous suspension of the ferrites, in which the solutions were tuned by using nitric acid or sodium hydroxide. These curves demonstrated that the zeta potential values are negative under the studied experimental conditions, and a pH dependency was also verified, once the ZP values become more negative increasing the pH of the aqueous suspensions.

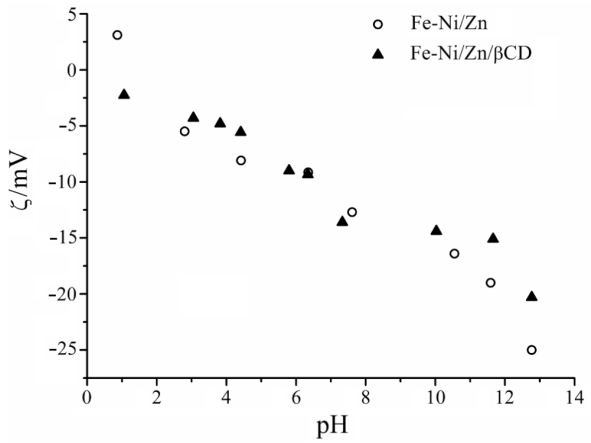

Figure 5: Zeta potential curves as a function of pH for the (○) Fe-Ni/Zn and (▲) Fe-Ni/Zn/βCD.

The negative values in the pH range could be attributed to (i) ionization of R–OH groups after pH 6.5, which causes the formation of negative charges on the ferrite surface [38], and/or (ii) preferential adsorption of nitrate anions on the particle surface before this pH, since ferrites can become less hydrophilic upon protonation, and it is known that NO_3^- exhibits a preferential adsorption on weakly hydrated surfaces [39]. The isoelectric point (IP) of ferrites is close to pH 7 [40], thus inflexions observed close to this value for both systems may be an apparent IP, which was masked by competition between the ionization of Fe–OH groups and preferential NO_3^- adsorption. In other materials, negative ZP values have been also found in the pH range scanned from 1 to 13 [41-43].

Although the potentiometric titration demonstrated that ferrites present different transitions due to the different ionization sites, ZP titrations did not show the same behavior. A reasonable explanation for this phenomenon is based on the sensitivity of these analytical techniques. Potentiometry measures the electrical potential difference established through the electrode membrane, being directly dependent on the activity of H_3O^+ ions in the bulk solution, since its rate of diffusion is proportional to the concentration. ZP measurements obtained by Doppler electrophoresis are dependent on the Brownian diffusion of the particles in an electric field, which depends on the surface charge and size, and the size and charge polydispersities, as well as the aggregation state, among other phenomena; which are hard to control in a suspension material.

Sedimentation studies

Information about the colloidal stability of these ferrite suspensions can be inferred from the optical obscuration changes of the optic path by visible light at 700 nm as a function of time [40]. Figure 6 shows the obscuration (O_b) relative to its absorbance at time t = 0 s ($O_{b,0}$), plotted as a function of time for different pH values. Although the overall tendency of O_b/

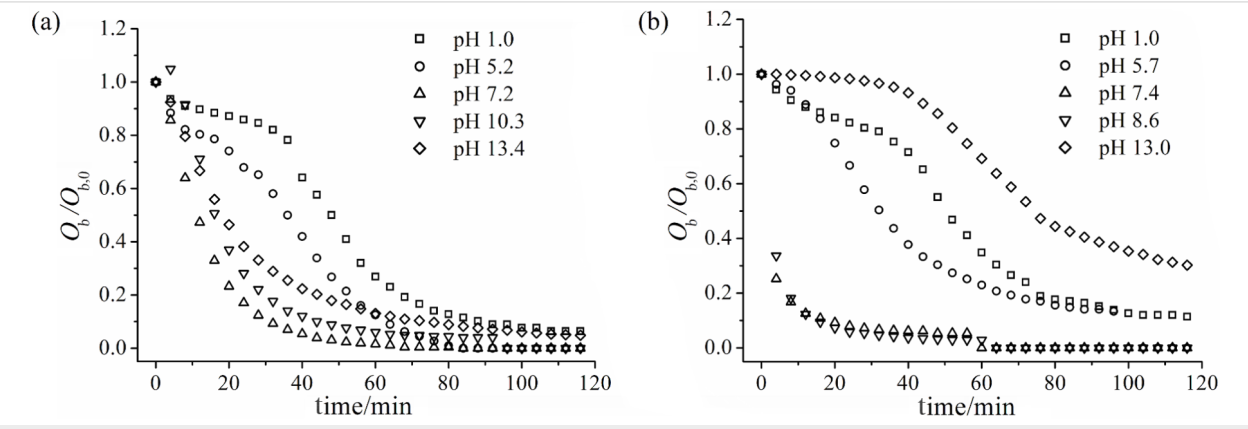

Figure 6: Relative optical obscuration ($O_b/O_{b,0}$) as a function of time for (a) Fe-Ni/Zn and (b) Fe-Ni/Zn/βCD.

$O_{b,0}$ is to decrease over time due to particle sedimentation, the results obtained at different pH do not overlap, indicating that there is a clear pH dependence on the sedimentation rate. This pH dependence corresponds to the charge variation on the ferrite surface, which was also observed in the ZP titrations.

Since light scattering and absorption properties upon sedimentation are complicated phenomena, only the initial slopes, $S = d(O_b/O_{b,0})_{t\rightarrow 0}/dt$, of the obscuration curves were used in order to evaluate the sedimentation rate, as suggested by Plaza et al. [40]. Figure 7 shows the initial sedimentation rate for both magnetic systems. It can be observed that S values are greater in magnitude for the Fe-Ni/Zn/βCD than for the Fe-Ni/Zn: once at neutral pH the initial sedimentation is faster. The maximum absolute S (i.e., $|S|$) can be related to the absence of electrostatic repulsion between the particles in the pH vicinity of the apparent IP, and particle aggregation could occur under these conditions. This is a direct consequence of the greater number of hydroxy groups in the Fe-Ni/Zn/βCD system.

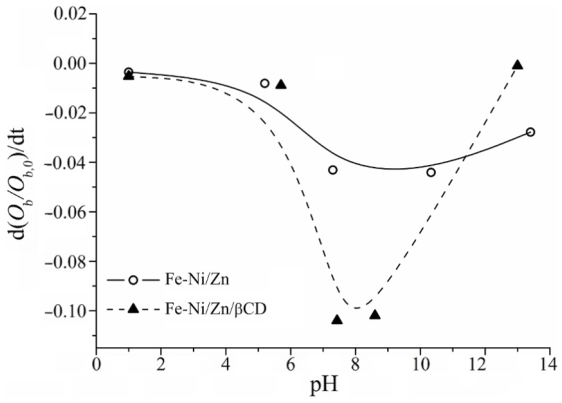

Figure 7: Obscuration curves for the Fe-Ni/Zn (○) and Fe-Ni/Zn/βCD (▲) as a function of pH.

At pH ≈ 1, both ferrites have approximately the same and slow rate of sedimentation, probably due to NO_3^- adsorption. However, at pH ≈ 13, $|S|$ is smaller for the Fe-Ni/Zn/βCD than for pure ferrite; in spite of the fact that the ZP results demonstrated the same values for both materials. The smaller particles and the greater presence of hydroxy groups of the Fe-Ni/Zn/βCD could be responsible for the slower sedimentation rate at this pH value.

Adsorption studies

Adsorption studies were carried out in order to compare the ion adsorption capacity of these magnetic materials in aqueous solution. ZP measurements were used to gain insights into the adsorption processes of Cr^{3+} and $Cr_2O_7^{2-}$ ions. Figure 8 shows how the ZP values change as a function of the ion concentration. The ZP titration curves indicated that the MHM is able to adsorb both ions (Cr^{3+} and $Cr_2O_7^{2-}$) on its surface, since the ZP values (|ZP|) increase in their presence. These data suggest an amphoteric characteristic of Fe-Ni/Zn/βCD, which can interact with positive and negative species through ion–dipole or ion–ion interactions. Changes in the ZP values have been observed in the literature for different ferrites after the ion-adsorption process, indicating the affinity between them [44].

Comparing qualitatively the interaction involving the MHM with both ions, it is possible to observe its greater affinity for the $Cr_2O_7^{2-}$ than the Cr^{3+}, since for the latter a constant ZP value was observed above 0.4 mmol L^{-1}, while a plateau was not reached for the $Cr_2O_7^{2-}$ titration. This result also demonstrated that the MHM are able to adsorb more than 10 mmol of this anion per liter (maximum concentration tested), which is greater than that of approximately 0.4 mmol L^{-1} for the Cr^{3+} cation. The MHM capacity to adsorb Cr^{3+} ions (about 19 mg g^{-1} of MHM) was higher than that observed for $MnFe_2O_4$ ferrite (7.6 mg g^{-1} of $MnFe_2O_4$) to remove Cr^{6+} from aqueous

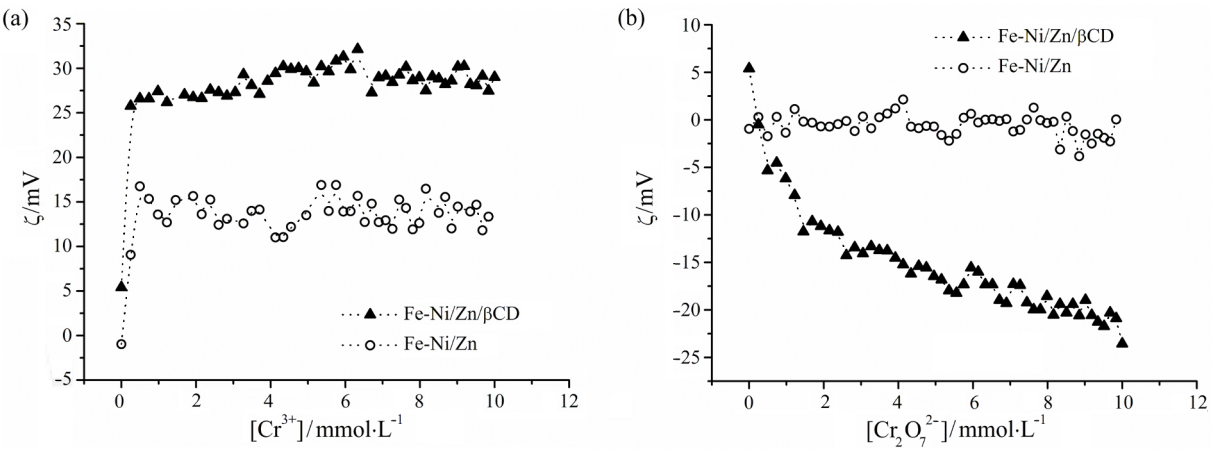

Figure 8: Adsorption curves of (a) Cr^{3+} and (b) $Cr_2O_7^{2-}$ ions using Fe-Ni/Zn and Fe-Ni/Zn/βCD aqueous suspensions.

solutions, described previously [4]. Thus, the inclusion of βCD in the inorganic matrix increased the ion adsorption, demonstrating the importance of choosing the organic component in a hybrid material carefully. Fe-Ni/Zn adsorption capacity for the Cr^{3+} cation was similar to that observed when βCD was used in the MHM. However without βCD, Fe-Ni/Zn was not able to adsorb the $Cr_2O_7^{2-}$, since no change in the ZP values was verified, indicating that Fe-Ni/Zn and the anion did not interact in aqueous suspension.

Conclusion

Hybrid magnetic nanoparticles based on ferrite and βCD were prepared and characterized in the solid state and in aqueous suspension, and their properties were compared with pure ferrite. Structural analysis pointed out that the synthesis approach was able to incorporate βCD in the ferrite matrix, which allowed us to keep the important βCD characteristics in the final magnetic material. Ferrite morphology in the solid state was affected by βCD insertion, probably due to its size and key role as modulator during inorganic nucleation. Ferrites presented at least three different organization scales, from the micrometric to the nanometric level, and on the nanometric scale it was possible to verify the material organization and particle size distribution. Lower domains, and greater specific area and free volume were observed for the Fe-Ni/Zn/βCD material. On the micrometric level, both ferrites have comparable behavior, with quite similar size distribution and ZP values, although Fe-Ni/Zn/βCD presents a slower sedimentation at high pH values. Finally, the MHM is more versatile for the adsorption of ions in aqueous solution than Fe-Ni/Zn due to its pronounced amphoteric characteristic, which was obtained by βCD incorporation in the inorganic matrix.

Experimental

Materials and Methods

Reagents and ferrite synthesis

βCD was obtained from Xiamen Mchem, Xiamen (China). Salts used for the ferrite synthesis ($FeSO_4{\cdot}7H_2O$, $NiSO_4{\cdot}6H_2O$ and $ZnSO_4{\cdot}7H_2O$) were obtained from Merck Laboratory and used without further purification. Magnetic nanoparticles of nickel/zinc (Fe-Ni/Zn) and nickel/zinc/cyclodextrin (Fe-Ni/Zn/βCD) were prepared by coprecipitation reaction of their metal sulfates at 80 °C and pH > 12 (with a sodium hydroxide concentration of 15 g L^{-1}), following the method described in the literature [21]. In the Fe-Ni/Zn/βCD synthesis, 5.0 g L^{-1} of βCD was used during the preparation process. Solid magnetic materials obtained were washed with hot distilled water and filtered, and then the freeze-dried material was used in the solid-state characterization. Part of the ferrite was kept in water to investigate the properties of the aqueous suspension.

Microscopy analysis

Scanning electron microscopy (SEM) was performed in a JEOL, JSM 840A at 4–10 KV in which samples were covered with a thin gold layer, for electronic contrast. Transmission electron microscopy (TEM) images were obtained in a FEI TECNAI G2 with a thermo-ionic gun at 200 kV. Atomic force microscopy (AFM) images were obtained with a Nanoscope IV MultiMode from Veeco Instruments operating in intermittent contact (tapping) mode, with standard Si probes. Phase-contrast images were acquired simultaneously with topographic images by monitoring, with a lock-in amplifier, the phase lag between the oscillation driver and the actual response of the cantilever.

Dynamic light scattering

Fe-Ni/Zn and Fe-Ni/Zn/βCD average hydrodynamic diameter was measured in a Malvern Zetasizer Nano Series ZS particle analyzer, by using polyethylene square cells. All suspensions were prepared by using Milli-Q water before and after the sonication process by using a Sonics Vibra Cell coupled with a microprobe, at 25% amplitude for 5 min. Samples were measured by monochromatic light (10 mW He–Ne laser, wavelength 632.4 nm) and the scattered light intensity was measured in an angle of 173°. Hydrodynamic diameters were measured five times independently and each one was obtained as the mean of 30 counts.

Gas adsorption/desorption isotherm studies

Textural characteristics of Fe-Ni/Zn or Fe-Ni/Zn/βCD samples were determined through nitrogen gas adsorption (Autosorb–Quantachrome Nova 1200) at liquid-nitrogen temperature. Nitrogen gas was used with a 25-point adsorption–desorption cycle. Samples were outgassed at 100 °C for 3 h before each analysis, and experiments were carried out in triplicate. The specific surface area and fractal dimension were obtained by the application of the Brunauer–Emmett–Teller (BET) equation and the Neimark–Kiselev (NK) methods.

Positron-annihilation-lifetime spectroscopy

PALS measurements of Fe-Ni/Zn or Fe-Ni/Zn/βCD were performed at 294 K by using a conventional fast–fast coincidence system (Ortec) with resolution time of 260 ps given by the ^{60}Co prompt curve. The ^{22}Na positron source, with approximately 20.0 μCi activity, was sandwiched between two 7.6 μm thick kapton foils, and the source correction was approximately 10%. The lifetime spectra (minimum of three measurements per sample) were satisfactorily resolved into three components by the Positronfit-Extended program [45], leading to intensities I_i and lifetimes τ_i. Subscript i = 1, 2, and 3 refers to p-Ps, e^+, and o-Ps, respectively.

Potentiometric titrations

Potentiometric titrations were performed in duplicate with a potentiometric system coupled with glass electrode at 25.0 °C. Each titration experiment consisted of approximately 130 successive injections of a concentrated aqueous solution of HNO_3 (14.0 mol L^{-1}) in a beaker loaded with 200 mL of a Fe-Ni/Zn or Fe-Ni/Zn/βCD basic aqueous suspension at an approximate pH of 13.0. The equivalence point was calculated by first-derivative method, which is well established in the literature [46].

Zeta potential

ZP measurements were carried out in a Malvern Zetasizer Nano Series ZS (Malvern Instruments, UK) with a 633 nm red laser, through the Malvern Standard M3 technique (with Doppler electrophoresis as the basic principle of operation) by using capillary cell (DPS1060) [37,47]. Average of the ZP values was calculated by ten independent measurements, each one obtained as the mean of 30 counts. ZP values were measured as a function of pH to evaluate the colloidal stability and these measurements were recorded by using different concentrations of nitric acid or sodium hydroxide. ZP titrations were also used to investigate the adsorption process, in which 51 injections of 5.0 μL increments of $Cr(NO_3)_3$ or $K_2Cr_2O_7$ at 50.0 mmol L^{-1} aqueous solution were titrated into 10.0 mL of Fe-Ni/Zn or Fe-Ni/Zn/βCD at concentrations of 5.1 mg L^{-1} and 4.6 mg L^{-1}, respectively. The pH of each solution was not regulated, since the net interaction between the ferrites and the heavy metal could have been disturbed, and moreover, using raw solutions would better represent the conditions in a practical application [4].

Sedimentation studies

The kinetic stability of the suspensions was evaluated by relative turbidity determinations as a function of time by using a FEMTO UV–visible spectrophotometer, in the wavelength of 700 nm and with a 1 cm light path quartz cell. Optical obscuration was recorded in intervals of 4 min over 120 min. Suspensions containing 4.6 mg L^{-1} of solid ferrite and 5.1 mg L^{-1} of solid MHM were analyzed at different pH values.

Supporting Information

Supporting Information File 1

Solid-state characterization of the magnetic hybrid materials.
[http://www.beilstein-journals.org/bjoc/content/supplementary/1860-5397-8-215-S1.pdf]

Acknowledgements

The authors would like to acknowledge financial support from the Brazilian Research agencies: CEFET-MG, CNPq, FAPEMIG and INCT-Nanobiofar (CNPq/MCT/FAPEMIG) and Centro de Microscopia–UFMG for electronic microscopy images.

References

1. Bar-Nahum, I.; Narasimhulu, K. V.; Weiner, L.; Neumann, R. *Inorg. Chem.* **2005,** *44,* 4900–4902. doi:10.1021/ic050473c
2. Hayashi, K.; Sakamoto, W.; Yogo, T. *J. Magn. Magn. Mater.* **2009,** *321,* 450–457. doi:10.1016/j.jmmm.2008.10.004
3. Dolbecq, A.; Dumas, E.; Mayer, C. R.; Mialane, P. *Chem. Rev.* **2010,** *110,* 6009–6048. doi:10.1021/cr1000578
4. Wang, Y.; Cheng, R.; Wen, Z.; Zhao, L. *Eur. J. Inorg. Chem.* **2011,** *2011,* 2942–2947. doi:10.1002/ejic.201100205
5. Hong, R. Y.; Feng, B.; Chen, L. L.; Liu, G. H.; Li, H. Z.; Zeng, Y.; Wei, D. G. *Bio. Chem. Eng. J.* **2008,** *42,* 290–300. doi:10.1016/j.bej.2008.07.009
6. Zeng, H.; Sun, S. *Adv. Funct. Mater.* **2008,** *18,* 391–400. doi:10.1002/adfm.200701211
7. Bocanegra-Diaz, A.; Mohallem, N. D. S.; Novak, M. A.; Sinisterra, R. D. *J. Magn. Magn. Mater.* **2004,** *272–276,* 2395–2397. doi:10.1016/j.jmmm.2003.12.975
8. Wu, R.; Qu, J.; Chen, Y. *Water Res.* **2005,** *39,* 630–638. doi:10.1016/j.watres.2004.11.005
9. Chung, H. J.; Lee, H.; Bae, K. H.; Lee, Y.; Park, J.; Cho, S.-W.; Hwang, J. Y.; Park, H.; Langer, R.; Anderson, D.; Park, T. G. *ACS Nano* **2011,** *5,* 4329–4336. doi:10.1021/nn201198f
10. Jang, J.-t.; Nah, H.; Lee, J.-H.; Moon, S. H.; Kim, M. G.; Cheon, J. *Angew. Chem., Int. Ed.* **2009,** *48,* 1234–1238. doi:10.1002/anie.200805149
11. Cornell, R. M.; Schwertmann, U. *The Iron Oxides: Structure, Properties, Reactions, Occurences and Uses,* 2nd ed.; Wiley-VCH: Weinheim, 2003.
12. De Sousa, F. B.; Guerreiro, J. D. T.; Ma, M.; Anderson, D. G.; Drum, C. L.; Sinisterra, R. D.; Langer, R. *J. Mater. Chem.* **2010,** *20,* 9910–9917. doi:10.1039/c0jm01903h
13. Harada, A.; Kobayashi, R.; Takashima, Y.; Hashidzume, A.; Yamaguchi, H. *Nat. Chem.* **2011,** *3,* 34–37. doi:10.1038/NCHEM.893
14. Lula, I.; De Sousa, F. B.; Denadai, Â. M. L.; Ianzer, D.; Camargo, A. C. M.; Santos, R. A. S.; Sinisterra, R. D. *J. Braz. Chem. Soc.* **2011,** *22,* 1765–1773. doi:10.1590/S0103-50532011000900020
15. Dos Santos, H. F.; Duarte, H. A.; Sinisterra, R. D.; De Melo Mattos, S. V.; De Oliveira, L. F. C.; De Almeida, W. B. *Chem. Phys. Lett.* **2000,** *319,* 569–575. doi:10.1016/S0009-2614(00)00087-7
16. Hedges, A. R. *Chem. Rev.* **1998,** *98,* 2035–2044. doi:10.1021/cr970014w
17. Loftsson, T.; Brewster, M. E. *J. Pharm. Sci.* **1996,** *85,* 1017–1025. doi:10.1021/js950534b
18. De Sousa, F. B.; Lima, A. C.; Denadai, Â. M. L.; Anconi, C. P. A.; De Almeida, W. B.; Novato, W. T. G.; Dos Santos, H. F.; Drum, C. L.; Langer, R.; Sinisterra, R. D. *Phys. Chem. Chem. Phys.* **2012,** *14,* 1934–1944. doi:10.1039/c2cp22768a
19. Loftsson, T.; Masson, M.; Brewster, M. E. *J. Pharm. Sci.* **2004,** *93,* 1091–1099. doi:10.1002/jps.20047

20. Messner, M.; Kurkov, S. V.; Flavia-Piera, R.; Brewster, M. E.; Loftsson, T. *Int. J. Pharm.* **2011,** *408,* 235–247. doi:10.1016/j.ijpharm.2011.02.008
21. Bocanegra-Diaz, A.; Mohallem, N. D. S.; Sinisterra, R. D. *J. Braz. Chem. Soc.* **2003,** *14,* 936–941. doi:10.1590/S0103-50532003000600011
22. Kim, D.-H.; Kim, K.-N.; Kim, K. M.; Lee, Y.-K. *J. Biomed. Mater. Res., Part A* **2009,** *88,* 1–11. doi:10.1002/jbm.a.31775
23. Pongpeerapat, A.; Wanawongthai, C.; Tozuka, Y.; Moribe, K.; Yamamoto, K. *Int. J. Pharm.* **2008,** *352,* 309–316. doi:10.1016/j.ijpharm.2007.10.052
24. Quickel, T. E.; Le, V. H.; Brezesinski, T.; Tolbert, S. H. *Nano Lett.* **2010,** *10,* 2982–2988. doi:10.1021/nl1014266
25. Peddis, D.; Cannas, C.; Musinu, A.; Piccaluga, G. *Chemistry* **2009,** *15,* 7822–7829. doi:10.1002/chem.200802513
26. Miretzky, P.; Fernandez Cirelli, A. *J. Hazard. Mater.* **2010,** *180,* 1–19. doi:10.1016/j.jhazmat.2010.04.060
27. Denadai, Â. M. L.; Santoro, M. M.; Texeira, A. V.; Sinisterra, R. D. *Mater. Sci. Eng., C* **2010,** *30,* 417–422. doi:10.1016/j.msec.2009.12.008
28. De Sousa, F. B.; Denadai, Â. M. L.; Lula, I. S.; Nascimento, C. S., Jr.; Fernandes Neto, N. S. G.; Lima, A. C.; De Almeida, W. B.; Sinisterra, R. D. *J. Am. Chem. Soc.* **2008,** *130,* 8426–8436. doi:10.1021/ja801080v
29. Bonini, M.; Ross, S.; Karlsson, G.; Almgren, M.; Nostro, P. L.; Baglioni, P. *Langmuir* **2006,** *22,* 1478–1484. doi:10.1021/la052878f
30. Boström, M.; Deniz, V.; Franks, G. V.; Ninham, B. W. *Adv. Colloid Interface Sci.* **2006,** *123–126,* 5–15. doi:10.1016/j.cis.2006.05.001
31. He, Y.; Ye, T.; Su, M.; Zhang, C.; Ribbe, A. E.; Jiang, W.; Mao, C. *Nature* **2008,** *452,* 198–U41. doi:10.1038/nature06597
32. Ooya, T.; Huh, K. M.; Saitoh, M.; Tamiya, E.; Park, K. *Sci. Technol. Adv. Mater.* **2005,** *6,* 452–456. doi:10.1016/j.stam.2005.01.006
33. Banaresmunoz, M. A.; Escribano, V. S. *Langmuir* **1991,** *7,* 1779–1783. doi:10.1021/la00056a034
34. Tao, S. J. *J. Chem. Phys.* **1972,** *56,* 5499. doi:10.1063/1.1677067
35. Jean, Y. C. *Macromolecules* **1996,** *29,* 5756–5757. doi:10.1021/ma960085h
36. Levine, I. N. *Physical Chemistry,* 4th ed.; McGraw-Hill: New York, 1995.
37. Xu, R. *Langmuir* **1993,** *9,* 2955–2962. doi:10.1021/la00035a037
38. Beattie, J. K. *Lab Chip* **2006,** *6,* 1409–1411. doi:10.1039/b610537h
39. Collins, K. D. *Methods* **2004,** *34,* 300–311. doi:10.1016/j.ymeth.2004.03.021
40. Plaza, R. C.; de Vicente, J.; Gomez-Lopera, S.; Delgado, A. V. *J. Colloid Interface Sci.* **2001,** *242,* 306–313. doi:10.1006/jcis.2001.7882
41. Elimelech, M.; Chen, W. H.; Waypa, J. J. *Desalination* **1994,** *95,* 269–286. doi:10.1016/0011-9164(94)00064-6
42. Fonseca, C. G.; Basaglia, R. M. F.; Brant, M. C.; Matencio, T.; Domingues, R. Z. *Powder Technol.* **2009,** *192,* 352–358. doi:10.1016/j.powtec.2009.01.022
43. Rao, K. H.; Forssberg, K. S. E.; Forsling, W. *Colloids Surf., A* **1998,** *133,* 107–117. doi:10.1016/S0927-7757(97)00130-1
44. Barale, M.; Lefevre, G.; Carrette, F.; Catalette, H.; Fédoroff, M.; Cote, G. *J. Colloid Interface Sci.* **2008,** *328,* 34–40. doi:10.1016/j.jcis.2008.09.007
45. Kirkegaard, P.; Eldrup, M.; Mogensen, O. E.; Pedersen, N. J. *Comput. Phys. Commun.* **1981,** *23,* 307–335. doi:10.1016/0010-4655(81)90006-0
46. Mendham, J.; Denney, R. C.; Barnes, J. D.; Thomas, M. J. K. *Vogel's Quantitative Chemical Analysis,* 6th ed.; Pearson Education Limited: Essex, 2000.
47. Tantra, R.; Schulze, P.; Quincey, P. *Particuology* **2010,** *8,* 279–285. doi:10.1016/j.partic.2010.01.003

License and Terms

Beilstein Journal of Organic Chemistry

Influence of intramolecular hydrogen bonds on the binding potential of methylated β-cyclodextrin derivatives

Gerhard Wenz

Full Research Paper

Open Access

Address:
Organic Macromolecular Chemistry, Saarland University, Campus Saarbrücken C4.2, 66123 Saarbrücken, Germany

Email:
Gerhard Wenz - g.wenz@mx.uni-saarland.de

Keywords:
binding constant; cyclodextrin; hydrogen bond; methylation; regioselective

Beilstein J. Org. Chem. **2012,** *8,* 1890–1895.
doi:10.3762/bjoc.8.218

Received: 21 June 2012
Accepted: 16 October 2012
Published: 06 November 2012

This article is part of the Thematic Series "Superstructures with cyclodextrins: Chemistry and applications".

Guest Editor: H. Ritter

Abstract

Various heptasubstituted derivatives of β-cyclodextrin (β-CD) bearing 1, 2 and 3 methyl substituents per glucose unit were synthesized by regioselective methods. Binding free energies and binding enthalpies of these hosts towards 4-*tert*-butylbenzoate and adamantane-1-carboxylate were determined by isothermal titration microcalorimetry (ITC). It was found that methyl substituents at the secondary positions of β-CD lead to a tremendous reduction of the binding potential, while methylation at the primary positions significantly improved binding. Stabilizing intramolecular hydrogen bonds between the glucose units were made responsible for the high binding potentials of those β-CD derivatives that possess secondary hydroxy groups.

Introduction

Cyclodextrins (CDs) are a well-known class of organic hosts able to include various guests, preferably in aqueous solution [1-3]. Inclusion is mainly driven by hydrophobic and van der Waals interactions [4-6]. The host–guest complexes, so-called cyclodextrin inclusion compounds, find many applications such as solubilization of pharmaceutical drugs, dispersion of cosmetics, catalysis, or chromatographic separation of enantiomers [2,7,8]. Application of β-CD **1** is hampered by its low solubility of 18.8 g L^{-1} at 25 °C [9]. Solubility of β-CD and its inclusion compounds can be significantly increased by the covalent attachment of neutral or ionic substituents [10]. Methylated β-CDs, such as heptakis(2,6-di-*O*-methyl)-β-CD **2** and heptakis (2,3,6-tri-*O*-methyl)-β-CD **3**, are well known for their high solubilities in water (**2**: > 300 g L^{-1}) and their

interesting inclusion behavior [11-13]. Because of the tedious synthesis of the disubstituted derivative **2** [11,14], the readily available randomly substituted derivative RAMEB with a degree of substitution DS = 1.7–1.8 is preferred nowadays and produced on an industrial scale [15].

Methylated CDs have already found several applications in drug delivery [10] and polymer chemistry [16]. They allow radical polymerizations of hydrophobic vinyl monomers in homogenous aqueous solution [17-20] and living RAFT polymerizations as well [21]. Methylated CDs are already applied industrially on a large scale, e.g., for switching the viscosity of polymeric thickeners [22], for decontamination of soil [23,24], or for cosmetic formulations [25]. High binding potentials of the methylated CDs are essential for their specific functions in these applications. Therefore, a quantitative understanding of the binding potential as a function of the degree and pattern of methylation is highly desirable.

The attachment of methyl groups to β-CD improves its solubility in water because it reduces formation of intermolecular hydrogen bonds. Methylation should also extend the hydrophobic cavity of β-CD and therefore improve the binding potential for hydrophobic guest molecules. Up to now, only little is known about the influence of methyl substituents on the inclusion potential of β-CD [26,27]. The dimethyl derivative **2** binds adamantane derivatives with a similar binding constants *K* to those of native β-CD, while the trimethyl derivative **3** binds much more weakly [28]. Similar differences in binding affinities between native **1** and permethylated β-CD **3** were observed for the inclusion of anti-inflammatory drugs [29].

For the systematic investigation of the influence of the pattern of methylation on the complexation of amphiphilic guests, we synthesized well-defined model compounds **2**–**6** (Figure 1) of methylated β-CD, using regioselective procedures already published [30]. 4-*tert*-Butylbenzoate and adamantane-1-carboxylate were chosen as representative guests. Complexation of these guests should sensitively respond to changes in the methylation pattern, because they fit tightly into the cavity of β-CD giving rise to high binding constants [26,27]. Binding data were measured by isothermal titration calorimetry (ITC) because it is known to be the most accurate method, and because it additionally yields binding enthalpies and entropies [31,32].

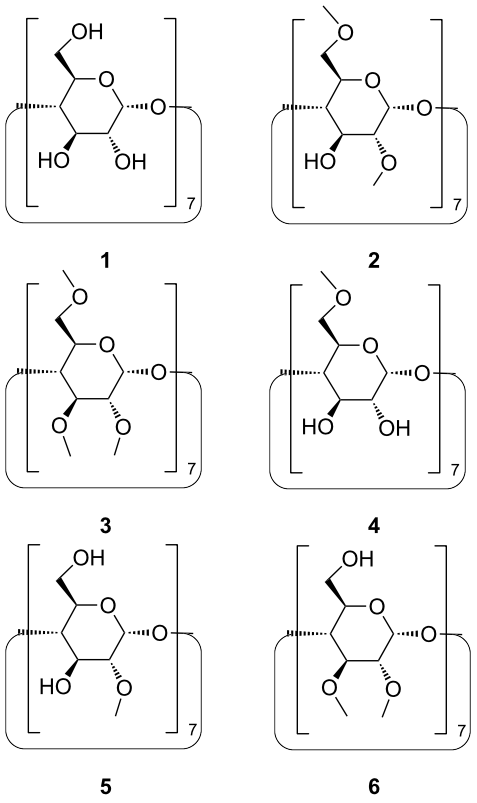

Figure 1: Structures of the methylated β-CD derivatives investigated.

Results

Since methylated β-CD derivatives **2**–**6** are highly water-soluble they are well suited for ITC. The ITC titration curves for all the β-CD derivatives **1**–**6** were exothermic and were in accordance with a 1:1 stoichiometry of the host–guest complexes. Thermodynamic data obtained for the guests 4-*tert*-butylbenzoate and adamantane-1-carboxylate are listed in Table 1 and Table 2, respectively.

Remarkable differences in the binding constants for 4-*tert*-butylbenzoate were found for the β-CD derivatives **2**–**7**. The completely methylated β-CD **3** and the 2,3-dimethylated derivative **6** showed the lowest binding constants *K*, less than one tenth of the one of native β-CD **1**. These very low binding constants are accompanied by positive values of the entropy term $-T\Delta S°$ weakening the binding free enthalpy $\Delta G°$. On the other hand, binding constants of the 2,6-di-*O*-methyl derivative **2** as well as the 6-*O*-methyl derivative were higher than the one of β-CD. Apparently, methylations of secondary hydroxy groups lead to a decrease of the binding constant, while methylation at primary hydroxy groups leads to an increase. For the 2,6-di-*O*-methyl derivative both effects seem to compensate each other giving rise to a binding constant *K* similar to the one of native β-CD. The randomly methylated β-CD **7** also showed an inclusion potential very similar to β-CD for the same reason.

The thermodynamic data (Table 2) measured for the inclusion of adamantane-1-carboxylate in β-CD and β-CD derivatives **2**–**6**, showed a similar trend to that observed before. This guest,

Table 1: Thermodynamics of the inclusion of 4-*tert*-butyl-benzoate in β-cyclodextrin **1** and its methyl derivatives **2**–**6**.

Host	No.	K (M^{-1})	$\Delta G°$ (kJ mol^{-1})	$\Delta H°$ (kJ mol^{-1})	$-T\Delta S°$ (kJ mol^{-1})
unsubstituted β-CD	**1**	16400 ± 4	−24.34	−19.00 ± 0.08	−3.82
2,6-di-*O*-methyl-β-CD	**2**	17000 ± 485	−24.13	−19.98 ± 0.14	−4.18
2,3,6-tri-*O*-methyl-β-CD	**3**	1190 ± 21	−17.54	−30.54 ± 0.37	12.98
6-*O*-methyl-β-CD	**4**	30700 ± 898	−25.60	−20.14 ± 0.12	−5.49
2-*O*-methyl-β-CD	**5**	12300 ± 428	−23.33	−14.30 ± 0.11	−9.05
2,3-di-*O*-methyl-β-CD	**6**	869 ± 28	−16.77	−19.24 ± 0.84	+2.45
RAMEB[a]	**7**	14700 ± 363	−23.77	−14.60 ± 0.09	−9.20

[a]randomly methylated β-CDs.

Table 2: Thermodynamics of the inclusion of adamantane-1-carboxylate in β-cyclodextrin **1** and its methyl derivatives **2**–**6**.

Host	No.	K (M^{-1})	$\Delta G°$ (kJ mol^{-1})	$\Delta H°$ (kJ mol^{-1})	$-T\Delta S°$ (kJ mol^{-1})
unsubstituted β-CD	**1**	38100 ± 1150	−26.13	−22.38 ± 0.09	−3.78
2,6-di-*O*-methyl-β-CD	**2**	20400 ± 975	−24.58	−20.75 ± 0.22	−3.87
2,3,6-tri-*O*-methyl-β-CD	**3**	606 ± 43	−15.87	−19.94 ± 0.82	+4.04
6-*O*-methyl-β-CD	**4**	56400 ± 2400	−27.10	−19.11 ± 0.15	−8.02
2-*O*-methyl-β-CD	**5**	18700 ± 275	−24.37	−20.85 ± 0.05	−3.57
2,3-di-*O*-methyl-β-CD	**6**	586 ± 65	−15.79	−12.72 ± 0.70	−3.09
RAMEB[a]	**7**	15300 ± 341	−23.87	−15.48 ± 0.09	−8.41

[a]randomly methylated β-CDs.

which is known as one of the most suitable guests for the β-CD cavity, was bound even more weakly by the 2,6-di-*O*-methyl derivative **2** than by native β-CD **1**. Again, all β-CD derivatives methylated at the secondary positions showed much lower affinities towards this guest than **1** did. Again, a positive value of the entropy term $-T\Delta S°$ was found for 2,3,5-tri-*O*-methyl-β-CD. As shown in Figure 2, this entropy term further grew with increasing temperature, compensating most of the strongly negative binding enthalpy $\Delta H°$. Taking into account these data and previous results from literature, the observed reduction of the binding potential by substitutions at the secondary positions appeared to be a general feature of β-CD.

In addition, the differential heat capacity, ΔC_p = −510 ± 30 J mol^{-1} K^{-1}, was calculated from the slope of the temperature dependence of $\Delta H°$. Negative ΔC_p are generally interpreted as the liberation of "hot" water molecules during complexation of the guest [33-35]. The liberation of water molecules of high energy from a cavity is regarded as a major driving force for the complexation of neutral guests by concave hosts in water, because it can lead both to entropy gains and enthalpic advantages [36]. The observed value for 2,3,5-tri-*O*-methyl-β-CD is even higher than that for native β-CD, ΔC_p = −320 ± 20 J mol^{-1} K^{-1} [37]. This difference was attributed to the larger internal hydrophobic surface of 2,3,5-tri-*O*-methyl-β-

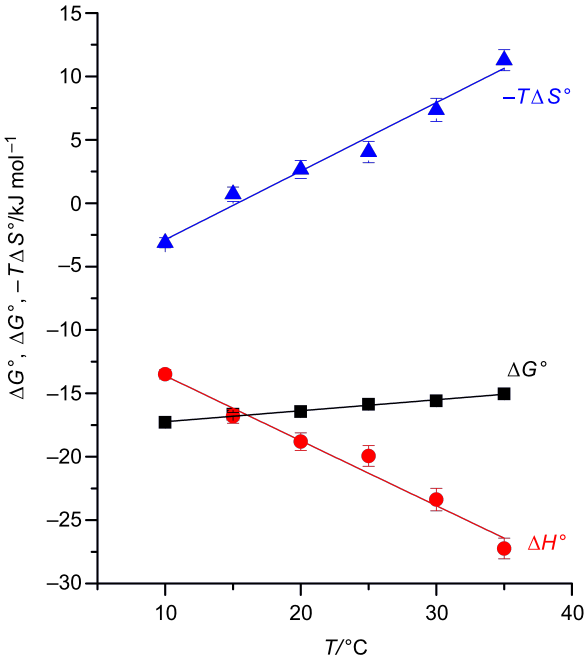

Figure 2: Temperature dependence of $-T\Delta S°$, $\Delta H°$ and $\Delta G°$ for the inclusion of 1-adamantane carboxylate in heptakis-2,3,6-tri-*O*-methyl-β-CD (**3**) measured by ITC.

CD compared to native β-CD leading to the liberation of more bound water molecules during complexation. Nevertheless, the effect of the negative heat capacity on binding adamantane carboxylate by 2,3,5-tri-*O*-methyl-β-CD is overcompensated by a strong increase of binding entropy leading in total to a reduction of the complex stability with increasing temperature.

Discussion

Only methylations at the primary positions lead to the anticipated increase of the binding potential of β-CD due to an elongation of the hydrophobic cavity of β-CD. The negative effect of methylations at the secondary positions was initially surprising. The discussion of the entropy term $-T\Delta S°$ appeared most appropriate to us to understand this behavior.

The entropy term $-T\Delta S°$ was negative (−3 to −9 kJ mol^{-1}) for those β-CD derivatives (**1**,**2**,**4**,**5** and **7**) equipped with free secondary hydroxy groups. This negative value is quite normal and attributed to the liberation of bound water molecules from the cavity, while the entropy of the host remains more or less unchanged [5,6]. Neutron scattering studies revealed that native β-CD is strongly rigidified by intermolecular hydrogen bonds (flip-flop bonds) between the secondary hydroxy groups of adjacent anhydroglucose units, as depicted in Figure 3 [38]. This finding was confirmed by MD calculations of CDs in the crystalline state and in aqueous environment [39,40]. A stabilization energy due to all $O_3H\cdots O_2$' hydrogen bonds of 14 to 23 kJ mol^{-1} was calculated by using density functional theory (basis set B3LYP) [41]. In addition, recent density-functional calculations also took into account strong intermolecular hydrogen bonds of these hydroxy groups with water molecules in aqueous solution [42].

The conformational stabilization of β-CD by these hydrogen bonds between the secondary hydroxy groups is lost upon methylation. Furthermore, methylated β-CDs are less hydrated than the native ones [44]. The lack of stabilizing hydrogen bonds leads to much higher ring flexibilities for derivatives **3** and **6**, which explains the low or even positive entropy contributions $-T\Delta S°$ to the binding free enthalpy $\Delta G°$. Especially for a guest such as adamantane-1-carboxylate, which fits well into the CD cavity, its inclusion will significantly reduce the conformational degrees of freedom of a flexible host, such as **3** or **6**, leading to an unfavorable decrease in entropy.

In contrast, primary hydroxy groups in β-CD are too far apart from each other to allow intramolecular hydrogen-bond formation. Hydrogen bonds between primary hydroxy groups were only found for α-CD, leading to a conical host conformation, which is unfavorable for the accommodation of a guest [45]. Therefore, methylation at the primary positions should not significantly diminish the rigidity of the CD torus. This explains why methylation at the primary position leads to the expected improvement of the binding potential. Also the substitution of the primary hydroxy groups with other hydrophobic groups, such as thioether moieties, is known to furnish host molecules with much higher binding potentials than native β-CD [46,47].

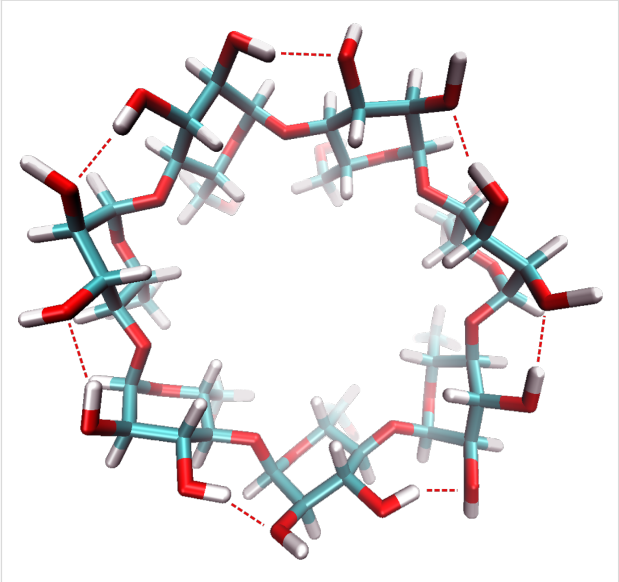

Figure 3: Structural drawing of β-CD [43], according to structural data (CSD-ID BUVSEQ03) from Zabel et al. [38], generated by VMD 1.8.4 showing the intramolecular hydrogen bonds between OH-3 and O-2.

Conclusion

The binding potential of β-CD can be improved significantly if hydrophobic substituents are exclusively attached at the primary positions. Intramolecular hydrogen bonds between secondary hydroxy groups of β-CD are crucial for achieving high binding constants. This result provides an example of a host, where intramolecular hydrogen bonds control the binding potential [48]. It will help to better understand binding mechanisms in supramolecular systems [48] and in the future help to design improved hosts based on β-CD for specific applications such as drug delivery [49], removal of pollutants [50-53], catalysis [54] or smart materials [55].

Experimental

4-*tert*-Butylbenzoic acid and adamantane-1-carboxylic acid and β-CD derivative **3** were purchased from Aldrich, β-CD **1** and RAMEB **7** from Wacker Chemie, β-CD derivative **2** from Cyclolab. β-CD derivatives **4**–**6** were synthesized from β-CD **1** following published procedures (Table 3) [30].

Binding data were measured with isothermal microcalorimetric titration at a temperature of 25.0 °C with an AutoITC isothermal titration calorimeter (MicroCal Inc., Northampton,

Table 3: List of the methylated β-CD derivatives used in this contribution.

Host	No.	CAS Registry No.	Reference
unsubstituted β-CD	**1**	7585-39-9	
2,6-di-*O*-methyl-β-CD	**2**	51166-71-3	[11]
2,3,5-tri-*O*-methyl-β-CD	**3**	55216-11-0	[11]
6-*O*-methyl-β-CD	**4**	84337-62-2	[30]
2-*O*-methyl-β-CD	**5**	60786-23-4	[30]
2,3-di-*O*-methyl-β-CD	**6**	123155-05-5	[30]
RAMEB[a]	**7**	343249-39-8	[15]

[a]randomly methylated β-CDs.

USA) by using 1.4144 mL sample and reference cells. The reference cell was filled with distilled water. The sample cell was filled with a 2 mM solution of the respective host in 50 mM phosphate buffer pH 6.8, and the contents were constantly stirred at 450 rpm. A 26 mM solution of the guest was prepared in the same buffer and adjusted by the addition of small quantities of HCl or NaOH to pH 6.8. This solution was automatically added by a syringe in 20 separate injections of 12.5 µL. The resulting 20 heat signals were integrated to yield the mixing heats, which were corrected by the corresponding dilution enthalpies of β-CD in the same buffer. The titration curve was fitted by nonlinear regression using the program Origin 7.0 for ITC. Thereby, a 1:1 stoichiometry of the guest and the host molecule was found to be most appropriate. The binding constant K and the molar binding enthalpy $\Delta H°$ were obtained as fitting parameters, from which the binding free energy $\Delta G°$ and binding entropy $\Delta S°$ were derived. For those titrations with high binding constants, i.e., $K > 5000\ M^{-1}$, titrations were repeated with [host] = 10/K in the cell and [guest] = 13[host] in the syringe to ensure optimal accuracy of the nonlinear-regression fitting procedure.

Acknowledgements

The author thanks Andreas Steffen for drawing the structure of β-CD (Figure 3), and Annegret Engelke for performing the ITC measurements.

References

1. Wenz, G.; Keller, B. *Angew. Chem., Int. Ed. Engl.* **1992,** *31,* 197–199. doi:10.1002/anie.199201971
2. Szejtli, J. *Pure Appl. Chem.* **2004,** *76,* 1825–1845. doi:10.1351/pac200476101825
3. Dodziuk, H., Ed. *Cyclodextrins and Their Complexes: Chemistry, Analytical Methods, Applications;* Wiley: Weinheim, 2006. doi:10.1002/3527608982
4. Connors, K. A. *Chem. Rev.* **1997,** *97,* 1325–1358. doi:10.1021/cr960371r
5. Lipkowitz, K. B. *Chem. Rev.* **1998,** *98,* 1829–1874. doi:10.1021/cr9700179
6. Liu, L.; Guo, Q.-X. *J. Inclusion Phenom. Macrocyclic Chem.* **2002,** *42,* 1–14. doi:10.1023/A:1014520830813
7. Szejtli, J. *Chem. Rev.* **1998,** *98,* 1743–1754. doi:10.1021/cr970022c
8. Singh, M.; Sharma, R.; Banerjee, U. C. *Biotechnol. Adv.* **2002,** *20,* 341–359. doi:10.1016/S0734-9750(02)00020-4
9. Jozwiakowski, M. J.; Connors, K. A. *Carbohydr. Res.* **1985,** *143,* 51–59. doi:10.1016/S0008-6215(00)90694-3
10. Szente, L.; Szejtli, J. *Adv. Drug Delivery Rev.* **1999,** *36,* 17–28. doi:10.1016/S0169-409X(98)00092-1
11. Szejtli, J.; Lipták, A.; Jodál, I.; Fügedi, P.; Nánási, P.; Neszmélyi, A. *Starch - Staerke* **1980,** *32,* 165–169. doi:10.1002/star.19800320506
12. Yannakopoulou, K.; Mentzafos, D.; Mavridis, I. M.; Dandika, K. *Angew. Chem., Int. Ed. Engl.* **1996,** *35,* 2480–2482. doi:10.1002/anie.199624801
13. Szejtli, J. *J. Inclusion Phenom.* **1983,** *1,* 135–150. doi:10.1007/BF00656816
14. Spencer, C. M.; Stoddart, J. F.; Zarzycki, R. *J. Chem. Soc., Perkin Trans. 2* **1987,** 1323–1336. doi:10.1039/p29870001323
15. Wimmer, T. Preparation of alkylated cyclodextrin derivatives, methylated cyclodextrin derivatives and their use. DE4333598 (A1), April 6, 1995.
16. Choi, S.; Amajjahe, S.; Ritter, H. Polymerization of Included Monomers and Behavior of Resulting Polymers. In *Inclusion Polymers;* Wenz, G., Ed.; Advances in Polymer Science, Vol. 222; Springer: Berlin Heidelberg, 2009; pp 79–113. doi:10.1007/12_2008_6
17. Jeromin, J.; Noll, O.; Ritter, H. *Macromol. Chem. Phys.* **1998,** *199,* 2641–2645. doi:10.1002/(SICI)1521-3935(19981201)199:12<2641::AID-MACP2641>3.0.CO;2-Y
18. Ritter, H.; Tabatabai, M. Polymerization in aqueous medium using cyclodextrin as host component. In *Advanced Macromolecular and Supramolecular Materials and Processes;* Geckeler, K. E., Ed.; Kluwer Academic Publishers/Plenum Publishers: New York, 2003; pp 41–53.
19. Choi, S.-W.; Ritter, H. *Macromol. Rapid Commun.* **2004,** *25,* 716–719. doi:10.1002/marc.200300181
20. Steffens, C.; Kretschmann, O.; Ritter, H. *Macromol. Rapid Commun.* **2007,** *28,* 623–628. doi:10.1002/marc.200600685
21. Köllisch, H.; Barner-Kowollik, C.; Ritter, H. *Macromol. Rapid Commun.* **2006,** *27,* 848–853. doi:10.1002/marc.200600067
22. Lau, W.; Shah, V. M. Method for improving thickeners for aqueous systems. U.S. Patent 5,376,709 (A), Dec 27, 1994.
23. Malton, P. J.; Holland, L. A. M.; Rizzi, G.; Heltovics, G. Cosmetic composition comprising cyclic oligosaccharides and fragrance. EP1176942 (A1), Feb 19, 2002.
24. Fava, F.; Ciccotosto, V. *Appl. Microbiol. Biotechnol.* **2002,** *58,* 393–399. doi:10.1007/s00253-001-0882-7
25. Fava, F.; Di Gioia, D.; Marchetti, L.; Fenyvesi, E.; Szejtli, J. *J. Inclusion Phenom. Macrocyclic Chem.* **2003,** *44,* 417–421. doi:10.1023/A:1023019903194
26. Rekharsky, M. V.; Inoue, Y. *Chem. Rev.* **1998,** *98,* 1875–1918. doi:10.1021/cr970015o
27. Höfler, T.; Wenz, G. *J. Inclusion Phenom. Mol. Recognit. Chem.* **1996,** *25,* 81–84. doi:10.1007/BF01041541
28. Gelb, R. I.; Schwartz, L. M. *J. Inclusion Phenom. Mol. Recognit. Chem.* **1989,** *7,* 537–543. doi:10.1007/BF01080464
29. Otagiri, M.; Uekama, K.; Imai, T.; Maeda, T.; Takadate, A.; Goya, S.; Janssen, L. H. M. *Acta Pharm. Suec.* **1984,** *21,* 357–366.

30. Takeo, K.; Mitoh, H.; Uemura, K. *Carbohydr. Res.* **1989,** *187,* 203–221. doi:10.1016/0008-6215(89)80004-7
31. Wiseman, T.; Williston, S.; Brandts, J. F.; Lin, L.-N. *Anal. Biochem.* **1989,** *179,* 131–137. doi:10.1016/0003-2697(89)90213-3
32. Cliff, M. J.; Ladbury, J. E. *J. Mol. Recognit.* **2003,** *16,* 383–391. doi:10.1002/jmr.648
33. Schneider, H.-J.; Yatsimirsky, A. *Principles and Methods in Supramolecular Chemistry;* John Wiley & Sons: Chichester, 2000; pp 105 ff.
34. Buchwald, P. *J. Phys. Chem. B* **2002,** *106,* 6864–6870. doi:10.1021/jp025711t
35. Terekhova, I. V.; De Lisi, R.; Lazzara, G.; Milioto, S.; Muratore, N. *J. Therm. Anal. Calorim.* **2008,** *92,* 285–290. doi:10.1007/s10973-007-8842-9
36. Biedermann, F.; Uzunova, V. D.; Scherman, O. A.; Nau, W. M.; De Simone, A. *J. Am. Chem. Soc.* **2012,** *134,* 15318–15323. doi:10.1021/ja303309e
37. Cameron, D. L.; Jakus, J.; Pauleta, S. R.; Pettigrew, G. W.; Cooper, A. *J. Phys. Chem. B* **2010,** *114,* 16228–16235. doi:10.1021/jp107110t
38. Zabel, V.; Saenger, W.; Mason, S. A. *J. Am. Chem. Soc.* **1986,** *108,* 3664–3673. doi:10.1021/ja00273a020
39. Koehler, J. E. H.; Saenger, W.; Van Gunsteren, W. F. *Eur. Biophys. J.* **1988,** *16,* 153–168. doi:10.1007/BF00261901
40. Koehler, J. E. H.; Saenger, W.; Van Gunsteren, W. F. *J. Biomol. Struct. Dyn.* **1988,** *6,* 181–198. doi:10.1080/07391102.1988.10506490
41. Deshmukh, M. M.; Bartolotti, L. J.; Gadre, S. R. *J. Comput. Chem.* **2011,** *32,* 2996–3004. doi:10.1002/jcc.21881
42. Heine, T.; Dos Santos, H. F.; Patchkovskii, S.; Duarte, H. A. *J. Phys. Chem. A* **2007,** *111,* 5648–5654. doi:10.1021/jp068988s
43. Steffen, A. Computational Approaches in Supramolecular Chemistry with a Special Focus on Virtual Screening. Ph.D. Thesis, Saarland University, 2007. http://scidok.sulb.uni-saarland.de/volltexte/2008/1417/
44. Starikov, E. B.; Bräsicke, K.; Knapp, E. W.; Saenger, W. *Chem. Phys. Lett.* **2001,** *336,* 504–510. doi:10.1016/S0009-2614(01)00160-9
45. Pinjari, R. V.; Joshi, K. A.; Gejji, S. P. *J. Phys. Chem. A* **2006,** *110,* 13073–13080. doi:10.1021/jp065169z
46. Wenz, G.; Strassnig, C.; Thiele, C.; Engelke, A.; Morgenstern, B.; Hegetschweiler, K. *Chem.–Eur. J.* **2008,** *14,* 7202–7211. doi:10.1002/chem.200800295
47. Steffen, A.; Thiele, C.; Tietze, S.; Strassnig, C.; Kämper, A.; Lengauer, T.; Wenz, G.; Apostolakis, J. *Chem.–Eur. J.* **2007,** *13,* 6801–6809. doi:10.1002/chem.200700661
48. Schneider, H.-J. *Angew. Chem., Int. Ed.* **2009,** *48,* 3924–3977. doi:10.1002/anie.200802947
49. Loftsson, T.; Vogensen, S. B.; Brewster, M. E.; Konrádsdóttir, F. *J. Pharm. Sci.* **2007,** *96,* 2532–2546. doi:10.1002/jps.20992
50. Shao, D.; Sheng, G.; Chen, C.; Wang, X.; Nagatsu, M. *Chemosphere* **2010,** *79,* 679–685. doi:10.1016/j.chemosphere.2010.03.008
51. Mahlambi, M. M.; Malefetse, T. J.; Mamba, B. B.; Krause, R. W. *J. Polym. Res.* **2010,** *17,* 589–600. doi:10.1007/s10965-009-9347-y
52. Rölling, P.; Lamers, M.; Staudt, C. *J. Membr. Sci.* **2010,** *362,* 154–163. doi:10.1016/j.memsci.2010.06.036
53. Baruch-Teblum, E.; Mastai, Y.; Landfester, K. *Eur. Polym. J.* **2010,** *46,* 1671–1678. doi:10.1016/j.eurpolymj.2010.05.007
54. Cassez, A.; Kania, N.; Hapiot, F.; Fourmentin, S.; Monflier, E.; Ponchel, A. *Catal. Commun.* **2008,** *9,* 1346–1351. doi:10.1016/j.catcom.2007.11.031
55. Celebioglu, A.; Uyar, T. *Chem. Commun.* **2010,** *46,* 6903–6905. doi:10.1039/c0cc01484b

License and Terms

Beilstein Journal of Organic Chemistry

Cyclodextrin-induced host–guest effects of classically prepared poly(NIPAM) bearing azo-dye end groups

Gero Maatz, Arkadius Maciollek and Helmut Ritter*

Full Research Paper

Open Access

Address:
Institute of Organic Chemistry and Macromolecular Chemistry, Heinrich-Heine-University Duesseldorf, Universitaetsstraße 1, D-40225 Duesseldorf, Germany

Email:
Helmut Ritter* - h.ritter@uni-duesseldorf.de

* Corresponding author

Keywords:
azo-dye; cyclodextrins; end-group functionalization; host–guest interaction; supramolecular aggregation

Beilstein J. Org. Chem. **2012,** *8,* 1929–1935.
doi:10.3762/bjoc.8.224

Received: 01 August 2012
Accepted: 29 October 2012
Published: 14 November 2012

This article is part of the Thematic Series "Superstructures with cyclodextrins: Chemistry and applications".

Associate Editor: P. J. Skabara

Abstract

A thermo-, pH- and cyclodextrin- (CD) responsive poly(*N*-isopropylacrylamide) (PNIPAM), with a *N*,*N*-dimethylaminoazobenzene end group was synthesized. Using 3-mercaptopropionic acid as a chain transfer agent, PNIPAM with a well-defined COOH end group was obtained. The acid end group was transferred to the corresponding acid chloride and then functionalized with *N*,*N*-dimethyl[4-(4'-aminophenylazo)phenyl]amine. This dye-end-group-labeled polymer showed acidochromic effects, depending on the pH and the presence of randomly methylated β-cyclodextrin (RAMEB-CD). Also higher cloud-point values for the lower critical solution temperature (LCST) in the presence of RAMEB-CD were observed. Additionally, this azo-dye-end-group-labeled polymer was complexed with hyperbranched polyglycerol (HPG) decorated with β-CD to generate hedgehog-like superstructures.

Introduction

Polymers bearing dyes, such as azo, stilbene, anthraquinone or fluorescence dyes, in the main or side chain have been widely described and investigated [1-15]. A few examples of dyes located at the end group of polymers are prepared preferably under anionic or controlled conditions such as reversible addition–fragmentation chain-transfer polymerization (RAFT) or atom-transfer radical polymerization (ATRP) [14-16]. However, up to now, only a little is known about the preparation of dye-end-group-labeled polymers by using classical free-radical polymerization techniques. Water-soluble polymers, which exhibit a lower critical solution temperature (LCST), e.g., many poly(*N*-alkylacrylamides), have found numerous practical applications in waterborne smart materials such as bioactive surfaces, selective bioseparation, or hyperthermia-induced drug delivery [14]. Several reports are available on the preparation and properties of thermally responsive

polyacrylamides containing azobenzene or stilbene dyes in the side chain [3,14]. Furthermore, the interaction of dye-containing polymers with CD in water is of some interest, because of their external, light-induced, reversible complexation [1-3,10,11]. In recent years, increasing attention has been given to supramolecular structures, the science of noncovalent assembly in biological systems and chemical processes [12]. Hyperbranched polymers such as polyglycerols (HPG), as a result of their inherent dendritic topology, attract considerable interest for a wide range of optical, medical or reagent-immobilization applications [16].

Results and Discussion

Here, we describe the free-radical polymerization of *N*-isopropylacrylamide (NIPAM, **1**) in the presence of a chain–transfer agent and its end-group functionalization by condensation with an azo dye. We also investigated the host–guest interaction of the azo-dye-labeled end group with randomly methylated β-cyclodextrin (RAMEB-CD), and with HPG bearing β-CD on top. Thus, the focus of the present study was directed towards the preparation and superstructure formation of a thermo- and pH-responsive polymer bearing an azo dye at the end group. In a first step, a chain-transfer polymerization (CTP) of *N*-isopropylacrylamide (**1**) was carried out in the presence of 3-mercaptopropionic acid (**2**) and with 4,4'-azobis(4-cyanovaleric acid) as initiator, to achieve a high degree of functionalization and yield of carboxy-terminated PNIPAM **3**. Then, the free carboxy end group was transferred in to the corresponding acid chloride by treatment with thionyl chloride, yielding polymers with a propionyl chloride end group (Scheme 1).

The final product **6** was obtained by condensation of **4** with the amino group of the dye *N*,*N*-dimethyl-[4-(4'-aminophenylazo)phenyl]amine (**5**, Supporting Information File 1). The molecular weight (M_n 3.4 kDa) and molecular weight distribution (D 1.3) of **6** were determined by size-exclusion chromatography (SEC). A M_n value of **5** was also calculated by end-group analysis based on ^{1}H NMR measurements, showing similar results (Supporting Information File 1).

The UV–vis absorption spectrum of **6** in water showed the characteristic broad band at λ_{max} 460 nm, which corresponds to the orange color at pH 7 [17]. However, upon decreasing of the pH from 7 to 2, a large bathochromic (red) shift takes place, due to the protonation of the azo dye of **6** [17]. As illustrated in Figure 1A this red shift corresponds to an increase of the absorption up to 500–550 nm, whereas the band at 420 nm decreases. Thus, the protonated azonium tautomer is considered to be the predominant form in the red acidic aqueous solution [17-19].

Due to our general interest in the use of CD in polymer chemistry [3], the interaction of polymer **6** with RAMEB-CD was investigated. The proposed formation of the host–guest structure between the azo-dye end group and the RAMEB-CD cavity was proved by use of 2D ROESY NMR spectroscopy (Supporting Information File 1). The correlation signals between the protons of the RAMEB-CD cavity and the aromatic protons of the azo dye were observed. However, the correlation signals between the RAMEB-CD cavity and the methyl protons of the *N*,*N*-dimethylamine group of the azo dye were not observed. This indicates a complete inclusion of the azo dye

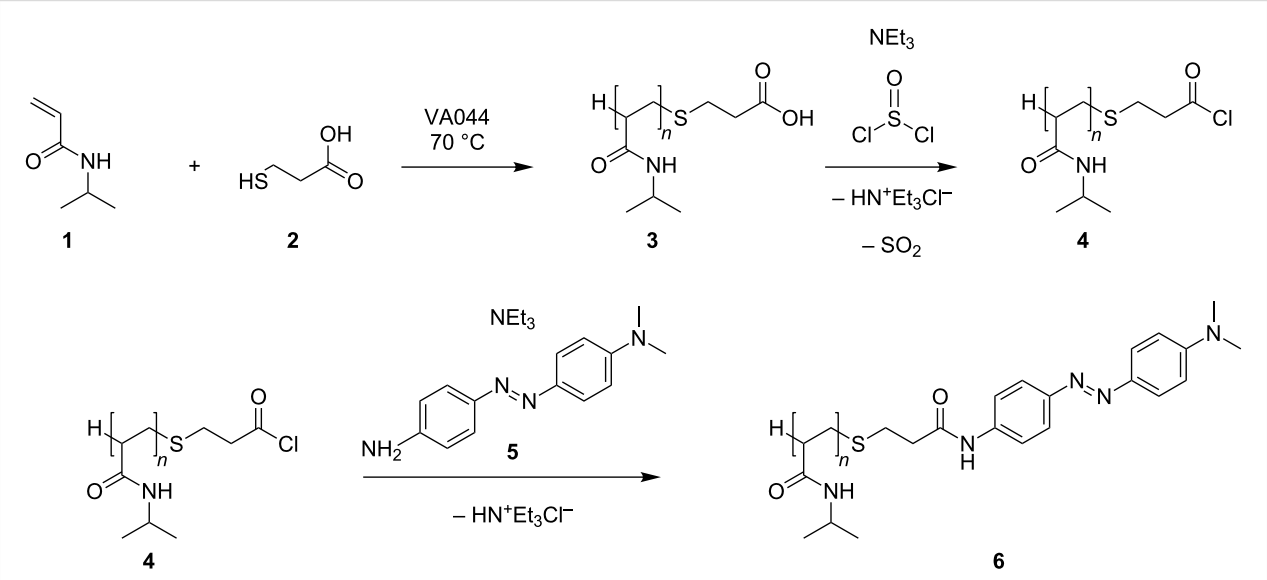

Scheme 1: CTP of **1** and end-group functionalization with **5** yielding the azo-dye-end-group-labeled polymer **6**.

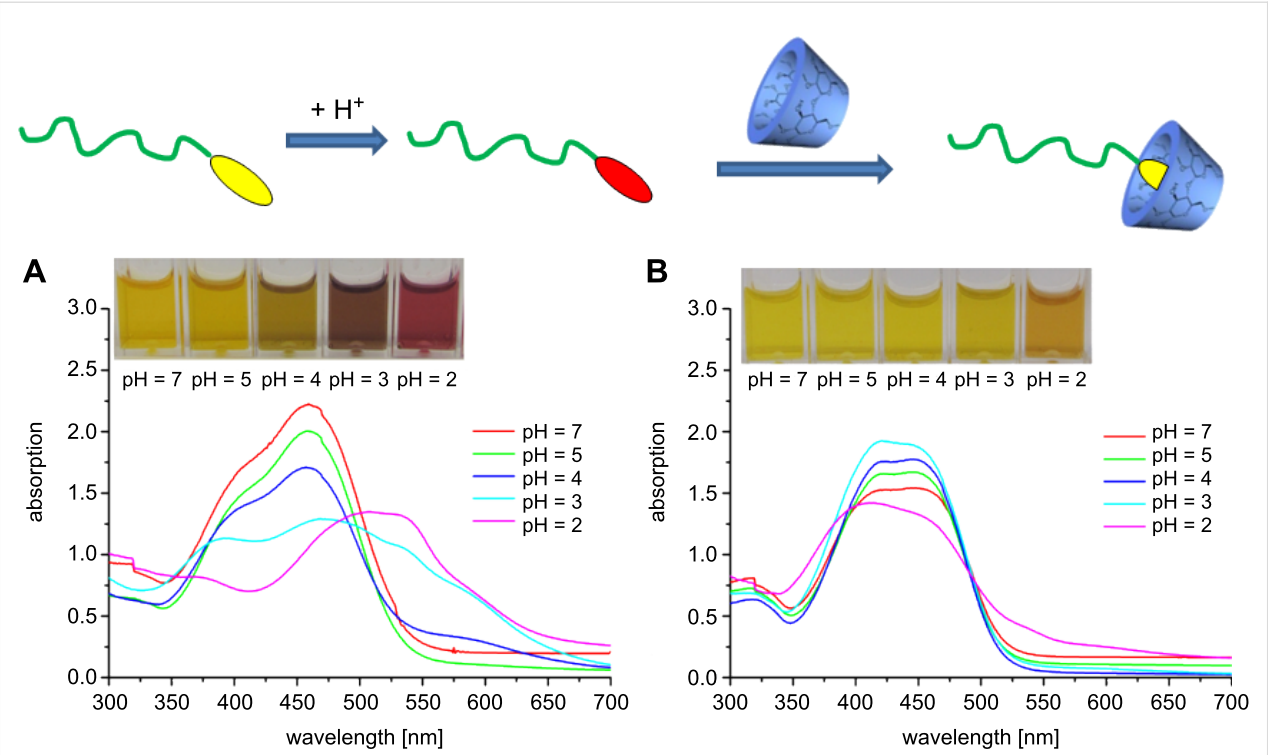

Figure 1: Absorption spectra of **6** in water in a pH range from 7 to 2 (A). Absorption spectra of **6** in water depending on the pH in the presence of RAMEB-CD (B).

inside the CD cavity with an orientation to the RAMEB-CD axis [1]. In addition, UV–vis absorption spectra of **6** were recorded in aqueous solution at a pH range from 7 to 2 and in the presence of RAMEB-CD. Hereby, a strong blue shift in the absorption spectra was observed (Figure 1B). As mentioned above, the absorption spectra of **6** after protonation indicate the formation of the azonium structure (Figure 1A). The subsequent complexation of this protonated azo dye with RAMEB-CD causes a hypsochromic shift. This strongly indicates that, due to the presence of RAMEB-CD, a shift of the equilibrium from the azonium to the amonium form of the azo dye takes place. Consequently, the azo group in **6** is supramolecularly protected from protonation by the surrounding CD ring, while the free dimethylamino group is easily protonated. These results correspond to the work of Toda et al. [19].

Furthermore, the solution properties of polymer **6**, depending on the temperature in the presence of RAMEB-CD, were investigated. As expected, **6** is soluble in cold water below the critical solution temperature (LCST). However, due to the hydrophobic azo-dye end group of **6**, a slight reducing effect on the cloud point in comparison to pure PNIPAM, from 32 down to 29.5 °C is detected. As a result of complexation of the hydrophobic azo-dye end group by RAMEB-CD, the cloud point increases from 29.5 back to 32 °C (Figure 2).

This is strong evidence for the interaction between the hydrophobic azo-dye end group and the hydrophilic RAMEB-CD ring. Based on this experience, the complexation of the azo-dye end group of **6** with hyperbranched polyglycerol (HPG, **7**) decorated with β-CD was investigated. This kind of supramolecular structure was generated to illustrate the broad applicability of **6** to generate, e.g., hedgehog-like nanoshapes. Therefore, **7** was prepared according to a procedure described in the literature recently [20-22]. The molecular weight of **7** (M_n 38 kDa) and the dispersity (D 1.7) were determined by SEC (Supporting Information File 1). To confirm the complexation between the azo-dye-labeled polymers **6** and **7** and the formation of a hedgehog-like superstructure **8**, DLS measurements in water were carried out. As expected, the complexation of **6** by **7** leads to an increase of the hydrodynamic diameters up to 18 nm (Figure 3).

The aggregation behavior of complex **8** in aqueous solution was also investigated by DLS measurements. Figure 4 shows the temperature dependence of the z-average diameter (D_Z) of the hedgehog-like nanoshaped polymer **8**. In the temperature range from 25 to 32 °C no change of D_Z was recorded.

At 33 °C the D_Z of **8** increased up to 21000 nm, but the values showed poor stability because of sedimentation. This means

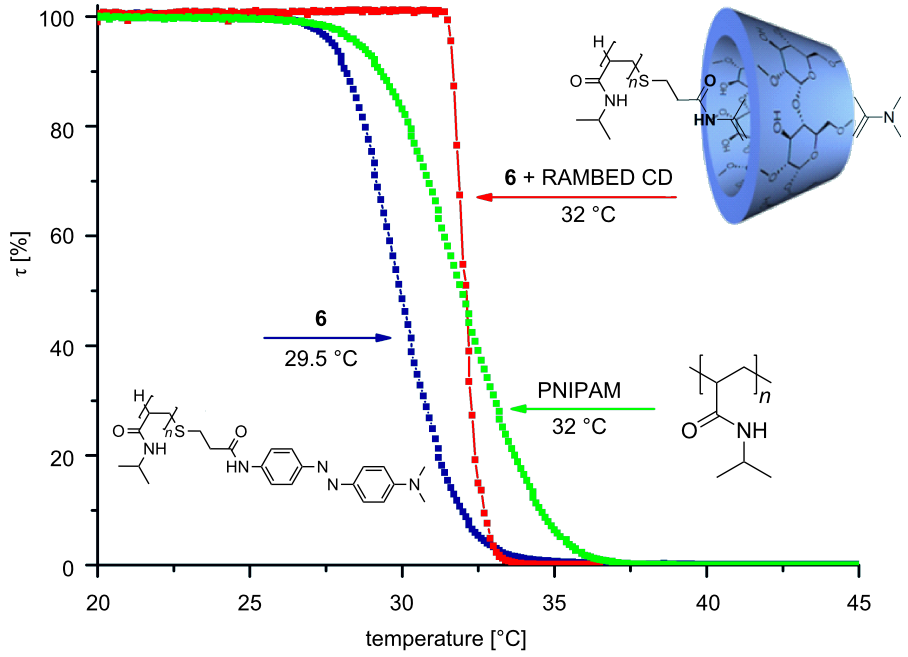

Figure 2: LCST measurements of **6**, the complex of **6** and RAMEB-CD, and in comparison to pure PNIPAM.

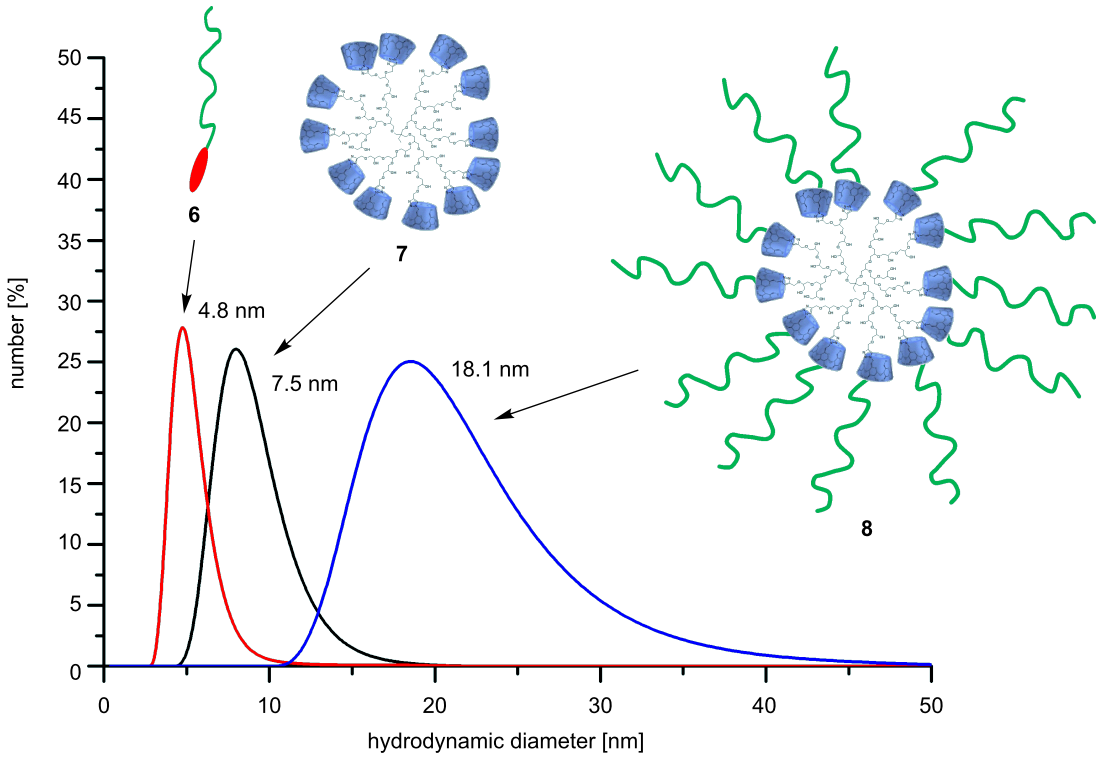

Figure 3: Hydrodynamic diameters of **6**, **7** and **8** (1 mg/mL) at 20 °C.

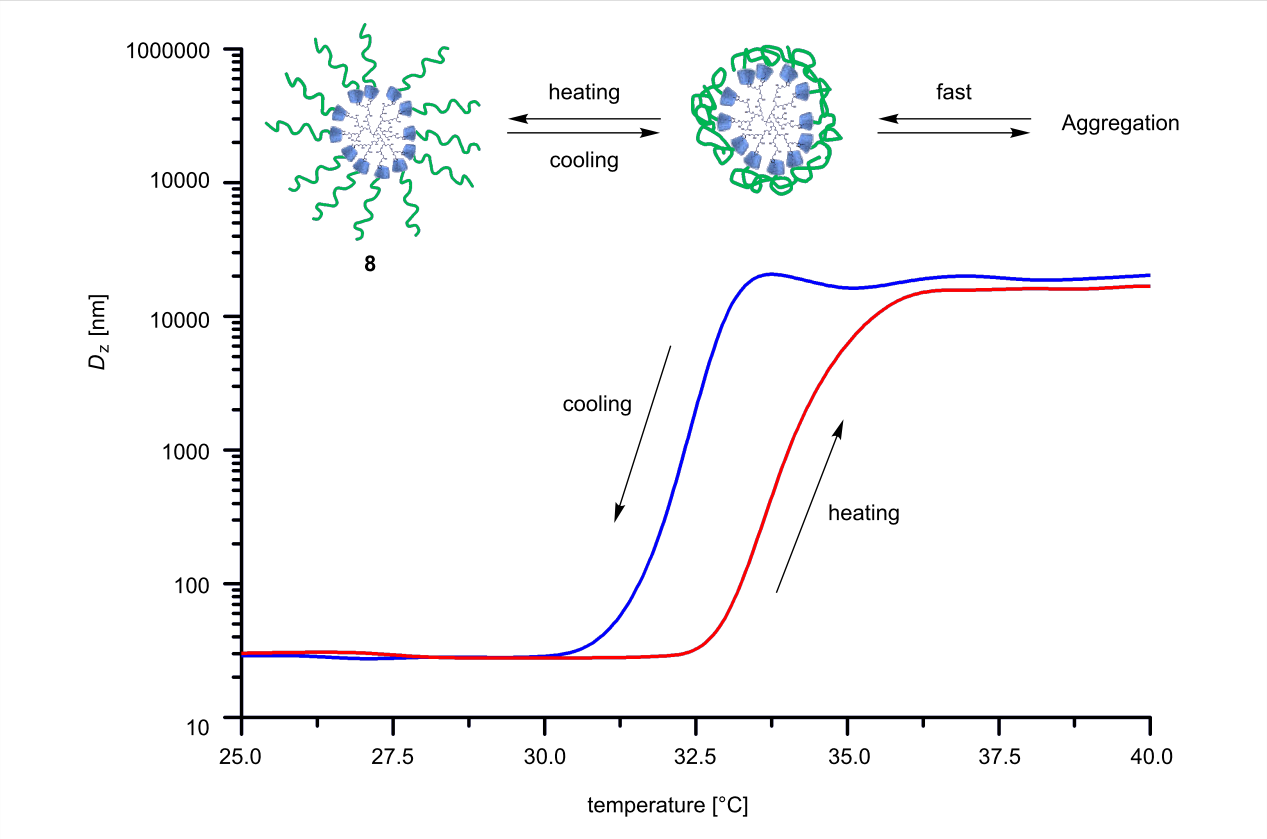

Figure 4: z-Average diameter (D_Z) of the complex **8** in water as a function of temperature (0.5 mg/mL, heating rate 0.5 °C/min).

that **8** is able to form larger particles above the LCST, even resulting in precipitation [23]. However, the change of D_Z showed a good reversibility upon cooling. The behavior can be interpreted by the hydrophobic shell of **8** and the strong hydrophobic interaction above the LCST, which causes the formation of the large particles.

Conclusion

In summary, we have presented the synthesis of an azo-dye-end-group-labeled PNIPAM by free-radical polymerization. The acidochromic and thermo-responsive behavior in aqueous solution was analyzed by absorption and cloud-point measurements. In addition, the influences of RAMEB-CD on both effects were investigated. The intermolecular interaction between the dye end group and RAMEB-CD was proven by absorption and 2D ROESY NMR experiments. Furthermore, we were able to show the formation of a hedgehog-like superstructure, based on a hyperbranched polyglycerol, bearing CD moieties, and the end-group-modified PNIPAM **6**.

Experimental

General remarks

All reagents used were commercially available (Sigma-Aldrich, Acros Organics) and used without further purification. RAMEB-CD and β-CD were obtained from Wacker Chemie GmbH, Burghausen, Germany and were used after being dried overnight with a vacuum oil pump over P_4O_{10}. *N*,*N*-Dimethylformamide (DMF) was purchased from Fluka, Germany. Dimethylsulfoxide-d_6 (99.9 atom % D) and deuterium oxide, D_2O were obtained from Deutero GmbH, Germany.

^{1}H NMR spectra were recorded on a Bruker Avance DRX 300 at 20 °C by using DMSO-d_6 or deuteriumoxide (99.9%) as solvents. FTIR spectra were recorded on a Nicolet 6700 FTIR spectrometer equipped with an ATR unit. The absorption spectra were measured in 1 cm quartz cells on a Specord 210 Plus UV–visible spectrophotometer (Analytik Jena AG, Germany). SEC-MALS measurements were carried out on a combined system comprising the following elements: refractive-index detector Optilabrex (Wyatt Technologies, laser wavelength 658 nm), three-angle light-scattering detector miniDawn TREOS (Wyatt Technologies, laser wavelength 658 nm, detector angles at 43.5°, 90.0° and 136.5°), UV detector Waters 486 (Waters), column set of HEMAbio 300 and HEMAbio 100 (MZ-Analysentechnik), pump, degasser and autosampler (Agilent 1200, Agilent technologies). The eluent was ultrapure water at a flow rate 1 mL/min. The molecular weight was calculated with Astra5 software from static-light-

scattering data, by using the Zimm model. As concentration source, the refractive index was used. Calibration of the system was performed with bovin serum albumin. Turbidity experiments were performed on a Tepper cloud-point photometer TP1. The relative transmission of a laser beam with a wavelength of 670 nm was recorded for each experiment. The measurements were performed in a temperature range between 5 and 60 °C and at a heating rate of 1 °C min^{-1} by using Hellma Suprasil precision cells 110 Q-S. Critical solution temperatures derived from these experiments were determined at 50% relative transmission. Dynamic light scattering (DLS) experiments were carried out with a Malvern Zetasizer Nano; ZS ZEN 3600 at a temperature of 20 °C. The particle size distribution is derived from a deconvolution of the measured intensity autocorrelation function of the sample by a general purpose method, i.e., the non-negative least squares algorithm, included in the DTS software.

Synthesis of 3. *N*-Isopropylacrylamide (**1**, 2 g, 0.02 mol) was dissolved in 10 mL of ethanol and flushed with argon for 15 min. To this solution, 3-mercaptopropionic acid (**2**, 0.1 mL, 1 mmol) and 4,4'-azobis(4-cyanovaleric acid) (24.7 mg, 0.09 mmol) were added under an argon atmosphere. After being stirred at 70 °C overnight, the corresponding polymer was separated by precipitation with cold diisopropyl ether. The precipitate was washed three times with diethyl ether and dried under reduced pressure. FTIR (diamond) ν (cm^{-1}): 3287 (NH), 2970 (CH), 2930 (CH),1712 (CO), 1640 (CO), 1539 (NH), 1456 (CH), 1365 (CH), 1230 (CH_2), 1171 (CC); ^{1}H NMR (300 MHz, D_2O) δ 7.19 (br, 1H, NH), 3.85 (br, 1H, CH), 2,67 (br, 2H, CH_2), 2,4 (br, 2H, CH_2), 1.3–2.2 (backbone), 1.02 ppm (s, 6H, CH_3).

Synthesis of 6. The carboxy-terminated PNIPAM (**3**, 2 g) was dissolved in 5 mL of dry DMF. To this solution, thionyl chloride (0.15 mL, 2 mmol) and triethylamine (0.28 mL, 2 mmol) were added and stirred for 3 h. The precipitated triethylammonium chloride was filtered and the excess of thionyl chloride was removed in vacuum from the DMF-solution. To the obtained solution, triethylamine (0.28 mL, 2mmol) and *N*,*N*-dimethyl-[4-(4'-aminophenylazo)phenyl]amine (**5**, 360 mg, 1.5 mmol) were added and stirred overnight at room temperature. The triethylammonium chloride was filtered off, and the terminated polymer was isolated by precipitation with cold diisopropyl ether. The precipitate was washed three times with diethyl ether and dried under reduced pressure. FTIR (diamond) ν (cm^{-1}): 3287 (NH), 2970 (CH), 2930 (CH), 1712 (CO), 1640 (CO), 1539 (NH), 1456 (CH), 1365 (CH), 1230 (CH_2), 1171 (CC), 881 (CN), 838 (aromatic C-H, 2 neighboring H atoms); ^{1}H NMR (300 MHz, DMSO-d_6) δ 7.97 (d, 8.88 Hz, ArH), 7.98 (d, 7.15 Hz, ArH), 7.58 (d, 7.17 Hz, ArH), 7.36 (d, 8.88 Hz, ArH) 7.20 (br, NH), 3.84 (s, CH), 2.62 (br, CH_2), 2.46 (br, CH_2), 1.3–2.2 (backbone), 1.04 ppm (s, 6H, CH_3); SEC measurements: M_n 3.4 kDa, P_D 1.3; ^{1}H NMR: 3.3 kDa.

Supporting Information

The Supporting Information contains experimental procedures for the preparation of **5**, HPG, propargyl-modified HPG, CD-monoazide, HPG bearing β-CD (**7**), and spectroscopic data of **6** and the complex of **6** and RAMEB-CD.

Supporting Information File 1

Experimental procedures and spectroscopic data.
[http://www.beilstein-journals.org/bjoc/content/supplementary/1860-5397-8-224-S1.pdf]

References

1. Tomatsu, I.; Hashidzume, A.; Harada, A. *J. Am. Chem. Soc.* **2006,** *128,* 2226–2227. doi:10.1021/ja058345a
2. Bergbreiter, D. E.; Osburn, P. L.; Li, C. *Org. Lett.* **2002,** *4,* 737–740. doi:10.1021/ol017198s
3. Harada, A.; Hashidzume, A.; Yamaguchi, H.; Takashima, Y. *Chem. Rev.* **2009,** *109,* 5974–6023. doi:10.1021/cr9000622
4. Pietsch, C.; Schubert, U. S.; Hoogenboom, R. *Chem. Commun.* **2011,** *47,* 8750–8765. doi:10.1039/c1cc11940k
5. Koopmans, C.; Ritter, H. *J. Am. Chem. Soc.* **2007,** *129,* 3502–3503. doi:10.1021/ja068959v
6. Jochum, F. D.; Theato, P. *Chem. Commun.* **2010,** *46,* 6717–6719. doi:10.1039/c0cc01288b
7. Beija, M.; Charreyre, M.-T.; Martinho, J. M. G. *Prog. Polym. Sci.* **2011,** *36,* 568–602. doi:10.1016/j.progpolymsci.2010.06.004
8. Bergbreiter, D. E.; Frels, J.; Heuze, K. *React. Funct. Polym.* **2001,** *49,* 249–254. doi:10.1016/S1381-5148(01)00087-6
9. Tomatsu, I.; Peng, K.; Kros, A. *Adv. Drug Delivery Rev.* **2011,** *63,* 1257–1266. doi:10.1016/j.addr.2011.06.009
10. Kuad, P.; Miyawaki, A.; Takashima, Y.; Yamaguchi, H.; Harada, A. *J. Am. Chem. Soc.* **2007,** *129,* 12630–12631. doi:10.1021/ja075139p
11. Goto, H.; Ohta, R. *Macromol. Chem. Phys.* **2010,** *211,* 2071–2080. doi:10.1002/macp.201000168
12. Yamaguchi, H.; Kobayashi, Y.; Kobayashi, R.; Takashima, Y.; Hashidzume, A.; Harada, A. *Nat. Commun.* **2012,** *3,* No. 603. doi:10.1038/ncomms1617
13. Bléger, D.; Liebig, T.; Thiermann, R.; Maskos, M.; Rabe, J. P.; Hecht, S. *Angew. Chem.* **2011,** *123,* 12767–12771. doi:10.1002/ange.201106879
14. Böhm, I.; Kreth, S. K.; Ritter, H. *Beilstein J. Org. Chem.* **2011,** *7,* 1130–1134. doi:10.3762/bjoc.7.130
15. Böhm, I.; Kreth, S. K.; Ritter, H.; Branscheid, R.; Kolb, U. *Macromol. Chem. Phys.* **2012,** *213,* 243–248. doi:10.1002/macp.201100259
16. Duan, Q.; Miura, Y.; Narumi, A.; Shen, X.; Sato, S.-I.; Satoh, T.; Kakuchi, T. *J. Polym. Sci., Part A: Polym. Chem.* **2006,** *44,* 1117–1124. doi:10.1002/pola.21208

17. Jochum, F. D.; Zur Borg, L.; Roth, P. J.; Theato, P. *Macromolecules* **2009,** *42,* 7854–7862. doi:10.1021/ma901295f
18. Sawunyama, P.; Jackson, M.; Bailey, G. W. *J. Colloid Interface Sci.* **2001,** *237,* 153–157. doi:10.1006/jcis.2001.7530
19. Kuwabara, T.; Nakamura, A.; Ueno, A.; Toda, F. *J. Phys. Chem.* **1994,** *98,* 6297–6303. doi:10.1021/j100076a011
20. Sunder, A.; Mülhaupt, R.; Haag, R.; Frey, H. *Macromolecules* **2000,** *33,* 253–254. doi:10.1021/ma9915881
21. Sunder, A.; Hanselmann, R.; Frey, H.; Mülhaupt, R. *Macromolecules* **1999,** *32,* 4240–4246. doi:10.1021/ma990090w
22. Sisson, A. L.; Papp, I.; Landfester, K.; Haag, R. *Macromolecules* **2009,** *42,* 556–559. doi:10.1021/ma802238e
23. Liu, Y.-Y.; Zhong, Y.-B.; Nan, J.-K.; Tian, W. *Macromolecules* **2010,** *43,* 10221–10230. doi:10.1021/ma1019973

License and Terms

Beilstein Journal of Organic Chemistry

Cyclodextrin-based nanosponges as drug carriers

Francesco Trotta*[1], Marco Zanetti[1] and Roberta Cavalli[2]

Review

Open Access

Address:
[1]Dipartimento di Chimica. University of Torino, Via Pietro Giuria 7 10125 Torino, Italy and [2]Dipartimento di Scienza e Tecnologia del Farmaco. University of Torino, Via Pietro Giuria 9 10125 Torino, Italy

Email:
Francesco Trotta* - francesco.trotta@unito.it

* Corresponding author

Keywords:
controlled release; cross-linked polymers; cyclodextrin; drug delivery; nanosponges

Beilstein J. Org. Chem. **2012,** *8,* 2091–2099.
doi:10.3762/bjoc.8.235

Received: 10 August 2012
Accepted: 06 November 2012
Published: 29 November 2012

This article is part of the Thematic Series "Superstructures with cyclodextrins: Chemistry and applications".

Guest Editor: H. Ritter

Abstract

Cyclodextrin-based nanosponges, which are proposed as a new nanosized delivery system, are innovative cross-linked cyclodextrin polymers nanostructured within a three-dimensional network. This type of cyclodextrin polymer can form porous insoluble nanoparticles with a crystalline or amorphous structure and spherical shape or swelling properties. The polarity and dimension of the polymer mesh can be easily tuned by varying the type of cross-linker and degree of cross-linking. Nanosponge functionalisation for site-specific targeting can be achieved by conjugating various ligands on their surface. They are a safe and biodegradable material with negligible toxicity on cell cultures and are well-tolerated after injection in mice. Cyclodextrin-based nanosponges can form complexes with different types of lipophilic or hydrophilic molecules. The release of the entrapped molecules can be varied by modifying the structure to achieve prolonged release kinetics or a faster release. The nanosponges could be used to improve the aqueous solubility of poorly water-soluble molecules, protect degradable substances, obtain sustained delivery systems or design innovative drug carriers for nanomedicine.

Review

Recent advances in nanotechnology demonstrate the increased attention that is now being paid to the supramolecular assembly of simple components for therapeutic and diagnostic purposes. The design of new biomaterials based on nanoscale structural characteristics can be expected to provide many potential applications in the field of nanomedicine.

Cyclodextrins [1-3] are nanometric biomaterials with a close relationship between molecular status and supramolecular properties. They are a class of cyclic glucopyranose oligomers and are synthesised by enzymatic action on hydrolysed starch. The main common native cyclodextrins are α, β and γ, which comprise six, seven and eight glucopyranose units, respectively.

They have a characteristic toroidal shape, which forms a well-defined truncated cone-shaped lipophilic cavity. Cyclodextrins are able to include compounds whose geometry and polarity are compatible with that of their cavity.

However, native cyclodextrins are not able to form inclusion complexes with certain molecules, such as hydrophilic or high-molecular-weight drugs. Moreover, β-cyclodextrin, the cheapest type, has low water solubility (1.85% w/v at 25 °C) and is toxic when injected intravenously. Consequently, many chemical modifications of cyclodextrins have been studied in an attempt to overcome their limitations and improve their technological characteristics. Well-structured molecules as well as random mixtures are described in the literature [4], and dimers [5], trimers [6], and polymers have also been obtained [7].

A different approach is to synthesise cross-linked cyclodextrin-based polymers so as to prepare insoluble multifunctional cyclodextrin derivatives [8-10]. These polymers can be obtained by reacting native cyclodextrins with a cross-linking agent that, after reaction, exerts its own properties and influences the behaviour of the cyclodextrin unit. Although insoluble cross-linked cyclodextrin polymers were first reported a long time ago, by reacting the parent cyclodextrin with dialdehydes, epoxides, epichlorohydrin, diacyl chlorides, etc., the term cyclodextrin nanosponges were first used by DeQuan Li and Min Ma in 1998 [11] to indicate a cross-linked β-cyclodextrin with organic diisocyanates leading to an insoluble network that showed a very high inclusion constant with several organic pollutants. For instance, *p*-chlorophenol was almost completely removed from waste water even at the parts per billion level [12]. However, no other applications were claimed or proposed.

It was not until the work performed by Trotta and co-workers [13] and the syntheses of new kinds of cyclodextrin nanosponges that they revealed their full potential in other fields, particularly as drug carriers.

Generally speaking, nanosponges are hyper-cross-linked cyclodextrins that can be obtained with α, β and γ cyclodextrins, either alone or as mixtures containing relevant amounts of linear dextrin, cross-linked with a suitable cross-linking agent. Interesting results have already been obtained as drug carriers by using an active carbonyl compound, e.g., carbonyldimiidazole, triphosgene, diphenyl carbonate, or organic dianhydrides (Scheme 1).

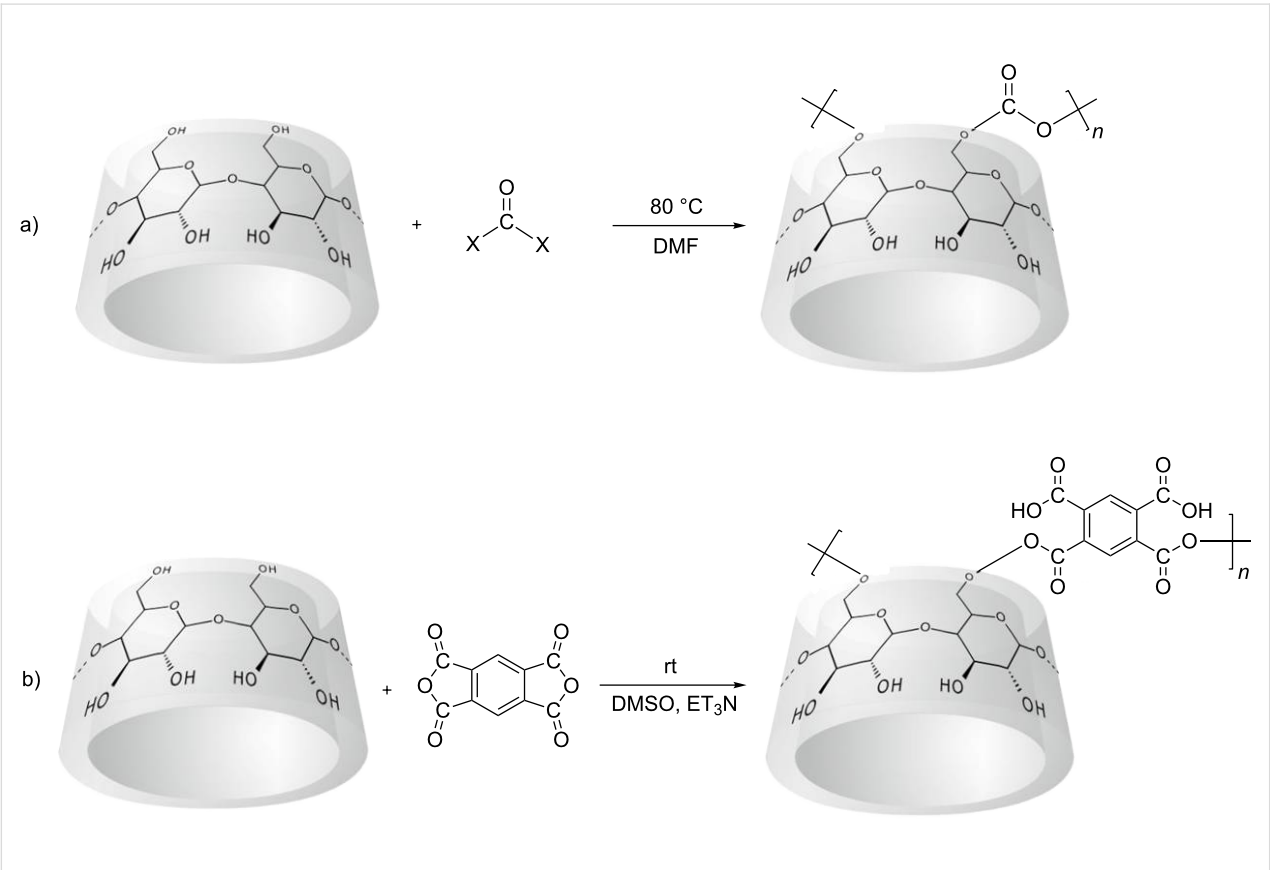

Scheme 1: Synthetic routes to cyclodextrin nanosponges. (a) Cyclodextrin carbonate nanosponges. (b) Cyclodextrin carboxylate nanosponges.

Detailed reaction conditions and parameters are reported elsewhere [14]. Here we simply wish to stress that primary hydroxy groups are mainly involved in the formation of a network as shown by FTIR–ATR, Raman and solid-state NMR analyses [15]. Moreover, the elastic properties of cyclodextrin nanosponges were determined by analysis of the spectral modification of the Boson peak and Brillouin frequency [16]. Using ultrasound-assisted synthesis and a suitable cross-linker molar ratio, spherical nanosponges of submicron size were obtained [17]. The cross-linking produces a powder consisting of cyclodextrin connected by nanochannels to form a cage-like structure (Figure 1).

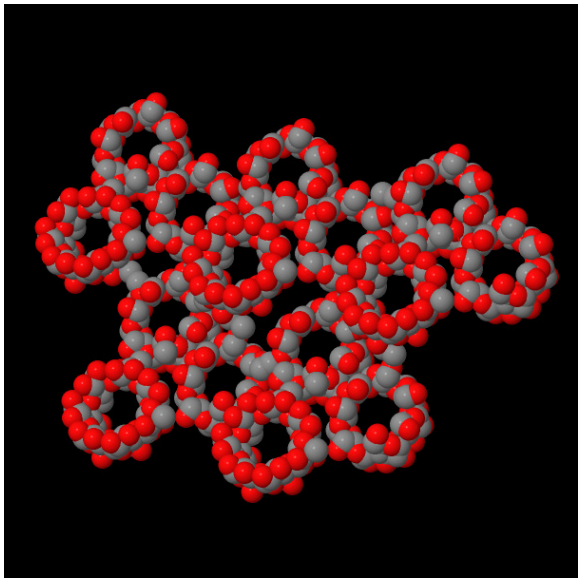

Figure 1: Molecular structure of cyclodextrin carbonate nanosponges.

By using different amounts of cross-linking agent, or by changing the type of cyclodextrin, it is possible to modulate the channels between the cyclodextrin molecules, thereby tuning the formation of the porous network and consequently affecting both the inclusion capacity and the solubilising ability of the nanosponges. Acid nanosponges carrying free carboxylic groups can be obtained using pyromellitic anhydride or other dianhydrides as a cross-linker, forming true cation exchange sites. The presence of free hydroxy groups in the nanosponges network allows further surface modification. For instance, carboxylated nanosponges can be obtained by reacting pristine carbonate nanosponges with succinic anhydride.

Detailed physicochemical characterisation is reported in the literature, demonstrating that carbonate nanosponges are thermally stable up to 300 °C and can therefore be sterilised by autoclaving at 121 °C and 2 bar for 15 minutes. FTIR and NMR analyses before and after sterilisation show their stability and the absence of degradation [13]. In addition, they do not act as surfactants and can be easily dispersed in water.

Nanosponges also have colloidal sizes with a mean diameter of less than 1 μm and narrow size distribution and form opalescent suspensions on dispersion in water. The zeta potential of carbonate nanosponges is about −25 mV, which is sufficiently high to produce stable water suspensions that do not undergo aggregation over time.

For parenteral application it is possible to synthesise nanosponges with a mean diameter in the range of 200–300 nm with narrow size distribution (Figure 2).

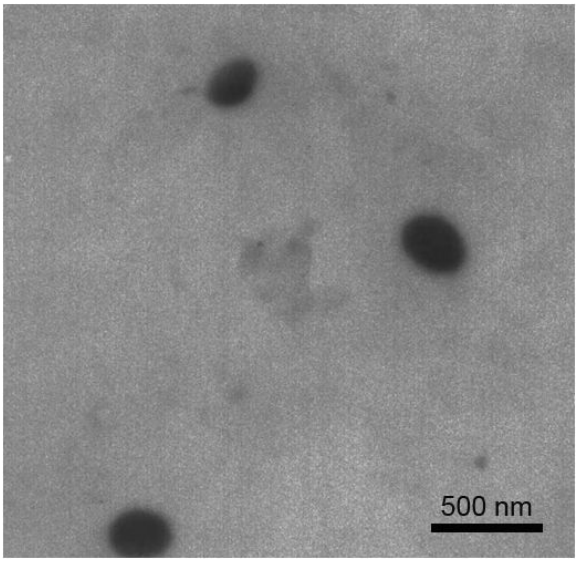

Figure 2: TEM microphotograph of cyclodextrin carbonate nanosponge (magnification 46,000×).

The stability of carbonate nanosponges was evaluated at 60 °C under both acidic and basic conditions. Under acidic conditions (0.1 N HCl) a limited release of cyclodextrin units was observed after 2 h due to degradation of the nanosponge structure, whereas the basic environment did not affect the nanosponge stability. On the other hand, carboxylated nanosponges obtained by using pyromellitic dianhydride as a cross-linker appear less chemically and thermally stable, but can swell more than 30-fold in water, they have more negative zeta potential, and can simultaneously host cations, organic molecules and even macromolecules.

Preliminary toxicity studies were carried out on carbonate nanosponges in order to assess their safety with respect to preclinical studies on laboratory animals.

The methods employed for cytotoxicity testing are those described in the literature [18].

In vitro cell culture toxicity assays were carried out on different cell lines (i.e., HELA; MCF7, COS) by using the MTT test. Cells were incubated for between 24 and 72 h and their viability determined. After incubation with nanosponges no cytotoxicity was observed. The percentage of cell viability did not change from untreated cells. Other in vitro methods for evaluating the toxicity of new materials include the determination of its haemolytic properties. When nanosponges were incubated with human erythrocytes for 90 minutes, no haemolytic activity was observed up to a concentration of 15 mg/mL, showing that the nanosponges possess good blood compatibility.

Acute systemic toxicity was evaluated after injection in mice. Unlike other cross-linked cyclodextrin polymers [19], nanosponges were found to be safe between 500 and 5000 mg/kg in Swiss albino mice: they did not show any sign of toxicity or adverse reactions. Nanosponges were then injected intravenously into mice and monitored for 24 h. Oral administration of nanosponges was also tested in mice [20] with no apparent side effects.

The nanoporous structure that is formed changes many properties of the native cyclodextrin. This peculiar and versatile structure is suitable for a broad range of potential and actual applications and was recently reviewed [13,21-23]. As a general characteristic, the nanosponge structure improves the ability of cyclodextrins to form specific complexes with guest molecules, compared to native cyclodextrins. The included substances can be either strongly retained or released in a controlled manner.

From an environmental standpoint this means that water pollutants, such as heavy metals and many organic molecules, can be removed and retained easily [24,25].

The use of nanosponges in water treatment has been found successful for aromatic chlorohydrocarbons, and nanosponges succeeded where their main competitor, activated carbon, failed, for example, in the removal of heavy metals. Furthermore, nanosponges have greater mechanical strength than activated carbon and are not affected by dust formation during application. Finally, they can be reused indefinitely after simple washing with an environmentally friendly solvent, such as ethanol.

Nanosponges can be used as supports for catalysis applications. One important result that has emerged from experiments on enzyme catalysis is the prolonged activity of the enzymes [26]. Nanosponges can preserve the activity of some enzymes far longer than other supporting media, such as agarose. Moreover, the possibility of including enzymes inside the structure prolongs their activity and makes it possible to obtain an efficaciously supported catalyst to promote chemical reactions and aid the destruction of chemical pollutants (detergents, POPs abatement) as well as biosensors.

Nanosponges can also be used in agriculture and have shown the interesting characteristic of encapsulating some important agricultural chemicals. In this case, release is controlled and has a slow profile [27]. Finally, nanosponges can also be used in polymer processing to improve flame-retardant properties [28,29] and in enantio-differentiating photoisomerization reactions [30].

Application of cyclodextrin nanosponges in drug delivery

By virtue of their biocompatibility and versatility, nanosponges have many potential applications in the pharmaceutical field. One recent EU commission report focused on the use of cyclodextrin nanosponges as a promising innovative system for drug delivery. They can be used as excipients in preparing tablets, capsules, pellets, granules, suspensions, solid dispersions, or topical dosage forms or as new nanotechnological, multifunctional carriers [31,32].

In particular, the design of new nanodelivery systems to improve drug administration is currently being studied. Many drugs show poor solubility, low permeability, a short half-life, low stability, and/or high molecular weight, and as a consequence their formulation is challenging.

Nanosponges have the capacity to incorporate drugs within their structure, either as inclusion complexes or as noninclusion complexes. There are far more interaction sites available for incorporation within a nanosponge structure than in β-cyclodextrin molecules, and they also show different mesh polarities (hydrophobic cyclodextrin cavities surrounded by hydrophilic nanochannels of the polymeric network) thereby enabling significant interactions between molecules with different lipophilicities and structures.

The ability of cyclodextrin nanosponges to encapsulate drugs has been studied in depth for both hydrophilic and lipophilic molecules, including dexamethasone, flurbiprofen, doxorubicin, itraconazole, resveratrol, paclitaxel, 5-fluorouracil and tamoxifen, as is shown in Table 1.

Table 1: Molecules complexed by using nanosponges.

Drug	log P	Therapeutic activity	Administration route	Reference
Dexamethasone	1.9	anti-inflammatory	oral, parenteral	[51]
Flurbiprofen	4.2	anti-inflammatory	oral	[51]
Doxorubicin	1.3	antineoplastic	parenteral	[51]
Progesterone	3.9	hormonal	oral	[51]
Itraconazole	5.7	antifungal	oral, topical	[33]
5-fluorouracile	−0.9	antineoplastic	parenteral, topical	[40]
Tamoxifen	4.0	antiestrogen	oral	[34]
Resveratrol	2.8	antioxidant	oral, topical	[48]
Paclitaxel	2.5	antineoplastic	parenteral	[36-46]
Camptothecin	1	antineoplastic	parenteral	[41,42]
Omeprazole	2.2	antiulcerative	oral	[38]
Nelfinavir mesylate	4.6	antiviral	oral	[38]
Acetylsalicylic acid	1.2	analgesic	oral	[36]
Acyclovir	−1.6	antiviral	oral, topical, parenteral	[39]
Gamma-oryizanol	–	antioxidant	topical	[49]
Telmisartan	7.7	antihypertensive	oral	[47]

Considering their versatility, nanosponges can act as multifunctional carriers, i.e., to enhance solubility, protect fragile molecules, and achieve sustained release. In many cases they act with two or more functions simultaneously.

In this review we summarise their potential capacities by classifying nanosponges according to their main applications, and some examples are reported as case studies.

Solubility enhancement

One of the greatest limits to the development of various pharmaceuticals is the low water solubility of many drugs. About 40% of new drugs are poorly soluble in water, which hinders their clinical application. The formulation of poorly water-soluble drugs constitutes a problem that is difficult to solve. Many technological approaches have been investigated. The ability of cyclodextrins to form inclusion complexes with various molecules is widely used in the pharmaceutical field as a strategy to increase the aqueous solubility and, consequently, bioavailability of lipophilic drugs. For hydrophilic or moderately polar drugs this approach is less effective, and consequently cyclodextrin derivatives have been investigated.

Nanosponges can improve the wetting and solubility of molecules with very poor solubility in water. The drugs can be molecularly dispersed within the nanosponge structure and then released as molecules, avoiding the dissolution step. Consequently, the apparent solubility of the drug can be increased.

Many formulation and bioavailability problems can be solved by enhancing the solubility and dissolution rate of a substance, and nanosponges can greatly enhance the drug solubility.

Swaminathan et al. studied a formulation of itraconazole in nanosponges [33], a drug with an aqueous solubility of about 1 ng/mL at physiological pH. The presence of nanosponges improved the solubility of the drug more than 27-fold; and when PVP was added as an auxiliary component of the nanosponge formulation, this rose to 55-fold. Moreover, the dissolution profiles of the drug for the two formulations were faster than for the formulations available on the market. Nanosponge formulation could thus increase the bioavailability of itraconazole.

The solubilisation efficiency of nanosponges with regard to tamoxifen, a nonsteroidal anti-estrogen molecule used for treating and preventing breast cancer, was observed by using a 0.5% aqueous suspension of β-CD nanosponges [34]. Encapsulation of tamoxifen in these nanosponges was more than 40% w/w, since 5 mg of nanosponges can solubilise 2.2 mg of tamoxifen. The in vitro release of tamoxifen from nanosponges showed pseudo-zero order kinetics. After 2 h about 60% of the encapsulated drug had been released at pH 7.4.

The anticancer agent paclitaxel is another drug difficult to formulate. Paclitaxel has a very low solubility in water, i.e., less than 0.3 μg/mL. As a consequence, the dosage form available for clinical administration requires the use of other pharmaceutical solvents or emulsifying agents, namely Cremophor EL (polyethoxylated castor oil). Unfortunately, Cremophor EL has

been seen to cause serious side effects, such as neurotoxicity, nephrotoxicity and cardiotoxicity [35].

Cyclodextrin-based nanosponges were used to prepare a Cremophor-free formulation for paclitaxel administration. Paclitaxel-loaded nanosponges were prepared by using the freeze-drying method to entrap the drug in a β-CD nanosponges network. The paclitaxel solubilisation efficiency of this formulation was compared to that of native β-cyclodextrin showing a marked increase. β-CD nanosponges loaded with paclitaxel have a mean diameter of about 350 nm with a rather narrow size distribution (polydispersity index below 0.2).

These nanosponges obtained using carbonyldiimidazole as a cross-linker showed good paclitaxel complexation ability: one millilitre of a 1.5% nanosponge aqueous suspension allows one to dissolve about 2 mg of paclitaxel, thus confirming their wetting and solubilising properties towards paclitaxel avoiding the use of surfactants. The paclitaxel-loaded nanosponges formed a stable colloidal system in water inhibiting the recrystallization of paclitaxel over time. Moreover, this study demonstrated that delivery of paclitaxel via nanosponges increased the amount of paclitaxel entering cancer cells and lowered the IC_{50} of paclitaxel, thereby enhancing its pharmacological effect [36].

Sustained delivery system

Modified-release dosage forms offer a number of advantages over the conventional release formulation of a drug. The design of a modified-release product is generally intended to optimise the treatment regimen by providing slow, continuous delivery of the drug over the entire dosing interval. This makes it possible to decrease the dose administered, change the pharmacokinetic profile, and decrease side effects.

Different drug delivery systems have been designed to modify the release kinetics of medicinal products. The drug release kinetics from nanosponges can be obtained with a prolonged release profile over time. Previous in vitro studies showed that flurbiprofen was released slowly from β-CD nanosponges [37], reaching a percentage of less than 10% after 130 minutes. A similar result was obtained with the incorporation of doxorubicin in nanosponges. In in vitro tests, doxorubicin was released very slowly at pH 1.2 (about 1% after 120 minutes) and the percentage increased with pH values. Doxorubicin release of about 29% was obtained at pH 7.4. This behaviour could suggest that the nanosponge formulation is able to protect the drug from the gastric environment, allowing delivery in the intestinal tract.

Vavia prepared nelfinavir mesylate loaded nanosponges to enhance the solubility of the drug [38]. Nelfinavir is a protease inhibitor with low bioavailability, used to treat HIV infections. In this case, the drug was released more slowly from nanosponges than from a β-CD complex. This behaviour shows that nanosponges are able to prolong drug release over time and consequently could also be proposed as a sustained drug-delivery system for oral administration.

Acyclovir is a medium polarity drug with a solubility in water of 1.5 mg/mL. Special carboxylated nanosponges, containing dissociable carboxylic groups in their structure were developed for its encapsulation. They represent a further electrostatic contribution for drug encapsulation, in addition to the cyclodextrin cavities. Electrostatic interactions may occur between the carboxylic groups present in the nanosponge structure and the amino group of acyclovir.

In vitro, acyclovir-loaded carboxylated nanosponges [39] showed prolonged release of the drug without the initial burst effect, and 20% drug release was obtained after three hours.

Protection from light or degradation

Nanosponges can also be used as carriers to protect encapsulated molecules from light or from chemical- and enzyme-induced degradation. To evaluate the potential protection application, 5-fluorouracile was used as a light-sensitive model drug. β-CD nanosponges were able to incorporate up to 30% of 5-fluorouracile [40]. The in vitro release of 5-fluorouracile, determined by using the dialysis-bag technique at pH 7.4, was about 60% of the encapsulated amount after 2 h showing an interaction between the drug and the nanosponge structure, despite the hydrophilicity of the drug. Moreover, encapsulation of 5-fluorouracile in nanosponges protected the drug and maintained its cytotoxicity against MCF-7 cells. Another paradigmatic example was established with the incorporation of camptothecin in cyclodextrin nanosponges.

The anti-tumour activity of camptothecin has been extensively investigated in both hematological and solid malignancies; however, its use is still limited due to its poor solubility and high chemical instability since the lactone ring of the molecule is very susceptible to hydrolysis under physiological conditions.

The encapsulation of camptothecin in nanosponges was used to prolong the shelf life and release of the drug [41]. The nanosponges solubilised large amounts of the drug and protected the lactone ring from opening due to its high inclusion abilities, thereby increasing stability.

Three types of nanosponges, i.e., β-CD-1/2 nanosponges, β-CD-1/4 nanosponges and β-CD-1/8 nanosponges, characterised by an increasing cross-linker/β-CD molar ratio, have been used as

delivery systems for camptothecin. All proved to solubilise camptothecin, thereby increasing its aqueous solubility, and formed inclusion complexes. FTIR, DSC and XRPD analyses confirmed the drug interaction with nanosponges. Moreover camptothecin loaded in nanosponges was seen to be more effective than the plain drug on HT29 cells.

The same formulation was recently shown to be an effective nanotechnology for the treatment of both androgen-sensitive and castrate-refractory prostate cancer in cell-line experiments [42].

Nanosponges can be used to store and prolong the release of volatile molecules, such as essential oils, following their encapsulation. Linalool, a liquid component of many essential oils and fragrances with a boiling point of 198 °C, was encapsulated in different types of nanosponges as a liquid oil model [43]. β-CD-1/4 nanosponges can incorporate 8% w/w of linalool within their structure. The entrapment of linalool in the nanosponge matrix was confirmed by DSC analysis. In vitro release studies were carried out by using the linalool β-cyclodextrin complex for comparative purposes. After 2 hours, linalool release from nanosponges was half that from the β-cyclodextrin complex, thereby showing that nanosponges stabilise the molecule in their structure.

Protein delivery

Swellable cyclodextrin-based nanosponges were purposely prepared for protein delivery by using a different synthetic route. New swellable cyclodextrin-based poly(amidoamine) nanosponges (PAA-NS) [44], named NS 10 and NS 11, were synthesised by cross-linking β-cyclodextrins with either 2,2-bis(acrylamidoacetic acid) or a short polyamido-amine chain deriving from 2,2-bis(acrylamidoacetic acid) and 2-methylpiperazine, respectively. These swellable nanosponges were shown to be sensitive to the pH of the surrounding media. PAA-NS were reduced in nanosuspensions by using the high-pressure-homoginisation technique. Bovine serum albumin (BSA) was used as a model protein to study the encapsulating capacity of these new β-cyclodextrin-based nanosponges. High protein-complexation capacity was achieved for both the nanosponges with a BSA-encapsulation efficiency greater than 90%. In vitro release studies were carried out, showing a prolonged release of albumin from the two swellable β-CD-nanosponges over a period of 24 h. The encapsulation of albumin and its prolonged release was also obtained with carbonate nanosponges (unpublished data).

NS10 and NS11 were recently used to incorporate lysozyme and showed a high loading capacity. The encapsulation efficiency and loading percentages were 89% and 17% for NS10 and 96% and 19.6 for NS11. These lysozyme-loaded nanosponges released the enzyme at a pH-dependent rate with prolonged kinetics, whilst maintaining its biological activity [44].

Oral delivery systems

The dissolution rate of a solid drug is a limiting factor for oral bioavailability. For hydrophobic drugs the dissolution process acts as the rate-controlling step and, therefore, determines the rate and degree of absorption. As a consequence, many hydrophobic drugs show erratic and incomplete absorption from the gastrointestinal tract.

The Biopharmaceutics Classification System (BCS) was developed by Amidon [45] in 1995 as a tool for predicting the extent of drug absorption after oral administration. This system divides drugs into four categories according to their solubility and intestinal permeability. Formulation strategies can be used to shift a drug from one class to another by improving their pharmaceutical characteristics.

Acetylsalicylic acid (ASA), a nonsteroidal anti-inflammatory drug belonging to BCS class III, was formulated into pyromellitic dianhydride cross-linked β-cyclodextrin nanosponges [36]. TEM studies showed that the particle sizes of ASA-loaded nanosponges have average diameters ranging from 40 to 60 nm and they were seen to have a regular spherical shape. Zeta potential was high enough to obtain a stable colloidal formulation. In vitro and in vivo studies indicated a slow and prolonged ASA release from pyromellitic cross-linked β-cyclodextrin nanosponges over a long period, i.e., 24 hours. In carrageenan-induced rat paw edema, administration of ASA as a nanosponge formulation administered by oral gavage reduced inflammation significantly ($P < 0.01$ and $P < 0.05$) compared to plain ASA and the control group. These results indicate that the ASA nanosponge formulation may be used for oral delivery of the drug.

Paclitaxel-loaded nanosponges were administered to rats by oral gavage using commercially available TAXOL® as the control. The oral bioavailability of the drug was increased about 3-fold after the administration of paclitaxel-loaded nanosponges, in comparison to the control [46].

More recently, Rao et al. studied the influence of carbonate nanosponges on telmisartan, an antihypertensive BCS class II drug characterised by an estimated solubility in water of just 9.9 μg/ml resulting in low bioavailability. The formation of a ternary complex of telmisartan with nanosponges and $NaHCO_3$ was seen to synergistically enhance the dissolution rate of telmisartan [47].

Topical delivery systems

Nanosponges can be used in gels or creams for topical application. In one recent work, resveratrol, a polyphenolic phytoalexin present in different plant sources and which plays an important role in the prevention of many human diseases, particularly due to its antioxidant properties, was encapsulated in nanosponges. Incorporation markedly increased the solubility and stability of the molecule.

Resveratrol-loaded nanosponges were seen to enhance drug permeation in in vitro studies on porcine skin. Enhanced permeation of resveratrol was also observed by using rabbit buccal mucosa [48].

Gamma-oryzanol is a ferulic acid ester mixture, used as sunscreen in the cosmetics industry. Its application is limited by its high instability and photodegradation. Gamma-oryzanol was encapsulated in nanosponges, showing a good protection from photodegradation. A gel and an O/W emulsion were formulated with the gamma-oryzanol-loaded nanosponges [49]. In vitro permeability and accumulation studies were then carried out on porcine skin. A high skin accumulation of gamma-oryzanol was observed over time. The ability of nanosponges to increase the uptake of the guest molecule by the skin can be attributed to the capacity to increase solubility at the surface of the skin, as already reported for cyclodextrins.

Gas delivery

Gas storage and delivery play an important role in biology, medicine, cosmetics and pharmaceuticals. The molecular encapsulation of gases in cyclodextrin cavities has already been proven. Nanosponge formulations can act as a reservoir for various types of gas. β-CD nanosponges have shown an ability to store large amounts of carbon dioxide, 1-methylcyclopropene and oxygen [8].

Three different cyclodextrin nanosponges were synthesised cross-linking α-, β- or γ-cyclodextrin with carbonyldiimidazole as oxygen-encapsulating formulations [50]. The nanosponges were able to release oxygen both in the presence and in the absence of ultrasound (US). Oxygen permeation through a silicone membrane was obtained by using a nanosponge/hydrogel combination system

All types of nanosponges were able to encapsulate, store and release oxygen for prolonged periods. Ultrasound enhanced the in vitro release and permeation of oxygen. The nanosponge/hydrogel system produces a slower sustained release of the gas. Therefore, nanosponges could be suitable carriers for topical oxygen delivery in the presence and in the absence of US and could act as an oxygen reservoir.

Conclusion

Nanosponges are a new type of biocompatible cross-linked polymer, whose production is flexible and cost-effective. Cyclodextrin nanosponges possess particular properties in terms of their encapsulation ability, biocompatibility and solubilisation capacity with regard to different types of molecules. Nanosponges could broaden the range of applications of cyclodextrins in pharmacy and medicine, as well as in other important fields, such as agriculture, cosmetics and the environment. They could be used to delivery two active substances simultaneously for combination therapy, or for simultaneous therapeutic and diagnostic applications. The surface engineering of nanosponges could lead to prolonged residence time in the blood or increased efficiency and specificity with ligands for targeting sites. In conclusion, nanosponges can be considered as multifunctional nanoscale systems suitable for the delivery of active molecules in nanomedicine.

References

1. Martin Del Valle, E. M. *Process Biochem.* **2004,** *39,* 1033–1046. doi:10.1016/S0032-9592(03)00258-9
2. Kurkov, S. V.; Loftsson, T. *Int. J. Pharm.* **2012,** in press. doi:10.1016/j.ijpharm.2012.06.055
3. Duchêne, D.; Ponchel, G.; Wouessidjewe, D. *Adv. Drug Delivery Rev.* **1999,** 29–40. doi:10.1016/S0169-409X(98)00053-2
4. Easton, C. J.; Lincoln, S. F. *Modified Cyclodextrins;* Imperial College Press: London, U.K., 1999.
5. Ishimaru, Y.; Masuda, T.; Iida, T. *Tetrahedron Lett.* **1997,** 3743–3744. doi:10.1016/S0040-4039(97)00742-9
6. Leung, D. K.; Atkins, J. H.; Breslow, R. *Tetrahedron Lett.* **2001,** 6255–6258. doi:10.1016/S0040-4039(01)01200-X
7. Renard, E.; Barnathan, G.; Deratani, A.; Sebille, B. *Macromol. Symp.* **1997,** 229–234. doi:10.1002/masy.19971220136
8. Pariot, N.; Edwards-Lévy, F.; Andry, M.-C.; Lévy, M.-C. *Int. J. Pharm.* **2000,** *211,* 19–27. doi:10.1016/S0378-5173(00)00576-7
9. Pariot, N.; Edwards-Lévy, F.; Andry, M.-C.; Lévy, M.-C. *Int. J. Pharm.* **2002,** *232,* 175–181. doi:10.1016/S0378-5173(01)00899-7
10. Rölling, P.; Lamers, M.; Staudt, C. *J. Membr. Sci.* **2010,** *362,* 154–163. doi:10.1016/j.memsci.2010.06.036
11. Li, D.; Ma, M. Cyclodextrin polymer separation materials. WO 9822197, May 28, 1998.
12. Li, D.; Ma, M. *Clean Technol. Environ. Policy* **2000,** *2,* 112–116.
13. Trotta, F. Cyclodextrin Nanosponges and Their Applications. In *Cyclodextrins in Pharmaceutics, Cosmetics and Biomedicine: Current and Future Industrial Applications;* Bilensoy, E., Ed.; John Wiley & Sons: Hoboken, NJ, USA, 2011; pp 323–342. doi:10.1002/9780470926819.ch17
14. Trotta, F.; Tumiatti, W. Cross-linked polymers based on cyclodextrins for removing polluting agents. WO 03/085002 A1, Oct 16, 2003.
15. Castiglione, F.; Crupi, V.; Majolino, D.; Mele, A.; Panzeri, W.; Rossi, B.; Trotta, F.; Venuti, V. *J. Inclusion Phenom. Macrocyclic Chem.* **2012**. doi:10.1007/s10847-012-0106-z
16. Rossi, B.; Caponi, S.; Castiglione, F.; Corezzi, S.; Fontana, A.; Giarola, M.; Mariotto, G.; Mele, A.; Trotta, F.; Petrillo, C.; Villani, G. *J. Phys. Chem. B* **2012,** *116,* 5323–5327. doi:10.1021/jp302047u

17. Trotta, F.; Cavalli, R.; Tumiatti, W.; Zerbinati, O.; Roggero, C.; Vallero, R. Ultrasound assisted synthesis of cyclodextrin based nanosponges. WO 0002814 A1, Jan 12, 2006.
18. Cavalli, R.; Donalisio, M.; Bisazza, A.; Civra, A.; Ranucci, E.; Ferruti, P.; Lembo, D. *Methods Enzymol.* **2012,** *509,* 1–19. doi:10.1016/B978-0-12-391858-1.00001-0
19. Van der Manakker, F.; Van Nostrum, C. F.; Hernik, W. E. *Biomacromolecules* **2009,** *10,* 3157–3175. doi:10.1021/bm901065f
20. Torne, S. Personal communication.
21. Subramanian, S.; Singireddy, A.; Krishnamoorthy, K.; Rajappan, M. *J. Pharm. Pharmaceut. Sci.* **2012,** *15,* 103–111.
22. Ahmed, R. Z.; Patil, G.; Zaheer, Z. *Drug Dev. Ind. Pharm.* **2012**. doi:10.3109/03639045.2012.694610
23. Rita, L.; Amit, T.; Chandrashekhar, G. *Int. J. Res. Ayurveda Pharm.* **2011,** *2,* 1520–1526.
24. Berto, S.; Bruzzoniti, M. C.; Cavalli, R.; Perrachon, D.; Prenesti, E.; Sarzanini, C.; Trotta, F.; Tumiatti, W. *J. Inclusion Phenom. Macrocyclic Chem.* **2007,** *57,* 631–636. doi:10.1007/s10847-006-9273-0
25. Berto, S.; Bruzzoniti, M. C.; Cavalli, R.; Perachon, D.; Prenesti, E.; Sarzanini, C.; Trotta, F.; Tumiatti, W. *J. Inclusion Phenom. Macrocyclic Chem.* **2007,** *57,* 637–643. doi:10.1007/s10847-006-9270-3
26. Di Nardo, G.; Roggero, C.; Campolongo, S.; Valetti, F.; Trotta, F.; Gilardi, G. *Dalton Trans.* **2009,** *33,* 6507–6512. doi:10.1039/B903105G
27. Seglie, L.; Martina, K.; Devecchi, M.; Roggero, C.; Trotta, F.; Scariot, V. *Postharvest Biol. Technol.* **2011,** *59,* 200–205. doi:10.1016/j.postharvbio.2010.08.012
28. Alongi, J.; Poskovic, M.; Frache, A.; Trotta, F. *Carbohydr. Polym.* **2011,** *86,* 127–135. doi:10.1016/j.carbpol.2011.04.022
29. Alongi, J.; Poskovic, M.; Visakh, P. M.; Frache, A.; Malucelli, G. *Carbohydr. Polym.* **2012,** *88,* 1387–1394. doi:10.1016/j.carbpol.2012.02.038
30. Liang, W.; Yang, C.; Nishijima, M.; Fukuhara, G.; Mori, T.; Mele, A.; Castiglione, F.; Caldera, F.; Trotta, F.; Inoue, Y. *Beilstein J. Org. Chem.* **2012,** *8,* 1305–1311. doi:10.3762/bjoc.8.149
31. http://www.observatorynano.eu/project/filesystem/files/HMN%20report.pdf.
32. Moya-Ortega, M. D.; Alvarez-Lorenzo, C.; Concheiro, A.; Loftsson, T. *Int. J. Pharm.* **2012,** *428,* 152–163. doi:10.1016/j.ijpharm.2012.02.038
33. Swaminathan, S.; Vavia, P. R.; Trotta, F.; Torne, S. *J. Inclusion Phenom. Macrocyclic Chem.* **2007,** *57,* 89–94. doi:10.1007/s10847-006-9216-9
34. Torne, S.; Darandale, S.; Vavia, P.; Trotta, F.; Cavalli, R. *Pharm. Dev. Technol.* **2012,** 1–7. doi:10.3109/10837450.2011.649855
35. Gelderblom, H.; Verweji, J.; Nooter, K.; Sparreboom, A. *Eur. J. Cancer* **2011,** *37,* 1590–1598. doi:10.1016/S0959-8049(01)00171-X
36. Mognetti, B.; Barberis, A.; Marino, S.; Berta, G.; De Francia, S.; Trotta, F.; Cavalli, R. *J. Inclusion Phenom. Macrocyclic Chem.* **2012,** *74,* 201–210. doi:10.1007/s10847-011-0101-9
37. Cavalli, R.; Trotta, F.; Tumiatti, W. *J. Inclusion Phenom. Macrocyclic Chem.* **2006,** *56,* 209–213. doi:10.1007/s10847-006-9085-2
38. Vavia, P. R.; Swaminathan, S.; Trotta, F.; Cavalli, R. Applications of nanosponges in drug delivery. In *Proceedings XIII International Cyclodextrin Symposium,* Turin, Italy, May 14–17, 2006; p 207.
39. Lembo, D.; Swaminathan, S.; Donalisio, M.; Civra, A.; Pastero, L.; Aquilano, D.; Vavia, P.; Trotta, F.; Cavalli. R. *Int. J. Pharm.* Submitted.
40. Cavalli, R.; Trotta, F.; Tumiatti, W.; Serpe, L.; Zara, G. P. 5-Fluorouracile loaded β-cyclodextrin nanosponges: invitro characterization and cytotoxicity. In *Proceedings XIII International Cyclodextrin Symposium,* Turin, Italy, May 14–17, 2006; p 207.
41. Swaminathan, S.; Pastero, L.; Serpe, L.; Trotta, F.; Vavia, P.; Aquilano, D.; Zara, G.; Cavalli, R. *Eur. J. Pharm. Biopharm.* **2010,** *74,* 193–201. doi:10.1016/j.ejpb.2009.11.003
42. Minelli, R.; Cavalli, R.; Ellis, L.; Pettazoni, P.; Trotta, F.; Barrera, G.; Fantozzzi, R.; Dianzani, C.; Pili, R. *Eur. J. Pharm. Sci.* **2012,** *47,* 686–694. doi:10.1016/j.ejps.2012.08.003
43. Cavalli, R.; Carlotti, E.; Trotta, F.; Torne, S.; Tumiatti, V.; Roggero, C.; Trotta, M. Nanospugne a base di ciclodestrine per la veicolazione del linaiolo. In *Proceedings Adritelf conference,* Catania, Italy, Oct 4–7, 2006; p 151.
44. Ranucci, E.; Ferruti, P.; Manfredi, A.; Cavalli, R. Cross-linked Resins by Stepwise Polyaddition of β-Cyclodextrin with Bisacrylamides and Assessment of Their Potential as pH-Sensitive NPs for Site-Specific Protein Delivery. In *In Proceedings CRS 2012,* Quebec City, Canada, July 15–17, 2012; p 99.
45. Amidon, G. L.; Lennernäs, H.; Shah, V. P.; Crison, J. R. *Pharm. Res.* **1995,** *12,* 413–420. doi:10.1023/A:1016212804288
46. Torne, S. J.; Ansari, K. A.; Vavia, P. R.; Trotta, F.; Cavalli, R. *Drug Delivery* **2010,** *17,* 419–425. doi:10.3109/10717541003777233
47. Rao, M.; Bajaj, A.; Khole, I.; Mumjapara, G.; Trotta, F. *J. Inclusion Phenom. Macrocyclic Chem.*, in press. doi:10.1007/s10847-012-0224-7
48. Ansari, K. A.; Vavia, P. R.; Trotta, F.; Cavalli, R. *AAPS PharmSciTech* **2011,** *12,* 279–286. doi:10.1208/s12249-011-9584-3
49. Sapino, S.; Carlotti, M. E.; Cavalli, R.; Ugazio, E.; Berlier, G.; Gastaldi, L.; Morel, S. *J. Inclusion Phenom. Macrocyclic Chem.*, in press. doi:10.1007/s10847-012-0147-3
50. Cavalli, R.; Ansari, K. A.; Bisazza, A.; Giustetto, P.; Trotta, F.; Vavia, P. *Int. J. Pharm.* **2010,** *402,* 254–257. doi:10.1016/j.ijpharm.2010.09.025
51. Trotta, F.; Cavalli, R. *Compos. Interfaces* **2009,** *16,* 39–48. doi:10.1163/156855408X379388

License and Terms

Beilstein Journal of Organic Chemistry

New enzymatically polymerized copolymers from 4-*tert*-butylphenol and 4-ferrocenylphenol and their modification and inclusion complexes with β-cyclodextrin

Adam Mondrzyk, Beate Mondrzik, Sabrina Gingter and Helmut Ritter*

Full Research Paper

Open Access

Address:
Heinrich-Heine-Universität Düsseldorf, Institut für Organische Chemie und Makromolekulare Chemie, Universitätsstrasse 1, 40225 Düsseldorf, Germany, Fax: (+49) 211-811-5840

Email:
Helmut Ritter* - h.ritter@uni-duesseldorf.de

* Corresponding author

Keywords:
copolymer; ß-cyclodextrin; enzymatic polymerization; 4-ferrocenylphenol; polyphenol; 4-*tert*-butylphenol; horseradish peroxidase; HRP oxidative coupling; inclusion complexes; polymer-analogous modification

Beilstein J. Org. Chem. **2012,** *8,* 2118–2123.
doi:10.3762/bjoc.8.238

Received: 17 September 2012
Accepted: 16 November 2012
Published: 04 December 2012

This article is part of the Thematic Series "Superstructures with cyclodextrins: Chemistry and applications".

Associate Editor: N. Sewald

Abstract

The enzymatically catalyzed synthesis of a copolymer of 4-*tert*-butylphenol and 4-ferrocenylphenol by horse radish peroxidase (HRP) in the presence of H_2O_2 in a 1,4-dioxane/water system is described. Furthermore, polymer-analogous alkylation of the free hydroxy groups and subsequent click reaction with mono-6-azido-6-desoxy-β-cyclodextrin (N_3-β-CD) was carried out. The formation of inter- and intramolecular inclusion complexes was investigated by DLS measurement.

Introduction

Polyphenols in general play an important role in nature, e.g., lignin and suberin. In industry, Bakelite represents the first practically successful polyphenol resin [1]. In the latter case, the phenol moieties are covalently connected by formaldehyde condensation. Alternative methods include electrochemical polymerization, metal catalysis or treatment with enzymes, which lead to phenyl–phenyl connected polyphenols [2-5]. In particular, oxidoreductase enzymes have the great advantage of nontoxicity and regioselective phenol–phenol coupling [6-8]. Several oxido-reductases and their catalytic mechanisms are well-studied; the most common are soybean peroxidase, bilirubin peroxidase, laccase and horse radish peroxidase (HRP) [8-12].

Taking the latter case, horse radish peroxidase catalyzes the oxidative polycondensation of electron-rich phenols in water/

organic-solvent systems in the presence of hydrogen peroxide. In recent studies it was demonstrated that several *para*-substituted phenols, i.e., 4-*tert*-butylphenol, can be polymerized with HRP in high yield and relatively high molecular weights [13]. Also several polyphenols with further functional groups, such as nitrones, double bonds and imides, have been synthetized and investigated in our group [14-18]. There are also several natural phenols such as flavonoides, or isoflavonoides, which were also polymerized successfully [19].

4-Ferrocenylphenol (**2**) has been the subject of several studies, especially with regard to its electrochemical properties. After electrochemical oxidation of the Fe(II) ion to Fe(III) a one-electron transfer from the phenol moiety takes place, in which a proton is transferred simultaneously [20]. Furthermore, 4-ferrocenylphenol shows an antianemic activity in mongrel rabbits [21].

Metal-containing polymers have drawn a lot of interest in the past decade because of their combined chemical, electrochemical, magnetic and optic properties. Potential applications include polymeric materials for light-emitting electrodes, solar cells or field-effect transistors [22].

Attempts to polymerize **2** in the presence of enzymes have been carried out by several research groups but lead to undesired, electrochemically inactive products [23]. Nevertheless, the copolymerization of **2** and 4-*tert*-butylphenol (**3**) to obtain electrochemically active products has not been investigated until now. Hence, in the present paper we report the HRP-catalyzed synthesis of novel copolymers from **2** and **3**. Click reaction of the propargyl modified polyphenol **5** with mono-(6-azido-6-deoxy)-β-cyclodextrin (**6**) was also investigated. Based on former studies, host–guest structures were created [24-30].

Results and Discussion

4-Ferrocenylphenol (**2**) was prepared according to the literature [31], in high purity (Scheme 1). It was then enzymatically copolymerized with 4-*tert*-butylphenol (**3**) in the presence of HRP and H_2O_2. The resulting copolymer **4** with a weight-average molecular weight of $\overline{M}_W$ = 6000 g/mol and a dispersity of D = 2.1 (SEC) was received. The ^{1}H NMR of the copolymer gave a broad signal in the range of 4.54–3.86 ppm (ferrocenyl group) and a broad signal between 1.79–0.06 ppm originating from the protons of the *tert*-butyl group.

As suggested in former studies, the enzyme-catalytic polymerization of phenols in general with HRP as catalyst leads to the formation of a copolymer containing phenylene and oxyphenylene moieties [32,33]. Accordingly, in the range of 1024–1174 cm^{-1} IR signals of the C–O stretching vibration of ether functionalities can be observed in the IR spectrum of

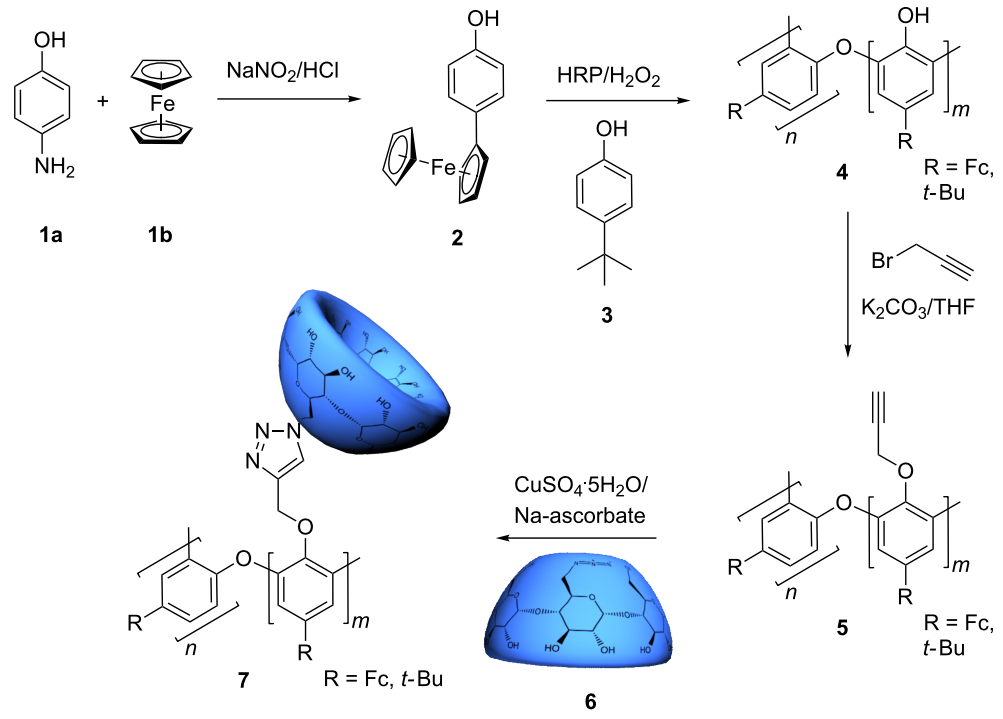

Scheme 1: Synthetic pathway to the desired polymer **7**.

copolymer **4**. Therefore, **4** is a copolymer comprising the *ortho–ortho*- and oxy-*ortho*-connected phenyl moieties.

The modified copolymer **5** was synthetized from copolymer **4** by alkylation with propargyl bromide under alkaline conditions. Then, the alkyne-functionalized copolymer **5** was combined successfully with mono-6-azido-6-deoxy-β-cyclodextrin (**6**) in a click-type reaction to give copolymer **7** (Scheme 1). ROESY measurements show some weak interaction of the protons of β-CD with the protons of the ferrocene (Fc) moiety and the *tert*-butyl-moiety (Supporting Information File 1).

Furthermore, the behavior of polymer **7** clicked with β-CD was studied electrochemically (Figure 1, Table 1). The cyclic voltammetry (CV) data of copolymer **7** shows an anodic peak potential at 0.97 V, which shifts to 1.09 V with each oxidation/reduction cycle due to formation of a polymer layer on the electrode (Figure 1A). The anodic peak potential at 0.44 V and both cathodic peak potentials are poorly resolved. After complexation of potassium adamantylcarboxylate (Ad-COOK) in the β-CD moieties, the CV measurements of this system show well resolved signals at 0.74 V as the anodic and 0.58 V as the cathodic peak potential. Other signals are poorly resolved (Figure 1B). In comparison, the CV measurements of **2** show anodic peak potentials of 0.66 and 0.90 V and cathodic peak potentials of 0.58 and 0.77 V. According to the literature, Fc-oxidation/reduction takes place at lower voltages than phenol oxidation/reduction [20]. The shift of peak potentials of polymerized 4-ferrocenylphenol in comparison to monomeric 4-ferrocenylphenol is +0.08 V for Fc oxidation/reduction and +0.19 V for phenol oxidation/reduction.

In conclusion, phenol-moieties are oxidized preferably in copolymer **7**, because the ferrocenyl moieties are sterically shielded by β-CD. Accordingly, adamantylcarboxylate as a competing guest for β-CD-moieties disassembles the ferrocenyl complexes. The Fc-moieties are now readily available for oxidation/reduction on top of the electrode. This result implies successful complexation and decomplexation.

Table 1: Summary of peak potentials acquired by cyclic voltammetry (ferrocenyl oxidation or reduction/phenol oxidation or reduction).

	Anodic peak potential [V]	Cathodic peak potential [V]
2	0.66/0.90	0.58/0.77
7	0.44[a]/1.09	0.23[a]/0.87[a]
7 + Ad-COOK	0.74/1.00[a]	0.58/0.83[a]

[a]poorly resolved signals.

In addition, hydrodynamic diameters also indicate strongly that supramolecular structures were formed (Figure 2). The hydrodynamic diameter of copolymer **5** (7 nm) in DMF is much smaller than the value of the cyclodextrin-modified copolymer **7** (70 nm). After breaking of supramolecular structures by addition of potassium adamantylcarboxylate as a competing guest for β-CD, the observed hydrodynamic diameter reduces to 5 nm. After measurement of compound **2** with native β-CD it is clear that self-agglomeration of the described system is a property of the modified copolymer **7**.

Experimental

Materials and Methods

All reagents used were commercially available (Sigma-Aldrich, Acros Organics) and were used without further purification unless stated otherwise. β-Cyclodextrin was obtained from Wacker Chemie GmbH, Burghausen, Germany, and used after drying overnight with the aid of a vacuum pump, over P_4O_{10}. Dimethylsulfoxide-d_6 (99.9 atom % D) and $CDCl_3$ were

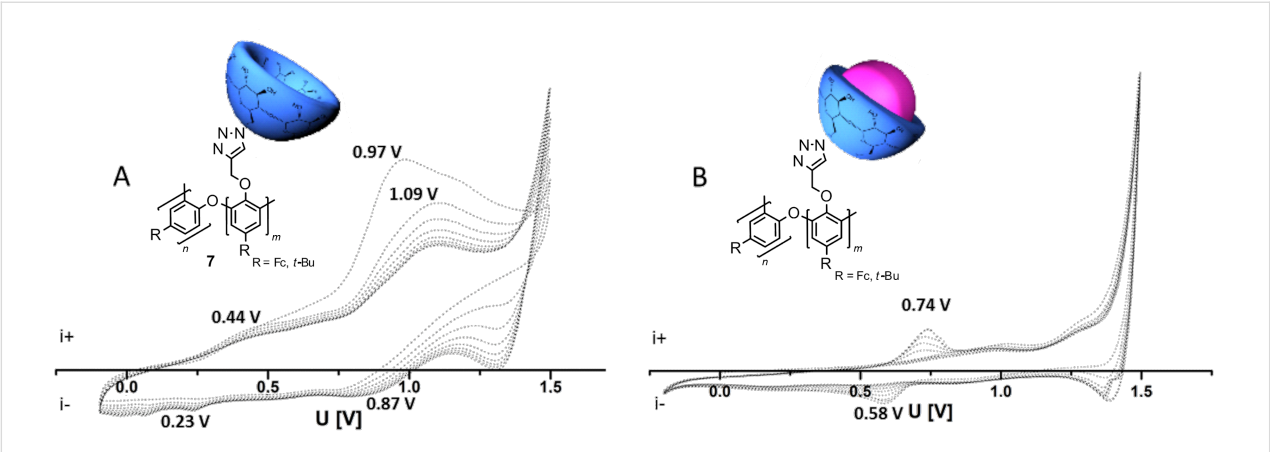

Figure 1: Cyclic voltammetry results of (A) clicked copolymer **7**, (B) clicked copolymer **7** with Ad-COOK (●).

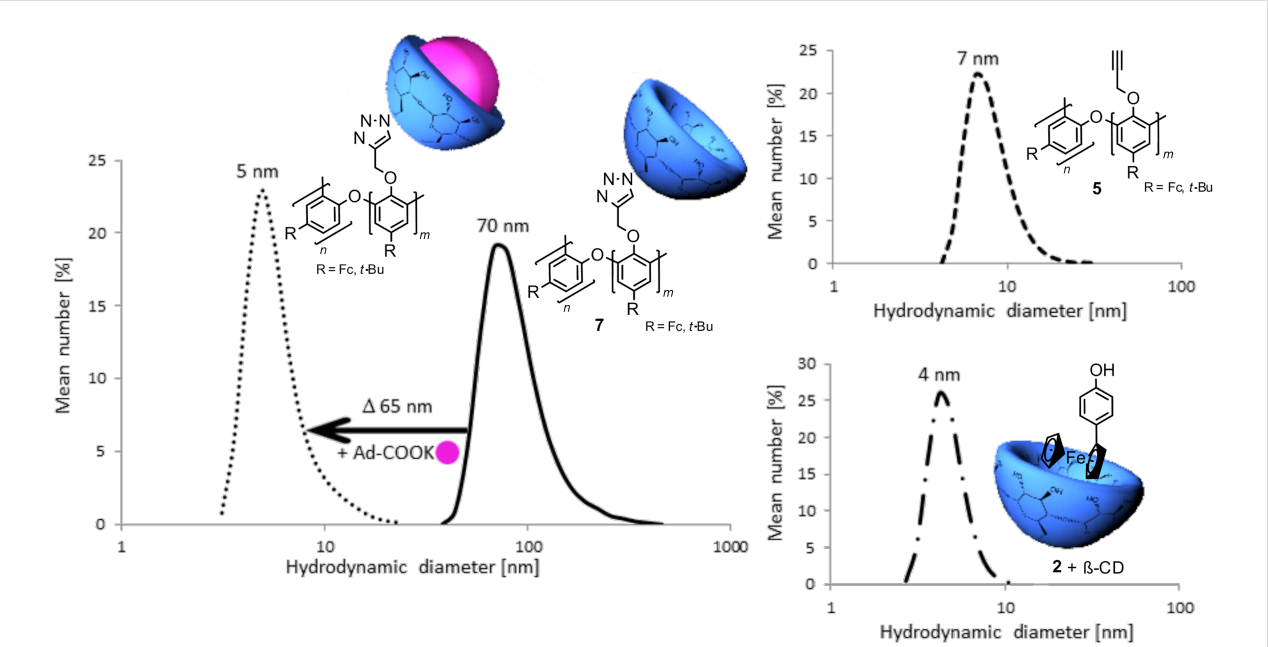

Figure 2: DLS measurement of compound **2** with β-cyclodextrin (— •), alkylated polyphenol **4** (- -), product **7** (—) and its complex with adamantylcarboxylate (•••).

obtained from Deutero GmbH, Germany. 4-Ferrocenylphenol was prepared according to synthetic routes reported in the literature [31]. The inclusion complexes of potassium adamantylcarboxylate were formed by stirring a solution of the β-CD-containing polymer in DMSO with excess potassium adamantylcarboxylate overnight. The residue was then filtered off and the remaining filtrate was used for measurement.

NMR experiments (^{1}H, ROESY) were performed on a Bruker Avance DRX 200 spectrometer operating at 200.13 or 500 MHz for protons with DMSO-d_6 or $CDCl_3$ 99.9% as solvents. The chemical shifts (δ) are given in parts per million (ppm) using the solvent peak as an internal standard.

FTIR spectra were recorded on a Nicolet 6700 FTIR spectrometer equipped with an ATR unit.

SEC measurements were performed at room temperature with THF (HPLC grade, unstabilized - Biosolv Kat.Nr. 202220602) as eluent and with a flow rate of 1 mL/min. The SEC system consists of a Gastorr BG 12 degasser (Schambeck), an Intelligent Pump AL-12 (FLOW), a S5200 sampler (Schambeck SFD) and a combination of columns (MZ Analysentechnik GmbH). The columns contain a styrene–divinylbenzene copolymer and are distributed over three main columns of porosity 10000, 1000 and 100 Å, and one column upstream of porosity 100 Å (type: Gel Sd plus). A 486 tunable absorbance detector (Waters) and a SFD RI 2000 differential-refractometer (Schambeck) were used as detectors. Calibration took place with polystyrene standards in a range of 575 to 3,114,000 g/mol. Toluene was used as the internal standard.

Dynamic light scattering (DLS) experiments were carried out with a Malvern Zetasizer Nano ZS ZEN 3600 at a temperature of 20 °C. The particle size distribution was derived from a deconvolution of the measured intensity autocorrelation function of the sample by the general purpose method (non-negative least squares) algorithm included in the DTS software. Each experiment was performed at least five times.

Microwave-assisted synthesis was performed by using a CEM Discover synthesis unit (monomode system). The temperature was measured by infrared detection with a continuous-feedback temperature control and maintained at a constant value by power modulation. Reactions were performed in closed vessels under controlled pressure.

Cyclic voltammetry (CV) measurements were performed with a computer-controlled potentiostat (SIMPOT) with a resolution in the range <100 pA. A gold electrode and an Ag/AgCl electrode were chosen as working electrode and reference electrode, respectively. The electrochemical measurements started at −0.2 V and the potential was reversed at 1.6 V. As electrolyte, a solution of 0.1 M tetra-*n*-butylammoniumhexafluorophosphate (n-$Bu_4N^+PF_6^-$) as conducting salt in DMSO was used (pH 6). Every experiment was carried out eight times.

Poly(4-ferrocenylphenol-co-4-*tert*-butylphenol) **4**

15 mg HRP are dissolved in 20 mL acetate buffer (pH 7); 1.39 g (5 mmol) **2** and 1.76 g (11 mmol) **3** are dissolved in 80 mL of 1,4-dioxane. The solutions are combined in a 250 mL one-neck flask and stirred vigorously. Then 1 mL of 30% hydrogenperoxide solution is added in 20 equiv portions every 15 minutes. The solution is stirred again for 12 h. The polymer precipitates to give 0.83 g (30%) yield. FTIR (diamond) $\tilde{\nu}$: 3279, 2957, 2904, 2863, 1653, 1603, 1507, 1479, 1394, 1363, 1253, 1215, 1174, 1119, 1081, 1042, 975, 872, 828 cm^{-1}; ^1H NMR (500 MHz, $CDCl_3$, 24 °C) δ 8.44–6.11 (m, 4H), 4.54–3.86 (m, 9H), 1.21 (s, 9H); SEC (THF) $\overline{M}_W$ = 6000, D = 2.1.

Poly(4-ferrocenylphenol-co-4-*tert*-butylphenol)-propargyl ether **5**

0.3 g of **2** (0.7 mmol) with 0.12 g (1.0 mmol) propargyl bromide and 0.14 g (1.0 mmol) potassium carbonate are dispersed in 20 mL dry THF in a one-neck flask under an argon atmosphere. The dispersion is stirred under reflux for 24 hours. The product is precipitated in hexane and dried in vacuo to give 0.28 g (80% yield). FTIR (diamond) $\tilde{\nu}$: 2962, 2864, 2361, 2334, 1635, 1593, 1447, 1394, 1362, 1264, 1218, 1172, 1065 cm^{-1}; ^1H NMR (300 MHz, DMSO-d_6, 25 °C) δ 8.06–6.13 (m, 4H), 4.26–4.03 (m, 11H), 3.61 (m, 2H), 1.22 (s, 9H).

Poly(4-ferrocenylphenol-co-4-*tert*-butylphenol-click-cyclodextrin) **7**

In a pressure vial, 0.20 g (0.41 mmol) of **5**, 0.72 g (0.62 mmol) of **6**, 0.008 g (0.03 mmol) of $CuSO_4{\cdot}5H_2O$ and 0.012 g (0.06 mmol) of sodium ascorbate are dissolved in 2 mL of DMF. The reaction mixture is stirred in a microwave oven for 1 h at 90 °C (30–70 W). The product is precipitated in acetone and dried in vacuo. FTIR (diamond) $\tilde{\nu}$: 3282, 2963, 2929, 1635, 1439, 1412, 1386, 1360, 1293, 1260, 1152, 1077, 1021 cm^{-1}; ^1H NMR (300 MHz, DMSO-d_6, 25 °C) δ 8.43 (H-a), 7.47–7.13 (ArH, H-c), 5.95 (OH-2, OH-3), 4.82 (H-1), 4.55 (H-b, OH-6), 4.50–3.90 (Fc, H-d), 3.90–2.98 (H-6a,b, H-3, H-5, H-4, H-2), 1.38–0.92 (br, H-e).

Conclusion

We described the enzymatic copolymerization of 4-ferrocenylphenol with 4-*tert*-butylphenol. The 4-ferrocenylphenol obviously tolerates the oxidative environment of H_2O_2. Furthermore, *ortho*–*ortho*- and oxy-*ortho*-connected phenol monomers were found. However, the free hydroxy groups were subjected to alkylation with propargyl bromide and subsequent click chemistry with N_3-β-CD. The covalently bound cyclodextrin moiety and the covalently bound Fc or *tert*-butyl group form host/guest complexes as proven by DLS measurement. The cyclic voltammetry data shows that the central iron atom of the Fc moiety is present in the copolymer and can be oxidized and reduced, if a suitable competing guest for β-CD is present to disassemble Fc complexes.

Supporting Information

The Supporting Information features a copy of the ROESY NMR spectrum of ferrocene- and β-cyclodextrin-containing copolymer **7**.

Supporting Information File 1

ROESY of copolymer **7**.
[http://www.beilstein-journals.org/bjoc/content/supplementary/1860-5397-8-238-S1.pdf]

References

1. Baekeland, L. H. *J. Ind. Eng. Chem.* **1909,** *1,* 149–161. doi:10.1021/ie50003a004
2. Belhadj Tahar, N.; Savall, A. *Electrochim. Acta* **2009,** *54,* 4809–4816. doi:10.1016/j.electacta.2009.03.086
3. Hay, A. S.; Blanchard, H. S.; Endres, G. F.; Eustance, J. W. *J. Am. Chem. Soc.* **1959,** *81,* 6335–6336. doi:10.1021/ja01532a062
4. Shan, J.; Han, L.; Bai, F.; Cao, S. *Polym. Adv. Technol.* **2003,** *14,* 330–336. doi:10.1002/pat.316
5. Wang, J.; Jiang, M.; Lu, F. *J. Electroanal. Chem.* **1998,** *444,* 127–132. doi:10.1016/S0022-0728(97)00583-4
6. Mita, N.; Tawaki, S.-i.; Uyama, H.; Kobayashi, S. *Chem. Lett.* **2002,** *31,* 402–403. doi:10.1246/cl.2002.402
7. Reihmann, M. H.; Ritter, H. *J. Macromol. Sci., Part A: Pure Appl. Chem.* **2002,** *39,* 1369–1382.
8. Wang, L.; Kobatake, E.; Ikariyama, Y.; Aizawa, M. *J. Polym. Sci., Part A: Polym. Chem.* **1993,** *31,* 2855–2861. doi:10.1002/pola.1993.080311123
9. Kobayashi, S. *J. Polym. Sci., Part A: Polym. Chem.* **1999,** *37,* 3041–3056. doi:10.1002/(SICI)1099-0518(19990815)37:16<3041::AID-POLA1>3.3.CO;2-M
10. Kobayashi, S.; Higashimura, H. *Prog. Polym. Sci.* **2003,** *28,* 1015–1048. doi:10.1016/S0079-6700(03)00014-5
11. Akkara, J. A.; Senecal, K. J.; Kaplan, D. L. *J. Polym. Sci., Part A: Polym. Chem.* **1991,** *29,* 1561–1574. doi:10.1002/pola.1991.080291105
12. Ayyagari, M.; Akkara, J. A.; Kaplan, D. L. *Acta Polym.* **1996,** *47,* 193–203. doi:10.1002/actp.1996.010470501
13. Mita, N.; Maruichi, N.; Tonami, H.; Nagahata, R.; Tawaki, S.-i.; Uyama, H.; Kobayashi, S. *Bull. Chem. Soc. Jpn.* **2003,** *76,* 375–379. doi:10.1246/bcsj.76.375
14. Reihmann, M. H.; Ritter, H. *Macromol. Biosci.* **2001,** *1,* 85–90. doi:10.1002/1616-5195(20010301)1:3<85::AID-MABI85>3.0.CO;2-N
15. Mejias, L.; Schollmeyer, D.; Sepulveda-Boza, S.; Ritter, H. *Macromol. Biosci.* **2003,** *3,* 395–399. doi:10.1002/mabi.200350008
16. Pang, Y.; Ritter, H.; Tabatabai, M. *Macromolecules* **2003,** *36,* 7090–7093. doi:10.1021/ma021678x
17. Reihmann, M. H.; Ritter, H. *Macromol. Chem. Phys.* **2000,** *201,* 798–804. doi:10.1002/(SICI)1521-3935(20000401)201:7<798::AID-MACP798>3.0.CO;2-X

18. Reihmann, M. H.; Ritter, H. *Macromol. Chem. Phys.* **2000,** *201,* 1593–1597. doi:10.1002/1521-3935(20000901)201:14<1593::AID-MACP1593>3.0.CO;2-D
19. Mejias, L.; Reihmann, M. H.; Sepulveda-Boza, S.; Ritter, H. *Macromol. Biosci.* **2002,** *2,* 24–32. doi:10.1002/1616-5195(20020101)2:1<24::AID-MABI24>3.3.CO;2-Y
20. Razumiene, J.; Meškys, R.; Gureviciene, V.; Laurinavicius, V.; Reshetova, M. D.; Ryabov, A. D. *Electrochem. Commun.* **2000,** *2,* 307–311. doi:10.1016/S1388-2481(00)00024-2
21. Askarov, I. R.; Kirgizov, S. M.; Nurimdinova, G. T. *Pharm. Chem. J.* **1988,** *22,* 372–376. doi:10.1007/BF00769649
22. Ho, C.-L.; Wong, W.-Y. *Coord. Chem. Rev.* **2011,** *255,* 2469–2502. doi:10.1016/j.ccr.2011.01.052
23. Ryabov, A. D.; Kurova, V. S.; Goral, V. N.; Reshetova, M. D.; Razumiene, J.; Simkus, R.; Laurinavičius, V. *Chem. Mater.* **1999,** *11,* 600–604. doi:10.1021/cm980729v
24. Del Valle, E. M. M. *Process Biochem.* **2004,** *39,* 1033–1046. doi:10.1016/S0032-9592(03)00258-9
25. Szejtli, J. *J. Mater. Chem.* **1997,** *7,* 575–587. doi:10.1039/a605235e
26. Godinez, L. A.; Patel, S.; Criss, C. M.; Kaifer, A. E. *J. Phys. Chem.* **1995,** *99,* 17449–17455. doi:10.1021/j100048a022
27. Harada, A.; Takahashi, S. *J. Inclusion Phenom. Macrocyclic Chem.* **1984,** *2,* 791–798. doi:10.1007/BF00662247
28. Luong, J. H. T.; Brown, R. S.; Schmidt, P. M. *J. Mol. Recognit.* **1995,** *8,* 132–138. doi:10.1002/jmr.300080123
29. Menger, F. M.; Sherrod, M. J. *J. Am. Chem. Soc.* **1988,** *110,* 8606–8611. doi:10.1021/ja00234a005
30. Yang, Z.; Breslow, R. *Tetrahedron Lett.* **1997,** *38,* 6171–6172. doi:10.1016/S0040-4039(97)01427-5
31. Nyamori, V. O.; Bala, M. D. *Acta Crystallogr., Sect. E: Struct. Rep. Online* **2008,** *64,* m1630. doi:10.1107/S1600536808039524
32. Kurioka, H.; Komatsu, I.; Uyama, H.; Kobayashi, S. *Macromol. Rapid Commun.* **1994,** *15,* 507–510. doi:10.1002/marc.1994.030150609
33. Uyama, H.; Kurioka, H.; Sugihara, J.; Kobayashi, S. *Bull. Chem. Soc. Jpn.* **1996,** *69,* 189–193. doi:10.1246/bcsj.69.189

License and Terms

Beilstein Journal of Organic Chemistry

Influence of cyclodextrin on the solubility and the polymerization of (meth)acrylated Triton® X-100

Melanie Kemnitz and Helmut Ritter*

Full Research Paper

Open Access

Address:
Institute of Organic Chemistry and Macromolecular Chemistry II, Heinrich-Heine-University, Universitätsstraße 1, 40255 Düsseldorf (Germany)

Email:
Helmut Ritter* - h.ritter@uni-duesseldorf.de

* Corresponding author

Keywords:
(meth)acrylated Triton®; randomly methylated β-cyclodextrin (RAMEB-CD); rheology; Triton® X-100 (poly(ethylene glycol)*tert*-octylphenyl ether)

Beilstein J. Org. Chem. **2012,** *8,* 2176–2183.
doi:10.3762/bjoc.8.245

Received: 28 August 2012
Accepted: 18 November 2012
Published: 13 December 2012

This article is part of the Thematic Series "Superstructures with cyclodextrins: Chemistry and applications".

Associate Editor: P. R. Schreiner

Abstract

Triton® X-100 (poly(ethylene glycol) *tert*-octylphenyl ether) was (meth)acrylated and polymerized in the absence and presence of randomly methylated β-cyclodextrin (RAMEB-CD). Triton®-polymers that were polymerized with RAMEB-CD in water were compared with polymers that were synthesized in organic solvents after the addition of RAMEB-CD. The polymers were characterized by ^{1}H NMR and FTIR spectroscopy, matrix-assisted laser desorption ionization mass spectrometry (MALDI-TOF MS), dynamic light scattering (DLS), gel-permeation chromatography (GPC) and turbidity measurements. Additionally, the viscosity change of the methacrylic homopolymer with RAMEB-CD was evaluated.

Introduction

Triton® X-100 (**1**) is a macromolecular, nonionic surfactant with an average number of ethylene oxide units of 9.5. The *tert*-octylphenyl group is a hydrophobic moiety whereas the poly(ethylene glycol) substituent is hydrophilic. Because of this amphiphilic character, Triton® X-100 can be described as a short AB block co-oligomer [1]. Long amphiphiles are relatively flexible and provide a lower critical micelle concentration (CMC) [2]. The CMC of Triton® X-100 is 0.22 mM [3]. Accordingly, below this concentration isolated molecules can be found; above this concentration micelles are formed.

Equilibrium constants of β-CD and Triton® X-100 complexes listed in the literature span a range of 145–171000 M^{-1}. Different methods, e.g., surface tension, isothermal titration calorimetric, and fluorescence studies, were used to determine the equilibrium constant [4-12]. The results also differ in the stoichiometry of the formed complexes [4,7,9-11]. Host/guest ratios of 1:1 [4,7], 2:1 [9] and the coexistence of 1:1 and 2:1 [10,11] complexes of β-CD and Triton® X-100 are reported in literature. In our previous paper, the coexistence of a 1:1 and 2:1 complex with an extraordinary high ($K_1 = 1.71 \times 10^5$ M^{-1})

and a lower equilibrium constant (K_2 = 260 M^{-1}) was described [12]. Due to the fact that the *tert*-octyl group represents the preferred binding site of the molecule it can be assumed that complexation takes place at this position first. In excess of β-CD an additional complexation of the phenyl ring occurs.

The synthesis and polymerization of methacrylic Triton® has already been described in the literature [2]. It was found that the reactivity of the methacrylic double bond was not affected by the length of the poly(ethylene oxide) side chain [13].

In the present work, we depict the homopolymerization and characterization of methacrylic and acrylic Triton® in the absence and presence of RAMEB-CD for the first time. The dissociation of the polymer-CD-complex was monitored by viscosity measurements.

Results and Discussion

Complexation study of Triton® X-100 with RAMEB-CD

The complexation behavior of Triton® X-100 (**1**) with RAMEB-CD was investigated by means of an ITC experiment (Supporting Information File 1, Figure S1). Assuming the sequential-binding model with two binding sites, values of K_1 = 6.08 × 10^4 M^{-1} and K_2 = 445 M^{-1} were obtained, which are extremely high compared to the other CD-complexes which show *K*-values rarely higher than 5 × 10^4 M^{-1} [14].

^{1}H NMR spectroscopy experiments indicate that Triton® is complexed at its hydrophobic *tert*-octyl-moiety as expected. The ^{1}H NMR signals of the aliphatic protons **a** and **c** at 0.66 and 1.24 ppm (Figure 1) shifted strongly after the addition of a small amount of RAMEB-CD. With increasing amount of RAMEB-CD, the signals of the aromatic protons **d** and **e** also shifted from 7.16 and 6.78 ppm to 7.34 and 6.93 ppm. Assumingly, the hydrophobic *tert*-octyl group is complexed first; secondly the aryl group is complexed by RAMEB-CD [12].

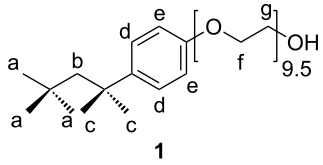

Figure 1: Chemical structure of Triton® X-100 (**1**).

To evaluate the size of Triton® X-100 (**1**) and its supramolecular complexes with CD in water, DLS measurements were carried out. The number-average hydrodynamic diameter (d_h) increased from 0.7 nm at concentrations lower than 0.22 mM up to 106 nm indicating the formation of micelles above the CMC. The formation of micelles was inhibited by the addition of RAMEB-CD to the Triton® solution, because the hydrophobic component of **1** slips into the cavity of RAMEB-CD. The addition of 1 equiv of RAMEB-CD to **1** exhibited a hydrodynamic diameter of 1.4 nm and the diameter of the 1:2 complex was determined to 2.1 nm. The different hydrodynamic diameters of the complexes indicate that different complexes are formed.

Triton® X-100 (**1**) as a macromolecular surfactant becomes insoluble above 66 °C due to a typical LCST effect. By addition of 1 equiv of RAMEB-CD (**1a**) the cloud point is shifted from 66 to 71 °C. This can be attributed to the increasing hydrophilicity. Figure 2 shows the changes of the transmittance

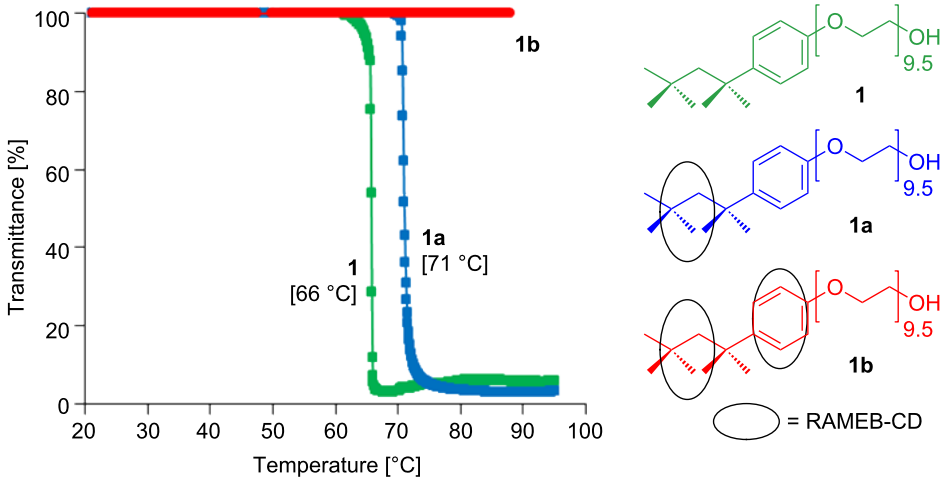

Figure 2: Solubility in water of 0.2 wt % Triton® X-100 (**1**) and its different assumed complexes with RAMEB-CD (**1a** and **1b**) according to the transparence measurement.

as a function of the temperature. After the addition of a second equiv of RAMEB-CD (**1b**) no LCST behavior could be observed over the whole temperature range from 5 to 95 °C. This was due to the much more hydrophilic character of the complex, which is a result of coverage of the hydrophobic part of **1**.

Complexation of the (meth)acrylic monomer derived from Triton® (**2** and **3**) with RAMEB-CD

The reaction of Triton® X-100 (**1**) with methacryloyl chloride and acryloyl chloride gave the corresponding methacrylic ester **2** [2] and acrylic ester **3**, respectively. Both monomers **2** and **3** were insoluble in water, but readily formed water-soluble host–guest complexes with RAMEB-CD (**4** to **7**) within a few minutes (Scheme 1).

In the solid state, the complex formation could be proved by FTIR, as the ether-band shifted from 1102 to 1033 cm^{-1}. By using 2D-ROESY NMR, the interactions between the inner protons H-3 and H-5 of 2,6-dimethyl-β-cyclodextrin (DIMEB-CD) and the protons of the tert-octyl and aryl group of **3** were analyzed (Supporting Information File 1, Figure S2). DIMEB-CD was used with the intention to gain information on the orientation of the RAMEB-CD molecules on Triton®. However, after the complexation, the signals of the inner protons were superimposed and no conclusions about the orientation of the CD ring could be drawn. An interaction between CD and the (meth)acrylic group could not be detected.

In the course of DLS experiments with dimethylformamide (DMF) as solvent a hydrodynamic diameter of 1.4 nm for pure RAMEB-CD and 1.2 nm for **3** was found. For each complexed RAMEB-CD the diameter increased by about 0.6 nm. Therefore, it can be concluded that RAMEB-CD forms stable complexes with the modified (**2** and **3**) and unmodified Triton® X-100 (**1**) even in DMF as solvent (Table 1).

Furthermore, the water-insoluble monomers **2** and **3** can be transferred into the aqueous phase by addition of RAMEB-CD. Above 27 °C the 2:1 complex of RAMEB-CD with the methacrylic monomer **2** precipitates as a result of slipping off the RAMEB-CD. If the solution is cooled down the complex is reformed and the dispersion became completely transparent again. With increasing concentration of RAMEB-CD and decreasing hydrophobicity of the modified monomers **2** and **3** the LCST increases significantly (Table 1).

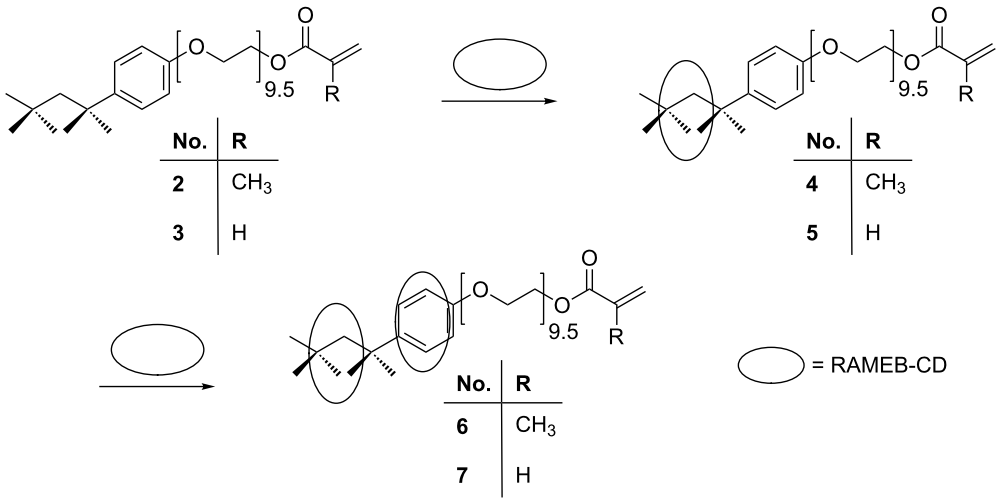

Scheme 1: Idealized reaction of the complexation of the (meth)acrylic monomer derived from Triton® (**2** and **3**) with one and 2 equiv of RAMEB-CD.

Table 1: Comparison of the hydrodynamic diameters and the LCSTs of **1**, **2** and **3** and their complexes with 1 and 2 equiv of RAMEB-CD.

compound	hydrodynamic diameter (nm) in DMF			LCST (°C) in water		
	without RAMEB-CD	with RAMEB-CD		without RAMEB-CD	with RAMEB-CD	
		1 equiv	2 equiv		1 equiv	2 equiv
1	106	1.4	2.1	66	71	not measurable
2	1.3	1.8	2.5	insoluble	10	27
3	1.2	1.8	2.5	insoluble	18	63

Homopolymerization of the uncomplexed (meth)acrylic monomers **2** and **3** in DMF

The macromonomers **2** and **3** respectively were homopolymerized in DMF with 2,2′-azobis(2-methylpropionitrile) (AIBN) as initiator (Scheme 2). The glass-transition temperature (T_g) of the methacrylic polymer **8** was found to be −40 °C, which is similar to the value that can be found in the literature [2]. Due to higher flexibility of the new acrylic polymer **9**, a lower T_g of −50 °C was detected.

According to DLS measurements, the addition of 1 equiv of RAMEB-CD to the dissolved polymer does not significantly influence the hydrodynamic diameter of 10.4 nm (**8**) and 11.7 nm (**9**) (+1 nm) in DMF. In contrast, the complexation with 2 equiv of RAMEB-CD induces a remarkable shift in d_h from 10.4 up to 18.4 nm (Table 2). This observation indicates that a total complexation of the hydrophobic component is required to prevent the intermolecular aggregation of the coil, which results in a higher rigidity of the polymer chain.

The addition of 2 equiv of RAMEB-CD to **8** leads to a water soluble polymer with a cloud point of 11 °C. For the single and double RAMEB-CD-complexed acrylic polymer **9** no cloud points could be observed over the whole temperature range, probably because the complexes are too stable in water.

Homopolymerization of RAMEB-CD complexed (meth)acrylic monomer derived from Triton® (**4** to **7**) in water

A solution polymerization in water was possible after the complexation of (meth)acrylated Triton® X-100 (**2** and **3**) with RAMEB-CD (Scheme 3). The polymers **10** and **12** complexed with 1 equiv of RAMEB-CD precipitated during the polymerization, whereas the double complexed polymers **11** and **13** did not precipitate, as a consequence of the stronger host–guest interactions.

The successful polymerization of **10**–**13** was demonstrated, e.g., by ^{1}H NMR spectroscopy. The signals of the olefinic protons between 5.5 and 6.2 ppm vanished; whereas the signals of the polymer backbone at 0.67 ppm were clearly visible. As expected, the signals of the protons of the *tert*-octyl group were broader after the polymerization. The 2D-ROESY spectrum indicates that the complex was still intact after the polymerization (Supporting Information File 1, Figure S3).

DSC measurements of the dried samples indicate a high influence of RAMEB-CD. The T_g value was found to be about 52 °C for the single complexed acrylic polymer **12** and about 85 °C for the double complexed acrylic polymer **13**. Compared to this a T_g value of −50 °C was found for the model polymer **9**. Obviously, RAMEB-CD reduces the mobility of the system, as suggested above. A similar behavior was observed for the single complexed methacrylic polymer **10**. The hydrodynamic diameters of the complexed, modified monomers are between 1.4 and 2.5 nm. For the polymers **10**–**13**, which were first complexed with RAMEB-CD and then polymerized in water, and the polymers **8** and **9**, which were homopolymerized in DMF and then complexed with RAMEB-CD, similar hydrodynamic diameters were observed (Supporting Information File 1, Table S1). To determine the molecular weight of the polymers RAMEB-CD had to be removed first. This was achieved by a dialysis at 45 °C (Table 3). The molecular weights of the polymers **11** and **13** derived from the double-complexed monomers **6** and **7** are

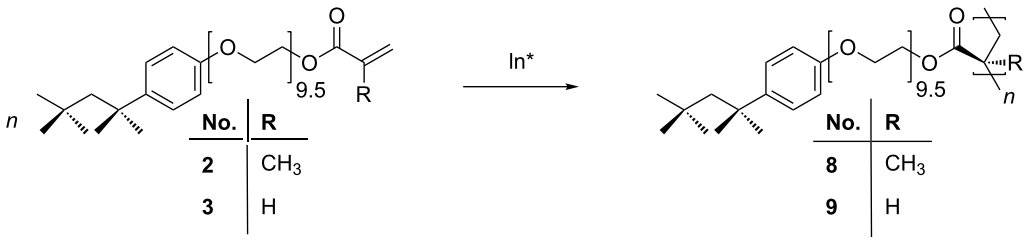

Scheme 2: Homopolymerization of the uncomplexed monomers **2** and **3** to the polymers **8** and **9** in DMF with AIBN as initiator.

Table 2: The hydrodynamic diameters and molecular weights of the polymers **8** and **9** and their complexes with RAMEB-CD in DMF.

compound	hydrodynamic diameter (nm) in DMF			GPC (DMF)	
	without RAMEB-CD	with RAMEB-CD			
		1 equiv	2 equiv	$\overline{M_n}$	*D*
8	10.4	11.4	18.4	80900	4.9
9	11.7	12.5	16.3	46800	6.5

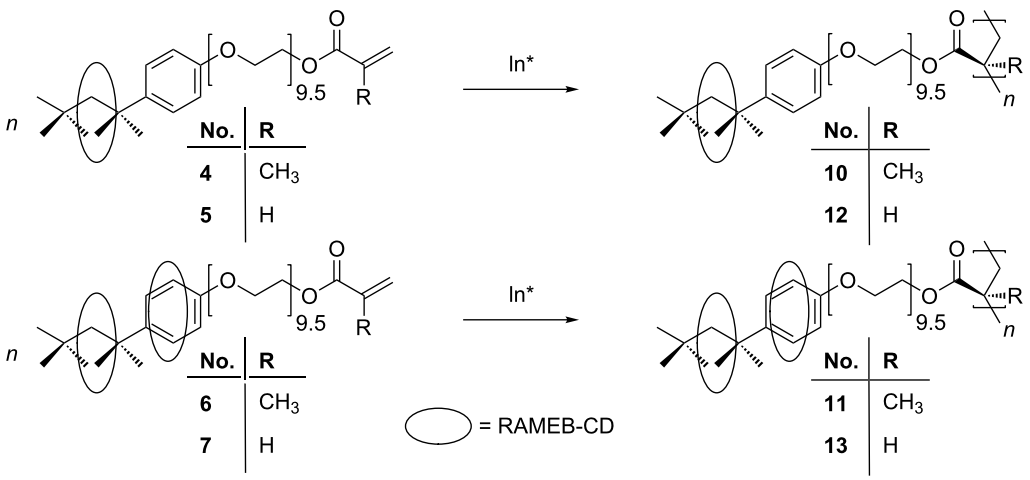

Scheme 3: Polymerization of the RAMEB-CD complexed monomers **4**, **5**, **6** and **7** to the homopolymers **10**, **11**, **12** and **13** in water with VA-044 as initiator.

higher than the molecular weights of the polymers **10** and **12,** which were prepared from the single-complexed monomers **4** and **5**. This may be a result of the increasing solubility of the monomers **2** and **3** if CD is added in molar excess.

Table 3: Molecular weights of the polymers **10**–**13** after dialysis at 45 °C.

compound	$\overline{M}_n$	*D*
10	119200	7.3
11	175300	3.4
12	54700	3.3
13	68400	3.2

Temperature-dependent behavior of the RAMEB-CD-double-complexed methacrylic homopolymer (**8**)

The rheological experiments were performed in a temperature range of 25 to 85 °C for constant shear rates. Below 30 °C the viscosity of an aqueous polymer solution decreases with increasing temperature (Figure 3, I). Surprisingly, above 30 °C the viscosity increases (Figure 3, II). Probably this result is caused by a gradual decomplexation of the polymer. Some RAMEB-CD molecules slip off from the polymer side chain and aggregates are formed. The agglomeration causes an increase in the viscosity, with its maximum at about 60 °C. Above this temperature, the polymer precipitates (Figure 3, III). Similar curves were determined for different shear rates and the solution showed shear-thinning behavior. The results found by rheometer were confirmed by DLS and turbidity measurements. The cloud point was around 56 °C. Figure 3 shows the transmittance and the zero-shear-viscosity as a function of the temperature in a range of 25 and 85 °C for a 50 wt % aqueous solution of **8**. Approaching the LCST, the hydrodynamic diameters increase (16 nm at 25 °C, 29 nm at 30 °C, 62 nm at 35 °C, 77 nm at 40 °C and 95 nm at 45 °C). The results of hydrodynamic diameters and the transmittance support the described explanation for the viscosity curve on the rheometer.

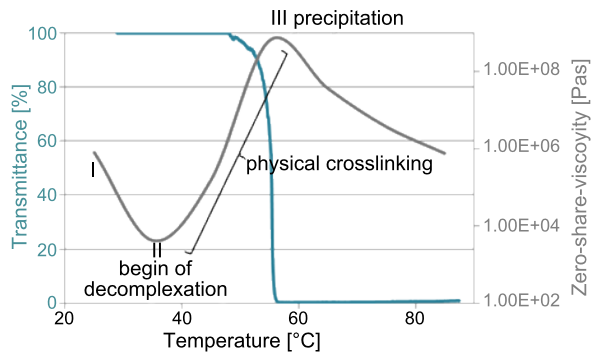

Figure 3: Transmittance [%] and zero-shear-viscosity [Pas] as a function of temperature for a 50 wt % solution of polymer **8**. (**I** → **II**: Viscosity decreases with higher temperature; **II** → **III**: Gradual decomplexation of the polymer, RAMEB-CD molecules slip off from the polymer side chain, aggregates are formed; **III**: Precipitation of the polymer).

Conclusion

It was possible to polymerize (meth)acrylated Triton® as a stable complex with RAMEB-CD in water (**10** to **13**). Even after the polymerization, the complex with RAMEB-CD still existed. Water is an environmentally friendly and favorable solvent. The molecular weights, LCSTs and hydrodynamic diameters of the resulting polymers prepared in water are similar to those of the uncomplexed model polymers, which

were synthesized in DMF (**8** and **9**). As an important result, it was possible to follow the decomplexation of double-complexed polymer **8** above 30 °C by DLS, turbidity measurements and also by viscosity changes.

Experimental

Materials

Triton® X-100 was purchased from Acros Organics and was used as received. RAMEB-CD was bought from the Wacker Chemie AG, and DIMEB-CD was bought from Acros Organics. They were dried in a microwave drying system SAM 255 (CEM). Methacryloyl chloride (Fluka), acryloyl chloride (Fluka), triethylamine (Acros Organics), AIBN (Sigma-Aldrich), VA-044 (Wako Chemicals) and DMF (VWR) were used as received.

Measurements

Isothermal titration calorimetry experiments were performed on a VP-ITC MicroCalorimeter from MicroCal, Northampton MA, and were controlled by MicroCal VP viewer 2000 ITC software. Experiments were conducted at 25 °C. A 2.5 mM solution of RAMEB-CD was titrated against a 0.2 mM solution of Triton® X-100. Titration was carried out by 30 injections of 5 × 1 μL, 5 × 2 μL, 5 × 5 μL, 15 × 15 μL with a spacing time of 180 s. The stirring speed was set to 300 min^{-1}. In a separate experiment the heat of dilution was measured and was subtracted from the binding isotherm. The results were calculated with Origin 7.0 and the MicroCal LLC ITC software.

2D-ROESY and ^{1}H NMR measurements were performed on a Bruker AVIII-300 spectrometer at 300.13 MHz. The δ scale relative to tetramethylsilan was calibrated to the solvent value δ 7.26 ppm for $CDCl_3$ and δ 4.79 ppm for D_2O.

Infrared (IR) spectra were determined on a Nicolet 6700 FTIR spectrometer equipped with an ATR unit at rt. The measurements were performed in the range of 4000–300 cm^{-1}.

DLS data were recorded in backscattering mode on a Malvern Zetasizer Nano ZS ZEN 3600 at a temperature of 20 °C with a laser wavelength of 633 nm and a detection angle of 173°. Measured solutions contained 5 mg/mL substance in DMF and were performed in a glass cuvette with a layer thickness of 1 cm. Each experiment was performed at least ten times to obtain statistical information and the number-averaged diameters were used for characterization.

For turbidity measurements a TP1 turbidity photometer within a temperature range of 5 to 95 °C was used. Measured solutions contained 20 mg/mL substance in water. During continuous stirring the transparency of the sample was determined. The values of the LCST were taken as the temperature where the transmission decreases by 50%.

GPC measurements were performed by using a Viscotek GPCmax VE2001 system. The system has a column set with one Viscotek TSK guard column HHR-H 5.0 mm (ID) × 8 cm (L) and two Viscotek TSK GMHHR-M 7.8 mm (ID) × 30 cm (L) columns. The columns were constantly heated at a temperature of 60 °C. DMF (0.1 M LiCl) was used as eluent at a flow rate of 1 mL/min. For detection a Viscotek VE 3500 RI detector was used. The system was calibrated with polystyrene standards within a molecular range from 575 to 3,114,000 g/mol.

On a Mettler Toledo DSC 822 instrument the DSC measurements were determined in a range of −50 to 200 °C at the heating rate of 10 °C/min. The T_g values were estimated as the average of three measurements by using the midpoint method.

Viscosities were measured with a rotational viscometer model Haake MARS II rheometer equipped with plate–plate (PP35Ti) and cone–plate (DC60/2°) configuration. A temperature control system DC30/K10 from Thermo scientific was used to ensure constant temperatures with deviations of 1 °C. Measured solutions contained 50 wt % aqueous solution of the polymer. To determine the viscosity a temperature range of 25 to 85 °C (ΔT = 5 °C) for constant shear rates (10, 20, 100 and 200 s^{-1}) was applied. For the zero-shear viscosity, different shear rates (10^{-5}–0.1 s^{-1}) at constant temperatures from 25 to 85 °C (Δ = 5 °C) were used.

Syntheses

Monomer syntheses

The methacrylic derivate of Triton® X-100 (**2**) was synthesized in a similar way as already described by San Román et al. [2]. To a solution of 9 g (14 mmol) Triton® X-100 (**1**) in methylene chloride with a 20% excess triethylamine (1.7 g, 16.7 mmol), a solution of 20% excess methacryloyl chloride (1.75 g, 16.7 mmol) was added dropwise at 0 °C under stirring. After being stirred for 24 h at rt, the solution was washed with aqueous NaOH (5 wt %) several times. The solvent was removed under reduced pressure. The acrylic derivate of Triton® X-100 (**3**) was synthesized in the same way; instead of methacryloyl chloride, acryloyl chloride (1.5 g, 16.5 mmol) was used.

Methacrylic derivate of Triton® X-100 (**2**)

Yield: 82%; FTIR (diamond, cm^{-1}): ν 2949/2868 (-CH_3, -CH_2-), 1718 (-COOR), 1638 (-C=C-), 1610/1511 (-aryl), 1454, 1365, 1349, 1319, 1296, 1245 (aryl-C-O-C), 1103 (-C-O-C-), 1039, 942 (R_2C=CH_2), 829/732 (1,4-disubstitute aromatic), 683, 659, 589, 522; ^{1}H NMR (300 MHz, $CDCl_3$) δ 7.25 (dd, ^3J

= 8.83 Hz, ^4J = 2.18 Hz, 2H, aryl-CH), 6.82 (dd, ^3J = 8.83 Hz, ^4J = 2.18, 2H, aryl-CH), 6.13 (m, 1H, -CH_3), 5.57 (m, 1H, =CH_2), 4.29 (t, ^3J = 4.86 Hz, 2H, -CH_2-), 4.10 (t, ^3J = 4.86 Hz, 2H, -CH_2-), 3.64 (s, polyethoxy, 37H), 1.94 (t, ^4J = 1.13 Hz, ^4J = 1.33 Hz, 3H, =CH_2), 1.69 (s, 2H, -CH_2-), 1.33 (s, 6H, -$(CH_3)_2$), 0.70 (s, 9H, -$(CH_3)_3$); MALDI-TOF ($CHCl_3$, *n* = number of ethoxy groups) *m/z*: 561 (*n* = 6), 605 (*n* = 7), 649 (*n* = 8), 693 (*n* = 9), 737 (*n* = 10), 781 (*n* = 11), 825 (*n* = 12), 869 (*n* = 13), 913 (*n* = 14), 957 (*n* = 15), 1001 (*n* = 16), 1045 (*n* = 17), 1089 (*n* = 18).

Acrylic derivate of Triton® X-100 (**3**)

Yield: 97%; FTIR (diamond, cm^{-1}): ν 2952/2868 (-CH_3, -CH_2-), 1724 (-COOR), 1636 (-C=C-), 1610/1511 (-aryl), 1455, 1407, 1365, 1350, 1319, 1295, 1245 (aryl-C-O-C), 1188, 1102 (-C-O-C-), 1066, 942 (R_2C=CH_2), 829/732 (1,4-disubstitute aromatic), 683, 659, 589, 522; ^{1}H NMR (300 MHz, $CDCl_3$) δ 7.24 (dd, ^3J = 8.83 Hz, ^4J = 2.16, 2H, aryl-CH), 6.80 (dd, ^3J = 8.87 Hz, ^4J = 2.16, 2H, aryl-CH), 6.41 (dd, ^2J = 1.50 Hz, ^3J = 17.39 Hz, 1H, -H), 6.14 (dd, ^3J = 17.39 Hz, ^3J = 10.44 Hz, 1H, =CH_2), 5.82 (dd, ^2J = 1.50 Hz, ^3J = 10.44 Hz, 1H, =CH_2), 4.30 (t, ^3J = 4.86 Hz, 2H, -CH_2-), 4.10 (t, ^3J = 4.93 Hz, 2H, -CH_2-), 3.63 (s, 37H, polyethoxy), 1.68 (s, 2H, -CH_2-), 1.32 (s, 6H, -$(CH_3)_2$), 0.69 (s, 9H, -$(CH_3)_3$); MALDI-TOF ($CHCl_3$, *n* = number of ethoxy groups) *m/z*: 547 (*n* = 6), 591 (*n* = 7), 635 (*n* = 8), 679 (*n* = 9), 723 (*n* = 10), 767 (*n* = 11), 811 (*n* = 12), 855 (*n* = 13), 899 (*n* = 14), 943 (*n* = 15), 987 (*n* = 16), 1031 (*n* = 17), 1075 (*n* = 18), 1119 (*n* = 19).

Homopolymerization in the absence of RAMEB-CD in DMF

The (meth)acrylic derivate of Triton® X-100 (**2** = 10 g, 13.99 mmol; **3** = 10 g, 14.27 mmol) was homopolymerized at 70 °C in a thermostatic bath, with 1 mol % AIBN (0.14 mmol) as radical initiator and 50 wt % dimethylformamide as solvent for 24 h. The polymerization reactions were carried out under an oxygen-free N_2 atmosphere. The polymer was precipitated in methanol, filtered off and vacuum dried at room temperature until a constant weight was reached.

Methacrylic polymer **8**

Yield: 65%; FTIR (diamond, cm^{-1}): ν 2948/2868 (-CH_3, -CH_2-), 1728 (-COOR), 1609/1512 (-aryl), 1455, 1394, 1364, 1349, 1325, 1294, 1245 (aryl-C-O-C), 1149, 1101 (-C-O-C-), 1038, 947, 829/748 (1,4-disubstitute aromatic), 732, 683, 588, 554, 521; GPC (DMF): $\overline{M_n}$ = 80,900, $\overline{M_w}$ = 396,700, *D* = 4.9.

Acrylic polymer **9**

Yield: 74%; FTIR (diamond, cm^{-1}): ν 2946/2868 (-CH_3, -CH_2-), 1733 (-COOR), 1610/1512 (-aryl), 1455, 1391, 1365, 1349, 1294 (aryl-C-O-C), 1245, 1185, 1103 (-C-O-C-), 1039, 948, 829 (1,4-disubstitute aromatic), 683, 588, 522; ^{1}H NMR (300 MHz, $CDCl_3$) δ 7.24 (d, ^3J = 8.76 Hz, 2H, aryl-CH), 6.80 (d, ^3J = 8.76 Hz, 2H, aryl-CH), 4.09 (t, ^3J = 4.87 Hz, 2H, -CH_2-), 3.83 (t, ^3J = 4.87 Hz, 2H, -CH_2-), 3.63 (s, 37H, polyethoxy), 2.21 (d, ^3J = 8.58 Hz, 2H, backbones), 1.68 (s, 2H, -CH_2-), 1.32 (s, 6H, -$(CH_3)_2$), 0.70 (s, 9H, -$(CH_3)_2$); GPC (DMF): $\overline{M_n}$ = 46,800, $\overline{M_w}$ = 303,800, *D* = 6.5.

Homopolymerization in the presence of RAMEB-CD in water

The (meth)acrylic derivate of Triton® X-100 (**2** = 1 g, 1.4 mmol; **3** = 1 g, 1.43 mmol) and 1 or 2 equiv of RAMEB-CD were dissolved in water (20 wt % with reference to the monomer) and stirred until the solution became clear. The complexed monomers were homopolymerized at 40 °C in a thermostatic bath, with 1 mol % VA-044 (for **2** 4.6 mg, 0.014 mmol; for **3** 4.8 mg, 0.015 mmol) as radical initiator for 24 h. The polymerization reactions were carried out under an oxygen-free N_2 atmosphere. The polymers were purified by dialysis for two days.

Methacrylic polymer with 1 equiv of RAMEB-CD (**10**) and 2 equiv of RAMEB-CD (**11**)

Yield **10**: 37%; yield **11**: 89%; FTIR (diamond, cm^{-1}): ν 3404 (-OH), 2924/2886/2832 (-CH_3, -CH_2-, -OCH_3), 1728 (-COOR), 1610/1512 (-aryl), 1454, 1407, 1364, 1325, 1299, 1246 (aryl-C-O-C), 1188, 1147, 1083, 1034 (-C-O-C-), 965, 858/757 (1,4-disubstitute aromatic), 701, 571; ^{1}H NMR (300 MHz, D_2O, **10** and **11** have identical chemical shifts, but the integral of RAMEB-CD for **11** is a 1.8 times bigger than for **10**) δ 7.35 (d, 2H, ^3J = 8.43 Hz, aryl-CH), 6.95 (d, ^3J = 8.43 Hz, 2H, aryl-CH), 5.20 (2s, RAMEB-CD), 4.34 (m, 2H, -CH_2-), 4.23 (m, 2H, -CH_2-), 3.88 (s, RAMEB-CD), 3.81 (s, RAMEB-CD), 3.69 (s, 37H, polyethoxy), 3.67 (s, RAMEB-CD), 3.58 (s, CH_3-RAMEB-CD), 3.54 (s, RAMEB-CD), 3.40 (s, CH_3- RAMEB-CD), 2.07 (s, 1H, -CH_3), 1.77 (s, 2H, -CH_2-), 1.68 (s, 2H, backbones), 1.51 (s, 6H, -$(CH_3)_2$), 0.85 (s, 9H, -$(CH_3)_2$); GPC (**10**, DMF): $\overline{M_n}$ = 119,200, $\overline{M_w}$ = 876,100, *D* = 7.3; GPC (**11**, DMF): $\overline{M_n}$ = 175,300, $\overline{M_w}$ = 593,500, *D* = 3.4.

Acrylic polymer with 1 equiv of RAMEB-CD (**12**) and 2 equiv of RAMEB-CD (**13**)

Yield **12**: 45%; yield **13**: 84%; FTIR (diamond, cm^{-1}): ν 3405 (-OH), 2924/2896/2832 (-CH_3, -CH_2, -OCH_3), 1731 (-COOR), 1610/1512 (-aryl), 1453, 1404, 1364, 1325, 1299, 1246 (aryl-C-O-C), 1189, 1150, 1083, 1033 (-C-O-C-), 1002, 965, 857/758 (1,4-disubstitute aromatic), 701, 571; ^{1}H NMR (300 MHz, D_2O, **12** and **13** have identical chemical shifts, but the integral of RAMEB-CD for **11** is 1.8 times larger than for **10**) δ 7.35 (d, ^3J = 8.73 Hz, 2H, aryl-CH), 6.94 (d, ^3J = 8.73 Hz, 2H, aryl-CH),

5.27 (2s, RAMEB-CD), 4.34 (m, 2H, -CH_2-), 4.23 (m, 2H, -CH_2-), 3.87 (s, RAMEB-CD), 3.70 (s, RAMEB-CD), 3.67 (s, 37H, polyethoxy), 3.67 (s, RAMEB-CD), 3.59 (s, CH_3-RAMEB-CD), 3.53 (s, RAMEB-CD), 3.40 (s, CH_3- RAMEB-CD), 1.77 (s, 2H, -CH_2-), 1.68 (s, H, backbone), 1.50 (s, 6H, -$(CH_3)_2$), 1.27 (s, 3H, -H), 1.27 (s, H, backbone), 0.87 (s, 9H, -$(CH_3)_2$); GPC (**12**, DMF): $\overline{M}_n$ = 54700, $\overline{M}_w$ = 182,700, D = 3.3; GPC (**13**, DMF): $\overline{M}_n$ = 68,400, $\overline{M}_w$ = 218,700, D = 3.2.

Supporting Information

Supporting Information File 1

Additional ITC results, 2D NMR ROESY and hydrodynamic diameters.
[http://www.beilstein-journals.org/bjoc/content/supplementary/1860-5397-8-245-S1.pdf]

References

1. Lindman, B. *Amphiphilic block copolymers: self-assembly and applications;* Elsevier Science: Amsterdam, 2000.
2. Larraz, E.; Elvira, C.; San Román, J. *J. Polym. Sci., Part A: Polym. Chem.* **2003,** *41,* 1641–1649. doi:10.1002/pola.10710
3. Tiller, G. E.; Mueller, T. J.; Dockter, M. E.; Struve, W. G. *Anal. Biochem.* **1984,** *141,* 262–266. doi:10.1016/0003-2697(84)90455-X
4. Du, X.; Lu, W.; Ding, N.; Dai, H.; Teng, X.; Deng, H. *J. Photochem. Photobiol., A: Chem.* **2006,** *177,* 76–82. doi:10.1016/j.jphotochem.2005.05.014
5. Smith, V. K.; Ndou, T. T.; Muñoz De La Peña, A.; Warner, I. M. *J. Inclusion Phenom. Macrocyclic Chem.* **1991,** *10,* 471–484. doi:10.1007/BF01061077
6. Eli, W.; Chen, W.; Xue, Q. *J. Inclusion Phenom. Macrocyclic Chem.* **2000,** *36,* 439–445. doi:10.1023/A:1008105200081
7. Nelson, G.; Warner, I. M. *Carbohydr. Res.* **1989,** *192,* 305–312. doi:10.1016/0008-6215(89)85188-2
8. Turco Liveri, V.; Cavallaro, G.; Giammona, G.; Pitarresi, G.; Puglisi, G.; Ventura, C. *Thermochim. Acta* **1992,** *199,* 125–132. doi:10.1016/0040-6031(92)80256-V
9. Saito, Y.; Ueda, H.; Abe, M.; Sato, T.; Christian, S. D. *Colloids Surf., A* **1998,** *135,* 103–108. doi:10.1016/S0927-7757(97)00235-5
10. He, Y.; Shen, X.; Gao, H.; He, Y. *J. Photochem. Photobiol., A: Chem.* **2008,** *193,* 178–186. doi:10.1016/j.jphotochem.2007.06.023
11. Buschmann, H.-J.; Cleve, E.; Schollmeyer, E. *J. Inclusion Phenom. Macrocyclic Chem.* **1999,** *33,* 233–241. doi:10.1023/A:1008069213946
12. Müller, B.-K.; Ritter, H. *J. Inclusion Phenom. Macrocyclic Chem.* **2012,** *72,* 157–164. doi:10.1007/s10847-011-9955-0
13. Larraz, E.; Elvira, C.; Gallardo, A.; San Román, J. *Polymer* **2005,** *46,* 2040–2046. doi:10.1016/j.polymer.2005.01.029
14. Rekharsky, M. V.; Inoue, Y. *Chem. Rev.* **1998,** *98,* 1875–1918. doi:10.1021/cr970015o

License and Terms

Beilstein Journal of Organic Chemistry

Theoretical study on β-cyclodextrin inclusion complexes with propiconazole and protonated propiconazole

Adrian Fifere[1], Narcisa Marangoci[1], Stelian Maier[2], Adina Coroaba[1], Dan Maftei[3] and Mariana Pinteala[*1]

Full Research Paper

Open Access

Address:
[1]Centre of Advance Research in Bionanoconjugates and Biopolymers, "Petru Poni" Institute of Macromolecular Chemistry, 700487 Iasi, Romania, [2]Faculty of Textiles & Leather Engineering and Industrial Management, "Gheorghe Asachi" Technical University of Iasi, 700050 Iasi, Romania and [3]Faculty of Chemistry, "Al. I. Cuza" University Iasi, Iasi 700506, Romania

Email:
Mariana Pinteala* - pinteala@icmpp.ro

* Corresponding author

Keywords:
β-cyclodextrin; inclusion complexes; PM3; propiconazole

Beilstein J. Org. Chem. **2012,** *8,* 2191–2201.
doi:10.3762/bjoc.8.247

Received: 31 August 2012
Accepted: 26 November 2012
Published: 17 December 2012

This article is part of the Thematic Series "Superstructures with cyclodextrins: Chemistry and applications".

Guest Editor: H. Ritter

Abstract

The synthesis of the β-cyclodextrin/propiconazole nitrate inclusion complex and the advantages of the encapsulation of this drug were recently reported, but the experimental data only partially revealed the structure of the supramolecular complex due to the limitations in understanding the intermolecular association mechanism. The present work describes the equilibrium molecular geometries of β-cyclodextrin/propiconazole and β-cyclodextrin/protonated propiconazole, established by the AM1 and PM3 semi-empirical methods. The affinity between different parts of the guest molecule and the cyclodextrin cavity was studied considering that propiconazole possesses three residues able to be included into the host cavity through primary or secondary hydroxyl rims. The results have revealed that the most stable complex is formed when the azole residue of the propiconazole enters the cavity of the cyclodextrin through the narrow hydroxyl's rim.

Introduction

The occurrence of fungal diseases has dramatically increased during the past 20 years. Extremely rare ten years ago, nowadays, antifungal drug resistance has become an important problem in treatment of fungal diseases for various categories of patients, especially those infected with HIV. Excessive and prolonged treatment with azole-containing medicines has led to fungal resistance to this class of compounds, especially in the case of HIV patients with repeated recurrent episodes [1,2]. Today, the number of reported cases of clinic resistance to antifungal drugs is growing and mycologists have warned about an

increasingly large-scale expansion of this phenomenon [3]. Consequently, the development of new therapeutic conjugates able to combine new antifungal properties with water solubility of the drug has become a major direction of research in the field of antifungal therapy. In this respect, one of the expected methods consists of the complexation of antifungals with cyclodextrins and/or with soluble polymers.

Propiconazole (PP) is a triazole derivative effective as a fungicide, with a broad spectrum, designed and launched by Janssen Pharmaceutics (Belgium). It is widely used in agriculture as a systemic foliar fungicide and, lately, for its fungistatic action. Propiconazole nitrate was tested in order to reduce the toxicity of the unmodified PP, but little information is available on this topic. Recently synthesized positively charged protonated propiconazole (PPH^+) showed an increased antifungal activity compared to unmodified PP. The inclusion compound based on β-cyclodextrin (β-CD) and PPH^+ (further abbreviated as β-CD/PPH^+) was preliminarily investigated in vitro, and its antifungal activity was reported [4].

Cyclodextrins (CDs) are macrocyclic oligosaccharides consisting of six to twelve glucopyranose units joined in a truncated cone-shaped structure [5]. They exhibit a hydrophobic cavity delimited by two rims, a wide and a narrow one, composed of secondary and primary hydroxy groups. By virtue of this structure, CDs are able to generate inclusion complexes with a wide variety of hydrophobic organic compounds in aqueous solution. The driving forces leading to complexation are numerous, varying from van der Waals to hydrophobic and to dipole–dipole interactions [6,7]. Since CDs and their complexes are widely used in pharmaceutical sciences and synthesis, there is currently a great interest in the theoretical study of their supramolecular associates.

Accurately representing the size of CD cavities and their chain flexibility represents a challenge for molecular simulation when quantum methods are employed. Since the ab initio approach is time consuming for this kind of molecule, quantum semi-empirical methods, such as CNDO, AM1 and PM3 were widely used in the theoretical investigation of CDs. The PM3 method has proved to be a powerful tool in the conformational study of supramolecular systems, such as CD inclusion compounds and provides better performance compared to the AM1 method for molecular geometry optimization, due to its improved description of hydrogen bonds and steric effects [8-10]. Advanced methods, such as Hartree–Fock (HF) and density functional theory (DFT), were also applied in cyclodextrin chemistry to explain experimental data [11,12]. Very often, ab initio methods are used in tandem with the semi-empirical PM3 method [13-17].

Because of the experimental limitations, the geometric details and the interactions that stabilize the molecular architecture of β-CD/PPH^+ inclusion compounds are still poorly understood. For this reason the present study theoretically investigates the interaction between PP, PPH^+ and β-CD molecules by means of AM1 and PM3 semi-empirical quantum-mechanical calculations, to examine in detail the insertion pathways and to determine the intimate configurations of the β-CD/propiconazole (β-CD/PP and β-CD/PPH^+) inclusion complexes. Bearing in mind that the CD cavity cannot fully incorporate the guest molecule, the aim of this work is to identify the part of the molecular cavity that is more suitable for complexation with the PPH^+. This information can be useful to predict which of the hydroxy groups of cyclodextrin can be chemically modified (by pegylation for example) in order to avoid the shielding of the cavity during the inclusion process, and, as a consequence, to improve the systemic bioavailability and pharmacokinetics of the inclusion complexes.

Results and Discussions

The most stable conformations of the β-CD/PP and β-CD/PPH^+ inclusion compounds were selected by considering the binding energy as being the difference between the heat of formation of the complex and the heat of formation of the involved free molecules:

$$\Delta E = E_{CD/PP} - (E_{CD} + E_{PP}) \quad (1)$$

where $E_{CD/PP}$, E_{PP} and E_{CD} represent the heat of formation of the complex, of the free β-CD, and of the free guest molecule, respectively. The higher the negative value of the stabilization energy, the more thermodynamically favorable is the pathway of inclusion-complex formation. The particular shape of the PP molecule allows its inclusion into the β-CD cavity following three different ways. Additionally, each residue of PP can be well accommodated either by the secondary or the primary face of the β-CD cavity (Figure 1a). Therefore, six configurations must be considered in pursuing the most stable molecular struc-

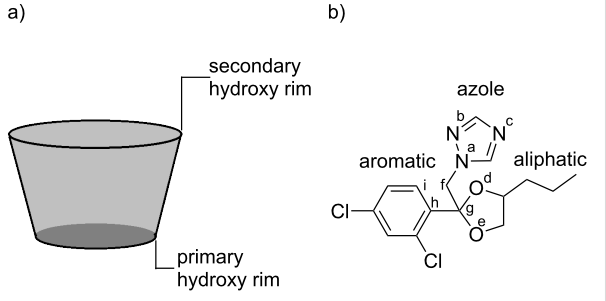

Figure 1: Schematic representation of the β-cyclodextrin (a) and propiconazole (b) molecules.

ture of the inclusion complex. For simplicity, let us note each PP residue as it is shown in Figure 1b. The orientation of PP toward β-CD will be named according to the PP residue that is first included through the wider (A) or narrower (B) cavity rim (e.g., aliphatic A, aliphatic B, if the aliphatic residue is included through the wider or narrower hydroxy rim of the cyclodextrin). A suitable methodology for finding the equilibrium molecular geometry of cyclodextrin inclusion complexes is to place the guest on the cavity axis and to move it through the cavity in steps, simultaneously optimizing the conformations. Since there are six possible configurations, it is crucial to find which propiconazole residue has maximum compatibility with the cyclodextrin cavity. To save computational resources, this can be achieved by the methodology described in the computational method section of the paper. The first step in attaining this goal involves the setting of some conformational constraints, followed by the energetic minimization of the resulted conformation. Hence, the optimized molecular geometries will contain the guest molecule inside or outside of the β-CD, depending on the molecular hindrance and on the affinity between the guest residues and CD cavities. Finally, the structures are to be subjected to PM3 calculations, without any constraints, to obtain the heats of formation and to compare the stability of the conformers.

Looking at Figure 2 it is obvious that all structures are stable since, in all cases, negative binding energies were obtained. It can also be observed that the PP deeply entered into the cavity during the calculation, demonstrating a high probability of complex formation. The binding energy is not very high, which could be explained by the absence of hydrogen bonds that strongly stabilize the molecular association. Analyzing the numerical values summarized in Figure 2, one can see that the stability of the complexes is inversely related to their global electric dipoles. There is an obvious correlation between the global electric dipole moments (p) of the complexes and their binding energies, for each paired situation including the PP residues. Such a fact suggests that a dipole–dipole coupling mechanism could be involved in the complex formation. The inclusion of the triazole ring is energetically favored, since the resulting binding energy is the lowest. The obtained theoretical results confirm the experimental data published on complexation of β-CD and PP, which highlights the inclusion of the triazole ring in the cyclodextrin cavity [4]. Hence, the developed interaction model is accurate.

Inclusion compounds with non-protonated propiconazole (β-CD/PP)

In order to determine the exact structure of the obtained complex, further calculations were carried out. Taking into account previous theoretical and experimental results, we assumed that the β-CD/PP complex is formed by triazole ring inclusion into the cyclodextrin cavity. The further study was performed considering two orientations of the triazole ring in relation to the CD cavity: one with the triazole ring pointing toward the negative sense of the *z* axis, denoted by A (Figure 3a), and the other with the triazole ring pointing toward the positive sense of the cavity axis, denoted by B (Figure 3b). The intermolecular distance was measured between the cavity center and the "dummy" atom of the triazole ring (marked with an asterisk). Initially, the triazole ring was placed in the center of the cavity and a complete rotation was performed to establish the preferred angular orientation of PP during the inclusion process. Keeping constant the resulting angular orientation, PP was then moved along the *z* axis simultaneously with geometry optimization, in the absence of any symmetry constraints (Figure 3a and Figure 3b) as discussed above.

Scanning the binding energy during the movement along the *z* axis, by using the PM3 method, always provided negative values for both A and B configurations (Figure 4a and Figure 4b).

The most stable equilibrium molecular geometry is obtained when PP is deeply included in the β-CD cavity, suggesting an enthalpically driven process (Figure 5a and Figure 5b). The obtained results confirm that PP penetration through the rim of the primary hydroxy is thermodynamically favored, and that the complex is stabilized in the B orientation, which has a stabilization energy about ~20 kJ smaller as compared to the A configuration (Table 1). These facts are in good agreement with those exposed in Figure 2, confirming a higher probability of azole ring inclusion into the β-CD cavity through the narrow rim, according to the B configuration. The results are also consistent with the DFT single-point computations applied on the PM3 equilibrium geometries.

The results are similar to those reported by Fatiha [18], where the imidazole ring of sulconazole enters through the narrow rim into the β-cyclodextrin cavity. The β-CD/sulconazole is stabilized by van der Waals interactions and hydrogen bonds. In fact, the author explained the difference between the A and B orientations in the case of sulconazole by the occurrence of hydrogen bonds. In the present case, no hydrogen bonds were evidenced and, since there are no steric constraints to explain the difference between the A and B orientations in terms of stability, other forces must be considered. It is already known that cyclodextrin molecules have a rather high electric dipole moment; the correlation between this parameter and the complex stability by means of quantum-mechanical calculations has been previously reported [19,20]. The PP molecule has a permanent electric dipole, and the dipole–dipole interaction can

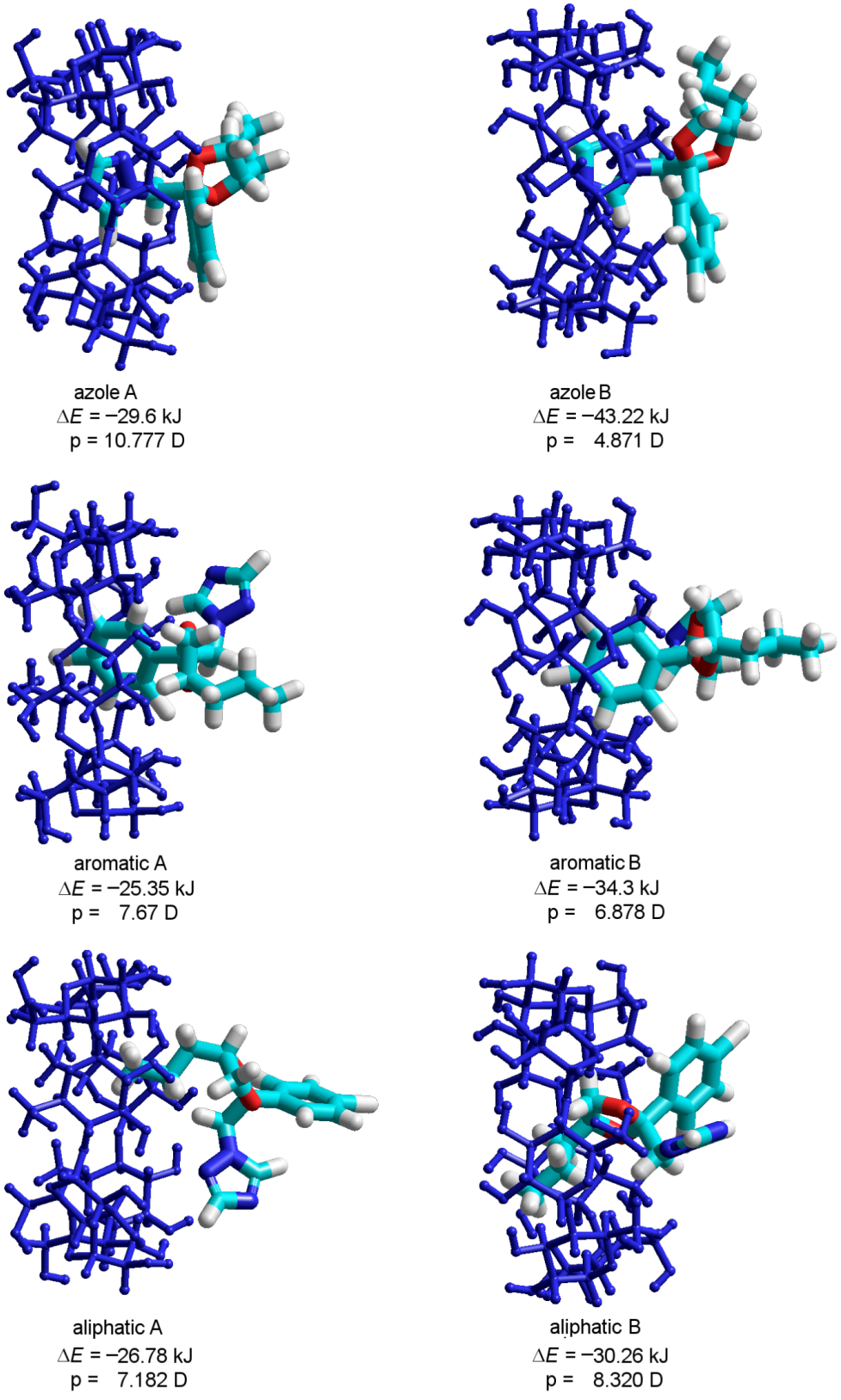

Figure 2: PM3 optimized molecular geometries of the β-CD/PP inclusion compounds involved in the assessment of PP inclusion into the β-CD cavity by each of its residues.

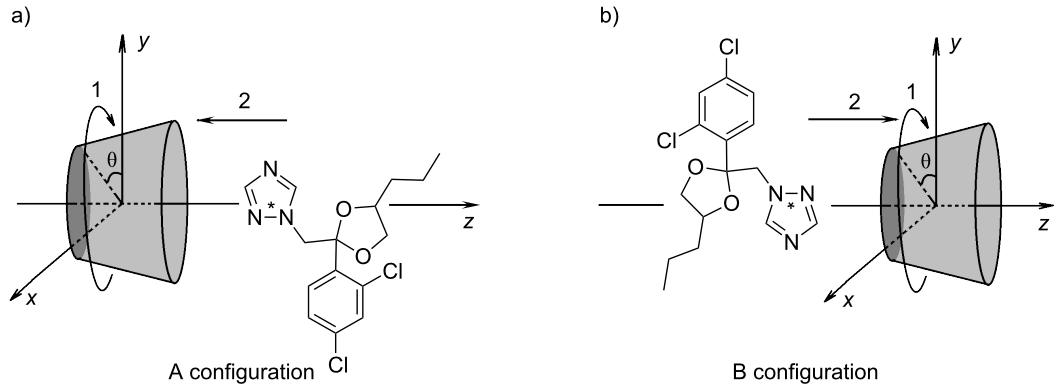

Figure 3: Molecular coordinates used to describe the relative position between the β-CD and guest molecules.

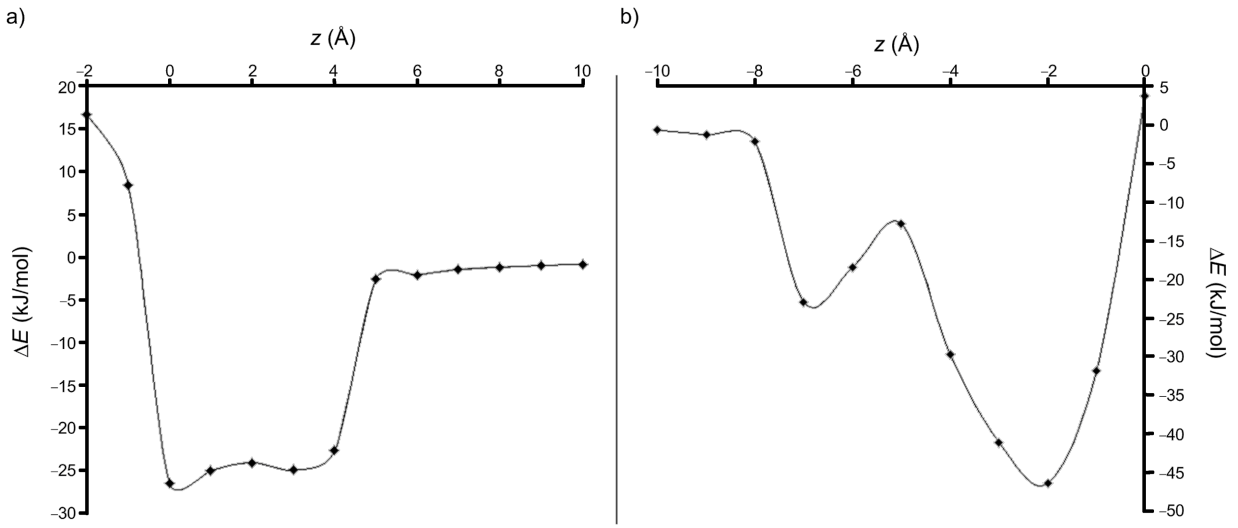

Figure 4: Evolution of the stabilization energy during the movement along the *z* axis in the case of (a) A and (b) B orientations of PP relative to the cavity of β-CD (PM3 calculation).

Table 1: Molecular parameters of the most stable β-CD/PP inclusion compounds in both A and B configurations, as given by AM1 and PM3 calculations and by B3LYP/6-31G(d)+ single-point calculations applied on the PM3 optimized geometries.

Parameter	Method of calculation[a]	β-CD (kJ/mol)	PP (kJ/mol)	β-CD/PP A configuration	β-CD/PP B configuration
E (kJ/mol)	AM1	−6895.59	21.08	−6879.92	−6889.54
	PM3	−6091.27	−91.71	−6209.44	−6229.34
	DFT	−11224754.47	−4770267.2	–	–
Δ*E* (kJ/mol)	AM1	–	–	−5.40	−15.02
	PM3	–	–	−26.45	−46.35
	DFT	–	–	−29.39	−49.64
p (D)	AM1	5.028	3.613	7.36	1.037
	PM3	6.915	3.945	9.633	4.644
	DFT	8.181	4.034	10.987	5.521

[a]In the case of DFT calculations, total energies were taken into account.

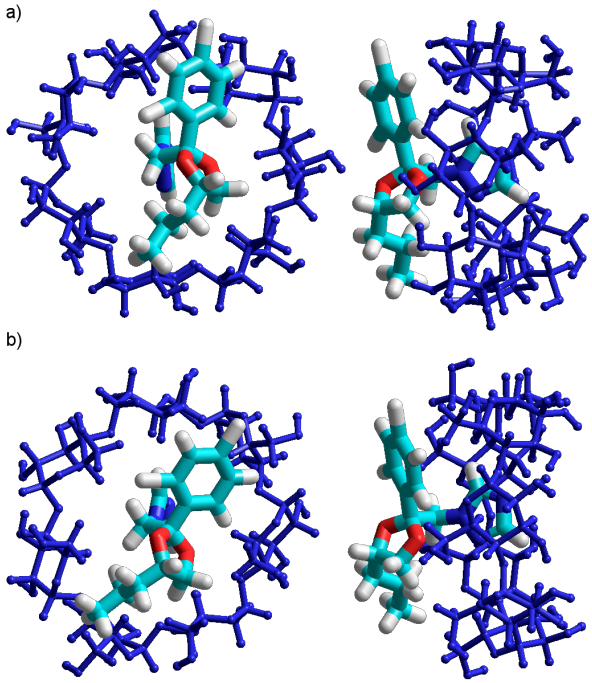

Figure 5: PM3 optimized molecular geometry of the β-CD/PP inclusion compounds in (a) A configuration and in (b) B configuration.

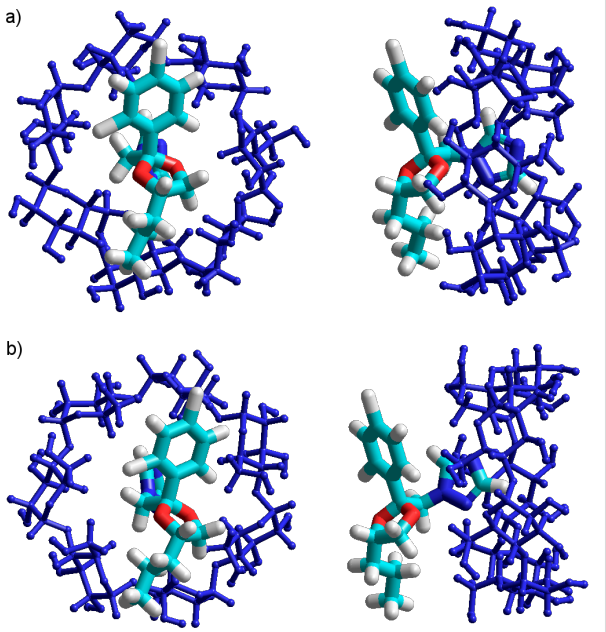

Figure 6: AM1 optimized molecular geometry of the β-CD/PP inclusion compounds, for both (a) A and (b) B configurations.

make the difference between the A and B configurations. The decrease of the global dipole moment together with the increase of the binding energy (see Table 1), points to the dipole–dipole interactions as a major contributor to the stabilization of the B structure.

As depicted in Figure 6a and Figure 6b, the molecular geometry of the AM1 optimized inclusion compounds shows that the PP molecule is deeply inserted in the cavity of β-CD for both A and B configurations.

In terms of binding energy, the difference between the A and B orientations was found to be 9.62 kJ. Similarly to the preceding PM3 calculation, the AM1 optimized B configuration of the β-CD/PP complex has a higher stability and no hydrogen bonds where identified. After AM1 optimization too, the same correlation between the stabilization energies and dipole moments of the inclusion compounds was revealed (Table 1).

Inclusion compounds with protonated propiconazole (β-CD/PPH$^+$)

In order to study the complex formation between β-CD and the positively charged guest molecule, a model of PPH$^+$ was built. The proton affinity (PA) was calculated for each of the five protonation sites of the azole ring (according to the notation scheme shown in Figure 1b). According to reference [21,22], PA was defined as the energy variation in the proton-addition equilibrium:

$$\mathrm{PPH^+} \rightleftharpoons \mathrm{PP} + \mathrm{H^+}$$
$$PA = H_f(\mathrm{PP}) + H_f(\mathrm{H^+}) - H_f(\mathrm{PPH^+}) \quad (2)$$

In this model the heat of formation of the proton was taken to be zero because of the lack of electrons, and the reaction system was considered in vacuo, at 0 K. The method does not provide the exact value of the PA parameter, but the calculation is useful to compare the stability of different protonation forms of the PP molecule. Table 2 shows that the PA values are considerably higher when PP is protonated at the iminic nitrogen atom (in the c position), this position being therefore the best protonation site.

Table 2: The calculated values of the proton affinity of the denoted atoms in the PP molecule (see Figure 1b).

PPH$^+$	PA (kJ/mol)
PPH$^+$ a	758.05
PPH$^+$ b	848.22
PPH$^+$ c	907.99
PPH$^+$ d	734.36
PPH$^+$ e	760.32

To find the energy-minimized molecular geometry of the β-CD/PPH^+ complex, only the inclusion of the protonated azole ring into the β-CD cavity was considered. The procedure was similar to that used in the case of the β-CD/PP inclusion complex, the azole ring being progressively introduced into the β-CD cavity. Also, similar to the β-CD/PP complex, two orientations of the guest molecule relative to the β-CD cavity were taken into account and the same notations are kept.

Scanning the binding energy by using the PM3 method revealed that, for all step intervals along the *z* axis, the energy of the complex is substantially lower compared with the sum of the energies of the isolated host and guest molecules (Figure 7a and Figure 7b). According to the values of the energy of the two configurations, it results that the B orientation of the PPH^+ molecule relative to the β-CD cavity provides the most stable inclusion complex, the difference being about 13.8 kJ/mol when compared to the A configuration (Table 3). Results are also consistent with the DFT single point computations applied on the PM3 equilibrium geometries.

As depicted in Figure 8a and Figure 8b, the equilibrium molecular geometries of the A and B PM3 optimized inclusion compounds are quite different. In the A orientation, the stable complex is formed with the protonated azole ring located outside of the β-CD cavity (Figure 8a), while in the B orientation, the azole ring is completely included in the cavity (Figure 8b).

The AM1 method shows the same trend as the PM3 regarding the inclusion pathway of PPH^+ in the β-CD cavity, where the

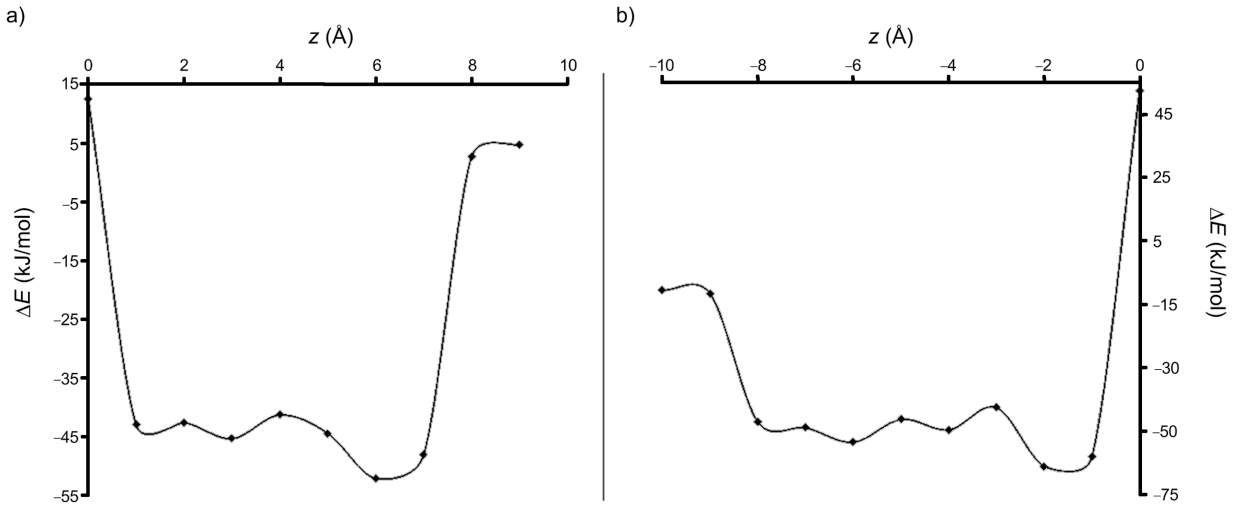

Figure 7: Variation of the stabilization energy during the movement along the *z* axis, in the case of (a) A and (b) B orientations of PPH^+ relative to the β-CD cavity (PM3 calculations).

Table 3: Molecular parameters of the most stable β-CD/PPH^+ inclusion compounds in both A and B configuration, as given by AM1 and PM3 calculations and by B3LYP/6-31G(d)+ single-point calculations applied on the PM3 optimized geometries.

Parameter	Method of calculation[a]	β-CD	PPH^+	β-CD/PPH^+ A orientation	β-CD/PPH^+ B orientation
E (kJ/mol)	AM1	−6895.59	150.66	−6308.95	−6352.23
	PM3	−6091.27	537.16	−5606.27	−5620.07
	DFT	−11224754.47	−4771227.68	–	–
Δ*E* (kJ/mol)	AM1	–	–	−44	−87.28
	PM3	–	–	−52.16	−65.96
	DFT	–	–	−28.63	−38.61
p (D)	AM1	5.028	13.077	17.476	1.09
	PM3	6.915	12.086	19.531	7.123
	DFT	8.181	10.898	10.987	7.145

[a]In the case of DFT calculations, total energies were taken into account.

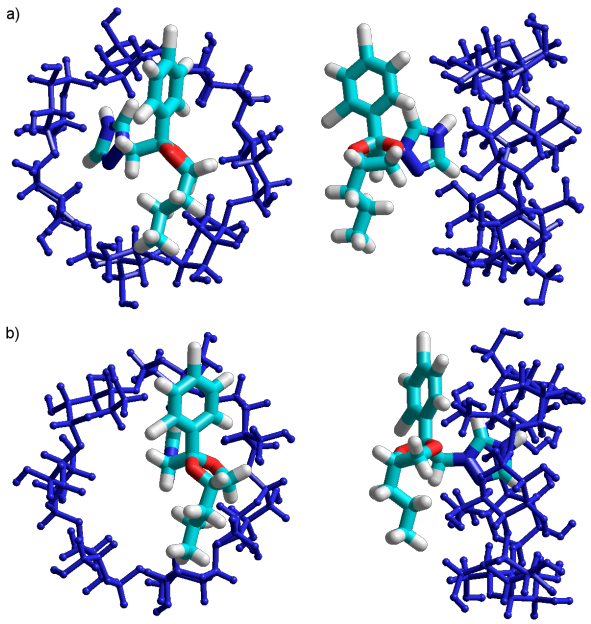

Figure 8: PM3 optimized molecular geometry of β-CD/PPH$^+$ inclusion compounds in the (a) A and (b) B configurations.

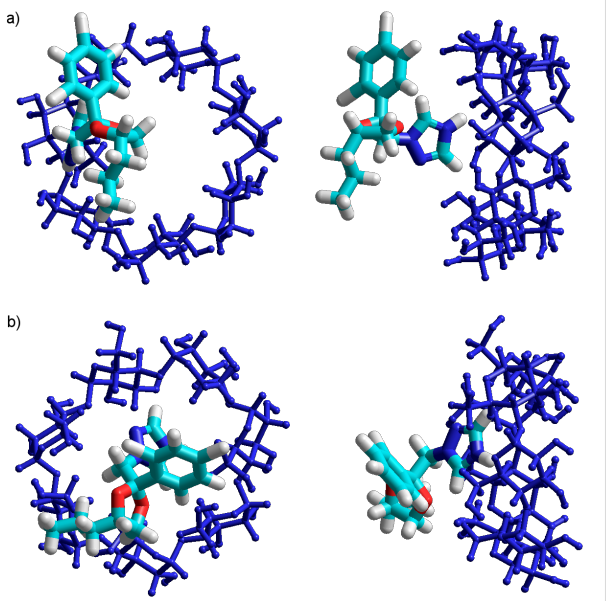

Figure 9: AM1 optimized molecular geometry of the inclusion compounds β-CD/PPH$^+$ in the (a) A and (b) B configurations.

complex has the highest stability in the B configuration. The binding energy of the B configuration is 43.28 kJ/mol lower than that in the A configuration (Table 3). The significant difference between stabilization energies leads to a rather big difference between molecular structures. Thus, while in the more stable B configuration the PPH$^+$ is included with the azole ring in the β-CD cavity, at the level of the wider rim (Figure 9a), in the A configuration, the PPH$^+$ molecule is completely outside of the cavity (Figure 9b). Both AM1 and PM3 calculations indicate a strong correlation between the stabilization energy and the electric dipole moments (Table 3).

Modeling the inclusion pathway of PP and PPH$^+$ by means of semi-empirical PM3 and AM1, a strong correlation between the values of binding energy and electric dipole moments is revealed, which indicates a major contribution of dipole–dipole coupling to the molecular stability of the inclusion complexes.

The energy minimization of the β-CD/PP and β-CD/PPH$^+$ inclusion compounds with the PM3 and AM1 methods leads to equilibrium geometries with the guest molecules partially inserted in the β-CD cavity for both A and B orientations of the guests. When the protonated form of PP is considered, the process minimization generates very different molecular architectures for the A and B starting configurations. While the complex in the A configuration contains the PPH$^+$ molecule completely outside of the β-CD cavity, in the case of the B configuration, PPH$^+$ is deeply inserted in the cavity with the protonated azole ring entering through the narrow rim. By protonating the PP, a regional selectivity of the inclusion process relative to the β-CD cavity was noticed, with the complexation path through the narrow rim being the favored one.

As Table 4 shows, PP and PPH$^+$ experience some conformational transformations during the complexation process. The variation of molecular parameters is not significant, but it seems that the PP molecule changes its shape in order to augment the complex stability. The magnitude of the variation is higher for the β-CD/PP complex than for the β-CD/PPH$^+$ one, and is significant at the level of dihedral angles of the molecules. In the case of the β-CD/PP complex, the magnitude of the variation of the molecular parameters is higher for the A orientation, while in the case of β-CD/PPH$^+$ the trend is reversed. Since for both PP and PPH$^+$, the most stable complex occurs in the B orientation, and because the magnitude of the conformational change is not correlated with any of the two configurations, we suppose that regional selectivity of cyclodextrin complexation is not governed by steric driving forces or by conformational effort of the PP during the inclusion process.

The effect of solvent on the orientation of a guest molecule toward the β-CD cavity

Since all the previously discussed molecular geometries were optimized in vacuo, it is important to know if the orientation of the guest molecules toward the β-CD cavity remains the same in the presence of water molecules. In this respect, the geometries

Table 4: Relevant geometric parameters of the PP and PPH^+ molecules in their inclusion compounds with β-CD, as given by PM3 calculations.

Molecular parameter	PP	β-CD/PP A	β-CD/PP B	PPH^+	β-CD/PPH^+ A	β-CD/PPH^+ B
Bond N_a–C_f	1.47	1.47	1.47	1.47	1.47	1.47
C_f–C_g	1.56	1.56	1.56	1.57	1.57	1.57
C_g–C_h	1.52	1.52	1.52	1.52	1.52	1.523
Angle N_a–C_f–C_g	114.18	114.23	114.27	113.90	113.85	114.31
C_f–C_g–C_h	110.82	111.25	110.68	111.1	111.01	111.77
C_f–C_g–O_d	110.81	110.29	110.89	108.17	108.68	107.84
C_g–C_h–C_i	120.46	120.34	120.80	120.54	120.50	120.27
Dihedral angle N_a–C_f–C_g–C_h	74.68	86.61	71.29	73.60	72.08	78.69
N_a–C_f–C_g–O_d	−48.92	−37.25	−52.19	−50.31	−51.77	−45.52
C_f–C_g–C_h–C_i	−110.26	−112.83	−110.56	116.23	−114.14	−119.59

of the complexes were optimized in aqua, by combining techniques of molecular mechanics and quantum mechanics [23].

The results given in Table 5 shows that, as solvent, water does not affect the most stable orientation of PP and PPH^+ toward the β-CD cavity, and that the binding energy permanently remains negative. Likewise with the case of in vacuo calculations, the B orientations of the guests are favored for both β-CD/PP and β-CD/PPH^+ inclusion complexes. It is important to note that both in vacuo and in aqua, the guest molecules are deeply inserted in the β-CD cavity, according to the B configurations (Figure 10), and no hydrogen bonds can be evidenced. The decrease of the global dipole moment by the increase of binding energy, suggests again that dipole–dipole interactions are the major contributor to the stabilization of the B structure.

Table 5: Molecular parameters of the most stable β-CD/PP and β-CD/PPH^+ inclusion complexes in A and B configurations, as given by the in aqua PM3 calculations.

Parameter	β-CD/PP		β-CD/PPH^+	
	A orientation	B orientation	A orientation	B orientation
ΔE (kJ/mol)	−11.4	−17.1	−12.15	−34.44
p (D)	10.587	4.278	20.429	4.559

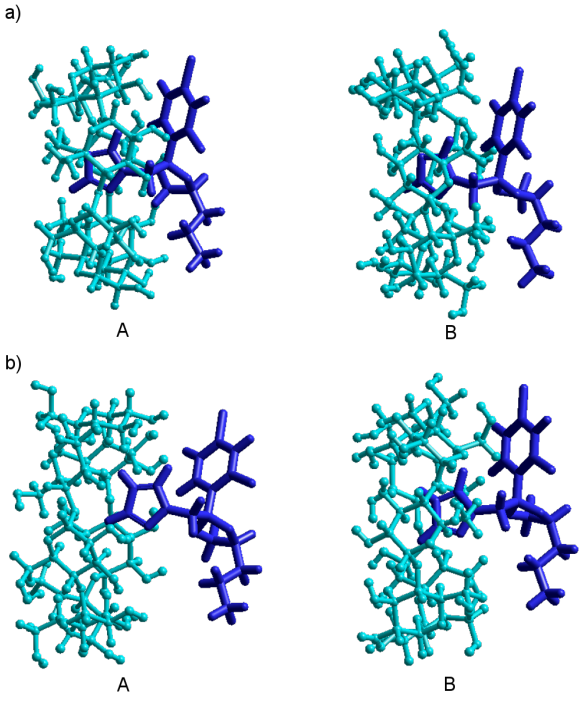

Figure 10: MM+ optimized molecular geometry of the (a) β-CD/PP and (b) β-CD/PPH^+ inclusion complexes, in both A and B configurations. For clarity, water molecules have been removed.

Conclusion

The molecular geometry of the inclusion complexes of β-CD with PP and PPH^+ as guests was studied by using the MM+, AM1 and PM3 methods. The results have revealed that the PP and PPH^+ azole rings were included into the cavity of the β-CD through the narrower hydroxy rim. A strong correlation between the binding energy and the global dipole moments was proved, pointing to the fact that dipole–dipole coupling acts as a major force in stabilizing the complexes.

The presence of water molecules as a solvent does not affect the orientation of PP and PPH^+ toward the β-CD cavity: both guests penetrating through the narrow rim is always favored. The strong correlation between the binding energy and the global dipole moment is obviously maintained, no matter if the inclusion process is simulated in vacuo or in the presence of water molecules.

Experimental

Computational method

The starting molecular conformations of β-CD, PP and PPH^+ were built by using the graphical tool of the HyperChem 7.52 software application [24]. β-CD was built up starting from α-D-glucopyranose residues (found in HyperChem data base) by interconnection with α-(1,4)-glycosidic oxygen bridges. The resulting molecular geometries where fully optimized by AM1 and PM3 quantum-mechanics semi-empirical methods, under HyperChem software application. DFT single-point calculations were performed using GAUSSIAN 09 software package [25], at the level of B3LYP/6-31G(d)+. The equilibrium molecular geometries were validated by comparing the obtained molecular parameters with those reported in the literature [10].

It is known that the calculation of the entire potential surface of CD inclusion complexes requires large computational resources and is time consuming. Because the three entering pathways of the PP molecule into the molecular cavity of the β-CD take place according to complexation mechanisms, several methods were developed to prove the compatibility of the molecular residue of the guest with the host cavity [26-29].

A molecular coordinate system was defined having the glycosidic oxygen atoms in the *x*O*y* plane, and with the *z* axis orthogonal to *xy* plane, so that *z* axis becomes the cavity axis. The primary hydroxy groups of cyclodextrin are therefore oriented toward the negative sense of *z*, while the secondary ones are directed toward the positive sense of the axis. In our approximation, the inclusion processes take place with the guest molecule moving along the cavity axis. To determine which PP residue has the highest affinity for the β-CD cavity, the PP molecule was placed on the cavity axis with one of the residues (either aromatic, aliphatic or azole ring) in front of the β-CD cavity. As a first stage, a MM+ calculation was applied to the guest PP molecule, while keeping the β-CD conformation frozen. The result was a deep insertion of the PP into the cavity, along with the advance of the calculation process. In the next stage, the whole system was fully optimized by using the PM3 quantum method, without any conformational constraints.

The molecular equilibrium geometries of the β-CD inclusion compounds with PP and PPH^+ were calculated by placing the drug molecule on the cavity axis. To find the favorable angular orientation, the guest molecule was placed in the center of the cavity and a complete rotation was performed, optimizing the molecular geometry by PM3 methods at equal intervals of 20°, in the absence of any conformational constraints. While keeping the favorable angular orientation constant, the guest was moved along the cavity axis through the β-CD cavity, and complete geometry-optimization calculations were performed for equal intervals of 1 Å, by the PM3 method.

To compare the results delivered by the two semi-empirical methods, the molecules with initial coordinates corresponding to their PM3 minimum energy were subjected to AM1 calculations and also to B3LYP/6-31G(d)+ single-point investigations.

The most stable inclusion complexes found by PM3 computations were placed in a cubic box with 36 × 36 × 36 Å, containing 1541 water molecules. The systems were firstly equilibrated by optimizing water molecules with the MM+ method, keeping the inclusion complexes frozen. Then a complete optimization of the whole system was performed for each system, without any constraints [23]. The resulting molecular geometries were finally subjected to singlepoint calculation by the PM3 method, in order to extract the heat of formation, after the removal of water molecules. A full optimization of the equilibrium geometries after removing water molecules would have led to a complete loss of information concerning the solvent effect.

Acknowledgements

This research was financially supported by the European Social Fund "Cristofor I. Simionescu" Postdoctoral Fellowship Programme (ID: POSDRU/89/1.5/S/55216), Sectoral Operational Programme Human Resources Development 2007–2013, and the PN-II-ID-PCCE-2011-2-0028 Grant.

References

1. Pfaller, M. A.; Diekema, D. J.; Rinaldi, M. G.; Barnes, R.; Hu, B.; Veselov, A. V.; Tiraboschi, N.; Nagy, E.; Gibbs, D. L.; the Global Antifungal Surveillance Group. *J. Clin. Microbiol.* **2005,** *43,* 5848–5859. doi:10.1128/JCM.43.12.5848-5859.2005
2. Ostrosky-Zeichner, L.; Pappas, P. G. *Crit. Care Med.* **2006,** *34,* 857–863. doi:10.1097/01.CCM.0000201897.78123.44
3. Stephenson, J. *JAMA, J. Am. Med. Assoc.* **1997,** *277,* 283–284. doi:10.1001/jama.1997.03540280021013
4. Marangoci, N.; Mares, M.; Silion, M.; Fifere, A.; Varganici, C.; Nicolescu, A.; Deleanu, C.; Coroaba, A.; Pinteala, M.; Simionescu, B. C. *Results Pharma Sci.* **2011,** *1,* 27–37. doi:10.1016/j.rinphs.2011.07.001
5. Tiwari, G.; Tiwari, R.; Rai, A. K. *J. Pharm. BioAllied Sci.* **2010,** *2,* 72–79. doi:10.4103/0975-7406.67003
6. Morari, C.; Bogdan, D.; Bogdan, M. *Rom. J. Phys.* **2005,** *50,* 995–1002.

7. Martin Del Valle, E. M. *Process Biochem.* **2004,** *39,* 1033–1046. doi:10.1016/S0032-9592(03)00258-9
8. Zheng, Y.-J.; Merz, K. M., Jr. *J. Comput. Chem.* **1992,** *13,* 1151–1169. doi:10.1002/jcc.540130916
9. Castro, R.; Berardi, M. J.; Córdova, E.; Ochoa de Olza, M.; Kaifer, A. E.; Evanseck, J. D. *J. Am. Chem. Soc.* **1996,** *118,* 10257–10268. doi:10.1021/ja960700x
10. Li, X.-S.; Liu, L.; Mu, T.-W.; Guo, Q.-X. *Monatsh. Chem.* **2000,** *131,* 849–855. doi:10.1007/s007060070062
11. Cheng, X.; Wang, Q.; Lu, C.; Meng, Q. *J. Phys. Chem. A* **2010,** *114,* 7230–7240. doi:10.1021/jp103118z
12. Stachowicz, A.; Styrcz, A.; Korchowiec, J.; Modaressi, A.; Rogalski, M. *Theor. Chem. Acc.* **2011,** *130,* 939–953. doi:10.1007/s00214-011-1014-9
13. Nascimento, C. S., Jr.; Dos Santos, H. F.; De Almeida, W. B. *Chem. Phys. Lett.* **2004,** *397,* 422–428. doi:10.1016/j.cplett.2004.09.026
14. Jimenez, V.; Alderete, J. B. *J. Phys. Chem. A* **2008,** *112,* 678–685. doi:10.1021/jp073011o
15. Xing, S.-K.; Zang, C.; Ai, H.-Q.; Zhao, Q.; Zhang, Q.; Sun, D.-Z. *J. Theor. Comput. Chem.* **2009,** *8,* 57–69. doi:10.1142/S0219633609004484
16. Jin, X.; Wang, X.; Ren, C.; Miao, Y.; Yi, L. *J. Mol. Model.* **2011,** *17,* 913–920. doi:10.1007/s00894-010-0781-x
17. Bhattacharya, P.; Sahoo, D.; Chakravorti, S. *Ind. Eng. Chem. Res.* **2011,** *50,* 7815–7823. doi:10.1021/ie2004797
18. Fatiha, M.; Khatmi, D. E.; Largate, L. *J. Mol. Liq.* **2010,** *154,* 1–5. doi:10.1016/j.molliq.2010.03.004
19. Kitagawa, M.; Hoshi, H.; Sakurai, M.; Inoue, Y.; Chûjô, R. *Carbohydr. Res.* **1987,** *163,* c1–c3. doi:10.1016/0008-6215(87)80176-3
20. Sakurai, M.; Kitagawa, M.; Hoshi, H.; Inoue, Y.; Chûjô, R. *Carbohydr. Res.* **1990,** *198,* 181–191. doi:10.1016/0008-6215(90)84291-2
21. DeKock, R. L.; Jasperse, C. P. *Inorg. Chem.* **1983,** *22,* 3839–3843. doi:10.1021/ic00168a004
22. Olivella, S.; Urpi, F.; Vilarrasa, J. *J. Comput. Chem.* **1984,** *5,* 230–236. doi:10.1002/jcc.540050304
23. Fatiha, M.; Khatmi, D. E.; Largate, L. *Orbital: Electron. J. Chem.* **2009,** *1,* 26–37.
24. *HyperChem 7.52 for Windows;* Hypercube, Inc.: Gainesville, FL, 2003.
25. *Gaussian 09,* Revision A.02; Gaussian, Inc.: Wallingford, CT, 2009.
26. Liu, L.; Guo, Q.-X. *J. Inclusion Phenom. Macrocyclic Chem.* **2004,** *50,* 95–103. doi:10.1007/s10847-003-8847-3
27. Bratu, I.; Gavira-Vallejo, J. M.; Hernanz, A. *Biopolymers* **2005,** *77,* 361–367. doi:10.1002/bip.20245
28. Farcas, A.; Jarroux, N.; Guégan, P.; Fifere, A.; Pinteala, M.; Harabagiu, V. *J. Appl. Polym. Sci.* **2008,** *110,* 2384–2392. doi:10.1002/app.28760
29. Farcas, A.; Fifere, A.; Stoica, I.; Farcas, F.; Resmerita, A.-M. *Chem. Phys. Lett.* **2011,** *514,* 74–78. doi:10.1016/j.cplett.2011.08.007

License and Terms

Beilstein Journal of Organic Chemistry

Inclusion of the insecticide fenitrothion in dimethylated-β-cyclodextrin: unusual guest disorder in the solid state and efficient retardation of the hydrolysis rate of the complexed guest in alkaline solution

Dyanne L. Cruickshank[1], Natalia M. Rougier[2], Raquel V. Vico[2], Susan A. Bourne[1], Elba I. Buján[*2], Mino R. Caira[*1] and Rita H. de Rossi[*2]

Full Research Paper

Open Access

Address:
[1]Department of Chemistry, University of Cape Town, Rondebosch 7701, South Africa and [2]Instituto de Investigaciones en Físico Química de Córdoba (INFIQC-CONICET), Departamento de Química Orgánica, Facultad de Ciencias Químicas, Universidad Nacional de Córdoba, Ciudad Universitaria, X5000HUA, Córdoba, Argentina

Email:
Elba I. Buján[*] - elba@fcq.unc.edu.ar; Mino R. Caira[*] - Mino.Caira@uct.ac.za; Rita H. de Rossi[*] - ritah@fcq.unc.edu.ar

* Corresponding author

Keywords:
crystal structure; cyclodextrin; fenitrothion; hydrolysis; inclusion complex

Beilstein J. Org. Chem. **2013,** *9,* 106–117.
doi:10.3762/bjoc.9.14

Received: 31 August 2012
Accepted: 12 December 2012
Published: 17 January 2013

This article is part of the Thematic Series "Superstructures with cyclodextrins: Chemistry and applications".

Guest Editor: H. Ritter

Abstract

An anhydrous 1:1 crystalline inclusion complex between the organophosphorus insecticide fenitrothion [*O*,*O*-dimethyl *O*-(3-methyl-4-nitrophenyl)phosphorothioate] and the host compound heptakis(2,6-di-*O*-methyl)-β-cyclodextrin (DIMEB) was prepared and its structure elucidated by single-crystal X-ray diffraction. This revealed two independent host molecules in the asymmetric unit. In one of these, the cavity is occupied by two disordered guest components (distinguishable as rotamers with respect to the P–OAr bond) while in the other, three distinct guest components with site-occupancies 0.44, 0.29 and 0.27 appear, the last having a reversed orientation relative to all the other components. Kinetic studies of the alkaline hydrolysis of fenitrothion in the presence of DIMEB showed a remarkable reduction of 84% in the rate of this reaction relative to that for the free substrate, a value exceeding those previously attained with the native hosts, β- and γ-cyclodextrin, and fully methylated β-cyclodextrin.

Introduction

Whereas cyclodextrins (CDs) have been employed for many years in the pharmaceutical industry to modify drug-delivery properties, the application of CD technology to the improvement of agrochemicals is a more recent innovation [1,2]. Nevertheless, very significant advantages of encapsulating agrochemicals such as pesticides (insecticides, herbicides, fungicides) in CDs may be gained [1], including, e.g., the conversion of toxic volatile liquids into solids, more localised pesticide application

to improve delivery and reduce wastage, and stabilisation of the included pesticide against undesired degradation reactions.

Fenitrothion [*O*,*O*-dimethyl *O*-(3-methyl-4-nitrophenyl)phosphorothioate] (**1**, Figure 1) is an organophosphorus insecticide and acaricide [3]. It is effective against a wide range of pests that damage forests and various crops and it can also be used in the form of a residual contact spray to control flies, mosquitoes and cockroaches. Fenitrothion has also been employed in antimalarial programmes, where spraying of houses and animal shelters with this insecticide over extended periods significantly reduced the incidence and prevalence of the disease [4].

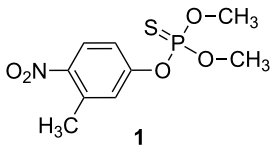

1

Figure 1: Chemical structure of fenitrothion (**1**).

In our recent reports on the interaction between CDs and the organophosphorus insecticide **1** we gave an account of the X-ray crystal structures and thermal decomposition profiles of two solid inclusion complexes between permethylated α- and β-cyclodextrins, hexakis(2,3,6-tri-*O*-methyl)-α-CD (TRIMEA) and heptakis(2,3,6-tri-*O*-methyl)-β-CD (TRIMEB) and the guest [5]. We have also described the results of solution-based kinetic studies aimed at determining the effect of the presence of various CDs on the rate of alkaline hydrolysis of fenitrothion in aqueous solution containing 2% dioxane at 25 °C [6]. A crystalline inclusion complex (TRIMEA)$_2$·**1** was isolated and shown by X-ray analysis to contain a novel capsule formed by head-to-head contact of the secondary rims of two TRIMEA molecules [5]. The encapsulated fenitrothion molecule showed minor disorder in the form of two rotamers (with respect to the P–OAr bond). In contrast, with the host TRIMEB, a monomeric inclusion complex TRIMEB·**1** was obtained, the guest molecule being statistically disordered over two positions [5]. In both crystalline complexes, however, the sensitive phosphate ester moiety was found to be buried deep within the CD cavity and we suggested that if this feature were to be obtained in solution, it would account for earlier observations that the rate of alkaline degradation of the ester is retarded in the presence of CDs [7,8].

Subsequently, a study of the kinetics of hydrolysis of the insecticide **1** in aqueous solution containing 2% dioxane at 25 °C and in the presence of the native cyclodextrins α-CD, β-CD, γ-CD as well as the permethylated derivatives TRIMEA and TRIMEB, was performed [6]. This revealed weak host–guest association in the case of α-CD and insoluble complex formation in the case of the host TRIMEA [9], whereas for β-CD, γ-CD and TRIMEB the association constants for the inclusion complexes of **1** had the respective values 417, 99 and 511 M^{-1} [6], the hydrolytic decomposition of **1** being significantly retarded by all three CDs.

The present study relates to the interaction between **1** and heptakis(2,6-di-*O*-methyl)-β-CD (DIMEB), the latter molecule having properties intermediate between those of the native and fully methylated counterparts [10]. The preparation and physicochemical characterization of the crystalline inclusion complex DIMEB·**1** are presented, this complex crystallizing in a novel arrangement and showing severe guest disorder, which was eventually resolved and successfully modelled. In addition, the results of a kinetic study of the hydrolytic degradation of **1** in the presence of DIMEB are reported and compared with those observed for the other CDs under the same reaction conditions.

Results and Discussion

Thermal analysis

Figure 2 shows representative thermogravimetric (TGA) and differential scanning calorimetric (DSC) traces for the novel inclusion complex DIMEB·**1**. Three reproducible thermal events occur in the DSC trace, the first of which is a small endotherm at 132 °C, which we interpret as a minor solid–solid phase change, based on supporting hot stage microscopic (HSM) observations that show the initially colourless crystals turning opaque in this temperature region. A significantly larger endotherm follows at 158 °C accompanying the major phase of guest loss, while the broad exotherm at ~230 °C is interpreted as indicating the onset of host decomposition. The latter event is also confirmed by HSM showing the opaque crystals turning brown in the temperature region following guest loss. In the TG trace, major host decomposition is seen to occur above 300 °C.

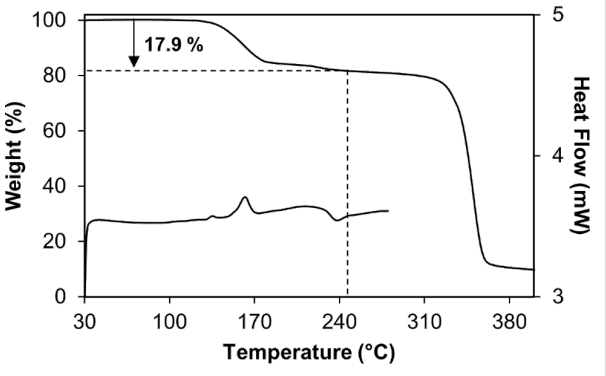

Figure 2: Representative TGA (top) and DSC (bottom) traces for DIMEB·**1**.

Complete loss of the guest from the inclusion complex resulted in an estimated 17.9 ± 0.3% (n = 2) mass loss, which is in good agreement with the theoretical value of 17.2% for a 1:1 host–guest complex. The complex stoichiometry deduced from thermal analysis was subsequently confirmed by NMR spectroscopy, as described below.

NMR spectroscopy

From the ^{1}H NMR spectrum of the solid complex dissolved in $CDCl_3$, a 1:1 DIMEB·**1** stoichiometry was calculated. Table 1 lists the relevant host and guest proton integrations, showing however, that a small excess of DIMEB, cocrystallized with the complex, was present in the sample.

Fenitrothion is known to decompose at elevated temperature [11]. Since the complex crystals had been isolated at 60 °C, the possibility that the fenitrothion may have degraded thermally was checked by ^{31}P NMR spectroscopy. Pure, uncomplexed fenitrothion dissolved in $CDCl_3$ shows a single peak at 65.60 ppm. The complex crystals dissolved in $CDCl_3$ also showed the presence of only one signal at 65.47 ppm confirming the structural integrity of the included insecticide molecule.

The ^{31}P NMR spectrum of a solution of **1** (2 mM) in 2% dioxane-d_8/D_2O gave a single peak at 65.14 ppm, while in the same solution but in the presence of DIMEB (2 mM) the signal appears at 66.82 ppm, in agreement with data reported for **1** in water [6,12-14]. The shift observed indicates that a complex is formed.

The ^{1}H NMR spectrum shows that the protons H3 and H5 of the cyclodextrin rings that are located inside the cavity are slightly shifted downfield, confirming the inclusion of the guest into the cavity.

X-ray analysis

Table 2 lists the crystal data and data-collection parameters for the complex. No DIMEB-containing crystals with similar unit cell dimensions and the same space group as those of the

Table 2: Crystal data and data-collection parameters.

Compound	DIMEB·**1**
Chemical formula	$C_{56}H_{98}O_{35}·C_9H_{12}O_5NPS$
Formula weight / (g mol^{-1})	1608.57
Crystal system	Monoclinic
Space group	$P2_1$
A / (Å)	19.626(2)
B / (Å)	15.049(2)
C / (Å)	26.854(3)
α / (°)	90
β / (°)	96.451(2)
γ / (°)	90
V / (Å^3)	7881.0(15)
Z	4
D_c / (Mg m^{-3})	1.356
μ[MoKα] (mm^{-1})	0.156
F(000)	3432
Temperature of data collection / (K)	173(2)
Crystal size / (mm)	0.46 × 0.35 × 0.26
Range scanned θ/ (°)	2.04–28.39
Index ranges ±h, ±k, ±l	−26, 26; −20, 19; −35, 35
Φ and ω scan angles / (°)	0.5
Total no. of frames	2494
Crystal to detector distance / (mm)	50.00
Total no. of reflections collected	125785
No. of independent reflections	20368
No. of reflections with I > 2σ(I)	17090
R_{int}	0.0383
No. of refined parameters	1636
No. of least-squares restraints	75
Goodness-of-fit, S	1.019
R_1 [I > 2σ(I)]	0.0770
No. of reflections omitted	34
wR on F^2	0.2129
Weighting scheme parameters	a = 0.144 and b = 7.338
$(\Delta/\sigma)_{mean}$	<0.001
Δρ excursions (eÅ^{-3})	1.30 and −0.98
CCDC no.	898328

Table 1: Integrals of the NMR signals for the protons of solid complex DIMEB·**1** dissolved in $CDCl_3$ used to confirm the complex stoichiometry.

[Theoretical number of protons](DIMEB·**1**)	δ (ppm)	Experimental integration of peaks	Experimental peak integral/theoretical proton number
[7 × H1] (DIMEB)	4.952	9.02	1.3
[7 × H2] (DIMEB)	3.271	8.47	1.2
[3 × CH] (Ar-CH_3, **1**)	2.621	3.00[a]	1

[a]Reference integral.

DIMEB·**1** crystals were identified in the Cambridge Crystallographic Database [15], which necessitated its ab initio structural solution by using direct methods. Density considerations indicated an asymmetric unit containing two complex molecules. In addition, prior to structural solution, a special feature was evident from the X-ray diffraction pattern, namely the general alternation of strong and weak intensities for the reciprocal lattice levels *hkl* with *h* even and odd, respectively. This immediately indicated that the unit cell contents at *x*, *y*, *z* and *x* + 1/2, *y*, *z* are quite similar and that the correct direct-methods solution should be consistent with this prediction.

This pseudo-translational symmetry was indeed a feature of the structural solution and is illustrated in Figure 3, where it relates the two complex units A and B in the crystal asymmetric unit of DIMEB·**1**.

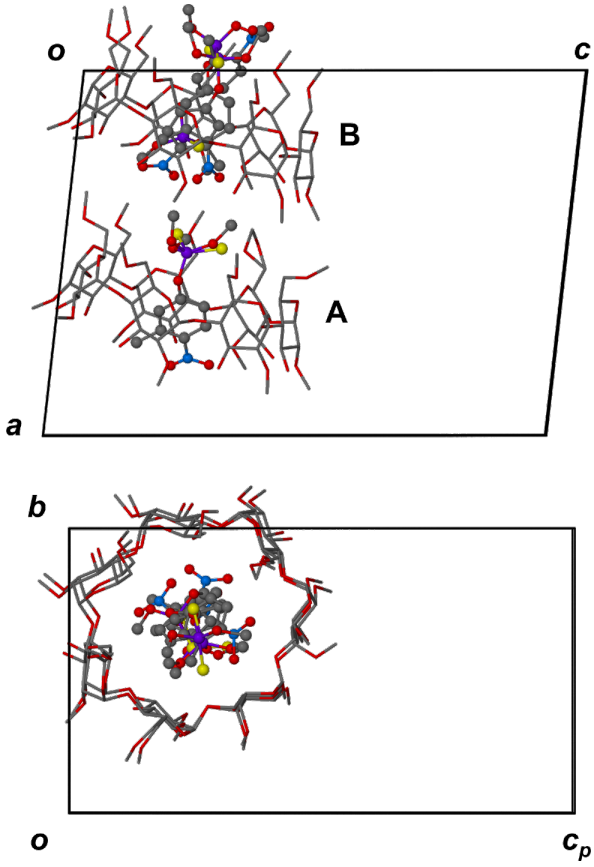

Figure 3: The asymmetric unit in DIMEB•**1** viewed along [010] (top) and [100] (bottom). H atoms are omitted for clarity.

While the gross structures of the independent complex units appear similar, there are obvious differences in the conformations of the two independent host molecules, and in particular, the images of the respective guest molecules are very different, as described further below. This is due to an unusually high level of guest disorder occurring in this complex, despite the low temperature of the data collection. Figure 4 shows the structures and atomic numbering of the two independent host molecule A and B, whose conformational parameters are listed in Table 3.

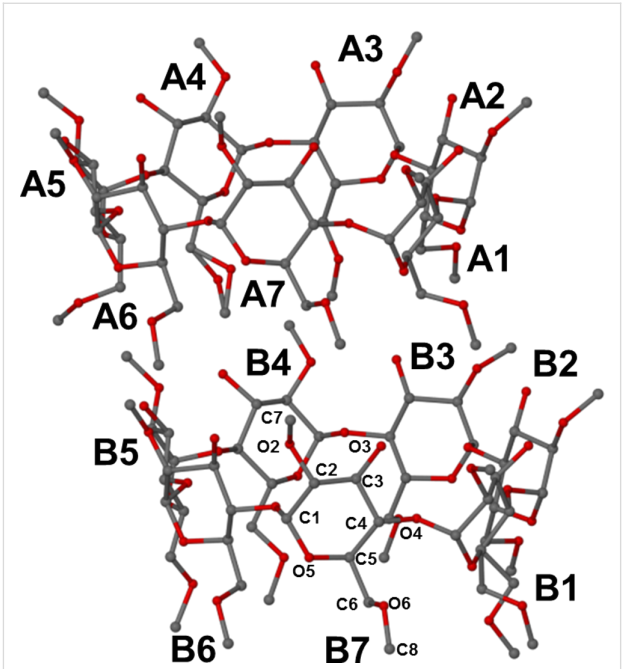

Figure 4: The host molecules in the asymmetric unit of DIMEB·**1** with the labelling of both residues and atoms indicated. H atoms are omitted for clarity.

The parameters in Table 3 that define the host structures include commonly employed descriptors of the O4-heptagon of each cyclodextrin molecule as well as the inclinations of the individual dimethylglucose residues (A1–A7, B1–B7, headed *Res* in Table 3) relative to the mean plane of the O4 atoms. These parameters are defined as follows: ***l***, the distance of each O4 atom from the centroid of the O4-polygon; *D*, the glycosidic O4···O4′ distance; Φ the O4···O4′···O4″ angle; *d*, the O4···O4′···O4″···O4‴ torsion angle; *α*, the deviation of each O4 atom from the O4 mean plane; D_3, the O2···O3′ intramolecular hydrogen bond distance; tilt angle τ_1, the angle between the six atoms of the glucopyranose ring (C1, C2, C3, C4, C5, O5) and the line orthogonal to the O4 mean plane; tilt angle τ_2 between the O4 plane and the mean plane through atoms O4, C4, C1 and O4′ of a given glucose ring.

All the dimethylglucose rings of host molecules A and B adopt the $^4C_1$ chair conformation. On their primary sides, with few exceptions, the values of the torsion angles ω (O5–C5–C6–O6) indicate (−)-*gauche* conformations, with the C6–O6 bonds thus directed away from the centres of the respective cavities. This

Table 3: Conformational parameters of the host molecules.[a]

Res	*l* (Å)	*D* (Å)	Φ (°)	*d* (°)	α (Å)	D_3 (Å)	τ_1 (°)	τ_2 (°)
A1	5.18	4.35	123.6	−11.0	−0.240	2.864	18.5	18.1
A2	4.74	4.51	135.9	0.3	0.122	2.849	14.7	19.7
A3	5.09	4.32	125.2	7.8	0.169	3.049	6.1	6.6
A4	5.20	4.34	125.7	0.4	−0.171	2.831	19.8	19.1
A5	4.97	4.40	128.7	−13.5	−0.134	2.744	15.9	17.0
A6	4.80	4.37	132.3	9.5	0.268	2.715	8.8	12.6
A7	5.11	4.22	126.8	5.5	−0.014	2.954	11.3	12.3
B1	5.31	4.42	121.1	−6.5	−0.078	2.991	15.5	16.5
B2	4.65	4.56	137.7	4.7	0.147	2.925	14.5	17.0
B3	5.03	4.23	127.4	3.3	0.018	2.906	13.9	13.4
B4	5.33	4.32	123.1	−2.6	−0.137	2.841	17.4	17.5
B5	4.97	4.47	129.4	−6.8	0.009	2.796	10.1	11.5
B6	4.72	4.42	134.0	10.7	0.174	2.755	9.9	11.9
B7	5.18	4.16	126.5	−2.5	−0.132	2.887	2.0	4.1

[a]The mean e.s.d.s for α, D_3, τ_1 and τ_2 are 0.003 Å, 0.005 Å, 0.1° and 0.2° respectively.

results in relatively open cavities, contrary to the usual situation in inclusion complexes of the fully methylated host analogue TRIMEB, where the primary methoxy groups typically act as a "lid", sealing that side of the macrocycle. In the DIMEB·**1** complex, there is thus no distinct "boundary" separating the guest molecules within the cavity of host molecule A from those within host molecule B.

The tilt angles (τ_1 and τ_2) are all positive indicating that each ring has its primary side tipped towards the centre of the cavity. The slight ellipticity in the host conformations, reflected in the values of *l, D* and Φ (Table 3) is a compromise between the tendency for "roundness" (induced by the intramolecular O2···O3′ hydrogen bonds with lengths D_3) and slight distortion due to guest inclusion. The O4 mean planes of host molecules A and B are slightly offset from one another but are nearly parallel (interplanar angle 2.65(2)°).

Details of the guest disorder within the host A cavity are illustrated in Figure 5.

Here, a single molecule of fenitrothion occupies the cavity, being present as two rotamers whose phosphorothioate groups are related by a rotation of 126° around the O11–P12 bond. The phosphorothioate group of each disordered component of the guest **1** is located near the primary side of the host molecule.

Instead, within the cavity of host molecule B, as many as three disordered guest components (B, C, E) were observed and modelled, as shown in Figure 6. These disordered components (B, C, E) are shown in green, blue and pink, respectively, in the stereoview of Figure 6.

The major disordered guest components B and C, with respective site-occupancy factors (sofs) 0.44 and 0.29, adopt the same

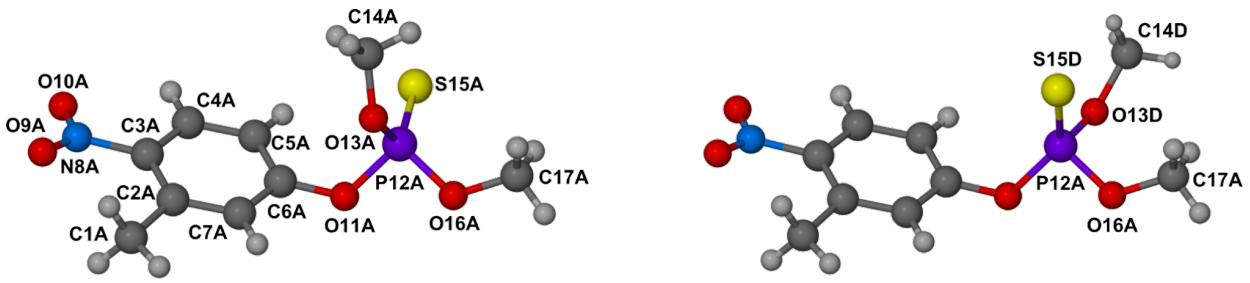

Figure 5: The rotamers of **1** occupying the cavity of host molecule A. Common atoms have labels with suffix A, while in the component on the right the alternative sulfur and methoxy group positions are labelled with suffix D. These disordered guest components (labelled A, D) have site occupancies 0.70 and 0.30, respectively.

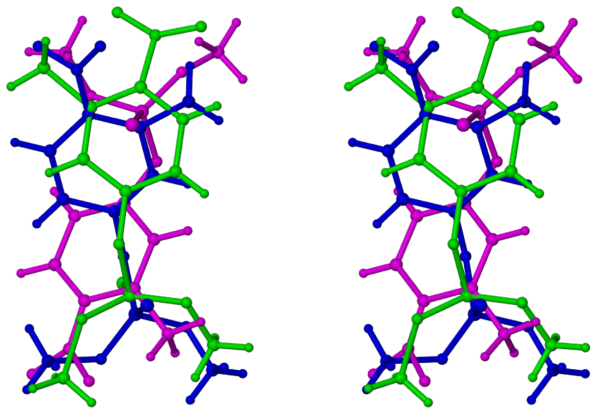

Figure 6: Stereoview of the three disordered guest components that occupy the cavity of host molecule B. Guest components B (green) and C (blue) have similar orientations while component E (pink) adopts the opposite orientation.

orientation, their phosphorothioate groups being located near the primary side of host molecule B (analogous to the situation in host molecule A). However, the third guest component E, with the lowest sof (0.27), adopts the opposite orientation to those of components B and C. This low sof indicates that the guest orientations adopted by the other four disordered components (A–D) is the preferred one in the solid state.

Host molecules A and B have slightly different geometries (e.g., extents of ellipticity), as indicated by the parameters in Table 3. More detailed analysis shows that these differences are attributable to their accommodation of different assemblies of disordered guest components.

An analysis of hydrogen bonding in the crystal of DIMEB·**1** revealed several types of interactions. These can be summarised as follows: (a) For the two independent host molecules A and B, a total of 14 intramolecular H-bonds O2*n*···H–O3(*n*−1) characteristic of the DIMEB molecule (O···O distances in the range 2.715(5)–3.049(5) Å), linking contiguous glucose residues and thus inducing a "round" host conformation (parameter D_3 in Table 3); (b) intramolecular H-bonds C6–H6···O5′/O6′ and C7–H7···O3′, which also contribute to stabilisation of the host conformation; and (c) 10 unique host–host intermolecular C–H···O hydrogen bonds that stabilise the host framework.

All guest molecules are fully encapsulated by the host molecules and there are no close contacts between the disordered guest molecules and host molecules. Figure 7 shows space-filling diagrams that illustrate representative modes of guest inclusion.

Crystal packing is shown in Figure 8. The complex units stack head-to-tail in infinite columns parallel to the *x*-direction.

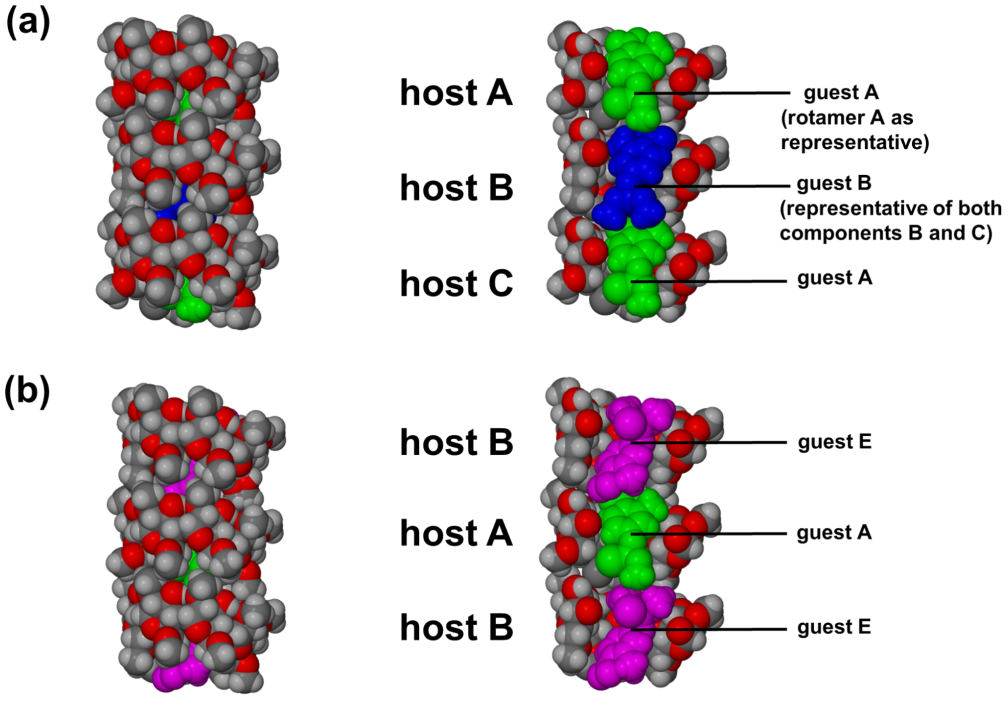

Figure 7: Space-filling diagrams showing the relative orientations of guest molecules within the cavities of the independent DIMEB molecules. Side-views of the complexes and cross-sectional views showing guest molecules (a) A and B, and (b) guest molecules A and E, encapsulated by their respective host molecules.

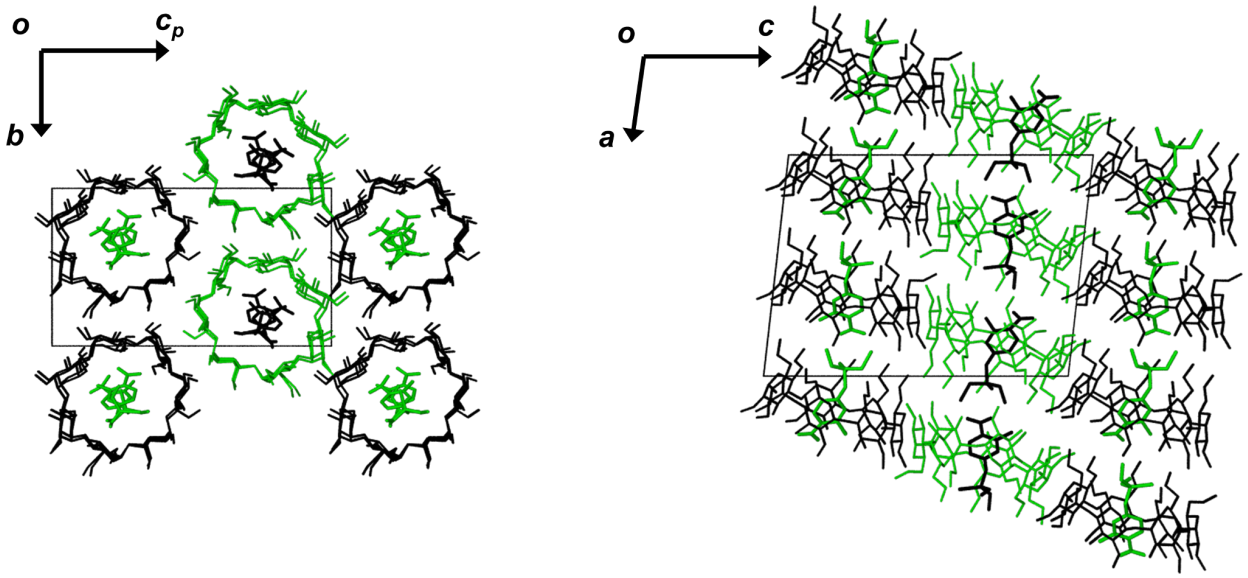

Figure 8: Packing diagrams of the DIMEB·**1** structure, viewed along [100] (left) and [010] (right). The symmetry related molecules are distinguished by the reverse green and black host and guest molecules. For clarity, only guest molecules A and B are shown and the hydrogen atoms have been omitted.

Owing to the twofold screw axis parallel to the *b*-axis, the adjacent columns are antiparallel. The slight ellipticity of the host molecules and the extension of the primary methoxy groups into the interstitial sites assist in the close packing of the complex units.

UV–vis and ICD studies

Spectroscopic methods are frequently used to determine association constants between cyclodextrins and different guests [16]. We attempted to determine the binding constant of **1** with DIMEB by UV–vis spectroscopy; however, when we recorded the spectra of **1** in the presence of DIMEB, only a small hypsochromic shift was noted and the change in absorbance was not large enough for an accurate determination of the binding constant.

The induced circular dichroism (ICD) spectrum of DIMEB and **1** is shown in Figure 9a, where the spectrum recorded for β-CD and TRIMEB with **1** is also shown for comparison.

It can be seen that the native β-CD and DIMEB show a negative and a positive peak (Figure 9a). The negative peaks appear at 320 and 324 nm and the positive ones at 260 and 265 nm for β-CD and DIMEB, respectively. The positive peak in the circular dichroism spectrum is slightly displaced from the maximum of the UV–vis spectrum as was observed in other cases where cyclodextrin was the chiral component [17-20].

The ICD spectrum of fenitrothion in the 200–300 nm wavelength range in the presence of β-CD was reported in the literature [21] and the spectrum shows a negative peak at ≈220 nm and a positive peak at ≈280 nm. This spectrum was measured for a basic solution and in the paper it is not stated what time had elapsed between the preparation of the solution and the running of the spectrum. We suspect that the spectrum reported corresponds to that of the hydrolysis product, namely 3-methyl-4-nitrophenol **2**. We carried out measurement of the ICD spectrum of **2** in a 3% dioxane–water solution, and the spectrum obtained was similar to that reported by Kamiya et al. [21] for fenitrothion (**1**).

It is remarkable that the sign of the peaks in the ICD spectrum of **1** in the presence of TRIMEB is inverted when compared with the spectra of β-CD and DIMEB with **1**. As suggested previously [6,8,22], the change in the sign of an ICD spectrum may indicate extrusion of the guest or a change in orientation of the guest in the cavity.

There are two possible modes of inclusion of the insecticide molecule in the cavity of a CD, either with the phosphorothioate moiety (type A) or with the aromatic moiety (type B) inside the cavity [6]. For most of the esters having an aromatic group it is proposed that this residue is included in the cavity of the CDs. This was suggested for parathion, methyl parathion, and paraoxon [17,21,23]. Theoretical calculation of the ener-

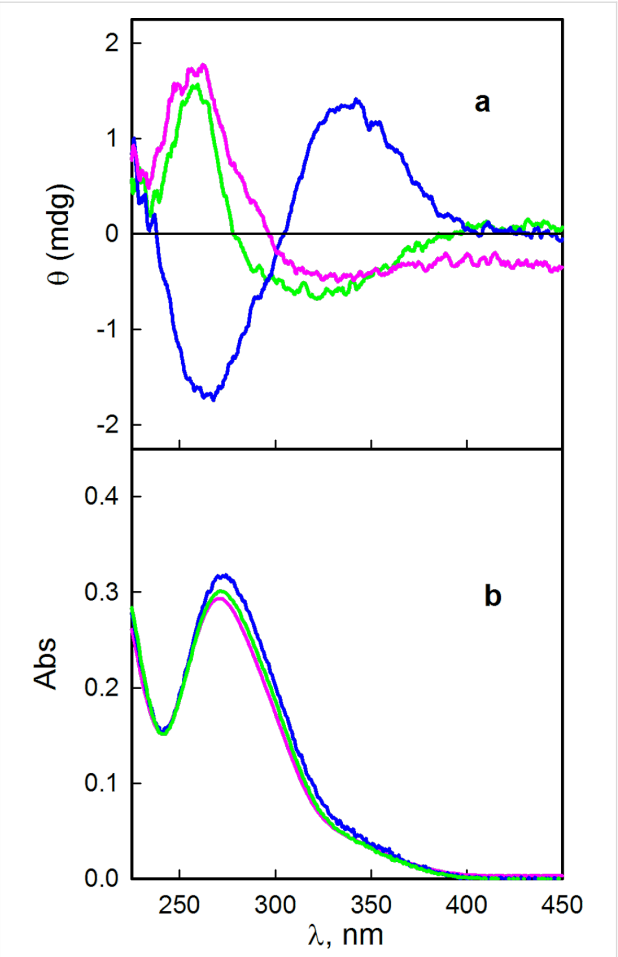

Figure 9: Induced circular dichroism (a) and UV–vis (b) spectra of **1** in the presence of β-CD (10 mM, green), DIMEB (2.5 mM, pink) and TRIMEB (10 mM, blue).

gies of the two types of complexes in the gas phase indicates that there is no significant difference in their values [24]. Single-crystal X-ray analysis shows that for β-CD and TRIMEB, complexes of type A are formed while for DIMEB (see above) in the unit cell a small percentage of the inclusion complexes exhibit the type B orientation.

By comparing the ICD spectra of the three complexes it seems that, in solution, the fenitrothion molecule adopts the same orientation in the β-CD and DIMEB cavities, which is different from that in the complex with TRIMEB. It appears that the presence of OH in the rim of the cavity has an important role in determining the orientation of the included guest molecule.

Based on the fact that the ICD spectra of *p*-nitrophenol and fenitrothion are similar, Kamiya [21] suggested that the inclusion of both compounds should be similar. This is not the case under our reaction conditions; therefore we think that the type A complex is predominant for β-CD and DIMEB.

Kinetic studies

The hydrolysis reaction of fenitrothion takes place with P–O bond fission as shown in Scheme 1 [12] and it was studied in the presence of constant HO^- and variable DIMEB concentrations, as reported previously with other CDs [6].

In Figure 10 a plot of the observed pseudo-first-order rate constants k_{obs} as a function of the concentration of DIMEB is

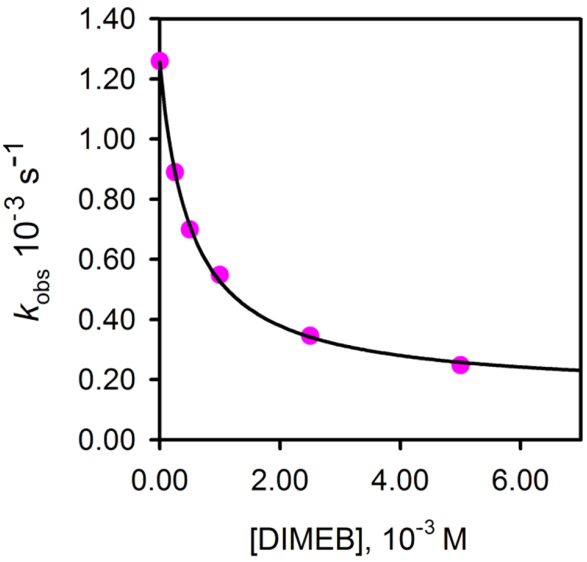

Figure 10: Plot of k_{obs} versus [DIMEB] for the hydrolysis reaction of fenitrothion with HO^- at different concentrations of DIMEB. T = 25 °C, [NaOH] = 0.5 M, ionic strength = 1 M (NaCl). Solvent: water with 2% 1,4-dioxane. The line was drawn by using the data calculated for k_0, k_2 and K_2 in Equation 1.

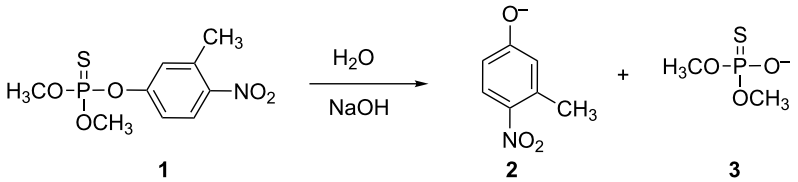

Scheme 1: Reaction of fenitrothion in basic media.

shown. The highest concentration of DIMEB used was 0.005 M. At a cyclodextrin concentration higher than this, precipitation of the DIMEB occurred under the conditions of our studies (ionic strength 1 M, NaOH 0.5 M aqueous solution with 2% 1,4-dioxane). This was confirmed by performing an experiment with DIMEB at a concentration of 0.01 M without the addition of substrate; a day later there was a solid precipitate at the bottom of the flask, which was confirmed by ^{1}H NMR spectroscopy to be DIMEB.

The reaction of **1** with NaOH in the presence of DIMEB may take place as shown in Scheme 2 [7,8], where k_0 and k_2 represent the reactions of the free substrate and of the substrate complexed with ionized cyclodextrin (DIMEB$^-$), respectively [25]. The observed rate constant for Scheme 2 is shown in Equation 1.

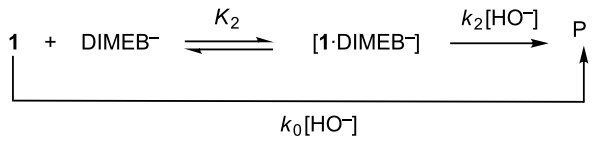

Scheme 2: Mechanism of the hydrolysis reaction of **1** mediated by DIMEB.

$$k_{obs} = \frac{k_0\left[HO^-\right] + k_2K_2\left[HO^-\right]\left[DIMEB\right]}{1 + K_2\left[DIMEB\right]} \qquad (1)$$

The values of the rate and equilibrium constants were obtained by treating the kinetic data as previously published [6] and they are (1.20 ± 0.01) × 10^{-3} s^{-1}, (0.24 ± 0.04) M^{-1} s^{-1} and (1.69 ± 0.09) × 10^3 M^{-1}, for k_0[HO$^-$], k_2K_2[HO$^-$], and K_2, respectively. From these data k_2 = 0.14 × 10^{-3} s^{-1} can be obtained and this is a measure of the rate of the reaction taking place within the DIMEB cavity.

The association constant determined for DIMEB and **1**, viz. (1.69 ± 0.9) × 10^3 M^{-1} is significantly higher than the values previously measured for complexation of **1** with β-CD and TRIMEB, namely 417 and 511 M^{-1} [6]. Furthermore, the inhibition effect as measured by the ratio k_0/k_2 is also significantly higher, namely 7.5, 8.6 and 5.0 for TRIMEB, DIMEB and β-CD, respectively, indicating that DIMEB is more effective in terms of protecting the substrate against the reaction with the nucleophile. The value of K_2 obtained by other authors under similar but not equal reaction conditions is 189 M^{-1} [21]. Part of the discrepancy with our results can be attributed to the different reaction conditions, but we think that the main difference may come from the sample of DIMEB used in each work. It is remarkable that the kinetic data obtained for β-CD are in much better agreement.

The large difference in the inhibitory effect when compared to the native CDs may be due to the methyl groups present on DIMEB and TRIMEB, which elongate the cavity of the CD molecules and provide a slightly larger pocket in which the fenitrothion molecules can situate themselves. Furthermore, the methyl groups have the ability to block the entering hydroxide ions, thereby preventing nucleophilic attack at the phosphorus atom. From the X-ray crystal structures of the CD complexes of fenitrothion with TRIMEB [6] and DIMEB (see above), it is clear that the major components of the fenitrothion molecules have their reactive phosphorothioate moieties positioned at the narrower primary rims of the cyclodextrin cavities. The stronger inhibition of fenitrothion hydrolysis in the presence of DIMEB in comparison with TRIMEB may indicate that the phosphorothioate unit is more protected from nucleophilic attack when it is in the cavity of DIMEB. A DIMEB molecule has a more rounded shape when compared to TRIMEB, due to the intramolecular O2···H–O3' hydrogen bonds that link neighbouring methylglucose residues. As a result, there is more available space in the cavity of a DIMEB molecule than in that of a TRIMEB molecule, and therefore the guest fenitrothion can penetrate further into the cavity.

Conclusion

Single-crystal X-ray analysis of the 1:1 DIMEB fenitrothion inclusion complex revealed that the mode of inclusion of the disordered guest molecules is predominantly of type A (phosphorothioate group near the host primary side). ICD spectra of the DIMEB and β-CD complexes indicated that analogous type A inclusion prevails in solution. The significantly higher association constant reported here for fenitrothion complexation with DIMEB in aqueous solution compared with previous data for its complexation with β-CD and TRIMEB results in more effective protection of the insecticide molecule from hydrolytic degradation.

Kinetic data of the type established in this and previous studies that we have undertaken, give indications of which type of cyclodextrin may be best suited in an agrochemical formulation to ensure resistance of sensitive bioactive compounds to chemical degradation, thus maximising their intended biological effect. Thermodynamic data, such as complex association constants, are also relevant parameters, especially in the context of CD-mediated remedial treatment of soils that are contaminated by persistent pesticides. As regards fenitrothion, a peripheral but important advantage of its inclusion in CDs is the significant reduction in its volatility (and hence toxicity) by conversion of the liquid pesticide into a solid phase.

Experimental

The compounds used in this study were purified as indicated before [6].

Crystal preparation and X-ray diffraction analysis

Fenitrothion (**1**, 20 mg, ~0.072 mmol) was added to a saturated aqueous solution of DIMEB (96 mg, 0.072 mmol) at 20 °C. Continuous stirring for 6 h, as well as several heating and cooling cycles between 20 and 60 °C led to formation of a clear solution, which was then filtered into a clean vial, capped and placed in an oven at 60 °C. Colourless single crystals of the complex DIMEB·**1** appeared over a 24 h period.

Collection of intensity data was performed on a Bruker KAPPA APEX II DUO diffractometer with the crystal cooled in a constant stream of nitrogen vapour (Oxford Cryostream, UK). Upon inspection of the reciprocal lattice layers with the program LAYER [26], the X-ray diffraction pattern revealed Laue symmetry 2/*m*, corresponding to the monoclinic crystal system. The intensity-weighted reciprocal lattice also revealed alternation in intensity of the layer lines perpendicular to *a**, from which it was deduced that the structural motif at *x*, *y*, *z* repeats itself at approximately *x* + ½, *y*, *z*. The space group $P2_1$ was identified from the reflection conditions *hkl*: none; *h*0*l*: none; 0*k*0: *k* = 2*n* (the alternative, centric space group $P2_1/m$ was eliminated since it could not accommodate the chiral cyclodextrin host). Owing to the alternating strong and weak reflections it was possible to deduce the presence of two DIMEB molecules in the asymmetric unit.

As no isostructural DIMEB complex could be found in the literature, the program SHELXD [27] was employed to solve the structure by ab initio direct methods. The initial structural solution (correlation coefficient = 84.9) revealed most of the nonhydrogen host atoms of the two DIMEB molecules and a partial guest molecule in one of the DIMEB host cavities. Before the first refinement in SHELXH-97 [28] the carbon and oxygen atoms of the host were correctly assigned, as were the atoms of the first guest molecule. The remaining host atoms were located in the initial and subsequent difference Fourier maps. The methyl glucose moieties of two independent CD molecules in the asymmetric unit were labelled A1–A7 and B1–B7.

One primary methoxy group per host molecule was disordered over two positions (on glucose residues B1 and A4). In the case of the primary methoxy group on methyl glucose unit B1, all three atoms (C6, O6 and C8) were disordered and the major component refined with a sof of 0.53, while methyl glucose unit A4 contained only atom O6, which was disordered over two positions (sof = 0.69) while C8 was shared. All ordered host atoms were refined anisotropically, except atoms C7A3, C7A7, C8B4 and C8B5, which had reasonable isotropic thermal parameters but unacceptable thermal ellipsoids when refined anisotropically.

The host hydrogen atoms were placed by using a riding model and were refined isotropically with thermal displacement parameters 1.2 times those of their parent atoms. For the hydroxy groups on each methyl glucose unit a hydrogen-bond searching model (AFIX 83) was used to place the hydrogen atoms in geometrically reasonable hydrogen-bonding positions. However, this procedure was not suitable for all the hydroxy groups, and thus, distance restraints were applied between the hydrogen atom of the hydroxy group and the hydrogen-bond-acceptor oxygen atom on the adjacent glucopyranose unit. This was necessary for hydroxy groups on methyl glucose units A4, A5, A6, A7, B6 and B1.

When both host molecules had been located, the first guest molecule that resulted from the initial SHELXD solution was modelled, followed by another in the second crystallographically independent DIMEB molecule. After refinement, the thermal displacement parameters of the guest in host molecule A were reasonable, with the exception of those of the atoms belonging to the *O,O*-dimethyl phosphorothioate moiety. The two disordered guest molecules were found to be rotamers that result from rotation of substituents around the O11–P12 bond. Distance restraints were applied to atoms of the phosphorothioate moiety and an AFIX 66 instruction was applied to the phenyl group, which constrained the ring as a rigid hexagon. The common atoms of the guest molecule were labelled A while the second sulfur and methoxy group were labelled D. The refined values of the sofs of the two rotamers were 0.70 and 0.30. All the ordered atoms of guest molecule A were refined anisotropically, with the exception of atoms O9A, O10A and C17A.

The first disordered guest component molecule modelled in host molecule B had many additional high electron-density peaks surrounding it and the entire molecule had unacceptably high thermal displacement parameters. There was an abnormally large peak situated close to the phenyl ring but it was not in the plane of the phenyl group. Two additional hexagonal rings were discerned in the difference Fourier map, suggesting two other guest-molecule positions. After many attempts at modelling the disorder, three disordered components within host molecule B were evident. The relative population of each was unknown and required an analysis of the initial electron-density peak heights for the phosphorus atoms of each component. Guest components B, C and E had initial phosphorus electron-density peaks

of 4.66, 3.07 and 2.86 eÅ^{-3}, respectively, which resulted in fixed sof values of 0.44, 0.29 and 0.27 being applied to the three disordered components. Owing to the excessive and unusual type of disorder of the guests present in this particular structure, many distance restraints and three AFIX 66 commands were applied to maintain reasonable geometries. Global isotropic thermal displacement parameters were assigned to each component and these refined to values of 0.10, 0.07 and 0.13 Å^2 for guest molecules B, C and E, respectively. The guest hydrogen atoms were placed in idealised positions in a riding model with isotropic thermal displacement parameters in the range 1.2–1.5 times those of their parent atoms.

CCDC 898328 contains the supplementary crystallographic data for this paper. These data can be obtained free of charge at http://www.ccdc.cam.ac.uk/products/csd/request/ [or from the Cambridge Crystallographic Data Centre (CCDC), 12 Union Road, Cambridge CB2 1EZ, UK; fax: +44(0)1223-336033; email: deposit@ccdc.cam.ac.uk].

Thermal analysis

Mass loss on heating the crystals of DIMEB·**1** was measured on a TA-Q500 Thermogravimetric Analyzer, TA instruments, equipped with Universal Analysis 2000 software. The differential scanning calorimetric trace was recorded on a DSC-Q200 calorimeter, TA instruments. For both techniques, a heating rate of 10 K min^{-1} and dry nitrogen purge gas flowing at a rate of 30 mL min^{-1} were employed. Crystals were transferred to an open alumina or aluminium crucible in the case of TG measurements and closed vented aluminium pans for DSC measurements. Sample masses were between 0.5 and 2.0 mg for DSC measurements and between 2 and 8 mg for the TG runs.

Kinetic procedures

The kinetic procedures were described previously [6].

The DIMEB molecule has hydroxy groups that can be deprotonated by hydroxide ions in basic media; therefore, when calculating the NaOH concentration required for preparation of the solutions it is necessary to take this fact into account. Since we did not find values for the pK_a of DIMEB in the literature, we used the pK_a value of β-CD, viz. 12.20 [29,30].

Acknowledgements

This material is based upon work supported by the National Research Foundation under UID 75868. M.R.C. and D.L.C. express their thanks to the NRF and the University of Cape Town for financial assistance.

Financial assistance from CONICET, FONCYT, MINCyT-Córdoba (Argentina) and support from the Universidad Nacional de Córdoba are gratefully acknowledged. This work was carried out as part of a bilateral cooperation project supported by the NRF (South Africa) and MINCyT (Argentina). The assistance of Dr. Gloria Bonetto with the NMR experiments is greatly appreciated. N.M.R. is a grateful recipient of a fellowship from CONICET, and R.V.V., E.I.B. and R.H.deR are members of the research career, CONICET (Argentina).

References

1. Lucas-Abellán, C.; Gabladón-Hernández, J. A.; Penalva, J.; Fortea, M. I.; Nuñez-Delicado, E. *J. Agric. Food Chem.* **2008,** *56,* 8081–8085. doi:10.1021/jf8015046
2. Morillo, E. Application of Cyclodextrins in Agrochemistry. In *Cyclodextrins and their Complexes: Chemistry, Analytical Chemistry, Applications;* Dodziuk, H., Ed.; Wiley-VCH: Weinheim, Germany, 2006; pp 459–466.
3. http://pmep.cce.cornell.edu/profiles/extoxnet/dienochlor-glyphosate/fenitrothion-ext.html. (accessed Aug 16, 2012).
4. http://www.ncbi.nlm.nih.gov/pmc/articles/PMC2395585/ (accessed Aug 16, 2012).
5. Cruickshank, D.; Rougier, N. M.; Vico, R. V.; de Rossi, R. H.; Buján, E. I.; Bourne, S. A.; Caira, M. R. *Carbohydr. Res.* **2010,** *345,* 141–147. doi:10.1016/j.carres.2009.10.023
6. Rougier, N. M.; Cruickshank, D. L.; Vico, R. V.; Bourne, S. A.; Caira, M. R.; Buján, E. I.; de Rossi, R. H. *Carbohydr. Res.* **2011,** *346,* 322–327. doi:10.1016/j.carres.2010.06.016
7. Vico, R. V.; Buján, E. I.; de Rossi, R. H. *J. Phys. Org. Chem.* **2002,** *15,* 858–862. doi:10.1002/poc.560
8. Vico, R. V.; de Rossi, R. H.; Buján, E. I. *J. Phys. Org. Chem.* **2009,** *22,* 691–702. doi:10.1002/poc.1502
9. In later work from our labs (unpublished), we succeeded in measuring the kinetics of the hydrolysis reaction of **1** in the presence of TRIMEA and found that in solution complexes of stoichiometry 1:1 and 1:2 (guest–host) were also formed and the reaction was strongly retarded.
10. Frömming, K.-H.; Szejtli, J. *Cyclodextrins in Pharmacy;* Kluwer Academic Press: Dordrecht, 1994; pp 25–27.
11. Fukuto, T. R.; Hornig, E. O.; Metcalf, R. L. *J. Agric. Food Chem.* **1964,** *12,* 169–171. doi:10.1021/jf60132a020
12. Rougier, N. M.; Vico, R. V.; de Rossi, R. H.; Buján, E. I. *J. Org. Chem.* **2010,** *75,* 3427–3436. doi:10.1021/jo100541y
13. Balakrishnan, V. K.; Han, X.; vanLoon, G. W.; Dust, J. M.; Toullec, J.; Buncel, E. *Langmuir* **2004,** *20,* 6586–6593. doi:10.1021/la049572d
14. Han, X.; Balakrishnan, V. K.; vanLoon, G. W.; Buncel, E. *Langmuir* **2006,** *22,* 9009–9017. doi:10.1021/la060641t
15. *Cambridge Structural Database and Cambridge Structural Database system,* Version 5.32; Cambridge Crystallographic Data Centre, University Chemical Laboratory: Cambridge, England, 2012.
16. Connors, K. A. Binding Constants. *The Measurement of Molecular Complex Stability;* John Wiley & Sons: New York, 1987; pp 139–216.
17. Kawamura, M.; Higashi, M. *J. Inclusion Phenom. Macrocyclic Chem.* **2005,** *51,* 11–15. doi:10.1007/s10847-004-5390-9
18. Shimizu, H.; Kaito, A.; Hatano, M. *Bull. Chem. Soc. Jpn.* **1979,** *52,* 2678–2684. doi:10.1246/bcsj.52.2678
19. Shimizu, H.; Kaito, A.; Hatano, M. *Bull. Chem. Soc. Jpn.* **1981,** *54,* 513–519. doi:10.1246/bcsj.54.513
20. Kamiya, M.; Mitsuhashi, S.; Makino, M.; Yoshioka, H. *J. Phys. Chem.* **1992,** *96,* 95–99. doi:10.1021/j100180a021

21. Kamiya, M.; Nakamura, K. *Pestic. Sci.* **1994,** *41,* 305–309. doi:10.1002/ps.2780410404
22. Hamai, S.; Ikeda, T.; Nakamura, A.; Ikeda, H.; Ueno, A.; Toda, F. *J. Am. Chem. Soc.* **1992,** *114,* 6012–6016. doi:10.1021/ja00041a017
23. Kamiya, M.; Nakamura, K.; Sasaki, C. *Chemosphere* **1995,** *30,* 653–660. doi:10.1016/0045-6535(94)00431-S
24. Coscarello, E. N.; Barbiric, D. A.; Castro, E. A.; Vico, R. V.; Buján, E. I.; de Rossi, R. H. *J. Struct. Chem.* **2009,** *50,* 671–679. doi:10.1007/s10947-009-0103-2
25. Under the condition of our study all the DIMEB present is expected to be ionized.
26. Barbour, L. J. *J. Appl. Crystallogr.* **1999,** *32,* 351–352. doi:10.1107/S0021889898012667
27. Sheldrick, G. M. In *Direct Methods for Solving Macromolecular Structures;* Fortier, S., Ed.; Kluwer Academic Publishers: Dordrecht, 1998; pp 401–411.
28. Sheldrick, G. M. *Acta Crystallogr., Sect. A* **2008,** *64,* 112–122. doi:10.1107/S0108767307043930
29. Gelb, R. I.; Schwartz, L. M.; Bradshaw, J. J.; Laufer, D. A. *Bioorg. Chem.* **1980,** *9,* 299–304. doi:10.1016/0045-2068(80)90039-5
30. Maeztu, R.; Tardajos, G.; González-Gaitano, G. *J. Inclusion Phenom. Macrocyclic Chem.* **2011,** *69,* 361–367. doi:10.1007/s10847-010-9753-0
In this publication the value of the pK_a of β-CD is reported as 12.36, but recalculating all the data using this value does not change the results significantly.

License and Terms

Beilstein Journal of Organic Chemistry

The β-cyclodextrin/benzene complex and its hydrogen bonds – a theoretical study using molecular dynamics, quantum mechanics and COSMO-RS

Jutta Erika Helga Köhler* and Nicole Grczelschak-Mick

Full Research Paper

Open Access

Address:
Wacker Chemie AG, Consortium für elektrochemische Industrie, Zielstattstrasse 20, D-81379 München, Germany

Email:
Jutta Erika Helga Köhler* - jutta.koehler@wacker.com

* Corresponding author

Keywords:
AM1; benzene; COSMO-RS; cyclodextrin; hydrogen bonds; inclusion complex; molecular dynamics; quantum mechanics

Beilstein J. Org. Chem. **2013,** *9,* 118–134.
doi:10.3762/bjoc.9.15

Received: 18 September 2012
Accepted: 12 December 2012
Published: 18 January 2013

This article is part of the Thematic Series "Superstructures with cyclodextrins: Chemistry and applications".

Guest Editor: H. Ritter

Abstract

Four highly ordered hydrogen-bonded models of β-cyclodextrin (β-CD) and its inclusion complex with benzene were investigated by three different theoretical methods: classical quantum mechanics (QM) on AM1 and on the BP/TZVP-DISP3 level of approximation, and thirdly by classical molecular dynamics simulations (MD) at different temperatures (120 K and 273 to 300 K). The hydrogen bonds at the larger O2/O3 rim of empty β-CDs prefer the right-hand orientation, e.g., O3-H···O2-H in the same glucose unit and bifurcated towards ···O4 and O3 of the next glucose unit on the right side. On AM1 level the complex energy was −2.75 kcal mol^{-1} when the benzene molecule was located parallel inside the β-CD cavity and −2.46 kcal mol^{-1} when it was positioned vertically. The AM1 HOMO/LUMO gap of the empty β-CD with about 12 eV is lowered to about 10 eV in the complex, in agreement with data from the literature. AM1 IR spectra displayed a splitting of the O–H frequencies of cyclodextrin upon complex formation. At the BP/TZVP-DISP3 level the parallel and vertical positions from the starting structures converged to a structure where benzene assumes a more oblique position (−20.16 kcal mol^{-1} and −20.22 kcal mol^{-1}, resp.) as was reported in the literature. The character of the COSMO-RS σ-surface of β-CD was much more hydrophobic on its O6 rim than on its O2/O3 side when all hydrogen bonds were arranged in a concerted mode.

This static QM picture of the β-CD/benzene complex at 0 K was extended by MD simulations. At 120 K benzene was mobile but always stayed inside the cavity of β-CD. The trajectories at 273, 280, 290 and 300 K certainly no longer displayed the highly ordered hydrogen bonds of β-CD and benzene occupied many different positions inside the cavity, before it left the β-CD finally at its O2/O3 side.

Introduction

Cyclodextrins (CD) are a family of conical shaped cyclic oligosacharides consisting of 6–8 (or up to 10) glucopyranose units linked by α-(1→4) glycosidic bonds. At the narrower rim of the truncated cone (O6 side) there is one primary hydroxy group per glucose unit whereas at the wider rim there are two secondary hydroxy groups (O2/O3 side) [1]. Cyclodextrins have many possibilities of forming hydrogen bonds [2]: firstly, cyclodextrin monomers form some intramolecular hydrogen bonds or closed rings of hydrogen bonds at both rims of the cone; secondly, they form intermolecular hydrogen bonds with water molecules in aqueous solution or with included guest molecules that fit into their cavity. This fit is extremely specific: the orientation of one and the same guest molecule inside the cyclodextrin cavity may be opposite in solution and in crystalline state, as was found for 4-fluorophenol in α-CD [3]. The reactivity of aromatic guest molecules, radicals or excited states, was found to be altered because of complex formation with cyclodextrins [4].

Cyclodextrins form three types of dimers, O2/O3 to O2/O3, O2/O3 to O6, and O6 to O6. They can also associate to extended stacks in crystalline state or solution, with guest and solvent molecules located inside the cavities, between dimers, or in the channels next to the stacks [5]. The influence of cyclodextrin on a broad variety of molecules was reported: from changes of α-/β-sheet ratio upon complex formation of cyclodextrins with side chains of proteins [6], to size control of the electrostatic self assembly of nanoparticles [7]. Also a pH-controlled release of many cyclodextrins in long stacks on polymers, such as polyrotaxanes, combined with mesoporous silica particles was observed [8].

Complex formation with solvent molecules can take place at the same time in different positions: the crystal structure of heptakis(6-*O*-triisopropylsilyl)-β-CD benzene pyrene solvate is a nice example for competing solvents that intercalate in the cavity of one β-CD (benzene), between β-CD dimers (pyrene), and in channels outside β-CDs (benzene). The β-CD dimers are connected with hydrogen bonds on their O2/O3 sides (Figure 1).

Investigations of such "flat energy hypersurfaces" due to hydrogen bonds and noncovalent interactions demand several theoretical methods to capture the entire network of forces on

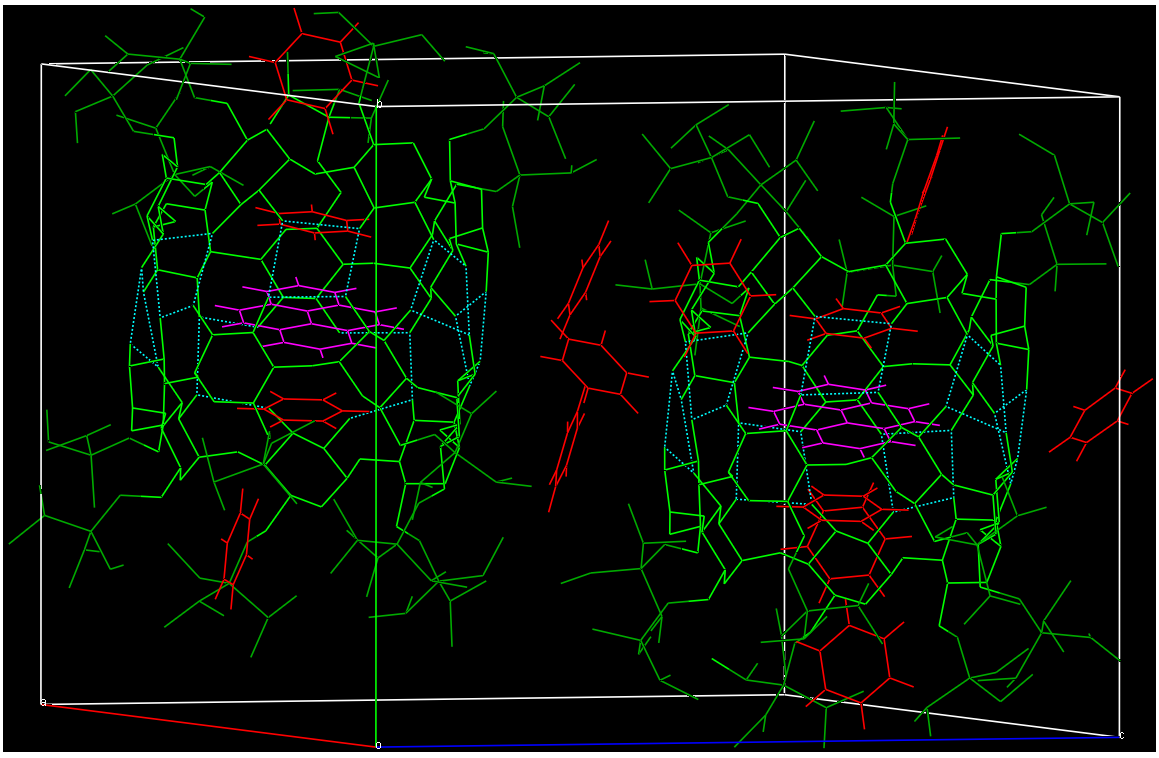

Figure 1: Crystal structure of heptakis(6-*O*-triisopropylsilyl)-β-cyclodextrin benzene pyrene solvate; [$C_{105}H_{210}O_{35}Si_{7,0.5}(C_{16}H_{10})_{,3.5}(C_6H_6)$], taken from The Cambridge Crystallographic Data Centre CCDC [9]. Colour code: benzene: red; pyrene: magenta; cyclodextrin corpus: light green; cyclodextrin side chains: dark green; hydrogen bonds: light blue, dotted lines.

which they rely. Molecular dynamics simulations displayed different hydrogen bond patterns of cyclodextrins in crystal and in solution and confirmed the experimental findings of soluble cyclodextrin complexes of cholesterol type versus precipitates of *cis*/*trans*-cyclohexadecenone//CDs [10-12]. MD with λ-dynamics and calculation of the solvation-free-energy differences was used to distinguish amylose helices from cellulose sheets by analysing the different reactivity of oxygen atoms O2, O3 and O6 of the sugar units with and without methylation, in line with experimental data [13]. Cyclodextrin-complex formation with substituted benzenes shows multiple topologies/configurations (guest up/down) in MD with λ-dynamics [14]. The association constant K_a for α- and β-CD inclusion complexes with several benzene derivatives was investigated by a genetic algorithm [15] and neuronal networks [16]. An overview of quantum mechanical methods to study cyclodextrin chemistry is given in [17]. The COSMO-RS solvation model [18] allows for calculations of several thermodynamic properties [19] once the polarisation charge surface of molecules has been determined by DFT calculations. With the current implementation of COSMO-RS, hydrogen-bond energies are predicted within 0.36 kcal mol^{-1} relative to QM dimer calculations [20].

The necessity to understand the function of cyclodextrins in all details arises from their many applications in industry [21], agriculture, food [22] and health care [23]. Cyclodextrins and their complexes are produced in large industrial processes [24-26]. Our intention for this study was to find a "modular, robust molecular-modelling workflow" for how to analyse the formation of cyclodextrin complexes for many guest molecules in general, before extensive experimental work is carried out. Lemon grass oil [27] or retinol [23] can serve as typical molecular examples of the "practical industrial workbench". To reach reasonable structures of these complexes we need to construct several models because of (a) isomers, (b) *n*:*m* guest/host stoichiometry, (c) preferred cyclodextrin cavity size, etc. We start here with the first step, the empty β-CDs, their subtle but strongly influential hydrogen bonds, and their complex formation with the simplest aromatic molecule of highest symmetry without substituents, i.e., benzene [28].

Methods

While calculating several cyclodextrin complexes with molecular dynamics [29], semi-empirical AM1, classical quantum mechanics [30] and COSMO-RS (Turbomole) [31], we observed that the orientation of all hydrogen bonds of the cyclodextrins already played a crucial role when the initial structures were constructed. It was not sufficient just to take the "normal route" of using the energetically lowest-lying structures from MD trajectories, and then proceed to AM1 and further to QM optimizations; on the contrary, these structures turned out not to be the best ones possible. The best ones in QM finally were those that had hydrogen bonds oriented as symmetrically as possible. Therefore, we started with such manually constructed models and their AM1 optimisations.

Step 1: Our four β-CD models are conformers; all the hydrogen bonds of each rim are oriented in the same direction. We named them BCDO23lO6l, BCDO23rO6l, BCDO23lO6r and BCDO23rO6r, referring to their manually constructed hydrogen-bond orientations when looking either at their O2/O3 or O6 rim (l = left hand, r = right hand orientation) by using GaussView [30]. Each model was optimised until convergence was reached "AM1 (opt=calcall, verytight)" by using the Gaussian9W program [30]. Molecular properties, such as energy, dipole moment, HOMO/LUMO molecular orbitals and IR spectral data, were analysed with GaussView.

Step 2: The four AM1 optimised β-CD models were used as starting structures in our QM calculations by using Turbomole v. 6.4 with COSMO-RS [31]. Two models were calculated for each structure, i.e., the structure in vacuo (.energy files) and the COSMO-RS structure (.cosmo files), the latter being optimised in a dielectric field with the dielectric constant of water (the value of the dielectric constant is a variable in the COSMO-RS program and can be chosen by the user). Up to now it was possible to calculate molecular structures with COSMO-RS on DMOL, BP/SVP or BP/TZVP level of approximation. Our trial to optimise the β-CD complexes with BP/TZVP failed: not always but in several cases, here, for example, the benzene guest was expelled for the BCDbenzeneO23lO6r conformers. Now, however, the current version of Turbomole allows the calculation of more detailed energy hypersurfaces especially for hydrogen bonds (keyword BP-TZVP-DISP3) since Grimme's dispersion corrections for nonbonded interactions were implemented recently [32]. The current release of COSMO-RS C30_1201 allows, for the first time, a more detailed σ-surface to be calculated (BP/TZVPD-FINE), but for the time being as single points (SP) only. COSMO-RS structures are saved in COSMO databanks to perform graphical and thermodynamic analysis with COSMOthermX [19]. In this study we used the BP/TZVP-DISP3 method to calculate the β-CD models, and with this method no benzene molecule was expelled from the β-CD cavity any more.

Step 3: Starting from the neutron diffraction study of β-CD [33] we constructed one model named "BCDcry" of one β-CD by adding hydrogen atoms using the Visualizer of Materials Studio v. 5.5 [29]. Additionally, we used the four empty β-CDs of the in vacuo runs (BP/TZVP optimised .energy files) and the two best structures from the AM1 optimisations, BCDO23rO6l/

benzene parallel and vertical. With Materials Studio molecular dynamics (Forcite plus program and Compass force field) we simulated their trajectories at 300 K. In detail: After force-field geometry optimisations the structures were heated up each from 0 to 3 K, to 100 K, to 200 K, and to 300 K. Finally at 300 K a trajectory of 6000 ps length was calculated using an integration step of 1 fs. From the last 2000 ps of the trajectories the averaged total energy E_{tot} <4000–6000>, averaged hydrogen-bond energy E_{HB} <4000–6000>, and the averaged hydrogen-bond distance and angle were calculated.

Next, the energetically two best optimised AM1 structures (BCDO23rO6l with benzene included in parallel and vertical positions) were used as starting structures and simulated at 300, 290, 280, and 273 K for 500 ps each, and their release of the guest was analysed from these trajectories.

Results and Discussion

AM1 Calculations

The four conformers of empty β-CD

The BCDO23rO6l structure turned out to be the lowest energy conformer, also having the lowest dipole moment of only 0.5618 Debye (dipole-moment components x = 0.0; y = 0.0; $-z$ = 0.5618) pointing from the O6 rim towards the O23 rim of the cone. This structure is so symmetric that all its Mulliken partial atomic charges on all types of oxygen atoms were identical, e.g., equal to each average number (Table 1). Second, with about 6 kcal mol^{-1} above, was conformer BCDO23rO6r. This oval structure has the highest dipole moment of 2.5639 D (x = +0.0268; y = +0.0236; z = −2.5637) and its O6 atomic charges display a range from −0.340 to −0.349 (average −0.344), but all O2 atoms still have the same charge of 0.325, and O3 and O4 oxygen charges vary very little (−0.337 to −0.338 and −0.300 to −0.301, respectively). The third conformer BCDO23lO6l, lying about 7 kcal mol^{-1} above, was again total symmetric as shown by its dipole moment components of x = 0.0; y = 0.0; z = −1.0687 and also with respect to all its oxygen charge values. The fourth conformer, BCDO23lO6r, had the highest energy of about 12.7 kcal mol^{-1} compared to the ground state BCDO23rO6l and the second largest dipole value of 2.4223 D (x = +0.5806; y = −0.0872; z = −2.3501). Its O6 oxygen atoms display a broad range of Mulliken partial charges from −0.338 to −0.360, although their average hardly differs from the average values of the other O6 types (see Table 1); O2 and O3 have small ranges (−0.333 to −0.335 and −0.345 to −0.347) but some differences can be observed in the O4 values, i.e., −0.288 to −0.296. These subtle differences were just given as a few examples here in the text (e.g., they are not given in Table 1) since they may be of importance during guest inclusion or reactivity. The Mulliken partial atomic charges of the benzene molecule in D_{6h} symmetry were C: −0.130 and H: +0.130.

The four conformers of the β-CD complexes with benzene in a parallel or vertical position

All four conformers of the complexes preferred the inclusion of benzene in a parallel position (Table 2). The energetic order of the benzene complexes and their sequence of dipole moments was qualitatively the same as for the empty ones: BCDO23rO6l,

Table 1: AM1 results for the four empty β-CD conformers. AM1 optimised energies [a.u.], relative energies [kcal mol^{-1}], dipole moments [D], LUMO/HOMO energies [a.u.] and gap [eV], and averaged Mulliken partial atomic charges of oxygen atoms. Benzene molecule with D_{6h} symmetry in vacuo. ΔE is the energy of each conformer with respect to the lowest conformer in this table, which is O23rO6l (bold).

AM1 β-CD empty[a]	abs. E [a.u.]	ΔE [kcal mol^{-1}]	μ [D]	LUMO/HOMO [a.u.]; gap [eV]	O2 atomic charge	O3 atomic charge	O4 atomic charge	O6 atomic charge
O23lO6l				+0.06271 −0.38469				
	−2.653658	7.06	1.0687	12.17	−0.335	−0.347	−0.291	−0.348
O23lO6r				+0.06083 −0.38424				
	−2.644708	12.68	2.4223	12.11	−0.334	−0.346	−0.293	−0.346
O23rO6l				**+0.06072** **−0.38650**				
	−2.664914	**0.00**	**0.5618**	**12.17**	**−0.325**	**−0.337**	**−0.297**	**−0.348**
O23rO6r				+0.05835 −0.38786				
	−2.655373	5.99	2.5639	12.14	−0.325	−0.337	−0.301	−0.344
benzene[b]				+0.02039 −0.35474				
	+0.034953		0.0000	10.21				

[a]All four β-CD conformers reached a RMS gradient norm of 0.00000001 [a.u.] in the geometry optimisations.
[b]Benzene reached a RMS gradient norm of 0.00000002 [a.u.].

Table 2: AM1 results for the four β-CD conformers with benzene placed in a parallel or vertical position. AM1 absolute energies, relative energies and dipole moments for the complexes: columns 1–3; for benzene alone: columns 4 and 5.

AM1 β-CD/benzene complex[a]	complex abs. *E* [a.u.]	complex Δ*E* [kcal mol^{-1}]	complex μ [D]	benzene abs. *E* [a.u.]	benzene μ [D]
O23lO6l					
parallel	−2.62313280	7.0374744	0.9544	0.03501077	0.0446
vertical	−2.62266055	7.3338160	0.7084	0.03499769	0.0092
O23lO6r					
parallel	−2.61493920	12.1790404	2.9750	0.03499519	0.0174
vertical	−2.61452474	12.4391182	1.5541	0.03500111	0.0104
O23rO6l					
parallel	**−2.63434772**	**0.00000000**	**0.4399**	**0.03502037**	**0.0543**
vertical	**−2.63388503**	**0.29034260**	**0.1579**	**0.03499812**	**0.0096**
O23rO6r					
parallel	−2.62574636	5.39743941	2.5365	0.03499903	0.0256
vertical	−2.62459809	6.11799032	1.9127	0.03499288	0.0138

[a]All four complexes reached a RMS gradient norm ≤ 3 × 10^{-8} [a.u.] in the geometry optimisations.

BCDO23rO6r, BCDO23lO6l, and BCDO23lO6r. Benzene was slightly distorted in each cavity, as can be seen from its energy and dipole moment inside the complex. Inside the β-CD/benzene complex the benzene neither in a parallel position nor in vertical position adopted an exact central position as displayed in Figure 2.

Our calculated AM1 HOMO/LUMO gaps of empty β-CD conformers, of benzene D_{6h} (Table 1) and the eight complexes (Table 3) are of the same order of magnitude as the values calculated with PM3 in the literature [34] where they found for β-CD 12.44 eV, for benzene 10.15 eV and for the β-CD/benzene complex 10.15 eV. These authors found β-CD/benzene

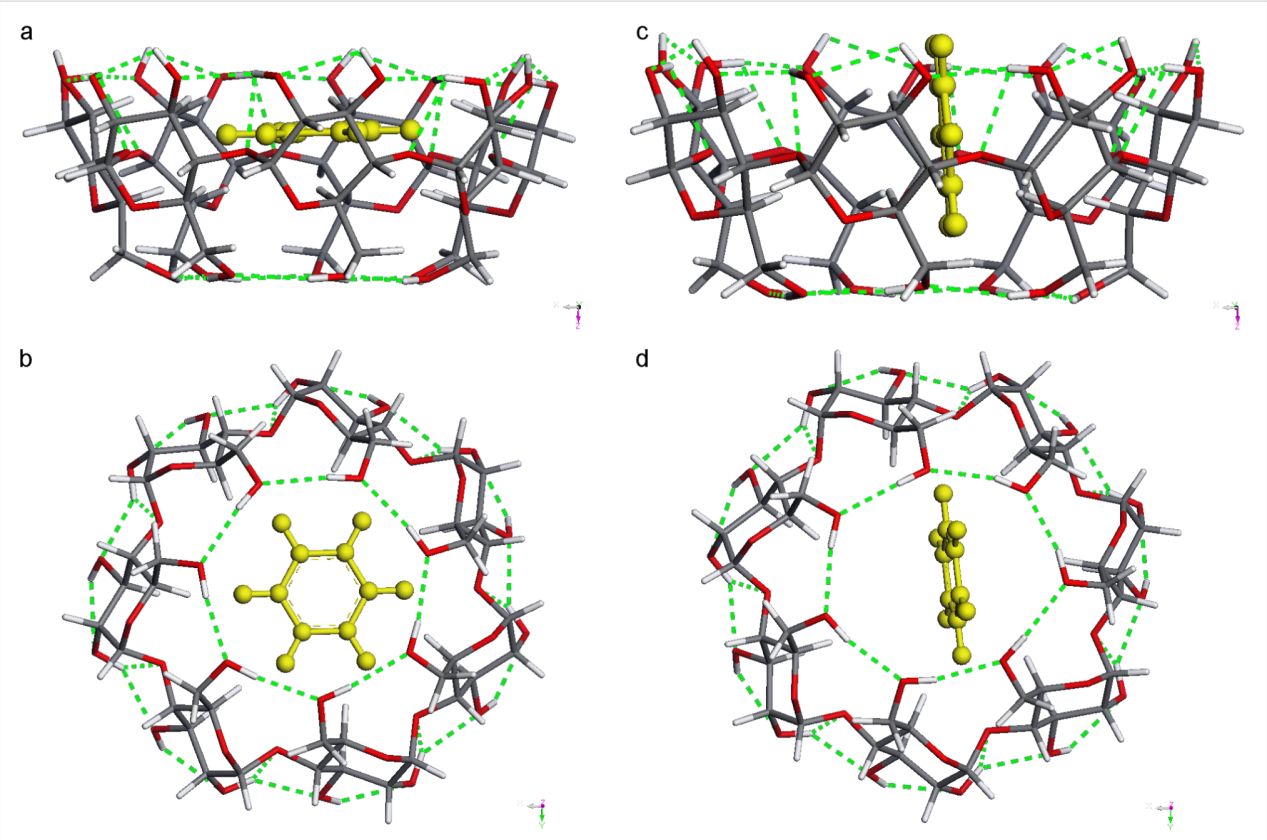

Figure 2: The two AM1-optimised stable conformers of BCDO23rO6l with benzene in a parallel (a and b) and vertical position (c and d). Top view from the O6 side.

Table 3: AM1 results for the four β-CD/benzene complex conformers with benzene placed in a parallel or vertical position. LUMO/HOMO energies and band gaps: columns 1–3. Absolute energies of complex formation $\Delta E_{complexation}$: columns 4,5. Data of column 5 are given in kilojoules per mole (kJ mol^{-1}) for easy comparison to the text above and [34].

AM1 β-CD/benzene complex	HOMO [a.u.]	LUMO [a.u.]	HOMO/LUMO gap [eV]	$\Delta E_{complexation}$ [kcal mol^{-1}]	$\Delta E_{complexation}$ [kJ mol^{-1}]
O23lO6l					
parallel	−0.34409	0.03063	10.196	4.29	17.93
vertical	−0.34163	0.03241	10.178	4.58	19.17
O23lO6r					
parallel	−0.35373	0.02092	10.195	9.43	39.44
vertical	−0.34592	0.02861	10.192	9.69	40.53
O23rO6l					
parallel	**−0.34784**	**0.02688**	**10.197**	**−2.75**	**−11.52**
vertical	**−0.34530**	**0.02866**	**10.176**	**−2.46**	**−10.30**
O23rO6r					
parallel	−0.35776	0.01689	10.195	2.65	11.07
vertical	−0.35353	0.02046	10.177	3.37	14.08

of 1:1 inclusion type in aqueous solution by experimental UV absorption spectra with various concentrations of β-CD. From their UV plots they calculated their stability constants K_s at three temperatures to be 116 L mol^{-1} at 291 K, 86 L mol^{-1} at 298 K and 68 L mol^{-1} at 303 K. According to the equation $\Delta G = -RT \ln K_s$ they obtained the corresponding three free energy values ΔG of −11.5 kJ mol^{-1}, −11.0 kJ mol^{-1} and −10.6 kJ mol^{-1}, indicating rather weak interactions between the guest and host molecule, but still a thermodynamically exothermic reaction of complex formation.

Here, our best conformer, BCDbenzeneparallelO23rO6l, displays an energy of complex formation

$$\Delta E_{\text{complexation}} = E_{\text{complex}} - E_{\text{BCDempty}} - E_{\text{benz}D_{6h}} \quad (1)$$

of −2.75 kcal mol^{-1} (Table 3), followed by the complex conformer BCDbenzeneverticalO23rO6l with −2.46 kcal mol^{-1}. This is in very good agreement with the experimental value from [34]. All our other complex conformers have positive $\Delta E_{complexation}$ values, up to BCDbenzeneverticalO23lO6r with +9.69 kcal mol^{-1}, and thus are endothermic, Table 3.

IR spectra of empty β-CD conformers and their inclusion complexes

The most important lines of the calculated AM1 IR spectra are given in Table 4. The IR bands of benzene at 744, 1145, 1579 and 3194 cm^{-1} were characteristically shifted in the parallel versus the vertical complex. Especially the 3194 cm^{-1} H–C benzene stretch was split into a range from 3150 to 3199 cm^{-1}. Very interesting and easy to see was the concerted movement of all hydrogen bonds at the O23 and O6 rim: the empty β-CD's

Table 4: AM1 results for benzene and the two stable O23rO6l β-CD conformers with benzene placed in a parallel or vertical position. All IR bands [cm^{-1}] and relative intensities are listed for benzene; in the case of β-CD, single bands are included only if their relative intensity is >200 or for "very close frequency clusters" (bold)[a].

AM1 IR freq. [cm^{-1}]	rel. intensity benzene D_{6h} sym.	rel. intensity β-CD O23rO6l empty	rel. Intensity β-CD O23rO6l parallel	rel. Intensity β-CD O23rO6l vertical	comment
443					H(O6) up/d
444		729		713	H(O6) up/d
445			741		H(O6) up/d
511				276	H(O2) up/d
513		2 × 346	286		H(O2) up/d
514				240	H(O2) up/d
516			335	230	H(O2) up/d

Table 4: AM1 results for benzene and the two stable O23rO6l β-CD conformers with benzene placed in a parallel or vertical position. All IR bands [cm^{-1}] and relative intensities are listed for benzene; in the case of β-CD, single bands are included only if their relative intensity is >200 or for "very close frequency clusters" (bold)[a]. (continued)

744	127				H–C up/d
757				122	H–C up/d
760			73		H–C up/d
1145	2 x 1.08				H–C in plane
1148				1.32	H–C in plane
1150			1.74		H–C in plane
1150			1.51		H–C in plane
1152				0.54	H–C in plane
1346				344	O4 and O5
1347		471	491		O4 and O5
1347		471	355		O4 and O5
1348				291	O4 and O5
1351		2 × 285			C-O6 frame
1356–1357			**534(3)**[a]		C-frame
1357		2 × 312			C-frame
1357–1358				**562(3)**[a]	C-frame
1418		346		338	H–C up/d
1419			339		H–C up/d
1577				14	C=C
1578			15		C=C
1579	2 × 12		15	10	C=C
3150				16	H–C benz.
3158				22	H–C benz.
3165				91	H–C benz.
3170				35	H–C benz.
3171			107		H–C benz.
3175	2 × 88		75		H–C benz.
3186			12		H–C benz.
3189				20	H–C benz.
3194					H–C benz.
3199				17	H–C benz.
3414–3421				**879(7)**[a]	H–O2 stretch
3418–3421			**861(7)**[a]		H–O2 stretch
3419		2 × 425			H–O2 stretch
3447–3455				**733(5)**[a]	H–O6 stretch
3449–3451			**1004(7)**[a]		H–O6 stretch
3453		2 × 536			H–O6 stretch
3455–3456			**563(7)**[a]		H–O3 stretch
3457		**532(3)**[a]			H–O3 stretch
3456–3461				**832(9)**[a]	H–O6/H–O3 stretch

[a]Sum of (*n*) intensities within the given frequency range for a cluster of the same type (bold).

H–O2 stretch at 3419 cm^{-1} was spread out to a range from 3414 to 3421 cm^{-1}, the H–O6 stretch at 3453 cm^{-1} was spread out from 3447 to 3453 cm^{-1}, and the β-CD's H–O3 stretch at 3457 cm^{-1} from 3455 to 3456 cm^{-1} as a result of the interaction with the guest molecule. In general, the shifts were subtle; it seemed that the benzene itself was influenced very little if at all, the cyclodextrin on the contrary was substantially influenced in its frame vibrations over a wider range, its splitting most probably being caused by the "rigid benzene wheel" it had included, see Figure 3. Interestingly, the concerted hydrogen-bond movements at the rims of β-CD rims were easily identified, for example in the BCDbenzeneparallelO23rO6l complex. Here, at 445 cm^{-1}, all hydrogen atoms bound to O6 atoms concertedly moved up and down the almost perfect plane of O6 oxygen atoms (marked H(O6) up/d in Table 4).

Since our two stable β-CD/benzene complex conformers (parallel and vertical) were energetically close neighbours with

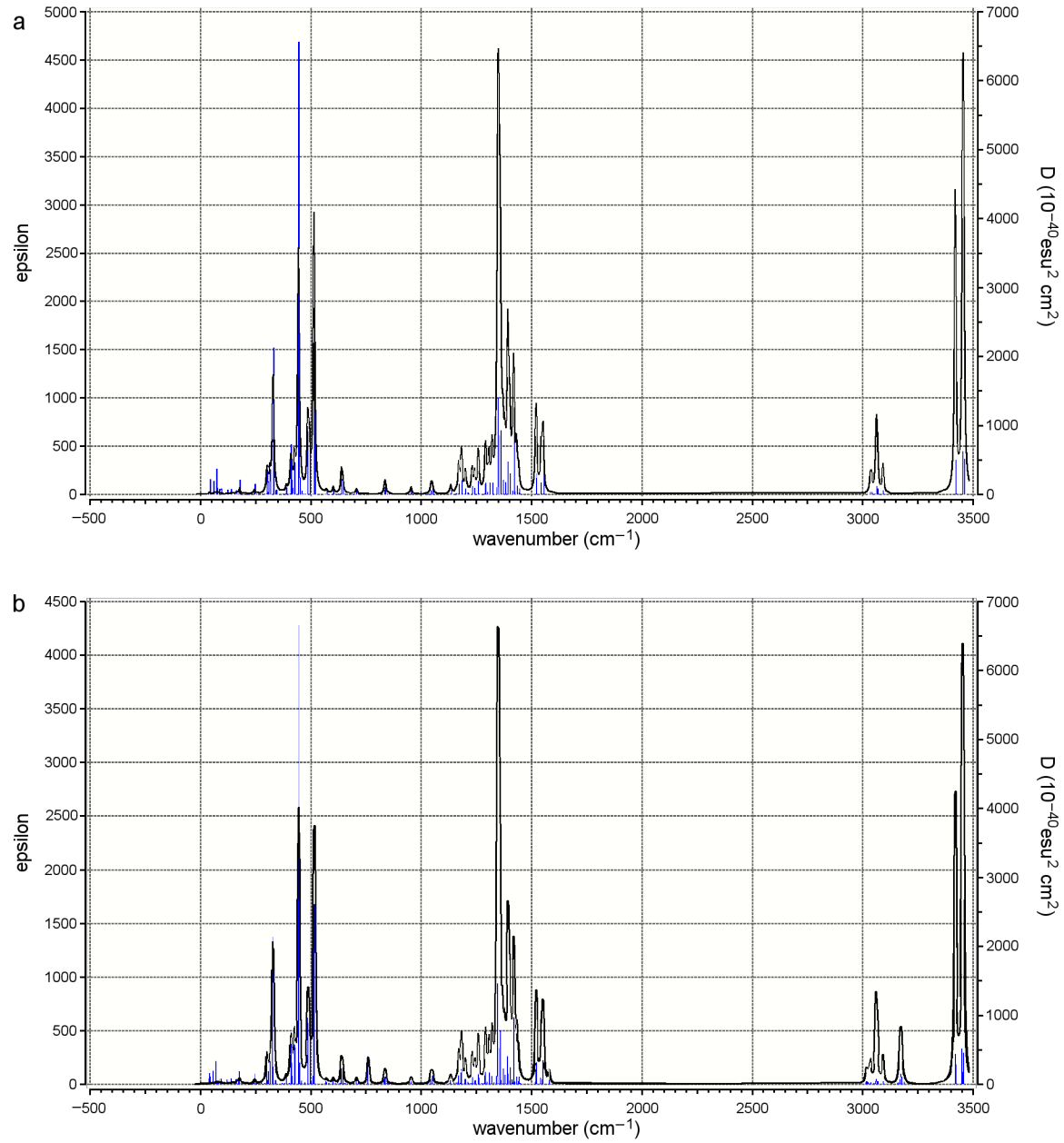

Figure 3: (a) AM1 calculated IR spectra of BCDO23rO6l empty and (b) the BCDO23rO6l/benzene inclusion complex with benzene in a parallel orientation.

only 0.29 kcal mol^{-1} energy difference calculated at 0 K, the experimental spectrum at room temperature should display all cyclodextrin absorptions, i.e., both our conformers exist at the same time.

Summarised result of the AM1 calculations

AM1 energy/geometry optimisations in vacuo at 0 K showed that the β-CD/benzene complex with all hydrogen bonds at the O2/O3 rim in a right-hand orientation and at the narrower O6 rim in a left-hand orientation can include benzene in a parallel (best energy) or vertical position (higher in energy by only 0.29 kcal mol^{-1}); both conformers were thermodynamically allowed. The HOMO/LUMO gap of the empty β-CD with about 12 eV was lowered to about 10 eV in the complex. The β-CD/benzene inclusion complex was formed only by weak noncovalent interactions, which influence the IR lines of the β-CD most at its frame frequencies and at highly ordered concerted movements of its hydrogen bonds. The IR frequencies of benzene were influenced only marginally upon inclusion.

COSMO-RS calculations with Turbomole

Quantum mechanical geometry/energy optimisations

For the four empty β-CD models, for benzene in D_{6h} geometry, and for all eight BCD/benzene complexes, quantum mechanical geometry/energy optimisations with Turbomole and the implemented COSMO-RS method were performed at 0 K. For all starting structures the AM1 optimised geometries were used, and the results are given in Table 5 for the calculations in vacuo, and in Table 6 for the calculations in the COSMO-RS dielectric field of water (no explicit water molecules, but instead dipoles that model the dielectric field of the solvent are used by this method [18]).

The empty BCDO23rO6l model is still the lowest energy conformer among the four in vacuo (Table 5), but now the BCDO23lO6l is second and energetically close (0.26 kcal mol^{-1}), followed by BCDO23rO6r with 2.17 kcal mol^{-1} and BCDO23lO6r with 2.3 kcal mol^{-1} higher. In aquo (Table 6) the empty hydrogen bond model BCDO23rO6l was again the most preferred (Figure 4).

Although all optimisations were started from the AM1-optimised parallel and vertical geometries (from which the naming stems), the BP/TZVP-DISP3 method with its enhanced description of dispersion forces led in general to structures in which the benzene molecule adopts a more oblique position [14,20,32]. The whole energy hypersurface of β-CD complexes is rather flat, and therefore it is difficult to identify the many local minima [17]. Therefore, geometry optimisations of β-CD complexes still remain a multiple-minimum problem in general. The COSMO-RS method combines these identified multiple-minima structures as a set of conformers in a databank (which is updated principally when new minima are identified by more sensitive theoretical methods). From these sets the thermodynamic properties of the material at various temperatures can be calculated (by analytical formulas with COSMOthermX) more realistically than for one structure only [18-20]. Molecules adopt many conformers at temperatures higher than 0 K, which will be shown for the β-CD/benzene complex by MD simulations in the next section. The energetically best structure of the BCD/benzene complex in vacuo due to the BP/TZVP-DISP3 method resulted from the BCDO23rO6l/benzenevertical starting structure. The AM1 favourite BCDO23rO6l/benzeneparallel model followed second with 0.06 kcal mol^{-1} above, and the others were higher up to a maximum of 2.34 kcal mol^{-1} (BCDO23lO6r/benzeneparallel), Table 5. All optimised BP/

Table 5: Optimised BP/TZVP-DISP3 energies in vacuo. Lowest energy conformer of each group in bold.

BP/TZVP-DISP3 in vacuo	$E_{abs.}$ [a.u.]	$E_{rel.}$ [a.u.]	$E_{rel.}$ [kcal mol^{-1}]
BCDO23lO6l	−4277.4641711793	0.0004226810	0.2652365729
BCDO23lO6r	−4277.4609298546	0.0036640057	2.2992002354
BCDO23rO6l	**−4277.4645938603**	**0.0000000000**	**0.0000000000**
BCDO23rO6r	−4277.4611238596	0.0034700007	2.1774601643
Benzene	−232.3358156576	0.0071740456	4.5017853670
parallelO23lO6l	−4509.8320598074	0.0005758687	0.3613633618
parallelO23lO6r	−4509.8289075499	0.0037281263	2.3394365033
parallelO23rO6l	−4509.8325394613	0.0000962148	0.0603757489
parallelO23rO6r	−4509.8291543743	0.0034813018	2.1845516926
verticalO23lO6l	−4509.8321043279	0.0005313482	0.3334263276
verticalO23lO6r	−4509.8289158257	0.0037198504	2.3342433180
verticalO23rO6l	**−4509.8326356761**	**0.0000000000**	**0.0000000000**
verticalO23rO6r	−4509.8291521426	0.0034835335	2.1859520815

Table 6: Optimised BP/TZVP-DISP3 COSMO-RS energies in aquo. Lowest energy conformer of each group in bold.

BP/TZVP-DISP3 in aquo	$E_{abs.}$ [a.u.]	$E_{rel.}$ [a.u.]	$E_{rel.}$ [kcal mol^{-1}]
BCDO23lO6l	−4277.5397933200	0.0044818408	2.8123999202
BCDO23lO6r	−4277.5390925770	0.0051825838	3.2521231603
BCDO23rO6l	**−4277.5442751608**	**0.0000000000**	**0.0000000000**
BCDO23rO6r	−4277.5432219210	0.0010532398	0.6609185069
Benzene	−232.3408624099	0.0021272933	1.3348978187
parallelO23lO6l	−4509.9064609135	0.0041674010	2.6150858014
parallelO23lO6r	−4509.9056675976	0.0049607169	3.1128994621
parallelO23rO6l	**−4509.9106283145**	**0.0000000000**	**0.0000000000**
parallelO23rO6r	−4509.9096646704	0.0009636441	0.6046963092
verticalO23lO6l	−4509.9004752425	0.0101530720	6.3711542109
verticalO23lO6r	−4509.9055329919	0.0050953226	3.1973658847
verticalO23rO6l	−4509.9106053475	0.0000229670	0.0144120224
verticalO23rO6r	−4509.9095882112	0.0010401033	0.6526752221

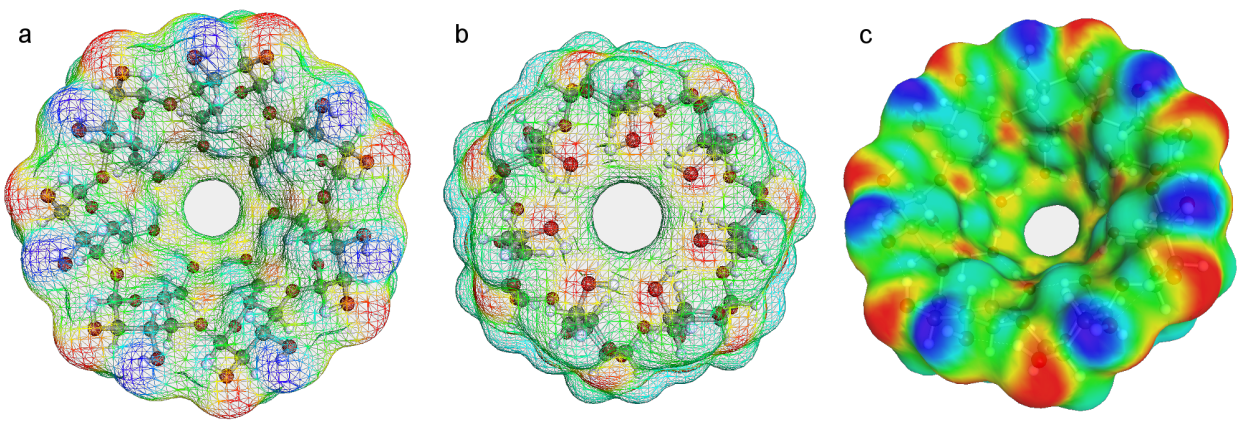

Figure 4: The lowest energy empty conformer BCDO23rO6l, COSMO-RS structure optimised with BP/TZVP-DISP3 (solvent = water), σ-surface with charge code: oxygen red, hydrogen blue, hydrophobic area yellow and green. View a: from O2/O3 side, view b: from O6 side, view c: from O2/O3 side.

TZVP-DISP3 COSMO-RS energies in aquo were lower than the corresponding ones in vacuo, which is reasonable (Table 6). Here the BCDO23rO6l hydrogen-bond starting models remained the best ones after energy/geometry minimisations, for the empty β-CD and for the complex as well.

The BP/TZVP-DISP3 energies of complex formation were calculated from the data of Table 5 and Table 6 by Equation 1 and are shown in Table 7. All energies of complex formation $\Delta E_{Complexation}$ in vacuo and in aquo were negative, indicating that the complexes will be formed. The complex structures of the reactions with the lowest energies were BCDO23rO6l/benzeneparallel in aquo and BCDO23rO6l/benzenevertical in vacuo.

Figure 4a–c and Figure 5a–c display different views of the best BCDO23rO6l empty model and the BCDO23rO6l/benzene complex with their COSMO-RS σ-surfaces. Hydrophilic areas are coloured in red (negative charge of oxygen atoms) or blue (positive charge of hydrogen atoms), which were mostly located at the O23 rim. Hydrophobic areas (coloured green/yellow) can be observed easily inside the BCDO23rO6l empty model (caused by its O6 highly ordered hydrogen-bond rim) and the whole surface of benzene while sitting inside the cyclodextrin cavity.

Consequences for thermodynamic analysis

The basis of thermodynamic analysis with COSMOthermX [18-20] is the so called σ-profiles and σ-potentials of each molecule,

Table 7: BP/TZVP-DISP3 energies of complex formation in vacuo and in aquo, calculated with the absolute data of BCDO23rO6l for $E_{BCDempty}$. Relative $\Delta E_{Complexation}$ with respect to the energetically lowest complex conformer, column 2 and column 4.

BP/TZVP-DISP3	abs. $\Delta E_{Complexation}$ in vacuo [kcal mol^{-1}]	rel. $\Delta E_{Complexation}$ in vacuo [kcal mol^{-1}]	abs. $\Delta E_{Complexation}$ in aquo [kcal mol^{-1}]	rel. $\Delta E_{Complexation}$ in aquo [kcal mol^{-1}]
parallelO23lO6l	−19.861	0.361	−13.381	2.615
parallelO23lO6r	−17.883	2.339	−12.883	3.113
parallelO23rO6l	−20.162	0.060	**−15.996**	**0.000**
parallelO23rO6r	−18.038	2.184	−15.391	0.605
verticalO23lO6l	−19.889	0.333	−9.625	6.371
verticalO23lO6r	−17.888	2.334	−12.798	3.198
verticalO23rO6l	**−20.222**	**0.000**	−15.981	0.015
verticalO23rO6r	−18.036	2.186	−15.343	0.653

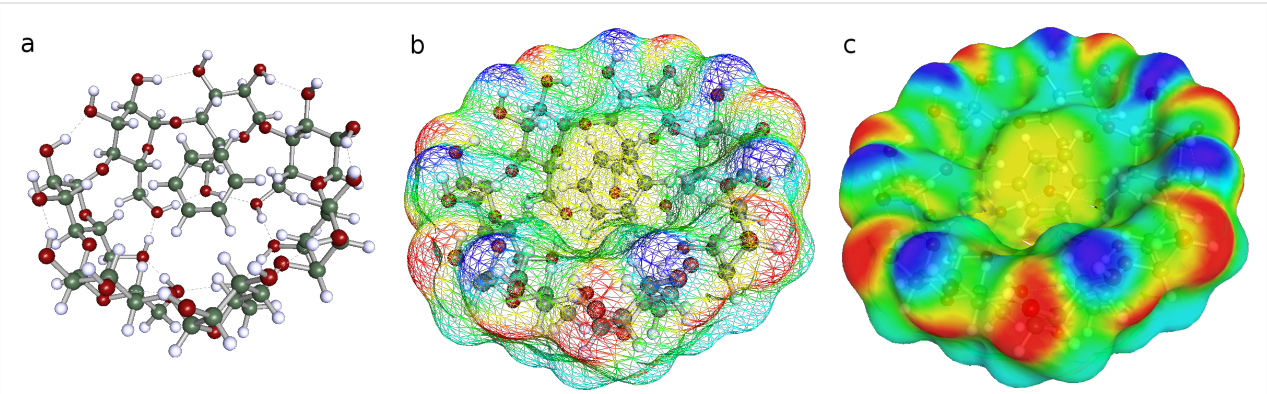

Figure 5: The lowest energy complex conformer BCDO23rO6l/benzene; benzene occupies an oblique position inside the cavity. COSMO-RS structure optimised with BP/TZVP-DISP3 (solvent = water), a: no surface, b,c: σ-surface with charge code: oxygen red, hydrogen blue, hydrophobic area yellow and green. All views from O2/O3 side.

which show the characteristic differences in the electrostatic molecular surfaces that are calculated quantum mechanically at 0 K for molecular conformers of up to 10 kcal mol^{-1} in the standard COSMO databases. These σ-profiles and σ-potentials were calculated with COSMOthermX for the empty β-CD models and are displayed in Figure 6 and Figure 7. Especially the σ-potentials (Figure 7) showed that the empty β-CD models were split into two groups. One group had the two hydrogen-bond models with all hydrogen bonds in the left-hand orientation (O23l), the other one with the two models with right-hand (O23r) orientation. This mirrored quantitatively the result of how much the two energetically preferred O23r models were closer to each other and were most different from the two O23l models, regardless of which orientation the hydrogen bonds had at the O6 rim. By the time these four empty β-CD models have been combined into one set of β-CD conformers and stored like this in the COSMO database, thermodynamic analysis with COSMOthermX will take into account these differences and give more accurate results for many material properties over a wider temperature range than with simple "one-molecule sets" [18-20].

Summarised result of the COSMO-RS calculations

In aquo the hydrogen-bond model BCDO23rO6l was again the most preferred, not only among the empty β-CD conformers but also as the BCDO23rO6l/benzene parallel complex model. According to the quantum mechanical COSMO-RS calculations, all empty β-CD and all complex conformers of β-CD/benzene were thermodynamically allowed, i.e., the complexes should be formed. The highest relative energy of all conformers was less than 2.4 kcal/mol^{-1} in vacuo and less than 6.4 kcal mol^{-1} in aquo. The benzene molecule adopted an oblique position in the inclusion complex. The σ-surface of the empty β-CD "looked" more hydrophilic from the outside at its O2/O3 side (red and blue) than from the O6 side (only red and yellow/green). From the inside, the O6 rim of β-CD "looked" hydrophobic.

Molecular-dynamics simulations

The empty cyclodextrin at 300 K

The "highly ordered hydrogen bonds" of the BCDO23lO6l, BCDO23rO6l, BCDO23lO6r and BCDO23rO6r models cannot be observed at 300 K where the temperature is high enough to

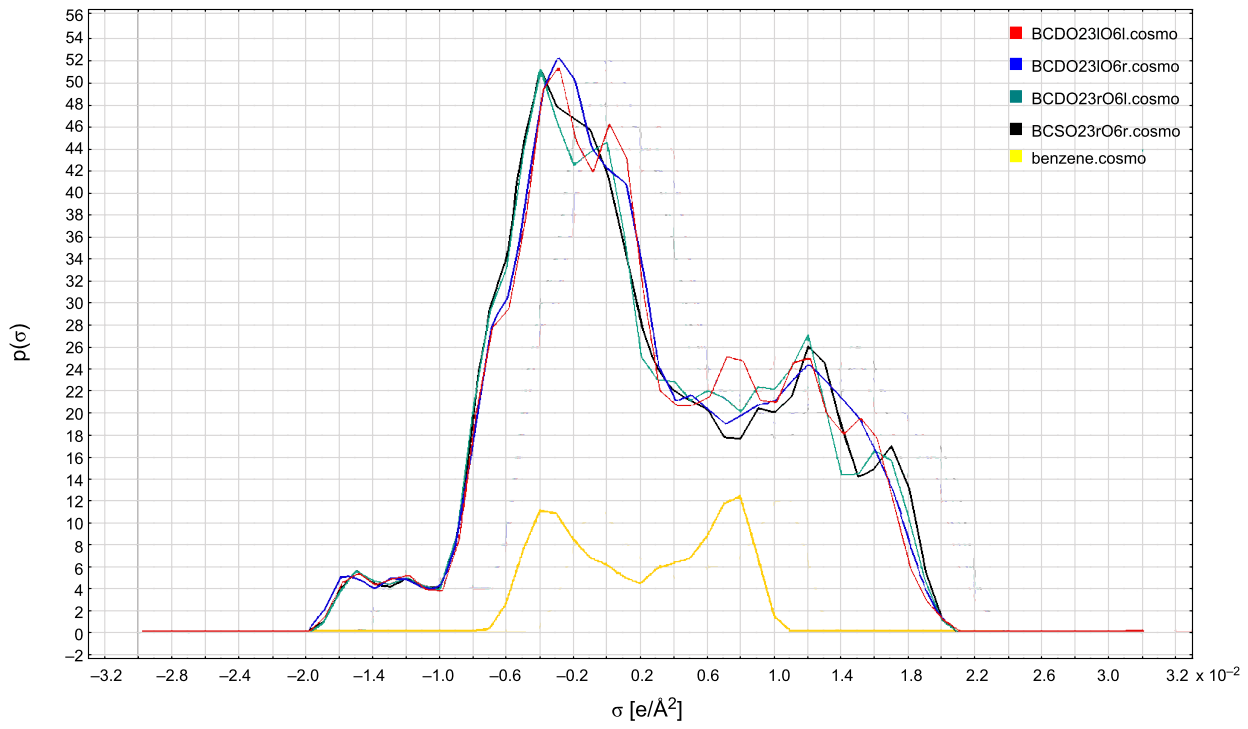

Figure 6: σ-Profiles of the COSMO-RS method for the four empty β-CD models and benzene (BP/TZVP-DISP3 method).

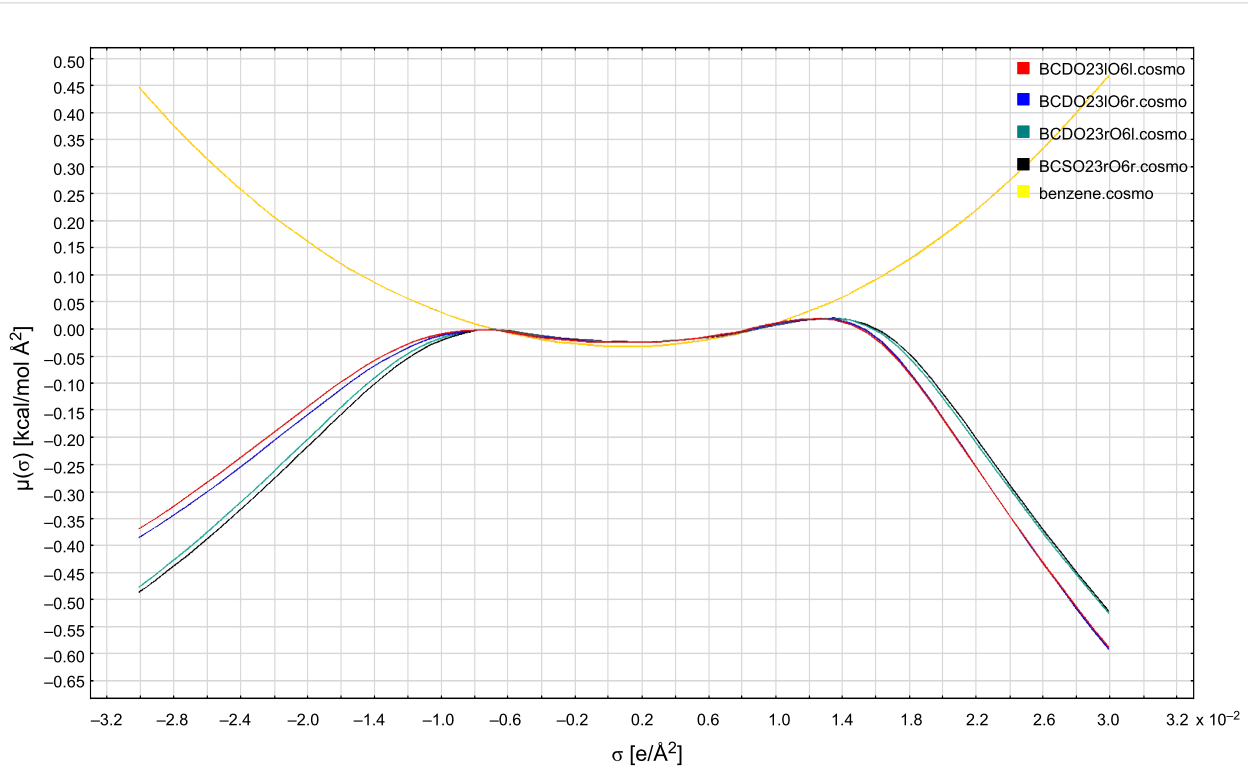

Figure 7: σ-Potentials of the COSMO-RS method for the four empty β-CD models and benzene (BP/TZVP-DISP3 method).

make the β-CDs flexible and the energy barriers of hydrogen bonds are overcome. As was observed in the neutron diffraction studies of β-CDs at 300 K [33] and 120 K [35] the temperature determined the hydrogen-bond distribution. In the MD simulations started from the "highly ordered" 0 K AM1 models the hydrogen bonds switched to more disordered arrangements. For comparison the crystal structure model of 300 K was added. The starting structures and the energetically best frame from the last 2000 ps of the 6000 ps trajectories are displayed in Figure 8, Figure 9 and Figure 10. Only the two energetically best models are shown: BCDO23rO6l and BCDO23rO6r. The Compass-E_{tot} energy of BCDcry was higher in the starting structure than in the best frame of the trajectory at 300 K, which accounts for the number of packing forces in the crystal that deformed the cyclodextrin monomer in vacuo. For the two other models BCDO23rO6l and BCDO23rO6r this was reversed;

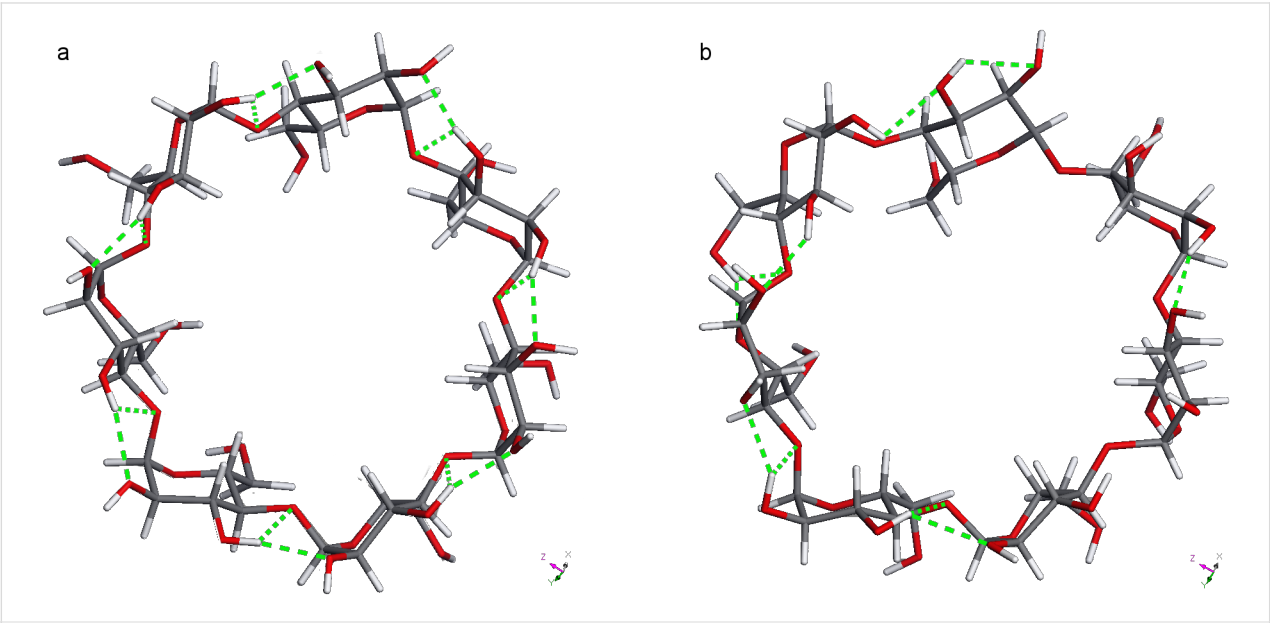

Figure 8: a: BCDcry (MD starting structure with Compass-E_{tot} = 389.99 kcal mol^{-1} and 14 hydrogen bonds with averaged Dreiding-E_{HB} = −3.04 kcal mol^{-1} => −42.56 kcal mol^{-1}) and b: BCDcry fr1662 (best frame from the last 2000 ps of the analysed MD-trajectory with Compass-E_{tot} = 308.01 kcal mol^{-1} and 11 hydrogen bonds with averaged Dreiding-E_{HB} = −0.93 kcal mol^{-1} => −10.23 kcal mol^{-1}).

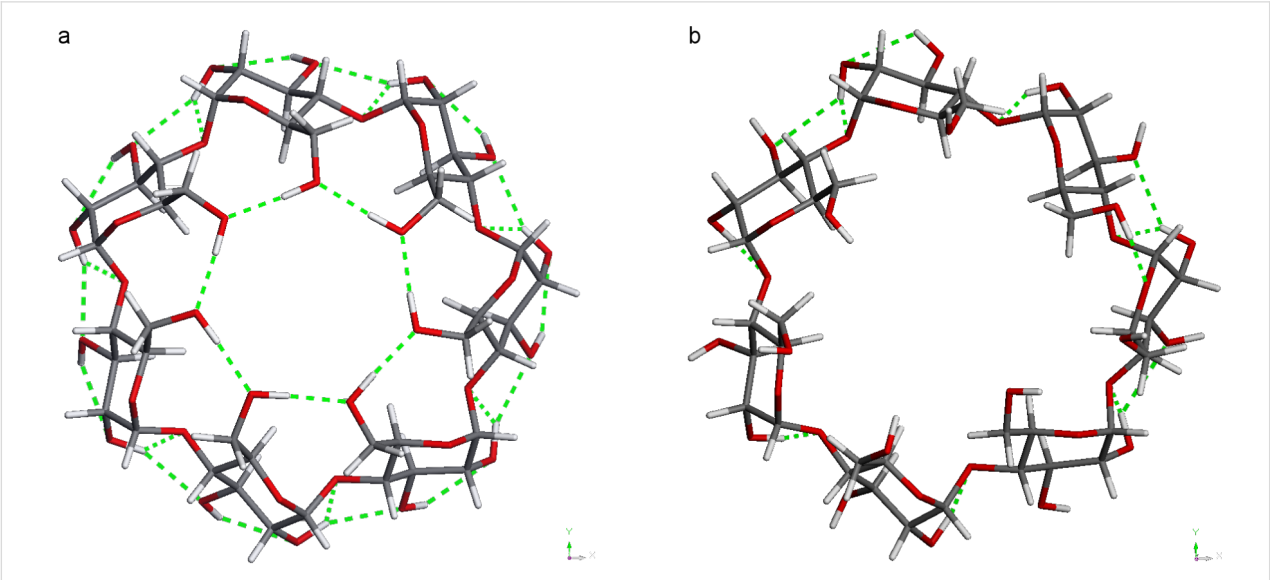

Figure 9: a: BCDO23rO6l (MD starting structure with Compass-E_{tot} = 221.52 kcal mol^{-1} and 28 hydrogen bonds with averaged Dreiding-E_{HB} = −4.71 kcal mol^{-1} => −131.88 kcal mol^{-1}) and b: BCDO23rO6l fr4739 (best frame from the last 2000 ps of the analysed MD-trajectory with Compass-E_{tot} = 292.47 kcal mol^{-1} and 13 hydrogen bonds with averaged Dreiding-E_{HB} = −0.63 kcal mol^{-1} => −8.19 kcal mol^{-1}).

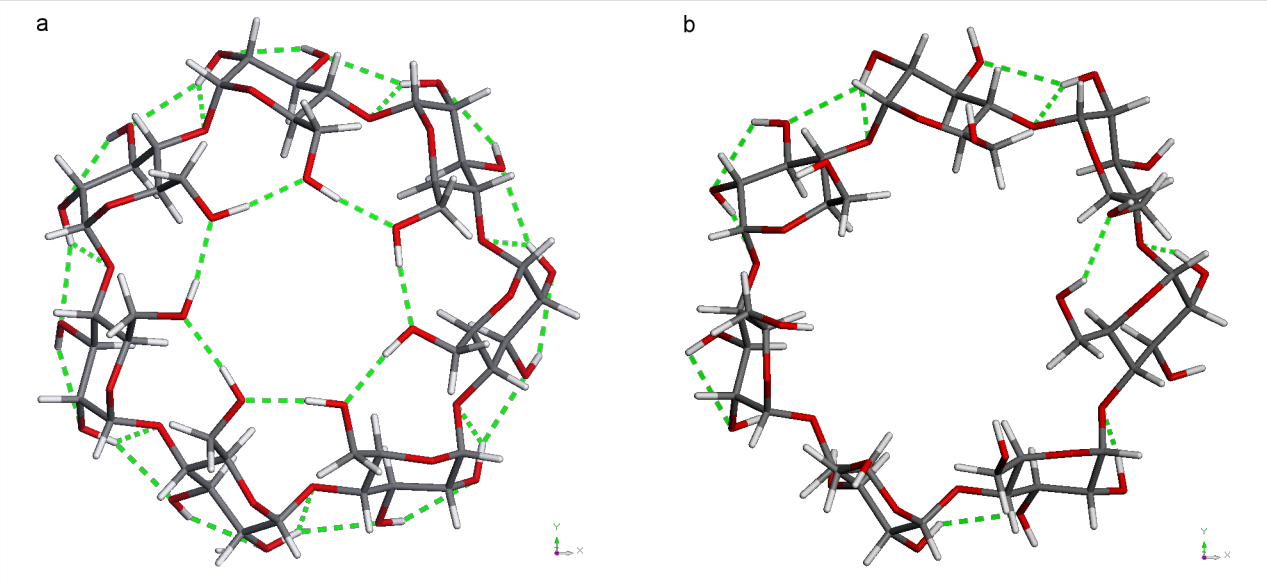

Figure 10: a: BCDO23rO6r (MD starting structure with Compass-E_{tot} = 217.25 kcal mol^{-1} and 28 hydrogen bonds with averaged Dreiding-E_{HB} = −4.59 kcal mol^{-1} => −128.52 kcal mol^{-1}) and b: BCDO23rO6r fr5418 (best frame from the last 2000 ps of the analysed MD-trajectory with Compass-E_{tot} = 290.26 kcal mol^{-1} and 14 hydrogen bonds with averaged Dreiding-E_{HB} = −0.65 kcal mol^{-1} => −9.1 kcal mol^{-1}).

their "highly ordered hydrogen-bond structures" in vacuo from the start were energetically lower than their structures from their best frames of the trajectories at 300 K, because they "lost their hydrogen-bond stabilisation" and became flexible instead. All starting structures had much higher hydrogen-bond energies (analysis using Dreiding force field) than the best structures from their trajectories.

The five MD trajectories of the empty β-CD models had the following averaged energies (Compass force field): BCDcry 311.15 kcal mol^{-1}, BCDO23lO6l 304.26 kcal mol^{-1}, BCDO23lO6r 304.02 kcal mol^{-1}, BCDO23rO6l 295.14 kcal mol^{-1} and BCDO23rO6r 291.22 kcal mol^{-1}. According to this the BCDO23rO6r model was the lowest energy conformer, closely followed by the BCDO23rO6l model, which was the best conformer in the AM1 method. This means, that the hydrogen bonds at the larger O2/O3 rim of empty β-CDs preferred the right-hand orientation, i.e., O3–H···O2–H in the same glucose unit and bifurcated towards O4 and O3 of the next glucose unit on the right side.

The β-CD/benzene complex at different temperatures from 300 K to 120 K

The MD trajectories of the parallel and vertical BCDO23rO6l model were practically the same since the benzene guest changed its position already in the first few pico seconds, and later a significant difference could not be observed any more. It was observed that the benzene guest left the cyclodextrin host at slightly different times, depending on the temperature, (Figure 11). At 120 K benzene was always inside the cyclodextrin cavity. "Inside the cavity" was defined by a distance of up to 2 Å between the centre of mass of benzene and the seven O4 oxygen atoms of the β-CD that define a plane in the middle of the torus. At 273 K this distance extended up to 3 to 4 Å starting at about 140 ps, and at about 320 ps it became longer than 5 Å indicating that now benzene had left the cavity without return. At 280 K and 290 K these events appeared earlier, at 140 ps/160 ps and 50 ps/125 ps, respectively. This was in good qualitatively agreement with the complex formation constants that were experimentally determined from UV spectra in [34] and showed that the complex was more stable at lower temperatures. At 300 K benzene tried to leave the cavity early at the O6 side, but always returned. It spent most of the time at a greater distance of about 4 to 5 Å to the O4-plane of β-CD and finally left the cavity on the O2/O3 side as all the others did, but later at 2400 ps. Benzene had a high mobility in many geometrical positions in these trajectories, and the most characteristic ones from the trajectory at 300 K are shown in Figure 12. Figure 13 displays how different the energies of the β-CD/benzene complex were during the MD trajectory at 290 K.

Summarised result of the molecular dynamics simulations

Molecular dynamics simulations at different temperatures (120 K to 300 K) displayed qualitatively correctly the dynamics of the β-CD/benzene complex. Benzene accepted many different positions inside the β-CD cavity before it finally left at the O2/O3 side. The highly ordered hydrogen bonds at the O6 or O2/O3 rim were not existent at these temperatures and thus were a phenomenon of very low temperatures.

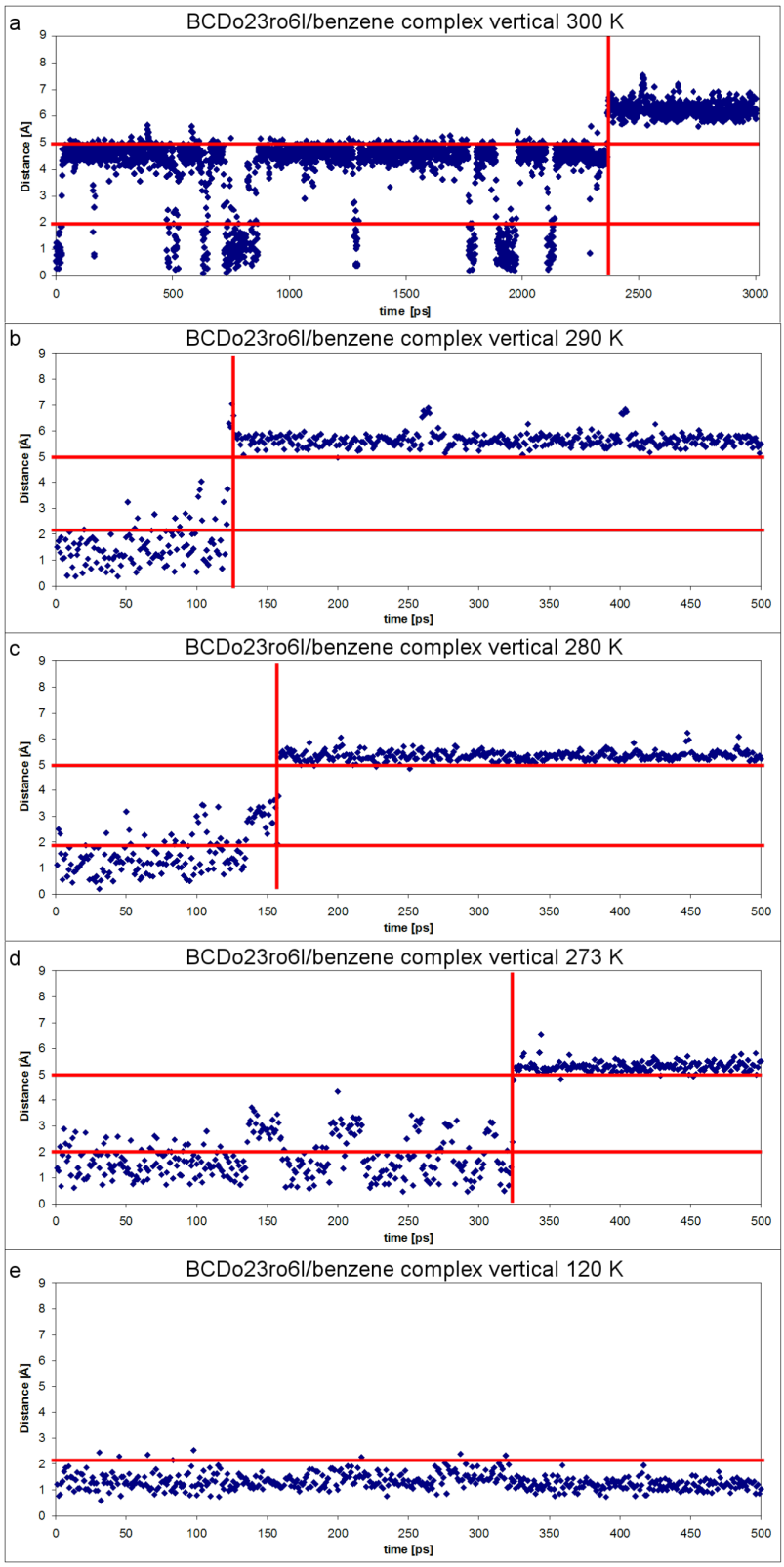

Figure 11: Distance plots from the MD trajectories of 500 ps each (*x* axis) for β-CD/benzene complex at different temperatures: a: 300 K, b: 290 K, c: 280 K, d: 273 K and e: 120 K. Distance [Å] (*y* axis) between the centres of mass of benzene and the seven O4 oxygen atoms of β-CD; horizontal red lines at distances of 2 Å and 5 Å, see text; vertical red lines indicate the time when the benzene left the β-CD cavity without return.

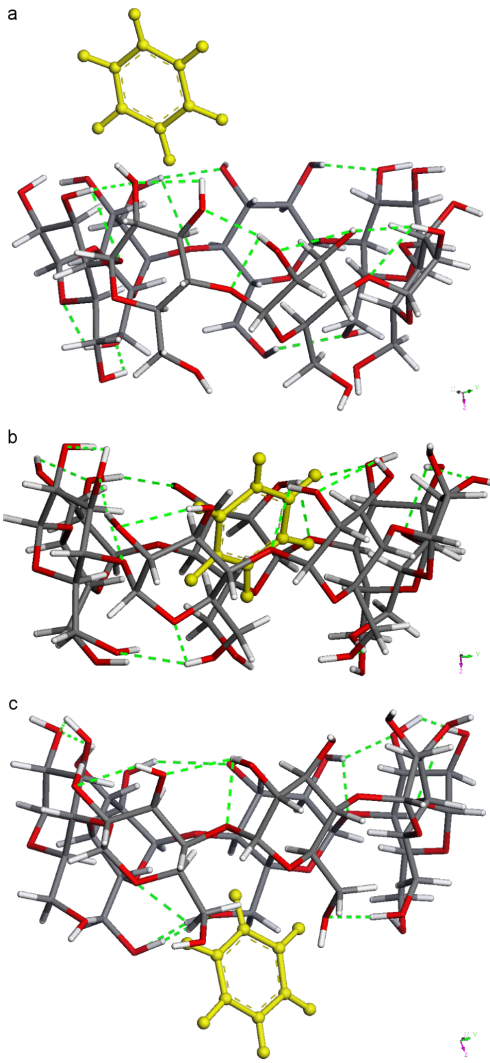

Figure 12: Three structures from the MD trajectory at 300 K: a: benzene left the β-CD at the O23 side; b: β-CD/benzene complex; c: benzene tried to leave the β-CD at the O6 side early, but always returned. Benzene finally left the cyclodextrin cavity also at the O23 side.

Since quantum-mechanical calculations lead to these highly ordered optimised structures, they represent the lowest energy conformers in vacuo at 0 K. Nevertheless, they will be the basis for the assumptions of the COSMO-RS method and its thermodynamic formulas and calculations/extrapolations based on the energetically lowest single-molecular states, plus conformers on top of that, up to 10 kcal mol^{-1}. These conformer ensembles will make it possible to calculate several thermodynamic properties at room temperature and above, not only for the gas phase but also for the liquid and solid states of matter made from these molecules.

Conclusion

The β-CD/benzene AM1 energies of complex formation after geometry optimisations for both positions of the guest, parallel and vertical were −2.75 kcal mol^{-1} and −2.46 kcal mol^{-1}, respectively. The concerted highly ordered hydrogen bonds at the O2/O3 and O6 rims of cyclodextrin had a strong influence on the structures. This was confirmed by the calculated AM1 IR spectra, which showed that the β-CDs O–H frequencies were mostly split up upon complex formation with benzene. The HOMO/LUMO gap of the empty cyclodextrin with about 12 eV was lowered to about 10 eV in the complex, in agreement with other calculations (PM3) from the literature. All four hydrogen-bond models studied here (BCDO23lO6l, BCDO23rO6l, BCDO23lO6r and BCDO23rO6r) were energetically advantageous after geometry optimisations with BP86/TZVP-DISP3 in vacuo and in aquo, their relative energies were, all but one, less than 3.2 kcal mol^{-1}. The character of the COSMO-RS σ-surface of β-CD was much more hydrophobic on its O6 rim than on its O23 side when all hydrogen bonds were arranged in a concerted mode. COSMO-RS BP/TZVP-DISP3 calculations in vacuo and in aquo (dielectric field approximation) preferred an oblique position (over parallel or vertical) of benzene inside the β-CD cavity and suggested energies of complex formation up to 20.2 kcal mol^{-1} in vacuo and of about 16 kcal/mol^{-1} in aquo.

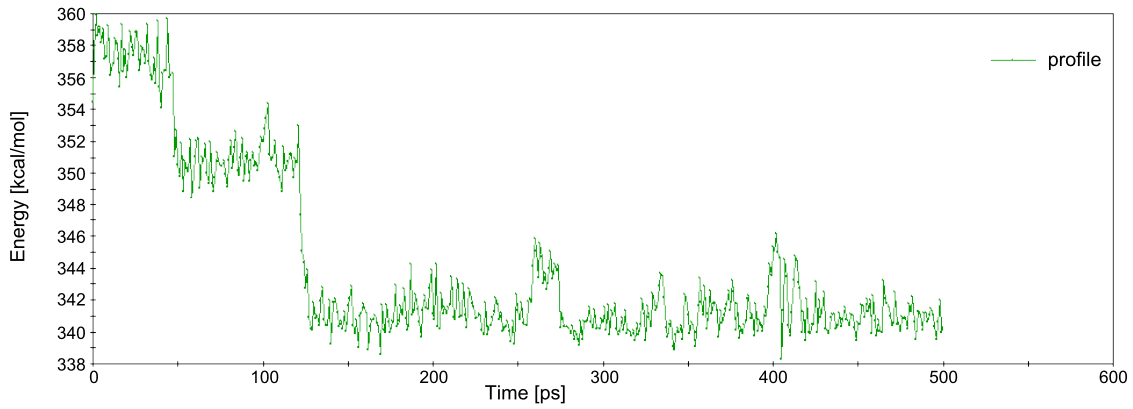

Figure 13: β-CD/benzene complex energy diagram (Forcite analysis – Hamiltonian) of the MD trajectory at 290 K.

The static picture of these energetically lowest structures of the β-CD/benzene complex at 0 K was extended by the molecular dynamics simulations at different temperatures (120 K to 300 K). They displayed qualitatively correctly the dynamics of the β-CD/benzene complex, which was more stable at lower temperatures, especially at 120 K. Benzene accepted many different positions inside the β-CD cavity before it finally left at the O2/O3 side (273 to 300 K). The highly ordered hydrogen bonds at the O6 or O2/O3 rim were a subtle phenomenon at very low temperatures. Still, we assume that hydrogen bonds of cyclodextrins nevertheless play a crucial role in all their special properties, i.e., their many inclusion complexes and remarkable influence on reactions, catalysis and supramolecular structures.

References

1. Szejtli, J. *Chem. Rev.* **1998,** *98,* 1743–1754. doi:10.1021/cr970022c
2. Jeffrey, G. A.; Saenger, W. Chapter 4. Theoretical calculations of hydrogen bond geometries. *Hydrogen Bonding in Biological Structures;* Springer Verlag: Berlin Heidelberg, 1991. See also Chapter 18, Cyclodextrins.
3. Alderfer, J. L.; Eliseev, A. V. *J. Org. Chem.* **1997,** *62,* 8225–8226. doi:10.1021/jo970772m
4. Schmid, B. V. K. J.; Hetzer, M.; Ritter, H.; Barner-Kowollik, C. *Macromolecules* **2011,** *44,* 7220–7232. doi:10.1021/ma2011969
5. Eliadou, K.; Yannakopoulou, K.; Rontoyianni, A.; Mavridis, I. M. *J. Org. Chem.* **1999,** *64,* 6217–6226. doi:10.1021/jo990021f
6. Aachmann, F. L.; Otzen, D. E.; Larsen, K. L.; Wimmer, R. *Protein Eng., Des. Sel.* **2003,** *16,* 905–912. doi:10.1093/protein/gzg137
7. Willerich, I.; Schindler, T.; Ritter, H.; Gröhn, F. *Soft Matter* **2011,** *7,* 5444–5450. doi:10.1039/c1sm05405h
8. Park, C.; Oh, K.; Lee, S. C.; Kim, C. *Angew. Chem., Int. Ed.* **2007,** *46,* 1455–1457. doi:10.1002/anie.200603404
9. Kida, T.; Iwamoto, T.; Fujino, Y.; Tohnai, N.; Miyata, M.; Akashi, M. *Org. Lett.* **2011,** *13,* 4570–4573. doi:10.1021/ol2017627
10. Koehler, J. E. H.; Saenger, W.; van Gunsteren, W. F. *J. Biomol. Struct. Dyn.* **1988,** *6,* 181–198. doi:10.1080/07391102.1988.10506490
11. Köhler, J.; Hohla, M.; Söllner, R.; Eberle, H.-J. *Supramol. Sci.* **1998,** *5,* 101–116. doi:10.1016/S0968-5677(97)00065-5
12. Köhler, J.; Hohla, M.; Söllner, R.; Amann, M. *Supramol. Sci.* **1998,** *5,* 117–137. doi:10.1016/S0968-5677(97)00066-7
13. Yu, H.; Amann, M.; Hansson, T.; Köhler, J.; Wich, G.; van Gunsteren, W. F. *Carbohydr. Res.* **2004,** *339,* 1697–1709. doi:10.1016/j.carres.2004.05.003
14. Damodaran, K. V.; Banba, S.; Brooks, C. L., III. *J. Phys. Chem. B* **2001,** *105,* 9316–9322. doi:10.1021/jp010361g
15. Liu, L.; Guo, Q.-X. *J. Phys. Chem. B* **1999,** *103,* 3461–3467. doi:10.1021/jp984545f
16. Liu, L.; Guo, Q.-X. *J. Chem. Inf. Comput. Sci.* **1999,** *39,* 133–138. doi:10.1021/ci980097x
17. Liu, L.; Guo, Q.-X. *J. Inclusion Phenom. Macrocyclic Chem.* **2004,** *50,* 95–103. doi:10.1007/s10847-003-8847-3
18. Klamt, A. *COSMO-RS From Quantum Chemistry to Fluid Phase Thermodynamics and Drug Design,* 1st ed.; Elsevier: The Netherlands, 2005.
19. Klamt, A.; Eckert, F.; Arlt, W. *Annu. Rev. Chem. Biomol. Eng.* **2010,** *1,* 101–122. doi:10.1146/annurev-chembioeng-073009-100903
20. Klamt, A.; Reinisch, J.; Eckert, F.; Hellweg, A.; Diedenhofen, M. *Phys. Chem. Chem. Phys.* **2012,** *14,* 955–963. doi:10.1039/c1cp22640a
21. Saenger, W. *Angew. Chem.* **1980,** *92,* 343–361. doi:10.1002/ange.19800920505
22. Ho, B. T.; Joyce, D. C.; Bhandari, B. R. *Food Chem.* **2011,** *129,* 259–266. doi:10.1016/j.foodchem.2011.04.035
23. Regiert, M. *SOFW J.* **2009,** *8,* 135.
24. Schmid, G. Preparation and industrial production of cyclodextrins. In *Comprehensive Supermolecular Chemistry;* Atwood, J.; Davies, E. D.; MacNicol, D. D.; Vogtle, F., Eds.; Pergamon Press: Oxford, U.K., 1996; pp 41–56.
25. van der Veen, B. A.; Uitdehaag, J. C. M.; Dijkstra, B. W.; Dijkhuizen, L. *Biochim. Biophys. Acta* **2000,** *1543,* 336–360. doi:10.1016/S0167-4838(00)00233-8
26. Li, Z.; Wang, M.; Wang, F.; Gu, Z.; Du, G.; Wu, J.; Chen, J. *Appl. Microbiol. Biotechnol.* **2007,** *77,* 245–255. doi:10.1007/s00253-007-1166-7
27. Rungsardthong Ruktanonchai, U.; Srinuanchai, W.; Saesoo, S.; Sramala, I.; Puttipipatkhachorn, S.; Soottitantawat, A. *Biosci., Biotechnol., Biochem.* **2011,** *75,* 2340–2345. doi:10.1271/bbb.110523
28. Hobza, P.; Selzle, H. L.; Schlag, E. W. *J. Am. Chem. Soc.* **1994,** *116,* 3500–3506. doi:10.1021/ja00087a041
29. *Materials Studio,* Version 5.5; Accelrys: San Diego, USA.
30. *Gaussian 09,* Revision A.1; Gaussian, Inc.: Wallingford, CT, 2009. GaussView v 5.0.9 Visualizer and Builder.
31. *Turbomole,* Version 6.4; COSMOlogic GmbH: Leverkusen, Germany.
32. Grimme, S.; Antony, J.; Ehrlich, S.; Krieg, H. *J. Chem. Phys.* **2010,** *132,* 154104. doi:10.1063/1.3382344
33. Betzel, C.; Saenger, W.; Hingerty, B. E.; Brown, G. M. *J. Am. Chem. Soc.* **1984,** *106,* 7545–7557. doi:10.1021/ja00336a039
34. Trofymchuk, I. M.; Belyakova, L. A.; Grebenyuk, A. G. *J. Inclusion Phenom. Macrocyclic Chem.* **2011,** *69,* 371–375. doi:10.1007/s10847-010-9757-9
35. Zabel, V.; Saenger, W.; Mason, S. A. *J. Am. Chem. Soc.* **1986,** *108,* 3664–3673. doi:10.1021/ja00273a020

License and Terms

Beilstein Journal of Organic Chemistry

Superstructures of fluorescent cyclodextrin via click-reaction

Arkadius Maciollek[1], Helmut Ritter[*1] and Rainer Beckert[*2]

Full Research Paper

Open Access

Address:
[1]Institute of Organic Chemistry and Macromolecular Chemistry, Heinrich-Heine-University Duesseldorf, Universitaetsstraße 1, 40225 Duesseldorf, Germany and [2]Institute of Organic Chemistry and Macromolecular Chemistry, Friedrich-Schiller-University, Humboldtstr. 10, 07743 Jena, Germany

Email:
Helmut Ritter[*] - h.ritter@uni-duesseldorf.de; Rainer Beckert[*] - c6bera@uni-jena.de

* Corresponding author

Keywords:
fluorescent dye; cyclodextrins; host–guest interaction; supramolecular polymer

Beilstein J. Org. Chem. **2013,** *9,* 827–831.
doi:10.3762/bjoc.9.94

Received: 17 December 2012
Accepted: 10 April 2013
Published: 29 April 2013

This article is part of the Thematic Series "Superstructures with cyclodextrins: Chemistry and applications".

Associate Editor: M. Rueping

Abstract

Mono-(6-azido-6-deoxy)-β-cyclodextrin (CD) was covalently attached to an alkyne-modified 5-methyl-2-(pyridin-2-yl)thiazol-4-ol yielding a fluorophore containing CD in a click-type reaction. Intermolecular complexes were formed by poly(host–guest)-interactions. The supramolecular structures were characterized by ^{1}H NMR-ROESY spectroscopy, dynamic light scattering, UV–vis spectroscopy, fluorescence spectroscopy, and asymmetric flow field-flow fractionation. By adding potassium adamantane-1-carboxylate, the thiazol dye is displaced from the CD-cavity and the elongated noncovalent polymeric structures collapse.

Introduction

Most small heterocyclic molecules show low fluorescence. However, as we reported earlier, substituted 4-hydroxythiazoles have a high fluorescent nature [1,2]. These optical properties can be used for the development of sensor molecules, blue emitting dyes, luminescent materials or as donor–(π-conjugated-bridge)–acceptor-type dyes in dye-sensitized solar cells [3-5]. The etherification of 4-hydroxythiazole by using propargyl bromide opens up a wide field of modification through click chemistry with azides or thioles [6,7]. Accordingly, following our former work with mono azide modified CD, we were encouraged to combine the fluorescent hydroxythiazole dye with CD [8-10]. Such water soluble spectroscopically active hosts can be used as potentially biological markers, as molecular sensors, or for chiral recognition in aqueous solution [11-13]. Thus, in this present paper we describe the spectroscopic and structural behavior of a "CD-Click-Fluorophore" in the absence and presence of a competitive guest in water.

Results and Discussion

The water-soluble fluorescent cyclodextrin was synthesized via copper-catalyzed cycloaddition (Scheme 1). The existence of the resulting product was confirmed by MALDI–TOF spec-

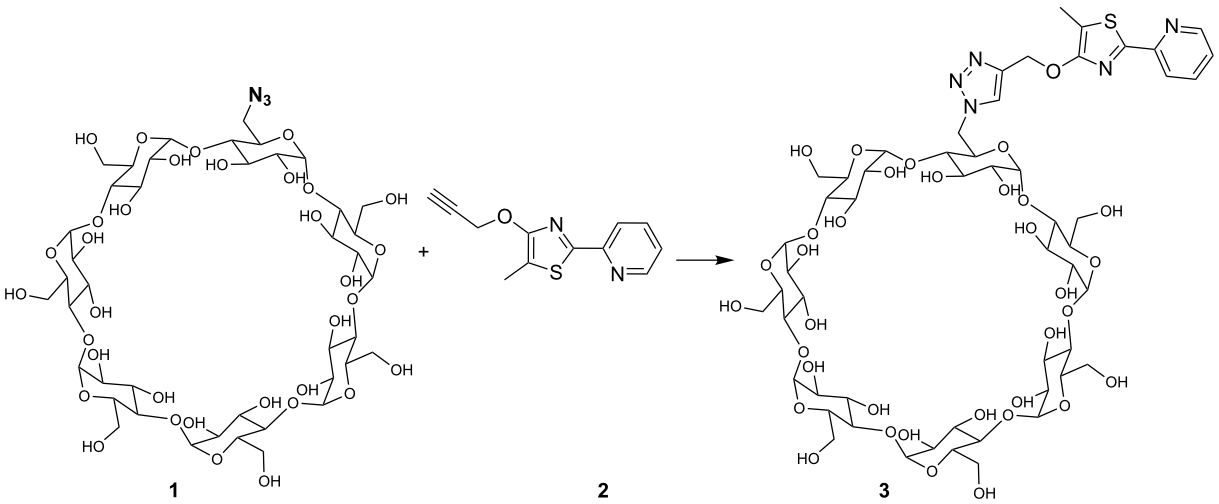

Scheme 1: Synthesis of fluorescent cyclodextrin **3** by click-chemistry.

trometry, ^{1}H NMR and IR spectroscopy. The formation of host–guest structures between the thiazole functionality and β-CD was proven by ^{1}H NMR rotating-frame Overhauser effect spectroscopy (ROESY) (Figure 1). NOE correlation signals of the β-CD cavity protons between 4 and 3.5 ppm and the aromatic protons of the pyridine moiety 8.6–7.4 ppm were observed, clearly proving the formation of complexes. However, no NOE interaction between protons of the methyl group of the thiazole and the triazole proton itself with CD is noticed. This indicates that only the inclusion of the pyridine moiety in the hydrophobic cavity of the CD takes place.

The formation of supramolecular structures was also proven by UV–vis spectroscopy and fluorescence spectroscopy. Figure 2

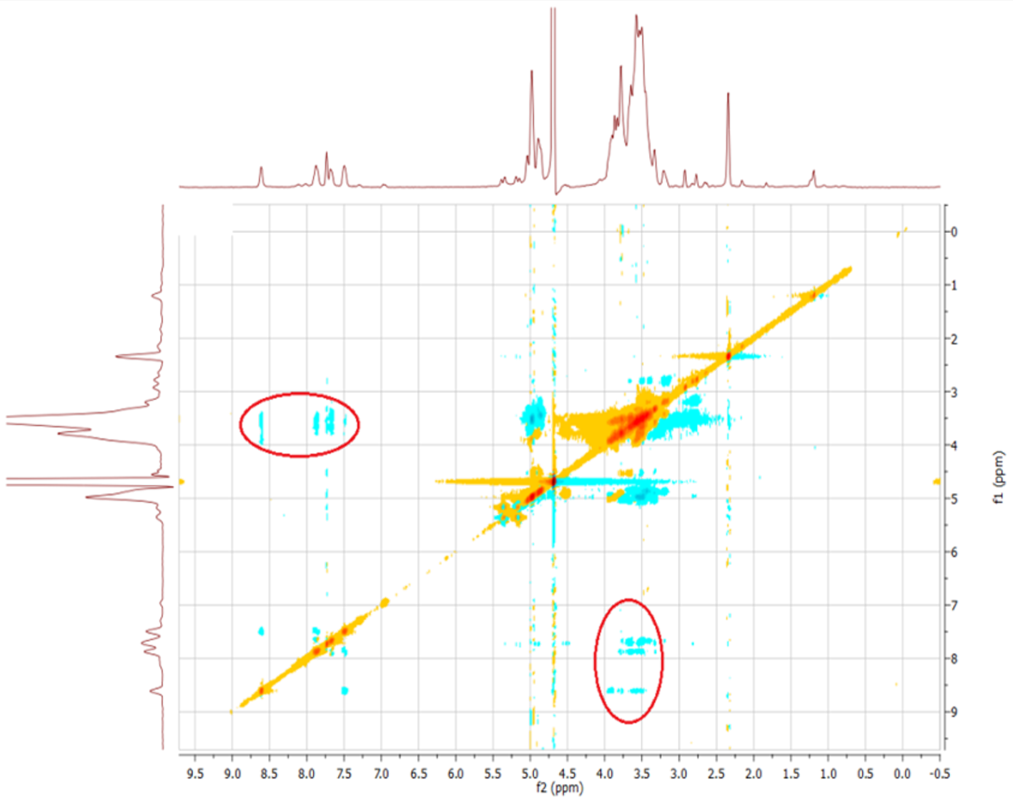

Figure 1: ^{1}H NMR-ROESY spectrum of the modified CD **3**.

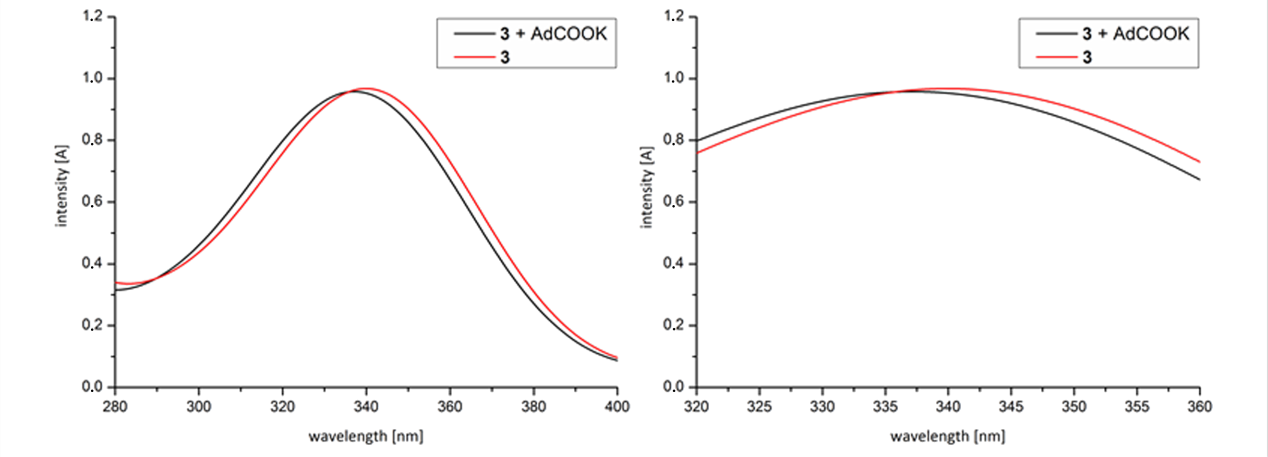

Figure 2: UV–vis spectrum of **3** (4 × 10^{-4} M) with and without a 10-fold excess of potassium adamantane-1-carboxylate.

shows the UV–vis absorption spectra of **3** in water with the characteristic band at λ_{max}= 340 nm. The addition of a 10-fold excess of potassium adamantane-1-carboxylate, as competitive guest for CD leads to a hypsochromic shift with λ_{max} = 336 nm, through the exclusion of the fluorophore moiety from the hydrophobic cavity of CD. This exchange causes a change in the HOMO–LUMO gap [14,15].

Figure 3 shows the fluorescence spectra of **3** in aqueous solution. Upon addition of potassium adamantane-1-carboxylate the maximum wavelength changes from 417 to 442 nm and the fluorescence intensity decreases. The inclusion of the fluorophore in the CD cavity causes an increase in the fluorescence intensity resulting from the decrease of the intramolecular rotational degrees of freedom of the molecule, compared to a solvent-accommodated fluorophore outside the cavity [12,14,16].

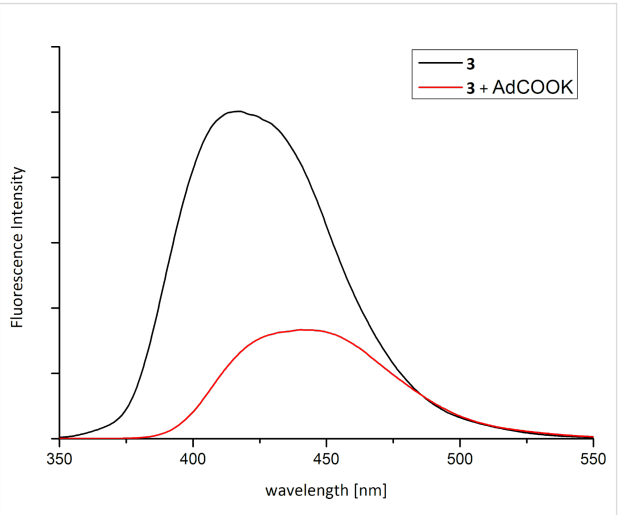

Figure 3: Fluorescence spectrum of **3** (4 × 10^{-4} M) with and without a 10-fold excess of 1-adamantanecarboxylic acid.

To investigate the expected intermolecular formation of supramolecular structures in aqueous solution, dynamic light scattering (DLS) experiments were performed (Figure 4). Hydrodynamic diameters up to 200 nm indicate the postulated formation of intermolecular complexes. Thus, repeating complexation of one rigid fluorophore moiety through the CD-function of the next monomer molecule takes place [17,18]. Accordingly, the formation of linear polymers via supramolecular monomer linkages can be claimed. Besides, intermolecular chain interactions may also take place due to hydrogen-bond interactions between the CD units.

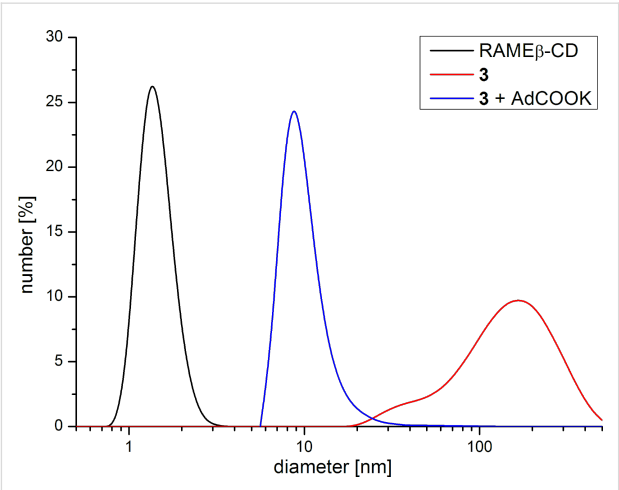

Figure 4: DLS measurement of **3** with and without a 10-fold excess of potassium adamantane-1-carboxylate; black: hydrodynamic diameter of randomly methylated β-CD, blue: mixture of monomer and oligomer after adding potassium adamantane-1-carboxylate, red: supramolecular polymer of **3**.

By adding potassium adamantane-1-carboxylate the pyridine moiety is displaced from the cavity. As a consequence, the noncovalent structures collapse to monomeric and oligomeric

CD units and the hydrodynamic diameter decreases by as much as 5 nm. Asymmetric flow field-flow fractionation experiments coupled with a three-angle light scattering detector confirm also the formation of intermolecular superstructures (Figure 5). Structures with a molar mass of M_n up to 100,000 g/mol and also a hydrodynamic diameter up to 200 nm were detected. The conformation plot, i.e., the plot of the log of the radius as a function of the log of the molar mass, with a value of 0.7 estimates an elongated shape of the noncovalent structures. Upon addition of potassium adamantane-1-carboxylate no signals of the polymeric structure were detected.

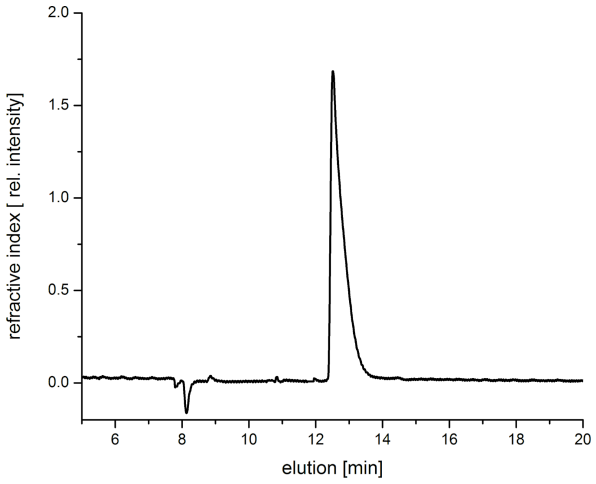

Figure 5: AF4 elution diagram of **3**.

Conclusion

In summary, we have presented the synthesis of a fluorescent cyclodextrin via click reaction. The changes in the spectroscopic properties of the fluorescent cycloadduct were investigated in the presence and absence of the competitive guest potassium adamantane-1-carboxylate. The intermolecular formation of polymeric structures with elongated shape, through poly(host–guest)-interactions, was found. Furthermore, we were able to show the collapse of the supramolecular polymers upon addition of potassium adamantane-1-carboxylate.

Experimental

General remarks

All reagents used were commercially available (Sigma-Aldrich, Acros Organics) and used without further purification. β-CD was obtained from Wacker Chemie GmbH, Burghausen, Germany and was used after drying overnight with a vacuum oil pump over P_4O_{10}. *N,N*-Dimethylformamide (DMF) was purchased from Fluka, Germany. Dimethyl sulfoxide-d_6 (99.9 atom % D) and deuterium oxide, D_2O, were obtained from Deutero GmbH, Germany. ^{1}H NMR spectra were recorded on a Bruker Avance DRX 300 at 20 °C, shifts (δ) are given relative to signals arising from the solvent.

FT IR spectra were recorded on a Nicolet 6700 FT IR spectrometer equipped with an ATR unit. Matrix-assisted laser desorption/ionization-time-of-flight mass spectrometry (MALDI–TOFMS) was performed on a Bruker Ultraflex TOF mass spectrometer. Ions were formed with a pulsed nitrogen laser (25 Hz, 337 nm) and the molecular masses were recorded in linear mode. 2,5-Dihydroxybenzoic acid (DBH) in acetonitrile/water was used as a matrix.

Mass spectrometric experiments (MS) were performed on a Thermo Finnigan Trace DSQ (Dual-Stage Quadrupole) mass spectrometer. Ionization was carried out by electron ionization (EI). The absorption spectra were measured on a Specord 210 Plus UV–visible spectrophotometer. Fluorescence spectra were recorded on a Perkin Elmer LS55 luminescence spectrometer. AF4 measurements in ultrapure water were carried out on a combined system comprising the following elements: refractive index detector Optilabrex (Wyatt Technologies, laser wavelength 658 nm), three angle light scattering detector miniDawn TREOS (Wyatt Technologies, laser wavelength 658 nm, detector angles at 43.5°, 90.0° and 136.5°), UV detector Waters 486 (Waters), pump, degasser and autosampler (Agilent 1200, Agilent technologies). The molecular weight was calculated with Astra5 software from static light scattering data, by using the Zimm model. As concentration source, the refractive index was used. Calibration of the system was performed with bovine serum albumin. Dynamic light scattering (DLS) experiments were carried out with a Malvern Zetasizer Nano; ZS ZEN 3600 at a temperature of 20 °C. The particle size distribution is derived from a deconvolution of the measured intensity autocorrelation function of the sample by a General Purpose Method (non-negative least squares) algorithm included in the DTS software. Microwave-assisted synthesis was performed using a CEM Discover Synthesis Unit (monomode system). The temperature was measured by infrared detection maintained at a constant value by power modulation. Reactions were performed in closed vessels.

Synthesis of mono-(6-azido-6-deoxy)-β-CD (1): Mono-(6-azido-6-desoxy)-β-cyclodextrin was synthesized according to the known procedure [8].

Synthesis of 2-[5-methyl-4-(prop-2-yn-1-yloxy)-1,3-thiazol-2-yl]pyridine (2): The alkyne modified thiazol was synthesized according to the literature procedure [2].

Synthesis of fluorescent β-cyclodextrin 3: 1.3 g (1.15 mmol) of mono-(6-azido-6-desoxy)-β-cyclodextrin (**1**), 396 mg

(1.73 mmol) 2-[5-methyl-4-(prop-2-yn-1-yloxy)-1,3-thiazol-2-yl]pyridine (**2**), 29 mg (147 µmol) sodium ascorbate and 18 mg (73.5 µmol) copper(II) sulfate pentahydrate were suspended in 5 mL dimethylformamide in a pressure-resistant microwave test tube provided with a magnetic stirring bar. The tube was sealed and placed in the microwave and irradiated at 140 °C and 100 W for 30 min. The product was precipitated in cold acetone, filtered and washed three times with acetone.

^{1}H NMR (300 MHz, DMSO-d_6, rt) δ 8.57 (br, 1H, ArH), 8.16–8.01 (br, 2H, CH, ArH), 7.98–7.86 (br, 1H, ArH), 7.47–7.38 (br, 1H, ArH), 5.79–5.68 (br, 14H, OH), 5.40 (br, 2H, CH_2), 4.89–4.79 (br, 7H, CH), 4.51–4.44 (br, 6H, OH), 3.75–3.53 (br, 28H, CH), 2.22 (br, 3H, CH_3) ppm; IR: 3301 (OH), 2923 (C-H), 1653 (C=C), 1548 (ring vibr.), 1329 (OH), 1153 (COH), 1078 (COC), 1027 (COH) cm^{-1}; MS (MALDI–TOF) (acetonitrile/water 1:10): m/z = 1412 $[M + Na]^+$.

References

1. Grummt, U.-W.; Weiss, D.; Birckner, E.; Beckert, R. *J. Phys. Chem. A* **2007,** *111,* 1104–1110. doi:10.1021/jp0672003
2. Täuscher, E.; Weiß, D.; Beckert, R.; Görls, H. *Synthesis* **2010,** 1603–1608. doi:10.1055/s-0029-1219759
3. Menzel, R.; Täuscher, E.; Weiß, D.; Beckert, R.; Görls, H. *Z. Anorg. Allg. Chem.* **2010,** *636,* 1380–1385. doi:10.1002/zaac.200900523
4. Happ, B.; Schäfer, J.; Menzel, R.; Hager, M. D.; Winter, A.; Popp, J.; Beckert, R.; Dietzek, B.; Schubert, U. S. *Macromolecules* **2011,** *44,* 6277–6287. doi:10.1021/ma201193e
5. Menzel, R.; Ogermann, D.; Kupfer, S.; Weiß, D.; Görls, H.; Kleinermanns, K.; González, L.; Beckert, R. *Dyes Pigm.* **2012,** *94,* 512–524. doi:10.1016/j.dyepig.2012.02.014
6. Lutz, J.-F. *Angew. Chem.* **2007,** *119,* 1036–1043. doi:10.1002/ange.200604050
7. Hoyle, C. E.; Lowe, A. B.; Bowman, C. N. *Chem. Soc. Rev.* **2010,** *39,* 1355–1387. doi:10.1039/b901979k
8. Choi, S.; Munteanu, M.; Ritter, H. *J. Polym. Res.* **2009,** *16,* 389–394. doi:10.1007/s10965-008-9240-0
9. Munteanu, M.; Choi, S.; Ritter, H. *Macromolecules* **2008,** *41,* 9619–9623. doi:10.1021/ma8018975
10. Maatz, G.; Maciollek, A.; Ritter, H. *Beilstein J. Org. Chem.* **2012,** *8,* 1929–1935. doi:10.3762/bjoc.8.224
11. Ogoshi, T.; Harada, A. *Sensors* **2008,** *8,* 4961–4982. doi:10.3390/s8084961
12. Tanabe, T.; Touma, K.; Hamasaki, K.; Ueno, A. *Anal. Chem.* **2001,** *73,* 1877–1880. doi:10.1021/ac001062a
13. Ueno, A. *Adv. Mater.* **1993,** *5,* 132–134. doi:10.1002/adma.19930050213
14. Nowakowska, M.; Smoluch, M.; Sendor, D. *J. Inclusion Phenom. Macrocyclic Chem.* **2001,** *40,* 213–219. doi:10.1023/A:1011820513256
15. Hamasaki, K.; Ikeda, H.; Nakamura, A.; Ueno, A.; Toda, F.; Suzuki, I.; Osa, T. *J. Am. Chem. Soc.* **1993,** *115,* 5035–5040. doi:10.1021/ja00065a012
16. Ikeda, H.; Nakamura, M.; Ise, N.; Oguma, N.; Nakamura, A.; Ikeda, T.; Toda, F.; Ueno, A. *J. Am. Chem. Soc.* **1996,** *118,* 10980–10988. doi:10.1021/ja960183i
17. Harada, A. *J. Polym. Sci., Part A: Polym. Chem.* **2006,** *44,* 5113–5119. doi:10.1002/pola.21618
18. Munteanu, M.; Kolb, U.; Ritter, H. *Macromol. Rapid Commun.* **2010,** *31,* 616–618. doi:10.1002/marc.200900754

License and Terms

Beilstein Journal of Organic Chemistry

Space filling of β-cyclodextrin and β-cyclodextrin derivatives by volatile hydrophobic guests

Sophie Fourmentin[1,2], Anca Ciobanu[1,2,3], David Landy[1,2] and Gerhard Wenz[*4]

Full Research Paper

Open Access

Address:
[1]University Lille Nord de France, F-59000 Lille, France, [2]ULCO, UCEIV, F-59140 Dunkerque, France, [3]University Vasile Alecsandri, 600115 Bacau, Romania and [4]Organic Macromolecular Chemistry, Saarland University, Campus Saarbrücken C4 2, 66123 Saarbrücken, Germany

Email:
Gerhard Wenz* - g.wenz@mx.uni-saarland.de

* Corresponding author

Keywords:
cyclodextrins; inclusion compound; molecular modelling; space filling; static headspace gas chromatography; vapor pressure

Beilstein J. Org. Chem. **2013,** *9,* 1185–1191.
doi:10.3762/bjoc.9.133

Received: 21 December 2012
Accepted: 31 May 2013
Published: 19 June 2013

This article is part of the Thematic Series "Superstructures with cyclodextrins: Chemistry and applications".

Guest Editor: H. Ritter

Abstract

The inclusion of volatile derivatives of benzene and cyclohexane in β-cyclodextrin (β-CD), hydroxypropyl-β-CD, and hydrophilic β-CD-thioethers was investigated by static headspace gas chromatography (HS-GC) and molecular modelling. The obtained binding constants strongly increase with the amount of space filling of the CD cavity and the salt concentration. β-CD thioethers show a 3–10 times higher binding potential than native β-CD.

Introduction

β-Cyclodextrin (β-CD, **1**), the cyclic α(1→4) heptamer of glucose, is known to form inclusion compounds with a great variety of guests [1], such as derivatives of benzene [2,3], cyclohexane [4], adamantane [5,6], other alicyclic guests [7], and also inorganic molecules or ions [1,8].

Generally, the binding constant K increases with the degree of space filling of the β-CD cavity. The volume of the guest is often expressed by the number of carbon atoms n of its hydrophobic part. The Gibbs free enthalpy $\Delta G°$ of binding decreases nearly linearly with n by $\delta\Delta G^0/\delta_n = -3.1$ kJ mol^{-1} for linear alkanols [1]. Similar values were found for cyclic and polycyclic alkanoic acids $\delta\Delta G^0/\delta_n = -3.3$ kJ mol^{-1} [7]. We found an even higher slope for a series of *p*-substituted benzoic acids $\delta\Delta G^0/\delta_n = -4.2$ kJ mol^{-1}, where the binding constant remarkably increased from K = 20 L mol^{-1} for benzoate to K = 18,400 L mol^{-1} for *p-tert*-butylbenzoate [3].

The observed increase of complex stability with increasing size of the hydrophobic part of the guest can be explained by the increase of hydrophobic interactions as well as other nonpolar interactions, e.g., van der Waals and dispersive interactions [9].

The molecular origin of hydrophobic interactions in general was already discussed controversially for many years [10-13]. Reliable quantitative predictive models are still missing [14]. Expulsion of "high energy water" from a cavity during space filling by a hydrophobic guest appears to be the main contributor to the driving force of complex formation [15]. The accumulation of basic understanding is essential for the formulation of precise docking programs, which estimate and screen the binding of drug candidates for biological receptors [16,17].

Practical applications of native β-CD, such as drug delivery [18,19], extraction of pollutants from soil [20-23], homogenous catalysis [24], and microbial degradation [25] are limited by both its low aqueous solubility (1.8 wt % at 25°C) and its moderate complexing ability. Especially hydrophobic guests form channel inclusion compounds with β-CD [26,27], which are nearly insoluble in water [28]. For instance the solubility of toluene in water is only 1.7 mM as a complex in β-CD compared to 5 mM in the free state.

Several β-CD derivatives have been synthesized to overcome these drawbacks. For instance, the statistical derivative hydroxypropyl-β-CD **2** was often employed, because it is much more water soluble than β-CD and can also be produced on an industrial scale [29,30]. Unfortunately, hydroxypropyl-β-CD **2** is not a single pure compound but a mixture of various similar homologues and isomers [31], and does not show formation constants superior to native β-CD. Thus, it was desirable to work with pure β-CD derivatives showing higher affinities.

We reported recently the synthesis and use of heptafunctional 6-S-substitued CD derivatives **3** and **4** (Figure 1) for the solubilization of sparingly water-soluble drugs [32,33]. These β-CD-thioethers are single pure compounds and they showed very promising binding constants and very high aqueous solubility.

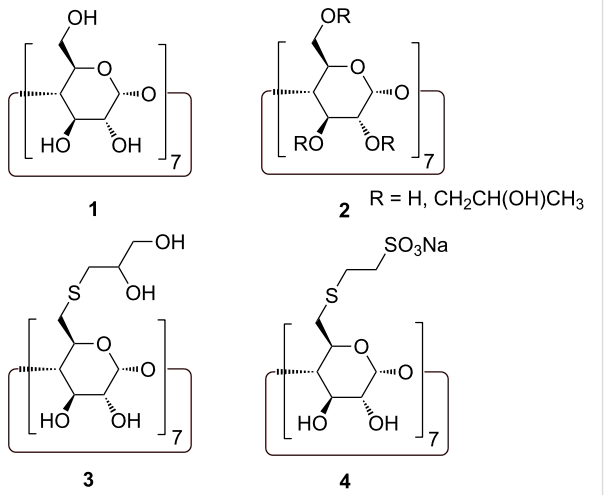

Figure 1: Chemical structures of β-CD **1**, hydroxypropyl-β-CD **2**, and β-CD-thioethers **3** and **4**.

In continuation of our investigations into the recognition of volatile organic compounds (VOCs) by CDs [34,35], we examined the potential of these β-CD-thioethers for the solubilization of VOCs. To demonstrate their versatility, two homologous series of volatile hydrophobic benzene and cyclohexane derivatives were chosen. These guests do not contain any hydrophilic substituents, therefore no attractive or repulsive polar interaction had to be taken into account.

Since static headspace gas chromatography (HS-GC) is a highly sensitive technique, it allows the investigation of the complexation of volatile guests in CD at very low concentrations, where guests, as well as their inclusion compounds, are still soluble in water [19,34-36]. Complexation of a guest is detected indirectly by the reduction of its vapor pressure due to complexation. This HS-GC method is applicable for a great variety of volatile guests [37].

The aim of this study was to investigate the binding ability of β-CD-thioethers toward hydrophobic VOCs in comparison to commercial β-CDs and to interpret the complexing abilities in terms of space filling of the cavities. Our systems are well-defined models for reaching a better understanding of hydrophobic interactions in general and are useful for the calibration of predictive tools.

Results and Discussion

A series of commercially available monosubstituted benzenes (Figure 2) was selected in analogy to the corresponding benzoates investigated previously [3].

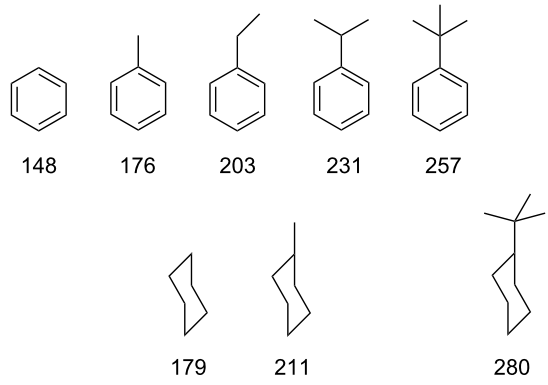

Figure 2: Chemical structures of the benzene and cyclohexane derivatives, with their calculated molecular volumes, $V_G = M/dN_A$ in Å^3, with M molecular weight, d density, N_A Avogadro's number.

These benzene derivatives were equilibrated in seated vials at very low concentrations (1 ppm) with solutions of β-CD derivatives (concentrations 1–10 mM). The partial pressures of these guests in the gas phase were determined by HS-GC. Because of the high separation efficiency of the GC column, all five guests could be determined simultaneously (Figure 3). Since interference of binding of the various guests was negligible because of the very large excess of β-CDs compared to the guests, binding constants could be determined for all of the five guests in parallel. The different decays of the signal intensities of the guests due to the complexation in β-CD are obvious in Figure 3.

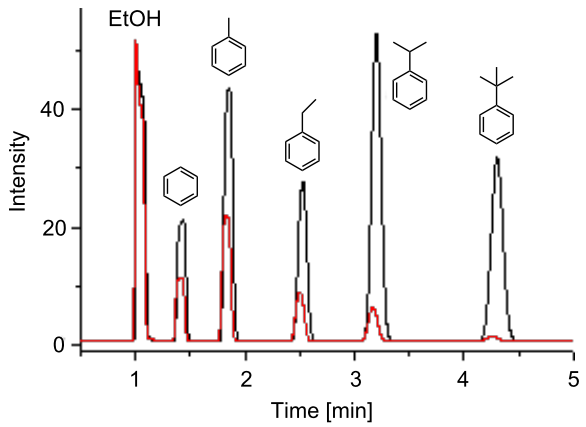

Figure 3: Chromatogram obtained by HS-GC for a mixture of aromatic guests (1 ppm) in water (black) and 10 mM solution of β-CD **1** (red).

The binding constant K was calculated from the ratio $y = A_0/A$ of the peak area of the guest without and with CD, A_0 and A, respectively, according to Equation 1, as derived in Supporting Information File 1 [36].

$$K = (fk_H + 1)\frac{A_0 / A - 1}{[\mathrm{CD}]_0} \quad (1)$$

For a validation of the method, the whole concentration dependence of the integrated GC signal intensity was measured as a function of the CD concentration $[CD]_0$ in the case of β-CD. The data points were fitted with the standard square root equation by nonlinear regression [19,34]. Within experimental error of ±10% the binding constant K, obtained by nonlinear regression, was identical to the value of K obtained according to Equation 1 from one data point. The latter method allows a fast and simultaneous determination of binding constant. The results for β-CD and the β-CD derivatives are summarized in Table 1 in comparison with values from the literature, which were in good agreement for β-CD **1** and in fair agreement for hydroxypropyl-β-CD **2** [2,4,29]. Deviations from literature values found for the statistical derivative **2** were attributed to slightly different substitution patterns.

The lower binding constant K of the host **2** compared to native β-CD was attributed to hydroxypropyl substituents at the 2- and 3-positions hindering the formation of intramolecular hydrogen bonds and thus destabilizing the β-CD framework. This destabilization leads to a reduction of the binding potential, because of an unfavorable negative binding entropy. Recently, we also found a diminished binding potential for those β-CD derivatives methylated at the 2- and 3-positions [38].

In contrast, the binding constants K of the β-CD thioethers were significantly higher by a factor of 3–10 than those of native β-CD. The higher binding potentials of the β-CD thioethers **3** and **4** compared to native β-CD could be attributed both to the higher hydrophobicity of sulfur compared to oxygen and to the exclusive localization of the substituents in position 6. This finding is consistent with previous observations of the high

Table 1: Binding constants K of benzene and cyclohexane derivatives in β-CD and β-CD derivatives as determined from HS-GC peak areas according to Equation 1.

guest\host	**1**	**2**	**3**	**4**	n[a]
	[M^{-1}]	[M^{-1}]	[M^{-1}]	[M^{-1}]	
benzene	128 (120[b], 111[c])	94 (99[c])	942	226	6
toluene	158 (140[b], 172[c], 142[d])	131 (170[c], 163[d])	1071	434	7
cyclohexane	341 (468[c])	227 (363[c])	4308	534	6
ethylbenzene	392 (330[b], 289[c])	303 (248[c])	2285	1427	8
methylcyclohexane	295 (332[c])	202 (253[c])	4032	893	7
cumene	1684 (1200[b])	1102	6992	6254	9
tert-butylbenzene	9503	1863	28081	24898	10
tert-butylcyclohexane	4092	2036	29345	44597	10

[a]n total number of carbon atoms; [b]from [2], [c]from [4], [d]from [35].

binding potentials of CD thioethers for other guests [32,33,39]. The binding constants of the neutral thioether **3** were in most cases higher than the ones of the anionic thioether **4**. The high hydrophilicity, introduced by the pendant sulfonate groups of **4**, seems to diminish the binding potential of the host.

Obviously, the binding constant K remarkably increased for all CD derivatives with the size of the guest, expressed by the number of carbon atoms n. The binding constant $K = 128\ M^{-1}$ for benzene in β-CD **1** was significantly higher than for benzoate $K = 20\ M^{-1}$ [3]. In contrast, the binding constant for *tert*-butylbenzene, $K = 9{,}503\ M^{-1}$ was lower than for *p*-*tert*-butylbenzoate, $K = 18{,}400\ M^{-1}$ [3]. The plot of $\Delta G°$ versus n was nearly linear (Figure 4). The slope $\delta\Delta G^0/\delta_n = -2.9$ kJ mol^{-1} was significantly smaller than the slope $\delta\Delta G^0/\delta_n = -4.2$ kJ mol^{-1} for the corresponding benzoate derivatives. This means that the carboxylate group at the guest can have either a repulsive or attractive interaction with β-CD, depending on the position of the carboxylate group within the β-CD cavity. The corresponding cyclohexane derivatives showed indeed a slope similar to the benzene derivatives, but free enthalpies more negative by $\Delta\Delta G° = 2$ kJ mol^{-1}, which was attributed to the larger diameter of cyclohexane compared to benzene filling the β-CD cavity more completely.

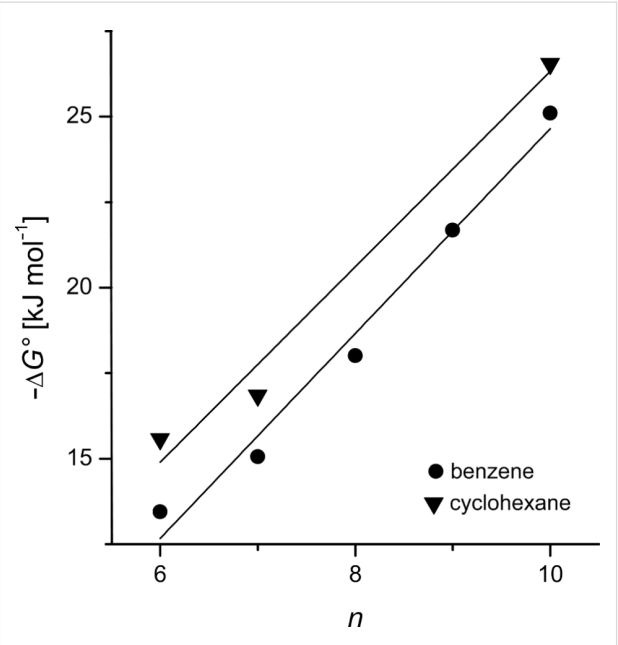

Figure 4: Gibbs free energy of formation of the inclusion compound of benzene derivatives, and cyclohexane derivatives in host **4** as a function of the total number of carbon atoms of the guest n.

For taking the space filling of the CD cavity better into account, the binding free energies $\Delta G°$ for host **4** were plotted as a function of the molecular volumes V_G from Figure 2 of the guests (Figure 5). A reasonable linear master plot was obtained for all guests. The slope with the dimension of a pressure was $p = -\delta\Delta G^0/\delta V_G = 0.107$ kJ mol^{-1}Å^{-3} = 1.8 kbar. Hydrophobic interactions causing high internal pressures of this magnitude are already known to accelerate dimerization reactions, such as the Diels–Alder addition [40]. The molecular volume of the largest guest, *tert*-butylcyclohexane, $V_G = 280$ Å^3 is close to the estimated volume of the β-CD cavity 262 Å^3 [41], which means that the β-CD cavity within host **4**, extended by the thioether substituents, is nearly completely occupied by it.

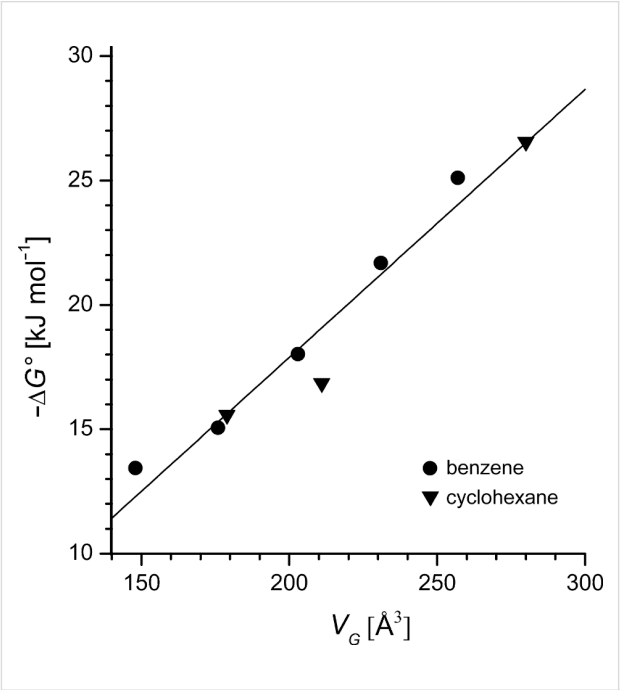

Figure 5: Gibbs free energy of formation of the inclusion compounds of benzene and cyclohexane derivatives in host **4** as a function of the molecular volume $V_G = M/dN_A$.

The ability of the program Macromodel (from Schrödinger Inc.) to predict the nonpolar interactions between host **4** and benzene derivatives was finally evaluated by means of docking simulations. Measured binding free energies were plotted as a function of the simulated inclusion enthalpies (Figure 6), defined as the enthalpy differences between the inclusion compounds and the free species. A significant linear correlation was obtained, confirming that the space filling of host cavity plays a dominant role within such series of complexes, and that the applied force field was reasonable. All guests fitted completely into the cavity of host **4** without steric hindrance. The slope of the experimental Gibbs free energy versus the simulated interaction enthalpy was still inferior to unity (0.69), which indicated that the host–guest interactions were partially compensated by reduced solvation and loss of freedom of the host–guest system.

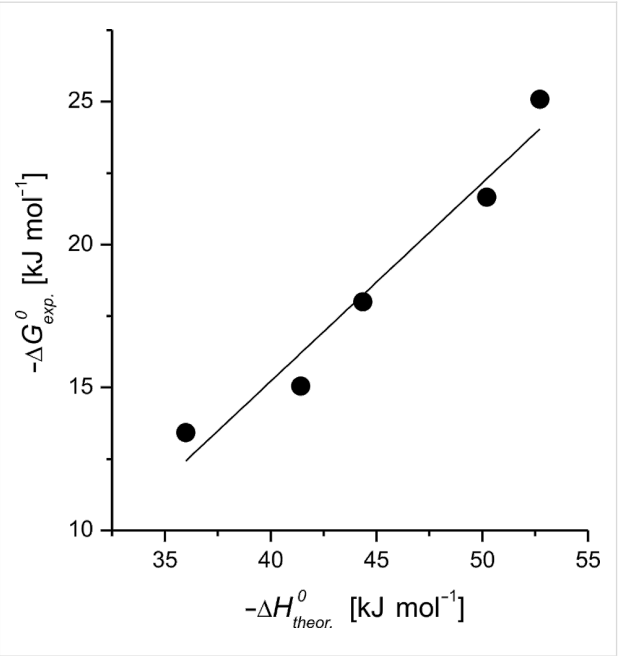

Figure 6: Gibbs free energy of formation of the inclusion compounds of benzene derivatives in host **4** as a function of the theoretical inclusion enthalpy, obtained by simulation by Macromodel (slope 0.69).

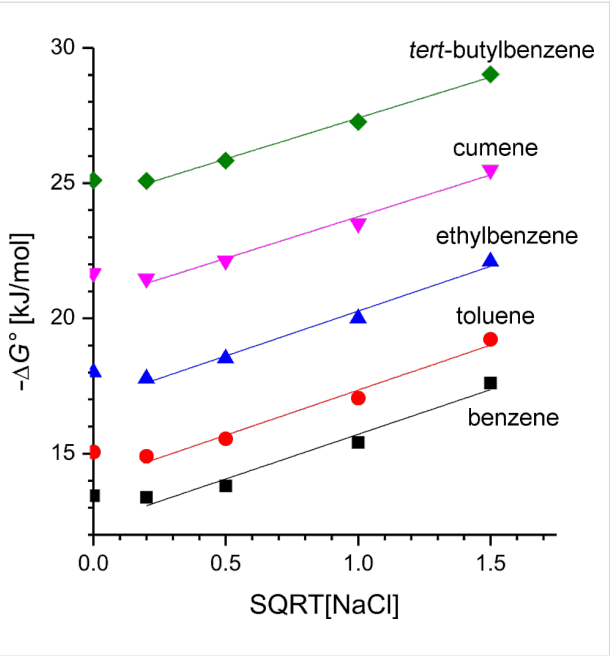

Figure 7: Free binding enthalpy for benzene, toluene, ethylbenzene, cumene, and *tert*-butylbenzene, in host **4** as a function of the square root of the salt concentration [NaCl].

One way to further improve the hydrophobic binding potential of a host in water is to add a salt such as NaCl [42]. From previous work we knew that $-\Delta G°$ increases linearly with the square root of the concentration of NaCl, equivalent to the ionic strength. We found a slope of

$$-\frac{\delta\Delta G°}{\delta\sqrt{I}} = 2 \text{ kJ mol}^{-1}\text{M}^{-0.5}$$

for binding in β-CD thioethers [43]. The investigation of the inclusion of the benzene derivatives in host **4** for various salt concentrations also provided a linear increase of the binding free enthalpy with the same slope as before,

$$-\frac{\delta\Delta G°}{\delta\sqrt{I}} = 2 \text{ kJ mol}^{-1}\text{M}^{-0.5}$$

(Figure 7). Consequently, this salt effect appears to be a unique feature of hydrophobic binding, as neither the hosts nor the guests are expected to interact significantly with NaCl. Very high binding constants of up to 120,000 M^{-1} could be reached for *tert*-butylbenzene with host **4**.

Conclusion

The GC-headspace technique is well suited for the determination of the stability constants of sparingly soluble inclusion compounds of volatile hydrophobic guests in CDs and their derivatives. β-CD thioethers **3** and **4** are good candidates for the solubilization of volatile hydrophobic compounds, because they are soluble in water at any concentration. Very high binding constants are obtained by attachment of hydrophobic substituents at both host and guest. However, substitution of CDs has to be performed at the primary positions of β-CD. Our binding data are well described by the space filling of the cavity, as defined either by the number of carbons *n*, the molecular volume of the guest V_G or by molecular modeling.

Experimental

Materials

Benzene and cyclohexane derivatives were purchased from Aldrich, β-CD and hydroxypropyl-β-CD (DS 5.6) from Wacker Chemie. β-CD derivatives **3** and **4** were synthesized from β-CD **1** following published procedures. Distilled water was used in all experiments.

Headspace analysis

Similar to those described in [44], measurements were conducted with an Agilent headspace autosampler. Sample solutions of 10 mL containing 1 ppm of guest were introduced into 20 mL headspace vials and sealed by using a silicone septa and aluminium foil. The vials were then thermostated at 25 ± 0.1 °C. After the equilibrium had been established (30 min), 1 mL of vapor from the above solution was withdrawn from the vial by using a gas-tight syringe and injected directly in the chromatographic column via a transfer line (250 °C). Each sample was then analyzed by gas chromatog-

raphy (Perkin Elmer Autosystem XL equipped with a flame-ionization detector using a DB624 column). The GC settings were set as follows: detector temperature, 280 °C; column temperature, 120 °C during 5 min.

Full equilibrium of the chemical solute between liquid and gas phases is required. For the chemicals tested, the equilibrium time was 30 min. Linear response of the GC detector to the chemical concentration range tested is another requirement for the successful application of the method. For all compounds, we verify that the GC detector responds linearly. The correlation coefficients are all better than 0.998.

The determination of the Henry's law constants were done with four different values of the aqueous volume V (3, 5, 7 and 10 mL for benzene derivatives and 7, 10, 12 and 15 mL for cyclohexane derivatives, respectively).

Molecular modelling

Simulations of inclusion compounds for each benzene derivative into the cavity of host **4** were realized by means of Macromodel [45] with MMFF force field and GB/SA simulation of water [46]. The host structure was based on a nondistorted β-CD with C_7 symmetry, on which primary hydroxyl groups were replaced by thioether arms (with a linear conformation, leading to a tubular extension of the cavity). Guests were constructed manually and submitted to minimization, prior to inclusion simulations. The docking of each guest inside host **4** was realized by means of Monte Carlo searches, with the generation of 5000 conformations (Polak–Ribiere conjugate gradient minimization, convergence fixed to 0.05 kJ $Å^{-1}$ mol^{-1}). During the search, host **4** was kept rigid, while the guest was freely modified. The most stable conformation for each inclusion compound was then completely relaxed (convergence fixed to 0.05 kJ $Å^{-1}$ mol^{-1}). Inclusion enthalpy was evaluated by the difference between the most stable inclusion-compound conformation and the free species.

Supporting Information

Supporting Information File 1

Derivation of Equation 1 and determination of Henry's law constant.
[http://www.beilstein-journals.org/bjoc/content/supplementary/1860-5397-9-133-S1.pdf]

Acknowledgements

We acknowledge support from UCEIV, which participates in the Institut de Recherche en ENvironnement Industriel (IRENI) financed by the Communauté Urbaine de Dunkerque, the Région Nord Pas-de-Calais, the Ministère de l'Enseignement Supérieur et de la Recherche, the CNRS and European Regional Development Fund (ERDF).

References

1. Rekharsky, M. V.; Inoue, Y. *Chem. Rev.* **1998,** *98,* 1875–1918. doi:10.1021/cr970015o
2. Sanemasa, I.; Akamine, Y. *Bull. Chem. Soc. Jpn.* **1987,** *60,* 2059–2066. doi:10.1246/bcsj.60.2059
3. Höfler, T.; Wenz, G. *J. Inclusion Phenom. Mol. Recognit. Chem.* **1996,** *25,* 81–84. doi:10.1007/BF01041541
4. Szaniszló, N.; Fenyvesi, É.; Balla, J. *J. Inclusion Phenom. Macrocyclic Chem.* **2005,** *53,* 241–248. doi:10.1007/s10847-005-0245-6
5. Gelb, R. I.; Schwartz, L. M. *J. Inclusion Phenom. Mol. Recognit. Chem.* **1989,** *7,* 537–543. doi:10.1007/BF01080464
6. Briggner, L.-E.; Ni, X.-R.; Tempesti, F.; Wadsö, I. *Thermochim. Acta* **1986,** *109,* 139–143. doi:10.1016/0040-6031(86)85015-8
7. Eftink, M. R.; Andy, M. L.; Bystrom, K.; Perlmutter, H. D.; Kristol, D. S. *J. Am. Chem. Soc.* **1989,** *111,* 6765–6772. doi:10.1021/ja00199a041
8. Hinze, W. L. *Sep. Purif. Methods* **1981,** *10,* 159–237. doi:10.1080/03602548108066011
9. Liu, L.; Guo, Q.-X. *J. Inclusion Phenom. Macrocyclic Chem.* **2002,** *42,* 1–14. doi:10.1023/A:1014520830813
10. Tanford, C. *J. Am. Chem. Soc.* **1962,** *84,* 4240–4247. doi:10.1021/ja00881a009
11. Israelachvili, J.; Wennerström, H. *Nature* **1996,** *379,* 219–225. doi:10.1038/379219a0
12. Schneider, H.-J.; Yatsimirsky, A. K. *Chem. Soc. Rev.* **2008,** *37,* 263–277. doi:10.1039/b612543n
13. Schneider, H.-J. *Angew. Chem., Int. Ed.* **2009,** *48,* 3924–3977. doi:10.1002/anie.200802947
14. Snyder, P. W.; Mecinović, J.; Moustakas, D. T.; Thomas, S. W., III; Harder, M.; Mack, E. T.; Lockett, M. R.; Héroux, A.; Sherman, W.; Whitesides, G. M. *Proc. Natl. Acad. Sci. U. S. A.* **2011,** *108,* 17889–17894. doi:10.1073/pnas.1114107108
15. Biedermann, F.; Uzunova, V. D.; Scherman, O. A.; Nau, W. M.; De Simone, A. *J. Am. Chem. Soc.* **2012,** *134,* 15318–15323. doi:10.1021/ja303309e
16. Eldridge, M. D.; Murray, C. W.; Auton, T. R.; Paolini, G. V.; Mee, R. P. *J. Comput.-Aided Mol. Des.* **1997,** *11,* 425–445. doi:10.1023/A:1007996124545
17. Moitessier, N.; Englebienne, P.; Lee, D.; Lawandi, J.; Corbeil, C. R. *Br. J. Pharmacol.* **2008,** *153,* S7–S26. doi:10.1038/sj.bjp.0707515
18. Wenz, G. *Clin. Drug Invest.* **2000,** *19* (Suppl. 2), 21–25. doi:10.2165/00044011-200019002-00003
19. Decock, G.; Landy, D.; Surpateanu, G.; Fourmentin, S. *J. Inclusion Phenom. Macrocyclic Chem.* **2008,** *62,* 297–302. doi:10.1007/s10847-008-9471-z
20. Shao, D.; Sheng, G.; Chen, C.; Wang, X.; Nagatsu, M. *Chemosphere* **2010,** *79,* 679–685. doi:10.1016/j.chemosphere.2010.03.008
21. Mahlambi, M. M.; Malefetse, T. J.; Mamba, B. B.; Krause, R. W. *J. Polym. Res.* **2010,** *17,* 589–600. doi:10.1007/s10965-009-9347-y
22. Rölling, P.; Lamers, M.; Staudt, C. *J. Membr. Sci.* **2010,** *362,* 154–163. doi:10.1016/j.memsci.2010.06.036
23. Baruch-Teblum, E.; Mastai, Y.; Landfester, K. *Eur. Polym. J.* **2010,** *46,* 1671–1678. doi:10.1016/j.eurpolymj.2010.05.007

24. Cassez, A.; Kania, N.; Hapiot, F.; Fourmentin, S.; Monflier, E.; Ponchel, A. *Catal. Commun.* **2008,** *9,* 1346–1351. doi:10.1016/j.catcom.2007.11.031
25. Schwartz, A.; Bar, R. *Appl. Environ. Microbiol.* **1995,** *61,* 2727–2731.
26. Mavridis, I. M.; Hadjoudis, E. *Carbohydr. Res.* **1992,** *229,* 1–15. doi:10.1016/S0008-6215(00)90476-2
27. Enright, G. D.; Udachin, K. A.; Ripmeester, J. A. *CrystEngComm* **2010,** *12,* 1450–1453. doi:10.1039/b920581k
28. Sanemasa, I.; Wu, J.-S.; Toda, K. *Bull. Chem. Soc. Jpn.* **1997,** *70,* 365–369. doi:10.1246/bcsj.70.365
29. Müller, B. W.; Brauns, U. *J. Pharm. Sci.* **1986,** *75,* 571–572. doi:10.1002/jps.2600750609
30. Brewster, M. E.; Loftsson, T. *Pharmazie* **2002,** *57,* 94–101.
31. Armstrong, D. W.; Li, W.; Chang, C. D.; Pitha, J. *Anal. Chem.* **1990,** *62,* 914–923. doi:10.1021/ac00208a006
32. Thiele, C.; Auerbach, D.; Jung, G.; Wenz, G. *J. Inclusion Phenom. Macrocyclic Chem.* **2011,** *69,* 303–307. doi:10.1007/s10847-010-9741-4
33. Steffen, A.; Thiele, C.; Tietze, S.; Strassnig, C.; Kämper, A.; Lengauer, T.; Wenz, G.; Apostolakis, J. *Chem.–Eur. J.* **2007,** *13,* 6801–6809. doi:10.1002/chem.200700661
34. Fourmentin, S.; Outirite, M.; Blach, P.; Landy, D.; Ponchel, A.; Monflier, E.; Surpateanu, G. *J. Hazard. Mater.* **2007,** *141,* 92–97. doi:10.1016/j.jhazmat.2006.06.090
35. Blach, P.; Fourmentin, S.; Landy, D.; Cazier, F.; Surpateanu, G. *Chemosphere* **2008,** *70,* 374–380. doi:10.1016/j.chemosphere.2007.07.018
36. Lantz, A. W.; Wetterer, S. M.; Armstrong, D. W. *Anal. Bioanal. Chem.* **2005,** *383,* 160–166. doi:10.1007/s00216-005-0030-9
37. Ciobanu, A.; Mallard, I.; Landy, D.; Brabie, G.; Nistor, D.; Fourmentin, S. *Carbohydr. Polym.* **2012,** *87,* 1963–1970. doi:10.1016/j.carbpol.2011.10.005
38. Wenz, G. *Beilstein J. Org. Chem.* **2012,** *8,* 1890–1895. doi:10.3762/bjoc.8.218
39. Wang, H. M.; Wenz, G. *Chem.–Asian J.* **2011,** *6,* 2390–2399. doi:10.1002/asia.201100217
40. Breslow, R. *Acc. Chem. Res.* **1991,** *24,* 159–164. doi:10.1021/ar00006a001
41. Szejtli, J. Chemistry, Physical and Biological Properties of Cyclodextrins. In *Cyclodextrins;* Szejtli, J.; Osa, T., Eds.; Comprehensive Supramolecular Chemistry, Vol. 3; Pergamon Press, 1996; pp 4–40.
42. Fini, P.; Castagnolo, M.; Catucci, L.; Cosma, P.; Agostiano, A. *J. Therm. Anal. Calorim.* **2003,** *73,* 653–659. doi:10.1023/A:1025498601192
43. Wenz, G.; Strassnig, C.; Thiele, C.; Engelke, A.; Morgenstern, B.; Hegetschweiler, K. *Chem.–Eur. J.* **2008,** *14,* 7202–7211. doi:10.1002/chem.200800295
44. Dron, P. I.; Fourmentin, S.; Cazier, F.; Landy, D.; Surpateanu, G. *Supramol. Chem.* **2008,** *20,* 473–477. doi:10.1080/10610270701358525
45. Mohamadi, F.; Richards, N. G. J.; Guida, W. C.; Liskamp, R.; Lipton, M.; Caufield, C.; Chang, G.; Hendrickson, T.; Still, W. C. *J. Comput. Chem.* **1990,** *11,* 440–467. doi:10.1002/jcc.540110405
46. Cheng, A.; Best, S. A.; Merz, K. M., Jr.; Reynolds, C. H. *J. Mol. Graphics Mod.* **2000,** *18,* 273–282. doi:10.1016/S1093-3263(00)00038-3

License and Terms

Beilstein Journal of Organic Chemistry

Linkage of α-cyclodextrin-terminated poly(dimethylsiloxanes) by inclusion of quasi bifunctional ferrocene

Helmut Ritter*, Berit Knudsen and Valerij Durnev

Full Research Paper

Open Access

Address:
Heinrich-Heine-Universität Düsseldorf, Institut für Organische Chemie und Makromolekulare Chemie, Lehrstuhl für Präparative Polymerchemie, Universitätsstraße 1, D-40225 Düsseldorf, Germany

Email:
Helmut Ritter* - H.Ritter@uni-duesseldorf.de

* Corresponding author

Keywords:
cyclodextrins; ferrocene; host–guest systems; polysiloxanes; supramolecular chemistry

Beilstein J. Org. Chem. **2013,** *9,* 1278–1284.
doi:10.3762/bjoc.9.144

Received: 25 March 2013
Accepted: 13 June 2013
Published: 01 July 2013

This article is part of the Thematic Series "Superstructures with cyclodextrins: Chemistry and applications".

Associate Editor: N. Sewald

Abstract

We report the noncovalent linkage of terminally substituted oligo(dimethylsiloxanes) bearing α-cyclodextrins (α-CD) as host end groups for the cyclopentadienyl rings of ferrocene. This double complexation of unsubstituted ferrocene leads to a supramolecuar formation of the siloxane strands. Structural characterization was performed by the use of ^{1}H NMR and IR spectroscopy and by mass spectrometry. Electron microscopy studies and dynamic light scattering measurements show a significant decrease of the derivative size after the complexation with ferrocene. In addition, further evidence for the successful complexation of the end groups was verified by the shifts of the protons in the ^{1}H NMR spectra and in the correlation signals of the 2D ROESY NMR spectra.

Introduction

Polymers containing cyclodextrins (CD) covalently or supramolecularly attached are of increasing interest in recent years. For example, polymers bearing β-CD as side or terminal groups and their interaction with classical guest groups such as adamantane or azo-dyes have been intensively studied [1-4]. The characterization of the inclusion complexes between cyclodextrin and ferrocene as a representative of metallocenes has been the subject of numerous works. Especially Takahashi and Harada were engaged in the analysis of ferrocene complexes with different cyclodextrins [5], which could be obtained in aqueous solution in high yields. In addition, the crystal structure of the α-CD:ferrocene complex has been analyzed by X-ray-diffraction [6]. These studies showed that the ferrocene molecule is encapsulated by two α-CD rings in a tail-to-tail orientation, where all carbon atoms of the cyclopentadienyl rings are in close contact with the cavity of the cyclodextrin macrocycles. The size of the ferrocene molecule is too large to penetrate completely into the α-CD cavity. Only a single cyclopentadienyl ring of the ferrocene is included. The binding mode, thermal stability, formation constants, and dielectric properties

[7] of this inclusion complex were also investigated by circular dichroism spectroscopy [8] and thermogravimetric analysis [9]. In addition, the complex of ferrocene and α-CD could be detected in the gas phase by mass spectrometry [10]. Recently, there have been many reports focusing on the use of α-CD in aqueous solution as a mobile phase for optical resolution of ferrocene derivates [11,12]. α-CD-functionalized siloxanes, however, have rarely been described in the literature. There are many reports on siloxanes bearing β-CD attached on the surface, which are used as stationary phases for chromatography and for drug-release systems [13-22]. In a previous paper we described the noncovalent AA–BB-type linkage of poly(dimethylsiloxanes) containing terminal ß-CD groups with terminally attached guest molecules on the poly(dimethylsiloxanes) [23]. With this in mind, the aim of our present study was to synthesize α-CD-terminated poly(dimethylsiloxanes) to create novel supramolecular linear or macrocyclic siloxan structures based on double inclusion complexes with ferrocene.

Results and Discussion

The syntheses of α-CD-terminated poly(dimethylsiloxanes) **4** and **5** were performed by hydrosilylation of mono-((6-*N*-allylamino)-6-deoxy)-peracetylated-α-CD (**3**) using a short-chain oligo(dimethylsiloxane) **1** or a long-chain poly(dimethylsiloxane) **2**, respectively, (Scheme 1).

During the reactions, samples were collected and investigated by IR spectroscopy in order to ensure the full conversion of the reactants to products (Figure 1).

The disappearance of the absorption bands at 2100 cm^{-1} clearly shows the successful hydrosilylation of the educts to the newly synthesized derivatives **4** and **5**.

The ^1H NMR spectra of the α-CD-functionalized poly(dimethylsiloxanes) (α-CD-DS **4** and α-CD-PDMS **5**) reveal the characteristic signals of the Si–CH_3 groups of the siloxane backbones at 0 ppm. In addition, the signals of the cyclodextrin-

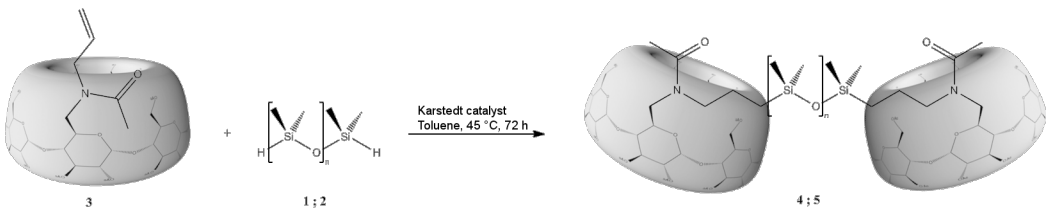

Scheme 1: Hydrosilylation of Si–H terminated poly(dimethylsiloxanes) **1** and **2** with mono-((6-*N*-(allylamino)-6-deoxy)-peracetylated-α-CD (**3**) to compounds **4** (*n* = 1) and **5** (*n* = 6–37).

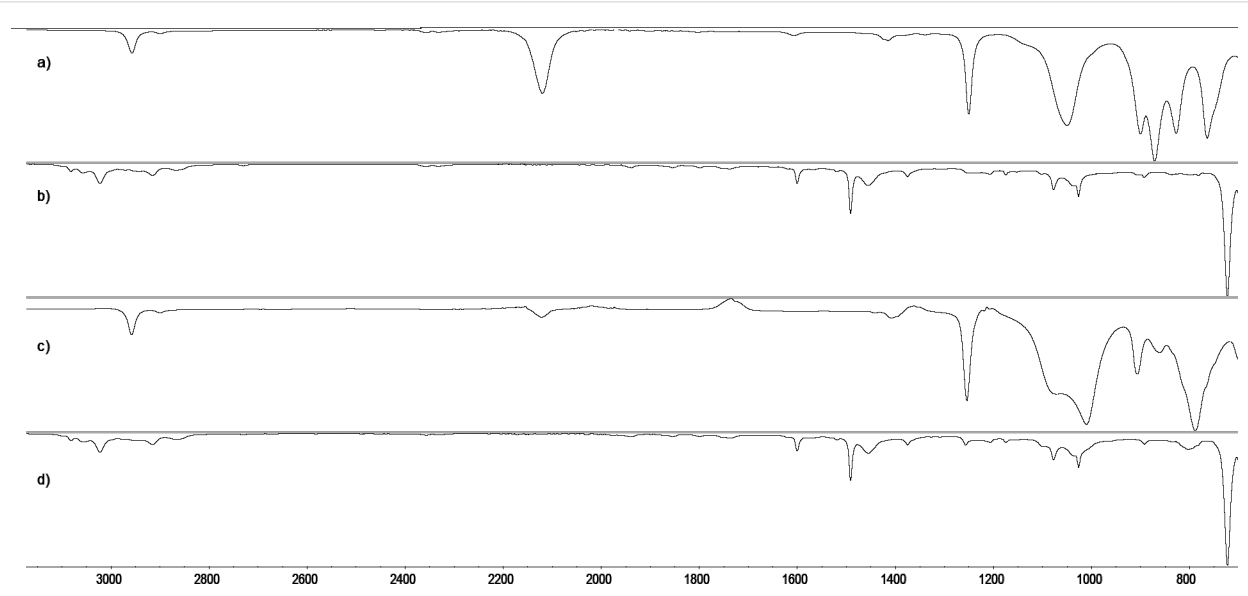

Figure 1: IR spectra of (a) H-terminated disiloxane (**1**), (b) α-CD-terminated disiloxane (α-CD-disiloxane) (**4**), (c) H-terminated polydimethylsiloxane (**2**) and (d) α-CD-terminated polydimethylsiloxane (α-CD-PDMS) (**5**).

substituents appear in the area of 3.50 to 6.00 ppm. New peaks at 0.43 and 1.25 ppm of the resulting dimethylene bridge between the siloxane and α-CD are detectable. Signals for the double bond of the vinyl group and the Si–H bond of the starting materials are absent, as expected. The MALDI–TOF spectra of the modified poly(dimethylsiloxanes) **4** and **5** show terminally substituted products of various chain lengths, wherein the distance of 74 g/mol between the mass signals exactly corresponds to one dimethylsiloxane unit. The results of the IR, ^{1}H NMR and mass spectroscopy strongly support the existence of the described derivatives. The terminally α-CD-functionalized poly(dimethylsiloxanes) **4** and **5** were subsequently used as host molecules component for the following complexation reactions.

Host–guest interactions of the siloxane derivatives with ferrocene

Linking of the obtained polydimethyl and disiloxane derivatives through host–guest interactions with single ferrocene molecules generates supramolecular, connected siloxane chains. The guest molecule ferrocene was therefore dissolved in chloroform and treated with the α-CD-siloxane derivatives. The solutions were stirred overnight and analyzed by ^{1}H NMR and 2D ROESY NMR.

As seen in Figure 2, ^{1}H NMR spectra of pure ferrocene and the resulting complexes are compared with regard to the proton signals of the cyclopentadienyl rings of the ferrocene. In the case of pure ferrocene (A) the signal of these protons appears at 4.22 ppm. After the complexation with the α-CD-modified disiloxane **4**, a shift of the cyclopentadienyl signals to 4.15 ppm can be observed (B). This phenomenon is explained by the penetration of the attached cyclopentadienyl rings of the guest molecule ferrocene into the cavity of the cyclodextrin and a subsequent change of the chemical environment of the cyclopentadienyl rings. The same studies were performed with the complex of α-CD modified polydimethylsiloxane **5** and ferrocene (C) to prove a successful complexation. As expected, a

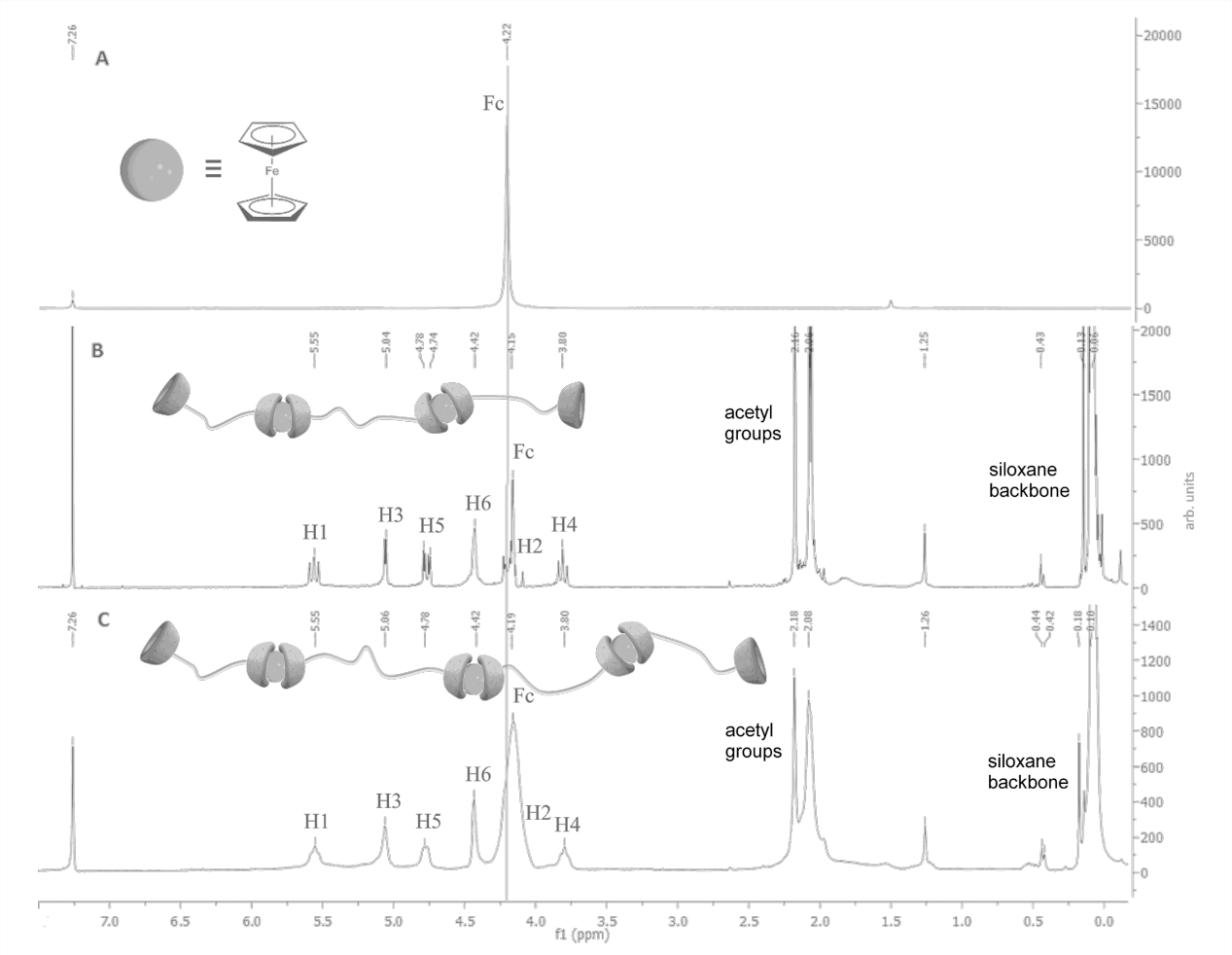

Figure 2: ^{1}H NMR spectra of ferrocene (A), complex of α-CD-disiloxane (α-CD-DS) **4** with ferrocene (B) and complex of α-CD-poly(dimethylsiloxane) (α-CD-PDMS) **5** with ferrocene (C).

clear shift of the ferrocene signal from 4.22 to 4.19 ppm can be detected, which also suggests that ferrocene molecules are completely complexed by the α-CD units.

The question about the formation of linear or macrocyclic suprastructures, cannot be answered by this method. Thus, the various polysiloxane strands can be linked with each other through the host–guest interactions of the terminal α-CD units and pure ferrocene without the need for covalent bonds. In order to complete the characterization of these host–guest interactions of the novel compounds, they were also examined by 2D ROESY NMR spectroscopy.

The 2D ROESY NMR spectra of the short-chain α-CD-disiloxane **4** with ferrocene (Figure 3) shows the correlation between the inner cavity protons H-3 and H-5 of the attached α-cyclodextrins and the protons of the cyclopentadienyl rings of the guest molecule ferrocene (Fc) (dotted lines) based on the characteristic cross-peaks of these protons (spots). The 2D ROESY NMR spectrum of the long-chain α-CD-polydimethylsiloxane **5** with ferrocene (Figure 4) also indicates the described proton interactions of the host and guest molecules. The noncovalent bonds of the siloxanes with the ferrocene leading to supramolecular structures are hereby established.

Thin-layer chromatography studies (toluene/ethanol 30:1 by volume) also indicate the presence of enclosed ferrocene in the cavity of the cyclodextrins. UV-active areas can be detected, which do not migrate with the solvent front in contrast to pure ferrocene.

Certainly, the viscosity of the poly(dimethylsiloxane) educts and the complexed systems is of great interest. However, a significant increase of the viscosity in solution could not be detected under the applied conditions, probably due to the relatively high shear forces, which cause the decomplexation of the derivatives mechanically.

In addition, the successful complexation of the α-CD-modified siloxanes and the formation of supramolecular structures via inclusion complexes with ferrocene can be illustrated in the TEM images of **4** (Figure 5). Figure 5A (α-CD-disiloxane **4**) shows a majority of globular structures of up to 400 nm. In the case of the complex of the compound **4** with ferrocene

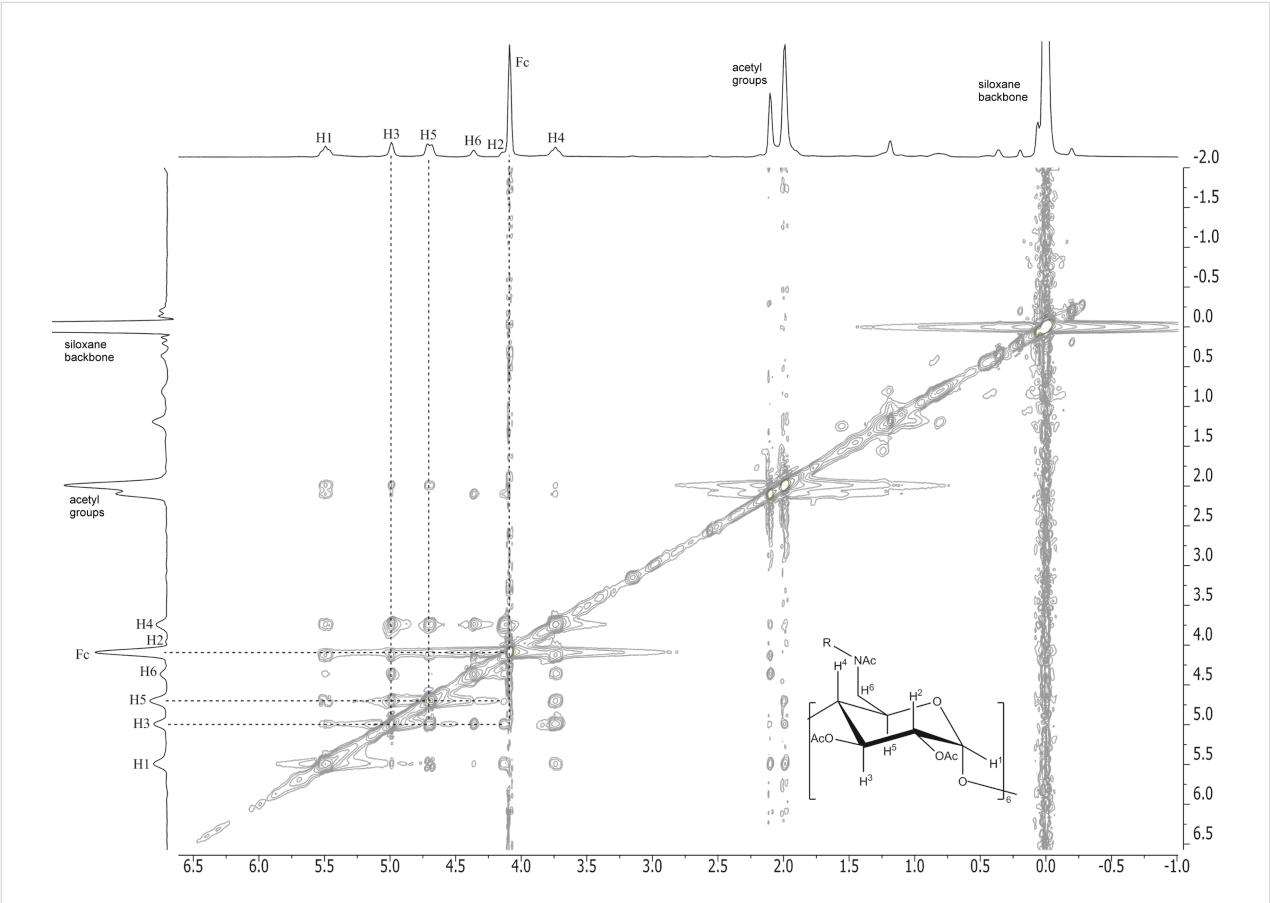

Figure 3: 2D ROESY NMR spectra of the complex of α-CD-disiloxane (α-CD-DS) **4** with ferrocene.

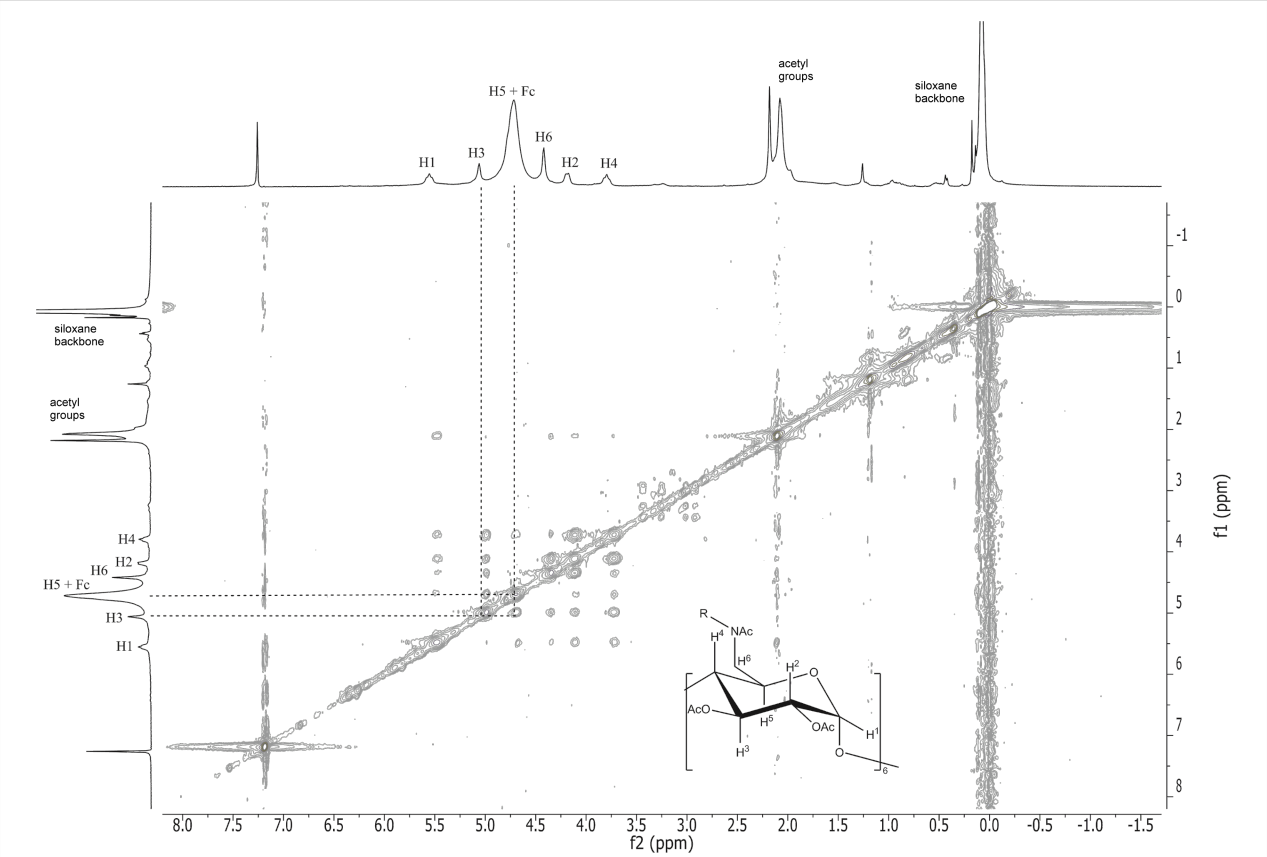

Figure 4: 2D ROESY NMR spectra of the complex of α-CD-polydimethylsiloxane (α-CD-PDMS) **5** with ferrocene.

(Figure 5B), elongated structures of up to 4000 nm can be observed. This phenomenon might be explained by the supramolecular linkage of the short-chain disiloxanes by interaction with the bifunctional ferrocene molecules, which leads to the formation of the larger structures.

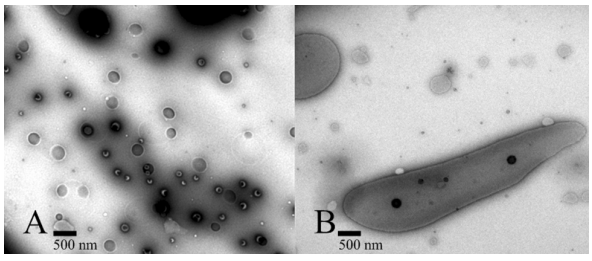

Figure 5: TEM images of α-CD-disiloxane **4** (A) and the supramolecular formation of α-CD-disiloxane **4** with ferrocene (B).

Finally, DLS (dynamic light scattering) analysis of **4** and **5** and their complexes with ferrocene were performed. Figure 6 illustrates the hydrodynamic diameters of α-CD-disiloxane **4** and α-CD-disiloxane with ferrocene. The average hydrodynamic diameter of α-CD-modified disiloxane **4** (dashed line) can be determined as 343 nm, which corresponds to the average sizes of the particles observed by TEM measurements. After the addition of ferrocene, the resulting complex with **4** was investigated by DLS (solid line) as well. The hydrodynamic diameter significantly shifts from 343 nm to 615 and 5489 nm. The hydrodynamic diameter of 615 nm can be explained by the formation of some macrocycles and oligomers by noncovalent interactions of the host and guest molecules. This phenomenon might also explain the almost unchanged viscosity increase of the complex in comparison to the uncomplexed educts, which is not influenced decisively by the presence of the smaller supramolecular structures. However, the peak at about 5000 nm indicates the presence of larger linear structures based on the complexation of α-CD-disiloxane **4** with the ferrocene molecules, which were also observed in the TEM images.

This further confirms the assumption that the terminally functionalized poly(dimethylsiloxanes) can assemble to supramolecular structures through noncovalent interactions.

Conclusion

We have demonstrated, for the first time, a chain extension of poly(dimethylsiloxanes) in chloroform as solvent, by host–guest

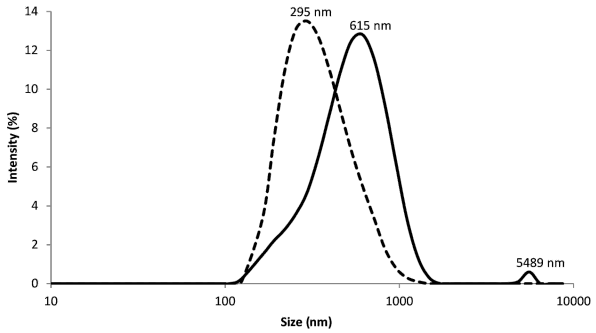

Figure 6: DLS measurements of α-CD-disiloxane **4** (A) (dashed line) and the supramolecular formation of α-CD-disiloxane **4** with ferrocene (B) (solid line).

interactions of terminally attached α-CD with ferrocene as a quasi-bifunctional single guest molecule. The formation of noncovalent linkages was proved by the use of NMR spectroscopy and TEM images. However, it turned out that the stability of linking functions is relatively poor with respect to shear forces during viscosity measurements.

Experimental

Materials and methods

Commercial reagents and solvents were purchased from ABCR and Sigma Aldrich and used as received. When necessary, solvents were dried and purified by appropriate standard procedures. Mono-(6-(*p*-toluenesulfonyl)-6-deoxy)-α-cyclodextrin (α-tosyl-CD), mono-(6-*N*-allylamino)-6-deoxy)-α-cyclodextrin (AAm-α-CD) and mono-((6-*N*-allylamino)-6-deoxy)-peracetylated-α-cyclodextrin (AAm-Ac-α-CD) [21] were synthesized according to the literature. MALDI–TOF mass spectra were recorded with a Bruker Ultraflex time-of-flight mass spectrometer. The device operates both in the linear mode and in reflector mode with a 337 nm nitrogen laser. The samples were dissolved in a suitable solvent. A dithranol (DIT) or 2,5-dihydroxybenzoic acid (DHB) matrix was used. The IR spectra were recorded with a Fourier transform infrared spectrometer FTIR Nicolet 5SXB. The calibration of the wave numbers was done by using a He–Ne laser. The ATR measurements were performed with a Specac Golden Gate diamond-ATR unit. For the NMR measurements at 300 MHz a Bruker Avance III - 300 (2010) spectrometer was used. The magnetic field strength was 7.05 T. This corresponds to an absorption frequency of 300 MHz for ^{1}H NMR and 75 MHz for ^{13}C {^{1}H} NMR. For ESI-measurements on an ion-trap mass spectrometer API Finnigan LCQ Deca, the substances were dissolved in a suitable solvent at a concentration of 2 mg·mL^{-1}. The ionization was carried out by electrospray ionization (ESI). The TEM images were obtained on a Zeiss EM 902A microscope at 80 kV. The samples were dissolved in chloroform and dripped on copper grids (Formvar/carbon film 400 mesh). After evaporation of the solvent, the remaining pure substances could be examined under a high vacuum (10^{-7} bar). The hydrodynamic diameters of the derivatives and their complexes were determined by use of dynamic light scattering (DLS) in the back scattering mode with a Malvern Zetasizer Nano ZS ZEN3600 at a laser wavelength of 633 nm and a detection angle of 173°. The samples were dissolved in chloroform (10 mg·mL^{-1}) and measured in quartz cuvettes of 1 cm thickness. The measurement data were evaluated with a nonnegative least squares (NNLS) algorithm. The number-averaged diameters were used to characterize the samples.

Synthesis of siloxane-derivatives

Synthesis of mono-((6-*N*-allylamino)-6-deoxy)-peracetylated-α-cyclodextrin-dimethyldisiloxane (α-CD-disiloxane) (4): Mono-((6-*N*-allylamino)-6-deoxy)-peracetylated-α-cyclodextrin (0.70 g, 0.40 mmol) is dissolved in 30 mL of dry toluene under an argon atmosphere at 45 °C. 1,1,3,3-Tetramethyldisiloxane (0.04 mL, 0.20 mmol) is added. In a period of 5 h, the Karstedt catalyst (50 µL, 2.1–2.4% Pt) is added in portions. After 72 h, the toluene is evaporated and the product is obtained by fractional precipitation as a solid (0.20 g, 20%). IR: 3026, 2919, 1746, 1605, 1495, 1459, 1260, 1140, 1081, 1029 cm^{-1}; ^{1}H NMR (300 MHz, $CDCl_3$) δ 0.00 (m, 12H), 0.43 (m, 4H), 1.25 (s, 4H), 2.06–2.16 (m, 108H, CH_3CO), 3.80 (m, 12H), 4.15 (m, 12H), 4.42 (m, 24H), 4.74–4.78 (m, 12H), 5.04 (m, 12H), 5.55 (m, 12H); ESI–MS *m*/*z*: 3148.34 $[M + Na]^+$.

Synthesis of mono-((6-*N*-allylamino)-6-deoxy)-peracetylated-α-cyclodextrin-polymethylsiloxane (α-CD-PDMS) (5): Mono-((6-*N*-allylamino)-6-deoxy)-peracetylated-α-cyclodextrin (0.70 g, 0.4 mmol) is dissolved in 60 mL of dry toluene under an argon atmosphere. Hydride-terminated poly(dimethylsiloxane) (0.3 mL, 0.22 mmol) is added and heated to 75 °C. The Karstedt catalyst (100 µL, 2.1–2.4% Pt) is added in portions over 1 h. After 72 h, the solvent is evaporated and the product is obtained by fractional precipitation as a solid (0.40 g, 35%). IR: 3026, 2919, 1746, 1605, 1495, 1459, 1260, 1140, 1081, 1029 cm^{-1}. ^{1}H NMR (300 MHz, $CDCl_3$) δ 0.00 (m, 78H), 0.44–0.42 (m, 4H), 1.26 (s, 4H), 2.06–2.16 (m, 108H, CH_3CO), 3.80 (m, 12H), 4.19 (m, 12H), 4.42 (m, 24H), 4.78 (m, 12H), 5.06 (m, 12H), 5.55 (m, 12H); MALDI–TOF–MS *m*/*z*: 3962.58 $[M + Na]^+$ for n = 12.

Complexation reactions

Complexation of α-CD-disiloxane (4) with ferrocene: α-CD-disiloxane (100 mg, 0.015 mmol) is dissolved in a solution of ferrocene (2.8 mg, 0.015 mmol) and 2.0 mL of chloroform and stirred at rt overnight. To isolate the product, the solvent is evaporated. The complex is obtained as a solid. ^{1}H NMR

(300 MHz, $CDCl_3$) δ 0.01–0.16 (m, 12H), 0.44–0.42 (m, 4H), 1.25 (s, 4H), 2.06–2.16 (m, 108H, CH_3CO), 3.69–3.85 (m, 2H), 4.15 (s, 10H, ferrocene), 4.25 (m, 2H), 4.42 (m, 2H), 4.74–4.78 (m, 38H), 5.04 (m, 14H), 5.55 (m, 14H).

Complexation of α-CD-PDMS (5) with ferrocene: α-CD-PDMS (40 mg, 0.01 mmol) is dissolved in a solution of ferrocene (1.5 mg, 0.01 mmol) and 2.0 mL of chloroform and stirred at rt overnight. To isolate the product, the solvent is evaporated. The complex is obtained as a solid. ^{1}H NMR (300 MHz, $CDCl_3$) δ 0.01–0.16 (m, 12H), 0.44–0.42 (m, 4H), 1.25 (s, 4H), 2.06–2.16 (m, 108H, CH_3CO), 3.69–3.85 (m, 2H), 4.19 (s, 10H, ferrocene), 4.25 (m, 2H), 4.42 (m, 2H), 4.74–4.78 (m, 38H), 5.04 (m, 14H), 5.55 (m, 14H).

Acknowledgements

The authors thank the Center of Advanced Imaging of the Heinrich-Heine-Universität Düsseldorf for support of this research. The authors also thank the Evonik Goldschmidt GmbH in Essen for financial support of this research and especially Dr. Wilfried Knott and Dr. Frauke Henning for the helpful discussions concerning this work.

References

1. Schmidt, B. V. K. J.; Hetzer, M.; Ritter, H.; Barner-Kowollik, C. *Macromolecules* **2013,** *46,* 1054–1065. doi:10.1021/ma302386w
2. Maatz, G.; Maciollek, A.; Ritter, H. *Beilstein J. Org. Chem.* **2012,** *8,* 1929–1935. doi:10.3762/bjoc.8.224
3. Stadermann, J.; Komber, H.; Erber, M.; Däbritz, F.; Ritter, H.; Voit, B. *Macromolecules* **2011,** *44,* 3250–3259. doi:10.1021/ma200048a
4. Weickenmeier, M.; Wenz, G. *Macromol. Rapid Commun.* **1996,** *17,* 731–736. doi:10.1002/marc.1996.030171008
5. Harada, A.; Takahashi, S. *J. Chem. Soc., Chem. Commun.* **1984,** 645–646. doi:10.1039/C39840000645
6. Odagaki, Y.; Hirotsu, K.; Higuchi, T.; Harada, A.; Takahashi, S. *J. Chem. Soc., Perkin Trans. 1* **1990,** 1230–1231. doi:10.1039/p19900001230
7. Kolivoška, V.; Gál, M.; Hromadová, M.; Valášek, M.; Pospíšil, L. *J. Organomet. Chem.* **2011,** *696,* 1404–1408. doi:10.1016/j.jorganchem.2011.01.007
8. Harada, A.; Hu, Y.; Yamamoto, S.; Takahashi, S. *J. Chem. Soc., Dalton Trans.* **1988,** 729–732. doi:10.1039/DT9880000729
9. Bai, Y.; Wang, J.; Bashari, M.; Hu, X.; Feng, T.; Xu, X.; Jin, Z.; Tian, Y. *Thermochim. Acta* **2012,** *541,* 62–69. doi:10.1016/j.tca.2012.04.029
10. Bakhtiar, R.; Kaifer, A. E. *Rapid Commun. Mass Spectrom.* **1998,** *12,* 111–114. doi:10.1002/(SICI)1097-0231(19980214)12:3<111::AID-RCM135>3.0.CO;2-D
11. Harada, A.; Saeki, K.; Takahashi, S. *J. Inclusion Phenom.* **1987,** *5,* 601–604. doi:10.1007/BF00662999
12. Harada, A.; Saeki, K.; Takahashi, S. *Carbohydr. Res.* **1989,** *192,* 1–7. doi:10.1016/0008-6215(89)85159-6
13. Lai, X.-H.; Ng, S.-C. *J. Chromatogr., A* **2004,** *1031,* 135–142. doi:10.1016/j.chroma.2003.11.018
14. Yi, G.; Bradshaw, J. S.; Rossiter, B. E.; Reese, S. L.; Petersson, P.; Markides, K. E.; Lee, M. L. *J. Org. Chem.* **1993,** *58,* 2561–2565. doi:10.1021/jo00061a035
15. Yi, G.; Bradshaw, J. S.; Rossiter, B. E.; Malik, A.; Li, W.; Petersson, P.; Markides, K. E.; Lee, M. L. *J. Org. Chem.* **1993,** *58,* 4844–4850. doi:10.1021/jo00070a019
16. Levkin, P. A.; Levkina, A.; Schurig, V. *Anal. Chem.* **2006,** *78,* 5143–5148. doi:10.1021/ac0606148
17. Armstrong, D. W.; Tang, Y.; Ward, T.; Nichols, M. *Anal. Chem.* **1993,** *65,* 1114–1117. doi:10.1021/ac00056a028
18. Zhang, Z.; Wu, M.; Wu, R.; Dong, J.; Ou, J.; Zou, H. *Anal. Chem.* **2011,** *83,* 3616–3622. doi:10.1021/ac200414r
19. Ruderisch, A.; Pfeiffer, J.; Schurig, V. *J. Chromatogr., A* **2003,** *994,* 127–135. doi:10.1016/S0021-9673(03)00423-0
20. Bai, Z.-W.; Lai, X.-H.; Chen, L.; Ching, C.-B.; Ng, S.-C. *Tetrahedron Lett.* **2004,** *45,* 7323–7326. doi:10.1016/j.tetlet.2004.08.007
21. Noomen, A.; Hbaieb, S.; Parrot-Lopez, H.; Kalfat, R.; Fessi, H.; Amdouni, N.; Chevalier, H. *Mater. Sci. Eng., C* **2008,** *28,* 705–715. doi:10.1016/j.msec.2007.10.057
22. Tian, W.; Fan, X.; Kong, J.; Liu, T.; Liu, Y.; Huang, Y.; Wang, S.; Zhang, G. *Macromolecules* **2009,** *42,* 640–651. doi:10.1021/ma8023848
23. Knudsen, B.; Kergl, B. E.; Paulsen, H.; Durnev, V.; Ritter, H. *J. Polym. Sci., Part A: Polym. Chem.* **2013,** *51,* 2472–2482. doi:10.1002/pola.26636

License and Terms

Beilstein Journal of Organic Chemistry

Topochemical control of the photodimerization of aromatic compounds by γ-cyclodextrin thioethers in aqueous solution

Hai Ming Wang and Gerhard Wenz*

Full Research Paper

Open Access

Address:
Organic Macromolecular Chemistry, Saarland University, Campus Saarbrücken C4 2, 66123 Saarbrücken, Germany

Email:
Gerhard Wenz* - g.wenz@mx.uni-saarland.de

* Corresponding author

Keywords:
acenaphthylene; anthracene; coumarin; cyclodextrins; photodimerization; quantum yield; stereoselectivity

Beilstein J. Org. Chem. **2013,** *9,* 1858–1866.
doi:10.3762/bjoc.9.217

Received: 16 May 2013
Accepted: 15 August 2013
Published: 12 September 2013

This article is part of the Thematic Series "Superstructures with cyclodextrins: Chemistry and applications".

Guest Editor: H. Ritter

Abstract

The formation of soluble 1:2 complexes within hydrophilic γ-cyclodextrin (γ-CD) thioethers allows to perform photodimerizations of aromatic guests under controlled, homogenous reaction conditions. The quantum yields for unsubstituted anthracene, acenaphthylene, and coumarin complexed in these γ-CD thioethers were found to be up to 10 times higher than in the non-complexed state. The configuration of the photoproduct reflected the configuration of the dimeric inclusion complex of the guest. Anti-parallel orientation of acenaphthylene within the CD cavity led to the exclusive formation of the *anti* photo-dimer in quantitative yield. Parallel orientation of coumarin within the complex of a CD thioether led to the formation of the *syn* head-to-head dimer. The degree of complexation of coumarin could be increased by employing the salting out effect.

Introduction

Photochemical reactions have been considered highly attractive for a long time because they often lead to products that are otherwise virtually inaccessible by thermal reactions. The syntheses of highly strained molecules such as cubane [1] and pagodane [2] are famous examples. However, it is often difficult to predict and control the outcome of photochemical transformations in homogeneous media, and various mixtures of products are obtained. Pre-organization of the reactants in the solid state [3] or by various templates in solution has been the best solution to this problem [4,5].

Cyclic host molecules large enough to accommodate two reacting molecules are the smallest possible templates for the control of photoreactions. Such a host provides a well-defined nano environment, a so-called molecular reaction vessel [6], which can catalyze and direct particular transformations.

Calixarenes [7], cucurbiturils [8,9], and cyclodextrins (CDs) [10-16] have already been employed in template controlled photoreactions. Among these hosts CDs offer the advantage of being soluble in water at neutral pH, which is the most favourable solvent for performing photoreactions because of its high transmittance and stability to UV light. Inclusion in CDs not only improves the quantum yields of photodimerizations but also gives rise to high regio- and stereo-selectivities [15-18] However, the application of native CDs for fully hydrophobic reactants is hampered by the fact that their inclusion compounds are nearly insoluble in water leading to undesirable heterogenous reaction conditions [19]. Yields of heterogenous photoreactions generally depend on the particle size of the educt phase because the penetration depth of the incident light is limited.

Recently, we synthesized a series of highly water-soluble per-6-deoxy-thioethers of β- and γ-CD, which are able to solubilize hydrophobic, nearly insoluble guest molecules, such as camptothecin [20], 1,4-dihydroxyanthraquinone [21], betulin [22], benzene and cyclohexane derivatives [23], and even C_{60} [24] in water. Furthermore, their respective γ-CD thioethers form highly water-soluble 1:2 complexes with polycyclic aromatics, such as naphthalene, anthracene (**ANT**), and acenaphthylene (**ACE**) [25]. In the following we report on the photochemistry of **ANT**, **ACE** and coumarin (**COU**), templated by complexation in several hydrophilic γ-CD thioethers **1**–**7** (Figure 1 and Figure 2). Special attention will be paid to both the quantum yields Φ and stereoselectivities of the photodimerizations.

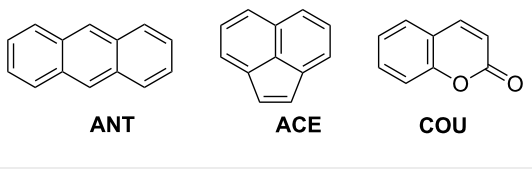

Figure 1: Chemical structures of selected aromatic guests: anthracene, **ANT**; acenaphthylene, **ACE**; and coumarin, **COU**.

Results and Discussion

Photodimerization of anthracene

Due to the fact that the inclusion compounds of **ANT** in native β-CD or γ-CD are completely insoluble in water, only the aqueous photochemistry of hydrophilic **ANT** derivatives, such as anthracene-2-carboxylate (**ANT**-2-COONa) [12], and anthracene-2-sulfonate (**ANT**-2-SO_3Na) [26], have been investigated so far. The quantum yields of photodimerization increase dramatically from 5 to up to 50% by complexation of these guests with β-CD or γ-CD, as found by Tamaki et al. [26,27]. Formation of 2:2 complexes with β-CD and 1:2 (host/guest) sandwich complexes with γ-CD were made responsible for the observed increase in the quantum yields.

The photodimerization of unmodified **ANT** could be performed for the first time homogenously in aqueous solution, because of the high solubilities of **ANT** complexed by γ-CD thioethers **1**–**7** in water. The highest concentration, [**ANT**] = 0.04 mM, was achieved with a 6 mM solution of host **1** [25]. The respective binding constants *K* [25], and quantum yields Φ for monochromatic irradiation, are listed in Table 1. The values of Φ in the presence of 6.0 mM γ-CD thioethers were very high (16–33%) depending on the side groups of the host. Derivative **4** with

Table 1: Influence of CDs on the quantum yield Φ of the photodimerization of **ANT** and 1:2 binding constant *K* [25].

Host[a]	Φ[b] [%]	$K/10^9$ [M^{-2}]
1	29	22.8
2	16	7.7
3	29	6.8
4	33	3.4
5	25	3.7
6	27	6.5
7	19	7.7

[a]Concentration of γ-CD thioethers **1**–**7** was 6.0 mM. [b]For λ = 350 nm, experimental error ± 5 %.

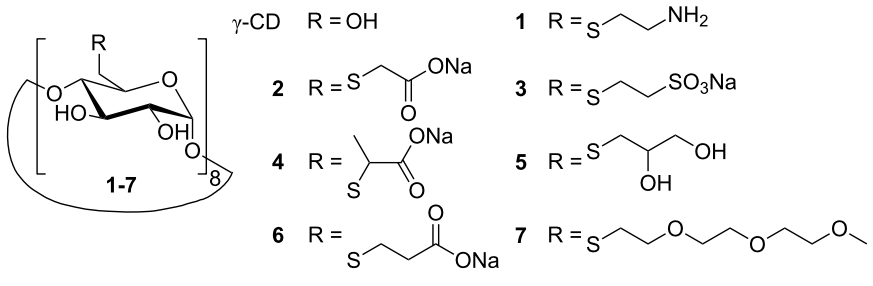

Figure 2: Structures of γ-CD and γ-CD thioethers **1**–**7**.

thiolactate side groups, performed best. The observed high quantum yields were attributed to the tight sandwich-like packing of the two **ANT** molecules within these hosts, which was already demonstrated previously by fluorescence measurements [25]. The quantum yield Φ did not correlate with the binding constant *K*, possibly because dissolved **ANT** is mainly converted in the complexed state in presence of hosts **1**–**7**. Only a small portion of **ANT** remains in the free state due to its low solubility (0.4 μM, [25]). Instead, packing of the two **ANT** molecules within the complex seems to determine the quantum yield Φ.

Stereoselective photodimerization of acenaphthylene

The photodimerization of **ACE** generally leads to mixtures of two isomeric cyclobutane derivatives, namely the *syn* and the *anti* dimers, as shown in Scheme 1. The quantum yields for the reactions in both aqueous and organic media are known to be rather low, 1% < Φ < 5%, as summarized in Table 2 [28,29]. Only the addition of solvents with heavy atoms, such as ethyl iodide, leads to satisfactory quantum yields (up to 17%). This increase is accompanied by an increase in the relative amount of the *anti* isomer. The increases of both the quantum yield and amount of the *anti* product – called the heavy atom effect – was attributed to an increased population of triplet states [29-31]. Heavy atoms close to the excited entity accelerate the rate of spin-orbit coupling interactions between states of different spin multiplicities and consequently facilitate intersystem crossing. However, supramolecular control of the packing of **ACE** leads to a significant improvement of the stereoselectivity. **ACE** was complexed in a cavitand nanocapsule [32] and in a Pd nanocage [33] in aqueous solution, both giving rise to the exclusive formation of the *syn* isomer. Unfortunately, the quantum yields have not been reported for these systems so far.

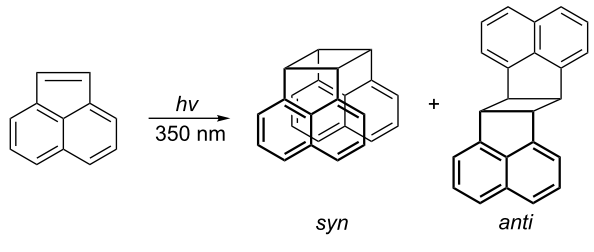

Scheme 1: Photodimerization of **ACE**.

ACE also formed inclusion compounds with β-CD thioethers **1**–**7,** which are soluble in aqueous medium. The highest concentrations of **ACE**, [**ACE**] = 1.7 and 1.3 mM, were achieved with 6 mM solutions of hosts **3** and **6**, respectively. The photodimerization of **ACE** complexed in hosts **3** and **6** proceeded under homogenous conditions and furnished nearly quantitatively the *anti* isomer within 12 h. The quantum yields, reaching Φ = 28%, were unprecedentedly high, significantly higher than that of free **ACE** in organic solvents such as toluene (5%), ethanol (4%), and methanol/water (20% v/v, 3%) [28]. The ^{1}H NMR signals of cyclobutane (for the *syn* photodimer, δ_H = 4.84 ppm; for the *anti* photodimer, δ_H = 4.10 ppm) were monitored to analyze the isomeric ratio [34,35]. As shown in Figure 3, only the proton signal at δ_H = 4.10 ppm was observed indicating the exclusive formation of the dimer in the *anti* configuration.

Table 2: Quantum yields Φ, distributions of the photodimers, and binding constants *K* [25] of **ACE** for various reaction media.

Medium	Φ [%]	*syn* [%]	*anti* [%]	$K/10^6$ M^{-2}
Water [32]	–	40	60	–
water/ methanol [28]	3	–	–	–
3[a]	28[b]	0[c]	100[c]	37
6[a]	12[b]	0[c]	100[c]	27

[a]This work, host concentration 6 mM. [b]For λ = 300 nm, experimental error ±5%. [c]Experimental error ±2%.

Because other hosts favored the *syn* dimer, the total preference of the *anti* dimer was indeed surprising at first, but there are several explanations for the observed *anti* specificity:

(a) **ACE** is tightly surrounded by the seven sulfur atoms of host **3**, which may lead to an increased population of the triplet state and consequently to a heavy atom effect, which favors the formation of the *anti* dimer. Other CD derivatives with heavy atoms attached, e.g., 6-deoxy-iodo-CDs, are known to even enable room temperature phosphorescence of an excited guest [36].

(b) Moreover, according to the results of the quantum mechanical calculations [25,34] the preferential anti-parallel alignment of the **ACE** dimer within the CD cavity also favors the formation of the *anti* dimer.

(c) The *anti* dimer appears to better fit into the γ-CD cavity than the *syn* isomer, as depicted in Figure 4.

Stereoselective photodimerization of coumarin

The photochemistry of **COU** and its derivatives is rather complex because the quantum yield and distribution of products strongly depend both on the solvent [38] and the concentration of **COU** [39]. In principle, four stereoisomeric dimers are conceivable: *syn* Head-to-Head (*syn*-HH), *anti*-HH, *syn*-Head-

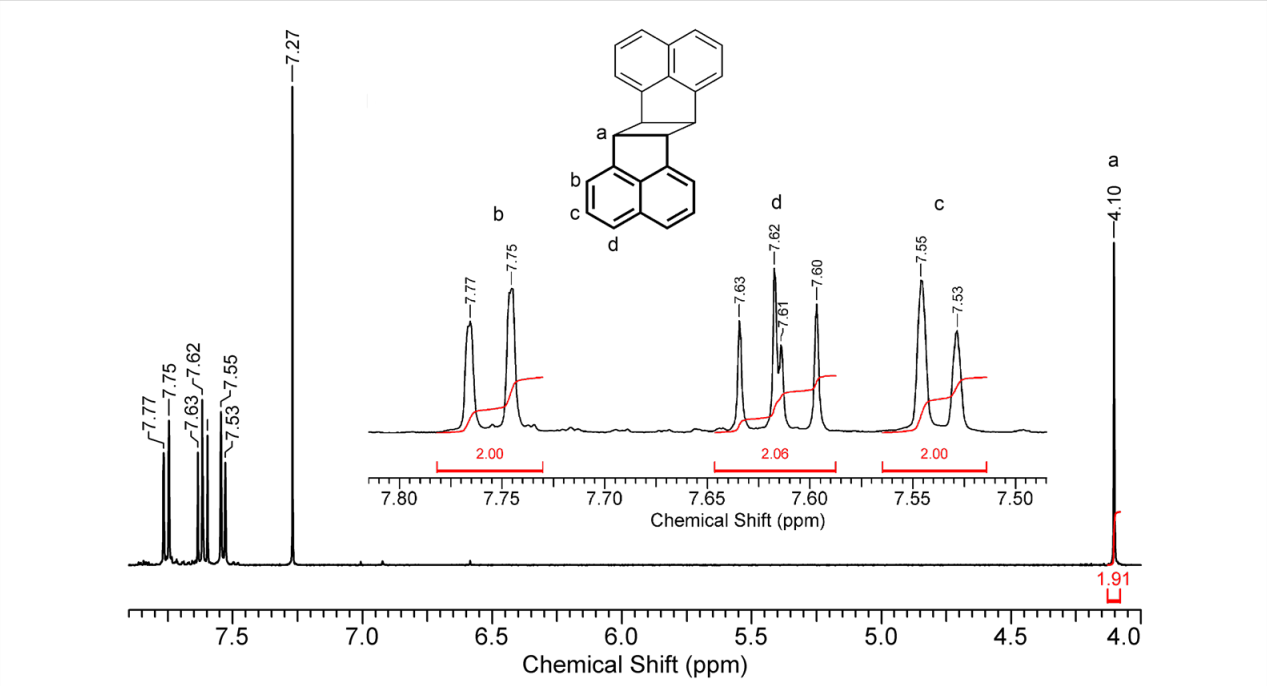

Figure 3: ^{1}H NMR spectrum of the photo product of **ACE** in the presence of γ-CD thioether **3** in $CDCl_3$.

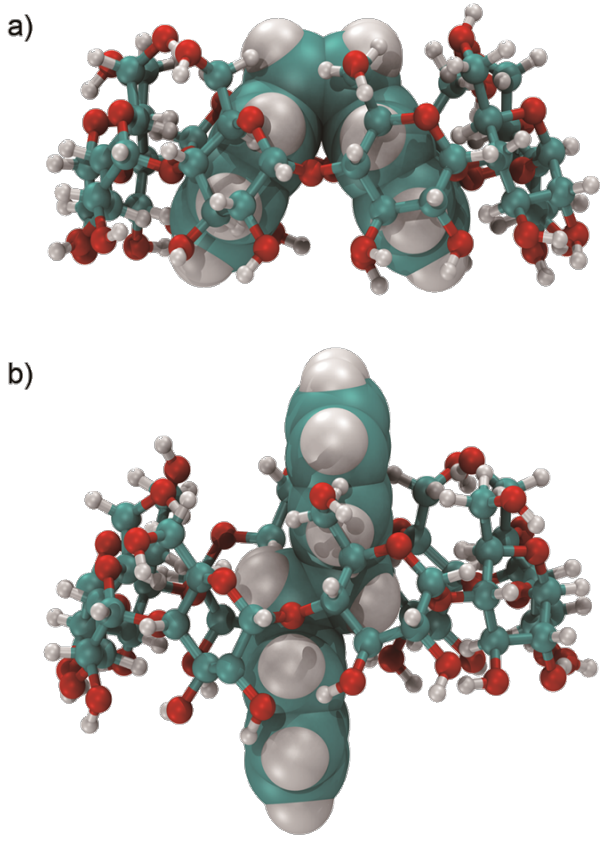

Figure 4: Schematic drawing of the **ACE** photodimers in γ-CD: a) the *syn* photodimer and b) the *anti* photodimer. The rendering was performed with VMD 1.8.7 [37].

to-Tail (*syn*-HT), and *anti*-HH, shown in Figure 5. The photodimerization is very slow in nonpolar media, $\Phi < 10^{-3}$% and mainly leading to the *anti*-HH dimer [39]. In contrast, polar protic solvents, like water, increase both the quantum yield and the amount of the *syn*-HH dimer, exemplified in Table 3. The singlet state has a very short lifetime because of rapid inter-system crossing and self-quenching and it reacts to form the *syn*-HH dimer, while the triplet state, with a longer lifetime,

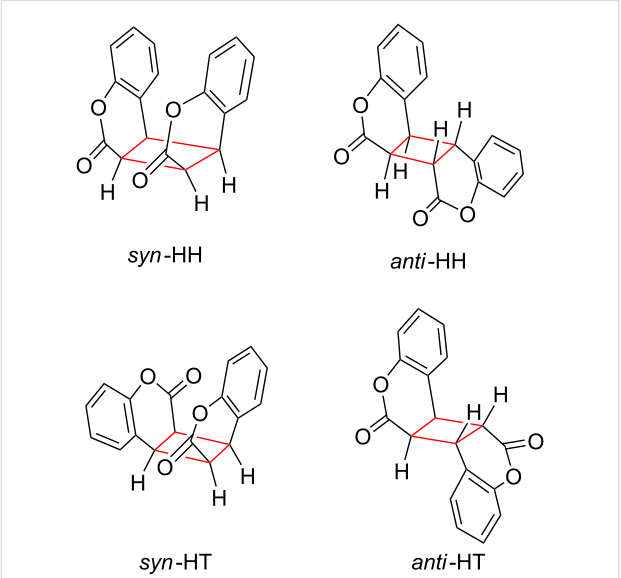

Figure 5: Structures of **COU** photodimers.

furnishes the *anti*-HH isomer [38,40]. Because most often mixtures of *syn* and *anti* isomers were obtained after irradiation of **COU**, any supramolecular control of the dimerization was highly desirable.

Table 3: Distribution of the photodimers of **COU** for various media.

Host	Product distribution [%][a]			
	syn-HH	*anti*-HH	*syn*-HT	*syn*/*anti*
water	59	9	32	10
γ-CD[b]	52	17	31	4.7
1[b]	58	16	26.5	5.4
2[b]	87	5	8.4	19.8
3[b]	57	16	26.6	5.1
4[b]	71	8	20.9	11.8
5[b]	72	9	19.1	10.0
6[b]	71	10	18.5	8.6
7[b]	51	10	38.6	8.5

[a]Experimental error ± 3%. [b]6 mM solutions in water.

Photodimerization of a 15 mM aqueous solution of **COU** proceeded with a low quantum yield Φ = 0.11% and afforded mainly the *syn*-HH isomer with a reasonable selectivity of *syn*/*anti* = 10, as previously described [38,39]. Photodimerization of 6-methyl-**COU** complexed in cucurbituril CB [8] furnished the *syn*-HT isomer as the main product [41,42]. The analogous effect of β-CD was investigated by Moorthy et al. in 1992. They isolated the *syn*-HH dimer in 64% yield after irradiation for 135 h of the *crystalline* (2:2) inclusion compound of **COU** in β-CD [43]. Therefore, it was very interesting to investigate the supramolecular control exerted by γ-CD thioethers **1**–**7** in aqueous solution. The composition of the mixture of isomeric photodimers was determined from the intensities of the ^{1}H NMR signals of the cyclobutane protons, which were assigned according to previous work [40]. The results including the respective *syn*/*anti* ratios are listed in Table 3. In comparison, a 6 mM solution of native γ-CD caused a diminished selectivity of *syn*/*anti* = 4.7.

Surprisingly, the γ-CD thioethers did not behave uniformly. The anionic host **2** increased the selectivity of *syn*/*anti* to 19.8, while the cationic host **1** produced low selectivity, similar to the native γ-CD. The 87% yield of the *syn*-HH dimer obtained with the best host **2** was still not sufficient for any preparative application.

The lower stereoselectivity of the photodimerization of **COU** compared to that of **ACE**, which was achieved with the γ-CD thioethers, was attributed to the much higher aqueous solubility of **COU** (15 mM) compared to the solubility of **ACE** (0.067 mM) [25]. Because the concentration of the free guest $[G]_{free}$ is determined by two coupled thermodynamic equilibria (Equation 1). The 2-phase solubility equilibrium is expressed by Equation 2 and the equilibrium of complexation by the CD host is formulated in Equation 3. The guest dissolves until the concentration of free guest is equal to the solubility of the guest, $[G]_0 = [G]_{free}$ [44,45]. Consequently, the lower the solubility of the guest in water, the lower the fraction of uncomplexed guests. The lower the concentration of the free guest, the lower the contribution of undesirable and non-specific photodimerization to the total quantum yield, according to Equation 4. Consequently, lowering the aqueous solubility of **COU** by the addition of salt, taking advantage of the so-called "salting-out effect" [46] appeared to be a plausible way to enhance the reaction selectivity of the *syn*-HH dimer.

$$G_{solid} \overrightarrow{\leftarrow} G_{free} \overrightarrow{\leftarrow} G \cdot CD \quad (1)$$

$$[G]_{free} = [G]_0 \quad (2)$$

$$[G]_{free} = \frac{[G \cdot CD]}{K[CD]} \quad (3)$$

$$\Phi = \frac{\Phi_{free}[G]_{free} + \Phi_{complex}[G \cdot CD]}{[G]_{free} + [G \cdot CD]} \quad (4)$$

The ^{1}H NMR spectra of the crude photoproducts indeed showed a striking effect from changes in the salt concentration. The signals of the *syn*-HT and *anti*-HH isomers significantly diminished as shown in Figure 6. At a high salt concentration,

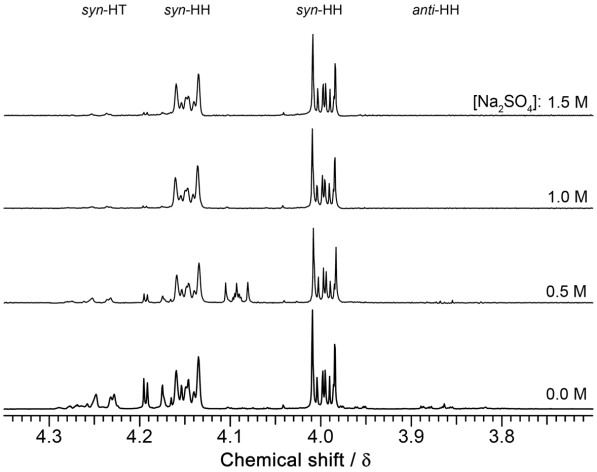

Figure 6: Partial ^{1}H NMR of the photodimers formed after irradiation of **COU** at various concentrations of Na_2SO_4 in the presence of 6 mM γ-CD thioether **2**.

$[Na_2SO_4]$ = 1.5 M, almost pure *syn*-HH dimer was formed exclusively. The compositions, obtained from the NMR intensities, are listed in Table 4. The observed improvement in the quantum yield and stereoselectivity by the addition of salt was quantitatively described taking into account the decrease of the solubility of **COU** by the salting-out effect. As shown in Table 5, the aqueous solubility of **COU** is diminished by nearly a factor of 6 as a result of raising the salt concentration to 1.5 M. In parallel, the quantum yield Φ_{free} of free **COU** is diminished approximately linearly from 2.2% to 1.2%.

Table 4: Influence of the sodium sulfate concentration on the quantum yield Φ and distribution of photoproducts of **COU** in a 6.0 mM solution of γ-CD thioether **2**.

$[Na_2SO_4]$	Φ[a]	Product distribution [%][b]		
M	%	*syn*-HH	*anti*-HH	*syn*-HT
0.0	3.8	86	5	9
0.5		89	0	11
1.0		95	0	5
1.5	13.0	97	0	3

[a]For λ = 300 nm, experimental error ±3%. [b]Experimental error ±2%.

Both effects based on the salt concentration led to a significant reduction in the contribution of the photodimerization of free **COU** to the total quantum yield Φ in Equation 4. Taking into account the molar fraction of the formation of *syn*-HH in water $X^{free}_{syn-HH} = 0.59$ from Table 3 and in the complex $X^{complex}_{syn-HH} = 1$, and assuming the quantum yield for the complex as $\Phi_{complex}$ = 19%, the total molar fraction X_{syn-HH} was calculated according to Equation 5, which was derived from Equation 4. The concentration of complexed **COU**, $[\mathbf{COU}]_C$, was determined as the increase in the solubility of **COU** upon the addition of the host. The calculated total quantum yields and molar fractions of the *syn*-HH isomer, listed in Table 5, are in good agreement with the measured values, listed in Table 4. It also shoes, that the binding constant *K*, calculated according to the law of mass action for the 1:2 (host/guest) complex, tremendously increases with the salt concentration leading to a strong increase of the complexed portion of **COU**. In contrast to the previous **ANT** system, the quantum yield of **COU** photodimerization increases with the binding const *K*, because *K* is much lower for **COU** than for **ANT** so that contribution of free **COU** is not negligible.

$$X^{calc}_{syn-HH} = \frac{\Phi_{free}[\mathbf{COU}]_0 X^{free}_{syn-HH} + \Phi_{complex} X^{complex}_{syn-HH}[\mathbf{COU}]_C}{\Phi_{free}[\mathbf{COU}]_0 + \Phi_{complex}[\mathbf{COU}]_C} \quad (5)$$

As a result, the *syn*-HH isomer is exclusively formed from the complex with CD derivative **2,** with a quantum yield approximately ten times higher than that observed without complexation. The tight packing of the two **COU** molecules within the host was made responsible for the significantly increased quantum yield. The heavy atom effect of the S-atoms of CD derivatives **1**–**7** should facilitate intersystem crossing to the triplet state and therefore support the formation of the *anti*-HH dimer. Because this preference does not hold true in this case, especially for host **2**, the multiplicity of the excited state seems not to be the dominant factor, but rather the pre-organization of the guest molecules in the CD cavity prior to excitation has the greatest effect. The distribution of the stereoisomers appears to be mainly topochemically [5] controlled because of the short lifetime of the excited state of **COU**.

Quantum mechanical calculations of the structures and interaction energies Δ*E* of the four **COU** dimers were performed using the Gaussian 03 software package to investigate the favored packing [47]. The aromatic dimers were fully optimized at the MP2/6-31G* level without any symmetry restriction during the computation. The interaction energies Δ*E* of the *syn*-HH, *anti*-HH, *syn*-HT, and *anti*-HT dimers of **COU** were −32.9, −29.3, −24.0, and −22.5 kJ·mol^{-1}, respectively. The Δ*E* value of the **COU** dimer with the *syn*-HH orientation was found to be significantly more negative than that of the dimer with the other orientation. This result can be attributed to relatively effi-

Table 5: The quantum yields, calculated according to (4) and the fractions of the *syn*-HH dimer, calculated according to (5), for the photodimerization of **COU** in a 6.0 mM solution of γ-CD thioether **2** and binding constant *K* as a function of salt concentration.

$[Na_2SO_4]$ M	$[\mathbf{COU}]_0$ mM	$[\mathbf{COU}]_C$ mM	Φ^{calc} %	X^{calc}_{syn-HH} %	$K/10^3$ M^{-2}
0.0	15.2	3.1	5.0	85	2
0.5	8.5	4.8		94	30
1.0	4.7	4.8		97	97
1.5	2.6	5.5	13.2	99	1000

$[\mathbf{COU}]_0$ solubility of **COU**, $[\mathbf{COU}]_C$ concentration of complexed **COU**, *K* binding constant of **COU** complexed in **2** from solubility measurements.

cient π–π stacking [48] The most stable *syn*-HH dimeric aggregate forms the most stable, and therefore, most abundant complex within the γ-CD cavity and consequently the main photoproduct. Hence, the photodimerization of **COU** within host **2** is a topochemical reaction. This type of topochemical control happening in solution is much more applicable than the classical topochemical control occurring in the crystalline state [3,43,49].

Conclusion

Aromatic guests **ANT**, **ACE**, and **COU** form 1:2 (host/guest) complexes within γ-CD thioethers **1**–**7**, which photodimerized approximately 10 times faster in aqueous medium than the same uncomplexed guests in aqueous solution. Since these photo dimerizations of hydrophobic guests are performable at neutral pH in optically clear solution in water they are suitable for preparative applications. Isolation of the photoproduct from aqueous solution by liquid/liquid extraction simplifies the scale up. Yields of photodimer based on the complex were nearly quantitative.

The observed supramolecular catalysis was explained by the high pre-organization resulting from the tight packing of the two guests in the cavity, which allows for photoreactions even for short-lived excited states. In comparison to other confined and ordered media, most γ-CD thioether complexes offer the advantages of very high quantum yields and excellent stereochemical control. Because the product formation is mainly topochemically controlled, photoproducts are predictable by quantum mechanical optimization of the corresponding dimeric aggregates in vacuo.

This work also showed that the addition of salt can further improve supramolecular control by suppression of the free photoactive species.

Experimental

General: Guests (**ANT**, **ACE**, and **COU)** and potassium ferrioxalate were purchased from Sigma-Aldrich. Unless otherwise stated, all chemicals were used as received. γ-CD was donated by Wacker and dried in vacuo at 100 °C overnight before use. The γ-CD thioethers were synthesized as previously described [25] and purified by nanofiltration (molecular weight cut-off of 1000 Da with demineralized water). Teflon syringe filters (0.22 μm) from Roth (Karlsruhe, Germany) were used to remove insoluble material before taking UV–vis and fluorescence measurements and the photoirradiation experiments. The UV–vis spectra of aqueous samples were taken on a Perkin Elmer Lambda 2 spectrometer (λ: 200–600 nm) using quartz cells with a 1 cm or 1 mm optical path at 298 K. The fluorescence spectra were recorded in a JASCO spectrophotometer using quartz cells of 10.0 mm path at 298 K. All of the NMR spectra were recorded on a Bruker 400 MHz NMR spectrometer at 298 K using the solvent peaks as internal references, and the coupling constants (J) were measured in Hz.

Photoreaction procedures: Aqueous solutions of the native CDs or γ-CD thioethers (25 mL, 6.0 mM) were added into glass vials containing excess amounts of the guest molecules. To evaluate the salting-out effect on the photo-product distribution of **COU**, different amounts of sodium sulfate were added to the vials to obtain the desired final salt concentration (Na_2SO_4 concentration: 0, 0.5, 1.0, and 1.5 M). Sample solutions were thoroughly degassed using sonication. The vials were tightly sealed, protected from light, and magnetically stirred at room temperature. After 72 h, the resulting suspensions were filtered through syringe filters. The concentrations of the reactants in the CD solutions were determined from the UV–vis extinction coefficients at the absorption maxima.

The aqueous solutions of the inclusion complexes were transferred into 50 mL quartz round-bottomed flasks and bubbled with nitrogen gas for 20 min with stirring before photo-irradiation. Photodimerization of the samples was carried out using a medium-pressure mercury lamp (166.5 W, Heraeus Noblelight GmbH, UVB) as a light source. After irradiation for 12 h at room temperature under a nitrogen atmosphere, the photoproducts formed were extracted with chloroform and then analyzed by ^{1}H NMR [34]. No starting material was found anymore after this time of reaction. It is worth mentioning that a precipitate was formed after irradiation of the aqueous solution of the inclusion complex of **ACE** with γ-CD thioether.

Molecular modeling: A previously described procedure was used [25]. The geometries of the orientational isomers of the **COU** gas-phase dimer were fully optimized without any symmetry restriction at the MP2/6-31G* level of theory by using the Gaussian 03 (E.01) software package [47]. Corrected interaction energies (ΔE) corresponding to the optimized aromatic dimers were evaluated using the equation $\Delta E = E_{dimer} - 2E_{monomer}$ at the MP2/6-31G* level, where E_{dimer} and $E_{monomer}$ are the energies of the aromatic dimer and the monomer, respectively [50].

Supporting Information

Supporting Information File 1

Quantum yield measurement.
[http://www.beilstein-journals.org/bjoc/content/supplementary/1860-5397-9-217-S1.pdf]

Acknowledgements

We thank the technical support from Annegret Engelke. We would also like to express our appreciation to Dagmar Auerbach, Christian Spies, and Prof. Dr. Gregor Jung from Saarland University (Biophysikalische Chemie) for their assistance in quantum yield measurements. Financial support from Saarland University and China Scholarship Council are gratefully acknowledged.

References

1. Eaton, P. E.; Cole, T. W. *J. Am. Chem. Soc.* **1964,** *86,* 3157–3158. doi:10.1021/ja01069a041
2. Fessner, W. D.; Sedelmeier, G.; Spurr, P. R.; Rihs, G.; Prinzbach, H. *J. Am. Chem. Soc.* **1987,** *109,* 4626–4642. doi:10.1021/ja00249a029
3. Schmidt, G. *Pure Appl. Chem.* **1971,** *27,* 647–678. doi:10.1351/pac197127040647
4. Ramamurthy, V. *Tetrahedron* **1986,** *42,* 5753–5839. doi:10.1016/S0040-4020(01)96063-6
5. Svoboda, J.; König, B. *Chem. Rev.* **2006,** *106,* 5413–5430. doi:10.1021/cr050568w
6. Murase, T.; Fujita, M. *Chem. Rec.* **2010,** *10,* 342–347. doi:10.1002/tcr.201000027
7. Kaliappan, R.; Ling, Y.; Kaifer, A. E.; Ramamurthy, V. *Langmuir* **2009,** *25,* 8982–8992. doi:10.1021/la900659r
8. Jon, S. Y.; Ko, Y. H.; Park, S. H.; Kim, H.-J.; Kim, K. *Chem. Commun.* **2001,** 1938–1939. doi:10.1039/B105153A
9. Chen, B.; Cheng, S.-F.; Liao, G.-H.; Li, X.-W.; Zhang, L.-P.; Tung, C.-H.; Wu, L.-Z. *Photochem. Photobiol. Sci.* **2011,** *10,* 1441–1444. doi:10.1039/c1pp05047h
10. Herrmann, W.; Wehrle, S.; Wenz, G. *Chem. Commun.* **1997,** 1709–1710. doi:10.1039/A703485G
11. Rao, K. S. S. P.; Hubig, S. M.; Moorthy, J. N.; Kochi, J. K. *J. Org. Chem.* **1999,** *64,* 8098–8104. doi:10.1021/jo9903149
12. Nakamura, A.; Inoue, Y. *J. Am. Chem. Soc.* **2003,** *125,* 966–972. doi:10.1021/ja016238k
13. Douhal, A. *Cyclodextrin materials photochemistry, photophysics and photobiology;* Elsevier Science, 2006; Vol. 1.
14. Luo, L.; Liao, G.-H.; Wu, X.-L.; Lei, L.; Tung, C.-H.; Wu, L.-Z. *J. Org. Chem.* **2009,** *74,* 3506–3515. doi:10.1021/jo900395v
15. Yang, C.; Nakamura, A.; Fukuhara, G.; Origane, Y.; Mori, T.; Wada, T.; Inoue, Y. *J. Org. Chem.* **2006,** *71,* 3126–3136. doi:10.1021/jo0601718
16. Yang, C.; Ke, C.; Liang, W.; Fukuhara, G.; Mori, T.; Liu, Y.; Inoue, Y. *J. Am. Chem. Soc.* **2011,** *133,* 13786–13789. doi:10.1021/ja202020x
17. Ramamurthy, V.; Eaton, D. F. *Acc. Chem. Res.* **1988,** *21,* 300–306. doi:10.1021/ar00152a003
18. Yang, C.; Fukuhara, G.; Nakamura, A.; Origane, Y.; Fujita, K.; Yuan, D. Q.; Mori, T.; Wada, T.; Inoue, Y. *J. Photochem. Photobiol., A: Chem.* **2005,** *173,* 375–383. doi:10.1016/j.jphotochem.2005.04.017
19. Sanemasa, I.; Wu, J. S.; Toda, K. *Bull. Chem. Soc. Jpn.* **1997,** *70,* 365–369. doi:10.1246/bcsj.70.365
20. Steffen, A.; Thiele, C.; Tietze, S.; Strassnig, C.; Kämper, A.; Lengauer, T.; Wenz, G.; Apostolakis, J. *Chem.–Eur. J.* **2007,** *13,* 6801–6809. doi:10.1002/chem.200700661
21. Thiele, C.; Auerbach, D.; Jung, G.; Wenz, G. *J. Inclusion Phenom. Macrocyclic Chem.* **2011,** *69,* 303–307. doi:10.1007/s10847-010-9741-4
22. Wang, H. M.; Soica, C. M.; Wenz, G. *Nat. Prod. Commun.* **2012,** *7,* 289–291.
23. Fourmentin, S.; Ciobanu, A.; Landy, D.; Wenz, G. *Beilstein J. Org. Chem.* **2013,** *9,* 1185–1191. doi:10.3762/bjoc.9.133
24. Wang, H. M.; Wenz, G. *Beilstein J. Org. Chem.* **2012,** *8,* 1644–1651. doi:10.3762/bjoc.8.188
25. Wang, H. M.; Wenz, G. *Chem.–Asian J.* **2011,** 2390–2399. doi:10.1002/asia.201100217
26. Tamaki, T.; Kokubu, T.; Ichimura, K. *Tetrahedron* **1987,** *43,* 1485–1494. doi:10.1016/S0040-4020(01)90264-9
27. Tamaki, T.; Kokubu, T. *J. Inclusion Phenom.* **1984,** *2,* 815–822. doi:10.1007/BF00662250
28. Livingston, R.; Wei, K. S. *J. Phys. Chem.* **1967,** *71,* 541–547. doi:10.1021/j100862a012
29. Cowan, D. O.; Koziar, J. C. *J. Am. Chem. Soc.* **1974,** *96,* 1229–1230. doi:10.1021/ja00811a049
30. Cowan, D. O.; Drisko, R. L. E. *J. Am. Chem. Soc.* **1970,** *92,* 6281–6285. doi:10.1021/ja00724a029
31. Cowan, D. O.; Drisko, R. L. E. *J. Am. Chem. Soc.* **1970,** *92,* 6286–6291. doi:10.1021/ja00724a030
32. Kaanumalle, L. S.; Ramamurthy, V. *Chem. Commun.* **2007,** 1062–1064. doi:10.1039/b615937k
33. Yoshizawa, M.; Takeyama, Y.; Kusukawa, T.; Fujita, M. *Angew. Chem.* **2002,** *114,* 1403–1405. doi:10.1002/1521-3757(20020415)114:8<1403::AID-ANGE1403>3.0.CO;2-6
34. Santos, R. C.; Bernardes, C. E. S.; Diogo, H. P.; Piedade, M. F. M.; Lopes, J. N. C.; da Piedade, M. E. M. *J. Phys. Chem. A* **2006,** *110,* 2299–2307. doi:10.1021/jp056275o
35. Bhat, S.; Maitra, U. *Molecules* **2007,** *12,* 2181–2189. doi:10.3390/12092181
36. Hamai, S.; Kudou, T. *J. Photochem. Photobiol., A* **1998,** *113,* 135–140.
37. Humphrey, W.; Dalke, A.; Schulten, K. *J. Mol. Graphics* **1996,** *14,* 33–38. doi:10.1016/0263-7855(96)00018-5
38. Wolff, T.; Gorner, H. *Phys. Chem. Chem. Phys.* **2004,** *6,* 368–376. doi:10.1039/b312335a
39. Muthuramu, K.; Ramamurthy, V. *J. Org. Chem.* **1982,** *47,* 3976–3979. doi:10.1021/jo00141a035
40. Yu, X. L.; Scheller, D.; Rademacher, O.; Wolff, T. *J. Org. Chem.* **2003,** *68,* 7386–7399. doi:10.1021/jo034627m
41. Barooah, N.; Pemberton, B. C.; Sivaguru, J. *Org. Lett.* **2008,** *10,* 3339–3342. doi:10.1021/ol801256r
42. Pemberton, B. C.; Singh, R. K.; Johnson, A. C.; Jockusch, S.; Da Silva, J. P.; Ugrinov, A.; Turro, N. J.; Srivastava, D. K.; Sivaguru, J. *Chem. Commun.* **2011,** *47,* 6323–6325. doi:10.1039/c1cc11164g
43. Moorthy, J. N.; Venkatesan, K.; Weiss, R. G. *J. Org. Chem.* **1992,** *57,* 3292–3297. doi:10.1021/jo00038a012
44. Higuchi, T.; Connors, K. *Adv. Anal. Chem. Instrum.* **1965,** *4,* 117–212.
45. Connors, K. A. *Chem. Rev.* **1997,** *97,* 1325–1357. doi:10.1021/cr960371r
46. Sau, S.; Solanki, B.; Orprecio, R.; Van Stam, J.; Evans, C. H. *J. Inclusion Phenom. Macrocyclic Chem.* **2004,** *48,* 173–180. doi:10.1023/B:JIPH.0000022556.47230.c8
47. *Gaussian 03,* Revision E. 01; Gaussian, Inc.: Wallingford, CT, 2004.
48. Guckian, K.; Schweitzer, B.; Ren, R. X.-F.; Sheils, C.; Tahmassebi, D.; Kool, E. *J. Am. Chem. Soc.* **2000,** *122,* 2213–2222. doi:10.1021/ja9934854
49. Wenz, G.; Wegner, G. *Mol. Cryst. Liq. Cryst.* **1983,** *96,* 99–108. doi:10.1080/00268948308074696

50. Boys, S. F.; Bernardi, F. *Mol. Phys.* **1970,** *19,* 553–566. doi:10.1080/00268977000101561

Beilstein Journal of Organic Chemistry

Oligomeric epoxide–amine adducts based on 2-amino-*N*-isopropylacetamide and α-amino-ε-caprolactam: Solubility in presence of cyclodextrin and curing properties

Julian Fischer and Helmut Ritter*

Full Research Paper

Open Access

Address:
Institute of Organic Chemistry and Macromolecular Chemistry, Heinrich-Heine-University Düsseldorf, Universitätsstraße 1, D-40225 Düsseldorf, Germany

Email:
Helmut Ritter* - h.ritter@uni-duesseldorf.de

* Corresponding author

Keywords:
amino acids; curing properties; cyclodextrin; epoxide–amine oligomers; LCST

Beilstein J. Org. Chem. **2013,** *9,* 2803–2811.
doi:10.3762/bjoc.9.315

Received: 05 August 2013
Accepted: 20 November 2013
Published: 05 December 2013

This article is part of the Thematic Series "Superstructures with cyclodextrins: Chemistry and applications".

Associate Editor: P. J. Skabara

Abstract

2-Amino-*N*-isopropylacetamide and α-amino-ε-caprolactam were reacted with glycerol diglycidyl ether to give novel oligomeric thermoresponsive epoxide–amine adducts. These oligomers exhibit a lower critical solution temperature (LCST) behavior in water. The solubility properties were influenced with randomly methylated β-cyclodextrin (RAMEB-CD) and the curing properties of the amine–epoxide mixtures were analyzed by oscillatory rheology and differential scanning calorimetry, whereby significant differences in setting time, viscosity, and stiffness were observed.

Introduction

Many partially hydrophobic polymers exhibit a lower critical solution temperature (LCST) behavior in water [1,2]. Below the critical temperature (T_c) these substances are completely soluble in water, whereas above the T_c they precipitate. Thereby, hydrogen bonds between polymer chains and water molecules in cold water lead to good solubility, whereas these bondings are increasingly disrupted on heating [3]. These LCST-type polymers are of interest for the development of e.g. hydrogels and drug delivery systems [2,4]. One of the most prominent LCST polymers is poly(*N*-isopropylacrylamide) (PNIPAM), which exhibits a LCST of about 32 °C [5]. The T_c can be influenced for example through copolymerization with hydrophobic or hydrophilic comonomers and further through supramolecular interactions of these comonomers with cyclodextrins (CD) [6-10]. Generally, CDs are water soluble and their ability of forming inclusion complexes with hydrophobic guest molecules is widely used in drug, food, cosmetics, textile, adhesives, plastics and more industries [11-13]. Interestingly, recently it

was confirmed that α- and β-CD cannot interact with PNIPAM. Only γ-CD has a tendency to include the PNIPAM main chain [14]. Normally, epoxy resins exhibit poor solubility in water [15-17]. Accordingly, epoxide–amine polymers are not yet deeply investigated in respect to LCST behavior [18,19]. At present, most available bio-based and water soluble epoxy resins are expensive and use petroleum-based curing agents [20]. Thus, in the present paper we wish to describe our results about preparation and solubility of novel bio-based amine–epoxy oligoadducts. Also, we present some effects of CD on the solubility of these oligomers.

Results and Discussion

Generally, primary amins are bifunctional towards diepoxides and are thus monomers for the formation of corresponding oligomers [16]. Inspired by the molecular structure of *N*-isopropylacrylamide, we synthesized a primary amine 2-amino-*N*-isopropylacetamide (**5**) that is based on the amino acid glycine (Scheme 1). This was achieved in a three-step reaction through protection of the primary amino function of glycine methyl ester hydrochloride (**1**) with di-*tert*-butyl dicarbonate [21], further amidation with isopropylamine (**3**), and finally deprotection in acidic solution.

We also synthesized as a further monomer the lysine based primary amine α-amino-ε-caprolactam (**7**) through cyclization [22]. Native amino acids are not suitable for fast reaction with epoxides at low temperatures, presumably due to protonation of their amine groups that results in a reduction of their nucleophilicity [23]. However, by means of the described α-amino-ε-caprolactam (**7**), we expect to increase the reactivity of the primary amine group towards epoxides due to the formation of activating hydrogen bonds. The subsequent epoxide–amine polyaddition was carried out with glycerol diglycidyl ether (**8**), which was directly used as a mixture of the structural isomers **8a** and **8b**. To facilitate the following discussion, figures will only illustrate an idealized structure of **8**, comprising only **8a** since it contains two primary glycidyl ether groups. Ring opening oligomerization of the epoxide functions of **8** with the primary amine functions of **5** or **7**, respectively were conducted in bulk at 25 °C. The product of **5** and **8** gave oligomer **9** and that of **7** and **8** gave oligomer **10,** respectively. Thereby, to reduce branching via the hydroxy or amide groups with the epoxide functions and to obtain amine end groups, **5** and **7** were added in low excess compared to the diepoxide (molecular ratio 1.2:1 (**5**/**7**:**8**)).

To investigate the solution properties of **9** and **10** in water, turbidity measurements were performed (Figure 1). It was observed, that **9** was soluble in cold water and exhibited a cloud point of about 27 °C due to heating.

To evaluate the effect of CD complexation on the solubility of that oligomer **9**, 150 mol % of randomly methylated β-cyclo-

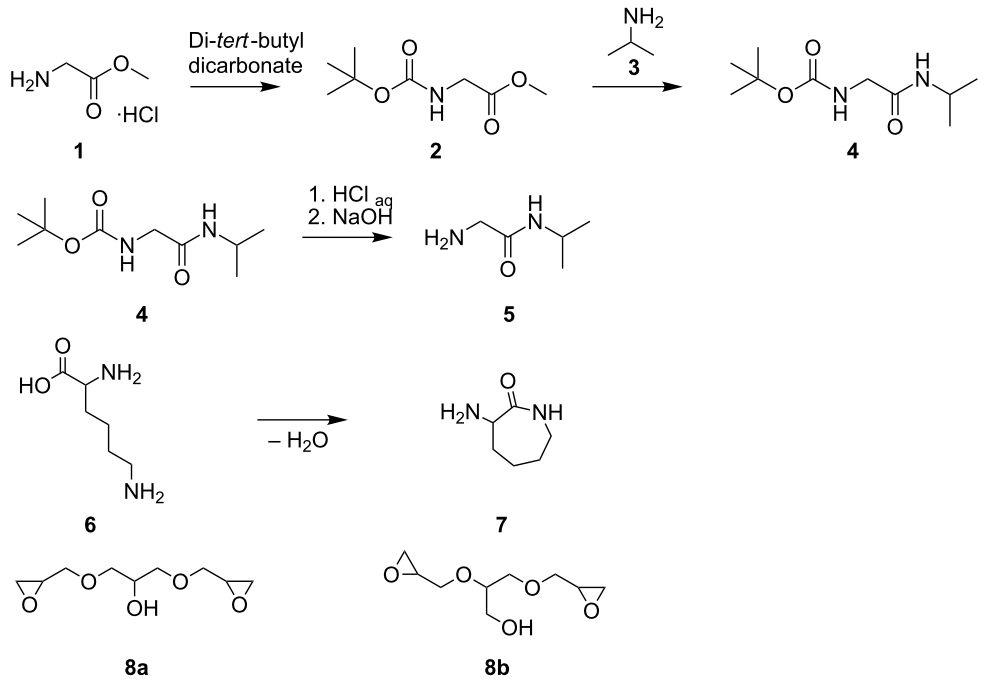

Scheme 1: Synthesis of the monomers **5** and **7**, as well as the chemical structure of the diepoxide **8**, comprising two structural isomers **8a** and **8b**.

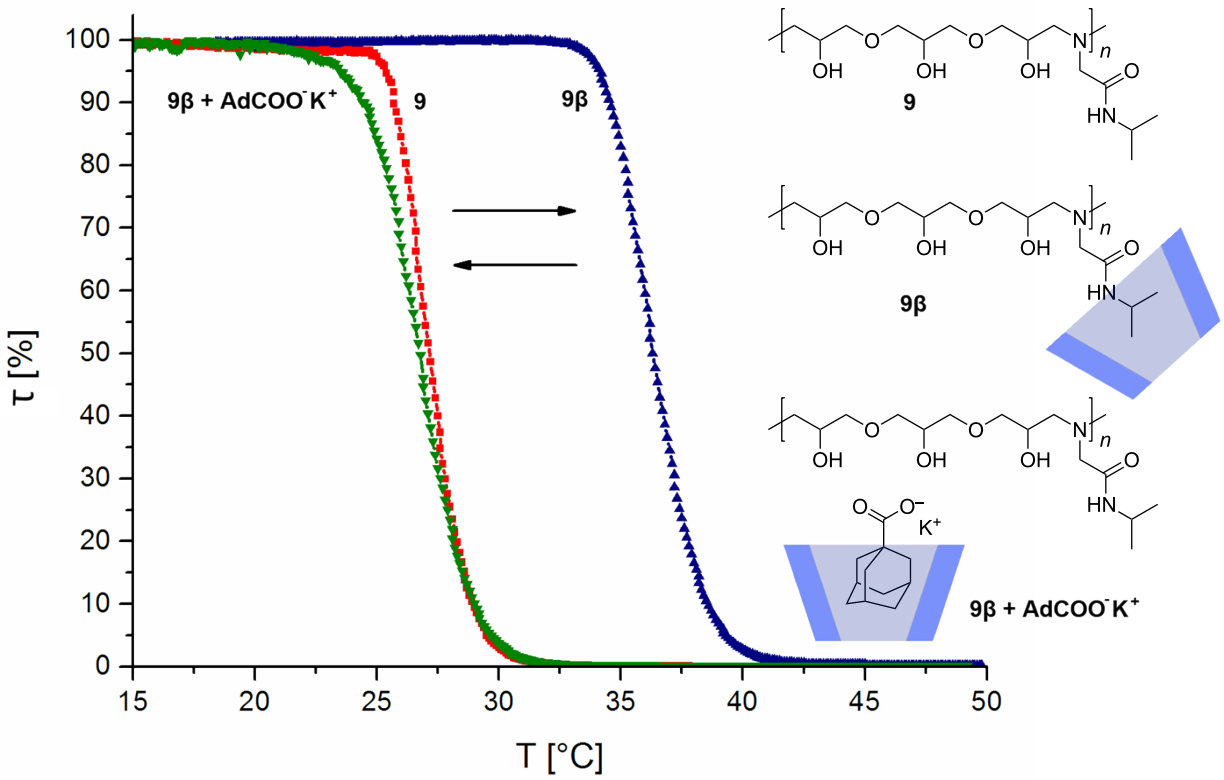

Figure 1: Heating curves of the LCST measurements of **9**, the complex of **9** with RAMEB-CD **9β**, and of **9** with RAMEB-CD with added $AdCOO^-K^+$.

dextrin (RAMEB-CD) were added (**9β**). After that, the cloud point shifted significantly up to 36 °C, which is remarkable since PNIPAM does not interact with β-CD [14]. Explanation for this can be steric effects, since the isopropyl group in our system **9** is placed not so close at the backbone as in PNIPAM. For further confirmation of these findings, the solution of **9** with RAMEB-CD was treated with potassium 1-adamantylcarboxylate ($AdCOO^-K^+$) in some excess, which should displace **9** from RAMEB-CD due to its high complexation properties [6,24,25]. As predicted, the cloud point shifted back to the initial temperature of about 27 °C. Oligomer **10** also exhibited LCST characteristics (Figure 2). It could be noticed that the solubility properties differ on heating and on cooling. While on heating a cloud point of about 35 °C was measured, on cooling a cloud point of about 30 °C was found. This effect is a result from insoluble to soluble transition which depends on the shape and size distribution of polymer particles.

Furthermore, **10** also showed an increase in water solubility by adding 150 mol % of RAMEB-CD **10β**. Hereby, a cloud point of about 49 °C on heating and 29 °C on cooling could be observed (Supporting Information File 1).

To confirm the interaction of the isopropyl, respectively lactam moiety with RAMEB-CD we performed 2D ROESY NMR spectroscopy in D_2O. The protons of the isopropyl group of **5** can be assigned to the proton resonances at 1.1 ppm. As illustrated in Figure 3a, these protons correlate with the protons of RAMEB-CD in the range of 3.2 ppm and 4.1 ppm. Also in case of **7**, similar findings can be observed. Hereby, the protons of the lower lactam ring between 1.1 ppm and 2.0 ppm show an interaction with the protons of RAMEB-CD (Figure 3b). 2D ROESY NMR of **9β** and **10β** were also conducted and as expected, the same correlation with RAMEB-CD as for **5** and **7** was observed (Supporting Information File 1). Unfortunately, the signals of the protons of the oligomer backbone are covered by the RAMEB-CD signals, whereby no clear correlation can be made. However, a further evidence for the self-agglomeration of RAMEB-CD with the side groups of **9** and **10** is a perceivable downfield shifting concurrent with a splitting of the concerned proton signals, since they are magnetically shielded by the CD cavity.

Kinetics of the curing process at a decent temperature (25 °C) of **9** and **10** were evaluated by applying oscillatory rheological

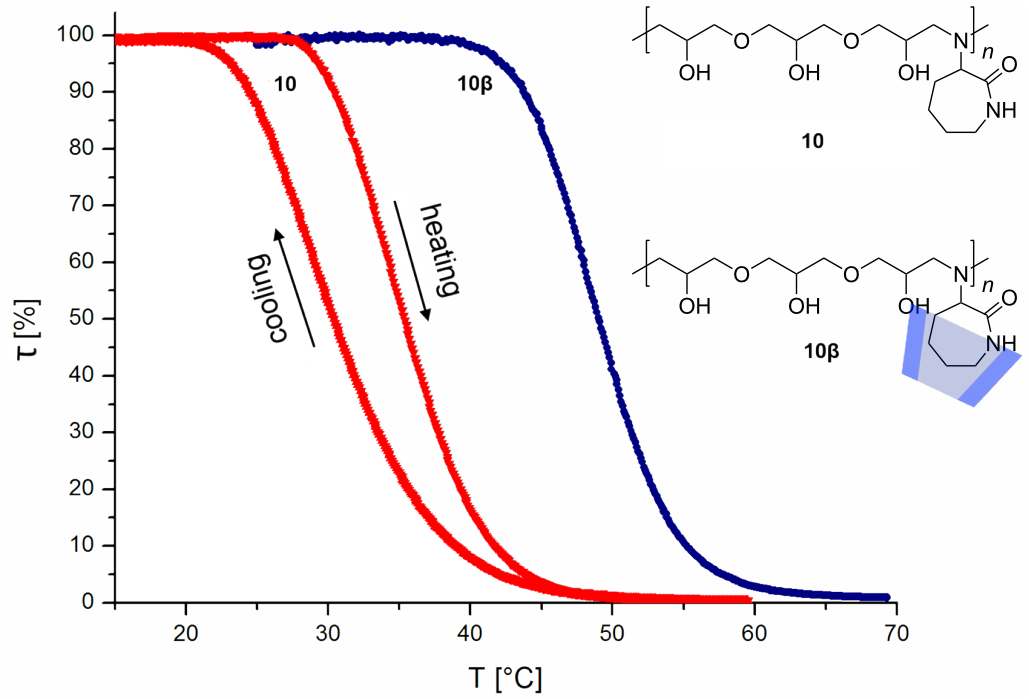

Figure 2: LCST measurements of **10** with illustrated heating and cooling curve, as well as the heating curve after addition of RAMEB-CD **10β**.

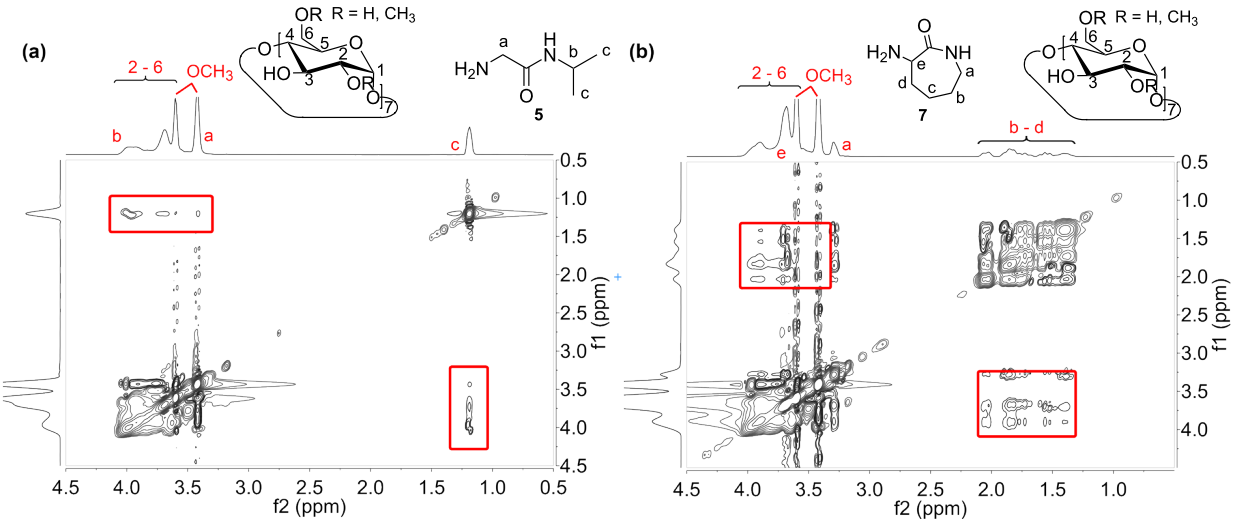

Figure 3: 2D NMR ROESY (300 MHz, D_2O) spectrum of the complex of **5** with RAMEB-CD (a), displaying the correlation of the isopropyl moiety with RAMEB-CD and of **7** with RAMEB-CD (b), illustrating the interaction of the lower lactam ring with RAMEB-CD.

measurements. A mixture of **5** and **8** showed a low viscosity before hardening. As illustrated in Figure 4a, the mixture exhibits one-digit values for storage modulus *G'* and loss modulus *G''* at first. With continuous reaction time the curves for *G'* and *G''* run almost parallel till they converge. It can be observed that the sol–gel transition ("gel point"), where *G'* is equal to *G''*, is reached after 21 h. In theory, after this point the mixture is not capable of flowing anymore. However, after gel point *G'* and *G''* do not diverge clearly, which can be a hint for still flowable or at least flexible parts of the product. Also, horizontal lines of *G'* and *G''* shortly after reaching the gel point are a sign of a completed reaction. The resulting oligomer **9** is dimensionally stable for a certain period, but can be stretched easily by applying a force (Figure 5b).

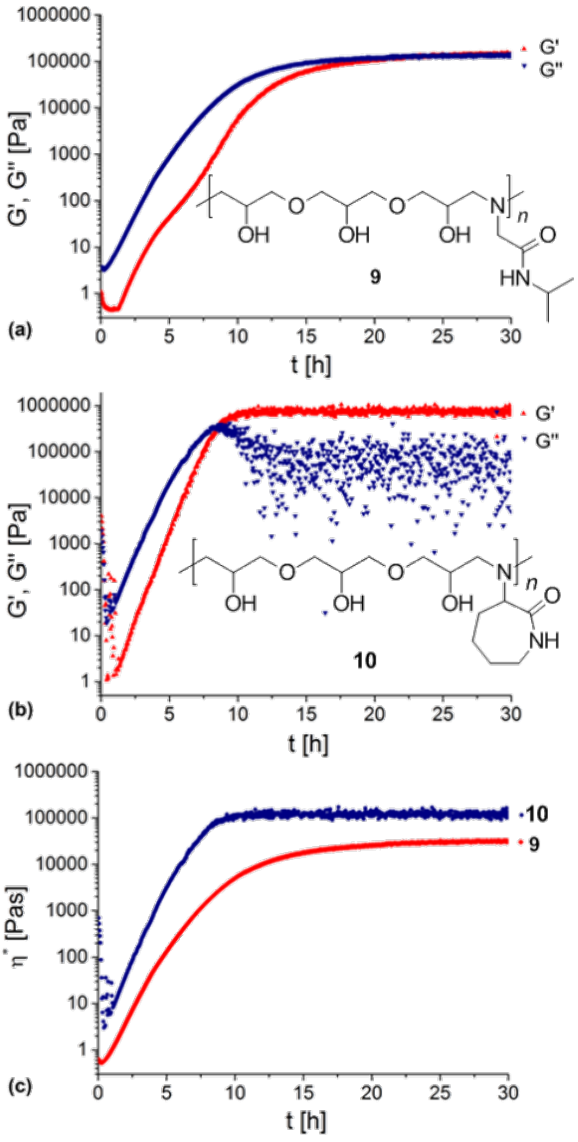

Figure 4: Oscillatory rheological measurements of the curing of **9** and **10**, respectively at 25 °C. Illustrated are exemplary *G'* and *G"* plots as a function of time for **9** (a) and **10** (b), as well as a comparison of the complex viscosity of **9** and **10** (c).

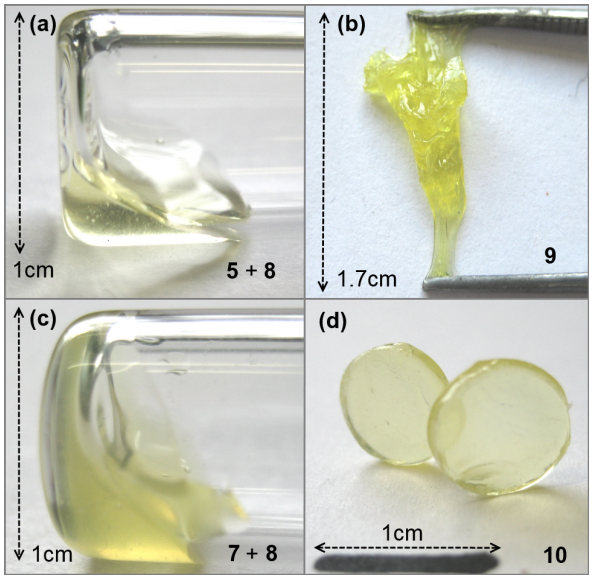

Figure 5: Illustration of the viscosity of a mixture of **5** and **8** (a), respectively **7** and **8** (c) before curing and the resulting materials **9** (b) and **10** (d), respectively after 24 h at 25 °C. **9** can be stretched easily by applying a force, whereas **10** can be shaped as a brittle disc.

Interestingly, a mixture of **7** and **8** yielding oligomer **10** displays 2.5-times faster curing than a mixture of **5** and **8**. In this case the gel point is reached already after about 8 to 9 h (Figure 4b). Horizontal lines for *G'* and *G''* are also observable shortly after. The resulting oligoadduct **10** can be shaped before curing and keeps this shape as a free-standing-disc after hardening (Figure 5d). This can be emphasized with the fact that *G'* and *G''* diverge considerably after the gel point transition.

A direct comparison of the curing properties of **9** and **10** is given in Figure 4c, which displays the complex viscosity (η*) calculated from *G'* and *G''*. As expected, the curves confirm the above described observations. In addition, η* at gel point transition of **10** compared to that of **9** is higher by factor of 2.8 (η* = 74 kPa*s (**10**), η* = 26 kPa*s (**9**)). The difference in rigidity of the cured products **9** and **10** is assumed to be caused by the different shape of side groups of the oligomers.

Additional proof of the different chain flexibility of the cured products **9** and **10** was conducted using DSC measurements. As expected, the T_g (glass transition temperature) of **9** (T_g = 6 °C) was significant lower than the value of the less flexible material **10** (T_g = 29 °C).

Furthermore, FTIR spectroscopy was performed to analyze the chemical process of oligoaddition of **8** with **5** directly after mixing of the monomers and after 24 h of curing at 25 °C (Figure 6). The epoxide-function of **8** exhibits two bands at 838 cm^{-1} and 908 cm^{-1} associated with its asymmetric, respectively symmetric ring deformation vibration and one peak at 1254 cm^{-1} caused by its C–O-stretching vibration. It becomes apparent that these bands vanish after 24 h due to the complete ring opening of the former epoxide group. However, the overlapping band at 1261 cm^{-1} assigned to the amine **5** (Supporting Information File 1) complicates the analysis in this band region. Furthermore, a broadening of the bands in the region of 3100 cm^{-1} and 3600 cm^{-1} can be attributed to increasing hydrogen bonded hydroxy stretching vibrations as a result of the ring opening. Generally, these observations are a strong evidence for a high conversion of the epoxide–amine adduct.

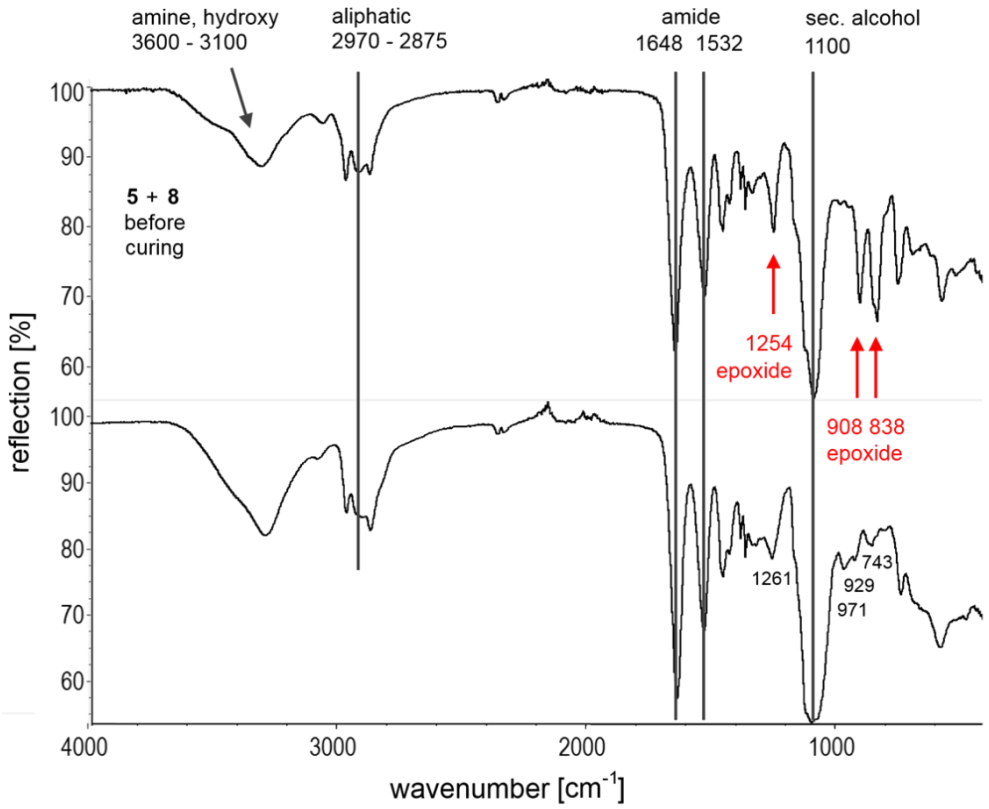

Figure 6: Comparison of the FTIR spectra of the monomer mixture of **5** and **8** and of the cured product **9** after 24 h.

The curing of **7** and **8** was also monitored by means of FTIR spectroscopy showing a similar disappearance of the specific bands of the epoxide function, accompanied by an increase of the hydroxy stretching vibrations (Supporting Information File 1).

Unfortunately, molecular weights of **9** and **10** could not yet be detected by use of size exclusion chromatography even under different conditions, probably due to the strong interaction of the functional groups with the column material. Also, because of its high thermosensitivity and tendency of cross linking on heating, mass spectrometry data were not useful for determination of that molecular weights. However, DLS measurements gave hydrodynamic diameters of 2.7 nm for **9** and 2.4 nm for **10** (Supporting Information File 1). This indicates the existence of oligomers rather than polymers. Comparing the hydrodynamic diameter of RAMEB-CD of ca. 1.4 nm in water (molecular weight = 1310 g/mol) with the hydrodynamic diameters of 2.7 nm for **9** and 2.4 nm for **10** these values correspond in a simple first approximation to molecular weights of around 1–3 thousands. Interestingly, the calculated values due to Carothers' equation (1.2-fold excess of the amine, complete conversion) gave an average molecular weight of 1760 g/mol for **9** and 1826 g/mol for **10**, respectively.

Conclusion

Two novel water soluble and thermoresponsive glycerol diglycidyl ether (**8**)–amine oligomers were obtained containing 2-amino-*N*-isopropylacetamide (**5**) and α-amino-ε-caprolactam (**7**), respectively. Complexation of RAMEB-CD with the side groups of the oligomers **9** and **10** influenced the LCST-behavior. In bulk, a mechanically flexible oligoadduct **9** and a rather brittle oligoadduct **10** were characterized.

Experimental

All reactants were commercially available and used without further purification. All solvents used were of analytical purity or freshly distilled. RAMEB-CD was obtained from Wacker Chemie GmbH, Burghausen, Germany and were used after being dried with a vacuum oil pump over P_4O_{10}. Glycine methyl ester hydrochloride (98%) and L(+)-lysine monohydrochloride (99+%) were purchased from Acros Organics, di-*tert*-butyl dicarbonate (97+%) and isopropylamine (99+%) were obtained from Alfa Aesar, glycerol diglycidyl ether and deuterium oxide (D_2O, 99.9% D) were purchased from Sigma Aldrich and chloroform-*d* ($CDCl_3$, 99.80% D) was obtained from Euriso-Top. ^{1}H NMR, ^{13}C NMR and ^{1}H-^{1}H-ROESY spectra were recorded on a Bruker Avance DRX 300 by using deuterium oxide or chloroform-*d* as solvents. The chemical

shifts (δ) are given in parts per million (ppm) using the solvent peak as an internal standard. Fourier transform infrared (FTIR) spectra were recorded on a Nicolet 6700 FTIR spectrometer equipped with an ATR unit. Turbidity measurements were conducted using a Tepper TP1 cloud-point photometer equipped with a laser with a wavelength of 670 nm. For all experiments a heating or cooling rate of 1 °C/min during continuous stirring was set and the critical temperature was determined at 50% of relative transmittance. Oscillatory rheological measurements were performed on a Haake Mars II rheometer by ThermoFisher Scientific. For this purpose a plate–plate construction (MP35, PP35Ti) was used. The temperature was set to 25 °C and was determined in the measuring plate with an accuracy of ±0.1 °C. The thermostat was regulated directly by software. For each sample the measurement period was set to 30 h. Sol–gel-transmission was determined by the arithmetic average of the first three intersections of *G'* and *G''* taking initial fluctuations due to homogenization and sheer-thinning processes not into account. Glass transition temperatures (T_g) were determined using a Mettler Toledo DSC 822e equipped with a sample robot TSO801RO. For calibration, standard tin, indium, and zinc samples were used. Heating and cooling curves were determined between −30 and 50 °C or −30 and 60 °C at a heating rate of 15 °C/min. The T_g values were calculated from the arithmetic average of the inflection points of the second, third and fourth heating curve. Electrospray ionization mass spectrometry (ESIMS) was conducted on a Bruker maXis 4G mass spectrometer and matrix-assisted laser desorption-ionization time-of-flight mass spectrometry (MALDI-TOF-MS) on a Bruker Dalomics Ultraflex 1 mass spectrometer. Melting points were obtained using a Büchi Melting Point B-545 apparatus at a heating rate of 1 °C/min. Dynamic light scattering (DLS) experiments were conducted on a Malvern Zetasizer Nano ZS ZEN 3600 at a temperature of 20 °C with a laser wavelength of 633 nm and a detection angle of 173°. The non-negative-least-squares algorithm was used for interpretation. The samples were dissolved in pure water of pH 7 and in a concentration of 1.5 mg/mL. Each measurement was performed at least five times and number-averaged diameters were used as result.

Synthesis of 2 [21]: 8.99 g (71.6 mmol) of glycine methyl ester hydrochloride (**1**) were suspended in 60 mL methylene chloride and 6.05 g (72.0 mmol) sodium hydrogen carbonate dissolved in 80 mL water and 12 g (205.3 mmol) sodium chloride were added. Under strong stirring a solution of 15.19 g (69.5 mmol) di-*tert*-butyl dicarbonate in 40 mL of methylene chloride was poured slowly into the mixture. Subsequently, the reaction batch was refluxed for 3 h and stirred at room temperature overnight. The phases were separated, the aqueous phase was washed twice with 30 mL of methylene chloride and the organic phases were combined. After drying over magnesium sulfate and filtration thereof methylene chloride was distilled off under reduced pressure and the product dried in vacuo. 11.9 g (62.9 mmol = 87.8%) of a colorless oil was obtained. FTIR (diamond) ν (cm^{-1}): 3500–3200 (br, NH), 1753 (s, ester), 1695 (vs, carbamate); ^{1}H NMR (300 MHz, $CDCl_3$) δ 5.22 (s, 1H, NH), 3.78 (d, J = 5.9 Hz, 2H, CH_2), 3.62 (s, 3H, OCH_3), 1.33 (s, 9H, $RC(CH_3)_3$); ^{13}C NMR (75 MHz, $CDCl_3$) δ 170.5 (1C, R-C(O)-OR), 155.4 (1C, RNH-C(O)-OR), 79.4 (1C, RO-C-Me_3), 51.7 (1C, OCH_3), 41.8 (1C, CH_2), 27.9 (3C, $RC(CH_3)_3$); ESIMS (acetone) *m*/*z*: 190.1 $[M + H]^+$, 212.1 $[M + Na]^+$.

Synthesis of 4: 9.39 g (49.7 mmol) of **2** were mixed with 11.21 g (189.7 mmol) isopropylamine (**3**) and 5.02 g (49.7 mmol) triethylamine. The mixture was stirred at room temperature for 3 days and subsequently refluxed for 2 days. In an adjacent step the solution was concentrated and precipitated in 500 mL of *n*-hexane. After drying in vacuo 8.6 g (39.8 mmol = 80.1%) of colorless crystals (melting point 102 °C) were obtained. FTIR (diamond) ν (cm^{-1}): 3292, 3222 (br, NH), 1692 (vs, carbamate), 1657, 1548 (vs, amide); ^{1}H NMR (300 MHz, $CDCl_3$) δ 6.41 (s, 1H, RC(O)-NH-R), 5.57 (s, 1H, R-NH-C(O)OR), 3.98 (m, 1H, CH-Me_2), 3.66 (d, J = 5.7 Hz, 2H, CH_2), 1.36 (s, 9H, $RC(CH_3)_3$), 1.06 (d, J = 6.6 Hz, 6H, $RHC(CH_3)_2$); ^{13}C NMR (75 MHz, $CDCl_3$) δ 169.1 (1C, R-C(O)-NHR), 156.7 (1C, RHN-C(O)-OR), 80.4 (1C, C-Me_3), 44.9 (1C, $CHMe_2$), 41.9 (1C, RHN-CH_2-C(O)R), 28.8 (3C, $RC(CH_3)_3$), 23.1 (2C, $RHC(CH_3)_2$); ESIMS (acetone) *m*/*z*: 217.2 $[M + H]^+$, 239.1 $[M + Na]^+$.

Synthesis of 5: 7.56 g (35.0 mmol) of **4** were suspended in 40 mL of water. On heavy stirring 30 mL of concentrated hydrochloric acid was added dropwise. The now homogenous solution was refluxed for 3 h and stirred at room temperature overnight. Afterwards, a pH value of 12–13 of the solution was adjusted by the addition of sodium hydroxide. The solution was concentrated and subsequently lyophilized. After extracting with methylene chloride the solvent was distilled off under reduced pressure and the resulting residue was dried in vacuo to give 1.14 g (9.8 mmol = 28.1%) of a colorless oil, that turns slightly yellow on heating or after time. FTIR (diamond), ν (cm^{-1}): 3600–3000 (br, NH, NH_2), 1644, 1544 (vs, amide); ^{1}H NMR (300 MHz, $CDCl_3$) δ 7.08 (s, 1H, NH), 3.82 (m, 1H, CH), 3.05 (s, 2H, CH_2), 1.49 (s, 2H, NH_2), 0.93 (d, J = 6.6 Hz, 6H, $RHC(CH_3)_2$); ^{13}C NMR (75 MHz, $CDCl_3$) δ 171.3 (1C, C(O)), 44.5 (1C, CH_2), 41.0 (1C, CH), 22.8 (2C, $RHC(CH_3)_2$); ESIMS (acetone) *m*/*z*: 117.1 $[M + H]^+$.

Synthesis of 7 [22]: A mixture of 20 g (109.5 mmol) L-lysine monohydrochloride (**6**), 4.38 g (109.5 mmol) sodium hydroxide, 60 g (589 mmol) aluminium oxide and 300 mL

n-butanol is heated to reflux for 48 h in a reaction vessel equipped with a water trap. Subsequently, the mixture is filtrated and the obtained pale yellow solution is concentrated under reduced pressure. After precipitation in diethyl ether, filtration, and drying in vacuo 8.1 g (63.2 mmol = 57.7%) of colorless/pale yellow crystals (melting point = 65–69 °C) are received. FTIR (diamond), ν (cm^{-1}): 3355, 3283 (br, NH), 2930, 2909, 2849 (m, CH), 1648 (s, amide); ^{1}H NMR (300 MHz, D_2O) δ 3.73 (dd, J = 11.0, 1.9 Hz, 1H, CH), 3.26 (m, 2H, RHN-CH_2-R), 2.02–1.30 (m, 6H, $(CH_2)_3$); ^{13}C NMR (75 MHz, D_2O) δ 181.3 (1C, C(O)), 52.7 (1C, CH), 41.3 (1C, RHN-CH_2-R), 32.4 (1C, RHC-CH_2-R), 27.7 (1C, CH_2), 27.6 (1C, CH_2); ESIMS (H_2O) *m*/*z*: 129.1 $[M + H]^+$.

Synthesis of 9: The viscous monomers **5** and **8** were mixed and stirred for several minutes. The obtained pale yellow oil was kept at 25 °C without stirring for 24 h to give a sticky and highly viscous material. FTIR (diamond), ν (cm^{-1}): 3600–3000 (br, NH, NH_2, OH), 2969, 2873 (m, CH), 1641, 1534 (vs, amide), 1101 (s, COH).

Synthesis of 10: Monomer **7** and monomer **8** were mixed thoroughly until a homogeneous solution was achieved. Afterwards, the mixture was kept at 25 °C without stirring for 24 h to give a brittle and dimensionally stable material. FTIR (diamond), ν (cm^{-1}): 3600–3000 (br, NH, NH_2, OH), 2924, 2858 (m, CH), 1650 (s, amide), 1077 (s, COH).

Supporting Information

The Supporting Information File 1 contains ^{1}H-^{1}H-ROESY spectra of oligomer **9** and **10**, respectively in presence of RAMEB-CD, additional FTIR spectra of the curing of **8** with **5** and **8** with **7**, respectively, and DLS measurements of **9** and **10**.

Supporting Information File 1

Additional ^{1}H-^{1}H-ROESY spectra, FTIR spectra and DLS data.
[http://www.beilstein-journals.org/bjoc/content/supplementary/1860-5397-9-315-S1.pdf]

References

1. Trellenkamp, T.; Ritter, H. *Macromol. Rapid Commun.* **2009,** *30,* 1736–1740. doi:10.1002/marc.200900250
2. Kretschmann, O.; Choi, S. W.; Miyauchi, M.; Tomatsu, I.; Harada, A.; Ritter, H. *Angew. Chem., Int. Ed.* **2006,** *45,* 4361–4365. doi:10.1002/anie.200504539
3. Saunders, B. R.; Vincent, B. *Adv. Colloid Interface Sci.* **1999,** *80,* 1–25. doi:10.1016/S0001-8686(98)00071-2
4. Schmaljohann, D. *Adv. Drug Delivery Rev.* **2006,** *58,* 1655–1670. doi:10.1016/j.addr.2006.09.020
5. Heskins, M.; Guillet, J. E. *J. Macromol. Sci., Part A* **1968,** *2,* 1441–1455. doi:10.1080/10601326808051910
6. Ritter, H.; Sadowski, O.; Tepper, E. *Angew. Chem., Int. Ed.* **2003,** *42,* 3171–3173. doi:10.1002/anie.200250814
7. Ritter, H.; Cheng, J.; Tabatabai, M. *Beilstein J. Org. Chem.* **2012,** *8,* 1528–1535. doi:10.3762/bjoc.8.173
8. Maatz, G.; Maciollek, A.; Ritter, H. *Beilstein J. Org. Chem.* **2012,** *8,* 1929–1935. doi:10.3762/bjoc.8.224
9. Zhu, J.-L.; Liu, K. L.; Zhang, Z.; Zhang, X.-Z.; Li, J. *Chem. Commun.* **2011,** *47,* 12849–12851. doi:10.1039/c1cc15965h
10. Choi, S.; Munteanu, M.; Ritter, H. *J. Polym. Res.* **2009,** *16,* 389–394. doi:10.1007/s10965-008-9240-0
11. Ritter, H.; Tabatabai, M. *Prog. Polym. Sci.* **2002,** *27,* 1713–1720. doi:10.1016/S0079-6700(02)00022-9
12. Wenz, G. *Angew. Chem., Int. Ed. Engl.* **1994,** *33,* 803–822. doi:10.1002/anie.199408031
13. Szejtli, J. *J. Mater. Chem.* **1997,** *7,* 575–587. doi:10.1039/a605235e
14. Wang, J.; Li, S.; Ye, L.; Zhang, A.-Y.; Feng, Z.-G. *Macromol. Rapid Commun.* **2012,** *33,* 1143–1148. doi:10.1002/marc.201200017
15. Klee, J.; Hörhold, H.-H.; Schütz, H. *Acta Polym.* **1987,** *38,* 293–299. doi:10.1002/actp.1987.010380509
16. Klee, J.; Hörhold, H.-H. Epoxide-amine addition polymers, linear. In *Polymeric Materials Encyclopedia;* Salamone, J. C., Ed.; CRC Press: Boca Raton, Florida, USA, 1996; Vol. 3, D-E, pp 2182–2192.
17. Ramesh, D.; Vasudevan, T. *Prog. Org. Coat.* **2009,** *66,* 93–98. doi:10.1016/j.porgcoat.2009.06.007
18. Swier, S.; Van Mele, B. *Polymer* **2003,** *44,* 2689–2699. doi:10.1016/S0032-3861(03)00138-1
19. Chen, J.-L.; Chang, F.-C. *Polymer* **2001,** *42,* 2193–2199. doi:10.1016/S0032-3861(00)00511-5
20. Liu, X.; Wang, Y.; Cao, Y.; Yadama, V.; Xian, M.; Zhang, J. *Carbohydr. Polym.* **2011,** *83,* 1180–1184. doi:10.1016/j.carbpol.2010.09.019
21. Biagini, S. C. G.; Gibsoné Thomas, S. E.; Keen, S. P. *J. Chem. Soc., Perkin Trans. 1* **1998,** 2485–2499. doi:10.1039/a804147d
22. Frost, J. W. Synthesis of caprolactam from lysine. WO Patent 2005/123669 A1, Dec 29, 2005.
23. Philippe, C.; Milcent, T.; Crousse, B.; Bonnet-Delpon, D. *Org. Biomol. Chem.* **2009,** *7,* 2026–2028. doi:10.1039/b902081k
24. Mondrzyk, A.; Mondrzik, B.; Gingter, S.; Ritter, H. *Beilstein J. Org. Chem.* **2012,** *8,* 2118–2123. doi:10.3762/bjoc.8.238
25. Obels, D.; Ritter, H. *Macromol. Rapid Commun.* **2013,** *34,* 879–882. doi:10.1002/marc.201300054

Beilstein Journal of Organic Chemistry

N,*N*′-(Hexane-1,6-diyl)bis(4-methyl-*N*-(oxiran-2-ylmethyl)benzenesulfonamide): Synthesis via cyclodextrin mediated *N*-alkylation in aqueous solution and further Prilezhaev epoxidation

Julian Fischer, Simon Millan and Helmut Ritter*

Full Research Paper

Open Access

Address:
Institute of Organic Chemistry and Macromolecular Chemistry, Heinrich-Heine-University Düsseldorf, Universitätsstraße 1, D-40225 Düsseldorf, Germany

Email:
Helmut Ritter* - h.ritter@hhu.de

* Corresponding author

Keywords:
alkylation; cyclodextrins; epoxy; rheology; sulfonamides

Beilstein J. Org. Chem. **2013,** *9,* 2834–2840.
doi:10.3762/bjoc.9.318

Received: 02 October 2013
Accepted: 18 November 2013
Published: 09 December 2013

This article is part of the Thematic Series "Superstructures with cyclodextrins: Chemistry and applications".

Associate Editor: C. Stephenson

Abstract

N-alkylation of *N*,*N*′-(hexane-1,6-diyl)bis(4-methylbenzenesulfonamide) with allyl bromide and subsequent Prilezhaev reaction with *m*-chloroperbenzoic acid to give *N*,*N*′-(hexane-1,6-diyl)bis(4-methyl-*N*-(oxiran-2-ylmethyl)benzenesulfonamide) is described. This twofold alkylation was performed in aqueous solution, whereby α-, and randomly methylated β-cyclodextrin were used as adequate phase transfer catalysts and the cyclodextrin–guest complexes were characterized by ^{1}H NMR and 2D NMR ROESY spectroscopy. Finally, the curing properties of the diepoxide with lysine-based α-amino-ε-caprolactam were analyzed by rheological measurements.

Introduction

Various diepoxides easily react with amines or diamines to form cross-linked, cyclic or linear addition-polymers, which are implemented in construction, electronic, aerospace, medical and dental industries [1,2]. Hereby, bisphenol A diglycidyl ether (BADGE) is often used [3,4]. However, non-bisphenol A based diepoxides are subject to intensive research [5-9]. The industrial synthesis of BADGE and other commercially available diepoxides proceeds mainly by using epichlorohydrin, whereby usually several side products and oligomers are formed in significant concentrations [10-12]. An alternative route is a two-step reaction via *N*-allylation and further Prilezhaev epoxidation with peroxides [13-15]. The solubility of hydrophobic reactants in water can be increased significantly by cyclodextrins (CD) and thereby the use of organic solvents can be reduced [16-18]. To our best knowledge, CD mediated *N*-alkylation of sulfonamides is not yet described. Generally, only a few exam-

ples are known in literature about CD assisted alkylation of amines in aqueous solution [19-22]. Hence, in this work, we wish to present our direct and CD mediated method to alternative sulfonamide based diepoxides, focusing on one characteristic example. Furthermore, the polymerization of these types of diepoxides was investigated with lysine-based α-amino-ε-caprolactam through rheological measurements.

Results and Discussion

N,*N*′-(Hexane-1,6-diyl)bis(4-methylbenzenesulfonamide) (**3**), as precursor for the subsequent *N*-alkylation and further Prilezhaev epoxidation, was synthesized easily from *p*-toluenesulfonyl chloride (**1**) and hexamethylenediamine (**2**) [23]. The resulting crystalline sulfonamide was first described in 1927 prepared from 1,6-dibromohexane and *p*-toluenesulfonamide [24]. The subsequent two-fold *N*-alkylation of **3** with allyl bromide (**4**) was conducted in *N*,*N*-dimethylformamide as solvent, as well as in aqueous solution via CD-complexation (Scheme 1).

Unmodified **3** is neither in a neutral nor in a basic milieu significantly soluble. However, by complexation of **3** with two equivalents of randomly methylated β-cyclodextrin (β-CD) to give **3β**, water solubility could be increased distinctively. Characterization of the inclusion complex of β-CD with **3** in D_2O solution was conducted using 2D NMR ROESY spectroscopy (Figure 1).

Thereby, proton signals at 7.0 and 7.4 ppm can be assigned to the aromatic protons of **3**. Furthermore, the protons of its *p*-methyl moiety demonstrate a singlet signal at 2.1 ppm. As illustrated in Figure 1, interaction of these protons with the inner protons of β-CD in the range of 3.3 to 3.8 ppm is visible.

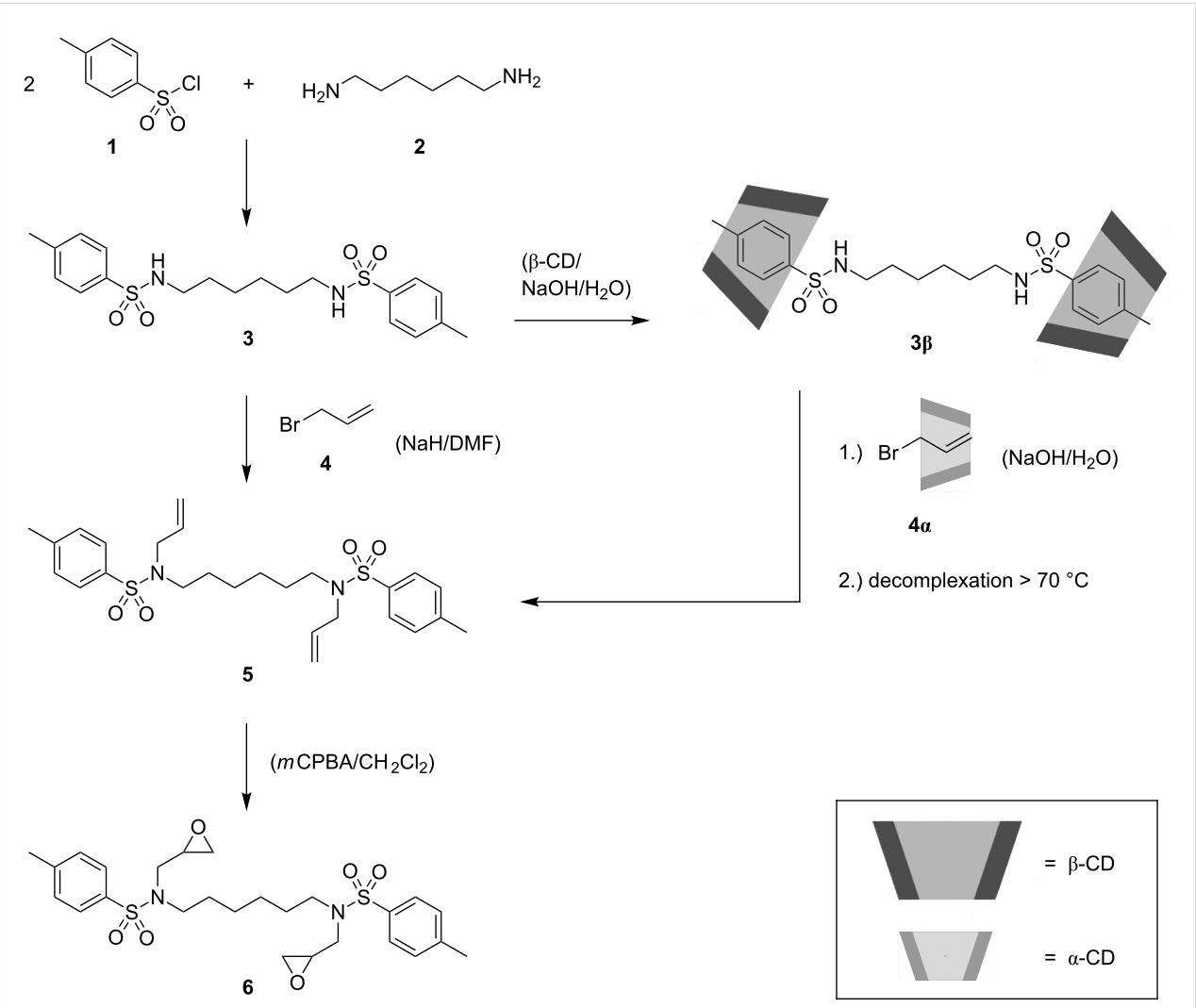

Scheme 1: Synthesis of sulfonamide **3**, *N*-alkylation of **3** in organic solution and of CD-complex (**3β**) in aqueous phase to obtain **5** and the subsequent epoxidation with *m*-chloroperbenzoic acid (*m*CPBA) to yield product **6**.

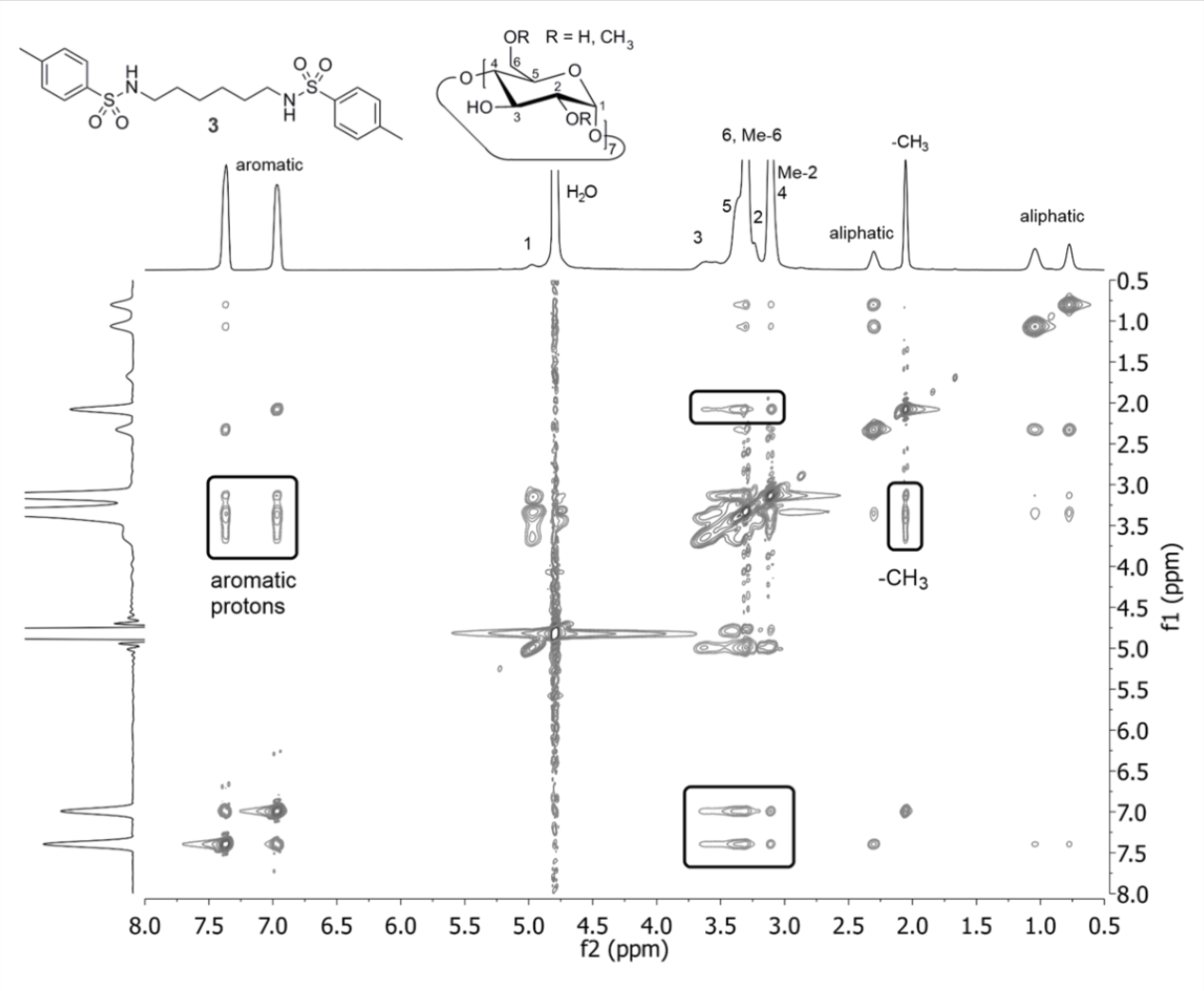

Figure 1: 2D NMR ROESY spectrum of the complex of **3** with β-CD in D_2O, displaying the interaction of the tosyl protons with the β-CD protons.

This strongly indicates a self-agglomeration of the tosyl groups of **3** with β-CD. Further confirmation of these findings is a perceivable downfield shifting of the proton signals of **3β** compared to **3** suspended in D_2O, since they are magnetically shielded by the β-CD cavity.

Additionally, the water solubility of **4** is limited as well (3.83 g L^{-1}) [25]. Since the stability of CD–guest complexes often depends on the size of the guest molecule relative to the CD cavity, stability constants of unbranched alkyl chains or vinyl groups are the highest with α-CD (six glucose units) and for tosyl groups with β-CD (seven glucose units), respectively [18]. Therefore, the water solubility of **4** was increased by addition of α-CD (**4α**). 2D NMR ROESY spectroscopy was also performed for **4α**. As expected, the protons of the allyl-group at 5.9 ppm, 5.1 ppm and 4.0 ppm correlate with the α-CD protons in the range of 3.9 to 3.5 ppm (Figure S1, Supporting Information File 1).

Two-fold *N*-alkylation of β-CD-complexed *N*,*N*′-(hexane-1,6-diyl)bis(4-methylbenzenesulfonamide) (**3β**) with **4α** in aqueous solution gave *N*,*N*′-(hexane-1,6-diyl)bis(*N*-allyl-4-methylbenzenesulfonamide) (**5**), which could easily be precipitated and separated from the CD-complex by heating, since decomplexation occurred over 70 °C. The remaining aqueous CD-solution can be reused in principle, since in an alkaline milieu CD-rings are stable. A comparison of the ^{1}H NMR spectra of **5** received in organic and in aqueous solution, respectively is given in Supporting Information File 1 (Figure S2) to show no significant differences. Also, CD signals in the range of 3.0 to 4.0 ppm are not observable. That indicates complete CD-decomplexation of **5**. Subsequently, **5** was epoxidized in a Prilezhaev reaction with *m*-chloroperbenzoic acid (*m*CPBA) in methylene chloride to obtain *N*,*N*′-(hexane-1,6-diyl)bis(4-methyl-*N*-(oxiran-2-ylmethyl)benzenesulfonamide) (**6**). The proceeding reaction was monitored by means of ^{1}H NMR spectroscopy, since the allyl protons of **5** in the range of 5.0 to 5.7 ppm vanish on

conversion (Figure S3, Supporting Information File 1). To illustrate the curing properties of the synthesized diepoxide, **6** was reacted in a ring-opening polymerization with the primary amine α-amino-ε-caprolactam (**8**). **8** was synthesized by cyclization of lysine (**7**) (Scheme 2). Hence, an increase of the reactivity of the primary amino group towards the epoxide function compared to the amino groups in native lysine was expected [26-28].

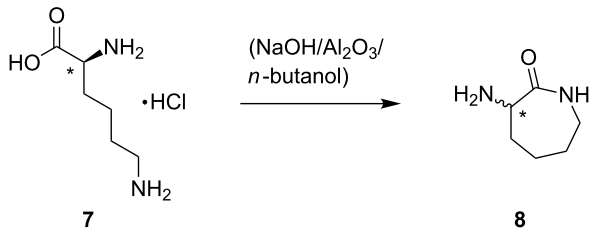

Scheme 2: Cyclization of L-(+)-lysine monohydrochloride to give racemate **8**.

As illustrated in Figure 2A, oscillatory measurements display an initial high viscosity for a mixture of **6** and **8**, since its complex viscosity (η*), calculated from storage modulus *G'* and loss modulus *G''*, exhibits low four-digit values at 50 °C. However, η* increases further on time until the sol–gel-transition (gelpoint), where *G'* is equal to *G''*, is reached after about 40 to 45 min (Figure 2B). Generally, by passing this point the mixture is no longer capable of flowing. Shortly after reaching the gelpoint, η* is not significantly rising further, which is a sign for completed conversion. The resulting poly-adduct **9** exhibits a glass transition temperature (T_g) of around 49 °C. Equivalent measurements of standard BADGE demonstrated a gelpoint after about 99 min and a T_g of about 74 °C (Figure S4, Supporting Information File 1). Thus, the curing properties for a mixture of **6** with **8** are relatively comparable to a mixture of BADGE with **8**, whereby the observed differences can be caused by different reactivity of the oxirane moieties or unequal solubility of the respective diepoxide with **8**.

By means of IR spectroscopy, ring opening polymerization of epoxides with amines can be monitored. The spectrum of **6** exhibits weak bands at 1253 and 895 cm^{-1}, which can be assigned to the C–O-stretching vibration and the symmetric ring deformation vibration, respectively, of its epoxide groups. On curing at 50 °C, a broad band between 3100 and 3600 cm^{-1} appears which is caused by hydrogen bonded hydroxy stretching vibrations originating from epoxide ring opening. The epoxide bands seem to vanish after curing, which is a sign

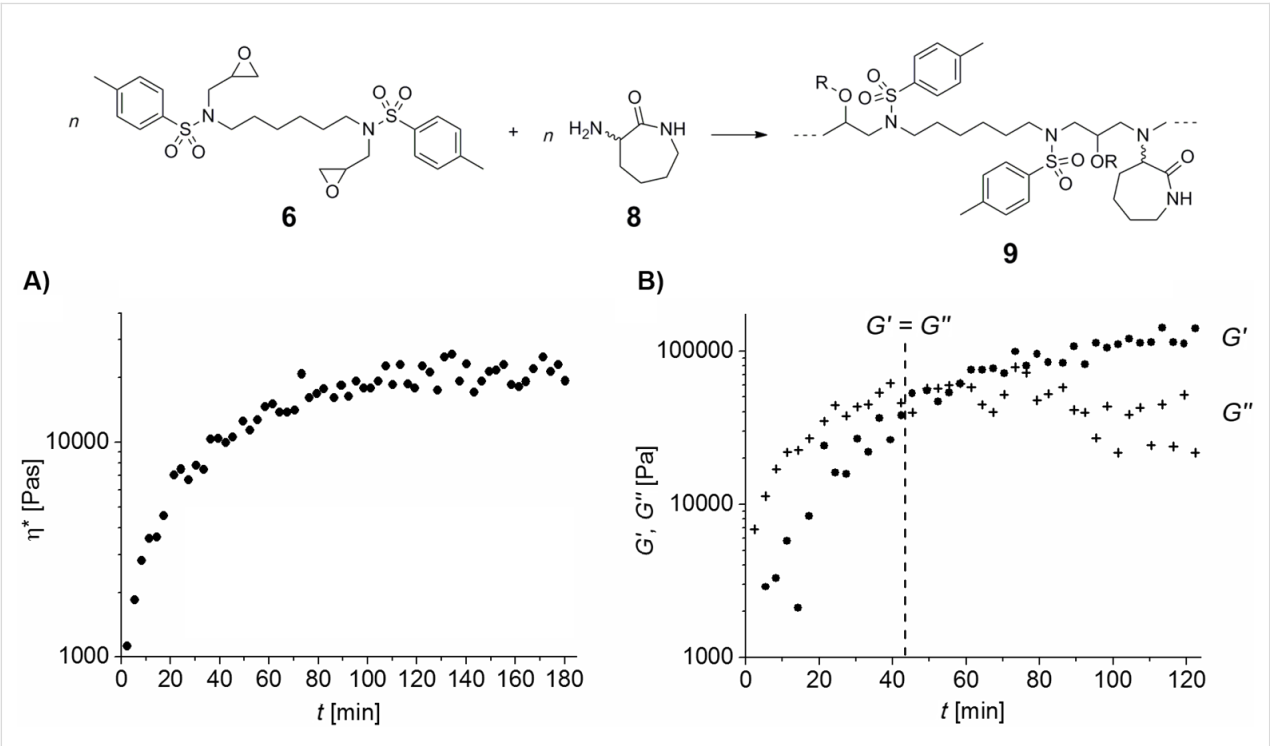

Figure 2: Oscillatory rheological measurements of an equimolar mixture of **6** and **8** at 50 °C. Illustrated is the complex viscosity (A), as well as *G'* and *G''* (B) in dependence of time. The polymer **9** is displayed as an idealized structure (R = H or polymer network; crosslinking via addition of epoxide moieties to the hydroxy functions is likely [2]).

for high conversion. However, due to overlaps of broader bands in adjacent areas, no clear statement can be made in this regard (Figure S5, Supporting Information File 1). Based on this work, future research could focus on conducting the entire synthesis of **6** CD mediated in aqueous solution. Also, the presented pathway for alkylation in aqueous media could be transferred to the solvent saving synthesis of further alkylated products.

Conclusion

An alternative route for the synthesis of *N*,*N*′-(hexane-1,6-diyl)bis(4-methyl-*N*-(oxiran-2-ylmethyl)benzenesulfonamide) (**6**) via *N*-alkylation of *N*,*N*′-(hexane-1,6-diyl)bis(4-methylbenzenesulfonamide) (**3**) and further oxidation was described. For the first time, the CD-mediated *N*-alkylation of a sulfonamide was conducted, whereby water solubility of **3** and **4** were increased by adding β-CD and α-CD, respectively. By applying oscillatory rheological measurements, a mixture of **6** and **8** reached the gelpoint after about 40 to 45 min at 50 °C. Thus, an environmentally more sustainable route for the synthesis of a bisphenol A free diepoxide was presented, which appears to be a suitable substitute for technically employed bisphenol A diglycidyl ether.

Experimental

All reactants were commercially available and unless otherwise stated used without further purification. All solvents used were of analytical purity or freshly distilled. β-CD and α-CD were obtained from Wacker Chemie GmbH and were used after being dried with a vacuum oil pump over P_4O_{10}. *p*-Toluenesulfonyl chloride (98%) was obtained from Alfa Aesar, allyl bromide (99%), 3-chloroperoxybenzoic acid (70–75%), 1,6-hexanediamine (99.5+%) and L-(+)-lysine monohydrochloride (99+%) were purchased from Acros Organics, bisphenol A diglycidyl ether and deuterium oxide (99.9%) were provided from Sigma Aldrich, chloroform-*d* (99.80%) was obtained from Euriso-Top and dimethyl sulfoxide-d_6 (99.9%) was purchased from Deutero. ^{1}H NMR, ^{13}C NMR and 2D ROESY spectra were recorded on a Bruker Avance DRX 300 and a Bruker Avance III – 600 by using deuterium oxide, dimethyl sulfoxide-d_6 or chloroform-*d* as solvents. The chemical shifts (δ) are given in parts per million (ppm) using the solvent peak as an internal standard. FTIR spectra were recorded on a Nicolet 6700 FTIR spectrometer equipped with an ATR unit. Oscillatory rheological measurements were performed on a Haake Mars II rheometer by ThermoFisher Scientific. For this purpose a plate-plate construction (MP35, PP35Ti) was used. The temperature was set to 50 °C and was determined in the measuring plate with an accuracy of ±0.1 °C. The Sol–gel-transmission was determined by the first intersection of G' and G''. Graphs were plotted using reduced data, calculated by the median of three following values. The glass transition temperature (T_g) was determined using a Mettler Toledo DSC 822e equipped with a sample robot TSO801RO. For calibration, standard tin, indium, and zinc samples were used. Heating and cooling curves were determined between −30 and 130 °C at a heating rate of 15 °C/min. The T_g value was taken from the inflection point of the second heating curve. Electrospray ionization mass spectrometry (ESIMS) was conducted on a Bruker maXis 4G mass spectrometer. Melting points were obtained using a Büchi Melting Point B-545 apparatus at a heating rate of 5 °C/min.

Synthesis of 5 in organic solution: 7.0 mmol of **3** were dissolved in 25 mL dried *N*,*N*-dimethylformamide and the solution was cooled to 0 °C in an ice bath. The apparatus was set under constant nitrogen-flow and 17.2 mmol of sodium hydride were added. Afterwards, the suspension was stirred for 2 h and subsequently, 35 mmol of allyl bromide (**4**), which was filtrated through neutral aluminium oxide, was added dropwise. The resulting mixture was stirred at 50 °C for 18 h and after cooling to room temperature it was diluted with 40 mL of saturated solution of ammonium chloride. The aqueous phase was washed threefold with 40 mL of ethyl acetate, the organic phases were combined and the solvent was evaporated under reduced pressure. After drying, 5.3 mmol (76% yield, not optimized) of brown slurry were received. The raw product was purified by column chromatography (*n*-hexane/ethyl acetate 2:1) to give 3.98 mmol (57% yield, not optimized) of **5**. ^{1}H NMR (300 MHz, DMSO-d_6, δ) 7.68 (d, J = 8.3 Hz, 4H, Ar-H), 7.40 (d, J = 7.9 Hz, 4H, Ar-H), 5.60 (ddt, J = 6.3, 10.1, 17.1 Hz, 2H, H_2C=C*H*-CH_2-), 5.19 (dd, J = 17.0, 1.6 Hz, 2H, CH_2, *trans*), 5.11 (dd, J = 10.1, 1.6 Hz, 2H, CH_2, *cis*), 3.73 (d, 4H, J = 6.4 Hz, allyl-CH_2-), 2.99 (t, J = 7.4 Hz, 4H, N-CH_2-), 2.39 (s, 6H, Ar-CH_3), 1.38 (m, 4H, -CH_2-), 1.14 (m, 4H, -CH_2-); ^{13}C NMR (75 MHz, DMSO-d_6, δ) 143.0 (2C, Ar(*C*)-CH_3), 136.6 (2C, RO_2S-(C)Ar), 133.5 (2C, R-*C*H=CH_2), 129.8 (4C, Ar(C)), 126.9 (4C, Ar(C)), 118.5 (2C, RHC=*C*H_2), 50.1 (2C, N-*C*H_2-CHR), 47.0 (2C, N-*C*H_2-CH_2R), 27.5 (2C, -CH_2-), 25.5 (2C, -CH_2-), 20.9 (2C, -CH_3); IR (diamond) ν (cm^{-1}): 2951, 2916, 2855 (m, -CH_2-, Ar-CH_3), 1652 (w, C=C), 1597 (m, Ar), 1336, 1155 (v, R-SO_2-NR_2), 1090 (m, Ar-S-), 965 (v, -CH_2-), 934 (m, R-SO_2-NR_2), 816 (s, Ar-H (neighbouring)); ESIMS *m*/*z*: 505.4 $[M + H]^+$, 527 $[M + Na]^+$; mp 70 °C.

Synthesis of 5 CD mediated in aqueous solution: 6.8 g of randomly methylated β-CD and 25 mmol of sodium hydroxide were dissolved in 15 mL double distilled water and 2.4 mmol of **3** were added. The initial suspension was stirred at 45 °C for some minutes until a homogenous solution was achieved. Simultaneously, a homogenous solution of 1.15 mmol of **4**, 13.8 mmol of sodium hydroxide and 1.6 mmol of α-CD in 10 mL of double distilled water was prepared. Subsequently, the solution of **4α** was added dropwise to the solution of **3β**.

The combined solutions were stirred at 50 °C and over the next 15 h further 8 mmol of **4** were added successively. After two days, the solution was heated to 70 °C for 30 min, filtrated and the precipitate dried in vacuo. 0.9 mmol (38% yield, not optimized) of a colorless powder of **5** was obtained. Spectral data of **5** synthesized in aqueous solution are given in the Supporting Information File 1.

Synthesis of 6: 3.0 mmol of **5** were dissolved in 15 mL of methylene chloride. Subsequently, 12.6 mmol of *m*CPBA dissolved in 20 mL methylene chloride were added. After two days of stirring at room temperature the reaction batch was treated with further 8.7 mmol of *m*CPBA and stirred for 4 days. Afterwards, the suspension was filtrated, the filtrate diluted with 20 mL of methylene chloride and washed three times with an aqueous solution of 10% sodium bisulfite. Then, the organic phase was treated twice with 50 mL each of sodium hydrogen carbonate solution and stirred for 1.5 h. Subsequently, the organic phase was dried over magnesium sulfate and the solvent removed under reduced pressure to obtain 1.7 mmol (57% yield, not optimized) of **6**. ^{1}H NMR (300 MHz, $CDCl_3$, δ): 7.67 (d, J = 8.3 Hz, 4H, Ar-H), 7.28 (d, J = 7.9 Hz, 4H, Ar-H), 3.59 (dd, J = 3.4, 15.2 Hz, 2H, N-CH_2-CH-, *trans*), 3.15 (m, 4H, N-CH_2-CH_2-), 3.05 (m, 2H, -CH-), 2.87 (dd, J = 6.5, 15.2 Hz, 2H, N-CH_2-CH-, *cis*), 2.74 (dd, J = 5.3, 4.2 Hz, 2H, O–CH_2, *cis*), 2.49 (dd, J = 2.6, 4.3 Hz, 2H, O–CH_2, *trans*), 2.40 (s, 6H, Ar-CH_3), 1.55 (m, 4H, -CH_2-), 1.27 (m, 4H, -CH_2-); ^{13}C NMR (75 MHz, $CDCl_3$, δ) 143.6 (2C, Ar(*C*)-CH_3), 136.8 (2C, RO_2S-(C)Ar), 130.0 (4C, Ar(C)), 127.3 (4C, Ar(C)), 51.2 (2C, epoxy), 51.0 (2C, N-*C*H_2-CH_2R), 49.4 (2C, N-*C*H_2-epoxy), 45.4 (2C, epoxy), 28.5 (2C, -CH_2-), 26.3 (2C, -CH_2-), 21.6 (2C, -CH_3); IR (diamond) ν (cm^{-1}): 2997, 2927, 2862 (m, -CH_2-, Ar-CH_3), 1597 (m, Ar), 1435 (m, -CH_2-), 1335 (v, R-SO_2-NR_2), 1253 (w, -C-O-C-), 1154 (v, R-SO_2-NR_2), 1090 (m, Ar-S-), 895 (w, -C-O-C-), 839 (m, C-C (ring)), 816 (s, Ar-H (neighbouring)); ESIMS m/z: 537.1 $[M + H]^+$, 559.1 $[M + Na]^+$.

Synthesis of 3 and 8: Sulfonamide **3** was obtained in a modified synthesis similar to that reported in [23]. The synthesis of **8** was performed according to [29].

Supporting Information

Experimental procedures and spectral data for the synthesis of **3** and **8** are given in the Supporting Information.

Supporting Information File 1

Additional spectra and experimental data.
[http://www.beilstein-journals.org/bjoc/content/supplementary/1860-5397-9-318-S1.pdf]

References

1. Klee, J. E.; Flammersheim, H.-J. *Macromol. Chem. Phys.* **2002,** *203,* 100–108. doi:10.1002/1521-3935(20020101)203:1<100::AID-MACP100>3.0.CO;2-J
2. Klee, J.; Hörhold, H.-H. Epoxide-amine addition polymers, linear. In *Polymeric Materials Encyclopedia;* Salamone, J. C., Ed.; CRC Press: Boca Raton, Florida, USA, 1996; Vol. 3, D-E, pp 2182–2192.
3. Wang, L.; Wu, Y.; Zhang, W.; Kannan, K. *Environ. Sci. Technol.* **2012,** *46,* 12968–12976. doi:10.1021/es304050f
4. Resende, L. M.; Rached-Junior, F. J. A.; Versiani, M. A.; Souza-Gabriel, A. E.; Miranda, C. E. S.; Silva-Sousa, Y. T. C.; Sousa Neto, M. D. *Int. Endodont. J.* **2009,** *42,* 785–793. doi:10.1111/j.1365-2591.2009.01584.x
5. Fenouillot, F.; Rousseau, A.; Colomines, G.; Saint-Loup, R.; Pascault, J.-P. *Prog. Polym. Sci.* **2010,** *35,* 578–622. doi:10.1016/j.progpolymsci.2009.10.001
6. Chiu, Y.-C.; Chou, I. C.; Tseng, W.-C.; Ma, C.-C. M. *Polym. Degrad. Stab.* **2008,** *93,* 668–676. doi:10.1016/j.polymdegradstab.2007.12.014
7. Shikha, D.; Kamani, P. K.; Shukla, M. C. *Prog. Org. Coat.* **2003,** *47,* 87–94. doi:10.1016/S0300-9440(02)00159-5
8. Tao, Z.; Yang, S.; Chen, J.; Fan, L. *Eur. Polym. J.* **2007,** *43,* 1470–1479. doi:10.1016/j.eurpolymj.2007.01.039
9. Pews, R. G. Diepoxide derivatives of *N,N**-disubstituted disulfonamides. U.S. Patent 0128978 A1, June 15, 2006.
10. Kolman, A.; Chovanec, M.; Osterman-Golkar, S. *Mutat. Res.* **2002,** *512,* 173–194. doi:10.1016/S1383-5742(02)00067-4
11. Braun, D.; Lee, D. W. *Angew. Makromol. Chem.* **1976,** *51,* 11–24. doi:10.1002/apmc.1976.050510102
12. Braun, D.; Lee, D. W. *Angew. Makromol. Chem.* **1977,** *57,* 111–122. doi:10.1002/apmc.1977.050570109
13. Prileschajew, N. *Ber. Dtsch. Chem. Ges.* **1909,** *42,* 4811–4815. doi:10.1002/cber.190904204100
14. Woods, K. W.; Beak, P. *J. Am. Chem. Soc.* **1991,** *113,* 6281–6283. doi:10.1021/ja00016a061
15. Mimoun, H. *Angew. Chem., Int. Ed. Engl.* **1982,** *21,* 734–750. doi:10.1002/anie.198207341
16. Ritter, H.; Tabatabai, M. *Prog. Polym. Sci.* **2002,** *27,* 1713–1720. doi:10.1016/S0079-6700(02)00022-9
17. Alupei, V.; Alupei, I. C.; Ritter, H. *Macromol. Rapid Commun.* **2005,** *26,* 40–45. doi:10.1002/marc.200400442
18. Wenz, G. *Angew. Chem., Int. Ed. Engl.* **1994,** *33,* 803–822. doi:10.1002/anie.199408031
19. Surendra, K.; Krishnaveni, N. S.; Sridhar, R.; Rao, K. R. *Tetrahedron Lett.* **2006,** *47,* 2125–2127. doi:10.1016/j.tetlet.2006.01.124
20. Zhang, Q.; Cheng, G.; Huang, Y.-Z.; Qu, G.-R.; Niu, H.-Y.; Guo, H.-M. *Tetrahedron* **2012,** *68,* 7822–7826. doi:10.1016/j.tet.2012.07.025
21. Yamaguchi, I.; Osakada, K.; Yamamoto, T. *Macromolecules* **1997,** *30,* 4288–4294. doi:10.1021/ma970051p
22. Li, W.; Zhang, W.; Ma, X.; Wang, P.; Du, M. *Appl. Catal., A: Gen.* **2012,** *419–420,* 210–214. doi:10.1016/j.apcata.2012.01.030
23. Stetter, H.; Roos, E.-E. *Chem. Ber.* **1954,** *87,* 566–571. doi:10.1002/cber.19540870421
24. Müller, A.; Sauerwald, A. *Monatsh. Chem.* **1927,** *48,* 727–732.
25. Tewari, Y. B.; Miller, M. M.; Wasik, S. P.; Martire, D. E. *J. Chem. Eng. Data* **1982,** *27,* 451–454. doi:10.1021/je00030a025
26. Philippe, C.; Milcent, T.; Crousse, B.; Bonnet-Delpon, D. *Org. Biomol. Chem.* **2009,** *7,* 2026–2028. doi:10.1039/b902081k

27. Brotzel, F.; Chu, Y. C.; Mayr, H. *J. Org. Chem.* **2007,** *72,* 3679–3688. doi:10.1021/jo062586z
28. Brotzel, F.; Mayr, H. *Org. Biomol. Chem.* **2007,** *5,* 3814–3820. doi:10.1039/b713778h
29. Frost, J. W. Synthesis of Caprolactam from Lysine. WO Patent 2005/123669 A1, Dec 29, 2005.

License and Terms